SAFETY ANALYSIS REPORT

FOR THE

NUPAC 10/140MB SHIPPING CASK

JULY, 1989

Prepared by: Nuclear Packaging, Inc.
1010 South 336th Street
Federal Way, WA 98003

NOTICE

This Safety Analysis Report for the NuPac Model 10/140MB Shipping Cask and all associated drawings including amendments thereto are the property of Nuclear Packaging, Inc., Federal, Washington. This material is being made available for the purpose of obtaining required certifications from the U. S. Nuclear Regulatory Commission and to enable others to register with the U.S.N.R.C. as a user of this package. No other use of this material is authorized unless by written consent of Nuclear Packaging, Inc. Parties who may come into possession of this material are cautioned that the information is not to be reproduced in any form without the prior written consent of Nuclear Packaging, Inc.

TABLE OF CONTENTS

1.0 GENERAL INFORMATION

1.1 Introduction

The NuPac 10/140MB Cask has has been developed for the purpose of safely transporting Type B quantities of radioactive material. The purpose of this Safety Analysis Report is to demonstrate compliance of the package with 10 CFR 71 regulatory requirements. The package is capable of safely transporting Type B quantities of radioactive materials. Authorization is sought for shipment by cargo vessel, motor vehicle and rail.

1.2 Package Description

1.2.1 Packaging

1.2.1.1 General Description

The NuPac 10/140MB reusable shipping package is designed to protect radioactive material from normal and hypothetical accident conditions of transport.

The NuPac 10/140MB Cask is a top and (optionally) bottom loading transport shield designed specifically for the safe transport of Type B levels of radioactive materials. The shield can accommodate full capacity liners, or miscellaneous form cargo such as 55 gallon drums, irradiated hardware, etc.

1.2.1.2 Materials of Construction, Dimensions and Fabricating Methods

General arrangement drawings of the NuPac 10/140MB are included in Appendix 1.3.1. These show the overall dimensions as well as materials of construction.

The cask body consists of external and internal steel shells separated by a 2.5 inch thick lead biological shield in the annular space between these two shells. The top and bottom ends of the cylindrical cask are constructed of stainless steel castings or forgings. The 0.75 inch thick inner steel shell is constructed of 304 stainless steel plate. The 1.25 inch thick outer steel shell is constructed of carbon steel.

The top (and as an option, the bottom) serves as a removable cask lid and is secured to the cylindrical cask body by eight 2-1/2 inch diameter bolts. Bolting material is ASTM A-320, Grade L43. A 29 inch diameter secondary cask lid is located in the center of the top primary lid and is secured to the primary lid by sixteen 1-1/4 inch bolts. Lifting lugs and tiedowns are a structural part of the package.

The top and bottom impact limiters consist of stainless steel sheet metal enclosing high-density polyurethane foam.

1.2.1.3 Containment Vessel

The inner shell together with the top and bottom end plates of the cask serve as the containment vessel. Its mechanical configuration is described in the foregoing paragraph.

Two pairs of butyl O-ring seals are employed in both the primary and secondary lid interfaces. These 'EnviroSeals^{tm}' are of a unique design, affording an easily maintained high level of containment to the contents of the 10/140MB.

Waste products will be contained in 55 gallon drums, in heavy gauge disposable steel liners, in crates or other suitable palletized forms.

1.2.1.4 Neutron Absorbers

There are no materials used as neutron absorbers or moderators in the NuPac 10/140MB package.

1.2.1.5 Package Weight

The gross, net and payload weights of the NuPac 10/140MB Package and components are as follows:

Component	Weight (lb.)
Top lid assembly	8,430
Cask body	26,960
Bottom plate/lid	6,460
2 impact limiters	11,150
Package total net weight	53,000
Maximum payload	15,000
Package total gross weight	68,000

1.2.1.6 Receptacles

There are no internal or external structures supporting or protecting receptacles, except as described in 1.2.1.7 below regarding the optional drain port.

1.2.1.7 Containment Penetrations

The casks are provided with a 0.44 inch diameter drain port in the bottom plate, suitably counter-drilled and tapped to accept an o-ring sealed pipe plug. The drain port is used for removal of entrapped liquids, such as rain or decontamination fluids. If a cask is configured to bottom-load, then no drain port is provided into containment.

1.2.1.8 Tiedowns

Tiedowns are a structural part of the package. From the attached general arrangement drawing, it can be seen that four reinforced tiedown locations are provided. Refer to Section 2.5.2 for a detailed analysis of their structural integrity.

1.2.1.9 Lifting Devices

Lifting devices are a structural part of the package. From the general arrangement drawing, it can be seen that three reinforced lifting locations are provided. Refer to Section 2.5.1 for a detailed analysis of their structural integrity.

1.2.1.10 Pressure Relief System

There are no pressure relief valves in the design of the NuPac 10/140MB packaging.

1.2.1.11 Heat Dissipation

There are no special devices used for the transfer or dissipation of heat. The package internal decay heat used for design is 95 watts.

1.2.1.12 Coolants

There are no coolants utilized in the package.

1.2.1.13 Protrusions

There are no outer or inner protrusions, except for the lifting and tiedown lugs described above.

1.2.1.14 Shielding

The contents will be limited such that the radiological shielding provided will assure compliance with DOT and IAEA regulatory requirements. Further details are provided in Section 5.0.

1.2.2 Operational Features

Refer to the General Arrangement drawing of the packaging, in Appendix 1.3.1. There are no complex operational requirements connected with the package, and none that have any transport significance. The top primary lid and optional bottom lid are both securily attached with standard bolts, which are readily removable, and which are completely recessed beneath the protective impact limiter to prevent inadvertent damage during normal or accident conditions of transport. Full and reliable containment is provided by NuPac's EnviroSeals,[tm] providing a reliably high level of containment to the package. These devices provide sealing surface protection during operational activities, and are themselves easily and quickly replaceable to maintain a sure and complete seal under all conditions. Full patent protection for the EnviroSeals[tm] is being sought.

1.2.3 Contents of Packaging

This application is for transporting the following radioactive materials as defined in U.S.A. and IAEA regulations:

- Contents include less than 2,000 times the Type A quantity of radioisotopes as defined in 10CFR71, Table A.

- Contents may be Type A or B quantities, including Low Specific Activity (LSA) in normal or special form.

- Contents total less than 95 watts of internal decay heat.

- Contents may be in dispersible or non-dispersible form (e.g., activated hardware) and may be contained within an internal liner not considered part of this application, or solidified in a stabilizing media, or both. The containment ability of any internal liner is not considered in this application.

- Contents shall be so limited that the external radiation dose rates are within the limits specified in 10 CFR 71. This shall be verified by pre-shipment inspection.

APPENDIX 1.3.A

NOTES: UNLESS OTHERWISE SPECIFIED

1. INTERPRET DRAWING PER ANSI Y-14.5

2. REFERENCE DATA: CASK WT 53,000 lbs
   PAYLOAD WT 15,000 lbs
   GROSS WT 68,000 lbs

3. ALL EXPOSED CARBON STEEL SURFACES (TIE-DOWN LUGS) SHALL HAVE A SURFACE PREPARATION PER SSPC-SP-10 AND PAINTED WITH A HIGH QUALITY 2 PART EPOXY COATING (ONE COAT INDUSTRIAL QUALITY PRIMER AND ONE COAT INDUSTRIAL QUALITY EPOXY FINISH COAT)

4. ALL WELDING PROCESSES, PROCEDURES, PERSONEL AND EXAMINATIONS SHALL BE QUALIFIED AND/OR PERFORMED IN ACCORDANCE WITH ASME CODE, SECTION III, DIVISION I, SUBSECTION NE. WELD PROCEDURES AND WELDER QUALIFICATIONS SHALL BE AVAILABLE FOR AUDIT OR REVIEW

5. ALL WELDS SHALL BE VISUALLY EXAMINED IN ACCORDANCE WITH AWS D1.1, SECTION 8.15

6. OPTIONAL 1-1/4-7UNC STUD (ASTM A320 L43) AND HEAVY HEX NUT (ASTM A194, GR 7) MAY BE USED IN PLACE OF THE HEX HD CAP SCREW

7. WELDS SHALL BE LIQUID PENETRANT INSPECTED ON FINAL PASS IN ACCORDANCE WITH ASME CODE, SECTION III, DIVISION I, SUBSECTION NB, ARTICLE NB-5000 AND SECTION V, ARTICLE 6

8. PRIOR TO ASSEMBLY, ALL COMPONENTS SHALL BE CLEANED OF CUTTING OILS, MARKING DYES, WELDING FLUX, SPATTER, SCALE, GRIME AND ALL OTHER FOREIGN MATERIALS. FINISHED ASSEMBLY AND ALL INTERIOR SURFACES SHALL BE CLEANED AND VISUALLY OR WIPE TEST INSPECTED IN ACCORDANCE WITH ASTM-A380

9. LEAD MATERIAL IN ACCORDANCE WITH ASTM B29-79, COPPER-BEARING

10. LEAD SHALL BE CAST IN PLACE

11. LEAD SHIELDING INTEGRITY SHALL BE DETERMINED BY GAMMA SCAN

12. POLYURETHANE FOAM SHALL HAVE A NOMINAL DENSITY OF 20 LB/FT^3. INSTALLATION TECHNIQUES, ACCEPTANCE TESTS AND ACCEPTABLE DEVIATIONS IN PROPERTIES ARE SUMMARIZED IN SECTION 2.10.2.4 OF 10/140B SAFETY ANALYSIS REPORT

13. FOAM: POLYURETHANE SHEET (2-3 LB/FT^3)

14. THREADS PER ASA B1.1 1960 EDITION

15. CASK SHALL BE LEAK TESTED TO DEMONSTRATE A LEAK RATE NOT TO EXCEED 1 x 10^{-7} STANDARD CUBIC CENTIMETERS PER SECOND OF AIR PER ANSI N14.5-1987

16. HOIST RINGS ARE PROVIDED FOR LIFTING AND HANDLING THE UPPER IMPACT LIMITER ONLY. EACH LOCATION SHALL BE LABELED WITH THE FOLLOWING WARNING "IMPACT LIMITER LIFT ONLY", VIA STENCILING WITH INDUSTRIAL ENAMEL PAINT, COLOR: BLACK. HOIST RINGS SHALL BE DISABLED WITH LOCKING WIRE DURING CASK TRANSPORTATION

17. TAMPER INDICATING SEALS SHALL BE INSTALLED AT ONE (1) UPPER LID PROTECTIVE COVER SECURING PIN, AT ONE (1) OPTIONAL DRAIN PLUG AND AT ONE (1) SECURING LUG ON EACH IMPACT LIMITER IN ACCORDANCE WITH 10 CFR 71.43 (b)

18. ALL CYLINDRICAL SHELLS SHALL COMPLY WITH THE TOLERANCE REQUIREMENTS OF ASME B AND PV CODE, SECTION III, DIVISION I, SUBSECTION NE, ARTICLE NE-4220

19. PROPRIETARY DATA

20. NOMINAL AIR GAP (MINIMUM .05 IN., MAXIMUM .42 IN). ADDITIONAL PERIODIC SPACERS MAY BE PLACED AT RANDOM LOCATIONS IN ORDER TO GUARANTEE THE MINIMUM AIR GAP. THE CUMULATIVE SPACER AREA SHALL NOT EXCEED 5% OF THE ENTIRE EXPOSED THERMAL SHIELD SURFACE

21. PACKAGE SHALL BE MARKED AND IDENTIFIED IN ACCORDANCE WITH THE REQUIREMENTS OF 10 CFR 71.85 (C)

22. ALL ASTM A516 GR70 AND ASTM A537 CLASS 1, NORMALIZED SHALL DEMONSTRATE A MINIMUM CHARPY V-NOTCH VALUE OF 15 FT/LBS AT 0°F

23. LIFTING LUGS SHALL BE LOAD TESTED TO 150% OF THE RATED LOAD AS SPECIFIED IN SECTION 2.5.1 OF THE 10-140B SAFETY ANALYSIS REPORT

24. TORQUE PRIMARY LID BOLTS (2 1/2-4UNC) TO 440-470 FT-LBS. TORQUE SECONDARY LID BOLTS (1 1/4-7UNC) TO 190-210 FT-LBS

25. THERMAL SHIELD TO BE INSTALLED AFTER GAMMA SCAN OF LEAD IS COMPLETE

26. IF PART IS MADE FROM TWO PIECES PRIOR TO FORMING, THE FABRICATOR'S WELDS SHALL BE FULL PENETRATION, RADIOGRAPHED AND INTERPRETED IN ACCORDANCE WITH ASME CODE, SECTION III, DIVISION I, SUBSECTION ND, ARTICLE ND-5000 AND SECTION V, ARTICLE 6

27. ALL IMPACT LIMITER PENETRATIONS SHALL BE WELDED CLOSED PER ASME CODE SECTION IX AND VISUALLY EXAMINED PER NOTE 5

28. PROPRIETARY DATA

29. ALL IMPACT LIMITER, THERMAL SHIELD AND CLADDING JOINTS AND SEAMS SHALL BE WELDED PER ASME CODE SECTION IX AND LIQUID PENETRANT INSPECTION PER NOTE 7

30. INSTALL LYTHERM ON ALL INTERIOR SURFACES OF IMPACT LIMITERS AND LID PROTECTIVE COVER PRIOR TO FOAM POUR. LYTHERM CERAMIC FIBER PAPER, via THE LYDALL, INC. NO. 153-LP, OR FIBERFRAX CERAMIC FIBER PAPER, via THE STANDARD OIL ENGINEERED MATERIALS NO. 550-A. ADHERE TO SURFACE WITH RTV SILICONE ADHESIVE, DOW CORNING NO. 732 OR 737

9910130940-01

PACIFIC NUCLEAR SYSTEMS

SHIPPING CASK
S.A.R.
NUPAC 10/140B

SCALE: NONE | SHEET 1 OF 7

DWG NO. D X-102-500SNP

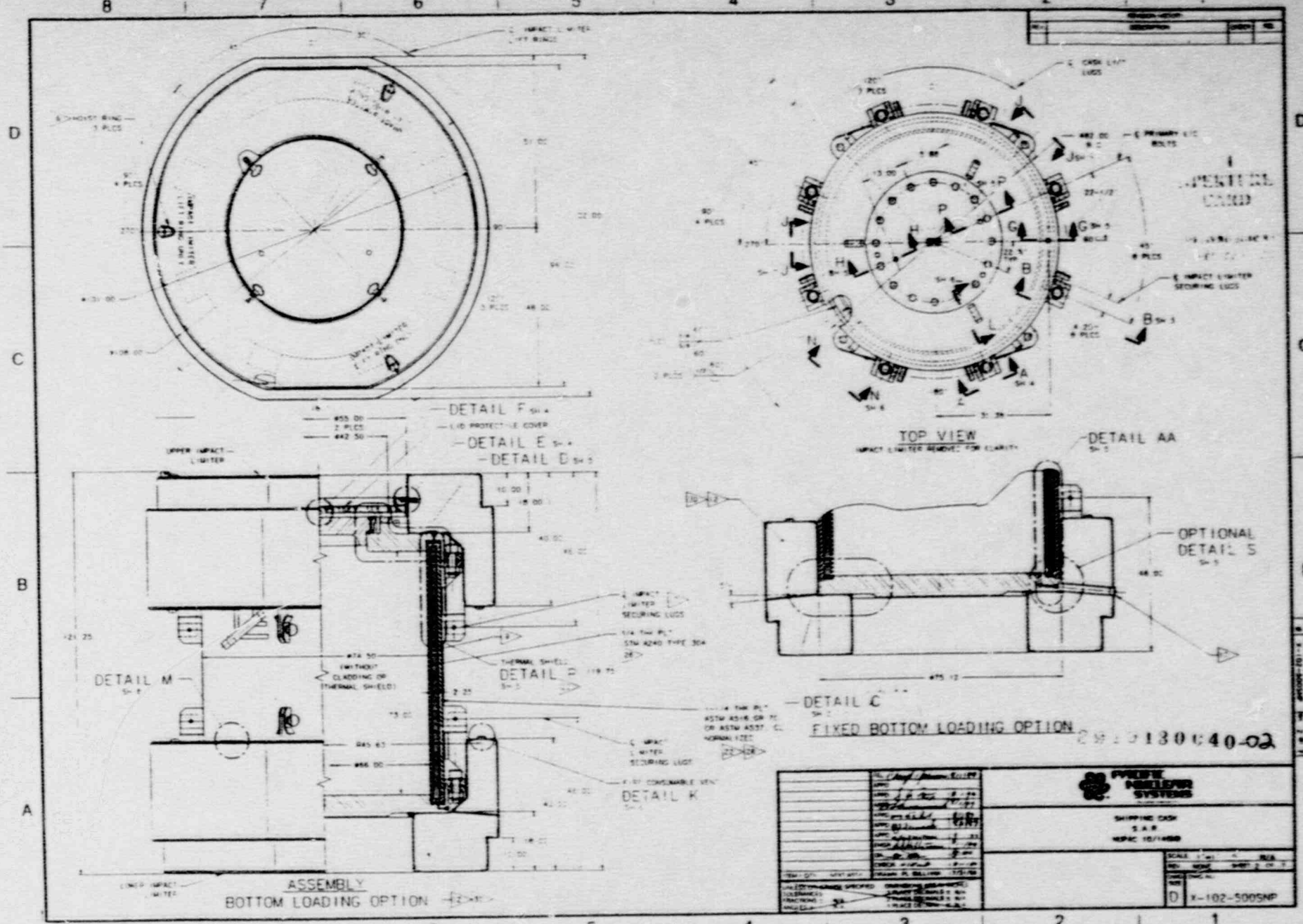
DETAIL F
DETAIL E
DETAIL D
TOP VIEW
DETAIL AA
OPTIONAL DETAIL S
DETAIL M
DETAIL P
DETAIL C
DETAIL K
ASSEMBLY
BOTTOM LOADING OPTION
FIXED BOTTOM LOADING OPTION
130040-02
X-102-500SNP

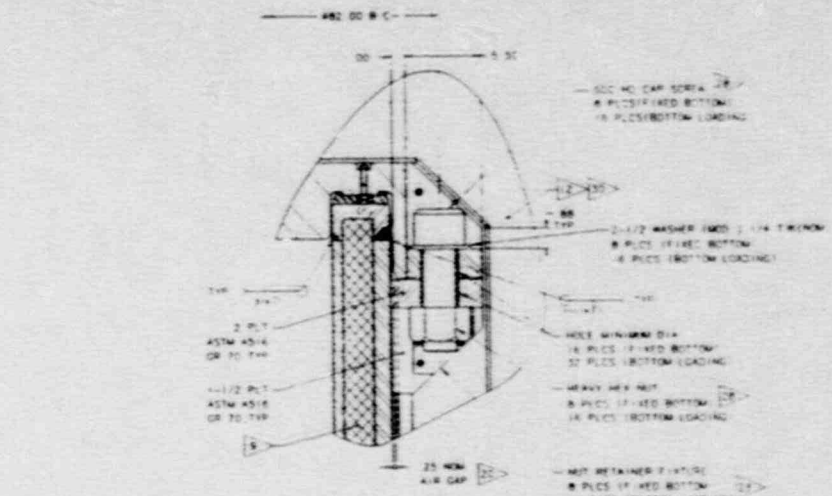

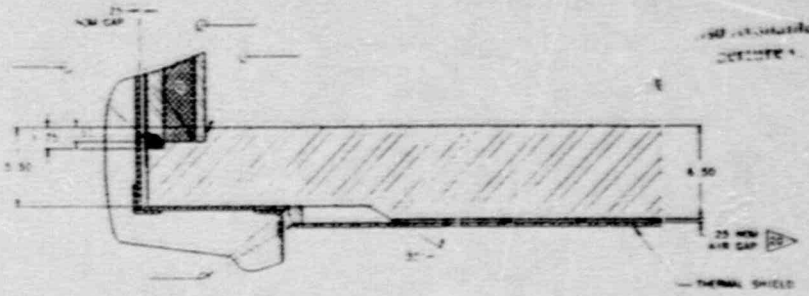

DETAIL C

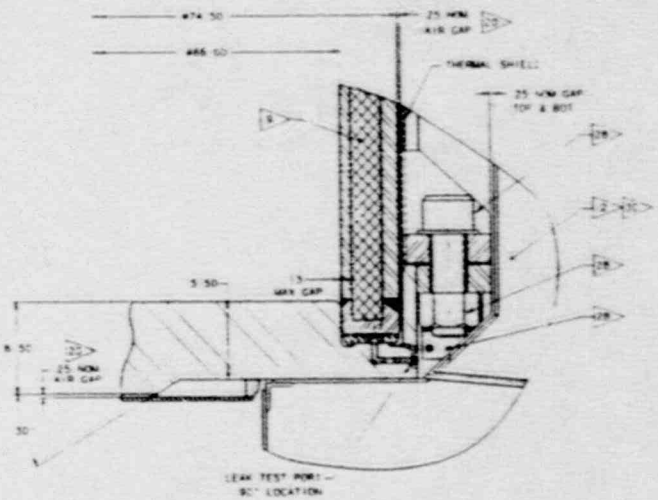

SECTION B-B

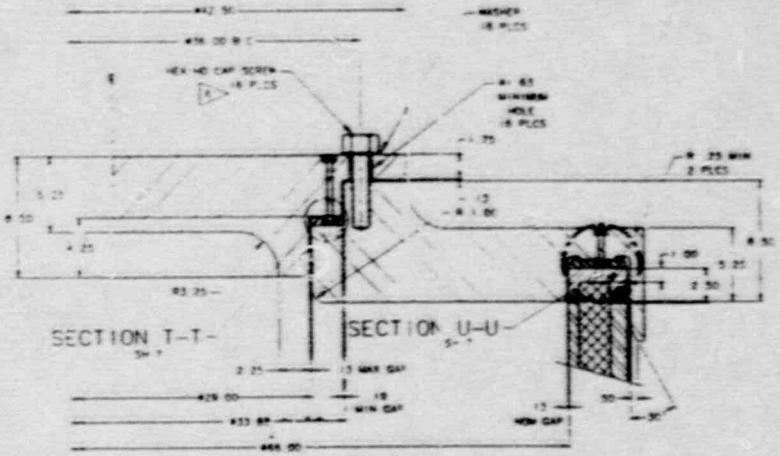

SECTION T-T

SECTION U-U

DETAIL D

S91C130040-03

X-102-5005NP

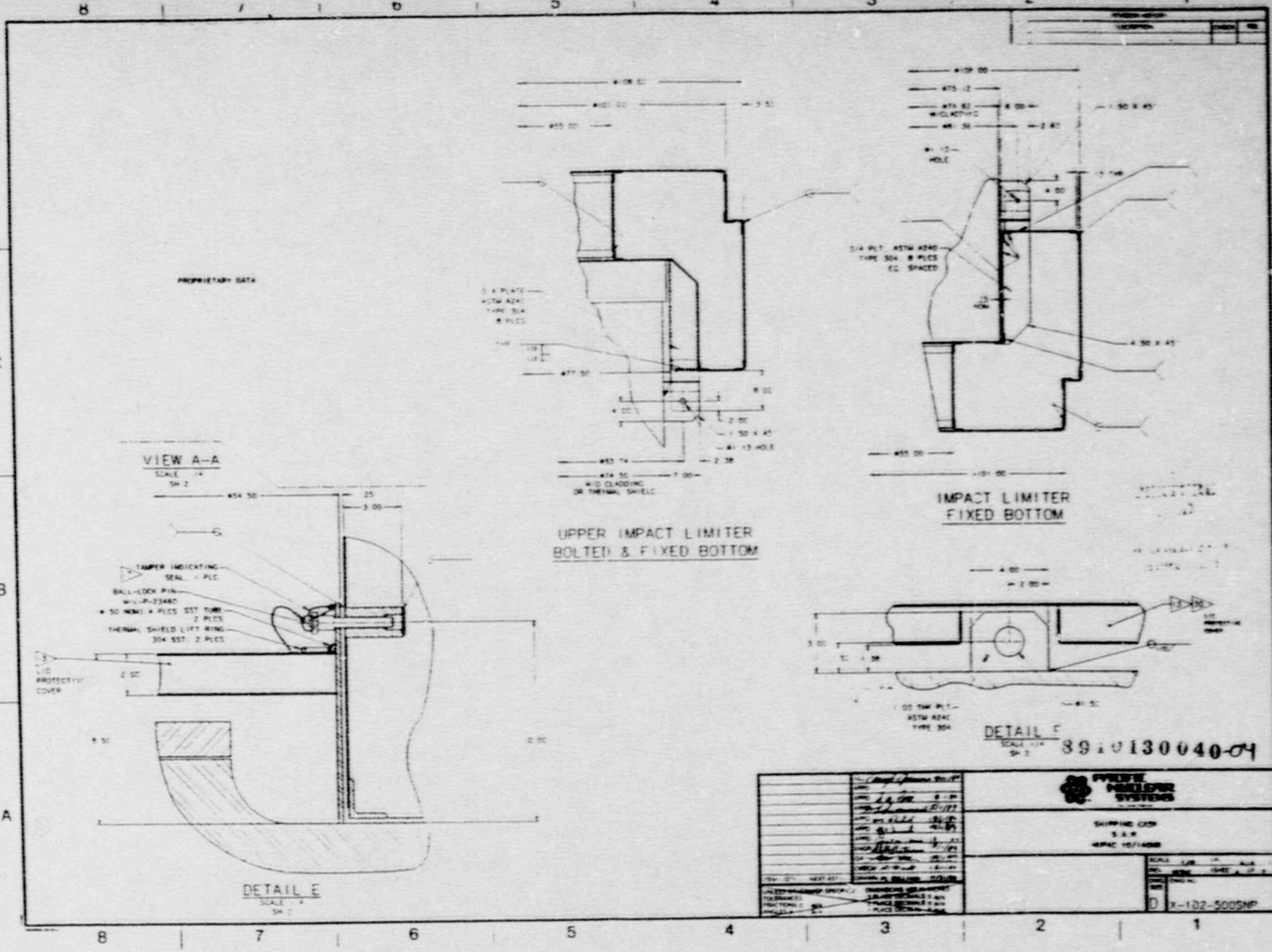
PROPRIETARY DATA
VIEW A-A
UPPER IMPACT LIMITER
BOLTED & FIXED BOTTOM
IMPACT LIMITER
FIXED BOTTOM
DETAIL E
DETAIL F
TAMPER INDICATING SEAL, 1 PLC
BALL-LOCK PIN
THERMAL SHIELD LIFT RING 304 SST, 2 PLCS
LID PROTECTIVE COVER
3/4 PLT, ASTM A240 TYPE 304, 8 PLCS EQ. SPACED
PACIFIC NUCLEAR SYSTEMS
SHIPPING CASK
S.A.R.
X-102-500SNP
8910130040-04

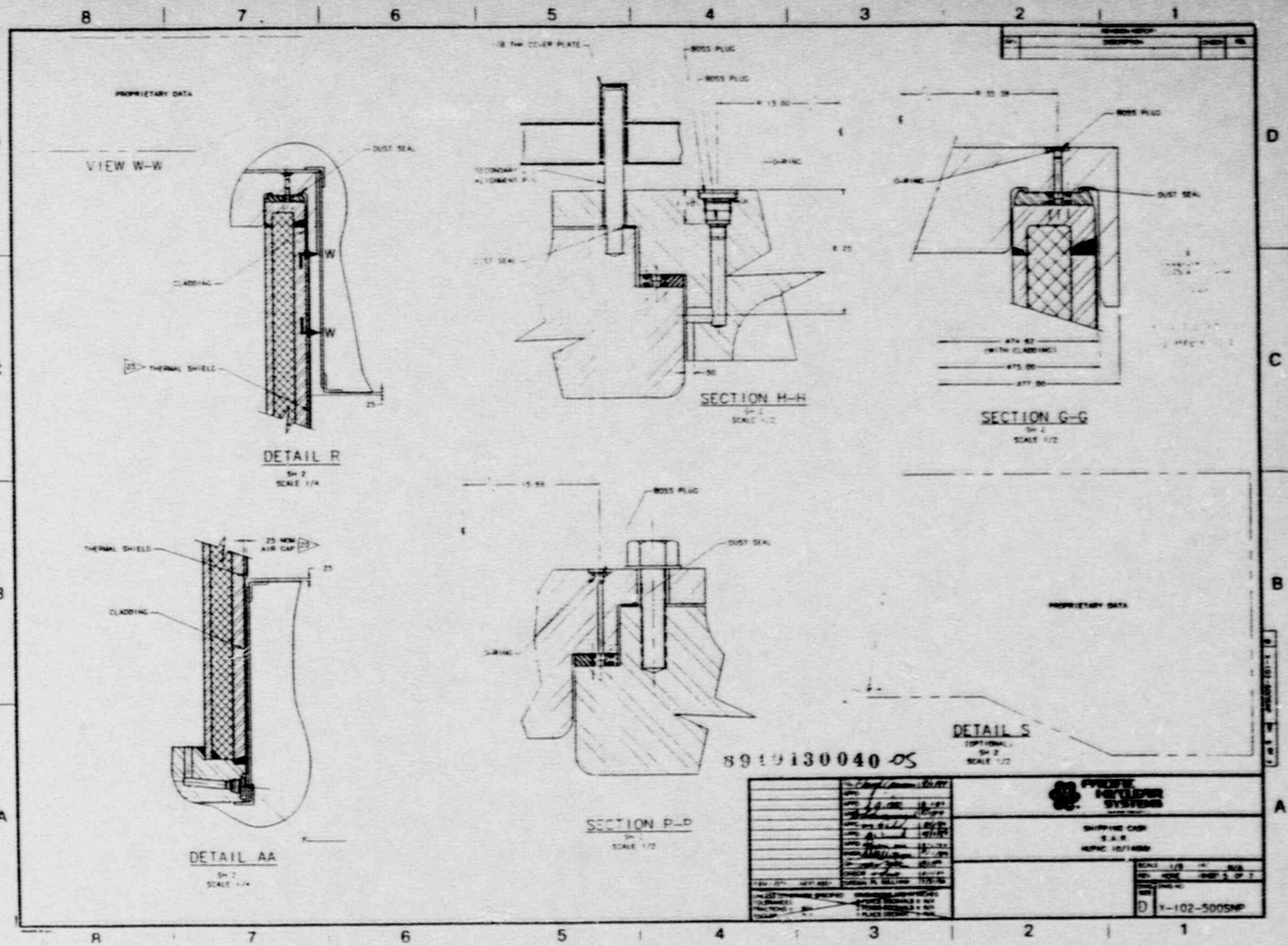
PROPRIETARY DATA
VIEW W-W
DUST SEAL
CLADDING
W
W
THERMAL SHIELD
25
DETAIL R
SH 2
SCALE 1/4
COVER PLATE
BOSS PLUG
BOSS PLUG
SECONDARY ALIGNMENT PIN
O-RING
DUST SEAL
.50
SECTION H-H
BOSS PLUG
O-RING
DUST SEAL
(WITH CLADDING)
SECTION G-G
SH 2
SCALE 1/2
THERMAL SHIELD
25 NOM AIR GAP
25
CLADDING
DETAIL AA
SCALE 1/4
BOSS PLUG
DUST SEAL
O-RING
SECTION P-P
SCALE 1/2
PROPRIETARY DATA
DETAIL S
(OPTIONAL)
SH 2
SCALE 1/2
8910130040-05
PACIFIC NUCLEAR SYSTEMS
SHIPPING CASK
S.A.R.
D
X-102-500SNP

DETAIL Y-

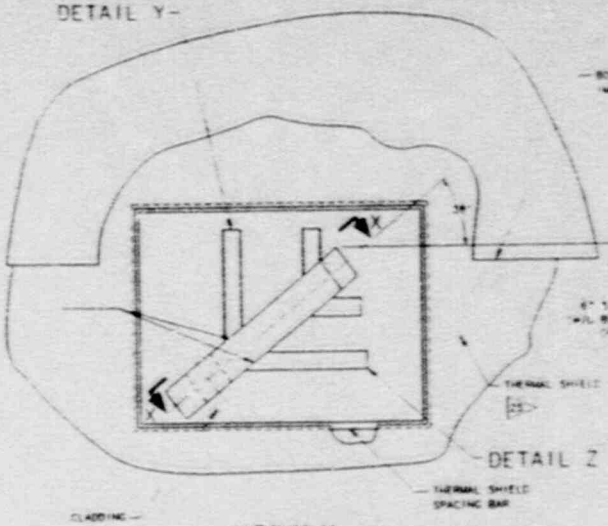

VIEW N-N

DETAIL Z

DETAIL M

SECTION L-L

DETAIL Z

PROPRIETARY DATA

PROPRIETARY DATA

PROPRIETARY DATA

DETAIL K

DETAIL Y

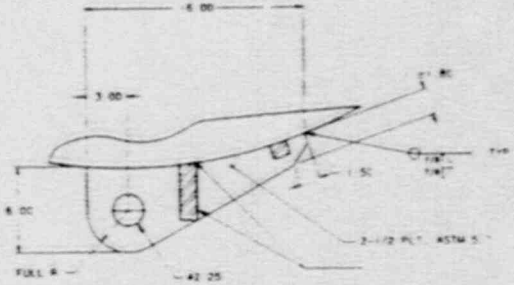

VIEW X-X

8910130040-06

X-102-500SNP

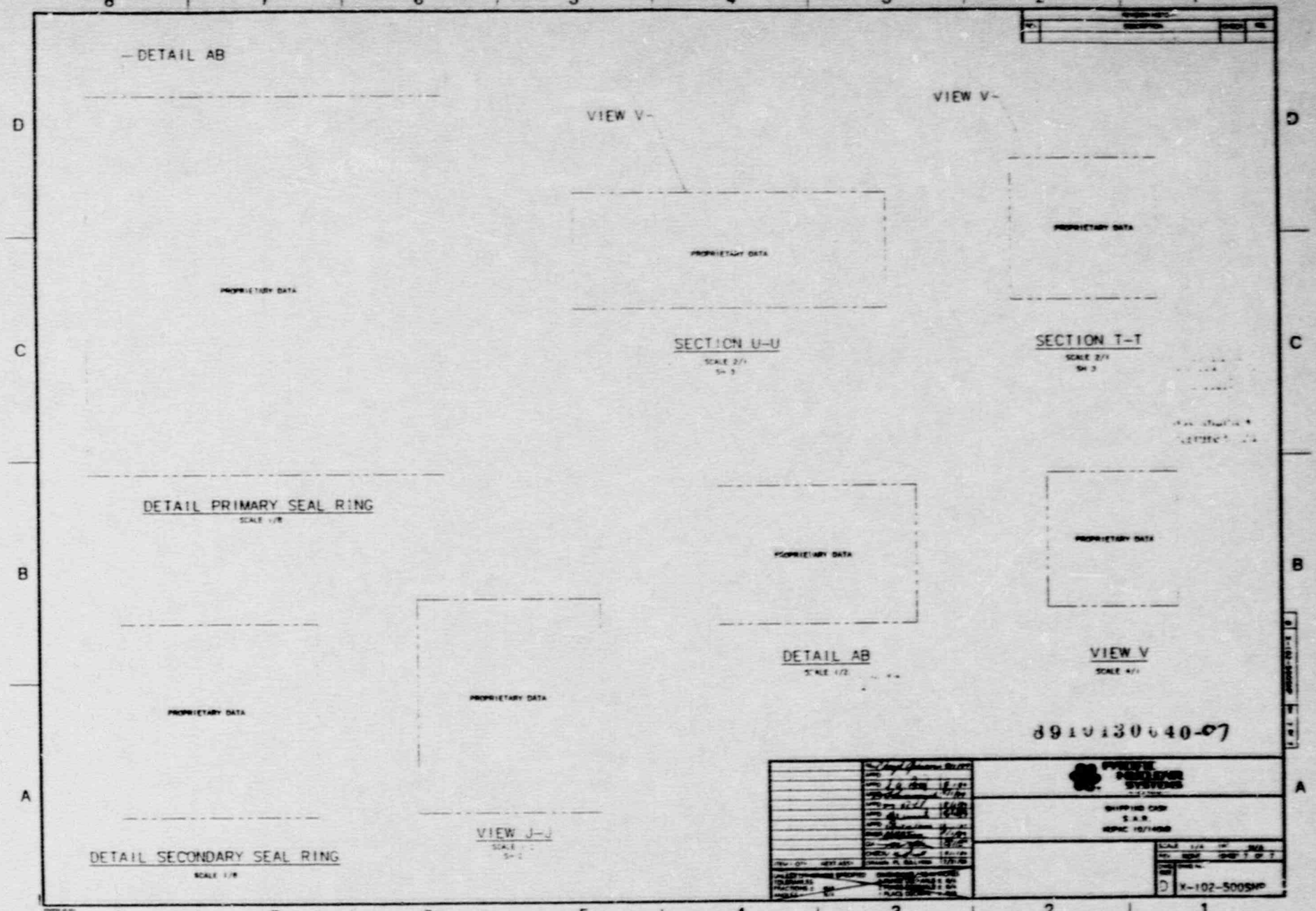
DETAIL AB
VIEW V
VIEW V
PROPRIETARY DATA
SECTION U-U
SECTION T-T
DETAIL PRIMARY SEAL RING
DETAIL AB
VIEW V
VIEW J-J
DETAIL SECONDARY SEAL RING
8910130640-07
X-102-500SNP

2.0 STRUCTURAL EVALUATION

This chapter presents structural evaluations demonstrating that the NuPac 10/140MB Shipping Cask design meets all applicable structural criteria. The cask is comprehensively evaluated and shown to provide adequate protection for the cask payload. Normal and hypothetical accident condition evaluations, using analytic and experimental techniques, are performed in accordance with 10 CFR 71 requirements. Analytic demonstration techniques comply with the methodology presented in Regulatory Guide 7.6. Experimental verifications and evaluations are of the following forms:

- 1/4-Scale Drop Tests have been performed to verify the behavior of the 10/140MB Shipping Cask under hypothetical accident condition loadings. Drop test results are summarized and compared with analytic results in Section 2.10.4. These comprehensive tests, coupled with appropriate analytic evaluations, demonstrate the capability of the package to meet the structural requirements associated with hypothetical accident conditions as set forth in 10 CFR 71. Reduced test data provide complete information defining deformations imposed upon the package's impact limiters. Those data, when correlated with analytic results and previous test results, provide accurate predictions of internal stresses and deformations for those combined loading events not explicitly tested.

- Component Tests were also performed to verify mechanical or physical properties. These tests are described within subsequent Sections where appropriate. Burn tests on the polyurethane foam used in the overpacks were performed to establish foam characteristics during exposure to the hypothetical fire event. A series of O-ring seal verification tests were performed to assure that selected O-ring material and gland geometry are adequate to assure leak-tight performance under all regulatory requirements.

Detailed test results are typically relegated to the relevant appendix of this report. In particular, Section 2.7 includes brief discussions of the 1/4 scale drop tests, but detailed comparisons of analytic and experimental results are only presented in Appendix 2.10.4.

Analytically determined minimum Margins of Safety obtained for the major cask components are summarized in Figure 2.0-1 and Table 2.0-1.

2.1 Structural Design

2.1.1 Discussion

The principal structural member of the NuPac 10/140MB package is the containment vessel described in Section 1.2.1. The above component is identified on the drawing as noted in Appendix 1.3.1. A detailed discussion of the structural design and performance of all cask components is provided below.

2.1.2 Design Criteria

2.1.2.1 Basic Design Criteria (Allowable Stresses)

This section defines the stress allowables for primary membrane, primary bending, secondary, bearing, shear, and buckling stresses for containment structures and fasteners, and non-containment structures and fasteners.

Regulatory Guide 7.6, Design Criteria for Structural Analysis of Shipping Cask Containment Vessels (Reference 2.11.1) is used in conjunction with Regulatory Guide 7.8, Load Combinations for the Structural Analysis of Shipping Casks (Reference 2.11.2) to evaluate the integrity of the NuPac 10/140MB. Where the loads specified by Regulatory Guide 7.8 conflict with those given in the current version of 10 CFR 71, the latter is used. Material properties and design stress intensity values, S_m, used in the analyses can be found in Table 2.3-1.

FIGURE 2.0-1

10/140MB Component Maximum Stresses

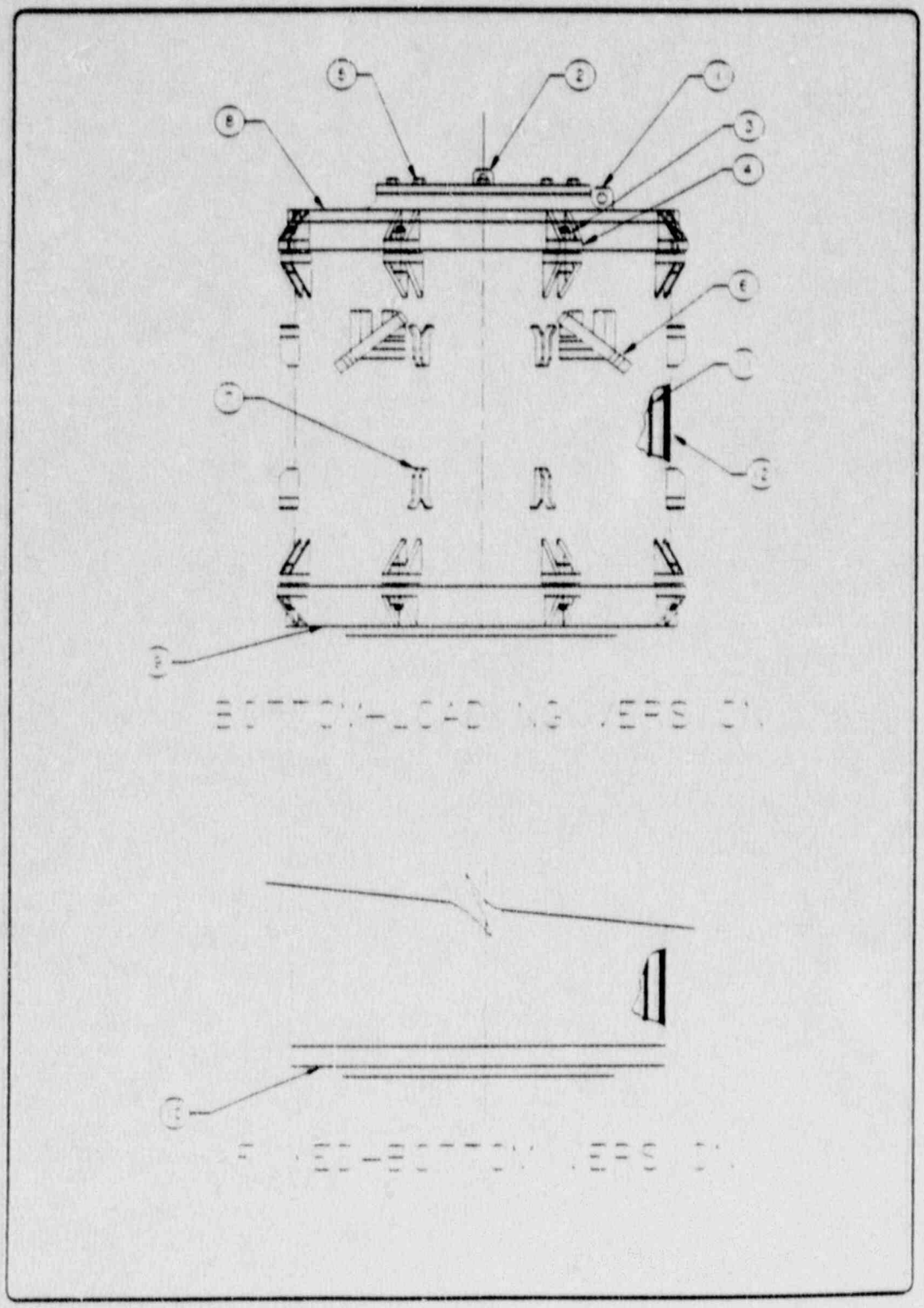

TABLE 2.6-1

10/140[redacted] Maximum Component Stresses

Component Ref. No.	Component Description	Location Within Component	Loading Condition ***	Load Combination	Type of Stress	Resultant Stress Component*, Stress Intensity, or Load	Acceptance Criteria	Allowable Value of Stress/Load	Margin of Safety	SAR Reference Location
1	Primary Lid Lifting Leg	Lug Eye	Lifting (Load Factor of 3)	Shear-Out	Shear	78520 lb	S_y	84106 lb	+0.07	2.5.1.1
2	Secondary Lid Lifting Leg	Lug Eye	Lifting (Load Factor of 3)	Shear-Out-	Shear	5100 lb	S_y	31540 lb	+5.18	2.5.1.2
3	Primary Lid Bolts	Shank	HAC Oblique Drop	Max. Payload +Pressure	Membrane	96610 psi	S_y	109000 psi	+0.07	2.7.1.2.5
4	Primary Lid Bolt Lugs	Cask Lug Weld	HAC Oblique Drop	Max. Payload +Pressure	Membrane +Bending	58750 psi	S_u	70000 psi	+0.19	2.7.1.2.5
5	Secondary Lid Bolts	Shank	HAC End Drop	Max. Payload +Pressure	Membrane	82000 psi	S_y	109000 psi	+0.26	2.7.1.1.5 2.10.7.4
6	Cask Tiedown Lug	Lug Eye	Tie-Down	Transportation Loads	Bearing	545850 lb	S_y	558225 lb	+0.02	2.5.1.3
7	Impact Limiter Attachment	Ball-Lock Pin	HAC Oblique Drop	Double Shear	Shear	25600 lb	1/5 Double Shear Capacity	29400 lb	+0.15	2.7.1.2.6
8	Top Lid Assembly	Secondary Lid O.D.	Puncture-Secondary Lid O.D.	Puncture	Membrane	47448 psi	$2.4S_m$	48000 psi	+0.01	2.7.2 2.10.8.3.2
9	Bottom Lid	Center of Lid	Puncture-Center	Puncture	Membrane +Bending	60598 psi	S_u	68785 psi	+0.13	2.7.2 2.10.8.2.1
10	Bottom Plate	Center of Plate	HAC End Drop	Min. Payload Load Slump	Membrane +Bending	21315 psi	S_u	68785 psi	+2.23	2.7.1.1.4
11	Inner Shell	Impact End	HAC End Drop	Min. Payload Load Slump	Buckling Interaction	σ_h = 6320 psi σ_a = 20086 psi	**	σ_{ha} = 26042 psi σ_{aa} = 27595 psi	+0.09	2.7.1.1.5(2)
12	Outer Shell	Adjacent to Tail End of Tie-Down Lug	Tie-Down	Transportation Loads	Membrane	36276 psi	S_y	37388 psi	+0.03	2.5.1.3

* σ_h = hoop compressive stress, σ_a = axial compressive stress

** Buckling Interaction: $[(\sigma_h/\sigma_{ha}) + (\sigma_a/\sigma_{aa})] \leq 1$

*** HAC - Hypothetical Accident Conditions

2.1.2.1.1 Containment Structures

Regulatory Guide 7.6 was used for all package containment boundaries for both the normal conditions of transport and the hypothetical accident conditions. Material data used in the evaluation correspond to the design stress values, S_m, yield strengths, S_y, and ultimate strengths, S_u, given in the ASME Code (Reference 2.11.3), Section III, Class I. The containment vessel is considered to be the 66.0 inch inside diameter, .75 inch thick inner shell of the cask, the castings or forgings at the top and bottom ends of the cask, the bolted secondary closure lid, and the drain port in fixed bottom models. A summary of allowable stresses used for containment structures, and fasteners is presented in Table 2.1.2-1. These data are consistent with Regulatory Guide 7.6 and Sections NB-3000 and Appendix F of ASME Section III.

2.1.2.1.2 Non-Containment Structures

Structural evaluations of non-containment components, such as tiedown and lifting devices, and the cask outer shell, use allowable stresses for normal and accident conditions as presented in Table 2.1.2-2. The impact limiter is allowed to exceed yield for all conditions. The acceptance criterion for all impact related loads within the impact limiters is that no cask 'hard points' directly come into contact with the impact surface. For normal lifting and handling loads, the material yield stress values of Table 2.3-1 are utilized in conjunction with a load factor of three (3), per 10 CFR 71.45. These lifting and handling criteria are applicable to all package components, including the impact limiter lift lugs.

TABLE 2.1.2-1

Allowable Stress Limits for Containment Structures

Item Ref. No.	Stress Category	Normal Conditions (A)	Accident Conditions (B)
1	Primary Membrane Stress Intensity	S_m	Lesser of: $2.4S_m$ $0.7S_u$
2	Primary Membrane + Bending Stress Intensity	$1.5S_m$	Lesser of: $3.6S_m$ S_u
3	Range of Primary + Secondary Stress Intensity	$3.0S_m$	Not Applicable
4	Bearing Stress	S_y	S_y for seal surfaces S_u elsewhere
5	Pure Shear Stress	$0.6S_m$	$0.42\ S_u$
	Buckling	Per Section 2.1.2.2.3	
		CONTAINMENT FASTENER ALLOWABLE STRESSES	
	Stress Category	Normal Conditions	Accident Conditions
6	Membrane Stress*	$2.0S_m$	S_y
7	Membrane + Bending Stress *	$3.0S_m$	S_y

* Not Considering Stress Concentrations

TABLE 2.1.2-2

Allowable Stress Limits for Non-Containment Structures

Item Ref. No.	Stress Category	Normal Conditions (A)	Accident Conditions (B)
1	Primary Membrane Stress Intensity	Greater of: S_m, S_y	$0.7S_u$
2	Primary Membrane + Bending Stress Intensity	Greater of: $1.5S_m$, S_y	S_u
3	Range of Primary + Secondary Stress Intensity	Greater of: $3.0S_m$, S_y	Not Applicable
4	Bearing Stress	S_y	S_u
5	Pure Shear Stress	Greater of: $0.6S_m$, $0.6S_y$	$0.42S_u$
	Buckling	Per Section 2.1.2.2.3	
		NON-CONTAINMENT FASTENER ALLOWABLE STRESSES	
	Stress Category	Normal Conditions	Accident Conditions
6	Membrane Stress*	Greater of: $2.0S_m$, S_y	Greater of: S_y, $0.7S_u$
7	Membrane + Bending Stress*	Greater of: $3.0S_m$, S_y	S_u

* Not Considering Stress Concentrations

2.1.2.2 Miscellaneous Structural Failure Modes

2.1.2.2.1 Brittle Fracture

With exception of the closure bolts, all containment structural components are fabricated of Type 304 austenitic stainless steel. Since this material does not undergo a ductile-to-brittle transition in the temperature range of interest (down to -40° F), it is safe from brittle fracture.

The primary and secondary lid closure bolts are fabricated of ASTM A-320, Grade L43, alloy steel. Per Section 5 of NUREG/CR-1815 (Reference 2.11.4) bolts are generally not considered as fracture-critical components because multiple load paths exist and because bolted systems are designed to be redundant. However, for purposes of comparison, the nil-ductility transition (NDT) temperature of the closure bolts will be calculated and compared with the requirements of NUREG/CR-1815.

According to Section 6.2.1.1 of the ASTM A-320, Grade L43, specification, the minimum impact energy absorption is 20 ft-lbs at -150 °F. The Charpy impact measurement may be transformed into a fracture toughness value by using the empirical relation developed in Section 4.2 of NUREG/CR-1815, as follows:

$$K_{ID} = [5E(C_v)]^{0.5}$$

Where:

K_{ID} = dynamic fracture toughness, psi-in$^{0.5}$

E = Modulus of Elasticity, psi
= 28.8(10)^6 psi at -150° F (Table I-5.0 of the ASME B and PV code, Reference 2.11.3)

C_v = Charpy impact measurement, ft-lbs
= 20 ft-lbs

Then,

$$K_{ID} = \{5[28.8(10)^6](20)\}^{0.5} = 53{,}665 \text{ psi-in}^{0.5}$$

The dynamic fracture toughness is translated to an equivalent nil-ductility transition (NDT) temperature by using the Pellini reference curve given as Figure 2 in NUREG/CR-1815.

By interpolation, the temperature relative to NDT is found as:

$$(T - NDT) = 30^{\circ}F$$

Accordingly, the nil-ductility transition temperature is:

$$NDT = -150-(+30)$$
$$= -180^{\circ}F$$

For Category I fracture critical components, and in section thicknesses of 1.25 and 2.5 inches (bolt diameters), Figure 3, NUREG/CR-1815, gives the minimum offset, 'A' as approximately 53°F for the 1.25 inch diameter bolt. Thus, the maximum NDT temperature value is:

$$T_{NDT} = LST - A = -20-53 = -73^{\circ}F$$

Where:

T_{NDT} = maximum NDT temperature per NUREG/CR-1815
LST = lowest service temperature
= -20°F (Reg Guide 7.6)
A = 53°F, per Figure 3, NUREG/CR-1815

The ASTM A-320, Grade L43, closure bolts experience a ductile to brittle transition temperature at -180°F whereas the criterion of NUREG/CR-1815 prescribes a maximum NDT temperature of -73°F. The 107°F margin between criteria requirements and material capability provide conservative assurance that brittle fracture failures will not occur in these ferritic closure bolt materials. Since bolts are acceptable under Category I rules, they are also acceptable for the Category II NuPac 10/140MB.

The 1.25 inch outer shell is fabricated from ASTM A-516 grade 70 (or alternatively, ASTM A-537 Class 1) material. Under Category II rules for qualification of 0.625 inch to 4.0 inch thick sections, Figure 6 of NUREG/CR-1815 (Reference 2.11.4) may be used to determine the nil-ductility transition temperature. Since the 10/140MB will be subjected to reduced loading rates and because the yield strength of ASTM A-516 grade 70 (or A-537 Class 1) steel is less than 60 ksi (it is actually 38 ksi for A-516 and 50 ksi for A-537), curve number 3 of that figure may be used. For the 1.25 inch thickness of A-516 Grade 70 (or A-537 Class 1) the NDT temperature T_{NDT} is given as:

$$T_{NDT} = LST - A$$

Where T_{NDT} = NDT temperatnre
LST = Lowest service temperature, -20°F
A = determined from Figure 6 of NUREG/CR-1815

$$T_{NDT} = -20-(-20)$$
$$T_{NDT} = 0°F$$

Therefore, all A-516 Grade 70 (or A-537 Class 1) components of the 10/140MB greater than 0.625 inches thick are required to have a tested nil-ductility transition less than 0°F. All A-516 Grade 70 (or A-537 Class 1) components less than 0.625 inches thick are required to be normalized only, consistent with the requirements of NUREG/CR-1815.

This NDT may be verified by noting that on Figure 2, the dynamic fracture toughness K_{ID} is defined as 40,000 psi-$in^{0.5}$ at the NDT temperature. The required Charpy V-notch measurement to demonstrate this fracture toughness can be calculated by the following equation from NUREG/CR-1815:

$$K_{ID}^2 = 5(C_v)E$$

Where K_{ID} = 40,000 psi-$in^{0.5}$
E = $30(10)^6$ psi
C_v = Charpy V-notch measurement, ft-lb.

So, $C_v = K_{ID}^2/5E$
C_v = 11 ft-lb.

Therefore, the requirement to have an NDT of less than 0°F may be demonstrated by showing that the Charpy measurement of 0°F or lower is at least 11 ft-lbs. in the A-516 Grade 70 (or A-537 Class 1) 1.25 inch (or thinner) plate. All A-516 Grade 70 (or A-537 Class 1) material greater than 0.625 inches thick used in the design of the NuPac 10/140MB possess Charpy values in excess of 15 ft-lbs. as shown on the drawings in Appendix 1.3.1.

2.1.2.2.2 Fatigue

Normal operating cycles do not present a fatigue concern for the NuPac 10/140MB cask components which have no stress concentrations. This is because the highest allowable stress for normal conditions ($3S_m$) is less than the allowable fatigue stress limit for the steels used in the 10/140MB design. For example, S_m for 304 stainless components is 20,000 psi in the temperature range of concern. Thus, assuming that the normal operating cycle stress actually equals the allowable ($3S_m$), Figure I-9.2.1 of Reference 2.11.3 may be used to determine the number of cycles which would be allowed. From that figure, it can be seen that over 10,000 cycles are allowed. For the A-516 grade 70 and A-537 Class 1 material, S_m is 23,300. Thus, for fatigue to become an important consideration, the cask would be required to undergo at least 1600 cycles at or near its normal stress allowable. Since under the most severe usage the cask might undergo 50 normal shipments per year, or 1000 cycles in 20 years of constant use, it seems clear that fatigue is not a problem for the cask components with no stress concentrations.

Fatigue considerations in the primary and secondary lid bolts follow a similar logic. The torque requirements in the bolts are 440 to 470 ft-lbs and 190 to 210 ft-lbs for the primary and secondary lid bolts, respectively. Using the simple torque-to-preload relationship and a torque coefficient of 0.13 (for cadmium-plated bolts), the maximum axial force in both fasteners may be determined:

$$P = T/KD$$

where P = bolt load, lbs.
T = torque, in-lb
K = 0.13

So for the 2-1/2 inch diameter primary lid bolts:

$$P = (470)(12)/(.13)(2.5) = 17,350 \text{ lbs maximum}$$

For the 1-1/4 inch diameter secondary lid bolts:

$$P = (210)(12)/(.13)(1.25) = 15,500 \text{ lbs maximum}$$

The stress area for the secondary lid bolt is 0.969 in^2. The primary lid bolt has only about a 12% higher load than the secondary lid bolt, and the secondary bolt has a much smaller tensile stress area (tensile stress area for a 2-1/2 in. diameter bolt is 4.0 in^2). The normal stress in the secondary bolt is therefore the worst case. The maximum normal stress is:

$$S_n = 15,500/0.969 = 16,000 \text{ psi}$$

The fatigue alternating stress amplitude is then (16,000)/2 = 8,000 psi.

This stress should be multiplied by the fatigue strength reduction factor (taken to be 4.0 per ASME NB-3232.3(c)) and using Figure I-9.4 from ASME Section III, Appendix I, the allowable number of cycles determined.

$$S_{range} = 4(8,000) = 32,000 \text{ psi}$$

Note that since S_{range} is very much less than $2.7S_m$ for the bolt (2.7 x 34,340 = 92,720 psi, where S_m = 34,340 psi at the maximum normal operating temperature of 133°F), the upper curve from Figure I-9.4 may be used. From that curve, it can be seen that the bolts may experience more than 10,000 cycles before exceeding the ASME fatigue criteria for the bolts. Clearly fatigue is not a serious consideration in the design of the NuPac 10/140MB cask.

2.1.2.2.3 Buckling

Buckling, per Regulatory Guide 7.6 (Reference 2.11.1), is an unacceptable failure mode for containment vessels. The intent of this provision is to preclude large deformations which would compromise the validity of linear analysis assumptions and quasi-linear stress allowables, as given in Paragraph C.6 of Regulatory Guide 7.6.

There are three sets of forces that can potentially cause buckling instabilities in cylindrical vessels. These are axial compression forces, bending moments, and external pressure. The remainder of this subsection defines techniques and criteria used in subsequent segments of this Safety Analysis Report to demonstrate that containment vessel buckling, and non-containment vessel buckling, does not occur.

There are two shells within the NuPac 10/140MB Cask where buckling prevention criteria are applicable - i.e., the inner and outer shells of the cask. For reference purposes the principal geometric features of these shells are as follows:

	Dimension (inches)		
Shell	Mean Radius (R)	Thickness (t)	Length (L)
Inner Shell	33.375	.75	75.5
Outer Shell	36.625	1.25	75.5

1. Elastic Buckling

Representative elastic buckling stress estimates for the shells and applicable loading modes are as follows:

Elastic Buckling Stresses (ksi)
(at 212°F)

Shell	Axial Compression	Bending	External Pressure
Inner Shell (304 SST)	261.7	280.4	177.5
Outer Shell (A-516 Gr.70 or A-537 Cl. 1)	440.1	469.8	N/A

The above elastic buckling values are all based upon a temperature of 212°F, consistent with the stress-strain data for 304 stainless steel given in Figure 2.3-1. Calculations discussing these elastic buckling estimates are found in the following paragraphs. Equations are taken from Structural Analysis of Shells, by Baker, Kovalevsky and Rish (Reference 2.11.5).

a) Crippling of Moderately Long Cylinders (Structural Analysis of Shells (Reference 2.11.5), p. 230) for the cask inner shell (containment vessel):

$$S_{cr}/\xi_a = (\gamma_a)CE(t/R)$$

Where:

S_{cr} = buckling stress
ξ_a = plasticity coefficient
γ_a = a factor which accounts for the difference between theoretical and experimental results
= 0.70 (at R/t = 44.5)
$C = [3(1 - \mu^2)]^{-0.5} = 0.605$
$E = 27.5(10)^6$ psi (at 212° F)
t = 0.75 in
R = 33.375 in
$\mu = 0.3$

Then,

$$S_{cr}/\xi_a = (0.70)(0.605)[27.5(10)^6](0.75/33.375)$$
$$= 261{,}700 \text{ psi}$$

Likewise, for the cask outer shell (non-containment):

$$S_{cr}/\xi_a = (\gamma_a)CE(t/R)$$

Where:

γ_a = 0.74 (at R/t = 29.3)
t = 1.25 in
R = 36.625 in
E = $28.8(10)^6$ psi (A516 at 200°F)

Then,

$$S_{cr}/\xi_a = (0.74)(0.605)[28.8(10)^6](1.25/36.625)$$
$$= 440{,}100 \text{ psi}$$

(b) Euler Column Buckling - The cask inner shell (containment) is laterally restrained and supported by the outer shell of the outer cask. Thus, Euler column buckling is governed by the geometric properties of the cask outer shell. The applied axial forces are distributed 'self weight' loads, thus buckling stresses are found as (per Theory of Elastic Stability by Timoshenko, (Reference 2.11.6) p. 118, Eq. 83):

$$S_{cr}/\xi_a = (qL)_{cr}/A = \pi^2 EI/(1.122L)^2 A$$

Where:

q = load per unit length (lb/in)
L' = column length = 75.5 in
L = L'/2 = 37.75 in
R = mean radius = 36.625 in
t = 1.25 in
A = $2\pi Rt$ in^2 = 287.65 in^2
I = $\pi R^3 t$ in^4 = 192,900 in^4
E = $28.8(10)^6$ psi (200° F)

Then,

$$S_{cr}/\xi_a = (E/2)[\pi R/(1.122)L]^2$$
$$= [28.8(10)^6/2][\pi(36.625)/(1.122)(37.75)]^2$$
$$= 1.063(10)^8 \text{ psi}$$

Thus, crippling is more critical for the outer cask shell than gross columnar instability.

c) Bending Moments (Structural Analysis of Shells (Reference 2.11.5) pp. 234-235) for the cask inner shell (containment vessel):

$$S_{cr}/\xi_a = (\gamma_b)CE(t/R)$$

Where:

$\gamma_b = 0.75$ (at $R/t = 44.5$)
$t = 0.75$ in
$R = 33.375$ in

Then,

$$S_{cr}/\xi_a = (0.75)(.605)[27.5(10)^6](0.75/33.375)$$
$$= 280,400 \text{ psi}$$

Likewise, for the cask outer shell (non-containment):

$$S_{cr}/\xi_a = (\gamma_b)CE(t/R)$$

Where:

$\gamma_b = 0.79$ (at $R/t = 29.3$)
$t = 1.25$ in
$R = 36.625$ in
$E = 28.8(10)^6$

Then,

$$S_{cr}/\xi_a = (0.79)(.605)[28.8(10)^6](1.25/36.625)$$
$$= 469,800 \text{ psi}$$

d) External Pressure, with external constraint. The case of a shell encased in a cavity is discussed in Pressure Buckling of Rings Incased in a Cavity James A. Cheney, ASCE EM Journal, April 1971, Vol. 97 (Reference 2.11.7). Upon buckling, the shell can only move inward. This case corresponds to the cask inner shell where external constraint is provided by the lead biological shield. From Equation 47 of the referred document, the critical buckling pressure is:

$$q_{cr} = (k^2 - 1)E(t/R)^3/12(1 - \mu^2)$$

Utilizing thin-walled pressure vessel theory, the critical buckling stress may be written as:

$$S_{cr} = q_{cr}R/t$$

Then,

$$S_{cr}/\xi_p = (k^2 - 1)E(t/R)^2/12(1 - \mu^2)$$

For the cask inner shell (containment)

$$k = 1.57(R/\rho)^{0.4} \quad \text{(Equation 29)}$$
$$= 11.78$$

$$R/\rho = R(12)^{0.5}/t \quad \text{(Equation 48)}$$
$$= 154.2$$

$t = 0.625$ in
$R = 33.3125$ in
$E = 27.5(10)^6$ psi (at 212° F)
$\mu = 0.3$

Then,

$$S_{cr}/\xi_p = [(11.78)^2 - 1][27.5(10)^6](0.75/33.375)^2/12[1 - (0.3)^2]$$
$$= 177,500 \text{ psi}$$

2. Buckling Criteria

The high elastic buckling stress limits estimated for the cask shells within the previous paragraph (177.5 to 469.8 ksi) provide solid generalized assurance that instability failure modes do not exist for compressively loaded components of the NuPac 10/140MB Cask. To quantify this assertion, all compressively loaded states of stress are tested versus the stability and buckling criteria set forth within Appendix 2.10.1. These criteria recognize that compressively loaded structures behave in different fashions depending upon the geometric aspect ratio of the structure. The nature of the criteria is such that the factors of safety vary with this geometric aspect ratio up to asymptotic values of 5 and 7.5, versus elastic buckling stresses, for accident and normal conditions of transport, respectively. These asymptotic factors of safety may be considered conservative for general use as radioactive materials package design criteria.

Appendix 2.10.1 defines both the rationale and the specifics of the applicable criteria. Briefly, the criteria are as follows:

Direct primary compressive membrane stresses, S_c in containment vessels shall be less than the lesser of S_e/R_d or S_j. S_e is defined as the appropriate elastic buckling stress limit considering adjustments resolving theoretical and experimental results, but neglecting plasticity corrections. The reduction coefficient R_d is to be taken as 7.5 for normal conditions of transport and 5 for accident conditions of transport. This reduction coefficient, R_d, corresponds to the intended factor of safety of the method at high aspect ratios of the structure. S_j is a generalized 'Johnson' parabolic transition curve having a value of S_s, at an aspect ratio, G, of zero. This parabolic transition curve is also tangent to the expression S_e/R_d at a stress level of 2/3 S_s. The term S_s denotes the applicable strength limit of the material -- S_m for normal conditions of transport and S_y for hypothetical accident conditions, both as defined within Reg Guide 7.6. The details of the criteria, in symbolic form are as follows:

Where G is less than G^*:

$$S \leq S_j.$$

Where G is greater than or equal to G^*:

$$S \leq S_e/R_d.$$

Where: S_e = The classical elastic buckling stress expression (including adjustments for theory versus tests) cast in the generalized form:

$$= K/G.$$

K = A numerical constant unique to each compressive loading mechanism reflecting materials properties (Young's Modulus, Poisson's ratio) and empirical or theoretical coefficients. See Table 2.10.1.1-1 for a summary versus typical loading mechanisms.

G = A non-dimensionalized geometric aspect ratio unique to each loading mechanism. See Table 2.10.1.1-1 for a summary versus typical loading mechanisms. For example:

$G = (L/\rho)^2$, for column type loadings [Note: $\rho = (I/A)^{1/2}$],

G = (R/t), for external pressures on long cylinders and axial compression loadings of cylinders.

R_d = 7.5, for Normal Conditions,
= 5.0, for Accident Conditions.

S_j = The parabolic transition from S_s to (S_e/R_d)

$$= S_s - \left[4S_s^3G^2/[27(K/R_d)^2]\right].$$

G^* = The aspect ratio, G, where the parabola defined by S_j intercepts and is tangent to the curve defined by (S_e/R_d); in other words, G^* corresponds to the aspect ratio where $S_j = (S_e/R_d)$, or:

= $(3/2)(K/R_d)/S_s$.

S_s = S_m, for Normal Conditions,
= S_y, for Accident Conditions.

S_m = Design Stress Intensity as used within Section III, ASME Boiler and Pressure Vessel Code (Reference 2.11.3).

S_y = Minimum Yield Stress per Reference 2.11.3.

3. Specific Buckling Limits

Application of these criteria to the specific shell geometries of the NuPac 10/140MB Cask are presented in Tables 2.1.2-3 thru 2.1.2-6 for normal and accident conditions, respectively. The allowable stresses based on the buckling criteria have been derived using a combination of the shell geometries introduced at the beginning of this Section and the criteria described immediately above. A single example serves to demonstrate the method for calculation of these allowables. For this example, consider normal conditions of transport and axial compression of the Cask Inner Shell at 250°F.

The parameters, K and G, are evaluated as follows:

$K = \gamma_a CE$, see preceding 'Elastic Buckling' discussion (Section 2.1.2.2.3, paragraph 1)

$= (.70)(.605)(27.3(10)^6) = 1.156(10)^7$

$G = R/t = 33.375/0.75 = 44.5$

TABLE 2.1.2-3

Normal Conditions of Transport
Crippling and Buckling Allowables
for Inner Shell

Loading Condition and Shell	••••• -20	70	TEMPERATURE (Deg-F) 100	150	200	••••• 250
Material Properties (psi):						
E	2870000•	28300000	281000000•	27900000•	27600000	27300000•
Sy	34100••	30000	30000	27500•	25000	23750•
Sm	20000••	20000••	20000	20000•	20000	20000•
Ss	20000	20000	20000	20000	20000	20000
Axial Compression Buckling Allowables (psi):						
	19106	19081	19068	19054	19034	19012
Bending Buckling Allowables (psi):						
	19222	19199	19188	19176	19158	19140
External Pressure Buckling Allowables (psi):						
	18004	17948	17919	17889	17843	17794

• Interpolated from ASME Code, Section III Appendix Data (See Table 2.3-1)

•• Extrapolated from ASME Code, Section III Appendix Data (See Table 2.3-1)

TABLE 2.1.2-4

Normal Conditions of Transport
Crippling and Buckling Allowables
for Outer Shell

Loading Condition and Shell	••••• -20	TEMPERATURE (Deg-F) 70	100	150	200	••••• 250
Material Properties (psi):						
E	2990000•	2950000	2930000•	2910000•	2880000	2860000•
Sy	40200••	38000	38000	36300•	34600	34200•
Sm	23800••	23500••	23300	23200•	23100	22800•
Ss	23800	23500	23300	23200	23100	22800
Axial Compression Buckling Allowables (psi):						
	23262	22968	22774	22674	22570	22283
Bending Buckling Allowables (psi):						
	23328	23033	22839	22738	22635	22346

• Interpolated from ASME Code, Section III Appendix Data (See Table 2.3-1)

•• Extrapolated from ASME Code, Section III Appendix Data (See Table 2.3-1)

TABLE 2.1.2-5

Accident Conditions of Transport
Crippling and Buckling Allowables
for Inner Shell

Loading Condition and Shell	••••• -20	TEMPERATURE (Deg-F) 70	100	150	200	••••• 250
Material Properties (psi):						
E	28700000•	28300000	28100000•	27900000•	27600000	27300000•
Sy	34100••	30000	30000	27500•	25000	23750•
Sm	20000••	20000••	20000	20000•	20000	20000•
Ss	34100	30000	30000	27500	25000	23750
Axial Compression Buckling Allowables (psi):	32131	28621	28602	26408	24161	23015
Bending Buckling Allowables (psi):	32385	28799	28782	26548	24269	23110
External Pressure Buckling Allowables (psi):	29704	26923	26877	25061	23200	22109

• Interpolated from ASME Code, Section III Appendix Data (See Table 2.3-1)

•• Extrapolated from ASME Code, Section III Appendix Data (See Table 2.3-1)

TABLE 2.1.2-6

Accident Conditions of Transport
Crippling and Buckling Allowables
for Outer Shell

Loading Condition and Shell	••••• -20	TEMPERATURE (Deg-F) 70	100	150	200	••••• 250
Material Properties (psi):						
E	2990000•	2950000	2930000•	2910000•	2880000	2860000•
Sy	40200••	38000	38000	36300•	34600	34200•
Sm	23800••	23500••	23300	23200•	23100	22800•
Ss	40200	38000	38000	36300•	34600	34200•
Axial Compression Buckling Allowables (psi):						
	39047	37000	36986	35404	33808	33424
Bending Buckling Allowables (psi):						
	39189	37122	37110	35514	33905	33519

• Interpolated from ASME Code, Section III Appendix Data (See Table 2.3-1)

•• Extrapolated from ASME Code, Section III Appendix Data (See Table 2.3-1)

Elastic Buckling stress, S_e, is:

$S_e = E/G = 259,800$ psi

For normal conditions

$R_d = 7.5$

$S_s = S_m = 20,000$ psi

The intercept tangent point G^* is:

$$G^* = (3/2)\ (E/R_d)/S_s$$
$$= (1.5)(1.156(10)^7/7.5)/20,000 = 115.6$$

Since $G << G^*$, the allowable stress is given by:

$$S_j = S_s - \left[4S_s^3\ G^2/\left[27(E/R_d)^2\right]\right]$$
$$= (20,000) - 4(20,000)^3(44.5)^2/\left[27(1.156(10)^7/7.5)^2\right]$$
$$= 19,012 \text{ psi}$$

4. Combined Buckling Stresses are treated in the following fashion:

(a) Stress ratios are calculated for each stress component at any point where compressive principal stresses exist:

$$R = S/S_{cr}$$

Where:

S = stress component under consideration

S_{cr} = buckling stress allowable for the stress component under consideration

(b) The stress ratios are summed linearly and compared with unity (Structural Analysis of Shells (Reference 2.11.5) pp. 240-241):

$$M.S. = [1/(R_a + R_b + R_p)] - 1$$

Where:

R_a = stress ratio for axial stress
R_b = stress ratio for bending stress
R_p = stress ratio for external pressure stress

2.1.2.3 Component Allowable Stresses

The allowable stress limits from Tables 2.1.2-1 and 2.1.2-2 and the buckling allowables from Tables 2.1.2-3 through 2.1.2-6 have been combined with the appropriate material properties from Table 2.3-1 below, at appropriate temperatures, taken from Section 3.0, to derive allowable stress levels for the various cask components under the different mandated loading conditions. In addition, lifting and tiedown stress allowables, generally one-third of the yield strength of the affected material, have been determined in Section 2.5 below. All these stress allowables have been conveniently summarized in Table 2.1.2-7. The derivations of these allowables can be found in the relevant portions of this SAR pertaining to the particular component and loading situation.

2.1.2.4 Impact Limiter Design Criteria

The NuPac 10/140MB package design incorporates energy-absorbing polyurethane foam-filled impact limiters to mitigate the consequences of many of the regulatory events. The foam used is a closed-cell polyurethane foam, with a nominal density of 20 lb per cubic foot (PCF). The properties of this rigid polyurethane foam have been studied at great length in preparation for this application. The foam was studied with regard to the effects of variations in as-poured density, temperature, and direction of load application on the stress-strain relationship of the foam.

TABLE 2.1.2-7
(Page 1 of 2)

10/140MB Allowable Stress Values

Component	Loading Type	Surface (Membrane + Bending)	Centroidal (Membrane)
Inner Shell	*NCT (Stress)	30000	20000
Inner Shell	NCT (Buckling)	-	17905 (Hoop) 19062 (Axial)
Inner Shell	**HAC (Stress)	72000	48000
Inner Shell	HAC (Buckling)	-	26042 (Hoop) 27593 (Axial)
Outer Shell	NCT (Stress)	37200	37200
Outer Shell	NCT (Buckling)	-	22728 (Axial)
Outer Shell	HAC (Stress)	70000	49000
Outer Shell	HAC (Buckling)	-	36258 (Axial)
Outer Shell	Operational (Transport)	37388	37388
Lids	NCT	30000	20000
Lids	HAC	68785	48000
Lids	Operational (Lifting)	(1/3)(28400)	(1/3)(28400)

* NCT - Normal Conditions of Transport
** HAC - Hypothetical Accident Conditions

TABLE 2.1.2-7
(Page 2 of 2)

10/140MB Allowable Stress Values

Component	Loading Type	Surface (Membrane + Bending)	Centroidal (Membrane)
Bolts	NCT	103000	58720
Bolts	HAC	103000	103000
Bolts	Operational (Lifting)	(1/3)(103000)	(1/3)(103000)
Bolt Lugs (Lid)	NCT	30000	20000
Bolt Lugs (Lid)	HAC	68785	48000
Bolt Lugs (Lid)	Operational (Lifting)	(1/3)(28400)	(1/3)(28400)
Bolt Lugs (Cask)	NCT	34855	23235
Bolt Lugs (Cask)	HAC	70000	49000
Bolt Lugs (Cask)	Operational (Lifting)	(1/3)(36900)	(1/3)(36900)
Tiedown Lugs	Operational (Transport)	99240	99240
Lifting Lugs	Operational (Lifting)	(1/3)(28400)	(1/3)(28400)

An initial test series was performed on many samples of 20 PCF foam at temperatures of -20°F, 75°F and 180°F. These samples were all compressed in the direction parallel to the rise of the foam (the foam is inserted into the impact limiters in liquid form, where it then rises and sets up in its final solid configuration). Later, a comprehensive test program was conducted to characterize behavior of several densities of foam over a wide range of temperatures. Foam densities tested included 5, 10, 15, 20 and 25 PCF foam, at temperatures of -20°F, 75°F, 100°F, 140°F and 180°F. Each density at each temperature was repeatedly tested in two different orientations: Parallel to direction of rise, and perpendicular to rise. In addition to the stress-strain data, other foam characteristics were also investigated. These included elastic modulus, yield stress, and thermal properties such as conductivity. From this large data base of test results, enveloping stress-strain relationships were developed for design.

An important consideration in impact limiter design and analysis involves the testing procedure used to derive the polyurethane foam stress-strain curves. These compression tests are performed in accordance with ASTM D1621-63 (Reference 2.11.8), which mandates cubical test specimens one inch on a side. For large-deformation materials, such as polyurethane foam, such a small test specimen tends to introduce an element of uncertainty at higher strain levels, where the material is essentially being crushed flat. At these high strain levels, where the foam cellular structure has collapsed, the character of the material begins to become sufficiently altered such that test results should be interpreted with a certain amount of caution. Additionally, the force required to crush foam specimens to higher strain levels begins to approach the limitations of the testing device, such that the specimen support system begins to exhibit internal deformations that may contribute a significant portion of the overall measured strains.

To ensure that these stipulated material properties are maintained, continuous monitoring of the foam takes place through the pouring operation, which occurs in several stages. During fabrication, the stress-strain properties of the foam are controlled by pouring samples from each batch in a special box. Test specimens are then prepared from each box and tested to determine their

FIGURE 2.1.2-1

Average Stress-Strain Properties
at Various Temperatures
Parallel to the Direction of Rise

THIS INFORMATION IS PROPRIETARY

FIGURE 2.1.2-2

Average Stress-Strain Properties
at Various Temperatures
Perpendicular to the Direction of Rise

THIS INFORMATION IS PROPRIETARY

stress-strain characteristics at 75°F. The impact limiter is considered acceptable if the average stress-strain properties from all pours, up to 75% strain, is within 15% of the mean curves at 75°F shown in Figures 2.1.2-1 and 2.1.2-2. Due to increasing uncertainties in measurement accuracy between 75% and 80% strain, the allowable measured variation from mean properties at 80% strain is conservatively increased to ±20%. Individual batches of foam exhibiting properties more than 20% from the required mean curve (25% at 80% strain) are rejected.

A number of factors were taken taken into consideration in attempting to characterize polyurethane foam properties for design purposes. The logic used in constructing enveloping foam stress-strain relationships is presented below:

First, while samples of foam of exactly the same density exhibit an extremely consistent stress-strain curve, it is difficult to reproduce that density to within better than five percent. The resulting variation in the stress-strain relationship can easily exceed the density variation. It was determined that foam placement techniques could not consistently hold the as-placed stress-strain relationship better than within plus or minus 15% of the mean value up to 75% strain, and ±20% at 80% strain. In order to envelope the behavior variations due to the slight variations in density, the stress data are thus scaled by plus or minus 15% (±20% for 80% strain), depending on whether stiff or soft foam is more detrimental.

Second, it was found that the stress-strain relationship of the foam varies with the temperature of the tested specimen. Interestingly, the properties of the foam at -20°F were very much stiffer and stronger than at the higher temperatures. At 180°F, the foam was considerably softer than at room temperature. However, it is important to note that the foam reacted to temperature in a very consistent manner -- that is, the stress-strain properties in all specimens tested were very consistent at a given temperature. To determine the behavior of the foam at an intermediate temperature, the stress at a given strain is linearly interpolated between the curves.

Finally, samples were tested to determine the variation of properties with respect to the orientation of the applied stress in relation to the direction

of foam rise. While this is an important concern for some rigid foams, it was found that the foam used in the NuPac 10/140MB exhibits relatively little directionality. In general, for all temperatures of interest, 20 PCF foam, when tested perpendicular to the direction of rise, is slightly stronger than that tested parallel to rise, up to strain levels of about 40 - 50%. At higher strain levels, the 'parallel' foam starts to become slightly stronger than the 'perpendicular' foam. The difference between stress levels for the two orientations runs about 3 - 4% in the 'plateau' region (a region of nearly constant stress between about 10% and 40% strain) for foam at -20°F. This percentage difference decreases as foam temperature increases.

In summary, there are a number of factors inherent in the polyurethane foam, which, in concert, dictate the strength level of any given foam under any given set of circumstances. For purposes of cask design, only two bounding cases are of practical interest. These cases are those where the foam exhibits its greatest strength, and where it exhibits minimum strength.

Maximum strength foam will tend to induce the greatest impact loads upon the package under the requirements of the Normal Condition and Hypothetical Accident Condition free drop tests. Minimum strength foam will tend to incur the largest deflections under the drop requirements, increasing the potential for 'bottoming out' of the cask. This would be a case where the foam does not remove enough energy to avoid a large acceleration spike at the end of the impact stroke. The integrity of the analysis methods used in this Report to evaluate the impact forces requires that none of the protrusions on the side of the cask or the cylindrical edge of the lead and steel shield actually strike the unyielding surface. While such an impact would not necessarily cause a loss of packaging effectiveness, the loads output from the various impact analysis programs used to verify the design would not be correct. A determination of the actual loads would involve a fairly complicated analysis for which there is little experimental data to verify the results.

Therefore, the impact limiters must be designed to insure that package 'hard spots' do not strike the impact surface under conditions of minimum foam strength. At the same time, the design must consider the effects of maximum strength foam to prevent excessive impact loading under conditions of minimum foam deformation. To successfully incorporate both these considerations into

the impact limiter design basically requires analysis which accounts for two bounding foam property extremes: Maximum strength for maximum impact loading, and minimum strength for maximum impact deflections.

In order to conservatively bound these two extremes in foam material properties, all the factors outlined above are taken into account. For maximum strength foam, the following parameters are considered: Minimum regulatory transport temperature of -20°F; maximum density -- 'nominal' -20°F stress data increased by a factor of 15% (20% at 80% strain); maximum directional properties -- strength perpendicular to rise up to 40 - 50% strain, and then strength parallel to rise at higher strains. Note that this latter assumption automatically eliminates drop orientation as a design consideration, since maximum foam properties will be in effect at all times. For example, a flat end drop would ordinarily mobilize foam mostly parallel to the direction of rise. In the lower strain regions, this would tend to induce lower load levels on the package than would be the case if the crush were in a direction primarily perpendicular to the rise. Flat side drop, where crush is primarily perpendicular to rise, would be just the opposite case: Larger deflections (greater than about 30% strain) would tend to induce lower load levels than would arise from parallel type crush. With maximum properties being utilized irregardless of rise direction, maximum impact loading is conservatively assured irregardless of impact orientation.

Minimum strength foam would be derived from the following combination of factors: Maximum anticipated foam temperature (169°F for Normal Conditions of Transport, and 105°F for foam prior to Hypothetical Accident Conditions -- see Sections 2.6.1, 2.7.1.1, and 3.1 for details); minimum foam density at these temperatures, e.g., 'nominal' stress derated by 15% (20% at 80% strain); minimum directionally dependent foam strength -- 'parallel' data at lower strains, and 'perpendicular' data at higher strains.

Note that the maximum temperatures utilized in the impact analyses are for relatively small, localized areas only, and are not indicative of the overall average foam temperature (refer to Section 3.0, 'Thermal Evaluation'). For instance, under Normal Conditions of Transport solar loading, the maximum temperature on the side of the upper impact limiter is only 123°F, as opposed to the 169°F shown near the top surface. Assuming that the entire impact limiter

is at the higher temperature is extremely conservative, and will tend to result in theoretical deflections much greater than would actually take place in real life conditions. Additional conservatism is introduced by evaluating both impact limiters at the maximum temperature, even though the temperature of the lower limiter will generally be lower under Normal Conditions of Transport, due to less solar loading. It should also be noted that Normal Condition impact limiter temperatures were derived by assuming constant solar loading. A more realistic, intermittent solar loading analysis will result in significantly lower temperature levels.

In addition to impact response evaluations at the temperature extremes discussed above, drop analyses were also performed for a nominal ambient temperature condition of 75°F. The results of these analyses can then be directly compared to drop test results to determine the approximate degree of accuracy of predicted impact limiter deflections and cask acceleration loads. Drop tests were performed utilizing impact limiters stabilized at approximately room temperature, so the comparison should be valid. For analysis purposes, the foam properties are taken at 'nominal' values for 20 PCF foam at 75°F, with no density bias. Since strength differences between 'parallel' and 'perpendicular' foam are minor, averages of 'parallel' and 'perpendicular' properties are utilized in the analyses. The effects of this assumption are expected to be insignificant for purposes of comparison to test results. Refer to Appendix 2.10.4 for a detailed discussion of drop test results.

Figures 2.1.2-1 and 2.1.2-2 present the average stress-strain behavior of the 20 PCF foam at the four temperatures of interest for strains parallel and perpendicular to the direction of rise, respectively. When the adjustments described above are made to this data, bounding design curves are generated. These bounding stress-strain properties are shown in Figure 2.1.2-3.

Because the force required to strain a sample of this foam much beyond 80% is greater than the capacity of the instrument used to measure it, the behavior of the foam beyond this point is not well defined. It is clear, however, that the foam neither disappears nor becomes perfectly rigid. In analyses where deflections are critical (such as when clearance between hard spots on the package and the essentially unyielding surface is required to maintain the

FIGURE 2.1.2-3

Stress-Strain Properties
Used for Design

THIS INFORMATION IS PROPRIETARY

integrity of the analysis), predicted strains may sometimes slightly exceed 80%. The force from foam stained beyond 80% is conservatively (for deflection prediction) linearly extrapolated from the stress-strain states at 75% and 80%. This is automatically done by the energy balance computer programs EYDROP, SYDROP, and CYDROP, which are discussed at length in Appendix 2.10.5. In such situations, the force of impact is slightly underpredicted. However, the highest impact forces occur when the foam is assumed to exhibit its stiffest stress-strain relationship. For EYDROP, SYDROP, and CYDROP analyses performed to determine the greatest forces on the package, the foam strain is not permitted to exceed 80%, thereby insuring a high degree of accuracy for the prediction of impact forces.

Additionally, it should be recognized that compression test results are valid for foam that is uniformly crushed between two essentially unyielding surfaces. Accordingly, foam strain can be idealized to a high degree of accuracy as a function of the depth of crushed foam between the cask surface and the impacted surface, for foam deformations arising from impacts. However, the nature of the impact limiter geometry is such that certain portions of foam mobilized during an impact event will lie outside of directly-crushed areas for most drop orientations. This characteristic precludes exact analysis of certain portions of the impact limiter. NuPac has found from experience (as discussed at the beginning of Section 2.0) that the response of these 'unbacked' portions of the mobilized impact limiter can be accurately approximated by assuming that the foam in these areas will exhibit a uniform stress corresponding to its 'plateau' region, 10 - 40% strain (refer to Figure 2.1.2-2). These assumptions have been borne out by drop test results.

Finally, the somewhat unconventional geometry of the impact limiter design has necessitated several simplifying assumptions for analysis purposes with regard to impact limiter configuration under the imposed drop conditions. These assumptions were made to develop equivalent geometries which are more amenable to NuPac's standard impact limiter analysis techniques. The resulting simplifications are conservative for the individual application, whether for purposes of maximizing loads or maximizing deflections. These geometry assumptions are summarized graphically in Figure 2.1.2-4. Brief explanations of the assumptions are provided in Table 2.1.2-8. Detailed explanations are given in the specific relevant sections shown in Table 2.1.2-8.

FIGURE 2.1.2-4
(Page 1 of 4)

Impact Limiter Geometry Assumptions

BASELINE REFERENCE GEOMETRY	CASE 1	CASE 2	CASE 3
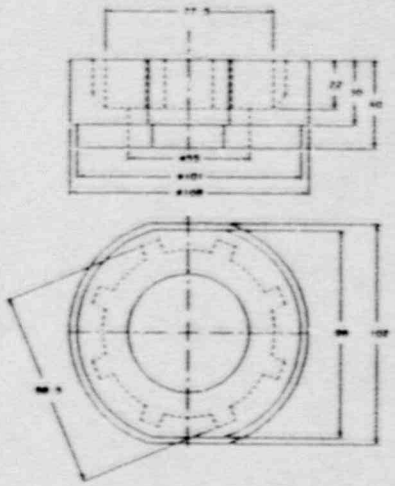 BOTTOM VIEW	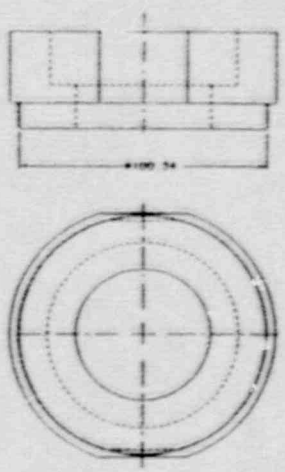 BOTTOM VIEW	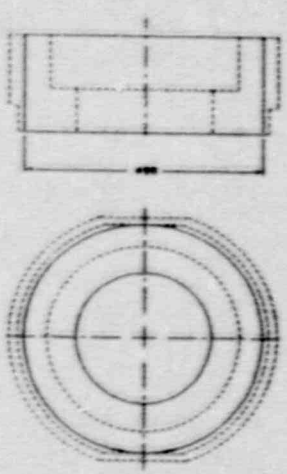 BOTTOM VIEW	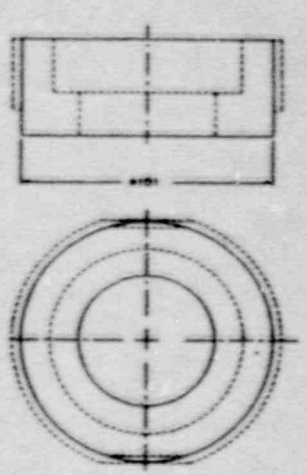 BOTTOM VIEW
IMPACT LIMITER BASIC GEOMETRY	IMPACT LIMITER ASSUMED GEOMETRY FOR FLAT END DROP MAXIMUM LOADS AND DEFLECTIONS	IMPACT LIMITER ASSUMED GEOMETRY FOR C.G. OVER STRUCK CORNER MAXIMUM DEFLECTIONS (CONFIGURATION 1)	IMPACT LIMITER ASSUMED GEOMETRY FOR C.G. OVER STRUCK CORNER MAXIMUM DEFLECTIONS (CONFIGURATION 2)

FIGURE 2.1.2-4
(Page 2 of 4)

Impact Limiter Geometry Assumptions

CASE 4	CASE 5	CASE 6	CASE 7
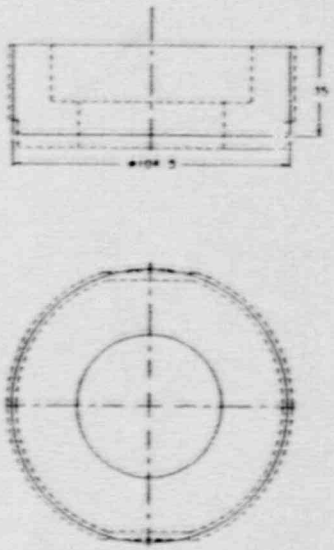	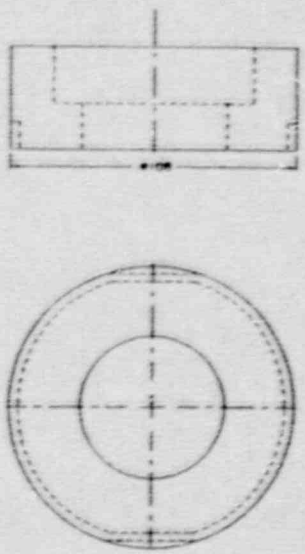	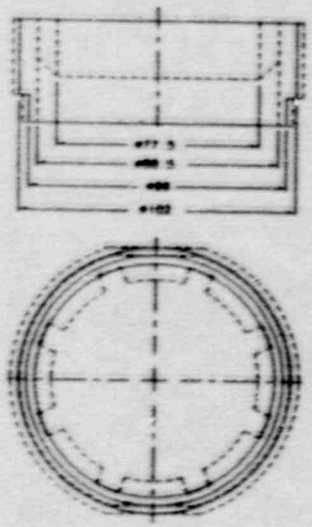	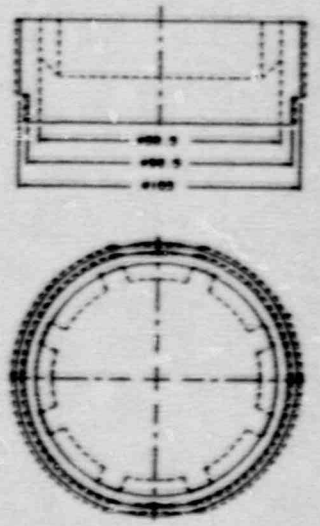
BOTTOM VIEW	BOTTOM VIEW	BOTTOM VIEW	BOTTOM VIEW
IMPACT LIMITER ASSUMED GEOMETRY FOR OBLIQUE DROP FORCE-DEFLECTION CURVES (MAXIMUM DEFLECTIONS) SEPARATION LOADS TEST GEOMETRY MAXIMUM OBLIQUE DEFLECTION TEST GEOMETRY	IMPACT LIMITER ASSUMED GEOMETRY FOR OBLIQUE DROP CASH INTERNAL FORCES (MAXIMUM LOADS)	IMPACT LIMITER ASSUMED GEOMETRY FOR SIDE DROP MAXIMUM LOADS AND DEFLECTIONS (NORMAL CONDITIONS OF TRANSPORT)	IMPACT LIMITER ASSUMED GEOMETRY FOR SIDE DROP MAXIMUM LOADS (PUNCTURE, ACCIDENT CONDITIONS)

FIGURE 2.1.2-4
(Page 3 of 4)

Impact Limiter Geometry Assumptions

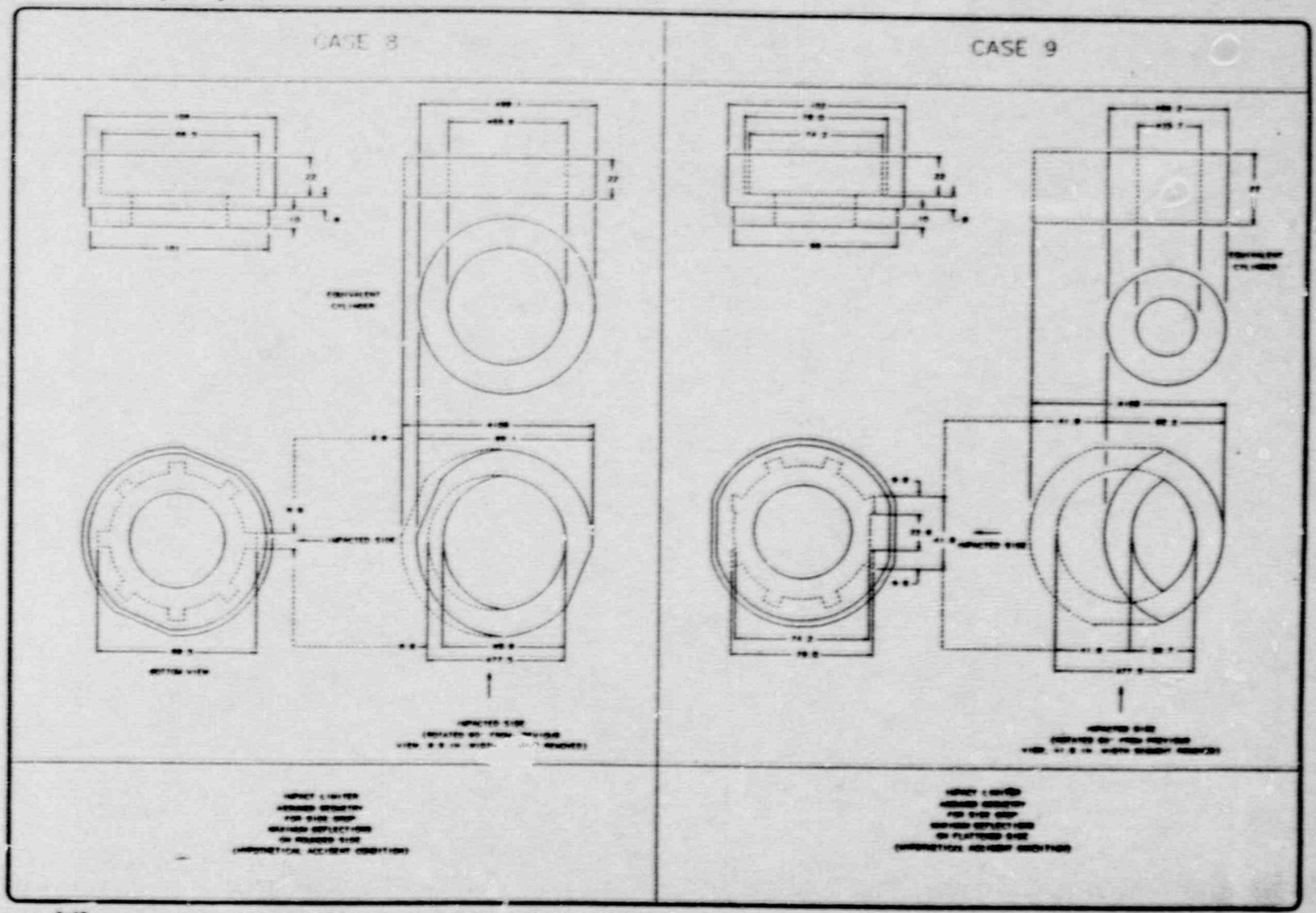

FIGURE 2.1.2-4
(Page 4 of 4)

Impact Limiter Geometry Assumptions

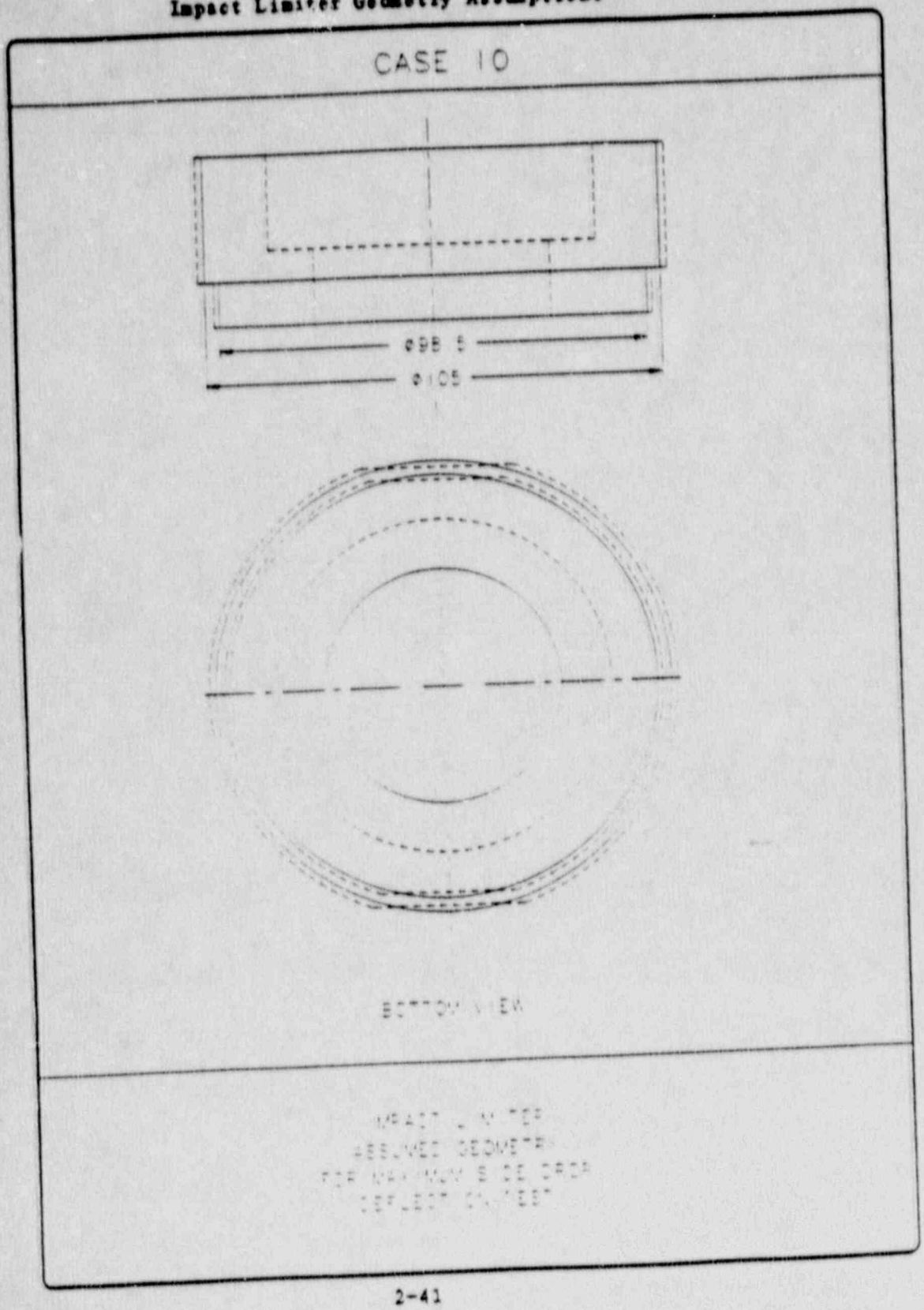

TABLE 2.1.2-8
(Page 1 of 8)

Impact Limiter Geometry Assumptions

Case No.	Explanation	Relevant SAR Section
Baseline Reference Geometry	The actual impact limiter geometry consists of two outside diameters, the major diameter being 108 inches, and the minor being 101 inches. The major diameter is flattened equally in two places, 180° apart. Distance between the two flattened surfaces is 102 inches. The minor diameter is flattened similarly, with the distance between flats being 96 inches. The portion of the impact limiter encompassing the major diameter is 30 inches deep, and the minor diameter portion is 10 inches deep. The cask is inserted 22 inches deep into the limiter, in a 77.5-inch diameter opening. Primary and bottom lid lug gussets are accomodated by individual 'pockets' built into the inside diameter of the impact limiter. For the fixed-bottom version, there are no lug 'pockets' on the lower impact limiter. A 55-inch diameter opening connects the cavity which contains the cask to the outside end surface of the limiter.	1.3.1

TABLE 2.1.2-8
(Page 2 of 8)

Impact Limiter Geometry Assumptions

Case No.	Explanation	Relevant SAR Section
1	The area of the minor diameter is resolved into a full circle (without flattened sides) of equivalent area. The diameter of this equivalent circle is 100.34 inches.	2.6.7.1 2.7.1.1 (Flat End Drop)
2	The diameter of the entire impact limiter is assumed to be equal to the distance across the flats on the actual minor diameter. This diameter is 96 inches.	2.6.7.2.1 2.7.1.2.1 (Max. Oblique Deflections)
3	The diameter of the entire impact limiter is assumed to be equal to the actual minor diameter. This diameter is 101 inches.	2.6.7.2.1 2.7.1.2.1 (Max. Oblique Deflections)
4	The diameter of the entire impact limiter is assumed to be the average of the major and minor diameters. This diameter is 104.5 inches. The total height of the impact limiter (40 inches) and the height of the section encompassing the major diameter (30 inches). This height is 35 inches.	2.6.7.2.2 2.7.1.2.2 2.10.4 (Oblique Force-Deflection Characteristics)

TABLE 2.1.2-8
(Page 3 of 8)

Impact Limiter Geometry Assumptions

Case No.	Explanation	Relevant SAR Section
5	The diameter of the entire impact limiter is assumed to be the same as the major diameter. This diameter is 108 inches.	2.6.7.2.3 2.7.1.2.3 (Oblique - Max. Loads)
6	The outside diameter of the major diameter portion of the impact limiter is assumed to be equal to the distance across the flats on the actual major diameter. This diameter is 102 inches. The outside diameter of the minor diameter portion of the impact limiter is assumed to be equal to the distance across the flats on the actual minor diameter. This diameter is 96 inches. For loads analysis, the inside diameter of the entire impact limiter is assumed to be equal to the distance across any opposing pair of bolt lug 'pockets'. This diameter is 88.5 inches. For deflection analysis, an inside diameter of 77.5 inches is assumed.	2.6.7.3.1 (Side Drop - Max. Normal Condition Deflections)

TABLE 2.1.2-8
(Page 4 of 8)

Impact Limiter Geometry Assumptions

Case No.	Explanation	Relevant SAR Section
7	The outside diameter of the major diameter portion of the impact limiter is assumed to be equal to the average of the major diameter and the distance across the flats of the major diameter. This diameter is 105 inches. The outside diameter of the minor diameter portion of the impact limiter is assumed to be the average of the minor diameter. This diameter is 98.5 inches. The inside diameter of the entire impact limiter is assumed to be equal to the distance across any opposing pair of bolt lug 'pockets'. This diameter is 88.5 inches.	2.7.1.3.1 (Side Drop - Max. Accident Condition Deflections)
8	For assumed impact on a rounded edge of the impact limiter, directly over a lid bolt lug 'pocket', the impact limiter is divided into four separate components for evaluation of maximum deflections. 1. The 10-inch length comprising the minor diameter is treated as a cylinder with outside diameter of 101 inches and inside diameter of 77.5 inches. Note that this portion of the ipact limiter does not begin	2.6.7.3.2 2.7.1.3.2 (Side Drop - Max. Accident Condition Deflections for Impact on Rounded Side)

TABLE 2.1.2-8
(Page 5 of 8)

Impact Limiter Geometry Assumptions

Case No.	Explanation	Relevant SAR Section
8 (Cont'd)	to crush until the portion comprising the major diameter (108 inches) has already compressed (108 - 101)/2 = 3.5 inches.	
	2. The 8-inch long segment comprising the portion of the major diameter which extends beyond the top of the bolt lug 'pocket' is treated as a cylinder with outside diameter of 108 inches and inside diameter of 77.5 inches.	
	3. The 22-inch long, 8.9-inch wide segment of the major diameter portion of the impact limiter directly over the bolt lug 'pocket' is treated as a rectangular slab, 22 inches long by 8.9 inches wide by (108 - 88.5)/2 = 9.75 inches deep.	
	4. The two 22-inch long sections of the major diameter portion of the impact limiter to the side of the lug bolt 'pocket' are rendered into an equivalent cylinder with an outside diameter of (108 - 8.9) = 99.1 inches,	

TABLE 2.1.2-8
(Page 6 of 8)

Impact Limiter Geometry Assumptions

Case No.	Explanation	Relevant SAR Section
	and an inside diameter of (77.5 - 8.9) = 68.6 inches.	
	The development of components 3 and 4 is illustrated in Figure 2.1.2.3-4.	
9	For assumed impact on a flattened edge of the impact limiter, straddling two adjacent bolt lug 'pockets', the impact limiter is divided into four separate components for evaluation of maximum deflections.	2.6.7.3.2 2.7.1.3.2 (Side Drop - Max. Accident Condition Deflections for Impact on Flattened Side)
	1. The 10-inche length comprising the minor diameter is treated as a cylinder with an outside diameter equal to the distance across the flattened areas (96 inches), and an inside diameter of 77.5 inches. Note that this portion of the impact limiter does not begin to crush until the portion comprising the flattened area of the major diameter (102 inches) has already compressed (102 - 96)/2 = 3.0 inches.	

TABLE 2.1.2-8
(Page 7 of 8)

Impact Limiter Geometry Assumptions

Case No.	Explanation	Relevant SAR Section
2.	The 8-inch long segment comprising the portion of the major diameter which extends beyond the top of the bolt lug 'pocket' is treated as a cylinder with outside diameter equal to the distance across the flattened areas (102 inches), and an inside diameter of 77.5 inches.	
3.	The 22-inch long, 41.8-inch wide segment of the major diameter portion of the impact limiter over the two adjacent bolt lug 'pockets' is treated as three rectangular slabs: The two directly over the lugs are 22 inches long by 9.6 inches wide by (102 - 79)/2 = 11.5 inches deep; The area between is treated as a single slab 22 inches long by 22.6 inches wide by (102 - 74.2)/2 = 13.9 inches deep.	

TABLE 2.1.2-8
(Page 8 of 8)

Impact Limiter Geometry Assumptions

Case No.	Explanation	Relevant SAR Section
	4. The two 22-inch long sections of the major diameter portion of the impact limiter to the side of the two adjacent lug 'pockets' are rendered into an equivalent cylinder with an outside diameter of (108 - 41.8) = 66.2 inches, and an inside diameter of 77.5 - 41.8) = 35.73 inches. The development of components 3 and 4 is illustrated in Figure 2.1.2.3-4.	
10	The major diameter portion of the impact limiter is assumed to be the average of the major diameter and the distance across the flats. This diameter is 105 inches. The minor diameter portion of the impact limiter is assumed to be the average of the minor diameter and the distance across the flats. This diameter is 98.5 inches.	2.10.4 (Side Drop - Max. Accident Condition Deflections for Comparison to Test Results)

The basic analysis techniques and assumptions are similar to those used to analyze the performance of the NuPac 125-B Fuel Shipping Cask (Certificate of Compliance No. 9200). An extensive drop test program was performed on that cask, showing that the assumptions and analytic techniques used on both that cask and the NuPac 10/140MB are both reasonably accurate and slightly conservative. These findings have been further reinforced by more recent scale model testing of the 10/140MB cask. Refer to Section 2.10.4 for details of this latter test program.

In conclusion, the NuPac 10/140MB employs a very efficient impact limiter design, which insures that protuberances such as the tie-down lugs and closure bolt gussets are adequately protected during the impact events, yet the sides of the cask are not protected more than required where there are no such protuberances. Such a design makes for a lighter impact limiter than might otherwise be required, but forces certain bounding calculations, since the impact analysis programs are written for a simpler design. These bounding calculations are described in detail in Sections 2.6.7 and 2.7.1.

2.2 Weights and Centers of Gravity

The weight of the cask and payload is approximately 68,000 lb. The center of gravity for the assembled package is located at the approximate geometric center of the assembly.

A package weight breakdown by major components is shown in the table below.

Component	Weight (lb)
Primary lid	6,730
Secondary lid	1,700
Bottom lid/plate	6,460
Cask body	26,960
Impact limiters (2)	11,150
Net Weight	53,000
Maximum payload	15,000
Gross Weight	68,000

In order to derive these component weights, as well as overall package center of gravity and inertial properties, the components were broken down into simple geometric shapes. This process simplifies the calculation procedure for defining section properties. As an example, the cask secondary lid is shown below:

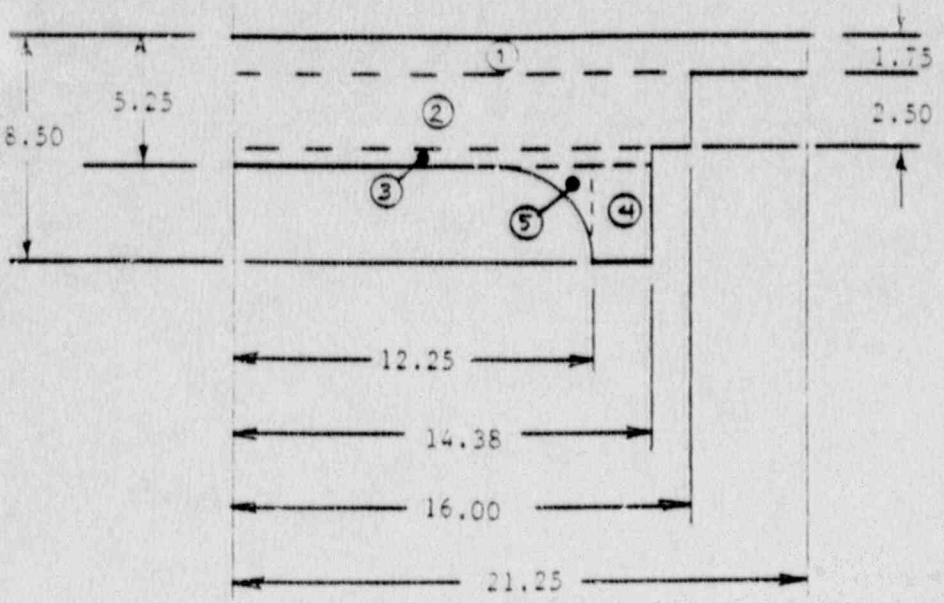

The weights of the individual portions of the lid are derived by calculating the volume of each portion, and then multiplying by the mass density of stainless steel. Thus, the weight of segment 1 above is:

$$w_1 = \pi(21.25)^2(0.29\ lb/in^3) = 411\ lb.$$

Similarly, all segments are calculated and summed to give the overall component weight. Individual component centers of gravity can be derived in a similar manner:

$$\bar{y} = \sum y_i A_i / \sum A_i$$

Where: y_i = location of individual segment c.g.
A_i = segment cross-sectional area

From this, the c.g. of the secondary lid is found to be 5.70 inches from the lowermost surface of the lid. Inspection of the drawings in Section 1.3 revels that this location corresponds to a height of 104.20 inches above the package baseline, defined as the bottom surface of the lower impact limiter.

In a similar manner, all component weights and centers of gravity can be derived. The overall package center of gravity can then be defined as:

$$\bar{Y} = \sum Y_i W_i / \sum W_i$$

Where: Y_i = distance of cask component from baseline
W_i = component weight

$$\bar{Y} = 61.17\ in.$$

In order to investigate the impact response of the package under the regulatory oblique drop requirements (refer to Sections 2.6.7.2.3 and 2.7.1.2.3), the mass moment of inertia about the center of gravity, perpendicular to the cask axis, must be derived. In order to simplify this procedure, while still maintaining accuracy, the cask components were

converted into equivalent simplified shapes. Again, as an example, the secondary lid is depicted as a simple disk. This was done by taking the total weight of the lid, as calculated above, and deriving a disk of equal weight. An equivalent lid diameter of 32.0 inches was assumed, and the equivalent lid thickness was then .ound:

$$t_{eq} = 1700 \text{ lb}/[(0.29 \text{ lb/in}^3)\pi(16.0)^2] = 7.29 \text{ in.}$$

This equivalent lid shape was then superimposed on the actual lid center of gravity. All cask components were treated in this manner, and an equivalent package was derived, as shown in Figure 2.?-1. In this equivalent package, the following additional assumptions were made:

Primary lid includes the weight of the thermal protective cushion, lid bolts, and bolt attachment gussets. It has equivalent diameters of 75.0 in. O.D. and 32.0 in. I.D., and an equivalent thickness of 5.78 in.

Cask body is treated as a homogeneous cylinder comprised of inner and outer steel shells and thermal shield, lead shielding, and appurtenances such as tiedown lugs and primary lid attachment bolt gussets. Outside diameter is 74.5 in., inside diameter is 66.0 in., and overall height is 79.0 in.

Impact limiters are treated as fully circular, homogeneous structures, with outside diameter of 108.0 in., major inside diameter of 75.0 in., minor I.D. of 55.0 in., and overall height of 40.0 in.

Payload was assumed to be a homogeneous cylinder weighing 15,000 lb., 73.0 in. high, with a diameter of 66.0 in.

FIGURE 2.2-1

Package Equivalent Geometry

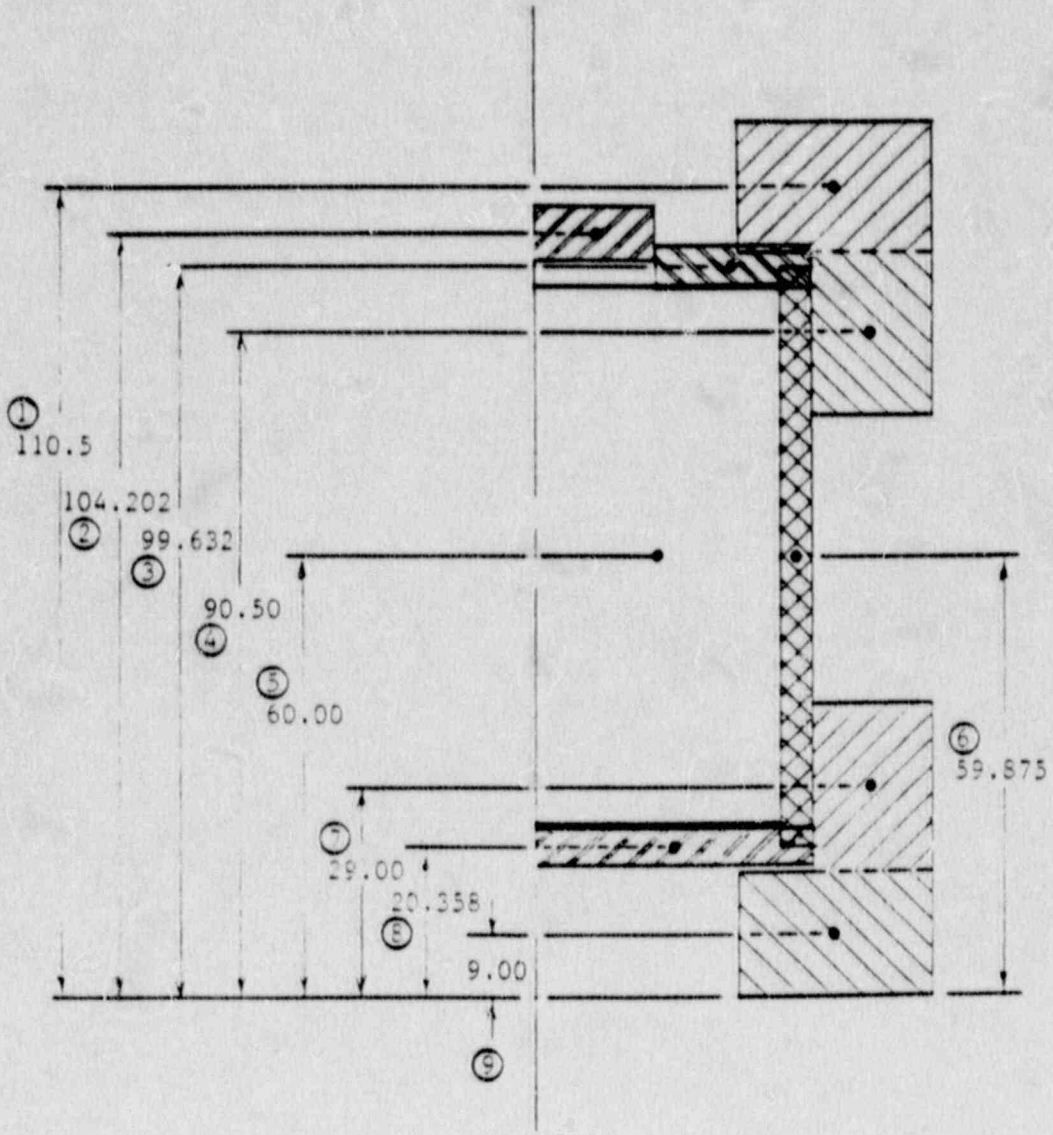

Component weights, corresponding to Figure 2.2-1, are summarized below:

Component number	Weight (lb)	
1	3,006	
2	1,700	
3	6,730	
4	2,569	
5	15,000	(payload)
6	26,960	
7	2,569	
8	6,460	
9	3,006	

The package mass moment of inertia was derived from individual equivalent component moments of inertia. These latter were calculated according to Shigley, Mechanical Engineering Design (Reference 2.11.9), Table A-32.

For solid cylinders (secondary lid, bottom plate, payload):

$$(I_x)_i = (m_i/48)(3d_i^2 + 4L_i^2)$$

Where: m_i = component mass = weight/386.4 in/sec^2
d_i = component diameter
L_i = component length

For hollow cylinders (primary lid, body, impact limiter components):

$$(I_x)_i = (m_i/48)[3(d_o)_i^2 + 3(d_i)_i^2 + 4L_i^2]$$

Where: $(d_o)_i$ = component outside diameter
$(d_i)_i$ = component inside diameter

The overall package mass moment of inertia was then found from the expression:

$$I_X = \sum[(I_x)_i + r_i^2 m_i]$$

Where: r_i = distance from component c.g. to package c.g.

$$I_X = 265{,}000 \text{ in-lb-sec}^2$$

2.3 Mechanical Properties of Materials

The cask outer shell and tiedown lug gussets are fabricated from ASTM A-516 Grade 70 or, alternatively, A-537 Class 1 carbon steel. The tiedown lugs are constructed of ASTM A-517 Grade P alloy steel plate. The inner shell is constructed of ASTM A-240 Type 304 stainless steel, and the top and bottom lids are either ASTM A-351 Grade CF8 or CF8A Type 304 stainless steel castings or ASTM A-182 Type F304 forgings. Bolts are ASTM A-320, Grade L43. Figures 2.3-1 and 2.3-2 show the tensile and compressive stress-strain curves for lead at various temperatures. Properties of these structural components are delineated in Table 2.3-1.

TABLE 2.3-1
Mechanical Properties of Materials Used in the NuPac 10/140MB Cask

Steel Material Specification	Class Type or Grade	Temperature (°F)	Strength (ksi) Yield[1] S_y	Ultimate[2] S_u	Allowable[3] S_m	Elastic Modulus[4] (10^6 psi)	Coefficient[5] of Thermal Expansion[6] (10^{-6} in/in/°F)
ASTM A-240	304	-100	-	-	-	29.1	
(Inner Shell		70	30.0[oo]	75.0[oo]	-	28.3	8.46
and Upper		100	30.0	75.0	20.0	-	8.55
Primary Lid		200	25.0	71.0	20.0	27.6	8.79
Bolt Lugs)		300	23.5	66.0	20.0	27.0	9.00
		400	20.7	64.4	18.7	26.5	9.19
		500	19.4	63.5	17.5	25.8	9.37
		600	18.2	63.5	16.4	25.3	9.53
		700	17.7	63.5	16.0	24.8	9.69
ASTM A-320	L43	-100	-	-	-	28.5	-
(Bolts and		70	105.0[oo]	125.0[oo]	-	27.8	6.20
Nuts)		100	105.0	-	35.0	-	6.27
		200	99.0	-	33.0	27.1	6.54
		300	95.7	-	33.9	26.7	6.78
ASTM A-351	CF8A/304	-100	-	-	-	29.1	-
(Lids and		70	35.0[oo]	77.0[oo]	-	28.3	8.46
Upper Primary		100	35.0	77.0	23.3	-	8.55
Lid Bolt Lugs)		200	29.1	72.8	23.3	27.6	8.79
		300	26.3	67.8	22.6	27.0	9.00
ASTM A-182	F304	-100	-	-	-	29.1	-
(Lids -		70	30.0[oo]	70.0[oooo]	-	28.3	8.46
Alternate		100	30.0	70.0	20.0	-	8.55
Mat'l)		200	25.0	66.2	20.0	27.6	8.79
		300	22.5	61.5	20.0	27.0	9.00
ASTM A-351	CF8/304	-100	-	-	-	29.1	-
(Lids -		70	30.0[oo]	70.0[oo]	-	28.3	8.46
Alternate		100	30.0	70.0	20.0	-	8.55
Mat'l)		200	25.0	66.2	20.0	27.6	8.79
		300	22.5	61.5	20.0	27.0	9.00
ASTM A-516	70	-100	-	-	-	30.2	-
(Outer Shell,		70	38.0[oo]	70.0[ooo]	-	29.5	5.42
Cask Tiedown		100	38.0	70.0	23.3	-	5.53
Lug Gussets, and		200	34.6	70.0	23.1	28.8	5.89
Lid Bolt Lugs)		300	33.7	70.0	22.5	28.3	6.26
		400	32.6	70.0	21.7	27.7	6.61
		500	30.7	70.0	20.5	27.3	6.91
		600	28.1	70.0	18.7	26.7	7.17
		700	27.4	70.0	18.3	25.5	7.41
ASTM A-51[7]	P	-100	-	-	-	30.4	-
(Tiedown Lugs)		70	100.0[oo]	115.0[ooo]	-	29.7	6.20
		100	100.0	-	38.3	-	6.27
		200	95.8	-	38.3	29.0	6.54
		300	93.0	-	38.3	28.5	6.78
ASTM A-53[7]		-100	-	-	-	30.2	-
(Outer Shell	1	70	30.0	70.0	-	29.5	5.42
Alternate		100	30.0	70.0	23.3	-	5.53
Material)		200	44.1	70.0	23.2	28.8	5.89
		300	40.5	68.6	22.9	28.3	6.26
		400	37.5	68.6	22.9	27.7	6.61
		500	35.2	68.6	22.9	27.3	6.91
		600	33.9	68.6	22.6	26.7	7.17
		700	32.1	68.6	21.4	25.5	7.41

Lead Material Specification	Type or Grade	Temperature (°F)	Strength (ksi) Proportional[1] S_p (Tens)	S_p (Comp)	Yield[2] S_y (Tens)	S_y (Comp)	Ultimate[2] S_u (Tens)	Elastic Modulus[4] (10^6 psi)	Coefficient[5] of Thermal Expansion[6] (10^{-6} in/in/°F)
ASTM B29	Copper	-99	----	----	----	----	----	2.50	15.28
	Bearing	70	----	----	----	----	----	2.34	16.07
		100	0.276	0.215	0.584	0.490	1.570	2.30	16.21
		175	0.293	0.107	0.509	0.428	1.162	2.20	16.58
		250	0.277	0.107	0.498	0.391	0.844	2.09	16.95
		325	0.189	0.093	0.311	0.320	0.642	1.96	17.54
		440	----	----	----	----	----	1.74	18.50
		620	----	----	----	----	----	1.36	20.39

References:

1. ASME Boiler and Pressure Vessel Code, Sect. III, Nuclear Power Plant Components, Division 1, 1983 Edition, Reference 2.11.3, Tables I-2.1, I-2.2, I-13.1 and I-13.3, except as noted.
2. Ibid, Tables I-3.1 and I-3.2, except as noted.
3. Ibid, Tables I-1.1, I-1.2, I-1.3 and I-11.1
4. Ibid, Table I-6.0
5. Ibid, Table I-5.0
6. WADC Technical Report 57-695, ASTIA Document No. 151165, Determination of the Mechanical Properties of a High Purity Lead and a 0.058% Copper-Lead Alloy, April 1958, by Thomas Tietz, Stanford Research Center, reference 2.11.10, pp. 21,26
7. Ibid
8. Ibid, p.14
9. NUREG/CR-0481, SAND77-1872, An Assessment of Stress-Strain Data Suitable for Finite Element Elastic - Plastic Analysis of Shipping Containers, H. J. Rack and G. A. Knorovsky, Sept. 1978, Reference 2.11.19, p.66
10. Ibid, p. 56

- • Mean from 70°F
- •• ASME Boiler and Pressure Vessel Code, Sect. II, Material Specifications, Part A, 1983 Edition
- ••• Ibid, minimum of specified range
- •••• Ibid, derated from 75 ksi for sections greater than 5.0 in. thick

Notes: Carbon steel density taken at 0.283 lb/in^3, Poisson's Ratio = 0.3
Stainless steel density taken at 0.29 lb/in.^{3}, Poisson's Ratio = 0.3
Lead density taken at 0.41 lb/in^3, Poisson's Ratio = 0.45, melting point = 620°F.

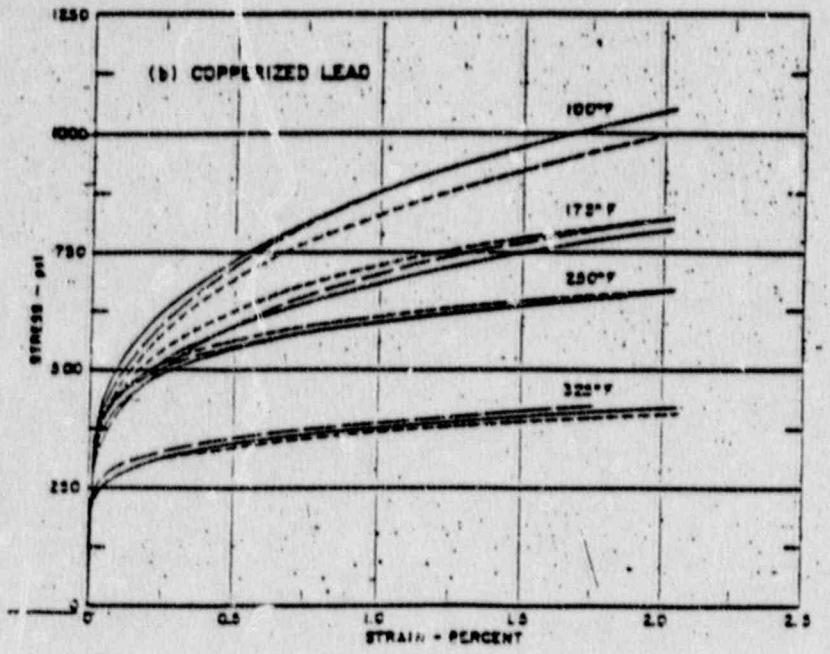

FIGURE 2.3-1

Tensile Stress - Strain Curves for Lead

Strain Rate 0.005 in/in/min.

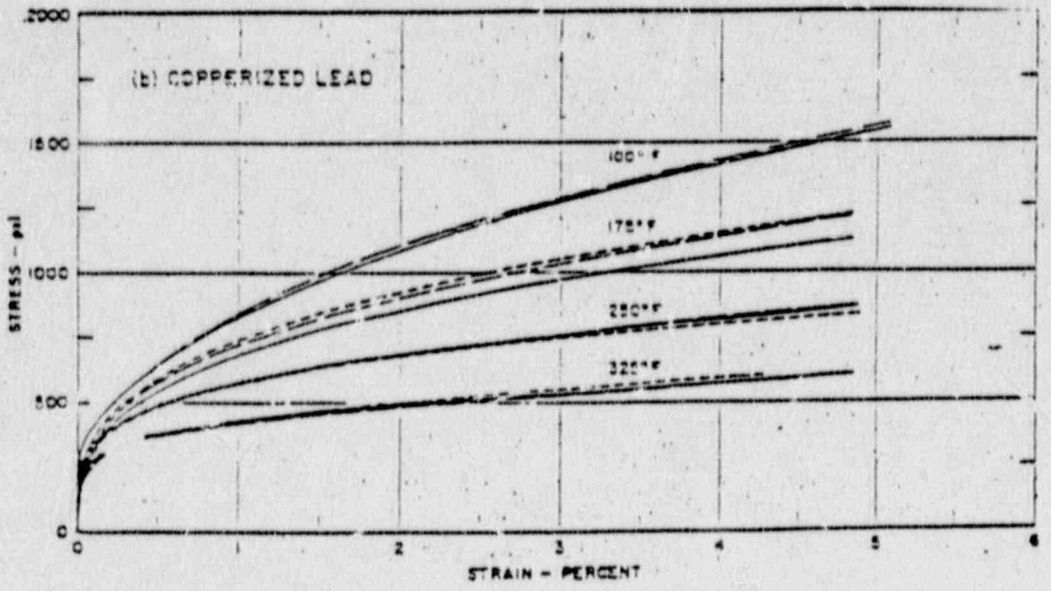

FIGURE 2.3-2

Compressive Stress - Strain Curves for Lead

Strain Rate 0.005 in/in/min.

The lead shielding will possess those properties referenced in WADC Technical Report 57-695, ASTIA Document No. 151165, Determination of the Mechanical Properties of a High-Purity Lead and a 0.058% Copper-Lead Alloy (Reference 2.11.10), April 1958, by Thomas Tietz, Stanford Research Institute, pp. 14, 21 and 26.

2.4 General Standards for All Packages

This section demonstrates that the general standards for all packages are met.

2.4.1 Minimum Package Size

The NuPac 10/140MB package does not have any overall dimension less than 4 inches.

2.4.2 Tamper-proof Feature

The NuPac 10/140MB cask will be sealed with an approved tamper indicating seal and suitable locks to prevent inadvertent and undetected opening.

2.4.3. Positive Closure

As described in Section 1.2.1, the positive closure system consists of a primary top (and, optionally, bottom) lid, secured by eight 2-1/2 inch diameter bolts, and a secondary lid affixed with sixteen 1-1/4 inch diameter bolts.

2.4.4. Chemical and Galvanic Reactions

The materials from which this package is fabricated (carbon, alloy and stainless steel, lead and polyurethane foam) will not cause significant chemical, galvanic, or other reaction in air, nitrogen, or water atmosphere. The technical basis for this fact is that all metallic materials of construction are essentially of equal potential in the Galvanic Series of Metals and Alloys.

2.5 Lifting and Tie-Down Standards for All Packages

All 10/140MB lifting and tie-down devices have been evaluated under their anticipated operational conditions. A summary of resulting critical component stresses is presented in Figure 2.5-1 and Table 2.5-1.

2.5.1. Lifting Devices

There are three lifting lugs for the lid assembly (primary and secondary lids), and there is a single lifting lug for the secondary lid. These lugs are fabricated from ASTM A-240 Type 304 stainless steel. All lifting lugs are evaluated per the requirements of 10 CFR 71, Section 71.45(a).

2.5.1.1. Primary Lid Lifting Lugs

The three primary lid lifting lugs will be utilized in handling both the entire cask as well as the primary lid assembly. For this reason, the following analysis will consider loads due to the maximum loaded cask weight. The net weight of the cask is 53,000 lb., and the maximum payload weight is 15,000 lb., for a combined gross weight of 68,000 lbs. 10 CFR 71 Para. 45(a) states that lifting attachments must be designed with a minimum safety factor of three against yielding. For three lifting lugs and a minimum lifting cable angle of 60° from the horizontal, the load per lug is:

$$P_L = (68{,}000 \text{ lbs}/\sin 60^\circ)(3)/(3 \text{ lugs})$$

$$P_L = 78{,}520 \text{ lbs/lug}$$

Using the conventional 40° shear-out equation, the yield capacity is:

$$P_s = F_{sy} 2t \, (e_d - d/2 \cos 40^\circ)$$

Where: $F_{sy} = (.6)(28{,}400 \text{ psi})$

$= 17{,}040$ psi

FIGURE 2.5-1

Lifting and Tie-Down Devices

Component Maximum Loads and Stresses

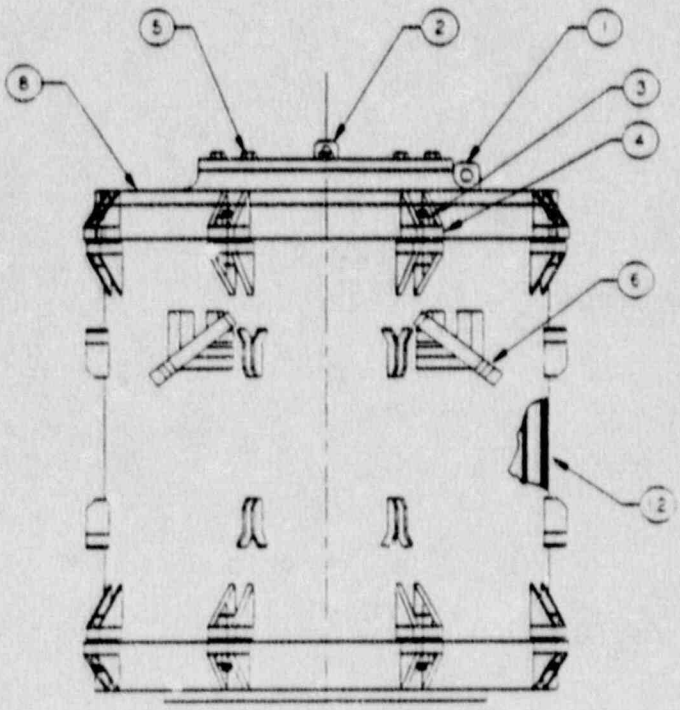

BOTTOM-LOADING VERSION

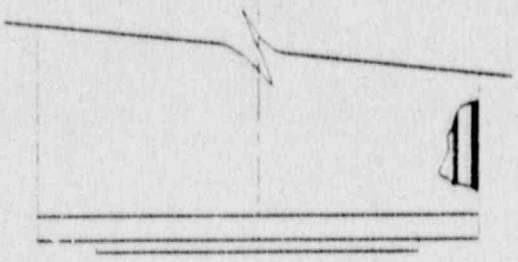

FIXED-BOTTOM VERSION

TABLE 2.5-1

10/140NB Component Stresses

Maximum Loads and Stresses for Lifting and Tie-Down

Component Ref. No.	Component Description	Location Within Component	Loading Condition	Load Combination	Type of Stress	Resultant Component Stress Intensity or Load	Acceptance Criteria	Allowable Value of Stress/Load	Margin of Safety	SAR Reference Location
1	Primary Lid Lifting Lug	Lug Eye	Lifting (Load Factor of 3)	Shear-Out	Shear	78520 lb.	S_y	84106 lb.	+0.07	2.5.1.1
2	Secondary Lid Lifting Lug	Lug Eye	Lifting (Load Factor of 3)	Shear-Out	Shear	5100 lb.	S_y	31540 lb.	+ 0	2.5.1.2
3	Primary Lid Bolts	Shank	Lifting (Load Factor of 3)	Tension	Membrane	25500 lb.	S_y	412000 lb.	+Large	2.5.1.1
4	Primary Lid Bolt Lugs	Cask Lug Weld	Lifting (Load Factor of 3)	Bending and Shear	Membrane +Bending	3877 psi	S_y	36900 psi	+8.52	2.5.1.1
5	Secondary Lid Bolts	Shank	Lifting (Load Factor of 3)	Tension	Membrane	5100 lb.	S_y	1596912 lb.	+Large	2.5.1.2
6	Cask Tiedown Lug	Lug Eye	Tie-Down (Transportation Loads)	Bearing	Bearing	545850 lb.	S_y	558225 lb.	+0.02	2.5.1.3
8	Top Lid Assembly	Inside Diameter	Lifting (Load Factor of 3)	Bending	Membrane +Bending	10875 psi	S_y	28400 psi	+1.61	2.5.1.1
12	Outer Shell	Adjacent to Tail Pad of Tie-Down Lug	Tie-Down (Transportation Loads)	Bending and Shear	Membrane	36276 psi	S_y	37288 psi	+0.03	2.5.1.3

Where 28,400 psi is the yield stress of the stainless steel lug material at the maximum anticipated normal operating temperature of 133°F (Refer to Table 2.3-1).

$t = 2.0$ in.
$d = 2.00$ in.
$e_d = 2.00$ in.

$$P_s = (17,040)(2)(2.0 \text{ in.})[2.00 - (2.00 \text{ in.}/2) \cos 40^\circ]$$
$$P_s = 84,106 \text{ lbs}$$

The yield Margin of Safety, using the maximum lug load, is:

$$M.S. = P_s/P_L - 1 = (84,106)/(78,520) - 1$$
$$M.S. = + 0.07$$

Because of the unconventional geometry of the lifting lug welds, as well as loading situations involving both tensile and bending loads, a detailed weld analysis will be undertaken. The basis for the analysis method derives from Shigley, Mechanical Engineering Design (Reference 2.11.9), pp. 421-423. Weldment details are shown below:

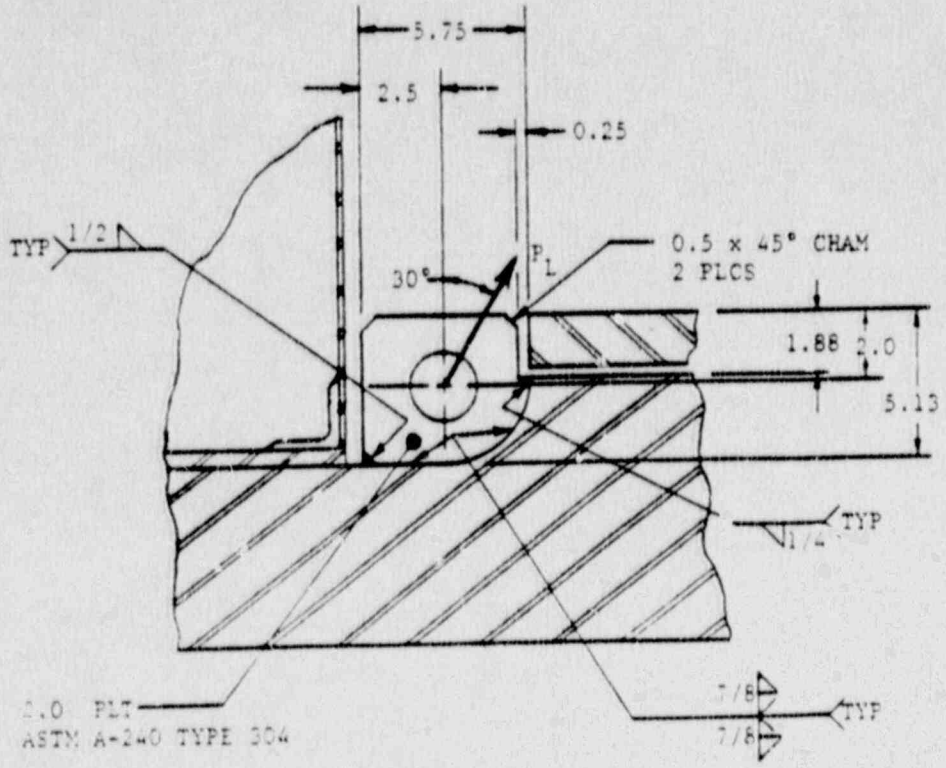

Since the weldment consists of a double weld comprised of two identical 7/8-inch beveled fillet welds, only one weld will be analyzed, using on-half the maximum lifting lug load. The 1/2-inch and 1/4-inch fillet welds along the edges of the lug will be conservatively ignored. The weld and load patterns are illustrated below:

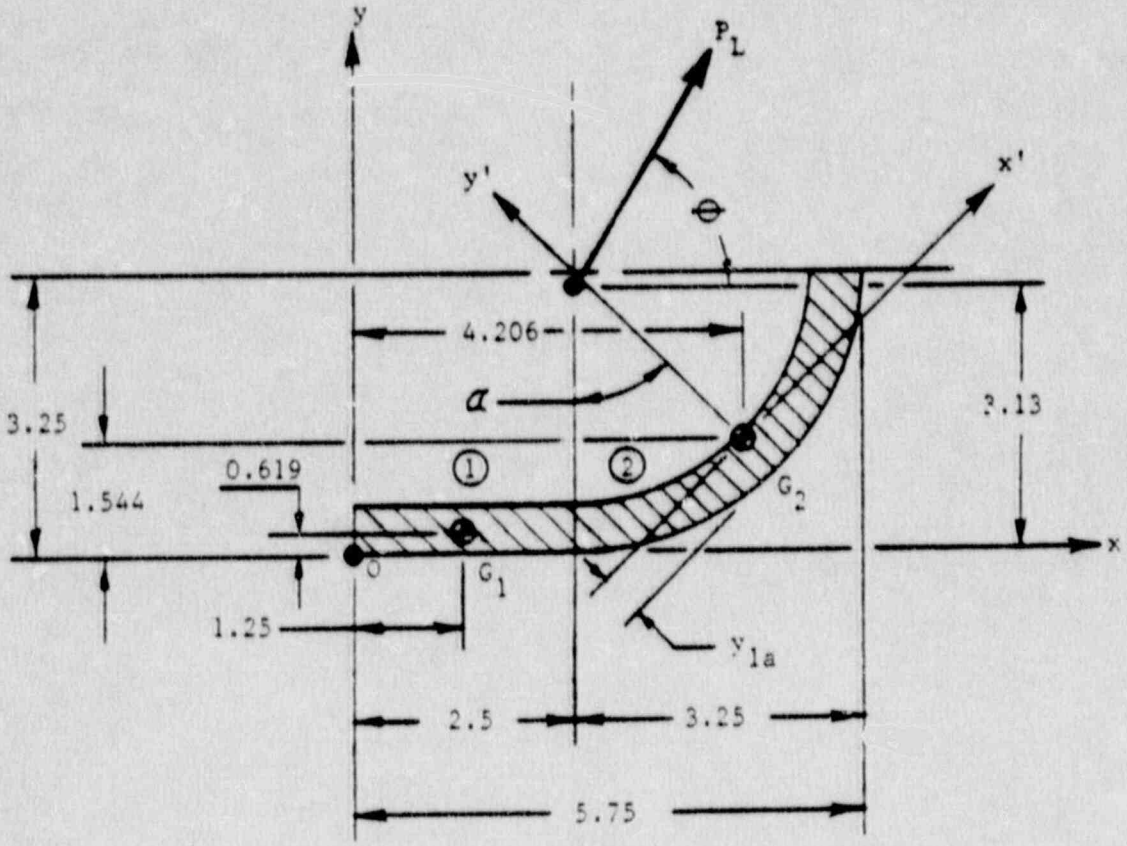

P_L = 78,520/2 = 39,260 lb.

θ = 60° = $\pi/3$ radians (minimum)

c = 45° = $\pi/4$ radians

For the 2.5 inch long straight section of weld, moments of inertia about the x-y coordinate axes may be defined as:

$$I_x = b_1 d_1^{\ 3}/12$$

Where d_1 = weld throat length = 0.875 in/sin 45°
= 1.237 in.

B_1 = weld length = 2.5 in.

$I_x = 0.395 \text{ in}^4$
$I_y = d_1 b_1{}^3/12 = 1.611 \text{ in}^4$

Weld torsional moment is:

$$J_{G1} = I_x + I_y = 2.006 \text{ in}^2$$

and weld shear area is:

$$A_1 = d_1 b_1 = 3.094 \text{ in}^2$$

For section properties of the curved, quarter-circle area of the weld, refer to Roark, Formulas for Stress and Strain, 5th Ed. (Reference 2.11.11), Table 1, Case 19. Moments of inertia about the x' - y' coordinate axes are as follows:

$$I_{x'} = R^3 d_2 [(1 - 3d_2/2R + d_2^2/R^2 - d_2^3/4R^3)(\alpha + \sin\alpha \cos\alpha - 2 \sin^2\alpha/\alpha) + (d_2^2 \sin^2 \alpha)(1 - d_2/R + d_2^2/6R^2)/3R^2 \alpha(2 - d_2/R)]$$

where: R = 3.25 in.
$d_2 = d_1 = 1.237$ in.

$I_{x'} = 0.809 \text{ in.}^4$
$I_{y'} = R^3 d_2 (1 - 3d_2/2R + d_2^2/R^2 - d_2^3/4R^3)(\alpha - \sin\alpha \cos\alpha)$
$= 6.790 \text{ in.}^4$

$$J_{G2} = I_{x'} + I_{y'} = 7.598 \text{ in.}^4$$

$$A_2 = \alpha d_2 (2R - d_2) = 5.115 \text{ in.}^2$$

$y_{1a} = R[1 - (2 \sin\alpha)(1 - d_2/R + 1/(2 - d_2/R))/3\alpha]$
$= 0.837$ in.

The center of gravity of the weld group is defined as:

$$\bar{x} = \sum x_n A_n / \sum A_n$$

$$= [(1.25)(3.094) + (4.206)(5.115)/(3.094 + 5.115)]$$
$$= 3.092 \text{ in.}$$

$$\bar{y} = \sum y_n A_n / \sum A_n$$

$$= [(1.237/2)(3.094) + (1.544)(5.115)/(3.094 + 5.115)]$$
$$= 1.195 \text{ in.}$$

Distances from the weld group center of gravity to individual weld component centers of gravity are:

$$r_1 = [(3.092 - 2.5/2)^2 + (1.195 - 0.619)^2]^{1/2} = 1.930 \text{ in.}$$

$$r_2 = [(3.092 - 4.206)^2 + (1.195 - 1.544)^2]^{1/2} = 1.167 \text{ in.}$$

Weld group torsional moment of inertia is:

$$J = (J_{G1} + A_1 r_1^2) + (J_{G2} + A_2 r_2^2)$$
$$= 28.098 \text{ in.}^4$$

The moment arm of load P_L with respect to the weld group center of gravity may be found by defining the line describing the load path, and then defining another line perpendicular to the first and intersecting the weld group c.g. The equation of the line defining the load path may be expressed as:

$$y - 3.13 = m(x - 2.50)$$

Where: m = slope of the line = $\tan 60^\circ = 1.732$

The equation of the line defining the moment arm can be written as:

$$y - 1.195 = (-1/m)(x - 3.092)$$

Solving these equations for the intersection point (x,y) yields x = 1.810 and y = 1.935, from which the moment arm length may be derived:

$$L = [(3.092 - 1.810)^2 + (1.195 - 1.935)^2]^{1/2}$$
$$= 1.480 \text{ in.}$$

The critical stress point on the weld will be point 'o', whose distance from the weld group c.g. is:

$$r = [(3.092)^2 + (1.195)^2]^{1/2}$$
$$= 3.315 \text{ in.}$$

The total weld shear stress is:

$$\tau = V/A + Mr/J$$
$$= P_L/(A_1 + A_2) + P_L\, Lr/J$$
$$= 11,638 \text{ psi}$$

Conservatively using base metal material properties (304 stainless steel plate) at a maximum normal operating temperature of 133°F, the maximum shear stress allowable is $(0.6)S_y = (0.6)(28,400 \text{ psi}) = 17,040$ psi. The margin of safety is thus:

$$M.S. = 17,040/11,638 - 1 = +0.46$$

It can therefore be concluded that the primary lid lifting lugs are adequate to resist a load equal to three times the maximum weight of the fully loaded cask.

To evaluate the effect of lifting lug loads on the primary containment system, consider stress levels in the primary lid and closure bolts. To conservatively analyze the lid structure, assume a flat circular plate of 5.25 in. constant thickness. Ignoring inner and outer edge 'lips', outside diameter is 65.75 in. and inner diameter is 33.25 in. Also assume lug load is uniformly distributed around the inner edge, and is:

$$w = P_v/\pi D_i$$

Where

P_v = Vertical Component of Lifting Lug Load
= (3)(68,000) = 204,000 lb.

$w = 204,000/\pi(33.25) = 1,953$ lb./in.

From Roark and Young, Formulas for Stress and Strain, 5th ed. (Reference 2.11.11), Table 24, case 1a, maximum bending moment is:

$$M_{max} = M_{tb}$$

Where:

$M_{tb} = K_{Mtb} wa$

a = Outside Radius = 65.75/2 = 32.88 in.

b = Inside Radius = 33.25/2 = 16.63 in.

$b/a = 16.63/32.88 = 0.506$

Therefore:

$$K_{Mtb} = 0.778$$

and:

$$M_{tb} = (0.778)(1,953)(32.88) = 49,957 \text{ in.-lb./in.}$$

Maximum bending stress thus becomes:

$$S_{max} = 6M_{tb}/t^2$$

Where:

t = Plate Thickness = 5.25 in.

S_{max} = (6)(49,957)/(5.25)^2 = 10,875 psi

Note that the horizontal component of the lifting load will tend to induce a bending moment of opposite sign as that resulting from the vertical component. This will act to reduce maximum bending stress. Therefore, the above stress value is the maximum possible bending stress that could result from the regulatory lifting requirements.

Maximum anticipated lid temperature at the inner edge (point of maximum stress) for normal conditions of transport will be 133°F (refer to Section 3.0, Thermal Evaluation for details). Interpolating Table 2.3-1 for the minimum strength lid material (ASTM A-182 Type F304 or A-351 Type CF8/304) at this temperature results in a minimum material yield strength of 28,400 psi. The Margin of Safety for 1/3 yield then becomes:

M.S. = 28,400/10,875 - 1 = + 1.61

The maximum primary lid bolt load that can be anticipated from lifting lug loads is:

P_B = (3)(68,000)/8 = 25,500 lb./bolt

Tensile yield strength of the bolting material at 133°F is given in Section 2.3 as 103,300 psi, and the bolt tensile stress area is 4.0 in.^{2}. The bolt yield load is then (103,000)(4.0) = 412,000 lb, and the Margin of Safety is thus:

M.S. = 412,000/25,500 - 1 = + Large

To evalute the strength of the primary lid bolt attachment lug welds, a simple beam bending analysis will be performed. Since the lug welds are all full penetration welds, the weld section will be treated as an area equivalent to the lug plate thicknesses, loaded in bending and shear. The lug geometry, as shown in the drawings of Section 1.3, is reproduced below:

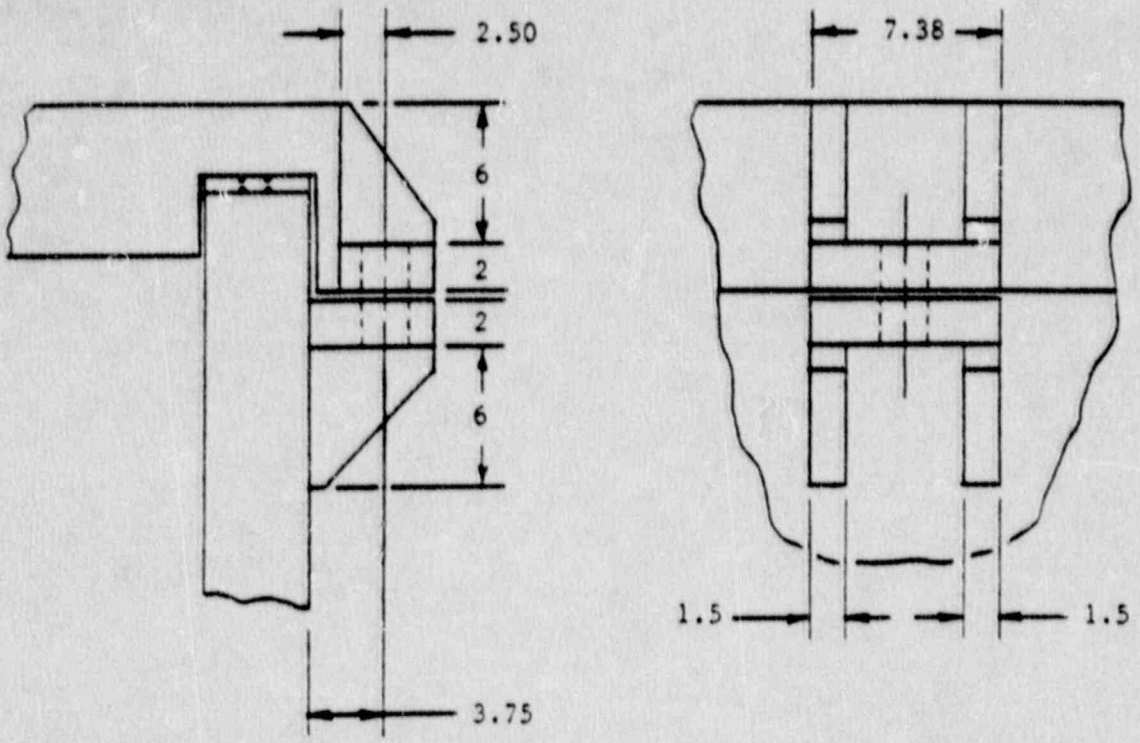

The weld areas of the upper and lower lugs are identical. The load offset on the lower lug is greater than on the upper, resulting in a greater bending moment. However, the minimum yield stress at normal transport temperatures (133°F maximum) for the lower lug (A-516) is 36,900 psi (See Table 2.3-1). This is greater than the yield stress of the 304 stainless steel lid components, which is 28,400 psi at the same temperature. Therefore, both lugs will be evaluated under the imposed lifting load of 25,500 lb/lug (same as the bolt load). The weld pattern is shown below. The loading configuration is the same for both lugs.

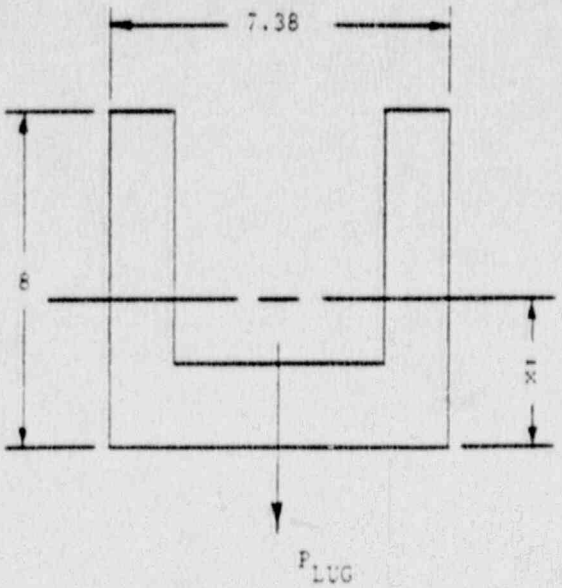

The distance to the centroid of the weld pattern is:

$$\bar{x} = [(1.0)(2.0)(7.38) + 2\ (5.0)(1.5)(6.0)/[(2.0)(7.38) + 2\ (1.5)(6.0)]$$

$$= 3.20 \text{ in.}$$

The moment of inertia of the section is:

$$I_x = (7.38)(2.0)^3/12 + (3.20 - 1.0)^2\ (7.38)(2.0) + 2(1.5)(6.0)^3/12 + 2(5.0 - 3.20)^2\ (1.5)(6.0)$$

$$= 188.68 \text{ in}^4$$

Bending stress for the upper (lid) lug is:

$$\sigma_B = Mc/I_x$$

$$= (25,500)(2.50)(8.0 - 3.20)/188.68$$

$$= 1,622 \text{ psi}$$

Bending stress for the lower (cask) lug is:

$$\sigma_B = (25,500)(3.75)(4.80)/188.68$$

$$= 2,433 \text{ psi}$$

Shear stress for both lugs is:

$$\tau = (25,500)/[(2.0)(7.38) + 2(1.5)(6.0)]$$

$$= 778 \text{ psi}$$

Maximum combined stress for the lug weld is then:

$$\sigma_C = \sigma_B + [(\sigma_B/2)^2 + (\tau)^2]^{1/2}$$

For the upper lug:

$$\sigma_C = 2,746 \text{ psi}$$

For the lower lug:

$$\sigma_C = 3,877 \text{ psi}$$

The margin of safety on one-third of yield stress is, for the upper lug:

$$\text{M.S.} = 28,400/2,746 - 1 = +9.34$$

For the lower lug:

$$\text{M.S.} = 36,900/3,877 - 1 = +8.52$$

The critically loaded lug is thus the lower lug, with the smaller margin of safety, though both lugs are more than adequate to carry the cask lifting load.

All the margins of safety for all components are larger than the 0.07 margin for the tear out of the eye of the lug. This indicates that excessive loading would not affect the containment integrity of the cask, since lug failure would occur before failure of any critical component could take place.

Thus, lifting forces will not significantly affect the containment capability of the cask.

2.5.1.2. Secondary Lid Lifting Lug

The secondary lid weight will be approximately 1,700 lbs. The total lug load is then:

$$P_L = (1,700 \text{ lbs})(3)$$

$$P_L = 5,100 \text{ lbs}$$

Using the conventional 40° shear-out equation, the yield capacity is:

$$P_s = F_{sy} 2t \, (e_d - d/2 \cos 40^\circ)$$

Where: $F_{sy} = 17,040$ psi (shear yield at 133°F)
$t = 1.0$ in.
$d = 1.5$ in.
$E_d = 1.5$ in.

$$P_s = (17,040)(2)(1.0)[1.5 - (1.5/2) \cos 40^\circ]$$
$$P_s = 31,540 \text{ lbs}$$

The yield Margin of Safety, using the maximum lug load, is:

$$M.S. = P_s/P_L - 1 = (31,540)/(5,100)$$
$$M.S. = + 5.18$$

The yield capacity of the lug-to-lid weld may be estimated as:

$$P_s = F_{sy} t_w$$

Where: $F_{sy} = 17,040$ psi
$A_w = L_w t_w$
$L_w = 2(4.0 \text{ in.} + 1.0 \text{ in.}) = 10.0 \text{ in.}$
$t_w = (0.707)(.50 \text{ in.}) = 0.35 \text{ in.}$
$A_w = (10.0)(.35) = 3.5 \text{ in.}^2$

Then: $P_s = (17,040)(3.5) = 59,640$ lbs.

The lug-to-lid weld Margin of Safety is:

$$M.S. = P_s/P_L - 1 = (59,640)/(5,100) - 1$$
$$M.S. = + \text{Large}$$

The secondary lid is held on by the use of sixteen 1-1/4 inch ASTM A-320 L43 bolts.

They have a yield load of:

$$P_y = (0.969)(103,000) = 99,800 \text{ lbs/bolt}$$

or

$$P_{y\text{-total}} = (16)(99,800)$$
$$= 1,596,800 \text{ lbs}$$

This gives a yield margin of safety of:

$$M.S. = P_{y\text{-total}}/P_L - 1 = 1,596,800/5,100 - 1 = + \text{Large}$$

Therefore, by comparing the margins of safety it can be concluded that the secondary lid lift eye will fail prior to any of the containment boundary components.

It can therefore be concluded that the secondary lid lifting lug is more than adequate to resist a load equal to three times its normal maximum load. Since the secondary lid lifting lug is not designed to react the full package load, it will be covered during transit.

2.5.2. Tie-down Devices

Four tie-down lugs are provided to resist transportation induced loads. From 10 CFR 71, Para. 71.45(b)(1), the required load factors are:

A_x = 10g (longitudinal)
A_y = 5g (lateral)
A_z = 2g (vertical)

The four tie-down lugs are located with their lug-eyes at 90° intervals around the package side wall. The lugs are positioned at an angle of 38° with respect to the horizontal, with their end tips at the same approximate elevation as the lower surface of the upper impact limiter. To evenly distribute the tie-down cable load from the lug into the cask outer shell, two pairs of gussets were added to the lug, as shown in Figure 2.5.2-1. The general tie-down arrangement for the NuPac 10/140MB Cask is shown in Figure 2.5.2-2.

From the geometry given in Figure 2.5.2-2, the cable tension due to horizontal accelerations can be determined by summing moments about the bottom corner of the package opposite the reacting cables. Conservatively ignoring the weight of the cask itself, the longitudinal acceleration case can be derived as follows:

$$(A_x c)W = 2\ (P_v d' + P_h h)$$

Where: W = Maximum package weight
P_v = Vertical (z - Direction) cable force component
P_h = Horizontal (x - Direction) cable force component
c, d', h are defined in Figure 2.5.2-1

But,

$$(A_x c)W = 2P_C(B_z d' + B_x h)$$

Where: B_x = Cable Direction Cosine with Respect to the X-axis
= x/Cable Length L
B_z = z/L
$L = (x^2 + y^2 + z^2)^{1/2}$

FIGURE 2.5.2-1
Tie-Down Lug Geometry

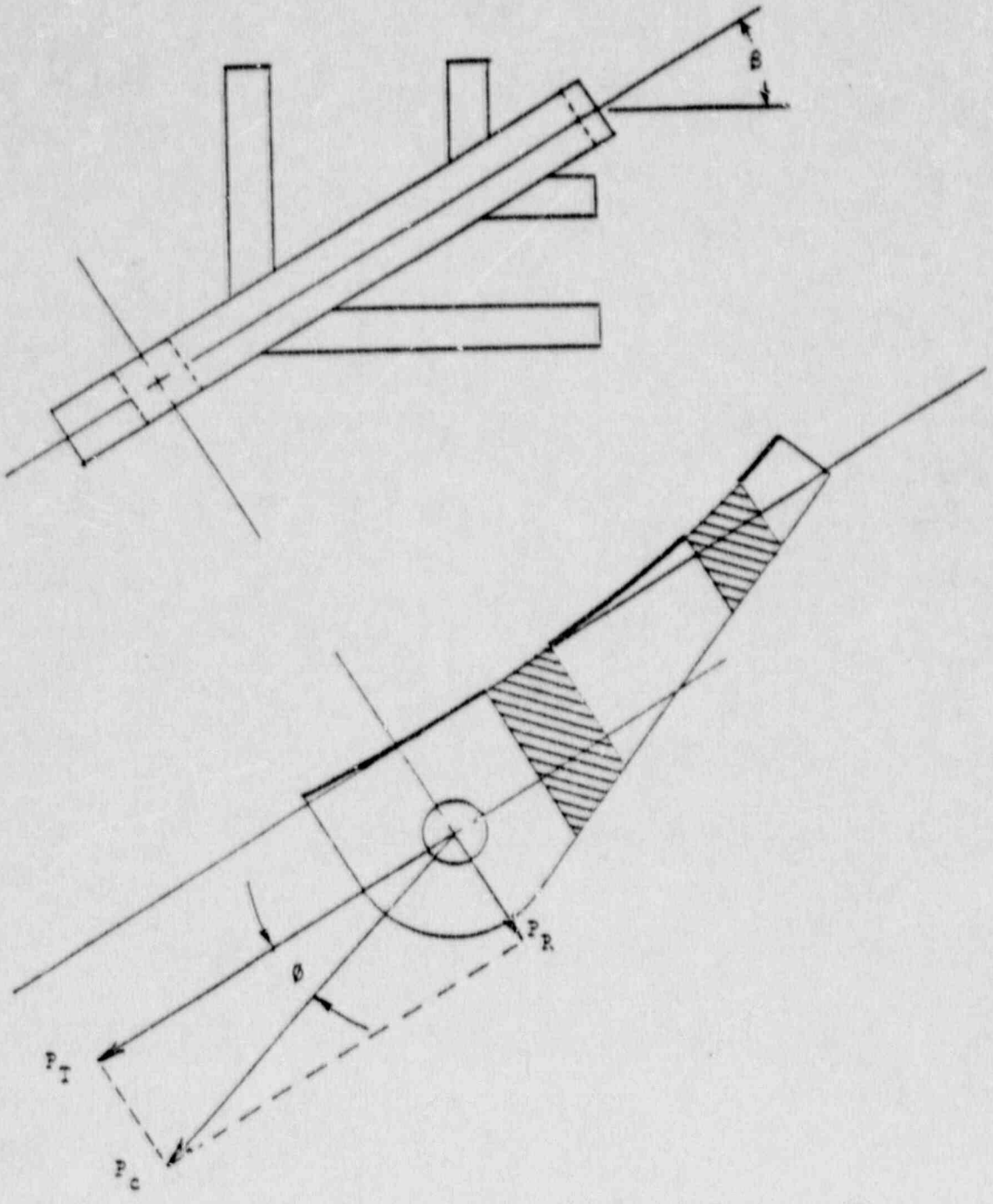

FIGURE 2.5.2-2

Tie-Down Cable Arrangement

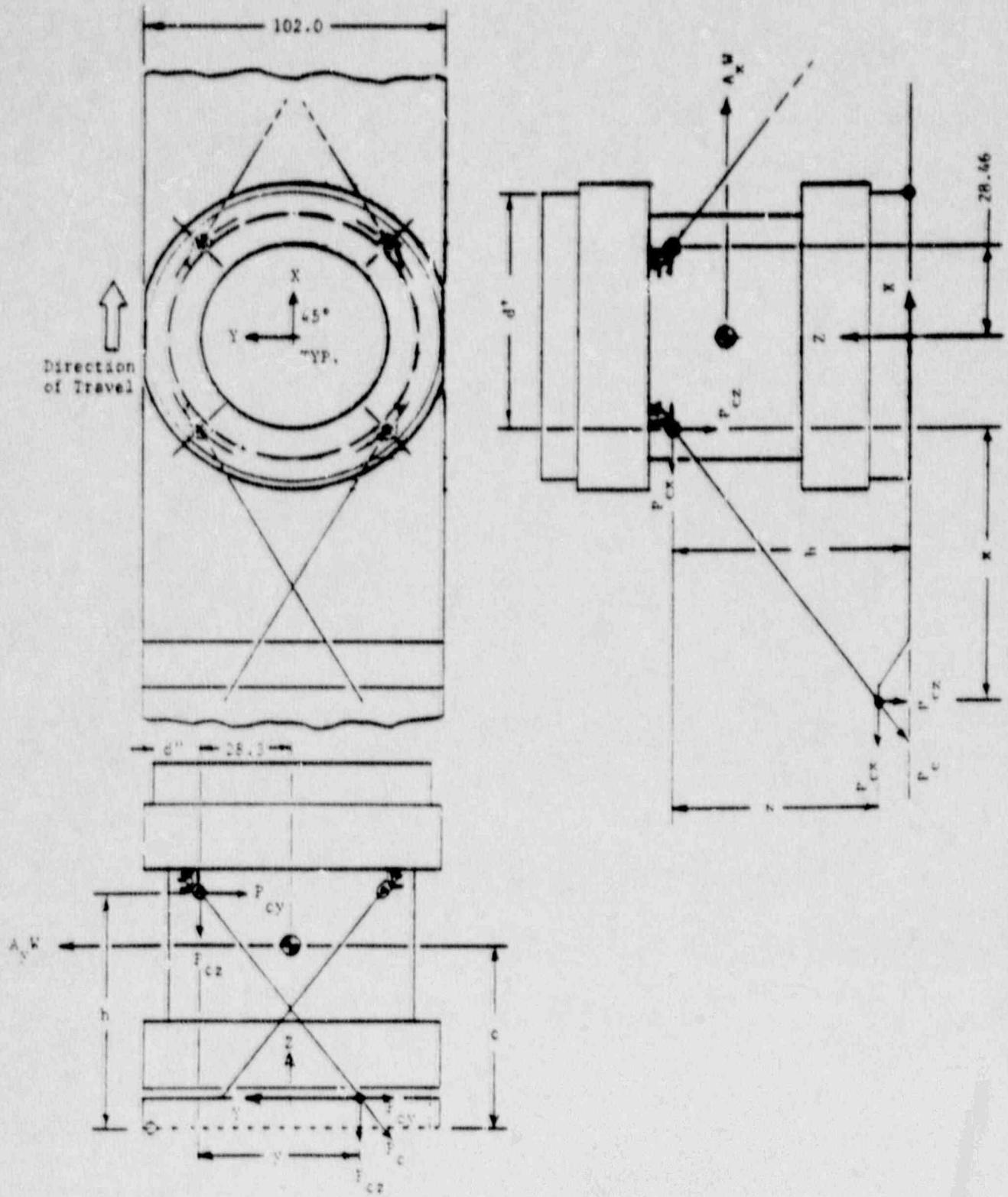

Solving for P_C:

$$P_{C_{long}} = (W/2)[(A_x c)/(B_z d' + B_x h)]$$

Similarly, the cable tension due to the lateral acceleration is:

$$P_{C_{lat}} = (W/2)[(A_y c)/(B_z d'' + B_y h)]$$

Where: $B_y = y/L$

The cable tension due to the vertical acceleration is simply:

$$4P_v = A_z W = 4B_z P_C$$

Solving for P_C:

$$P_{C_{vert}} = A_z W/4B_z$$

These three loads will coincide for the most severely loaded cable:

$$P_C = (W/2)[A_x c/(B_z d' + B_x h) + A_y c/(B_z d'' + B_y h) + A_z/2B_z]$$

Where, for the NuPac 10/140MB Cask:

W = Cask Gross Weight = 68,000 lb.
c = 61.17 in.
d' = 78.96 in.
d'' = 19.54 in.
h = 71.50 in.

To obtain the tie-down loads, the direction cosines of the tie-down cable must be defined. Since the cable will always lie in the plane of the tie-down lug, whose angle β is constant, the cable direction cosines will be entirely dependent on the cable angle ϕ. Cable angle is defined as the true angle which the tie-down cable makes with respect to the tangent line of the tie-down lug (refer to Figure 2.5.2-1).

Cable direction cosines can be determined as a function of lug angle β and cable angle ϕ in the following manner:

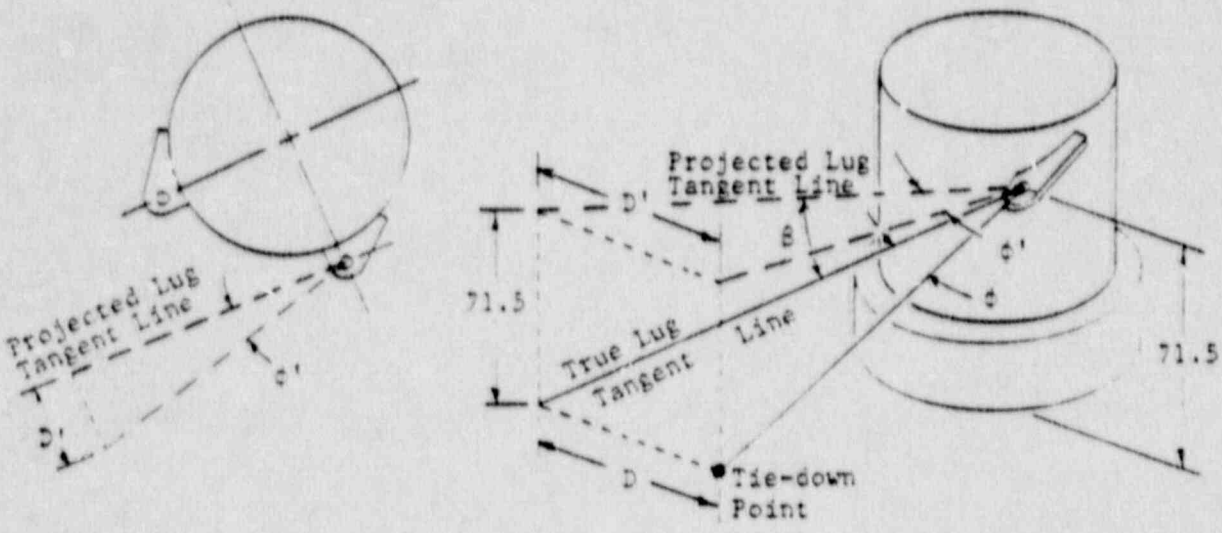

True Lug Tangent Line Length $T = h/\sin \beta$

True Deviation Distance D = Projected Deviation Distance $D' = T \tan \phi$

Projected Lug Tangent Line Length $T' = h/\tan \beta$

To allow some flexibility in the tie-down arrangement, two cable angles were investigated. One angle, 18°, corresponds to the angle at which the line of action of the cable describes a tangent with the centroid of the cask outer wall. This is considered to be the optimum configuration for obtaining the most uniform load distribution from the tie-down lug into the cask outer wall. Thus, tie-down location is:

True Lug Tangent Line Length T = 71.5/sin 38° = 116.1 in.

Deviation Distance D = (116.1)(tan 18°) = 37.7 in.

Projected Lug Tangent Line Length T' = 71.5/tan 38° = 91.5 in.

These dimensions were used to locate the trailer tie-down point, shown in Appendix 2.10.3. The coordinates of this location were then utilized in calculating direction cosines, as defined above (refer to Figure 2.5.2-2), with which the corresponding maximum tie-down load could be determined. This load, calculated in Appendix 2.10.3, was found to be 545,850 lb.

In order to obtain greater lateral support for the cask in its tied down position (refer to Figure 2.5.2-2), a smaller cable angle, 14°, was also selected for evaluation. In an analysis similar to that above and detailed in Appendix 2.10.3, the tie-down cable load for this angle was found to be 525,211 lb.

To ensure that lug and cask outer shell stresses did not exceed the regulatory limitation (material yield strength) under these tie-down loads, a detailed computer analysis was undertaken. This analysis was performed utilizing the finite element program ANSYS, Revision 4.1c, available on the Boeing Computer Services (BCS) National Network, MAINSTREAM - EKS. The capabilities of ANSYS are outlined in Appendix 2.10.2 and details of the analysis are given in Appendix 2.10.3.

From the above tie-down loads analysis, it is apparent that cable direction cosines, and thus loads, will change with varying cable angle. Since the finite element analysis is based entirely on elastic material properties, element stresses can be varied in direct proportion to the changing cable load. For analysis purposes, a 500,000 lb. cable load was applied to the lug eye. Adjusted stress levels for the varying cable loads are calculated in Appendix 2.10.3 and summarized in Table 2.5.2-1. Resulting stress Margins of Safety are also given in Table 2.5.2-1.

Each tie-down lug is made of 2.5 inch thick ASTM A-517 steel plate welded to the cask outer skin. The lug is designed and positioned so that the tie-down cable lies in the plane of lug, and there are no twisting moments induced in the lug. The finite element analysis results for the lug are outlined in Appendix 2.10.3 and summarized in Table 2.5.2-1.

To check lug shear yield capacity, the conventional 40° shear-out equation was utilized:

$$P_{sy} = F_{sy} 2t[e_d - (d/2)\cos 40^\circ]$$

Where: $F_{sy} = (.6)(99,240 \text{ psi}) = 59,546 \text{ psi}$

Where 99,240 psi is the yield strength of the tiedown lug material at the normal operating temperature of 114°F (refer to Table 2.3-1)

$t = 2.5$ in.
$e_d = 3.0$ in.
$d = 2.25$ in.

Then: $P_{sy} = (59,546)(2)(2.5)[(3.0) - (2.25/2)\cos 40^\circ]$

$= 636,610$ lb.

TABLE 2.5.2.-1

Tie-Down Lug Analysis Stress Levels and Margins of Safety

Structural Component	Tie-Down Cable Angle	
	18°	14°
Maximum Outer Skin Stress	36,276 psi	34,533 psi
Margin of Safety	+0.03	+0.08
Maximum Tie-Down Lug Stress	89,777 psi	81,398 psi
Margin of Safety	+0.11	+0.22
Maximum Tie-Down Lug Weld Shear Stress	17,125 psi	17,370 psi
Margin of Safety	+0.31	+0.29

Shear yield margin of safety is:

M.S. = (636,610/545,850) - 1 = +0.17

For shackle pin bearing stress, assume cable load is evenly distributed around one-half of the lug-eye diameter. The maximum cable load then becomes:

F_b = (99,240 psi)(2.25 in)(2.50 in)
= 558,225 lb.

Then: M.S. = (558,225/545,850) - 1 = +0.02

The cable load consists of both radial and tangential (to the cask wall) components, introducing both a bending moment and a shear load into the outer shell through the lug-to-shell weld. The weld stresses in the lug-to-shell weld are thus composed of pure shear and tension/compression due to the moments (refer to Figure 2.5.2-1).

With the tie-down cable acting in the plane of the lug, and assuming weld load components parallel to the lug tangent line, the lug weld stress components can be determined. Results are given in Appendix 2.10.3 and summarized in Table 2.5.2-1.

To ensure that excessive cable loads will not result in damage to the cask, the lug ultimate shear-out capacity was evaluated:

$$P_{su} = 2F_{su}t[e_d - (d/2)\cos 40^\circ]$$

Where: F_{su} = Maximum Shear Strength of Lug Material
= (.6)(115,000) = 69,000 psi

P_{su} = (2)(69,000)(2.5)[3.0 - (2.25/2)cos 40°]
= 737,680 lb.

Likewise, ultimate strength of the lug welds was checked for the two extreme cable angles, as shown in Appendix 2.10.3. The results indicated that the controlling failure load would be lug shear-out at 737,680 lb. Applying this load at the maximum cable angle of 18° (worst case load condition) and directly ratioing maximum stress obtained from the finite element analysis yields a cask outer shell stress of:

$$P_{shell} = (737,680/500,000)(33,229) = 49,025 \text{ psi}$$

Specified minimum ultimate strength of the A-516 Gr. 70 material comprising the cask outer shell is 70,000 psi at 114°F. Failure margin of safety for the cask is thus:

$$M.S. = 70,000/49,025 - 1 = +0.43$$

It can therefore be concluded that the tie-down lug is more than adequate to resist the loads specified in 10 CFR 71 Para. 45(b)(1), and yet not compromise the structural integrity of the cask under more extreme loading conditions.

2.6 Normal Conditions of Transport

The NuPac 10/140MB cask has been designed and the contents are so limited (as described in Section 1.2.3 above) that the performance requirements specified in 10 CFR 71.71 will be met when the package is subjected to the Normal Conditions of Transport specified therein. The ability of the NuPac 10/140MB to satisfactorily withstand the Normal Conditions of Transport has been assessed as described on the following pages. A summary of maximum stresses in the major cask components arising from Normal Conditions of Transport is presented in Figure 2.6-1 and Table 2.6-1.

2.6.1 Heat

A detailed thermal analysis can be found in Section 3.4 wherein the package was exposed to a combination of solar heating, 95 watts internal decay heat and 100°F ambient air. The steady state analysis conservatively assumed a 24-hour day as maximum solar heat load. The maximum steady state temperature in any cask component was found to be 174°F. This temperature will have no detrimental effect on the package.

2.6.2 Cold

For the cold condition, a -40°F steady state ambient temperature is assumed as is no internal heat generation. This will result in a uniform temperature throughout the cask of -40°F. The materials of construction for the cask are not adversely affected by the -40°F condition. In particular, brittle fracture is not a concern, as discussed in Section 2.1.2.2.1.

The only concern identified with the cold condition is with shrinkage of the lead onto the inner shell of the outer cask. As shown by the following calculations, a hoop stress of -2,914 psi and an axial stress of -2,820 psi can develop in the inner shell when cooled to -40°F. This case is independent of other load cases. To check buckling interaction, allowable hoop and axial stresses may be taken from Table 2.1.2-3. Conservatively using allowables for

FIGURE 2.6-1

Cask Components Affected by Normal Conditions of Transport

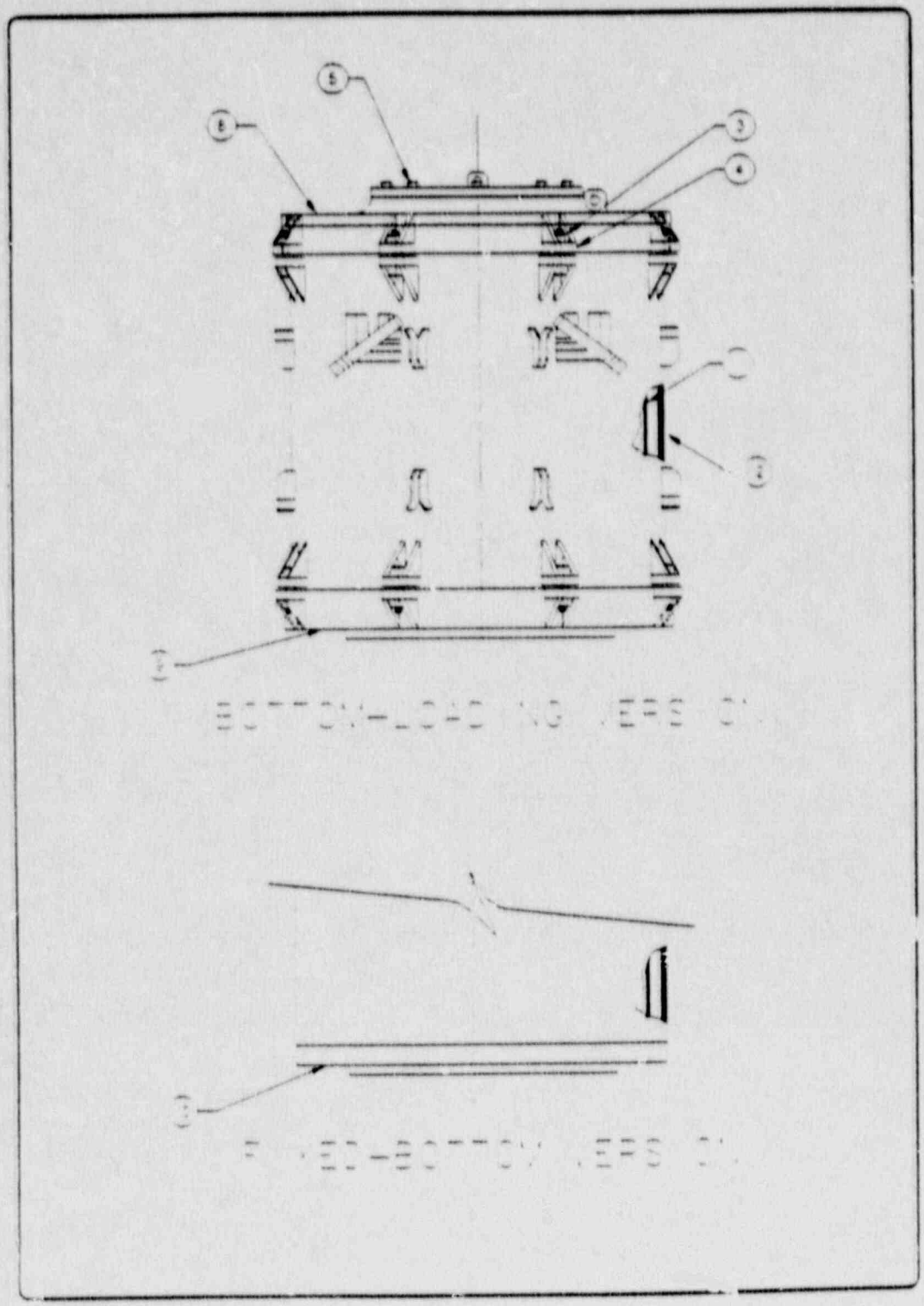

TABLE 2.6-1

Normal Conditions of Transport Maximum Stresses

Component Ref. No.	Component Description	Location Within Component	Loading Condition	Load Combination	Type of Stress	Resultant Stress Component*, Stress Intensity, or Load	Acceptance Criteria	Allowable Value of Stress/Load	Margin of Safety	SAR Reference Location
3	Primary Lid Bolts	Shank	Oblique Drop	Max. Payload +Pressure	Membrane	15732 psi	$2.0S_m$	68720 psi	+3.37	2.6.7.7.5
4	Primary Lid Bolt Lugs	Cask Leg Weld	Oblique Drop	Max. Payload +Pressure	Membrane +Bending	9567 psi	$1.5S_m$	34855 psi	+2.64	2.6.7.2.5
5	Secondary Lid Bolts	Shank	End Drop	Max. Payload +Pressure	Membrane	43487 psi	$2.0S_m$	68720 psi	+0.58	2.6.7.1.5 2.10.7..
8	Top Lid Assembly	Outside Dia.	End Drop	Max. Payload +Pressure	Membrane +Bending	13378 psi	$1.5S_m$	30000 psi	+1.24	2.6.7.1.4 2.10.7.5
9	Bottom Lid	Outside Dia.	End Drop	Max. Payload +Pressure	Membrane	6105 psi	S_m	20000 psi	+2.28	2.6.7.1.4 2.10.7.3
10	Bottom Plate	Center of Plate	End Drop	Max. Payload Load Cling	Membrane +Bending	8281 psi	$1.5S_m$	30000 psi	+2.62	5.7.1.4
11	Inner Shell	Impact End	End Drop	Min. Payload Load Cling	Buckling Interaction	σ_h = 2462 psi σ_a = 9619 psi	**	σ_{ha} = 17905 psi σ_{aa} = 19062 psi	+0.94	2.6.7.1.3(1)
12	Outer Shell	Impact End	End Drop	Min. Payload Load Slump	Bending Buckling	7596 psi	Buckling Allowable	22793 psi	+2.00	2.6.7.1.3(2) 2.10.6.4

* σ_h - loop compressive stress, σ_a - axial compressive stress

** Buckling Interation: $[(\sigma_h/\sigma_{ha}) + (\sigma_a/\sigma_{aa})] \leq 1$

a temperature of -20°F (lower temperature allowable stresses will be higher), a Margin of Safety may be calculated. The allowable stresses are 18,004 psi (hoop) and 19,106 psi (axial). The Margin of Safety against buckling is therefore:

$$M.S. = 1/[(2,914/18,004) + (2,820/19,106)] - 1 = +2.23$$

It can thus be seen that the -40°F minimum temperature requirement will have no adverse effect on the cask.

However, a -20°F case must be considered as a possible initial condition for other load cases per 10 CFR 71.71(b). The hoop stress will be approximately -2,462 psi and the axial stress approximately -2,705 psi at -20°F. These stresses are determined by conservatively neglecting lead creep effects.

Fabrication Stresses Due to Lead Pour:

Assume a uniform steel and lead temperature of 620°F. The static head (pressure) due to a column of lead is simply:

$$p = \rho h$$

Where:

$\rho = 0.386$ lb/in^3 (liquid lead)

$h = 77.5 + 10.0 = 87.5$ in (10.0 inches for overflow pipe)

Then,

$$p = (0.386)(87.5) = 33.78 \text{ psi}$$

The physical properties of ASTM A-240, Type 304, stainless steel used for the cask inner shell are extracted from Section 2.3, are:

Temperature (°F)	E (10^6 psi)	α (10^{-6} in/in/°F)	μ
70	28.3	8.46	0.3
100	28.1	8.55	0.3
200	27.6	8.79	0.3
300	27.0	9.00	0.3
400	26.5	9.19	0.3
500	25.8	9.37	0.3
600	25.3	9.53	0.3
620	25.2	9.56	0.3

The physical properties of ASTM A-516 Grade 70, and, alternatively, A-537 Class 1, carbon steel used for the cask outer shell are:

Temperature (°F)	E (10^6 psi)	α (10^{-6} in/in/°F)	μ
70	29.5	5.42	0.3
100	29.3	5.53	0.3
200	28.8	5.89	0.3
300	28.3	6.26	0.3
400	27.7	6.61	0.3
500	27.3	6.91	0.3
600	26.7	7.17	0.3
620	26.5	7.22	0.3

The physical properties of lead (copperized) are also taken from Section 2.3, as follows:

Temperature (°F)	E (10^6 psi)	α (10^{-6} in/in/°F)	μ
70	2.34	16.07	0.45
100	2.30	16.22	0.45
200	2.17	16.70	0.45
300	2.00	17.33	0.45
400	1.82	18.15	0.45
500	1.61	19.12	0.45
600	1.40	20.17	0.45
620	1.36	20.38	0.45

Where:

E = Young's (Elastic) Modulus

α = coefficient of thermal expansion (mean from 70°F)

μ = Poisson's Ratio

At 70°F, the steel shell geometry is as follows:

Geometry (at 70°F)	Inner Shell (in)	Outer Shell (in)
Inside Diameter, D_i	66.00	72.00
Outside Diameter, D_o	67.50	74.50
Shell Thickness, t	0.75	1.25
Mean Shell Radius, R	33.375	36.625

At 620°F, without load, the shells will grow as follows:

$$R' = R(1 + \alpha\Delta T)$$
$$t' = t(1 + \alpha\Delta T)$$
$$\Delta T = 620 - 70 = 550^\circ F$$
$$\alpha_s = 9.56(10)^{-6} \text{ in/in/}^\circ F \text{ (304 Stainless Steel)}$$
$$\alpha_c = 7.22(10)^{-6} \text{ in/in/}^\circ F \text{ (A-516 or A-537 Carbon Steel)}$$

Then:

$$R_i' = 33.375[1 + 9.56(10)^{-6}(550)] = 33.5505 \text{ in}$$
$$t_i' = 0.75[1 + 9.56(10)^{-6}(550)] = 0.7539 \text{ in}$$
$$R_o' = 36.625[1 + 7.22(10)^{-6}(550)] = 36.7701 \text{ in}$$
$$t_o' = 1.25[1 + 7.22(10)^{-6}(550)] = 1.2550 \text{ in}$$

When filled with molten lead, the inner and outer shells of the outer cask will be subjected to the 33.78 psi pressure head. This will decrease the radius of the inner shell and increase the radius of outer shell. Utilizing Roark, Raymond J., and Young, Warren C., Formulas For Stress and Strain, 5th ed. (Reference 2.11.11), Table 29, Case 1b, the change in radius for each shell is:

$$\Delta R_i' = q(R_i')^2/Et_i'$$
$$= (-33.78)(33.5505)^2/25.2(10^6)(0.7539) \quad -0.0020 \text{ in.}$$
$$\Delta R_o' = q(R_o')^2/E t_o'$$
$$= (33.78)(36.7701)^2/26.5(10)^6(1.2550) = 0.0014 \text{ in.}$$

In summary, the initial condition of the steel shells just before lead solidification at 620°F, $(R' + \Delta R' \pm t'/2)$ is:

Shell	Inner Radius (in)	Outer Radius (in)
Inner	33.1716	33.9255
Outer	36.1440	37.3990

Lead experiences a decrease in volume of approximately 3.85% upon solidification. As the lead solidifies, it will shrink and liquid lead from above will fill in between the solidifying lead and the outer cask inner and outer shells, thus maintaining a 33.78 psi pressure on the shells. Eventually, the full annular region between the shells will be filled with lead, subjected to a loading as illustrated below:

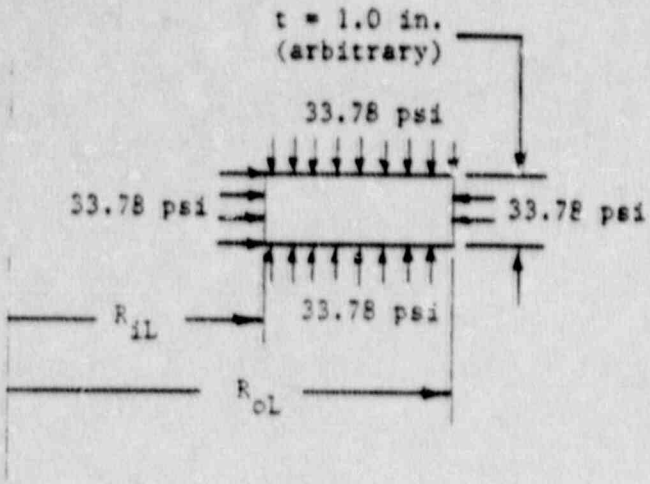

Note: the 33.78 psi pressure actually only exists at the base of the lead column and will linearly decrease toward the top of the column.

Under this loading, R_{i1} = 33.9255 inches and R_{o1} = 36.1440 inches, the outer radius of the inner shell and inner radius of the outer shell, respectively. Geometry of the unloaded lead shell is determined as follows:

$$R_{o1} = a + \Delta a$$
$$R_{i1} = b + \Delta b$$

a = outer radius
b = inner radius

Solve for a and b by superimposing Cases 1b and 1d, Table 32, of the Reference above with q = 33.78 psi:

$$\Delta a = qab^2(2 - \mu)/E(a^2 - b^2) - qa[a^2(1 - 2\mu) + b^2(1 + \mu)]/E(a^2 - b^2)$$
$$= R_{o1} - a$$

$$\Delta b = qb[a^2(1+\mu) + b^2(1-2\mu)]/E(a^2 - b^2) - qba^2(2-\mu)/E(a^2 - b^2)$$
$$= R_{i1} - b$$

Simplifying the two equations yields:

[1] $\Delta a = -qa(1-2\mu)/E$

[2] $\Delta b = -qb(1-2\mu)/E$

For $q(1-2\mu)/E = (33.78)\left[1-2(.45)\right]/1.36(10)^6 = 2.484(10)^{-6}$,

[1] $\left[1-2.484(10)^{-6}\right]a = R_{o1}$

[2] $\left[1-2.484(10)^{-6}\right]b = R_{i1}$

Where:

$E = 1.36(10)^6$ psi

$\mu = 0.45$

$R_{o1} = 36.1440$ in

$R_{i1} = 33.9255$ in

Then, solving for a and b:

$a = 36.14409$ in.

$b = 33.92558$ in.

At this point, the hoop stress in the inner and outer steel shells of the outer cask is:

$$\sigma_i = pR_i/t_i$$
$$= (-33.78)\left[(33.9255 + 33.1716)/2\right]/(33.9255 - 33.1716) = -1,503 \text{ psi}$$

$$\sigma_o = pR_o/t_o$$
$$= (33.78)\left[(37.399 + 36.144)/2\right]/(37.399 - 36.144) = 990 \text{ psi}$$

Again, utilizing Table 32, Cases 1b and 1d, of Reference 2.11.11, the stress in the lead shell, σ_1 = axial, σ_2 = hoop, σ_3 = radial, upon solidification, may be determined as:

$$\sigma_1 = \sigma_2 = \sigma_3 = -33.78 \text{ psi}$$

Determine the temperature at which lead will separate from the outer shell, T_{sep}. Separation initiates when the lead outer radius, R_{o1}, and outer steel shell inner radius, R_{os}, become equal. The unrestrained state of each of the above shells, at 620°F, is:

$$R_{os} = R_o' - t_o'/2 = 36.1426 \text{ in}$$
$$R_{o1} = a = 36.14409 \text{ in}$$

At 70°F, the lead outer radius, R, is such that $R + R\alpha\Delta T = 36.14409$ inches at 620°F. Then, solving for R:

$$R = 36.14409/(1 + \alpha\Delta T)$$
$$= 36.14409/[1 + 20.38(10)^{-6}(550)] = 35.7434 \text{ in}$$

At 70°F, the outer steel shell inner radius is 36.0 inches. At the temperature of separation, T_{sep}, the following relationship is true:

$$35.7434(1 + \alpha_1\Delta T) = 36.0(1 + \alpha_c\Delta T)$$

A solution for T_{sep} is achieved by trial and error. At approximately 600°F:

$$\Delta T = 600 - 70 = 530° \text{ F}$$
$$\alpha_1 = 20.17(10)^{-6} \text{ in/in/°F}$$
$$\alpha_c = 7.17(10)^{-6} \text{ in/in/°F}$$

and:

$$36.1255 < 36.1368$$

At 600°F, lead shell outer radius has decreased to less than the outer shell inner radius, e.g., separation has taken place between 620°F and 600°F.

At 520°F, $\Delta R = R_{os} - R_{ol} = -0.001465$ in.

At 600°F, $\Delta R = R_{os} - R_{ol} = 0.01610$ in.

Linearly interpolating for the temperature at $\Delta R = 0$:

$$(620 - T_{sep})/(620 - 600) = (-0.001465 - 0)/(-0.001465 - 0.01610)$$

Or:

$$T_{sep} = 618.3°F$$

That is, lead separation from the outer shell commences almost immediately when cool-down begins.

At 618.3°F, check press fit of the lead onto the inner steel shell. At 70°F, lead inner radius, R, is such that $R + R\,\alpha\,\Delta T = 33.92558$ inches at 620°F. Then, solving for R:

$$R = 33.92558/(1 + \alpha\Delta T)$$
$$= 33.92558/[1 + 20.38(10)^{-6}(550)] = 33.550 \text{ in}$$

At 70°F, the steel inner shell outer radius is 33.75 inches. At 618.3°F, the interference is calculated as:

$$\delta = -33.550[1 + 20.362(10)^{-6}(548.33)] + 33.75[1 + 9.56(10)^{-6}(548.33)]$$
$$= +0.002829 \text{ in}$$

Utilizing the press fit equation (2-67) from Shigley, Joseph E., Mechanical Engineering Design, 4th Ed. (Reference 2.11.9), for the interface pressure, p, at a temperature of 618.3°F, the interference is:

$$\delta = b_1 p[[(c^2 + b_1^2)/(c^2 - b_1^2)] + \mu_1]/E_1 + b_s p[[(b_s^2 + a^2)/(b_s^2 - a^2)] - \mu_s]/E_s$$

Where, from previous calculational techniques:

a = inner radius of inner steel shell = 33.1729 in
b_s = outer radius of inner steel shell = 33.9268 in
b_l = inner radius of lead shell = 33.92542 in
c = outer radius of lead shell = 36.14392 in
$E_s = 25.2(10)^6$ psi
$\mu_s = 0.3$
$E_l = 1.36(10)^6$ psi
$\mu_l = 0.45$

Thus,

$$\delta = p[4.04545(10)^{-4} + 5.94949(10)^{-5}] = 0.002829 \text{ in}$$
$$p = 47.6 \text{ psi interface pressure}$$

Using thick-walled pressure vessel theory, the inner shell hoop stress is:

$$\sigma_s = -p[(b_s^2 + a^2)/(b_s^2 - a^2)]$$
$$= -2,116 \text{ psi}$$

Likewise, the lead shell hoop stress is:

$$\sigma_l = p[(c^2 + b_l^2)/(c^2 - b_l^2)]$$
$$= 752 \text{ psi}$$

Note that at 325°F, the proportional limit of the lead is 189 psi, or with an offset of 0.2% strain, yield is 311 psi which indicates the lead will yield under such a pressure. To fully accommodate the 0.002829 inch interference, the lead would be required to see a strain of 0.002829/33.92542 = 0.000083 in/in, or 0.0083%. Utilizing Figure 2.3-1 from Section 2.3, the corresponding lead stress for a strain of 0.0083% would be approximately 270 psi. The interface pressure would then be:

$$p = \sigma_l/[(c^2 + b_l^2)/(c^2 - b_l^2)]$$
$$p = 17.1 \text{ psi interface pressure}$$

Now, cool to 70°F and summarize the steel and lead shell, stress-free dimensions from the analyses performed above. The geometry and properties are, at 70°F, as follows:

$$a = 33.00 \text{ in}$$
$$b_s = 33.75 \text{ in}$$
$$b_l = 33.550 \text{ in}$$
$$c = 35.7434 \text{ in}$$
$$E_s = 28.3(10)^6 \text{ psi}$$
$$\mu_s = 0.3$$
$$E_l = 2.34(10)^6 \text{ psi}$$
$$\mu_l = 0.45$$

and:

$$\delta = b_s - b_l = 0.200 \text{ in}$$

Utilizing the same press-fit equation as above, the interface pressure is:

$$\delta = b_l p[[(c^2 + b_l^2)/(c^2 - b_l^2)] + \mu_l]/E_l + b_s p[[(b_s^2 + a^2)/(b_s^2 - a^2)] - \mu_s]/E_s$$

$$\delta = [2.8587(10)^{-4}]p$$

Then:

$$p = 0.200/2.8587(10)^{-4} = 700 \text{ psi interface pressure}$$

This corresponds to a lead shell hoop stress of:

$$\sigma_l = p[(c^2 + b_l^2)/(c^2 - b_i^2)]$$
$$= 11{,}090 \text{ psi}$$

which, obviously, cannot be sustained.

To fully accommodate the 0.200 inch interference, the lead would be required to see a strain of 0.200/33.55 = 0.00596 in/in, or 0.60%. Extrapolating lead stress-strain data from Section 2.3, a hoop stress of approximately 725 psi

will exist in the lead for this strain. The effective interface pressure would be:

$$p = \sigma_l / [(c^2 + b_l^2)/(c^2 - b_l^2)]$$
$$= 45.85 \text{ psi interface pressure}$$

[NOTE: δ of inner shell for -45.85 psi = $2.43(10)^{-5}(-45.85) = -0.0011$ inches, which can be conservatively neglected.]

The hoop stress in the inner steel shell at 70°F would be:

$$\sigma_s = p[(b_s^2 + a^2)/(b_s^2 - a^2)]$$
$$= -2,041 \text{ psi}$$

Next, consider cooling to -20°F (-90 ΔT) for the worst hoop stress on the inner steel shell during all hypothetical accident drop events. The steel and lead properties may be extrapolated from Table 2.3-1 as:

$$\alpha_s = 8.21(10)^{-6} \text{ in/in/°F}$$
$$E_s = 29.0(10)^6 \text{ psi}$$
$$\alpha_l = 15.7(10)^{-6} \text{ in/in/°F}$$
$$E_l = 2.43(10)^6 \text{ psi}$$

The steel and lead shell initial shell conditions are determined as:

$$a = (33.00)[1 + 8.21(10)^{-6}(-90)] = 32.9756 \text{ in}$$
$$b_s = (33.75)[1 + 8.21(10)^{-6}(-90)] = 33.7251 \text{ in}$$
$$b_l = (33.550)[1 + 15.7(10)^{-6}(-90)] = 33.5026 \text{ in}$$
$$c = (35.7434)[1 + 15.7(10)^{-6}(-90)] = 35.6929 \text{ in}$$

and,

$$\delta = b_s - b_l = 0.2225 \text{ in}$$

To fully accommodate the 0.2225 inch interference, the lead would be required to see a strain of 0.2225/33.5026 = 0.0064 in/in, or 0.64%. Extrapolating from data given in Section 2.3, a hoop stress of approximately 875 psi will

exist in the lead for this strain. The effective interface pressure would be:

$$p = \sigma_l / [(c^2 + b_l^2)/(c^2 - b_l^2)]$$
$$= 55.8 \text{ psi interface pressure}$$

The hoop stress in the inner steel shell at -20°F, conservatively neglecting the beneficial effects of lead creep, would be:

$$\sigma_s = p[(b_s^2 + a^2)/(b_s^2 - a^2)]$$
$$= -2,462 \text{ psi}$$

Finally, consider cooling to -40°F (-110 ΔT) for the worst hoop stress on the inner steel shell. The steel and lead properties, extrapolated from Table 2.3-1, are:

$$\alpha_s = 8.15(10)^{-6} \text{ in/in/°F}$$
$$E_s = 29.0(10)^6 \text{ psi}$$
$$\alpha_l = 15.6(10)^{-6} \text{ in/in/°F}$$
$$E_l = 2.43(10)^6 \text{ psi}$$

The steel and lead shell initial shell conditions are determined as:

$$a = (33.00)[1 + 8.15(10)^{-6}(-110)] = 32.9704 \text{ in}$$
$$b_s = (33.75)[1 + 8.15(10)^{-6}(-110)] = 33.7197 \text{ in}$$
$$b_l = (33.550)[1 + 15.6(10)^{-6}(-110)] = 33.4724 \text{ in}$$
$$c = (35.7434)[1 + 15.6(10)^{-6}(-110)] = 35.6821 \text{ in}$$

and:

$$\delta = b_s - b_l = 0.227 \text{ in}$$

To fully accommodate the 0.227 inch interference, the lead would be required to see a strain of 0.227/33.4924 = 0.00679 in/in, or 0.68%. Extrapolating from the data given in Section 2.3, a hoop stress of approximately 1,035 psi will exist in the lead for this strain. The effective interface pressure would be:

$$p = \sigma_1/[(c^2 + b_1^2)/(c^2 - b_1^2)]$$
$$= 65.5 \text{ psi interface pressure}$$

The hoop stress in the inner steel shell at -40°F, conservatively neglecting the beneficial effects of lead creep, would be:

$$V_s = p[(b_s^2 + a^2)/(b_s^2 - a^2)]$$
$$= -2,915 \text{ psi}$$

The preceding calculations deal only with the calculation of hoop stresses. Axial stress will also develop in the inner steel and lead shells due to axial shrinkage of the lead. In cooling to -20°F, axial strain in the lead, assuming bonding of the lead to the inner steel shell, is:

$$\epsilon_a = [(\alpha_l - \alpha_s)\Delta T]_{620} + [(\alpha_l - \alpha_s)\Delta T]_{-20}$$
$$= [(20.38 - 9.56)(10)^{-6}(620 - 70)] - [(15.7 - 8.21)(10)^{-6}(-20 - 70)]$$
$$= 0.00663 = 0.663\% \text{ strain (tensile)}$$

Extrapolating from the data in Section 2.3, an axial stress of approximately 990 psi will exist in the lead for this strain. The effective force in the lead shell would be:

$$P_a = pA_l$$
$$= 990\pi[(36.6929)^2 - (33.7251)^2] = 424,854 \text{ lbs}$$

From equilibrium, this same force can develop in the inner steel shell. Thus, the compressive axial stress in the inner steel shell at -20°F is:

$$\sigma_a = P/A_i$$
$$= -424,854/\pi[(33.7251)^2 - (32.9756)^2] = -2,705 \text{ psi}$$

This is a conservative estimate in that it assumes the ends of the outer cask inner shell are free and that no load develops in the outer shell.

In cooling to -40°F, axial strain in the lead, assuming bonding of the lead to the inner steel shell, is:

$$\varepsilon_a = [(\alpha_l - \alpha_s)\Delta T]_{620} + [(\alpha_l - \alpha_s)\Delta T]_{-40}$$
$$= [(20.38 - 9.56)(10)^{-6}(620 - 70)] + [(15.6 - 8.15)(10)^{-6}(-40 - 70)]$$
$$= 0.00677 = 0.677\% \text{ strain (tensile)}$$

Extrapolating from the data in Section 2.3, an axial stress of approximately 1,035 psi will exist in the lead for this strain. The effective force in the lead shell would be:

$$P_a = pA_l$$
$$= 1,035\pi[(35.6820)^2 - (33.7197)^2] = 442,820 \text{ lbs}$$

From equilibrium, this same force can develop in the inner steel shell. Thus, the compressive axial stress in the inner steel shell at -40°F is:

$$V_a = P/A_i$$
$$= -442,820/\pi[(33.7197)^2 - (32.9704)^2] = -2,820 \text{ psi}$$

Again, this calculation conservatively assumed that the ends of the outer cask inner shell are free and that no load develops in the outer shell.

2.6.3 Reduced External Pressure

From Section 3.4.4, the maximum normal operating pressure of the NuPac 10/140MB is 6.8 psig, assuming the cask was loaded at standard atmospheric pressure (14.7 psia). An external pressure of 3.5 psia will result in an additional cask internal pressure differential of 11.2 psig. Total maximum differential pressure acting internally on the cask is thus 11.2 + 6.8 = 18.0 psig, which will be reacted by the lid and its associated closures, comprised of eight 2.5 inch diameter bolts for the primary lid and sixteen 1.25 inch diameter bolts for the secondary lid.

Stresses induced in the cylindrical portion of the cask are conservatively estimated by assuming the pressure differential is totally borne by the 0.75 in. thick inner shell without backing by the lead shielding. The hoop,

longitudinal and radial stresses are:

$$f_h = PR/T = (18.0)(33.375/0.75) = 801 \text{ psi}$$
$$f_l = PR/2T = (18.0)(33.375/0.75)(1/2) = 401 \text{ psi}$$
$$f_r = -P = -18.0 \text{ psi}$$

Since these are the principle stresses, the stress intensity may be calculated by subtracting the minimum value from the maximum:

$$S.I. = f_h - f_r$$
$$= 801 - (-18.0) = 819.0 \text{ psi}$$

The allowable membrane stress intensity for containment structures at Normal Conditions of Transport is S_m (Table 2.1.2-1, item reference number 1(A)). From Table 2.3-1, the value of S_m for the 304 stainless steel inner shell at its expected maximum operating temperature of 128°F is 20,000 psi. The Margin of Safety is:

$$M.S. = 20,000/819.0 - 1 = + \text{Large}$$

Pressure across the lids is carried in plate bending by the 6.00 in (average) thick steel plates top and bottom. For the bottom lid of the bottom-loading configuration assume a circular plate, uniformly loaded and with edges simply supported. The maximum stress can be calculated as follows (refer to Roark, Formulas for Stress and Strain, 4th ed., Reference 2.11.11, Table 24, Case number 10a). Conservatively assuming a uniform pressure distribution over the entire circular plate, the maximum bending moment (at the center of the plate) may be expressed as:

$$M_c = qa^2(3+\mu)/16$$

Where:

q = Pressure loading = 18.0 psig

a = Lid radius = 38.0 in

μ = Poisson's ratio = 0.3

$$M_c = (18.0)(38.0)^2(3 + 0.3)/16 = 5,361 \text{ in-lb/in}$$

The bending stress at this location may then be derived as:

$$\sigma_B = 6M_c/t^2 = (6)(5,361)/(6.0)^2$$
$$= 893 \text{ psi}$$

For purposes of verifying the above hand calculation, a finite element analysis was performed on the bottom lid under an assumed 10 psig internal pressure loading. The ANSYS finite element program, discussed in Appendix 2.10.2, was utilized for this analysis. The model used is discussed in Section 2.10.7.1 of Appendix 2.10.7, and is shown in Figure 2.10.7-5. The maximum surface (membrane plus bending) stress intensity was found to be 1,045 psi on the lid 'skirt' (overhanging the cask outer wall), at the primary bolt attachment point. The maximum centroidal (membrane) stress intensity was 756 psi, acting at the same location as the maximum bending stress. Since the analysis was linear, maximum stresses arising from the actual maximum pressure of 18.0 psig may be found by directly ratioing derived stresses by a factor of 18.0/10.0. At the actual maximum pressure of 18.0 psig, these stresses become 1,881 psi (surface) and 1,721 psi (centroidal). A (18.0/10.0)(479) = 862 psi bending stress was found on the inside surface at the center of the lid, and compares very well with the hand-calculated result of 893 psi given above.

Due to the complex geometry of the cask top lid assembly, a finite element analysis was also performed to determine stresses arising from internal pressure loading on this structural member. The model used is discussed in Section 2.10.7.1 of Appendix 2.10.7, and is shown in Figure 2.10.7-13. An intenal pressure of 10 psig was applied to the inner surface of the top lid, with a resulting maximum surface (membrane plus bending) stress intensity of 3,790 psi. This stress intensity was located on the outer surface of the secondary lid, near the secondary bolt circle diameter. A maximum centroidal (membrane) stress intensity of 1,194 psi was developed near the same location, at the midpoint of the secondary lid section. The actual surface stress intensity for 18.0 psig internal pressure is 6,822 psi, and the actual centroidal stress intensity is 2,149 psi.

The maximum allowable membrane stress intensity, from Table 2.1.2-1, item reference number 1(A), is S_m. For the lowest-strength material suitable for lid construction, according to Table 2.3-1, S_m is 20,000 psi (at the lid's maximum normal operating temperature of 133°F). The maximum centroidal stress, 2,149 psi, from the top lid finite element analysis, yields a Margin of Safety of:

$$M.S. = 20,000/2,149 - 1 = + 8.31$$

The maximum allowable membrane plus bending stress intensity, from Table 2.1.2-1, item reference number 2(A), is $1.5S_m$, or (1.5)(20,000) = 30,000 psi. From the top lid finite element analysis, the maximum surface stress intensity of 6,822 psi yields Margin of Safety of:

$$M.S. = 30,000/6,822 - \quad = + 3.40$$

It is thus demonstrated that both the top and bottom lids for the 10/140MB cask easily meet the reduced external pressure requirement. Since the fixed-bottom cask configuration has an essentially clamped-edge bottom plate, it may be assumed that the more flexible bottom-loading version will present the worst case.

Loads on the primary lid attachment bolts may be approximated as:

$$P_s = Ap/N$$

Where:

A = Area that the internal pressure acts on = $\pi D^2/4$
D = Maximum O-ring seal diameter = 69.0 in
p = Maximum internal pressure = 18.0 psi
N = Number of primary lid bolts = 8

For the worst case loading:

$$P_s = [\pi(69.0)^2/4](18.0)/8$$
$$= 8,413 \text{ lbs.}$$

Similiarly for the secondry lid bolts, the load is:

$$P_s = [\pi(32.0)^2/4](18.0)/16$$
$$= 905 \text{ lbs.}$$

Since both the bolt loads are well below the maximum bolt preload value of 17,350 lb and 15,500 lb, respectively (refer to Section 2.1.2.2.2), it would seem that bolt loads under the Reduced External Pressure requirement are inconsequential. However, inspection of the finite element results discussed above reveals that the simple approach to bolt loads used here is non-conservative.

The primary lid top and bottom bolt loads are indeed reduced to values below preload. For the top lid, the load decreases from the preload value of 16,774 lb/bolt to 14,152 lb/bolt, and the bottom lid bolt load is reduced from 16,750 lb/bolt to 13,883 lb/bolt, for an assumed internal pressure of 10.0 psig. It can be seen that the maximum residual primary bolt load will be that of the top lid bolts. The load on these bolts decreases under internal pressure loading an average of (16,774 - 14,152)/10.0 = 262.2 lb/psi. It can be expected then, that the maximum possible residual load on a primary lid bolt, assuming an initial preload to the maximum value of 17,350 lb/bolt, would be:

$$P_{bolt} = 17,350 - (18)(262.2) = 12,630 \text{ lb/bolt}$$

under 18.0 psig for the Reduced External Pressure case.

The secondary lid bolt load, on the other hand, actually increases, from the applied preload value of 14,756 lb/bolt to 15,380 lb/bolt, for 10.0 psig internal pressure. This represents a bolt load increase of (15,380 - 14,756)/10.0 = 62.4 lb per psi of applied internal pressure. If the secondary bolts were tightened up to their maximum preload of 15,500 lb, it can be expected that the bolt load calculated in the finite element analysis would increase to:

$$P_{bolt} = 15,500 + (18)(62.4) = 16,623 \text{ lb/bolt}$$

for an internal pressure of 18.0 psig. This would in turn induce a secondary bolt tensile stress of:

$$S_{bolt} = 16,623/0.969 = 17,155 \text{ psi}$$

The mechanism behind this unexpected result becomes clear upon inspection of the exagerated lid deflection plot shown in Figure 2.10.7-19 of Appendix 2.10.7. While this plot is for an end drop load with maximum payload distributed over the inner surface of the lid, the internal pressure loading will produce the same general effect. As can be seen from the plot, the deformation of the primary lid acts to impart a prying action on the secondary lid. The net result is an increased pressure on the secondary EnviroSeal™ plate, reacted by an increased secondary bolt load.

The allowable stress of the bolting material, from Table 2.1.2-1, item reference number 6(A), is $2S_m$. From Table 2.3-1, S_m for this material at the maximum anticipated operating temperature of 133°F is 34,360 psi. The allowable stress is then (2)(34,360) = 68,720 psi.

The maximum primary lid bolt stress will be conservatively taken as the maximum preload value of 17,350/4.0 = 4,340 psi. The resulting Margin of Safety of primary bolts is:

$$M.S. = 68,720/4,250 - 1 = + \text{Large}$$

For the secondary bolts, the Margin of Safety is:

$$M.S. = 68,720/17,155 - 1 = + 3.01$$

Even with the unexpected loading mechanism acting on the secondary bolts, bolt stresses are still well below allowable values for Reduced External Pressure.

It can thus be concluded from the above analyses that the packaging can safely react a reduced external pressure of 3.5 psia.

2.6.4 Increased External Pressure

Conservatively assuming the cask is loaded at the previously evaluated minimum atmospheric pressure of 3.5 psia, and increase of external pressure to 20 psia will result in a cask minimum external pressure of -16.5 psig. The absolute magnitude of this pressure is less than for Section 2.6.3 above, so cask lid margins of safety for this condition will be even larger than those calculated above.

For additional conservatism, assume that the negative pressure differential is applied directly to the inner shell, and utilizing the results of the previous section, the resulting compressive hoop and axial stresses are:

$$f_h = (-16.5/18.0)(801) = -734.3 \text{ psi}$$

$$f_l = (-16.5/18.0)(401) = -367.1 \text{ psi}$$

These are very much less than the same compressive stress components calculated in Section 2.6.2 above for a -40°F temperature. Therefore, no excessive compressive stresses will be applied to the critical inner shell under increased external pressure.

2.6.5 Vibration

The effects of vibrations normally incident to transport are of limited consequence to the 10/140MB Package. This conclusion is reached based on a relatively simple comparison of worst case truck transport vibratory accelerations with the tiedown accelerations addressed in Section 2.5.2 (10, 5 and 2 g's). As established herein, vibratory loadings are significantly less than the 10, 5 and 2 g tiedown loadings previously addressed. Since stresses due to the relatively large tiedown loads are required to remain less than yie[illegible] sulting from normal vibration will be considerably less than y[illegible] ltant stress levels are also readily shown to remain below t[illegible]s for the applicable materials of construction. Details a[illegible] prov[illegible] the following subsections.

2.6.5.1 Transport Vibratory Accelerations

Draft ANSI Standard N14.23, Reference 2.11.20, Design Basis for Resistance to Shock and Vibration of Radioactive Material Packages Greater than One Ton in Truck Transport, provides a basis for estimating peak truck bed vibration inputs and package response accelerations. Table 2 of ANSI N14.23 summarizes peak vibratory accelerations at the truck trailer bed for heavy loads (over 20 tons, which applies even for an empty 10/140MB), as follows:

Truck Bed Vibratory Accelerations

Direction	Magnitude
Longitudinal	0.3 g
Lateral	0.3 g
Vertical	0.6 g

Since some amplification of these input loads can occur, the package acceleration response can be somewhat greater than presented above. As a conservative estimate of the amplified response of the package, it will be assumed that the package responds at continuously cycling accelerations equal to the greater of twice the above tabulated truck bed vibratory accelerations or one half of the maximum shock acceleration response of the package. The maximum shock response of the package is readily available as Table 1 of ANSI N14.23. That table provides peak shock accelerations for the bed of the truck. Additionally, per the commentary provided within Section 4.2 of ANSI N14.23, these peak accelerations can also be directly used to estimate the maximum inertial loading acting on the cask tiedown system. The peak shock accelerations are as follows (Note: the vertical down acceleration from Table 1 of N14.23 is used, as this acceleration tends to separate the package from the truck bed, thus loading the tiedown system; the vertical up acceleration forces the package into the truck bed and does not load the tiedown system):

Peak Shock Acceleration Response of the Package

Direction	Magnitude
Longitudinal	2.3 g
Lateral	1.6 g
Vertical	2.0 g

By using the greater of one half of these peak shock accelerations, or twice the vibratory acceleration input at the bed of the truck, the maximum cyclic acceleration response of the package used for the analysis herein therefore becomes:

Maximum Cyclic Response Acceleration of the Package

Direction	Magnitude
Longitudinal	1.15 g
Lateral	0.8 g
Vertical	1.2 g

2.6.5.2 Transport Vibratory Stresses

Under normal vibration loadings, the most significantly stressed 10/140MB components will be those components which directly react the loads that develop in the tiedown system. The components to be addressed are therefore the tiedown lug, the welds attaching the tiedown lugs to the cask body, and the cask outer shell itself in the vicinity of the tiedown lugs. Nominal stress levels in these components are readily determined by ratioing the stress results available from Section 2.5.2. These resultant nominal stresses can then be multiplied by appropriate stress concentration factors to arrive at peak stress magnitudes. As the tiedown cables are tension-only components, the alternating stress to be considered in the fatigue evaluation is simply one half the peak stress magnitude. The remainder of this subsection develops

the alternating stresses to be considered in each component of interest.

2.6.5.2.1 Maximum Cable Load

The maximum cable load resulting from the simultaneous application of the package cyclic response accelerations of 1.15 g longitudinally, 0.8 g laterally and 1.2 g vertically, is readily determined using the methodology presented in Section 2.10.3.1 of Appendix 2.10.3. Using that methodology, the resultant cable load to be considered for this normal vibration case becomes:

For an 18° cable angle, F_C = 103,305 lb

For a 14° cable angle, F_C = 99,354 lb

2.6.5.2.2 Maximum Alternating Stress Intensity In Lug

The peak stress intensity in the lug will occur in the vicinity of the 2.25 inch diameter hole used to interface with the tiedown hardware, due to stress concentrations associated with the presence of the hole. To determine this peak stress intensity, the lug geometry is approximated as follows:

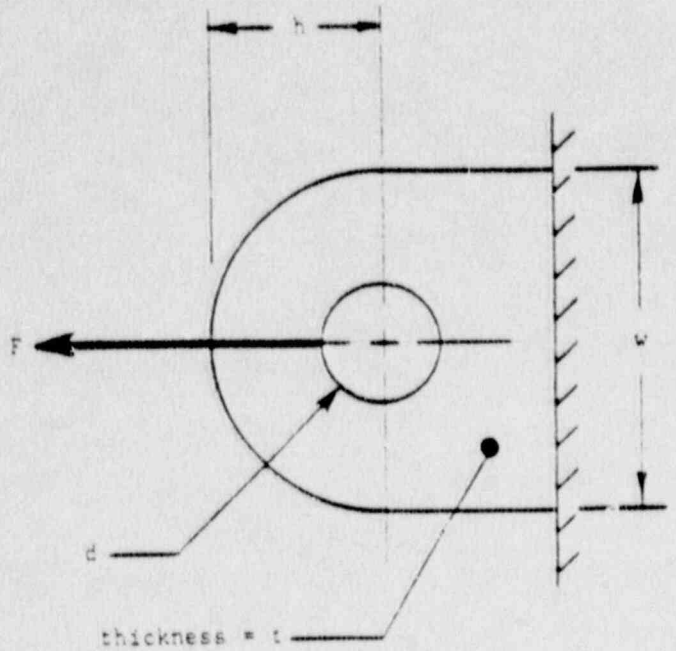

h = 3.0 inches
w = 6.0 inches
t = 2.5 inches
d = 2.25 inches

Utilizing Figure A-26-12 on page 842 of Shigley, Joseph E., Mechanical Engineering Design, 4th Ed. (Reference 2.11.9), the peak stress intensity in the lug becomes:

$$\sigma_p = K_t(\sigma_o) = K_t(F/A) = 37,465 \text{ psi}$$

Where:

K_t = 3.4 (directly from Figure A-20-12 for h/w = 0.5 and d/w = 0.375)
F = P_C = 103,305 lb
A = (w-d)t = 9.375 in^2

The maximum alternating stress intensity, σ_a, is one half of this peak value, or:

$$\sigma_a = 18,733 \text{ psi}$$

2.6.5.2.3 Maximum Alternating Stress Intensity In Lug to Body Weld

To determine the peak stress intensity in the lug to body weld, a nominal shear stress in the weld will first be determined by simply applying appropriate ratios to the results available from Table 2.5.2-1 of Section 2.5.2. The resultant nominal weld shear stresses therefore become:

(103,305/545,850)17,125 = 3,241 psi for an 18° cable angle

(99,354/525,211)17,370 = 3,286 psi for a 14° cable angle

To account for stress concentrations associated with the bevel/fillet weld, a factor of 3.7 will be applied to the above nominal weld shear stresses (per Table 9-5 on page 4[illegible] of Reference 2.11.9). Additionally, to obtain stress intensities, the resultant peak shear stresses must be further increased by an additional factor of two. The resultant peak stress intensities in the weld are therefore:

17,501 psi for an 18° cable angle

17,744 psi for a 14° cable angle

The maximum alternating stress intensity, σ_a, is one half of the worst case peak value of 17,744 psi (for the 14° cable angle), or:

σ_a = 8,872 psi

2.6.5.2.4 Maximum Alternating Stress Intensity In Cask Outer Shell

There are no stress concentration factors associated with the outer cask shell in the vicinity of the tiedown lug. For this reason, the peak stress intensity can be directly obtained by applying appropriate ratios to the stress intensity results available in Table 2.5.2-1 of Section 2.5.2. The resultant peak stress intensities in the cask outer shell therefore become:

(102,305/545,850)36,276 = 6,865 psi for an 18° cable angle

(99,354/525,211)34,533 = 6,533 psi for a 14° cable angle

The maximum alternating stress intensity, σ_a, is one half of the worst case peak value of 6,865 psi (for the 18° cable angle), or:

σ_a = 3,433 psi

2.6.5.3 Comparison of Vibratory Stresses With Allowable Limits

The allowable alternating stress intensity limits for the A-517 lug material and the A-516 or A-537 outer shell material are available from Figure I-9.1 and Table I-9.1 of Reference 2.11.3 (ASME B and PV Code, Section III). From that Figure and Table, the following allowable alternating stress intensities are obtained at $1(10)^6$ cycles.

20,000 psi for A-517

12,500 psi for A-516 or A-537

As Figure I-9.1 is based on a modulus of elasticity of $30(10)^6$ psi, the above allowable limits must be adjusted to reflect the modulus of elasticity of the A-517 lug and A-516 or A-537 cask outer shell at their normal operating temperature of 114°F ($29.44(10)^6$ psi and $29.24(10)^6$ psi respectively). The adjusted allowable alternating stress intensity limits therefore become:

19,625 psi for A-517

12,180 psi for A-516 or A-537

From Subsections 2.6.5.2.2 through 2.6.5.2.4, the maximum alternating stress intensity for the A-517 lug is 18,733 psi and the maximum alternating stress intensity for the A-516 or A-537 cask outer shell or weld attaching the lug to the shell is 8,872 psi. The corresponding Margins of Safety are therefore as follows:

M.S. = (19,625/18,733) - 1 = +0.05 for A-517

M.S. = (12,180/8,872) - 1 = +0.37 for A-516 or A-537

As indicated, the allowable limits are met and the response of the 10/140MB Package to normal vibrations is fully acceptable.

2.6.5.4 Stresses in the Polyurethane Foam Impact Limiters

To estimate the effect of transportation shock and vibration on the supporting impact limiter, use the maximum vertical up shock value from Table 1 of Reference 2.11.20. This value is 3.6 g's. Assuming that the cask is supported in transport on the 10 inch high, reduced diameter end section only, peak stress of the foam due to transportation shock may be derived by multiplying the peak shock loading by the support area. The area of the reduced diameter segment of the impact limiter can be determined by taking the area of an equivalent outside diameter, calculated in Section 2.7.1.1 as 100.34 inches, and subtracting the area of the 55 inch diameter center

opening.

$$\text{Area} = (\pi/4)[(100.34)^2 - (55.0)^2] = 5,532 \text{ in}^2$$

The cask gross weight is 68,000 lb, as derived in Section 2.2. Combined with the peak shock load factor of 3.6, the stress on the foam in the support base of the impact limiter is:

$$\sigma_{foam} = (68,000)(3.6)/5,532 = 44 \text{ psi}$$

The polyurethane foam used in the impact limiters experiences its lowest mechanical strength at elevated temperatures. Conservatively using the maximum foam temperature for Normal Condition of Transport of 169°F (actually found only in the upper impact limiter), the 'plateau' stress is found to be approximately 700 psi (refer to Figure 2.1.2-3). It can thus be seen that, even under worst case conditions, the polyurethane foam in the impact limiters remains well below its compressive yield strength, and its impact absorbing integrity will not be dimenished.

2.6.6 Water Spray

Since the package exterior is constructed of steel, this test will have no detrimental effects on the NuPac 10/140MB.

2.6.7 Free Drop

The NuPac 10/140MB Shipping Cask weighs approximately 68,000 pounds. Subpart F of 10 CFR 71 requires that a package in excess of 33,000 pounds be capable of resisting the effects of a one foot drop onto a flat, essentially unyielding, horizontal surface striking the surface in a position for which maximum damage is expected. The following subsections address free drops in any orientation, and show that the requirements of 10 CFR 71 are met.

For end and side impact events, the package is analyzed using Nuclear

Packaging's EYDROP and SYDROP programs, respectively. These programs are described in detail in Appendix 2.10.5. The programs predict a maximum acceleration imparted to the cask during the event, which is then applied statically to the package as a whole. Since the impact limiter foam stress-strain curve is dependent on temperature, the foam performance at the extreme temperatures predicted for the foam under Normal Conditions of Transport (-20° to 169°F) is assumed as a means of bounding the performance of the impact limiters. Additionally, since the programs assume a relatively simple cylindrical impact limiter surrounding a smaller cylinder, additional bounding analyses have been performed to account for the flat sections of the impact limiter, as well as the 'notch' in the side of the impact limiter.

For oblique impacts, the package was analyzed using Nuclear Packaging's CYDROP and OBLIQUE computer programs. These programs are also detailed in Appendix 2.10.5. Again, bounding calculations were performed to insure adequate consideration was taken with respect to the somewhat unconventional shape of the impact limiter and the temperature variation of the polyurethane foam.

A graphical and descriptive summary of the impact limiter geometry assumptions made for each type of analysis is given in Figure 2.1.2-4 and Table 2.1.2-8.

Polyurethane foam impact limiter behavior is becoming increasingly well understood, due to the many drop test programs that have been undertaken in the past few years. Notable among these programs are the tests performed in support of the 1-13[illegible] II package, the NuPac 125-B Fuel Shipping Cask (Docket Number 71-9200), and, most recently, the 10/140MB quarter-scale cask, as detailed in Appendix 2.10.4. These tests indicate that analysis methods and assumptions used in this application are reasonable and conservative.

It has been determined in the free drop analyses which follow, that drops in the various orientations produce different situations critical to overall cask design. For example, in general, flat end drops result in loads which tend to induce the governing stress resultants on the major cask components. Oblique drops tend to create maximum primary lid separation loads. Because of the various appurtenances extending from the side of the cask (tie-down lugs and primary lid bolt lugs), as well as the relatively 'soft' impact limiter res-

ponse in the side drop orientation (foam strain hardening effects are generally less for side drop than for other orientations), flat side drop will tend to result in the most critical deformations conducive to potential 'bottoming out' of the cask. All of these considerations are addressed in detail in the following sections.

An important consideration in the detailed analyses which follow is the fact that cask response to the regulatory drops is temperature dependent. At maximum temperature conditions, the structural material comprising the cask will exhibit lower mechanical strength than at lower temperatures. As a consequence, the stress and buckling allowables will also be lower. However, because the polyurethane foam in the impact limiters likewise exhibits lower mechanical strength at elevated temperatures, it will deform more on impact than would be the case at lower temperatures. The result will be smaller impact loads occuring at higher temperatures.

Conversely, at the minimum regulatory temperature, while the mechanical strength of the structural components will be greater, so will the mechanical strength of the foam The result will be greater impact loading at reduced temperatures.

In order to conservatively bound temperature effects in the free drop events that follow, the maximum impact loads, derived at the minimum temperature, will be applied to the cask. Simultaneously, the cask response will be evaluated utilizing mechanical properties at the highest normal operating temperature derived for the individual cask componenets at the maximum temperature condition. In this extremely conservative fashion, cask integrity will be demonstrated across the full range of temperatures expected under all Normal Conditions of Transport.

2.6.7.1 Flat End Drop

Analysis of the NuPac 10/140MB Cask behavior during normal condition drops from 1 foot is performed in the following steps:

1. Analyze the maximum impact limiter deformation using the EYDROP energy balance computer program.

2. Analyze the maximum impact force using the EYDROP computer program.

3. Analyze the axial and hoop stresses in the cask shells and lead.

4. Analyze the cask lid for bending, assuming that the payload acts as a uniform load on the inside surface of the lid, and the impact limiter foam pressure acts in the opposite direction in the appropriate place on the outside of the lid. Reanalyze the lid, omitting payload reaction.

5. Analyze the stresses in the primary and secondary lid bolts.

6. Analyze bearing stresses on the EnviroSeal^{tm} plates.

The flat end free drop event will tend to impose maximum loading on the major cask components, compared to other impact orientations. Lids will generally experience their greatest bending forces, while the cask shells will undergo maximum compressive loading conducive to buckling. In addition, there are a number of cask-specific considerations which could govern component loads and determine which are the most critical. These are as follows:

1. The NuPac 10/140MB cask has two different basic configurations -- a fixed-bottom and a removable-bottom version. Each will respond differently to the same imposed drop load.

2. Drop orientation could be an important factor. Impacts for both top-down and bottom-down end drops must be addressed.

3. The presence of the cask payload may, in certain circumstances, tend to counteract and relieve impact loading on some components. Response of the lids, for example, under uniform loadings applied externally by the impact limiters and internally by the payload will differ from the response where a payload is reduced or constrained from applying an evenly distributed loading. Consequently, two bounding cases are considered: One, where the impact is modelled as though the full 15,000 lb payload were present, and the other with no payload reaction at all.

4. The maximum normal condition internal pressure (6.8 psig, from Section 3.4.4) must be accounted for, when this will result in a worse-case stress condition. Generally, the presence of internal pressure will tend to increase the critical inner shell (containment boundary) buckling strength. Conversely, for lid analysis purposes, internal pressure will result in additional bending stress. Therefore, for the following shell analyses, internal pressure will be conservatively neglected. For lid and closure component stress evaluation, internal pressure will be applied.

5. The state of the lead shielding will be an important factor on cask shell loading. As demonstrated in Section 2.6.2, it is possible that the lead will shrink onto the cask inner shell during the cool-down process, and would be clinging to the shell during the drop event. Whether or not the force of the impact would be sufficient to cause the lead to slip down is an important consideration in how severely the shell is loaded during this event. Conversely, over a period of time, the lead could creep completly away from the inner shell. Response to end drop loading would vary accordingly.

In the analyses that follow, worst-case combinations of all these factors have been evaluated. Where simple geometries and load patterns allow, classical stress analysis techniques are utilized to determine component response to end drop loading. For more complex geometries, the ANSYS finite element program was used to determine maximum stresses.

A summary of all end drop analyses performed in Section 2.6.7.1 is presented in Tables 2.6.7-1 and 2.6.7-2. This summary details each component analysed, the initial conditions assumed, analysis technique utilized, and results. It is from these Tables that the worst-case end drop stress states detailed in Table 2.6-1 above are drawn.

Material properties of structural components utilized in the analyses were taken from Table 2.6-1. Stress allowables were drawn from Tables 2.1.2-1 and 2.1.2-2, and buckling allowables came from Tables 2.1.2-3 and 2.1.2-4. Polyurethane foam properties were derived from Figure 2.1.2-3

The impact limiter is modeled as having an outside diameter of 100.34 inches. This dimension corresponds to the diameter of a circle with the same area as a 101 inch diameter circle flattened to 96 inches on each side. Refer to Section 2.7.1.1 below for the derivation of this equivalent diameter. As a result, the impacted area calculated by EYDROP is exactly equivalent to the end contact area of the impact limiter. Tests performed on a variety of packages indicate that loads calculated in this manner are slightly conservative (overpredicted). The assumed impact limiter geometry is shown in Figure 2.6.7-1.

2.6.7.1.1 Impact Limiter Deflection:

Table 2.6.7-3 presents the results from the EYDROP energy balance program for an impact limiter at 169°F. This corresponds to the maximum temperature the polyurethane foam in the package might experience under normal conditions, as described in 10 CFR 71 (see Section 3.4.2). Note that the 169°F temperature represents the maximum foam temperature, which occurs in the upper impact limiter, and not the average temperature. The minimum temperature in the upper impact limiter is actually only 119°F. The lower impact limiter is considerably cooler, with temperatures ranging from 119°F to 129°F. It should also be noted that the foam properties assumed were taken at the lower bound that might be expected at that temperature. That is, foam strength was derated by 15% up to 75% strain, and by 20% thereafter. Refer to Section 2.1.2.4 for further details.

TABLE 2.6.7-1

(Page 1 of 2)

Normal Conditions of Transport

Flat End Drop Structural Component Analysis Parameters

Component	Case Ref. No.	Cask Configuration	Drop Orientation	Payload	Lead Status	Internal Pressure	Analysis Technique
INNER SHELL	1	Bottom Loading	Bottom Down	No	Slump	No	ANSYS
	2	Fixed Bottom	Bottom Down	Yes	Cling	No	Classical
	3	Fixed Bottom	Bottom Down	No	Cling	No	Classical
	4	Fixed Bottom	Bottom Down	Yes	Slump	No	Classical
	5	Fixed Bottom	Bottom Down	No	Slump	No	Classical
OUTER SHELL	6	Bottom Landing	Bottom Down	No	Slump	N/A	ANSYS
	7	Fixed Bottom	Bottom Down	Yes	Cling	N/A	Classical
	8	Fixed Bottom	Bottom Down	No	Cling	N/A	Classical
	9	Fixed Bottom	Bottom Down	Yes	Slump	N/A	Classical
	10	Fixed Bottom	Bottom Down	No	Slump	N/A	Classical
TOP LID	11	Both	Top Down	Yes	N/A	Yes	ANSYS
	12	Both	Top Down	No	N/A	No	ANSYS

TABLE 2.6.7-1

(Page 2 of 2)

Component	Case Ref. No.	Cask Configuration	Drop Orientation	Payload	Lead Status	Internal Pressure	Analysis Technique
BOTTOM LID	13	Bottom Loading	Bottom Down	Yes	N/A	Yes	ANSYS
	14	Bottom Loading	Bottom Down	No	N/A	No	ANSYS
BOTTOM PLATE	15	Fixed Bottom	Bottom Down	Yes	Cling	No	Classical
	16	Fixed Bottom	Bottom Down	No	Cling	No	Classical
	17	Fixed Bottom	Bottom Down	Yes	Slump	No	Classical
	18	Fixed Bottom	Bottom Down	No	Slump	No	Classical
PRIMARY LID BOLTS	19	Both	Top Down	No	N/A	No	Classical
BOLT LUGS	20	Both	Top Down	No	N/A	No	Classical
SECONDARY LID BOLTS	21	Both	Top Down	Yes	N/A	Yes	ANSYS

TABLE 2.6.7-2
(Page 1 of 3)

Normal Conditions of Transport
Flat End Drop Structural Component Stress Evaluation

Component	Case Ref. No.	Location Within Component	Load Combination	Type of Stress	Resultant Stress Component or Stress Intensity (psi)	Acceptance Criteria	Allowable Value of Stress (psi)	Margin of Safety	SAR Reference Location
INNER SHELL	1	Impact End	Min. Payload Lead Slump	Membrane + Bending	SI = 7524	$SI \leq 1.5S_m$	$1.5S_m$ = 30000	+2.99	2.6.7.1.3(2) 2.10.6.2
				Membrane	SI = 6498	$SI \leq S_m$	S_m = 20000	+2.08	
				Buckling Interaction	σ_h = 2558 σ_a = 6462	**	σ_{ha} = 17905 σ_{aa} = 19062	+1.00	
	2	Impact End	Max. Payload Lead Cling	Membrane	SI = 7888	$SI \leq S_m$	S_m = 20000	+1.54***	2.6.7.1.3(1)
				Buckling Interaction	σ_h = 2462 σ_a = 7888	**	σ_{ha} = 17905 σ_{aa} = 19062	+0.81	
	3	Impact End	Min. Payload Lead Cling	Membrane	SI = 9619	$SI \leq S_m$	S_m = 20000	+1.08	
				Buckling Interaction	σ_h = 2462 σ_a = 9619	**	σ_{ha} = 17905 σ_{aa} = 19062	+0.56	2.6.7.1.3(1)
	4	Impact End	Max. Payload Lead Slump	Membrane	SI = 5421	$SI \leq S_m$	S_m = 20000	+2.69***	
				Buckling Interaction	σ_h = 2462 σ_a = 5421	**	σ_{ha} = 17905 σ_{aa} = 19062	+1.37***	2.6.7.1.3(2)
	5	Impact End	Min. Payload Lead Slump	Membrane	SI = 7151	$SI \leq S_m$	S_m = 20000	+1.80	
				Buckling Interaction	σ_h = 2462 σ_a = 7151	**	σ_{ha} = 17905 σ_{aa} = 19062	+0.95	2.6.7.1.3(1)
OUTER SHELL	6	Impact End	Min. Payload Lead Slump	Membrane + Bending	SI = 7569	$SI \leq S_y$	S_y = 37200	+3.96	2.6.7.1.3(2) 2.10.6.2
				Membrane	SI = 5775	$SI \leq S_y$	S_y = 37200	+5.44	
				Buckling Interaction	σ_h = 1245 σ_a = 4418	**	σ_{aa} = 22728	+4.01	

* SI = Stress Intensity, σ_h = hoop compressive stress, σ_a = axial compressive stress
** Buckling Interaction: $[(\sigma_h/\sigma_{ha}) + (\sigma_a/\sigma_{aa})] \leq 1$
*** Not specifically presented herein - not a governing worst case

TABLE 2.6.7-2
(Page 2 of 3)

Normal Conditions of Transport
Flat End Drop Structural Component Stress Evaluation

Component	Case Ref. No.	Location Within Component	Load Combination	Type of Stress	Resultant Stress Component or Stress Intensity (psi)*	Acceptance Criteria	Allowable Value of Stress (psi)	Margin of Safety	SAR Reference Location
OUTER SHELL	7	Impact End	Max. Payload Lead Cling	Membrane	SI = 4616	$SI \leq S_y$	S_y = 37200	+7.06	2.6.7.1.3(1)
				Buckling Interaction	σ_h = 0 σ_θ = 4616	**	σ_{ss} = 22728	+3.92	
	8	Impact End	Min. Payload Lead Cling	Membrane	SI = 3670	$SI \leq S_y$	S_y = 37200	+9.14***	2.6.7.1.3(1)
				Buckling Interaction	σ_h = 0 σ_θ = 3670	**	σ_{ss} = 22728	+5.19***	
	9	Impact End	Max Payload Lead Slump	Membrane	SI = 6331	$SI \leq S_y$	S_y = 37200	+4.88	2.6.7.1.3(2)
				Buckling Interaction	σ_h = 0 σ_θ = 4937	**	σ_{ss} = 22728	+3.60	
	10	Impact End	Min. Payload Lead Slump	Membrane	SI = 5385	$SI \leq S_y$	S_y = 37200	+5.91***	2.6.7.1.3(2)
				Buckling Interaction	σ_h = 0 σ_θ = 3991	**	σ_{ss} = 22728	+4.69***	
TOP LID	11	Secondary Lid Outside Dia.	Max. Payload	Membrane	SI = 8514	$SI \leq S_m$	S_m = 20000	+1.35	2.6.7.1.4 2.10.7.5
				Membrane +Bending	SI = 13378	$SI \leq 1.5S_m$	$1.5S_m$ = 30000	+1.24	
	12	Outside Dia. Outside Dia.	Min. Payload	Membrane	SI = 7415	$SI \leq S_m$	S_m = 20000	+2.69	2.6.7.1.4 2.10.7.5
				Membrane +Bending	SI = 5656	$SI \leq 1.5S_m$	$1.5S_m$ = 30000	+4.30	

TABLE 2.6.7-2
(Page 3 of 3)

Normal Conditions of Transport
Flat End Drop Structural Component Stress Evaluation

Component	Case Ref. No.	Location Within Component	Load Combination	Type of Stress	Resultant Stress Component or Stress Intensity (psi)*	Acceptance Criteria	Allowable Value of Stress (psi)	Margin of Safety	SAR Reference Location
BOTTOM LID	13	Outside Dia.	Max. Payload	Membrane	SI = 6,05	SI $\leq S_m$	S_m = 20000	+2.28	2.6.7.1.4 2.10.7.3
		Center		Membrane + Bending	SI = 8788	SI $\leq 1.5S_m$	$1.5S_m$ = 30000	+2.41	
	14	Outside Dia.	Min. Payload	Membrane	SI = 3618	SI $\leq S_m$	S_m = 20000	+4.53	2.6.7.1.4 2.10.7.3
		Center		Membrane + Bending	SI = 5293	SI $\leq 1.5S_m$	$1.5S_m$ = 30000	+4.67	
BOTTOM PLATE	15	Center	Max. Payload Lead Cling	Membrane +Bending	SI = 3887***	SI $\leq 1.5S_m$	$1.5S_m$ = 30000	+6.72***	2.6.7.1.4
	16	Center	Max. Payload Lead Cling	Membrane + Bending	SI = 8281	SI $\leq 1.5S_m$	$1.5S_m$ = 30000	+2.62	2.6.7.1.4
	17	Center	Max. Payload Lead Slump	Membrane + Bending	SI = 4233***	SI $\leq 1.5S_m$	$1.5S_m$ = 30000	+6.09***	2.6.7.1.4
	18	Center	Min. Payload Lead Slump	Membrane + Bending	SI = 7935***	SI $\leq 1.5S_m$	$1.5S_m$ = 30000	+2.78***	2.6.7.1.4
PRIMARY LID BOLTS	19	Shank	Max. Payload	Membrane	SI = 5740	SI $\leq 2.0S_m$	$2.0S_m$ = 68720	+ Large	2.6.7.1.5
BOLT LUGS	20	Weld to Cask Body	Max. Payload	Membrane + Bending	SI = 3600	SI $\leq 1.5S_m$	$1.5S_m$ = 34855	+8.68	2.6.7.1.5
SECONDARY LID BOLTS	21	Shank	Max. Payload	Membrane	SI = 43487	SI $\leq 2.0S_m$	$2.0S_m$ = 68720	+0.58	2.6.7.1.5 2.10.7.3

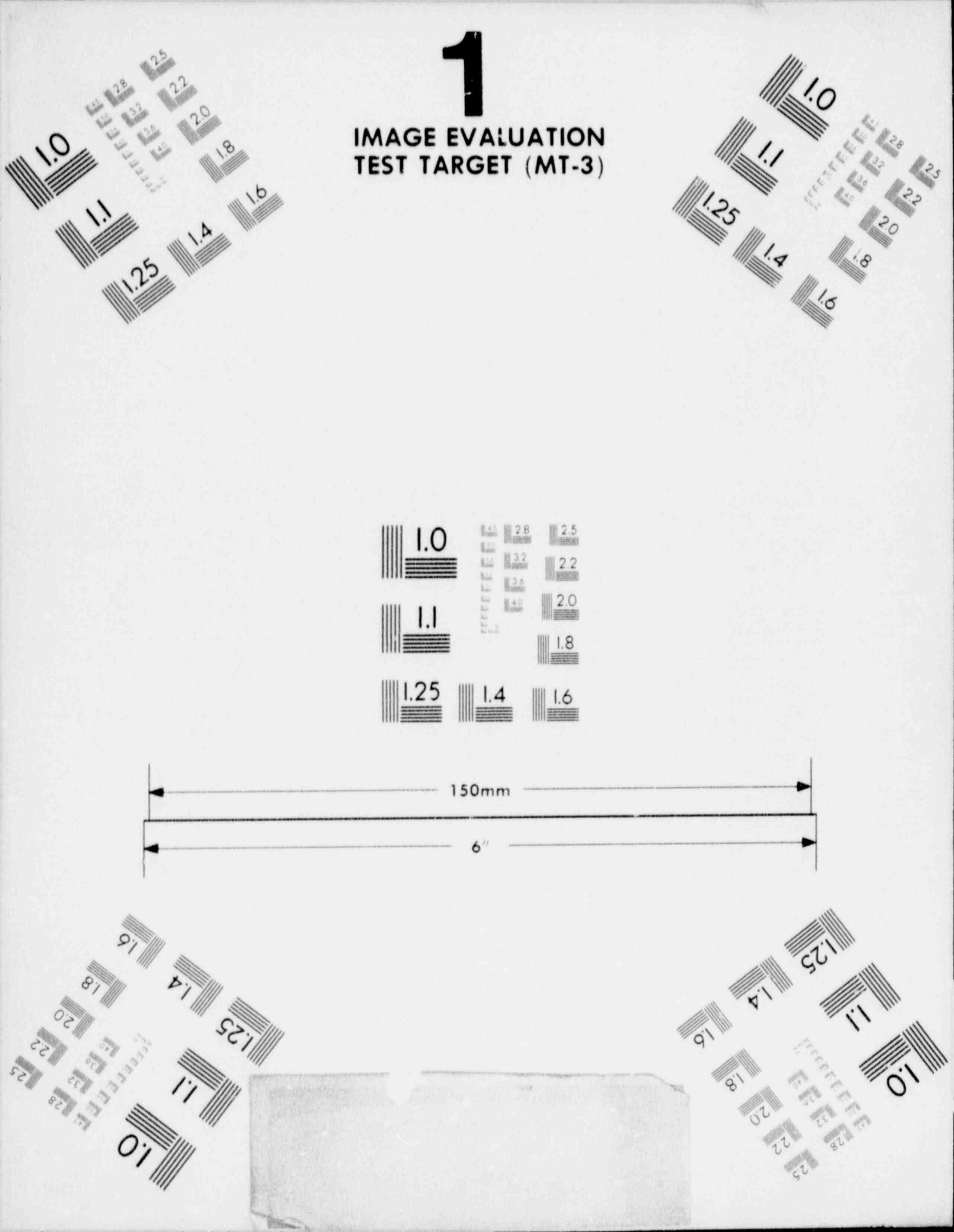
1
IMAGE EVALUATION
TEST TARGET (MT-3)
1.0
1.1
1.25
1.4
1.6
1.8
2.0
2.2
2.5
2.8
3.2
3.6
4.0
150mm
6"

1

IMAGE EVALUATION TEST TARGET (MT-3)

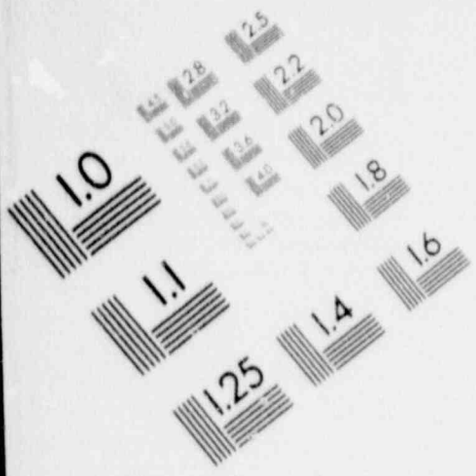

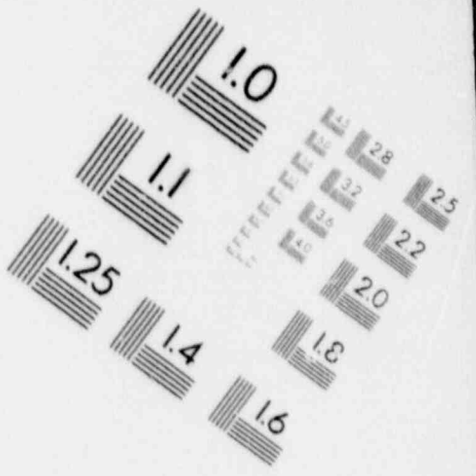

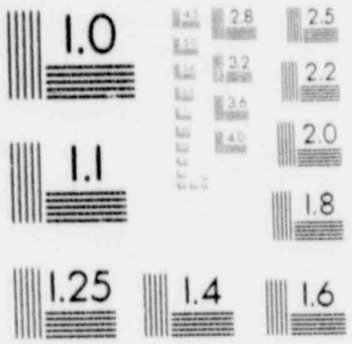

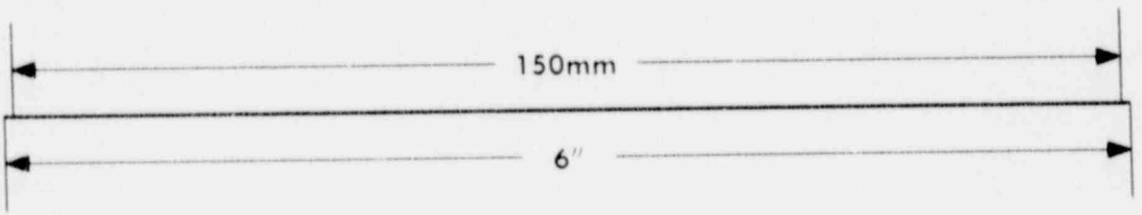

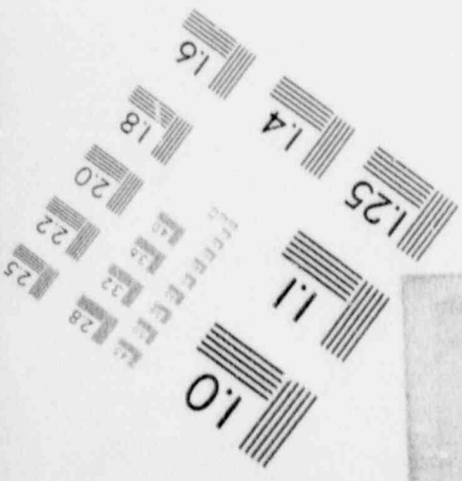

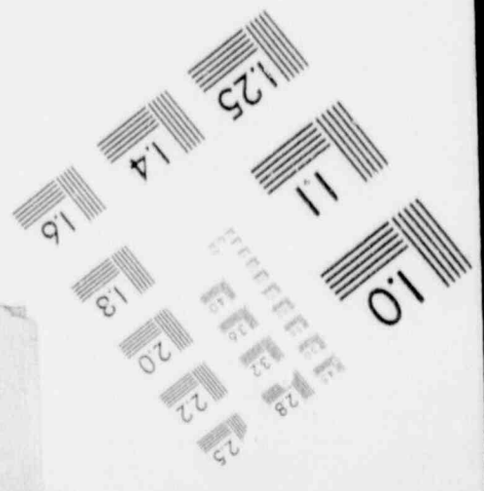

1

IMAGE EVALUATION TEST TARGET (MT-3)

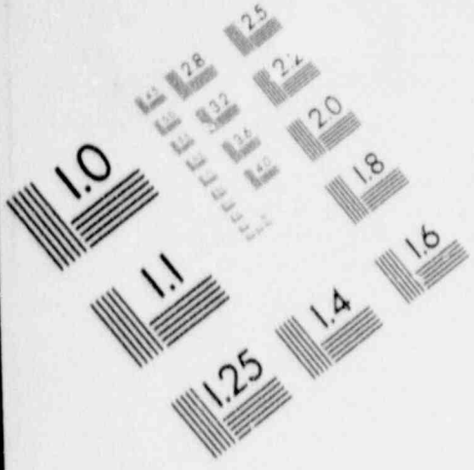

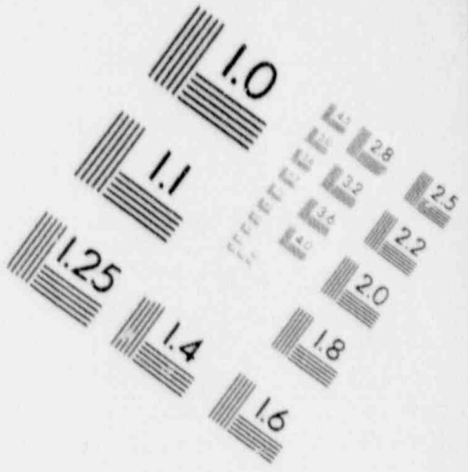

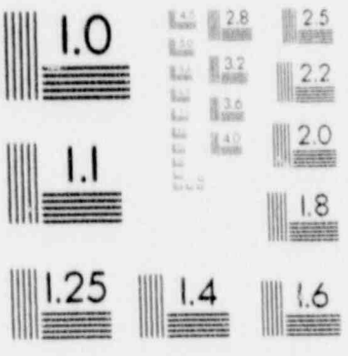

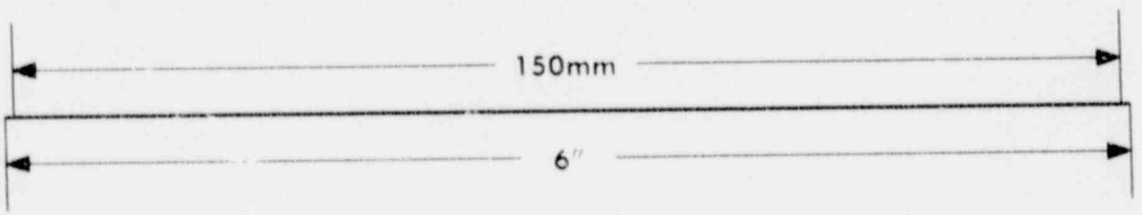

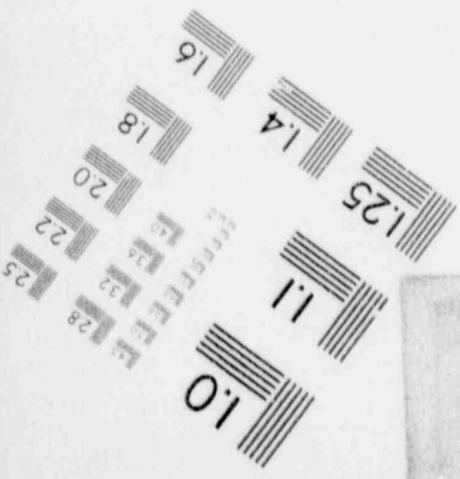

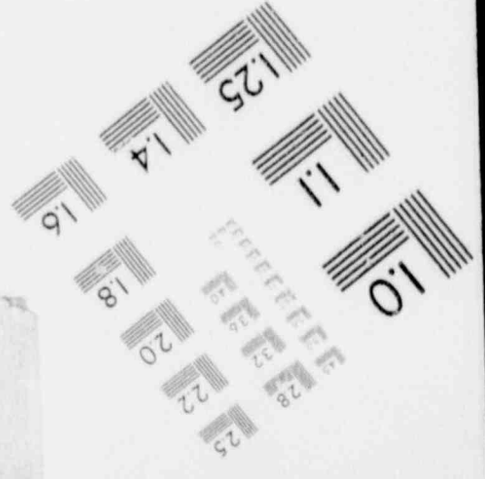

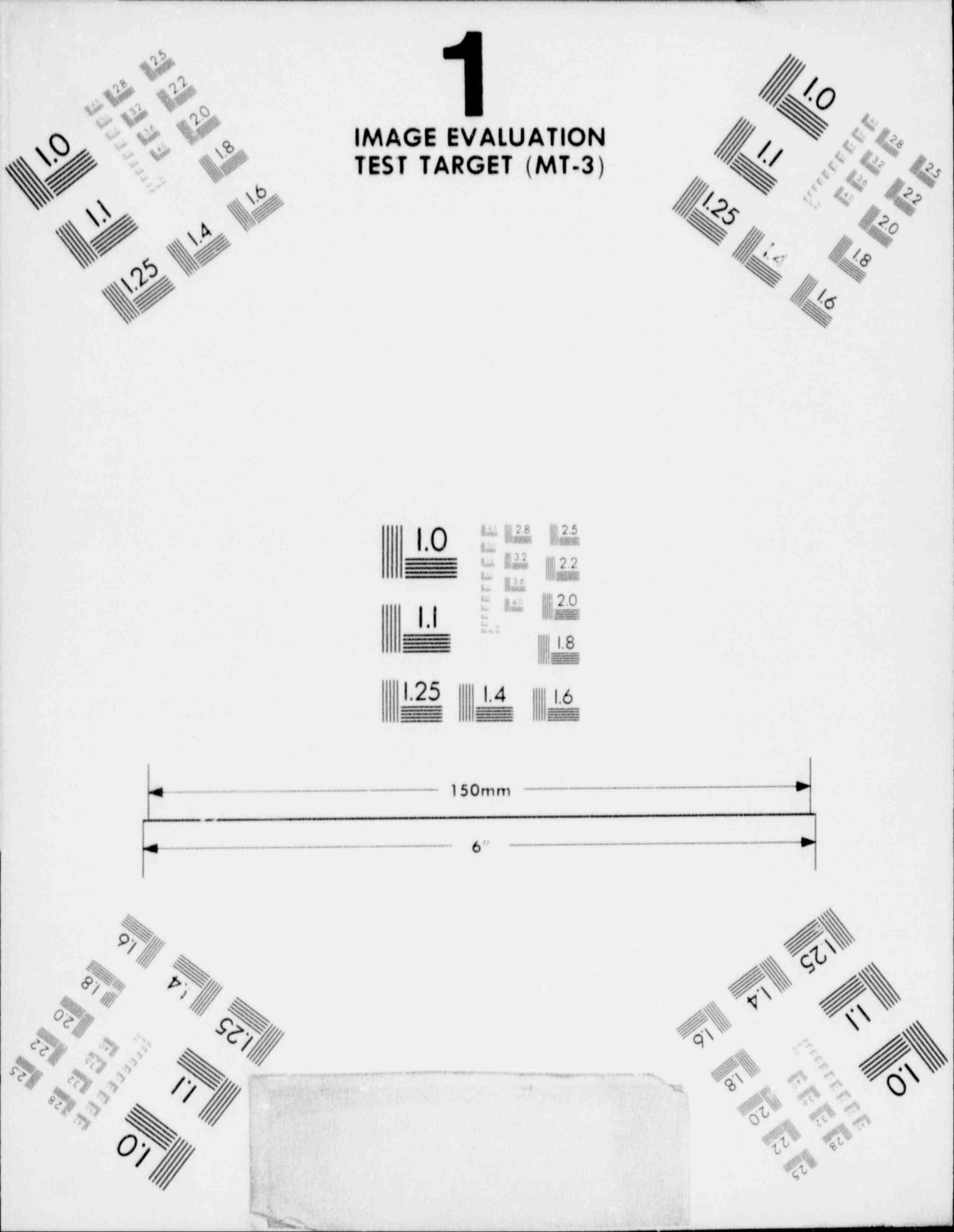
1
IMAGE EVALUATION
TEST TARGET (MT-3)
1.0
1.1
1.25
1.4
1.6
1.8
2.0
2.2
2.5
2.8
3.2
3.6
4.0
150mm
6"

FIGURE 2.6.7-1

Impact Limiter Assumed Geometry for Flat End Drop

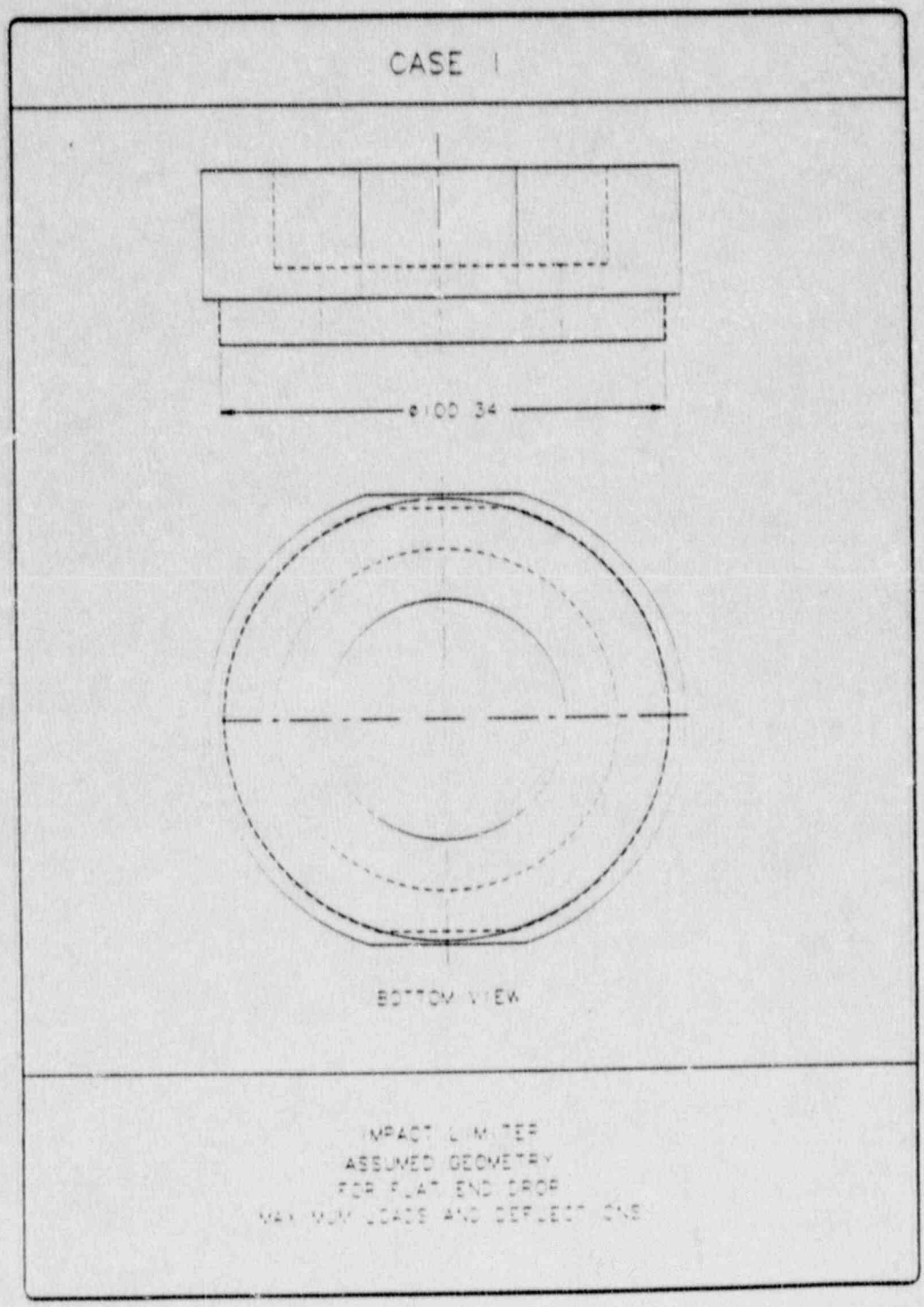

TABLE 2.6.7-3

EYDROP Results for 169°F Foam

EYDROP(END) NUPAC 10/140MB, HOT FOAM (169 DEG), N.C.T.

PACKAGE WEIGHT = 68000. (LBS)
PACKAGE DIAMETER = 100.34 (IN)
HOLE DIAMETER = 55.00 (IN)
OVERPACK DEPTH = 18.00 (IN)
DROP HEIGHT = 1.00 (FT)

CRUSH DEPTH (IN)	STRAIN	++++ IMPACT ++++ FORCE (LBS)	ACCEL. (G)	++++++ ENERGY ++++++ KINETIC (IN-LB)	STRAIN (IN-LB)	RATIO (SE/KE)	
.06	.003	302789.	4.5	820250.	9462.	.012	
.13	.007	605578.	8.9	824500.	37849.	.046	
.19	.010	908367.	13.4	828750.	85159.	.103	
.25	.014	1211156.	17.8	833000.	151395.	.182	
.31	.017	1513945.	22.3	837250.	236554.	.283	
.38	.021	1816735.	26.7	841500.	340638.	.405	
.44	.024	2119524.	31.2	845750.	463646.	.548	
.50	.028	2422313.	35.6	850000.	605578.	.712	
6.60 .56	.031	2663649.	40.2 39.2	854250.	766477.	.895	1.000
.63	.035	2795468.	41.1	858500.	945299.	1.089	
.69	.038	2918785.	42.8	862750.	1113651.	1.291	
.75	.042	3020600.	44.4	867000.	1299101.	1.498	
.81	.045	3115911.	45.8	871250.	1490867.	1.711	
.88	.049	3199720.	47.1	875500.	1688230.	1.928	
.94	.052	3268016.	48.1	879750.	1890347.	2.149	
1.00	.056	3322852.	48.9	884000.	2096311.	2.371	
1.06	.059	3368141.	49.5	888250.	2305405.	2.595	
1.13	.063	3405105.	50.1	892500.	2517069.	2.820	
1.19	.066	3434966.	50.5	896750.	2730821.	3.045	
1.25	.069	3458947.	50.9	901000.	2946256.	3.270	
1.31	.073	3485609.	51.3	905250.	3163273.	3.494	
1.38	.076	3510295.	51.6	909500.	3381895.	3.718	
1.44	.080	3533871.	51.9	913750.	3601963.	3.942	
1.50	.083	3550540.	52.2	918000.	3823288.	4.165	
1.56	.087	3566507.	52.4	922250.	4045696.	4.387	
1.63	.090	3579974.	52.6	926500.	4269024.	4.608	
1.69	.094	3591146.	52.8	930750.	4493121.	4.827	
1.75	.097	3600227.	52.9	935000.	4717852.	5.046	
1.81	.101	3608955.	53.1	939250.	4943138.	5.263	
1.88	.104	3622825.	53.3	943500.	5169132.	5.479	
1.94	.108	3636220.	53.5	947750.	5395977.	5.693	
2.00	.111	3649162.	53.7	952000.	5623645.	5.907	

From the Table, the deformation at which all the impact energy is absorbed by the impact limiter may be calculated by interpolation. Even with the conservative assumptions regarding foam strength, the maximum impact limiter deflection resulting from a 1 foot flat end drop was calculated to be only 0.60 inches. Considering the depth of foam on the bottom part of the impact limiter, it is obvious that this impact limiter deformation is insignificant, and that the impact limiter would be expected to perform nearly elastically.

Impact loading for this case was found to be 40.2 g's, which is significantly less than that calculated for the cold foam case below.

2.6.7.1.2 Impact Forces

Table 2.6.7-4 presents the results from EYDROP for an impact limiter at -20°F, corresponding to the coldest service temperature the polyurethane foam in the package might experience under normal conditions. Foam properties assumed for -20°F were taken at the upper bound that might be expected at that temperature.

From the Table, the acceleration at which all the impact energy is absorbed by the impact limiter is calculated to be 62.7 g's. This load is well below that reported in Section 2.7.1.1.2 for the hypothetical accident free drop event.

2.6.7.1.3 Axial and Hoop Stresses in the Shells

The response of the cask steel shells and lead shielding to the normal end drop event is determined using both hand calculations and finite element analyses. The principal concern for the cask is with buckling of the inner shell, which is the containment structure. As shown by the following calculations, buckling will not occur as the result of the hoop and axial compressive stresses which develop in the cask inner shell under normal end drop conditions.

Various initial conditions can be assumed for the normal drop event. In

TABLE 2.6.7-4

EYDROP Results for -20°F Foam

EYDROP(END) NUPAC 10/140MB, COLD FOAM (-20 DEG), N.C.T.

PACKAGE WEIGHT = 68000. (LBS)
PACKAGE DIAMETER = 100.34 (IN)
HOLE DIAMETER = 55.00 (IN)
OVERPACK DEPTH = 18.00 (IN)
DROP HEIGHT = 1.00 (FT)

CRUSH DEPTH (IN)	STRAIN	++++ IMPACT ++++ FORCE (LBS)	ACCEL. (G)	++++++ ENERGY ++++++ KINETIC (IN-LB)	STRAIN (IN-LB)	RATIO (SE/KE)	
.06	.003	677915.	10.0	820250.	21185.	.026	
.13	.007	1355829.	19.9	824500.	84739.	.103	
.19	.010	2033744.	29.9	828750.	190664.	.230	
.25	.014	2711659.	39.9	833000.	338957.	.407	
.31	.017	3389573.	49.8	837250.	529621.	.633	
0.40 .38	.021	4067488.	62.7	59.8 841500.	762656.	.906	1.000
.44	.024	4745403.	69.8	845750.	1038057.	1.227	
.50	.028	5423317.	79.8	850000.	1355829.	1.595	
.56	.031	6066297.	89.2	854250.	1714880.	2.007	
.63	.035	6617923.	97.3	858500.	2111262.	2.459	
.69	.038	7126539.	104.8	862750.	2540776.	2.945	
.75	.042	7592145.	111.6	867000.	3000735.	3.461	
.81	.045	8014740.	117.9	871250.	3488450.	4.004	
.88	.049	8396328.	123.4	875500.	4001234.	4.570	
.94	.052	8717933.	128.2	879750.	4535992.	5.156	
1.00	.056	8992200.	132.2	884000.	5089433.	5.757	
1.06	.059	9229781.	135.7	888250.	5658870.	6.371	
1.13	.063	9434629.	138.7	892500.	6242133.	6.994	
1.19	.066	9610697.	141.3	896750.	6837300.	7.625	
1.25	.069	9761936.	143.6	901000.	7442694.	8.260	
1.31	.073	9914781.	145.8	905250.	8057592.	8.901	
1.38	.076	10055176.	147.9	909500.	8681653.	9.546	
1.44	.080	10179857.	149.7	913750.	9313998.	10.193	
1.50	.083	10289657.	151.3	918000.	9953670.	10.843	
1.56	.087	10385408.	152.7	922250.	10599766.	11.493	
1.63	.090	10467946.	153.9	926500.	11251433.	12.144	
1.69	.094	10538103.	155.0	930750.	11907872.	12.794	
1.75	.097	10596713.	155.8	935000.	12568335.	13.442	
1.81	.101	10644821.	156.6	939250.	13232289.	14.088	
1.88	.104	10716210.	157.6	943500.	13899978.	14.732	
1.94	.108	10776966.	158.5	947750.	14571640.	15.375	
2.00	.111	10832[illegible]	159.3	952000.	15246929.	16.016	

particular, a temperature must be assumed in order to establish an initial fabrication stress for the inner shell. A lower assumed temperature will result in a higher initial hoop stress on the inner shell (see Section 2.6.2) but higher allowable stresses. For purposes of this analysis, drops at 126°F (maximum lead normal temperature per Section 3.4.2), 75°F, and -20°F are considered.

To adequately bound the consequences of the drop event at a given temperature, two initial lead conditions are also considered. These are: (1) The lead shielding clings to the cask inner shell for the duration of the drop event; and (2) The lead shielding is free to slump during the drop event. For additional conservatism, two analyses will be performed to determine maximum stress states. The first will assume a uniform payload weight distribution on the bottom plate in the form of a pressure load. The same computational technique will then be used to determine cask stresses without the payload reaction, to find out if this is a potential worse-case condition.

(1) Stresses in the Cask Shells and Lead (Maximum Fabrication Stress Condition Assumed)

The first condition assumes that the lead has shrunk onto the inner shell and away from the outer shell. In addition, due to the combined effects of friction between the lead and inner shell, and axial shrinkage of the lead relative to the inner and outer shells, axial gaps will develop between the lead and the steel structures at the top and bottom end of the lead column. These axial gaps are important in that, until friction is overcome, under increased axial loading, the lead will impose a direct axial load on the inner shell.

Once friction is overcome, the lead will become supported at its base (the bottom of the lead column) and will grow radially outward due to the 'Poisson Effect' under increased axial loading. This radial growth will tend to relieve the initial fabrication hoop stress as the lead separates from the inner shell. If sufficient axial load develops, the lead would grow out to the outer shell creating tensile hoop stresses therein. Under further

loading, the lead would eventually begin to yield and flow back inward into the inner shell, thereby developing compressive hoop stresses in the inner shell. Since the primary mechanism of this load case would be to relieve stresses on the critical inner shell, it is not considered to be worst-case condition.

From Section 2.6.2, hoop stress in the inner shell due to fabrication is as follows:

Temperature (°F)	Inner Shell Hoop Stress (psi)	
128	-1,793	(extrapolated)
75	-2,041	
-20	-2,642	

Note:

The outer shell hoop stress is considered negligible since the lead separates from the outer shell upon cooling.

The equivalent pressure at the lead/inner shell interface is as follows:

$$p = \sigma t / r$$

Where:

$t = 0.75$ in

$r = 33.375$ in

Thus, the interface pressures at the different temperatures are:

Temperature (°F)	Interface Pressure, p (psi)
128	40.3
75	45.9
-20	59.4

With a coefficient of friction, f, for lead on stainless steel assumed to fall in the 0.5 to 1.0 range (Refer to Mark's Standard Handbook for Mechanical Engineers, 8th ed., 1978, (Reference 2.11.12), pp. 3-26), the load, P, which can be supported by friction at the lead/inner shell interface, may be determined as follows:

$$P = \pi DLpf$$

Where:

D = 67.5 in (inner shell outside diameter)

L = 77.5 in (lead column height)

p = interface pressure, psi

f = 0.5 to 1.0 (coefficient of friction)

Applying the interface pressures determined earlier, the total load which may be supported is:

Temperature (°F)	Coefficient of Friction	Load Supported (lbs)
128	0.5	331,090
	1.0	662,179
75	0.5	376,885
	1.0	753,769
-20	0.5	487,863
	1.0	975,727

Total lead weight can be calculated as:

$$W_L = \pi(R_{Oi}^2 - R_{Io}^2)L_C\rho_L$$

Where:

R_{Oi} = Outer Shell Inside Radius = 36.0 in

R_{Io} = Inner Shell Outside Radius = 33.75 in

L_c = Height of Lead Column = 77.5 in

ρ_L = Lead Density = 0.41 lb/in^3

$$W_L = \pi[(36.0)^2 - (33.75)^2](77.5)(0.41) = 15,666 \text{ lb}$$

At the Normal Conditions of Transport maximum lead temperature of 128°F, the maximum g-load which can be supported by friction is (662,179/15,666) = 40.6 g's. Since this exceeds the maximum temperature Normal Condition end drop load of 40.2 g's, it is possible that the entire lead weight would cling to the inner shell during the drop event at the maximum Normal Condition temperature. Likewise, at the minimum temperature of -20°F, maximum sustainable g-load is (975,727/15,666) = 62.3 g's. End drop acceleration at this temperature condition is 62.7 g's, which is very near the maximum sustainable load. It is clear, therefore, that lead cling is a possible load condition across the entire anticipated normal condition temperature range.

To conservatively bound the end drop event, the maximum g-load of 62.7 g's (derived at -20°F) will be used to calculate shell stresses (and accompanying bottom plate deflections), while the minimum applicable stress intensity and buckling stress allowables and material properties (derived at 128°F) will be used to evaluate Margins of Safety. The geometry to be addressed is as follows:

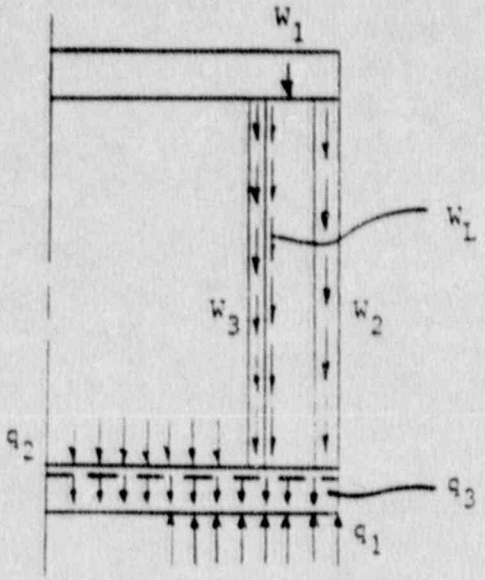

For calculating structural deflections, refer to Pilkey and Pin, Modern Formulas for Statics and Dynamics (Reference 2.11.13), Tables 11-1 and 11-2. Relevant structural weight components are:

W_1 = (Weight of top impact limiter and cask lid assembly) (62.7 g's)
= (14,000)(62.7) = 877,800 lbs

W_2 = (Weight of cask outer shell, thermal shield, etc.) (62.7 g's)
= (7,790)(62.7) = 488,430 lbs

W_3 = (Weight of cask inner shell) (62.7 g's)
= (3,510)(62.7) = 220,080 lbs

W_L = (Weight of lead) (62.7 g's)
= (15,666)(62.7) = 982,260 lbs

W_B = (Weight of bottom plate) (62.7 g's)
= (6,460)(62.7) = 405,040 lbs

q_2 = (Weight of payload) (62.7 g's)/$\pi(33.375)^2$
= (15,000)(62.7)/3,499.4 = 268.76 lb/in^2

$q_1 = [W_1 + W_2 + W_3 + W_L + W_B + q_2\pi(33.375)^2]/\pi(36.625^2 - 27.5^2)$
= 2129.2 lb/in^2

$q_3 = W_B/\pi(36.625)^2$
= 96.12 lb/in^2

Free-body diagrams of the outer cask inner and outer shells, and end plate are illustrated below:

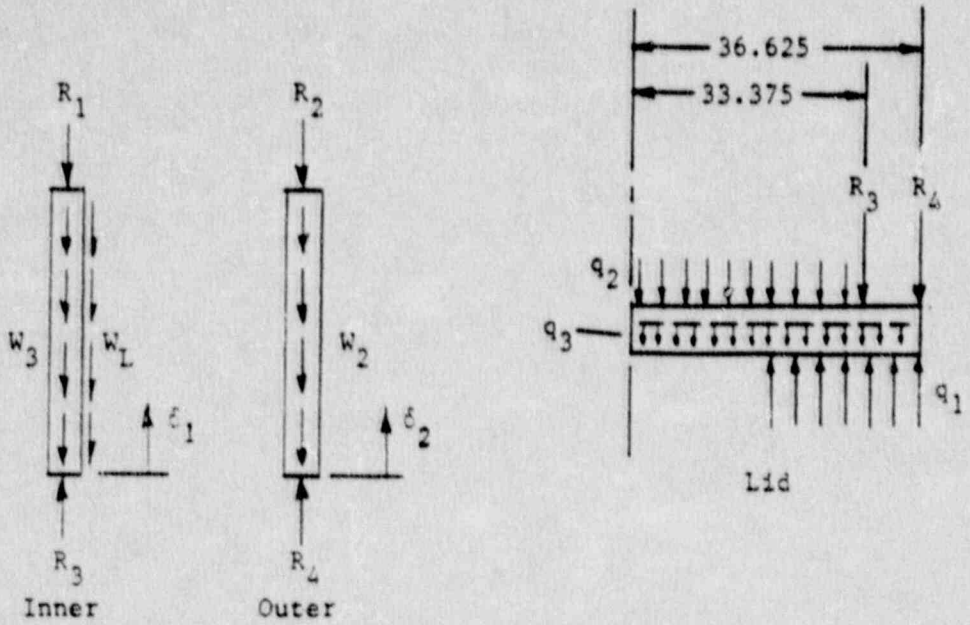

Assuming reaction R_3 does not affect the deflection of the lower end plate (conservative for maximum R_3), the differential deflection, $\delta_1 - \delta_2$, may be calculated. The analysis requires superposition of three pressure loads: q_1, due to the reaction force of the bottom impact limiter; q_2, due to the package payload; and q_3, due to the self-weight of the bottom plate. For the first load case, the differential deflection is:

$$\delta_1 - \delta_2 = y_c - M_c r^2/2D(1 + \mu) + F_v$$

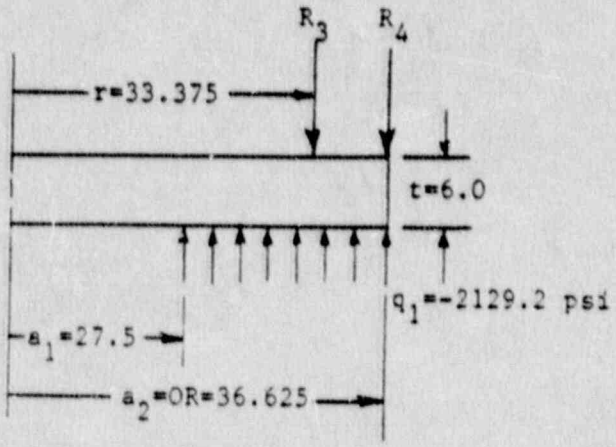

Where:

$$y_c = -\left[OR^2/2D(1 + \mu)\right]F_{M|r=OR} - F_{v|r=OR}$$

$$D = Et^3/\left[12(1 - \mu^2)\right]$$

$E = 28.0(10)^6$ psi (at 128°F)

$t = 6.0$ in (average lid thickness)

$\mu = 0.3$

$$D = 553.85(10)^6$$

$$F_{M|r=OR} = -(q_1/4)\left[F_{Mw1}(OR, a_1) - F_{Mw1}(OR, a_2)\right]$$

$$F_{Mw1}(OR,a_1) = \langle OR-a_1\rangle^0\left[(3+\mu)OR^2/4 - a_1^2 + (1-\mu)a_1^4/4OR^2 - (1+\mu)a_1^2\ln(OR/a_1)\right]$$

$OR = 36.625$ in.

$a_1 = 27.5$ in.

$\langle OR - a_1\rangle^0 = 1$ when $a_1 < OR$

$\langle OR - a_1\rangle^0 = 0$ when $a_1 \geq OR$

$$F_{Mw1}(OR,a_1) = 143.30$$

Similarly:

$$F_{Mw1}(OR,a_2) = 0, \text{ since } OR - a_2 = 0$$

Therefore:

$$F_M|_{r=OR} = 76,279$$

$$F_v|_{r=OR} = (q_1/8D)\left[F_{vw1}(OR,a_1) - F_{vw1}(OR,a_2)\right]$$

$$F_{vw1}(OR,a_1) = \langle OR - a_1\rangle^0\left[OR^4/8 - 5a_1^4/8 + a_1^2OR^2/2 - a_1^2(OR^2 + a_1^2/2)\ln(OR/a_1)\right]$$

$$F_{vw1}(OR,a_1) = 2,064.62$$

Similarly:

$$F_{vw1}(OR,a_2) = 0$$

$$F_v|_{r=OR} = -9.921(10)^{-4}$$

Then:

$y_c = -0.07007$ in. (positive downward)

$M_c = -F_M|_{r=OR} = -76,279$ in-lb/in

$$F_v = (q_1/8D)\left[F_{vw1}(r,a_1) - F_{vw1}(r,a_2)\right]$$

$$F_{vw1}(r,a_1) = \langle r - a_1\rangle^0 \left[r^4/8 - 5a_1^4/8 + a_1^2r^2/2 - a_1^2(r^2 + a_1^2/2)\ln(r/a_1)\right]$$

$$r = 33.375 \text{ in}$$

$$\langle r - a_1\rangle^0 = 1 \text{ when } a_1 < r$$

$$= 0 \text{ when } a_1 \geq r$$

$$F_{vw1}(r,a_1) = 376.81$$

Since $r < a_2$, $\langle r - a_2\rangle^0 = 0$ and $F_{vw1}(r,a_2) = 0$

$$F_v = -1.7675(10)^{-4}$$

Then:

$$\delta_1 - \delta_2 = -0.07007 - (-76,279)(33.375)^2/(2)(553.85(10)^6)(1.3) + (-1.7675(10)^{-4})$$

$$\delta_1 - \delta_2 = -0.01124 \text{ in (positive downward)}$$

The second load case represents the differential deflection due to the distributed payload pressure q_2.

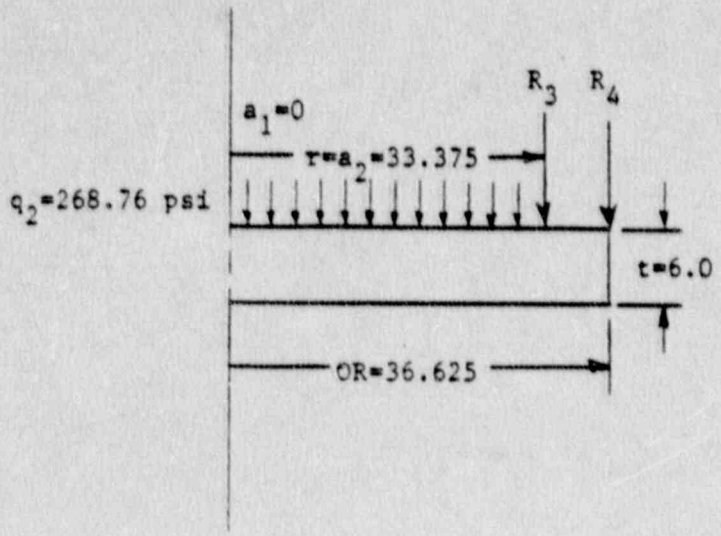

An analysis similar to that above yields a deflection of:

$\delta_1 - \delta_2 = 0.007301$ in (positive downward), and

$M_c = 73,007$ in-lb/in

The third load case represents the differential deflection due to an equivalent pressure q_3 of the bottom plate self-weight.

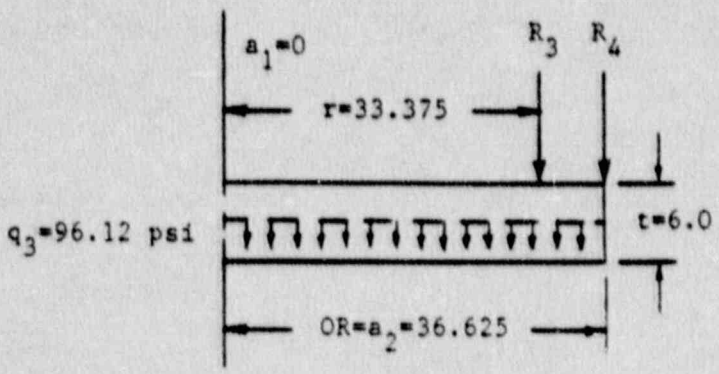

For this case, relative deflection at r = 33.375 in is:

$\delta_1 - \delta_2$ = 0.002686 in (positive downward), and

M_c = 26,593 in-lb/in

Superposition of the results of the three load cases yields:

$\delta_1 - \delta_2$ = -0.001253 in (positive downward)

M_c = 23,321 in-lb/in (positive for tension on bottom surface of base plate)

To neglect the effect of the payload on bottom plate deflections, the first and third load cases are superposed. Note that this conservatively assumes

that q_1 does not decrease when payload is eliminated. The resulting differential deflection and bending moment is:

$$\delta_1 - \delta_2 = -0.008554 \text{ in (positive downward)}$$

$$M_c = -44,686 \text{ in-lb/in (positive for tension on bottom surface)}$$

To obtain stresses in the cask inner and outer shells, the relative deflections obtained above will be utilized. The first case to be analysed will be that where full payload weight is applied as a uniform pressure load. The differential deflection for this case, as derived above, is $\delta_1 - \delta_2 = -0.001253$ in. It should again be emphasized at this point that this plate deflection is derived by conservatively ignoring the stiffening effect that the presence of the cask shells would induce. The bottom plate was analysed as simply-supported at the outer edge. This assumption corresponds to the finite element analysis procedure, which utilized the bottom-loading cask option (e.g., bottom lid configuration, with the bottom plate not rigidly attached to the cask walls).

The cask shell analysis will be performed by imposing these relatively large plate deflections on the shells as though shells and bottom plate were rigidly attached. As can be seen, this is a very conservative analysis procedure which maximizes both plate and shell stresses, while analytically bounding both the fixed-bottom and bottom-loading cask geometries.

From the free-body diagrams for the cask inner and outer shells, and axial stiffness relations for the shells ($\delta = PL/AE$ for an end load, and $\delta = PL/2AE$ for self-weight, i.e., distributed load), the deflections, δ_1 and δ_2, and reactions, R_3 and R_4, may be found:

$$\delta_1 = R_3 L/A_1E_1 - (W_3 + W_L)L/2A_1E_1$$

$$\delta_2 = R_4 L/A_2E_2 - W_2 L/2A_2E_2$$

Where:

$L = 77.5$ in

$$A_1 = \pi[(33.75)^2 - (33.0)^2]$$
$$= 157.28 \text{ in}^2$$

$$A_2 = \pi[(37.25)^2 - (36.0)^2]$$
$$= 287.65 \text{ in}^2$$

$$E_1 = 28.0(10)^6 \text{ psi (at } 128^\circ\text{F)}$$

$$E_2 = 29.2(10)^6 \text{ psi (at } 128^\circ\text{F)}$$

Then:

$$\delta_1 = (1.760(10)^{-8})R_3 - 0.01058$$

$$\delta_2 = (9.227(10)^{-9})R_4 - 0.00225$$

and:

$$R_3 + R_4 = W_1 + W_2 + W_3 + W_L = 2,568,570 \text{ lbs}$$

or:

$$R_4 = 2,568,570 - R_3$$

Solving simultaneously:

$$R_3 = 1,240,660 \text{ lbs}$$

$$R_4 = 2,568,570 - 1,240,660 = 1,327,910 \text{ lbs}$$

Therefore, assuming full payload reaction on the bottom plate, the axial compressive stress in the cask inner shell, σ_1, and outer shell, σ_2, is:

$$\sigma_1 = R_3/A_1 = 7,888 \text{ psi}$$

$$\sigma_2 = R_4/A_2 = 4,616 \text{ psi}$$

Using the same analysis procedure, shell stresses for the case where payload

reaction is ignored, can be derived as:

$$\sigma_1 = 9,619 \text{ psi}$$

$$\sigma_2 = 3,670 \text{ psi}$$

From Section 2.6.2, worst-case inner shell hoop stress for Normal Condition of Transport temperatures is -2,462 psi at -20°F. Conservatively taking radial stress (pressure) as zero, maximum inner shell stress intensity becomes:

$$S.I._1 = 0 - (-9,619) = 9,619 \text{ psi}$$

From Table 2.1.2-1, reference case number 1(A), the allowable membrane stress limit for the inner shell material is S_m = 20,000 psi at 128°F (Refer to Table 2.3-1). Stress Margin of Safety is therefore:

$$M.S. = 20,000/9,619 - 1 = +1.08$$

From Table 2.1.2-3, at 128°F, inner shell buckling allowables are 19,062 psi (axial) and 17,905 psi (hoop). Buckling Margin of Safety is thus:

$$M.S. = 1/\left[(9,619/19,062) + (2,462/17,905)\right] - 1$$
$$= +0.56$$

From Section 2.6.2, the outer shell will not be in contact with the lead, and will, therefore, undergo axial stress only.

$$S.I._2 = 0 - (-4,616) = 4,616 \text{ psi}$$

Table 2.1.2-2, reference case number 1(A), yields an allowable membrane stress (for non-containment componenets) of S_y = 37,200 psi (greater than S_m = 23,250) at 128°F. Stress Margin of Safety is thus:

$$M.S. = 37,200/4,616 - 1 = +7.06$$

Table 2.1.2-4 yields an axial compression buckling allowable of 22,728 psi at

128°F, for a Margin of Safety of:

$$M.S. = 1/(4,616/22,728) - 1 = +3.92$$

Therefore, the cask inner and outer shell structures are both well in excess of regulatory requirements for the Normal Conditions of Transport end drop event when the lead shielding is completely supported by the inner shell.

(2) Stresses in the Outer Cask Shells and Lead (Zero Fabrication Stress Condition Assumed)

The second initial lead condition assumes that the fabrication stress has fully crept away, resulting in a stress free column of lead just in contact with the inner and outer shells. This is a potential worst case, since any axial load imposed on the lead will directly load, radially, both the inner and outer shells (i.e., the lead need not flow away from the inner shell, into the outer shell and back into the inner shell to develop a compressive hoop stress in the inner shell).

For this condition, initial stresses in the lead and the steel shells are taken as zero. As axial load is applied to the lead and shells, the lead will attempt to move downward and outward and develop pressures on both the inner and outer shells.

Under acceleration, the lead column will experience a linearly increasing axial stress distribution from top to bottom:

$$\sigma_z = \gamma \rho_L z$$

Where:

σ_z = Lead Axial Stress (psi)

γ = Acceleration (g's)

ρ_L = Lead Density = 0.41 lb/in^3

z = Distance Down From Top of Lead Column (in)

However, from the lead stress-strain curves shown in Figures 2.3-1 and 2.3-2, it is apparent that, as the lead reaches a stress level around its yield point, the stress will tend to remain fairly uniform under continued loading. The resulting axial stress distribution can thus be illustrated as follows:

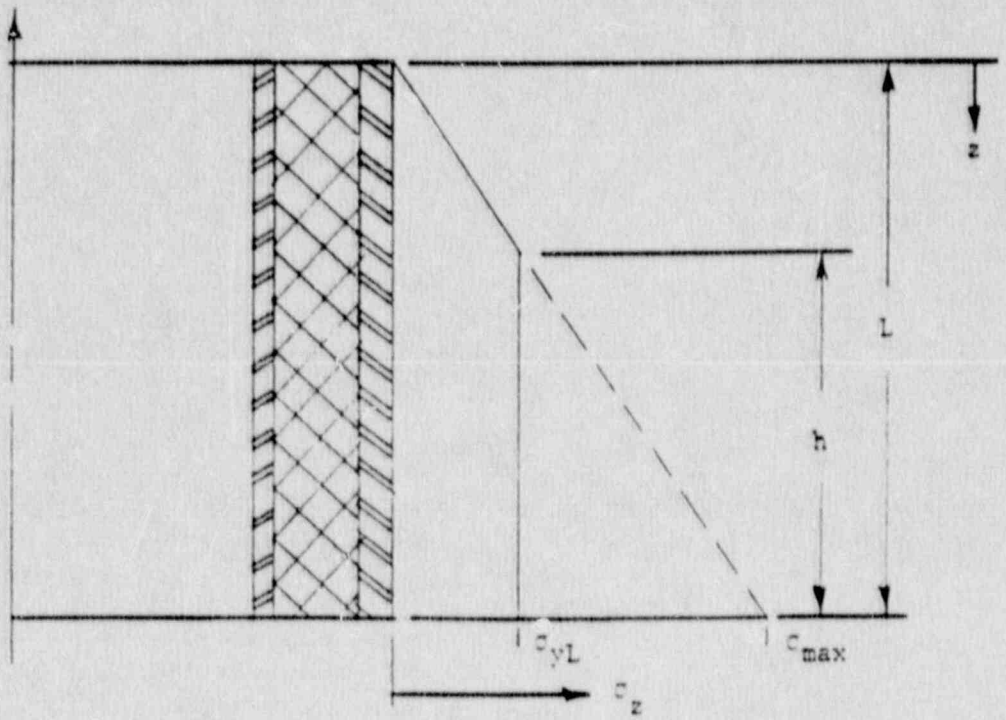

Where:

σ_{yL} = Yield Strength of Lead (psi)

σ_{max} = Maximum Stress at Applied Acceleration for Fully Elastic Material (psi)

L = Lead Column Height = 77.5 in

The height h at which the lead reaches its yield point can be found by:

$$L - h = \sigma_{yL}/\gamma\rho_L$$

Or:

$$h = L - \sigma_{yL}/\gamma\rho_L$$

For the maximum Normal Condition of Transport end drop acceleration of 62.7 g's, h becomes:

$$h = 77.5 - 600/(62.7)(0.41) = 54.16 \text{ in.}$$

Where σ_{yL} is conservatively taken as 600 psi, the approximate yield strength of lead at 128°F.

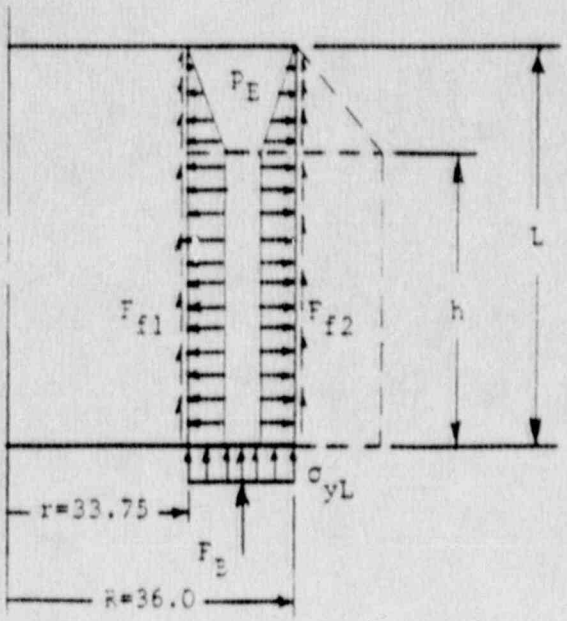

The sum of the axial forces acting on the lead column may now be expressed as:

$$W_L = F_B + F_{f1} + F_{f2}$$

Where:

$W_L = (15,666)(62.7) = 982,260$ lb.

$F_B = (600)\pi(36.0^2 - 33.75^2) = 295,820$ lb.

F_{f1} = Frictional Reaction Force of Inner Shell

F_{f2} = Frictional Reaction Force of Outer Shell

The above frictional forces result from radial forces exerted by the lead column onto the steel shells. These radial forces will be a function of the lead-to-steel coefficient of friction. Conservatively assuming the minimum friction coefficient of 0.5, the net radial forces become:

$F_{R1} = F_{f1}/0.5$, or $F_{f1} = 0.5\ F_{R1}$

$F_{R2} = F_{f2}/0.5$, or $F_{f2} = 0.5\ F_{R2}$

These radial forces can then be expressed in terms of a lead maximum radial pressure, p_E, which is assumed to be equal on both shells. For uniform pressure p_E in the lead yield region and linearly varying pressure in the lead elastic region, the radial force on the inner shell may be expressed as:

$$F_{R1} = p_E \pi D_1 h + 0.5\ p_E \pi D_1 (L-h)$$

Where:

D_1 = Inner shell outside diameter = 67.5 in

Or:

$$F_{R1} = 0.5\ p_E \pi D_1 (L+h)$$

From which:

$$F_{f1} = 0.25\, p_E \pi D_1\, (L+h)$$

Likewise, for the outer shell:

$$F_{f2} = 0.25\, p_E \pi D_2\, (L+h)$$

Where:

D_2 = Outer shell inside diameter = 72.0 in

The lead equilibrium equation may now be re-written as:

$$W_L - F_B = 0.25 \pi p_E\, (D_1 + D_2)\, (L+h)$$

or:

$$p_E = 4(W_L - F_B)/\left[\pi(D_1 + D_2)\, (L+h)\right]$$

Substituting in the proper terms, the equivalent shell pressure becomes:

$$p_E = 47.59 \text{ psi}$$

Therefore, the inner shell compressive hoop stress is:

$$\sigma_1 = -p_E R_1/t_1$$
$$= -(47.59)(33.375)/(0.75) = -2,118 \text{ psi}$$

The outer shell tensile hoop stress is:

$$\sigma_2 = p_E R_2/t_2$$
$$= (47.59)(36.625)/(1.25) = 1,394 \text{ psi}$$

To evaluate axial stresses in the shells, a similar approach to the previous analysis is utilized. Appropriate frictional forces are added to the inner and outer shells, and an applied pressure load q_4, representing the force to yield the lead column, is added to the bottom plate between the inner and

outer shells. From the above analysis, shell frictional forces may be calculated:

F_{f1} = 332,172 lbs

F_{f2} = 354,317 lbs

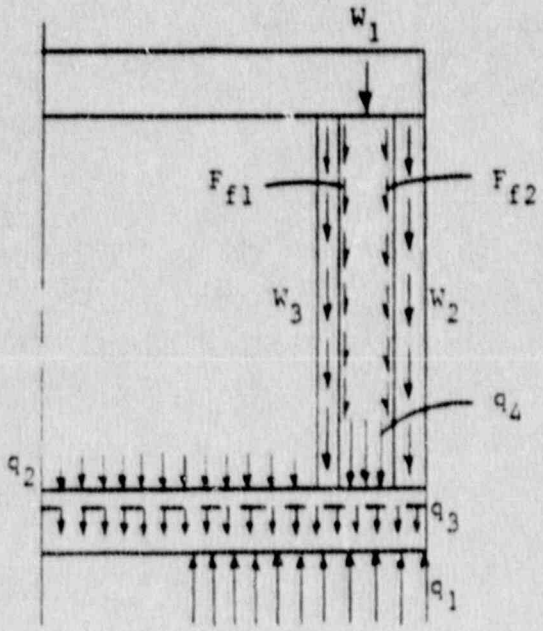

For this evaluation:

$q_4 = F_B/\pi(36.625^2 - 33.375^2) = 413.9$ psi

Repeating the previous calculational approach, and taking q_4 into account:

$\delta_1 - \delta_2 = -0.008229$ in (positive downward) for no payload reaction.

$\delta_1 = R_3L/A_1E_1 - (W_3 + F_{f1})L/2A_1E_1$

$$\delta_2 = R_4 L/A_2E_2 - (W_2 + F_{f2})L/2A_2E_2$$

$$R_4 = W_1 + W_2 + W_3 + F_{f1} + F_{f2} - R_3$$
$$= 2,272,800 - R_3$$

Also, the bending moment at the center of the plate for this pressure load combination is:

M_c = -47,609 in-lb/in (positive for tension on bottom surface)

Solving simultaneously, inner shell reaction load becomes:

R_3 = 1,124,730 lbs

Thus, outer shell reaction is:

R_4 = 1,148,070 lbs.

Therefore, assuming no payload reaction on the bottom plate, compressive axial stresses on the inner and outer shell are:

$\sigma_1 = R_3/A_1$ = 7,151 psi

$\sigma_2 = R_4/A_2$ = 3,991 psi

With payload reaction pressure q_2, the following results:

$\delta_1 - \delta_2$ = -0.000928 in. (positive downward)

M_c = 25,398 in-lb/in (positive for tension on bottom surface)

Resulting compressive axial stresses for the inner and outer shells are:

σ_1 = 5,421 psi

σ_2 = 4,937 psi

Conservatively ignoring shell radial pressure loading, the maximum inner shell stress intensity is:

$$S.I._1 = 0 - (-7,151) = 7,151 \text{ psi}$$

From the previous section, the stress allowable for the inner shell at 128°F is S_m = 20,000 psi. The stress Margin of Safety is thus:

$$M.S. = 20,000/7,151 - 1 = +1.80$$

The maximum inner shell hoop stress which would arise due to lead slump, as calculated above, is -2,118 psi. This is less than the inner shell hoop stress due to fabrication, as derived in Section 2.6.2. This value, which is -2,462 psi, will be used for the inner shell buckling evaluation.

Buckling allowables at 128°F are 19,062 psi (axial) and 17,905 psi (hoop). Buckling Margin of Safety is then:

$$M.S. = 1/\left[(7,151/19,062) + (2,462/17,905)\right] - 1 = +0.95$$

Maximum stress intensity of the outer shell is:

$$S.I._2 = 1,394 - (-4,937) = 6,331 \text{ psi}$$

With an allowable stress intensity of 37,200 psi at 128°F, the Margin of Safety becomes:

$$M.S. = 37,200/6,331 - 1 = +4.88$$

The axial buckling allowable at 128°F is 22,728 psi, and the buckling Margin of Safety is thus:

$$M.S. = 1/(4,937/22,728) - 1 = +3.60$$

This analysis indicates that the cask inner and outer shells will not be

adversely affected by the Normal Conditions of Transport end drop event with no fabrication stresses present in the lead shielding.

It should be noted that the assumptions made regarding the response of the lead shielding to end drop impact loads are approximations only. Prediction of the actual state of the lead is difficult to achieve by classical analysis techniques. To more accurately analyze the complex interaction of lead shielding with inner and outer steel shells during the end drop event, a finite element analysis was conducted with the ANSYS program. Details of this program are given in Appendix 2.10.2, the analysis results are shown in Appendix 2.10.6, and these results are summarized below.

While the minimum temperature condition for the drop event (-20°) induces the highest acceleration loading (62.7 g's), the material properties and buckling and stress intensity allowables are also at a maximum (refer to Sections 2.1 and 2.3 for details). Likewise, though the maximum temperature case results in lower impact loads (a maximum of 40.2 g's), material properties and buckling and stress intensity allowables are also reduced at the higher temperature condition. Refer to Section 2.1.2.4, Impact Limiter Design Criteria, as well as Sections 2.6.7.1.1 and 2.6.7.1.2 above for details of the effects of temperature variation on drop loads.

To conservatively bound the buckling and stress allowable calculations, the maximum g-load (obtained at the minimum temperature condition) was applied to the analysis while utilizing reduced material strength properties (found at the higher temperature), which will tend to maximize stresses. Therefore, the analysis utilized material properties based on a maximum expected normal condition of transport temperature of 128°F at the inner shell.

The smaller buckling and stress allowable values found at the higher temperature were then used to derive Margins of Safety. Thus, maximum possible loads were combined with minimum possible material strength conditions for a worst-case analysis and minimum possible Margins of Safety.

The results of the stress and buckling analyses for Normal Conditions of

Transport, detailed in Appendix 2.10.6, are summarized in Tables 2.6.7-5 and 2.6.7-6. Modelling assumptions used for the finite element analysis, and justification for their use, are detailed in Section 2.7.1.1.3.

As a point of interest, it should be noted that the finite element results indicate that inner and outer shell hoop stresses under end drop loading increase gradually from the top (non-impacted) end of the cask to a point approximately one-third of the way down. They then tend to remain fairly uniform down to the bottom (impacted) end of the cask. These results provide further justication for the lead slump pattern assumed in the hand calculations above.

2.6.7.1.4 Lid Stresses

The lid analyses performed for Normal Conditions of Transport utilize the same finite element techniques as outlined in Section 2.7.1.1.4 for the Hypothetical Accident Condition 30 foot drop. Note that the worst case impact under normal conditions is only 38.2% of the worst case for accident conditions (62.7/164.0 = 0.382, where 164.0 is the worst case accident condition g-load). Since the allowable membrane stress for normal conditions, derived at the same temperature as for accident conditions, is 41.7% of the accident allowable (S_m verses $2.4S_m$), and allowable bending stress is 43.6% ($1.5S_m$ versus S_u), then clearly the normal condition margins of safety will always be larger than the accident margins of safety for the lid during end impact.

A summary of the lid stresses and margins of safety during the normal condition 1 foot end drop is given below as Table 2.6.7-7. The Table is derived from lid analysis results detailed in Appendix 2.10.7. Allowable normal condition stresses are derived from column (A) of Table 2.1.2-1, in conjunction with Table 2.3-1. It should be noted that, since the lids are not directly attached to the cask shells, but instead pivot on the EnviroSeal^{tm} plates, their resonse to end drop loading will be independent of the state of the lead shielding (e.g., either clinging or slumping under load).

TABLE 2.6.7-5

End Drop Finite Element Shell Stress Analysis
Results Summary

Drop Load = 65 g's
(Actual Drop Load = 62.7 g's at -20°F)

Material Properties and Stress Allowables Temperature = 128°F

Maximum Inner Shell Stress Intensities		Maximum Outer Shell Stress Intensities	
Surface (Element 51)	Membrane (Element 51)	Surface (Element 60)	Membrane (Element 66)
7,524 psi	6,498 psi	7,596 psi	5,775 psi
Stress Intensity Allowables*		Stress Intensity Allowables**	
30,000 psi	20,000 psi	37,200 psi	37,200 psi
Margins of Safety		Margins of Safety	
+ 2.99	+ 2.08	+ 3.90	+ 5.44

* Interpolated from Table 2.1.2-1

** Interpolated from Table 2.1.2-2

TABLE 2.6.7-6
(Page 1 of 2)

End Drop Finite Element Shell Buckling Analysis
Results Summary

Drop Load = 65 g's
(Actual Drop Load is 62.7 g's at -20°F)

Material Properties and Stress Allowable Temperature = 128°F

Maximum Inner Shell Stresses		Maximum Outer Shell Stress
Axial	Hoop	Axial
(Element 57)		(Element 42)
-6,462 psi	-2,558 psi	-5,663 psi
Buckling Allowables*		Buckling Allowable**
19,062 psi	17,905 psi	22,728 psi
Margin of Safety		Margin of Safety
+ 1.08		+ 3.01

TABLE 2.6.7-6
(Page 2 of 2)

Banding (Element 51)	Banding (Element 60)
7,524 psi	7,596 psi
Buckling Allowable*	Buckling Allowable**
19,182 psi	22,793 psi
Margin of Safety	Margin of Safety
+ 1.55	+ 2.00

* Interpolated from Table 2.1.2-3

** Interpolated from Table 2.1.2-4

TABLE 2.6.7-7

End Drop Finite Element Lid Stress Analysis

Results Summary

	Lid	Max. Bending Stress (psi) (Margin of Safety)	Max. Membrane Stress (psi) (Margin of Safety)	Max. Primary Bolt Stress (psi) (Margin of Safety)	Max. Secondary Bolt Stress (psi) (Margin of Safety)
With Payload Reaction	Bottom	8788 (M.S. = +2.41)	6105 (M.S. = +2.28)	448 (M.S. = +Large)	---
	Top	13378 (M.S. = +1.24)	8514 (M.S. = +1.35)	5740 (M.S. = +Large)	43487 (M.S. = +0.58)
Without Payload Reaction	Bottom	5293 (M.S. = +4.67)	3618 (M.S. = +4.53)	3774 (M.S. = +Large)	---
	Top	5656 (M.S. = +4.30)	5415 (M.S. = +2.69)	4853 (M.S. = +Large)	16556 (M.S. = +3.15)

For the case of the fixed bottom configuration, the previously determined moments (Section 2.6.7.1.3) can be directly used to arrive at the maximum bending stress at the center of the end plate. The maximum moment at the center of the end plate was determined to be:

M_c = 49,686 in-lb/in (no payload, lead cling)

The corresponding bending stress is therefore:

$\sigma_B = 6M_c/t^2 = 8,281$ psi

Where t = 6.0 in (average bottom plate thickness)

With an allowable stress of $1.5S_m$ = 30,000 psi, the corresponding Margin of Safety becomes:

M.S. = 30,000/8,281 - 1 = +2.62

From the results generated in this section, it is apparent that the lids and bottom plate of the 10/140MB can withstand any worst-case 1 foot end drop.

2.6.7.1.5 Primary and Secondary Lid Bolts

From the finite element lid analysis results presented in Appendix 2.10.7 and summerized above in Section 2.6.7.1.4, it was found that neither the top or bottom primary lid closure bolts exceed their tensile prestress during the end impact event, with the full payload present. Without payload, the bottom lid bolts maintain a loading somewhat lower than their preload, while top lid bolts slightly exceed their preload value. The maximum bolt load (top lid, without payload) is 19,410 lb per bolt. This value will thus be taken as a worst case for normal condition end drops. The resulting stress on the 4.0 in^2 tensile stress area is thus:

σ_{bolt} = 19,410/4.0 = 4,853 psi

The material for all 10/140MB containment closure bolts is ASTM A-320 Grade

L43. The Margin of Safety on the allowable stress of $2S_m$ (taking S_m as 34,360 psi for ASTM A-320 Grade L43 at 133°F), is:

M.S. = 68,720/4,853 - 1 = + Large

From Section 2.5.1.1, it was determined that, for primary bolt loads, the most critically loaded bolt lug would be the lug attached to the cask body. In that Section, a bending stress intensity of 3,997 psi was calculated for a lifting load imposed on the bolts of 25,500 lb. For a bolt load of 19,410 lb, this stress intensity would be (19,410/25,500)(3,042) = 2,665 psi. The allowable membrane plus bending stress for the A-517 Grade 70 lug material is $1.5S_m$ = (1.5)(23,237) = 34,855 psi at a temperature of 133°F. The bolt lug Margin of Safety for bolt preload is then:

M.S. = 34,855/3,042 - 1 = + Large

Primary bolt loads will therefore not be a consideration for normal condition flat end drops.

The stresses in the secondary lid bolts are also derived from the lid analysis results given in Appendix 2.10.7 and summarized in Section 2.6.7.1.4 above. The maximum load in the secondary lid bolts from a 65 g impact acceleration was determined to be 42,139 lb, for the case of a top down impact with full payload present and 6.8 psig internal pressure. This results in a stress on the 0.969 in^2 tensile stress area of:

σ_{bolt} = 42,139/0.969 = 43,487 psi

Including the load in the bolts due to the normal condition maximum pressure is conservative for two reasons: (1) The maximum internal pressure occurs at a temperature for which the impact accelerations are considerably lower; and (2) The pressure load, being less than the bolt preload, will not actually result in additional bolt loading.

The margin of safety on the allowable stress of 2 S_m (taking S_m as 34,360 psi for ASTM A-320 Grade L43 at 133°F), is:

M.S. = 68,720/43,487 - 1 = +0.58

2.6.7.1.6 EnviroSeal[tm] Plate Bearing Stresses

In Section 2.7.1.1.6 below, positive Margins of Safety are calculated for bearing stresses on EnviroSeal[tm] plates and mating surfaces. Since the allowable stress (S_y) is the same for normal conditions as for accident conditions, with materials being evaluated at the same temperature, while imposed loads are considerably less, it may readily be seen that Margins of Safety for normal conditions will be much greater than for the more extreme accident condition loading. Therefore, bearing stresses in seal areas are of no consequence to package performance for Normal Conditions of Transport.

From all the above analyses, it is evident that Normal Conditions of Transport end drop will have no detrimental effect on the 10/140MB Cask integrity.

2.6.7.2 Oblique Impact

Analysis of the NuPac 10/140MB package behavior during normal condition drops from 1 foot proceeds in the following steps, using the same conservative assumptions made in the analysis of the hypothetical accident 30 foot drop event discussed in Section 2.7.1.2 below.

1. Use CYDROP to determine worst-case impact limiter deformations for minimum foam properties.

2. Use CYDROP with the highest (coldest) foam stress-strain data to determine a conservative estimate of the force-deflection relationship of the 10/140MB impact limiter design at various impact angles. This force deflection relationship is identical to the one used (and discussed in detail) for the analysis of the hypothetical 30 foot drop (see Section 2.7.1.2.2).

3. Use the OBLIQUE program to determine internal forces in the cask body. Geometry assumptions will be the same as used in Section 2.7.1.2.3 below.

4. Determine the worst case stress state from internal forces in the cask body.

5. Determine lid attachment forces and stresses in the lid closure system under-worst conditions. The OBLIQUE program will be utilized in the same conservative manner as outlined in Section 2.7.1.2.5.

2.6.7.2.1 Worst Case Corner Deformations

Under normal conditions as defined by 10 CFR 71, the polyurethane foam-filled impact limiters may range in temperature from -20°F to 169°F during normal operations. It is clear from an examination of the stress-strain properties of the polyurethane foam at various temperatures that the highest impact limiter deformations will occur at the highest temperature extreme, and that the highest impact forces would develop at the lowest temperature extreme.

Tables 2.6.7-8 and 2.6.7-9 present the output from NuPac's CYDROP energy balance program for impact limiters of 96-inch and 101-inch diameters, assuming an impact angle corresponding to the c.g. over struck corner cask. Foam properties are taken at the maximum temperature for Normal Conditions of Transport, 169°F. The two impact limiter diameters chosen for analysis provide a conservative estimate of the deformation which would occur in the actual impact limiter should it be subjected to this event. A more complete discussion of the conservative nature of these analyses appears in Section 2.7.1.2.1. The assumed geometries of the impact limiter appear in Figures 2.6.7-2 (96-inch diameter) and 2.6.7-3 (101-inch diameter).

The Tables show that a normal condition drop event would be expected to result in less than 8 inches of deformation under the worst conditions. Compared to the depth of foam in the impact limiters, and considering the conservatism of the analysis approach, this deflection can be considered inconsequential.

2.6.7.2.2 Force - Deflection Relationship

As stated above, the conservative force-deflection relationship for normal conditions is identical to the the hypothetical accident force-deflection relation, since the relationship is a function of impact limiter geometry, not drop height. A complete discussion on the conservative and reasonable nature of the force-deflection relationship used for the 10/140MB oblique impact analysis is presented in Section 2.7.1.2.2. The assumed impact limiter geometry used for developing the force-deflection relationship is shown in Figure 2.6.7-4.

2.6.7.2.3 Internal Forces During Oblique Impact

Cask internal forces are calculated by NuPac's OBLIQUE computer program, discussed in Appendix 2.10.3. The force-deflection relationship calculated using the assumptions presented in Section 2.7.1.2.2 was used in conjunction with the physical properties of the package calculated in Section 2.7.1.2.3 by OBLIQUE to determine a conservative estimate of cask internal forces. As

Table 2.6.7-8

Proprietary

Table 2.6.7-9

Proprietary

FIGURE 2.6.7-2

Impact Limiter Assumed Geometry for Center of Gravity Over Struck Corner Drop - 96 Inch Diameter Impact Limiter

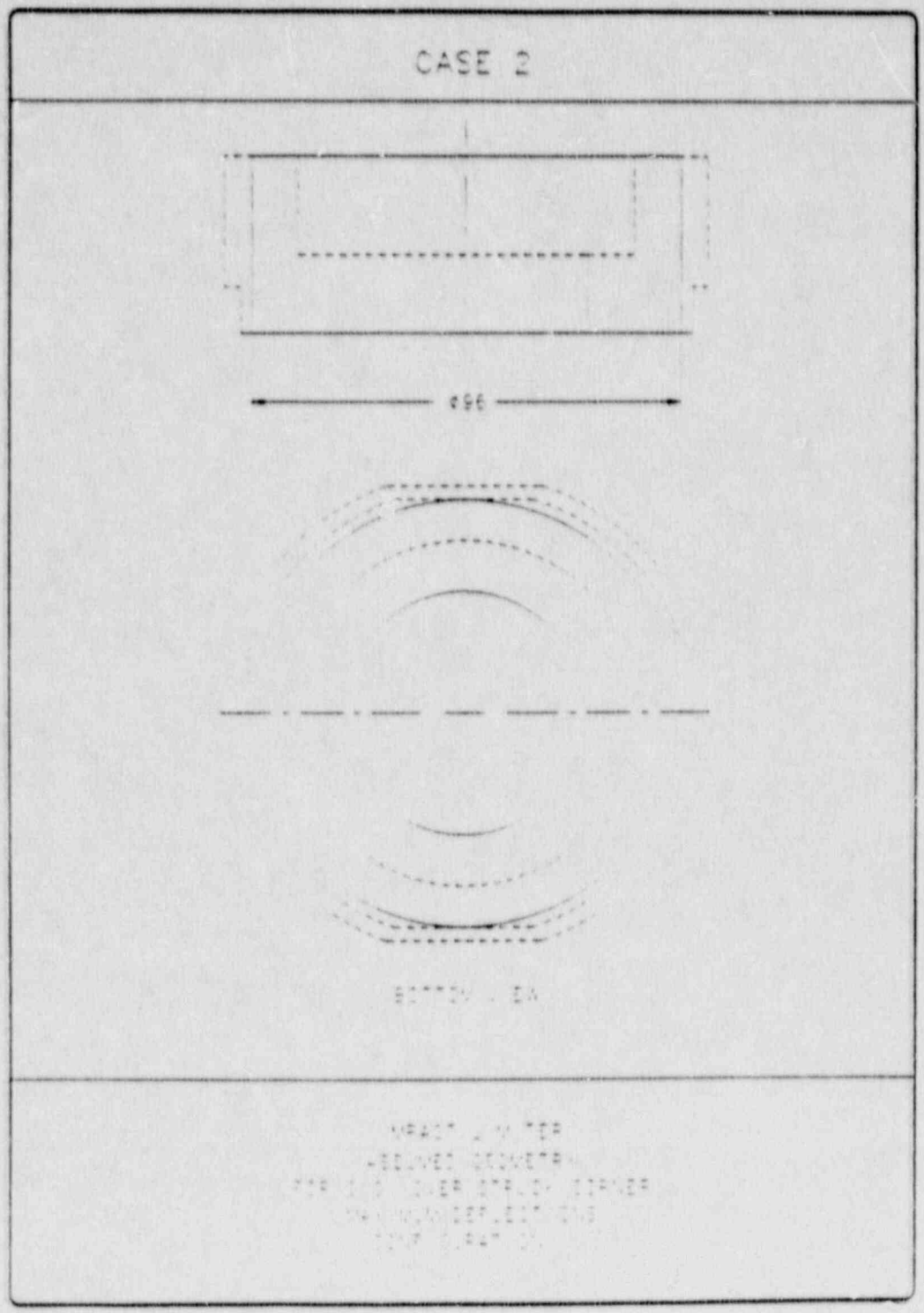

FIGURE 2.6.7-3

Impact Limiter Assumed Geometry for Center of Gravity Over Struck Corner Drop - 101 Inch Diameter Impact Limiter

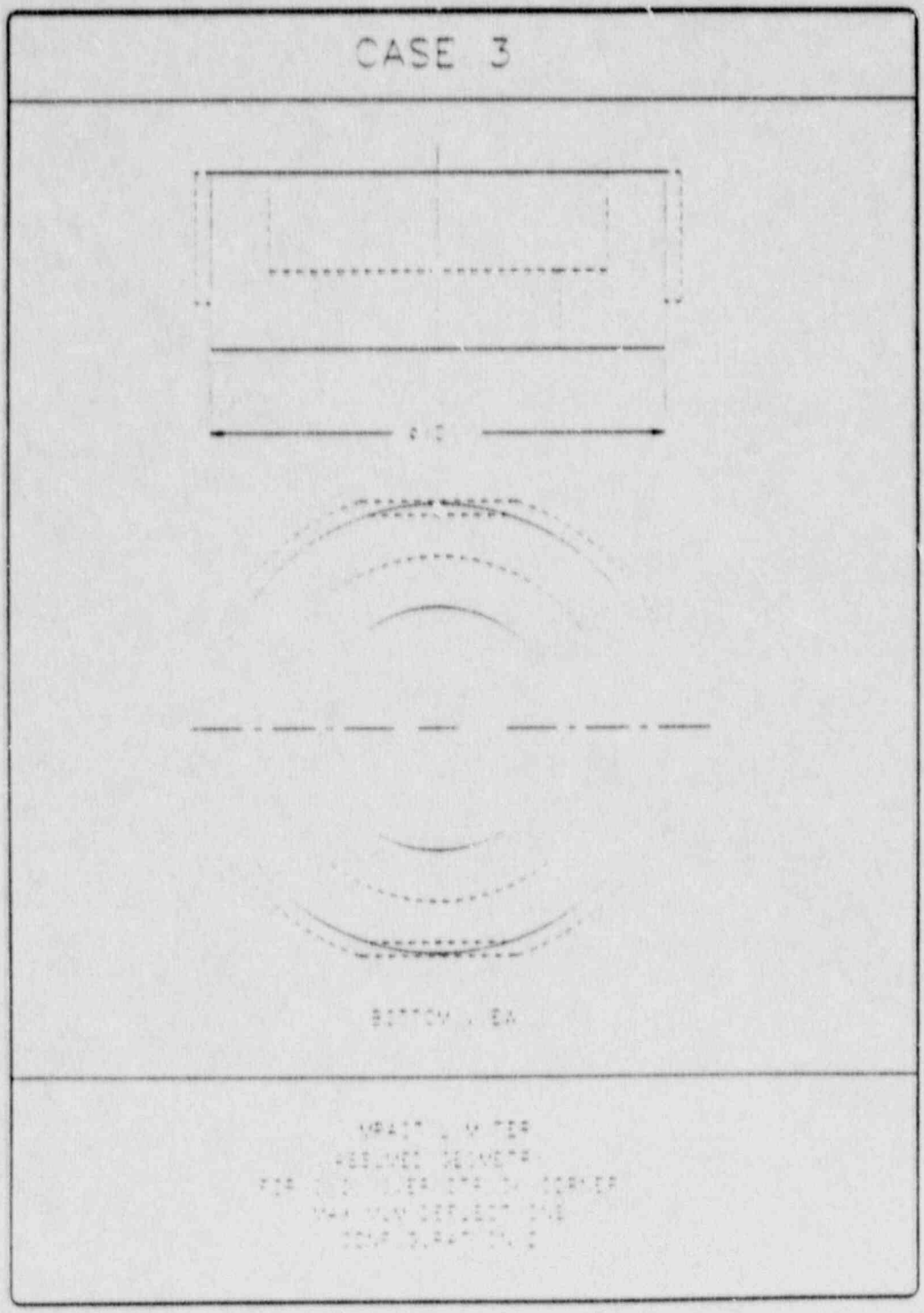

FIGURE 2.6.7-4

Impact Limiter Assumed Geometry for Oblique Drops
To Maximize Impact Forces

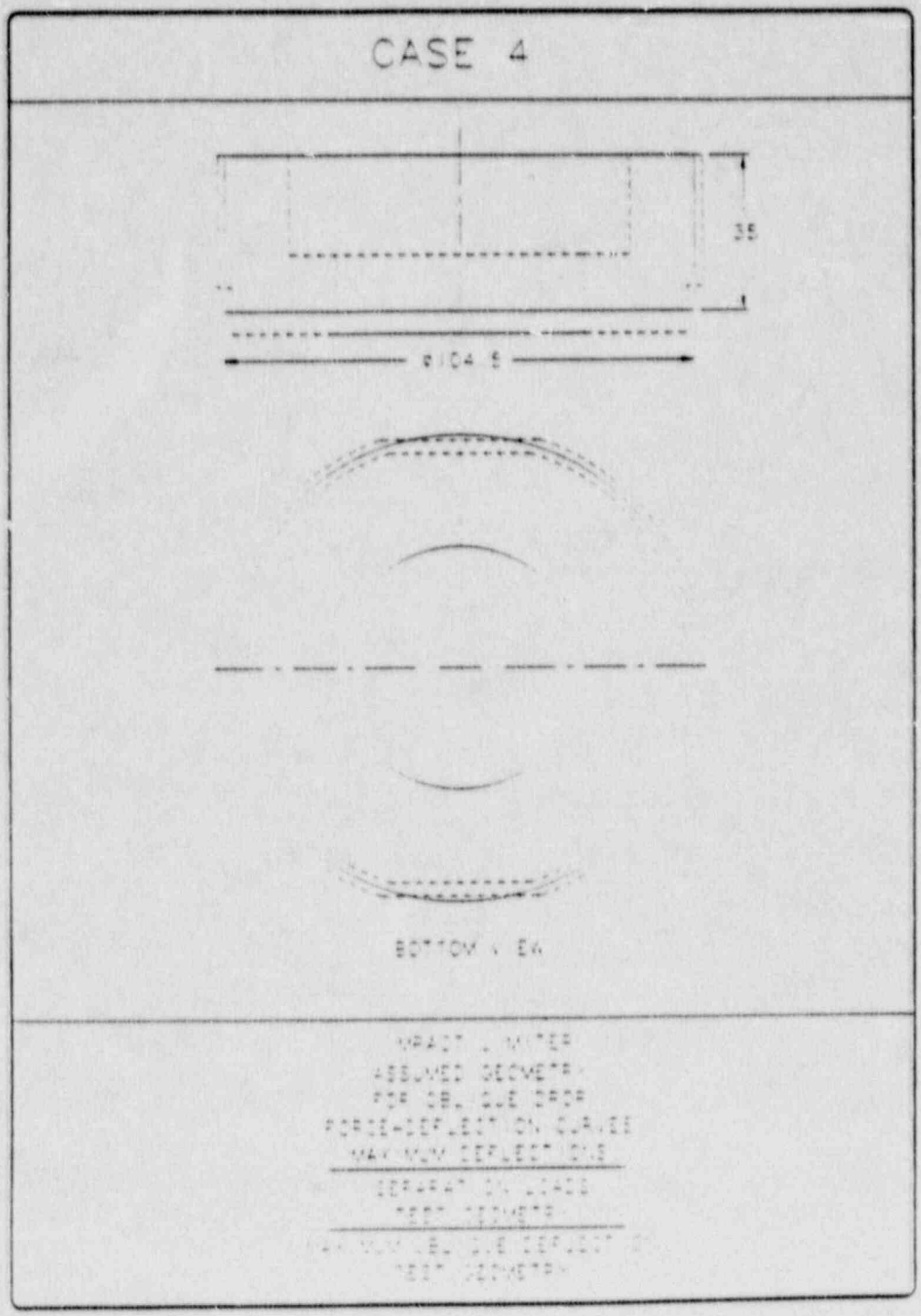

explained in that section, a maximum diameter impact limiter will tend to increase cask body forces for oblique impacts at drop angles where load combinations will be maximum. The assumed impact limiter geometry used for developing maximum cask internal loading is shown in Figure 2.6.7-5.

Table 2.6.7-10 presents a summary of these internal forces calculated by OBLIQUE for a drop of 1 ft. The forces and moments are presented graphically in Figures 2.6.7-6 (internal forces) and 2.6.7-7 (cask bending moments). Not surprisingly, the internal forces for a drop from one foot are very much less than for a drop from 30 feet (refer to Section 2.7.1.2.3).

2.6.7.2.4 Stress Calculations in Cask Body

From the summary of internal forces in Table 2.6.7-10, the worst case state of compressive stress may be found. From that table, it is evident that the worst stress state will occur during drops from angles between 65 and 30 degrees from horizontal. Using the standard formula for combined axial and bending stress:

$$\sigma = P/A + Mc/I$$

and conservatively assuming all stress is carried by the outer shell, the following table may be constructed:

Impact Angle	Thrust (10^6 lbs)	Moment (10^6 lb-in)	Stress (psi)
65	.5848	3.225	2655
60	.5554	3.820	2668
55	.5294	4.477	2705
50	.4895	5.055	2678
45	.4347	5.462	2566
40	.3701	5.636	2375
35	.3062	5.650	2155
30	.2526	5.694	1977

TABLE 2.6.7-10

OBLIQUE Results for -20°F Foam
With Assumed 108 Inch Diameter Impact Limiter

```
PROGRAM OBLIQUE VERSION 8, DATE 8/5/87

12345678901234567890123456789012345678901234567890123456789012345678901234567890
         V         V         V         V         V         V         V         V
NUPAC 10/140MB SHIPPING CASK ENVELOPE DIMENSIONS, COLD FOAM
     83.50     38.75       40.     15.25       18.
    175.98    265000.     386.4
       .25        17        .25       25.
       90.        87       87.5       85.      82.5       80.
       75.        70        65.       60.       55.       50.
       45.        40        35.       30.       25.       20.
       15.        10.       7.5        5.       2.5        1.
        0.
    -96.30        85.        5.       -5.        0.        .5
```

NUPAC OBLIQUE ANALYSIS-NUPAC 10/140MB SHIPPING CASK ENVELOPE DIMENSIONS, COLD FOAM

```
PACKAGE GEOMETRY-
     LENGTH                        =       83.500
     RADIUS                        =       38.750
     OVERPACK LENGTH               =       40.000
     OVERPACK SIDE THICKNESS       =       15.250
     OVERPACK BOTTOM THICKNESS     =       18.000
PACKAGE MASS PROPERTIES-
     MASS                          =      175.980
     MASS MOMENT OF INERTIA        =   265000.000
     GRAVITATIONAL CONSTANT        =      386.400
SOLUTION CHARACTERISTICS-
     IMPACT VELOCITY (YDOT)        =      -96.300
                     (XDOT)        =        0.000
                     (THETADOT)=            0.000
     FRICTION COEFFICIENT          =        0.000
     ESTIMATED CRUSH DEPTH         =         .500
```

THETA0	FMAX	SHEAR	THRUST	MOMENT	DEFLECTION	CLEARANCE
85.0000	966989.	79353.	963770.	981623.	1.07	18.12
80.0000	687032.	113462.	677687.	1403317.	1.64	18.62
75.0000	547193.	134303.	530640.	1661373.	2.30	18.87
70.0000	592434.	193408.	560111.	2392532.	3.21	18.76
65.0000	640168.	260737.	584765.	3225418.	4.05	18.59
60.0000	635336.	308778.	555418.	3819701.	4.49	18.65
55.0000	641274.	361938.	529371.	4477303.	4.87	18.60
50.0000	637704.	408674.	489543.	5055453.	5.12	18.47
45.0000	619648.	441555.	434734.	5462198.	5.20	18.29
40.0000	586996.	455636.	370082.	5636382.	5.10	18.08
35.0000	549862.	456748.	306152.	5650145.	4.87	17.82
30.0000	524602.	460342.	252573.	5694607.	4.52	17.49
25.0000	460863.	422044.	185471.	5220841.	3.97	17.20
20.0000	407766.	386149.	131509.	4776811.	3.29	16.92
15.0000	402188.	390303.	97653.	4828198.	2.71	16.41
10.0000	430903.	425342.	69669.	5261641.	2.17	15.74
5.0000	740655.	738619.	54884.	9136991.	2.17	14.37

FIGURE 2.6.7-5

Impact Limiter Assumed Geometry for Oblique Drops
to Maximize Cask Body Loads

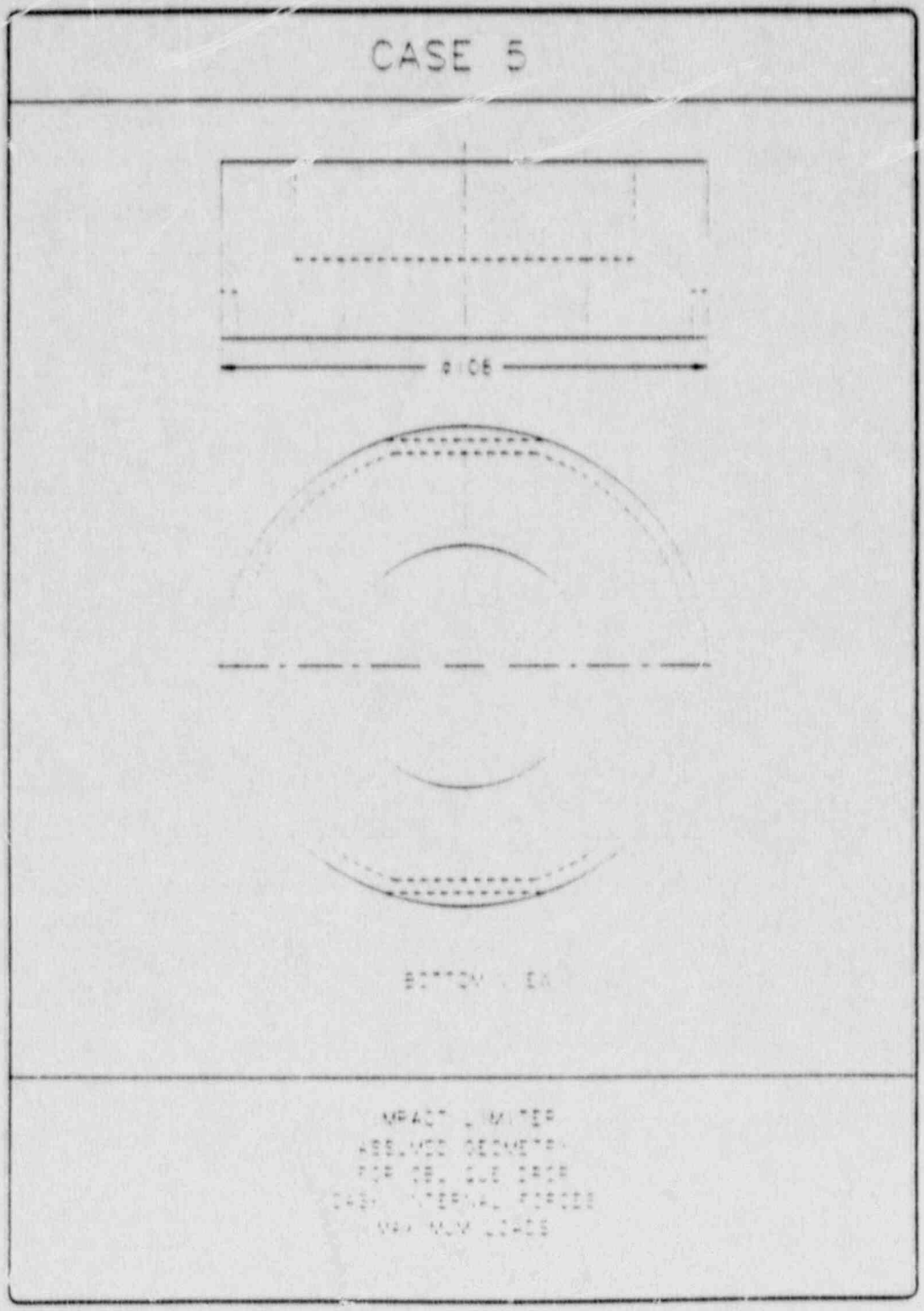

FIGURE 2.6.7-6

Oblique Impact Body Forces

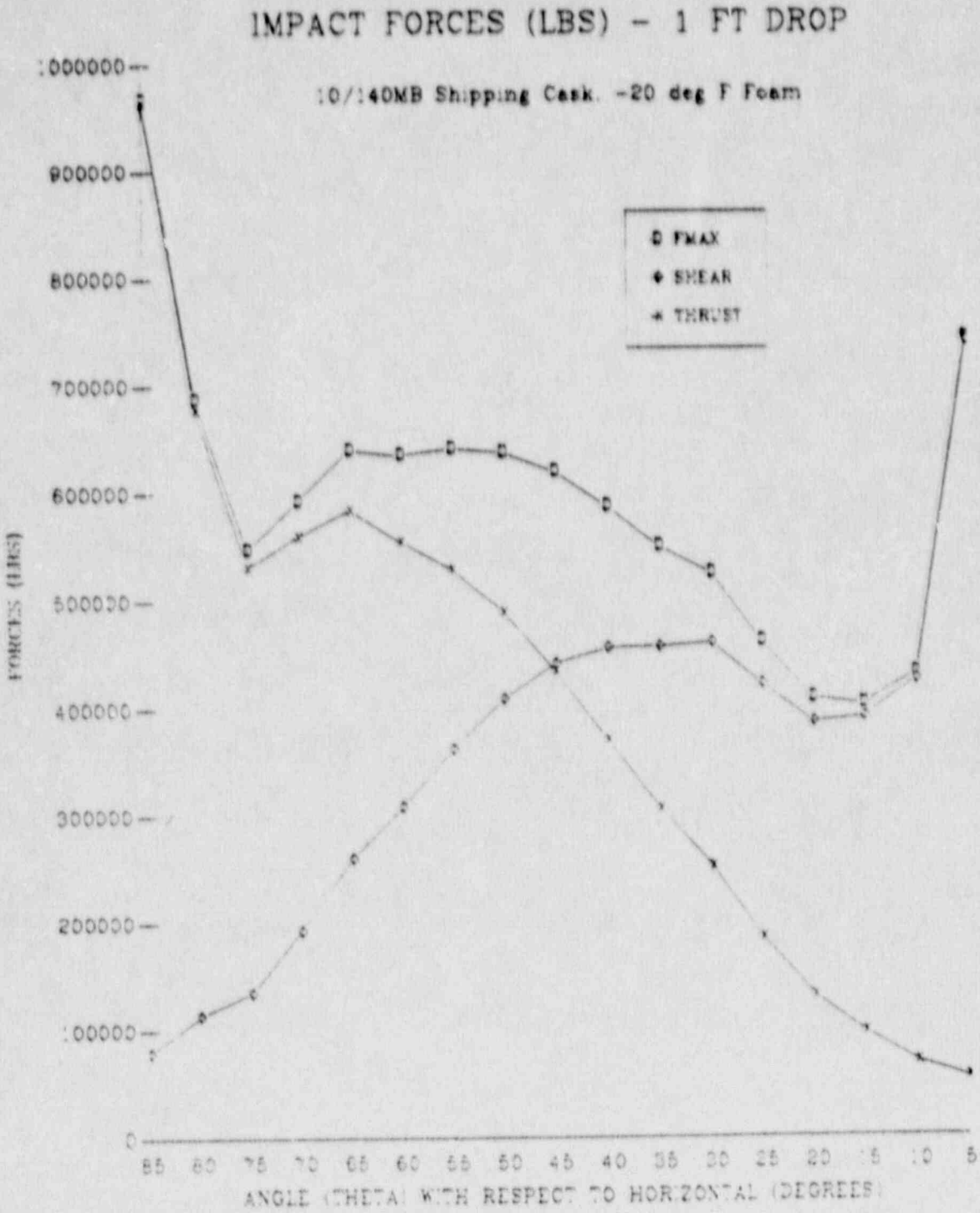

FIGURE 2.6.7-7

Oblique Impact Cask Bending Moments

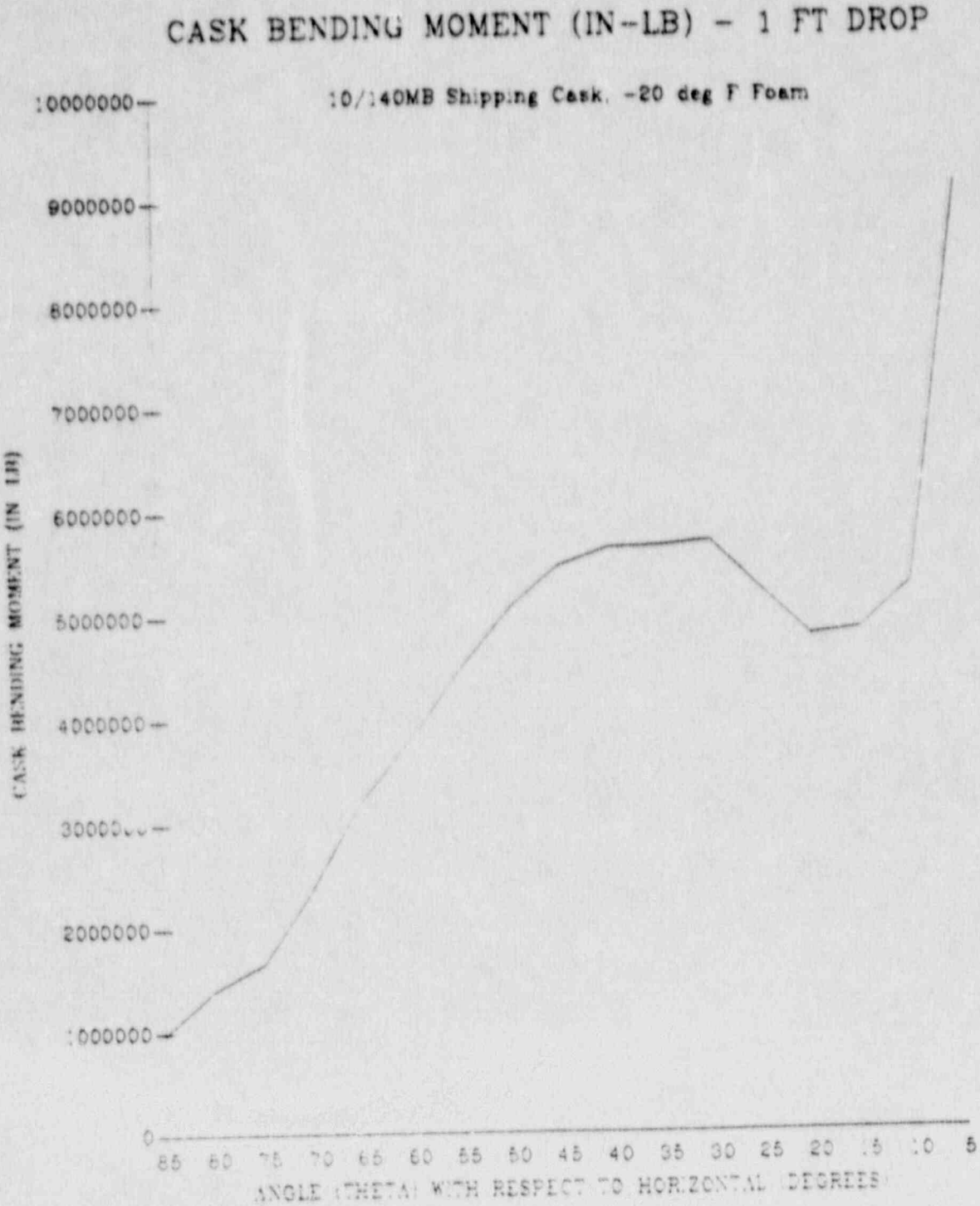

The stresses above were calculated assuming that all of the bending and axial forces are carried by the outer shell, which has a cross sectional area of 287.6 in^2 and moment of inertia of $1.93(10)^5$ in^4 (see Section 2.7.1.2.4). These stresses have been derived using extremely conservative techniques, as detailed in Section 2.7.1.2.4 below. In addition, the stress maximum for combined loading for the package for 1 foot oblique impacts occurs at the point of local peak in thrust load, 65°. From the table above, the maximum stress intensity due to combined loading is 2,705 psi, occuring at an impact angle of 55 degrees from horizontal.

For Normal Conditions of Transport, the maximum allowable membrane stress (conservatively ignoring the small bending contribution) for the non-containment outer shell is S_y (Table 2.1.2-2, reference case number 1(A)). From Table 2.3-1, this is 37,200 psi at the maximum normal outer shell temperature of 128°F. The Margin of Safety is therefore:

M.S. = 37,200/2,705 - 1 = + Large

The maximum cask bending moment for this oblique impact event is 9,136,991 in-lb, occuring at an angle of 5° with respect to horizontal. Cask bending moments are higher in side impacts, as demonstrated in Section 2.6.7.3 which follows. Therefore, bending effects will not be a significant factor for oblique drops.

2.6.7.2.5 Lid Attachment Forces

In order to evaluate the maximum forces acting on the 10/140MB closure system during the oblique impacts, a different set of assumptions regarding impact limiter geometry must be made. Separation forces are maximized through the use of an assumed minimum diameter impact limiter. The detailed logic behind this assumption is set out in Section 2.7.1.2.5 below, and basically revolves around minimizing cask inertial effects in order to maximize impact limiter deformation and consequent thrust loading. For this reason, another OBLIQUE analysis was performed, this time utilizing an assumed 96 inch diameter impact limiter. The impact limiter geometry used in this analysis is illustrated in Figure 2.6.7-2 above. The results of the analysis are listed in Table 2.6.7-

11.

A detailed evaluation of the cask closure system under oblique impact loading is set out in Section 2.7.1.2.5 below. This same approach will be utilized here.

The maximum thrust load for normal condition oblique drops is found from Table 2.6.7-11 to be 1,038,864 lb, derived at an impact angle of 85° with respect to horizontal. The resulting axial g-load is thus:

$$\gamma_{axial} = 1{,}038{,}864/(68{,}000)(\sin 85^{\circ})$$
$$= 15.3 \text{ g's}$$

It should be noted that thrust loads are significantly higher during end impacts (62.7 g's, as demonstrated in Section 2.6.7.1 above), so axial effects on the cask body itself will not be a factor for oblique impacts.

Impact on the cask closure system can be calculated by factoring the combined top lid assembly and maximum payload weights by the axial g-load:

$$P_{max} = (15.3)(23{,}430) = 358{,}479 \text{ lb}$$

The resulting lid separation moment can now be found:

$$M = (358{,}479)(41.0) = 14.698(10)^{6} \text{ in-lb}$$

Where 41.0 in is the radius of the primary lid bolt circle. In Section 2.7.1.2.5, it was demonstrated that the maximum force acting on any component of the cask closure system can be derived as:

$$f_m = 4M/3RN$$

Where: R = Lid bolt circle radius = 41.0 in
N = Number of closure attachments = 8

$$f_m = 4(14.698(10)^{6})/3(41.0)(8)$$

TABLE 2.6.7-11

OBLIQUE Results for -20°F Foam
With Assumed 96 Inch Diameter Impact Limiter

```
PROGRAM OBLIQUE VERSION 8. DATE 8/5/87

12345678901234567890123456789012345678901234567890123456789012345678901234567890
         V         V         V         V         V         V         V         V
NUPAC 10/140MB SHIPPING CASK ENVELOPE DIMENSIONS, COLD FOAM
    83.50     38.75       40.     9.25       18.
   175.98   265000.     386.4
      .25       12.       .75       25.
      90.       89.      87.5       85.     82.5       80.
      75.       70.       65.       60.      55.       50.
      45.       40.       35.       30.      25.       20.
      15.       10.       7.5        5.      2.5        1.
       0.
   -96.30       85.        5.       -5.       0.        1.
```

```
NUPAC OBLIQUE ANALYSIS-NUPAC 10/140MB SHIPPING CASK ENVELOPE DIMENSIONS, COLD FOAM

        PACKAGE GEOMETRY-
             LENGTH                      =        83.500
             RADIUS                      =        38.750
             OVERPACK LENGTH             =        40.000
             OVERPACK SIDE THICKNESS     =         9.250
             OVERPACK BOTTOM THICKNESS   =        18.000
        PACKAGE MASS PROPERTIES-
             MASS                        =       175.980
             MASS MOMENT OF INERTIA      =    265000.000
             GRAVITATIONAL CONSTANT      =       386.400
        SOLUTION CHARACTERISTICS-
             IMPACT VELOCITY (YDOT)      =       -96.300
                             (XDOT)      =         0.000
                             (THETADOT)  =         0.000
             FRICTION COEFFICIENT        =         0.000
             ESTIMATED CRUSH DEPTH       =         1.000
```

THETA0	FMAX	SHEAR	THRUST	MOMENT	DEFLECTION	CLEARANCE
85.0000	1042286.	85111.	1038864.	1052859.	1.13	17.56
80.0000	736147.	121072.	726240.	1497705.	1.75	17.52
75.0000	601592.	147389.	583394.	1823255.	2.47	17.24
70.0000	654960.	214278.	619154.	2650694.	3.38	16.65
65.0000	693618.	284060.	633114.	3513925.	4.21	15.99
60.0000	672650.	329423.	586541.	4075083.	4.64	15.59
55.0000	660048.	376174.	542362.	4653413.	4.95	15.11
50.0000	637684.	412197.	486554.	5099029.	5.12	14.59
45.0000	603590.	432687.	420836.	5352500.	5.12	14.06
40.0000	562687.	438301.	352859.	5421940.	4.98	13.52
35.0000	524250.	436241.	290744.	5396469.	4.74	12.94
30.0000	501120.	439532.	241040.	5437174.	4.40	12.36
25.0000	440342.	403385.	177237.	4990024.	3.87	11.82
20.0000	391950.	371203.	126621.	4591917.	3.21	11.31
15.0000	391722.	380215.	95318.	4703396.	2.65	10.64
10.0000	424683.	419205.	68740.	5185754.	2.14	9.85
5.0000	680043.	678313.	48478.	8390977.	2.06	8.45

= 59,747 lb

The 6.8 psig normal operating pressure, derived in Section 3.4.4, will exert an additional 3,180 lb on each primary lid bolt. Total bolt loading is therefore 59,747 + 3,180 = 62,927 lb. The 2-1/2 inch closure bolts have a 4.0 in^2 tensile stress area. Resulting bolt stress is therefore 62,927/4.0 = 15,732 psi. From Table 2.1.2-1, reference case number 6(A), the allowable stress for Normal Conditions of Transport is $2S_m$. From Table 2.3-1, S_m for the bolting material at the maximum service temperature of 133°F is 34,360 psi, so the allowable stress is (2)(34,360) = 68,720 psi. The Margin of Safety is:

M.S. = 68,720/15,732 - 1 = +3.37

From Section 2.7.1.2.5, it was found that the most severly loaded bolt attachment lug is the lower lug, attached to the cask wall. For this lug, the bolt circle is 3.75 inches from the lug attachment at the cask wall. The moment of inertia of the attachment section has been derived in Section 2.5.1 as 188.68 in^4, and the distance from the centroid of the attachment area to the tip of the lug gusset was found to be 4.8 in. So the bending stress acting on the lug under maximum oblique loading is:

$$\sigma_B = (62,927)(3.75)(4.8)/188.68$$
$$= 6,003 \text{ psi}$$

Shear stress on the attachment section is:

$$\tau = 62,927/32.76$$
$$= 1,921 \text{ psi}$$

Where 32.76 in^2 is the area of the lug attachment section. Combined stress for the section is:

$$\sigma_C = \sigma_B + [(\sigma/2)^2 + (\tau)^2]^{1/2}$$
$$= 9,567 \text{ psi}$$

From Table 2.1.2-1, reference case number 2(A), the allowable membrane plus bending stress on containment components is $1.5S_m$. For the A-516 lower lug material, S_m = 23,236 psi at 133°F, so the allowable is (1.5)(23,236) = 34,855 psi. The Margin of Safety is:

M.S. = 34,855/9,567 - 1 = +2.64

In Section 2.7.1.2.5 below, it is demonstrated that closure system bearing surfaces exhibit large margins of safety in bearing against an allowable of yield for the much more extreme accident condition loadings. It is therefore obvious that the smaller normal condition loadings will result in even higher margins for bearing stress with the same allowable stress at the same temperature.

It has thus been demonstrated that Normal Conditions of Transport oblique drop impacts will have negligible effect on the the 10/140MB cask.

2.6.7.3 Flat Side Impact

Analysis of the 10/140MB cask behavior during side impact from one foot follows the same approach described in Section 2.7.1.3 for the hypothetical accident impact event. Because the normal condition impact is much less severe than the accident condition impact, the evaluation of the event is somewhat less complicated.

The analysis presented here follows these steps:

1. Determine the maximum impact limiter deflections using the SYDROP computer program, utilizing conservative assumptions regarding impact limiter geometry.

2. Determine the impact forces using the SYDROP computer program as well as some hand analyses, utilizing conservative assumptions regarding impact limiter geometry.

3. Determine stresses in the outer shell assuming it reacts the entire impact bending load.

4. Determine stresses in the inner shell assuming it reacts the payload weight and half the lead weight in bending.

2.6.7.3.1 Side Impact Deflections

In order to conservatively maximize impact limiter deformations, the SYDROP energy balance program was used, with minimum impact limiter outside diameters assumed. These diameters correspond to the distances across the flattened sides of the major and minor portions of the impact limiter, and were 102 inches and 96 inches, respectively. The assumed outside diameters are illustrated in Figure 2.6.7-8. In this manner, impacts on both the rounded and flattened sides of the impact limiters are effectively bounded. The inside diameter was assumed to be the minimum value of 77.5 inches. This assumption conservatively ignores the presence of the bolt lug 'pockets'

FIGURE 2.6.7-8

Impact Limiter Assumed Geometry for Flat Side Drop

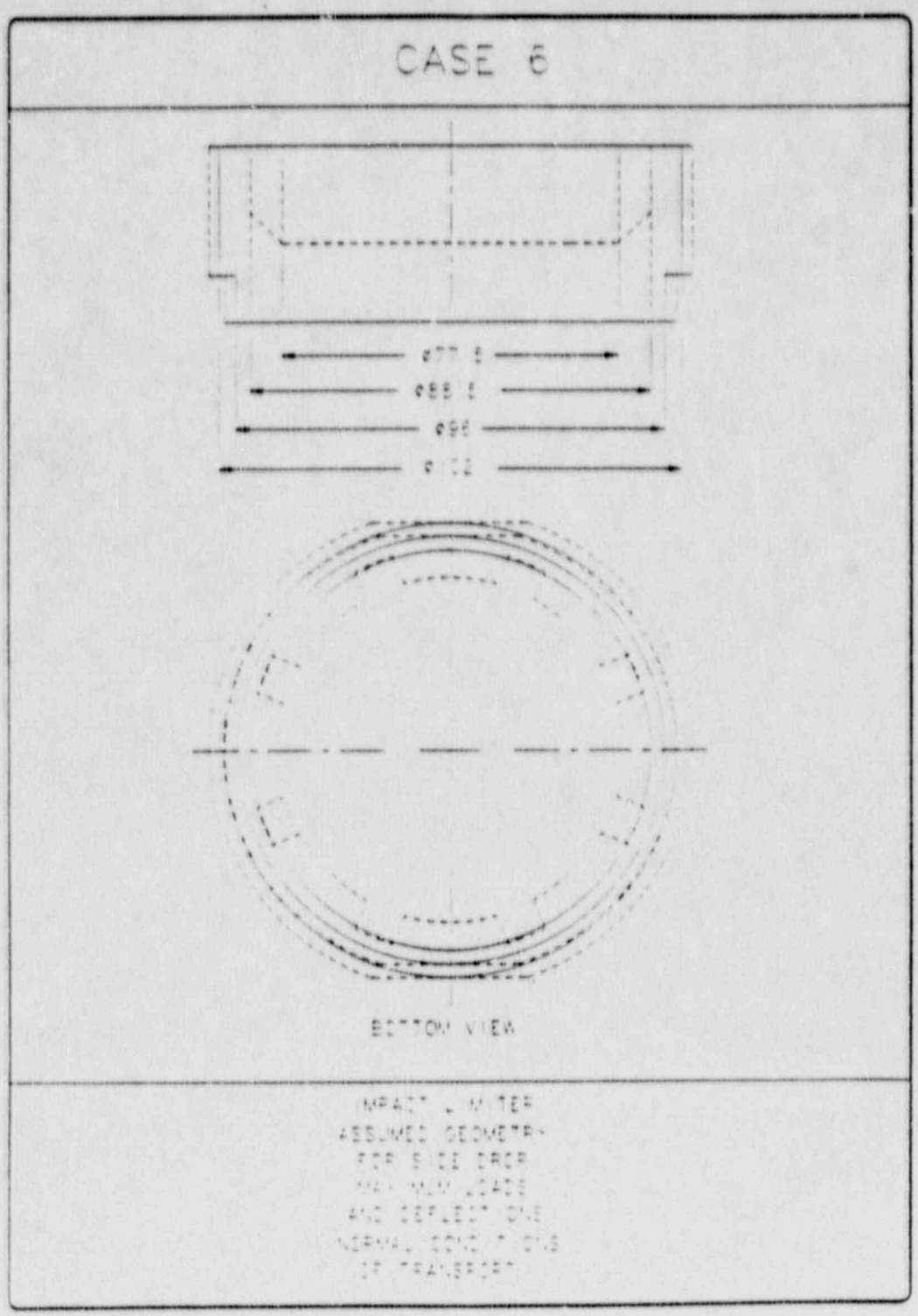

embedded in the sides of the impact limiters. As will be shown in Section 2.7.1.3.1 below, these pockets tend to induce local strain hardening effects in the polyurethane foam, and thus act to reduce deformations. Ignoring them will result in higher calculated deflections than would otherwise occur.

Additionally, the maximum temperature foam properties were utilized. Since the polyurethane foam is at its lowest strength at elevated temperatures, this assumption will tend to maximize deflections. Foam properties taken at the maximum normal condition temperature of 169°F were derated by 15% (20% at the maximum strain of 80%), as explained in Section 2.1.2.4. The results of the SYDROP analysis are given in Table 2.6.7-12. As can be seen, the maximum predicted deflection, even with the conservative assumptions made, is only 1.74 inches. It should be noted that, since the difference in radii of the impact limiters is (102 - 96)/2 = 3.0 inches, only the 30 inch long major diameter portion of the impact limiter will be affected by normal condition side drop. The 10 inch long, minor diameter 'cap' portion will not incur any damage.

In Section 2.7.1.3.1 below, it is shown that the minimum distance between an outer and an inner surface of the impact limiter is 8.1 inches. Normal condition impact limiter deflections are therefore of no consequence.

2.6.7.3.2 Side Impact Forces

Side impact forces were likewise determined using the SYDROP energy balance program. For this evaluation, the analysis was performed assuming foam properties at -20°F, increased 15% to 20%. At this minimum temperature condition, foam strength will be greatest, and ensuing impact loading will therefore be maximum. The same minimum outside diameters were used for this analysis as were used above in the deflection analysis. However, to conservatively maximize impact loading, a maximum inside diameter of 88.5 inches was assumed. This dimension corresponds to the distance across any opposing pair of bolt lug 'pockets' embedded within the impact limiter. The full 30 inch length of major diameter portion of the impact limiter on each end is assumed effective. This has been shown by test to be the most realistic model and results in higher loads.

Table 2.6.7-12

The results of the SYDROP evaluation are given in Table 2.6.7-13. The 10 inch 'cap' portion of the impact limiter is again shown to be unaffected by one foot drops, since the impact limiter does not deflect enough to mobilize this part of the foam. As shown in the Table, the maximum acceleration during a normal condition side impact would not be expected to exceed 28.2 g's.

2.6.7.3.3 Outer Shell Bending Stresses

The outer shell bending stresses for the hypothetical accident 30 foot side impact were determined using a linear analysis (see section 2.7.1.3.2). Therefore, the stresses derived from that analysis may be factored by the ratio of the normal condition impact acceleration to the hypothetical accident impact acceleration. The maximum stress intensity from hoop and longitudinal bending during the accident event is given in Section 2.7.1.3.2 as 17,380 psi, for an impact acceleration of 163.2 g's. Therefore, during normal conditions, the corresponding stress would be:

$$(28.2/163.2)(17,380) = 3,003 \text{ psi}$$

The allowable membrane stress under normal conditions for the non-containment A-516 Grade 70, or, alternatively, A-537 Class 1 steel outer shell is the greater of S_m or S_y (Table 2.1.2-2, reference case number 1(A)). At the maximum expected outer shell temperature of 128°F, the allowable is thus S_y = 37,200 psi (greater than S_m = 23,350 psi). So the Margin of Safety is:

$$M.S. = 37,200/3,003 - 1 = + \text{Large}$$

The normal condition bending buckling allowable is 22,793 psi (Table 2.1.2-4), so the Margin of Safety on bending buckling is:

$$M.S. = 22,793/3,003 - 1 = +6.59$$

2.6.7.3.4 Inner Shell Stresses

The inner shell stresses may be factored from the hypothetical accident

Table 2.6.7-13

Proprietary

conditions in the same manner that outer shell stresses were. Thus, the 19,150 psi maximum stress in the inner shell during the hypothetical accident side impact event becomes:

$$(28.2/163.2)(19,150) = 3,309 \text{ psi}$$

Using the membrane stress allowable of S_m = 20,000 psi for the stainless steel inner shell, the Margin of Safety is then :

$$M.S. = 20,000/3,309 - 1 = +5.04$$

The buckling bending allowable is 19,182 psi (Table 2.1.2-3), so the Margin of Safety on bending buckling is then:

$$M.S. = 19,182/3,309 - 1 = +4.80$$

It can thus be seen from the above analyses that Normal Conditions of Transport flat side drops will be of little consequence to the 10/140MB cask, even under the worst possible conditions.

2.6.8 Corner Drop

This requirement is not applicable, since the NuPac 10/140MB is constructed primarily of steel and lead, and exceeds 220 pounds gross weight.

2.6.9 Compression

This requirement is not applicable, since the NuPac 10/140MB exceeds 10,000 pounds weight.

2.6.10 Penetration

From previous container tests, as well as engineering judgement, it can be concluded that a 13 pound rod would have a negligible effect on the heavy gauge steel sheet impact limiter or cask.

2.6.11 Summary

As the result of the above assessment, it is concluded that in normal conditions of transport:

1. There will be no release of radioactive material from the package.

2. The effectiveness of the packaging will not be substantially reduced.

3. There will be no mixture of gases or vapors in the package which could, through any credible increase in pressure or an explosion, significantly reduce the effectiveness of the package.

2.7 Hypothetical Accident Conditions

The NuPac 10/140MB Cask, when subjected to Hypothetical Accident Conditions as specified in 10 CFR 71.73, meets the performance requirements specified in Subpart E of 10 CFR 71. This is demonstrated in the following subsections where each accident condition is addressed and shown to meet the applicable design criteria previously discussed in Section 2.1.2. A summary of maximum stresses in the major cask components arising from the Hypothetical Accident Conditions is presented in Figure 2.7-1 and Table 2.7-1.

2.7.1 Free Drop

Subpart F of 10 CFR 71 requires that a 30 foot free drop be considered for the NuPac 10/140MB Cask. The drop is to be onto a flat, essentially unyielding, horizontal surface, and the cask is to strike the surface in a position for which maximum damage is expected. Per 10 CFR 71.73(b) the initial temperature for the drop is to be the worst case constant ambient air temperature between -20°F and 100°F. Internal heat generation from the payload (95 watts) is also considered when it is conservative to do so. (Note: 10 CFR 71 does not require consideration of insolation as an initial condition for accident conditions). Regarding initial internal pressure, the maximum normal operating pressure must be considered unless a lower internal pressure consistent with the ambient temperature assumed to precede and follow the drop is more unfavorable.

The analyses in this section extract accelerations from NuPac's impact analyses programs (EYDROP, SYDROP, CYDROP, and OBLIQUE) and statically apply them to the package. Static application is justified since the natural frequencies of the cask are relatively high and the duration of the impact loadings relatively long. The cask frequencies are high as the result of using relatively thick, stiff shells in the cask design. The duration of impact loadings are relatively long as the result of using soft (relative to the steel structures) energy absorbing impact limiters to protect the cask during free drop events. In addition, inspection of accelerometer data available from previous drop

FIGURE 2.7-1

Cask Components Affected by Hypothetical Accident Conditions

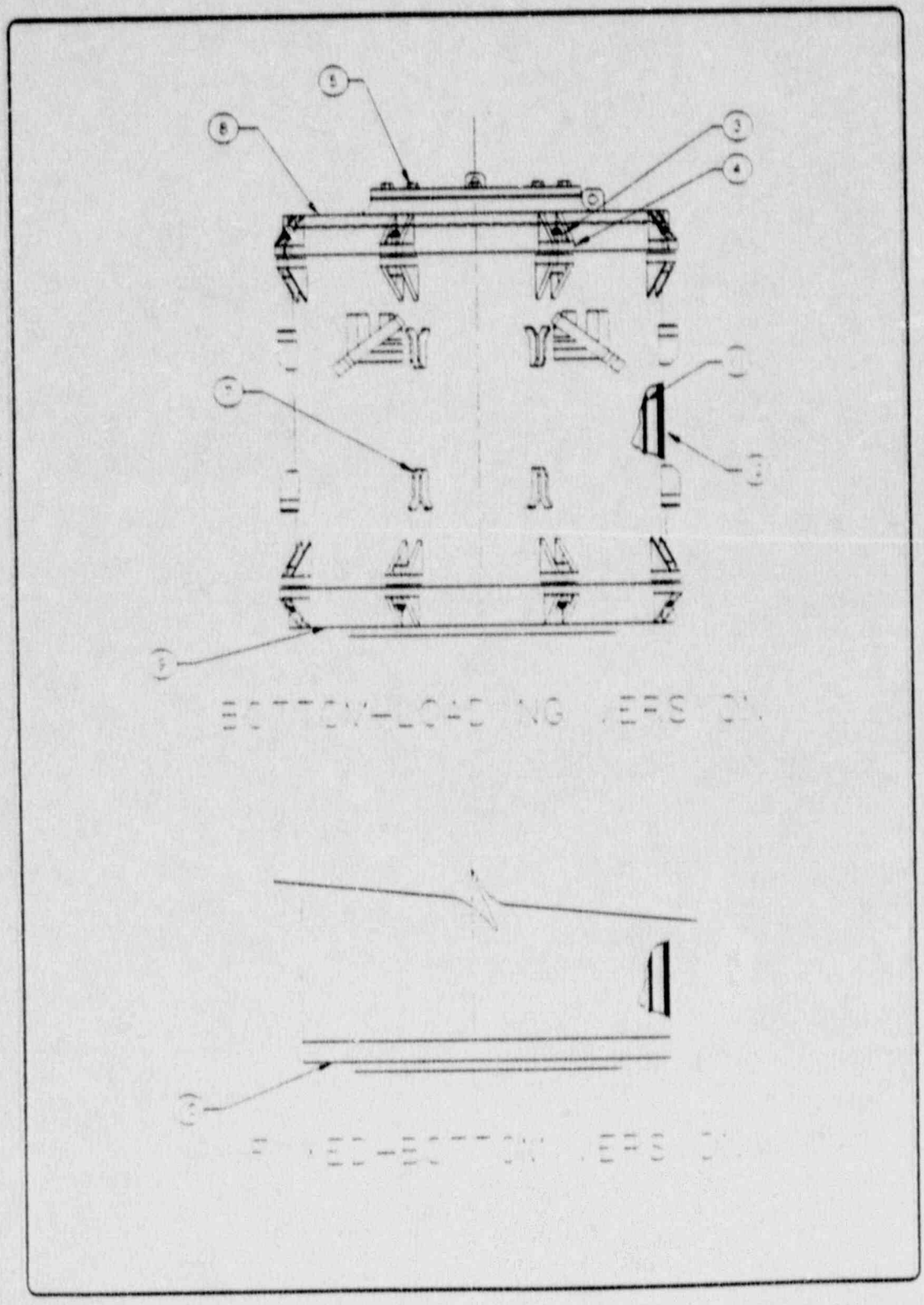

TABLE 2.7-1

Hypothetical Accident Conditions Maximum Stresses

Component Ref. No.	Component Description	Location Within Component	Loading Condition	Load Combination	Type of Stress	Resultant Stress Component*, Stress Intensity, or Load	Acceptance Criteria	Allowable Value of Stress (psi)	Margin of Safety	SAR Reference Location
3	Primary Lid Bolts	Shank	Oblique Drop	Max. Payload +Pressure	Membrane	96610 psi	S_y	103000 psi	+0.07	2.7.1.2.5
4	Primary Lid Bolt Lugs	Cask Lug Weld	Oblique Drop	Max. Payload +Pressure +Bending	Membrane	58750 psi	S_u	70000 psi	+0.19	2.7.1.2.5
5	Secondary Lid Bolts	Shank	End Drop	Max. Payload +Pressure	Membrane	82000 psi	S_y	103000 psi	+0.26	2.7.1.1.5 2.10.7.4
7	Impact Limiter Attachment	Ball-Lock Pin	Oblique Drop	Double Shear	Shear	25600 lb	1/5 Double Shear Capacity	29400 lb	+0.15	2.7.1.2.6
8	Top Lid Assembly	Secondary Lid O.D.	Puncture Secondary Lid O.D.	Puncture	Membrane	47448 psi	$2.4S_m$	48000 psi	+0.01	2.7.2 2.10.9.3.2
9	Bottom Lid	Center of Lid	Puncture Center	Puncture	Membrane +Bending	60898 psi	S_u	68785 psi	+0.13	2.7.2 2.10.8.2.1
10	Bottom Plate	Center of Plate	End Drop	Min. Payload Load Slump	Membrane +Bending	21315 psi	S_u	68785 psi	+2.23	2.7.1.1.4
11	Inner Shell	Impact End	End Drop	Min. Payload Load Slump	Buckling Interaction	σ_h = 6920 psi σ_a = 20086 psi	**	σ_{ha} = 26042 psi σ_{aa} = 27599 psi	+0.09	2.7.1.1.9(2)
12	Outer Shell	Center of Cask	Side Drop	Bending +Ovality	Bending Buckling	17586 psi	Buckling Allowable	37976 psi	+0.86	2.7.1.1.8

* σ_h = hoop compressive stress, σ_a = axial compressive stress

** Buckling Interaction: $[(\sigma_h/\sigma_{ha}) + (\sigma_a/\sigma_{aa})] \leq 1$

tests indicates that casks such as the 10/140MB respond essentially as a rigid body. This observation further justifies static application of g loads.

It has been determined in the free drop analyses which follow, that drops in the various orientations produce different situations critical to overall cask design. For example, in general, flat end drops result in loads which tend to induce the governing stress resultants on the major cask structural components. Oblique drops tend to create maximum primary lid and impact limiter separation loads. Because of the various appurtenances extending from the side of the cask (tie-down lugs and primary lid bolt lugs), as well as the relatively 'soft' impact limiter response in the side drop orientation (foam strain hardening is generally less for side drop than for other orientations), flat side drop will tend to result in the most critical deformations conducive to potential 'bottoming out' of the cask. All of the considerations are addressed in detail in the following sections.

An important consideration in the detailed analyses which follow is the fact that cask response to the regulatory drops is temperature dependent. At maximum temperature conditions, the structural material comprising the cask will exhibit lower mechanical strength than at lower temperatures. As a consequence, the stress and buckling allowables will also be lower. However, because the polyurethane foam in the impact limiters likewise exhibits lower mechanical strength at elevated temperatures, it will deform more on impact than would be the case at lower temperatures. The result will be smaller impact loads occuring at higher temperatures.

Conversely, at the minimum regulatory temperature, while the mechanical strength of the structural components will be greater, so will the mechanical strength of the foam. The result will be greater impact loading at reduced temperatures.

In order to conservatively bound temperature effects in the free drop events that follow, the maximum impact loads, derived at the minimum temperature, will be applied to the cask. Simultaneously, the cask response will be evaluated utilizing mechanical properties at the highest Normal Conditions of Transport temperature derived for the individual cask componenets at the

maximum temperature condition. This introduces additional conservatism, due to the fact that component temperatures at the start of the Hypothetical Accident Conditions will be significantly lower than for Normal Conditions of Transport. In this extremely conservative fashion, cask integrity will be demonstrated across the full range of temperatures expected under all Hypothetical Accident Conditions.

Finally, it should be noted that, while the following analyses are based on conservative assumptions derived from sound engineering judgement, the final evaluation of the 10/140MB Cask integrity rests in the results of the quarter-scale drop tests performed to verify the cask design. Details of this test program are given in Appendix 2.10.4. The results derived therefrom fully vindicate the accident condition analyses performed in this Section, and demonstrate that the NuPac 10/140MB is fully capable of meeting the most stringent regulatory requirements.

2.7.1.1 Flat End Drop

Analysis of the NuPac 10/140MB Cask behavior during the accident condition drops from 30 feet is performed in the following steps:

1. Analyze the maximum impact limiter deflections using the EYDROP energy balance computer program.

2. Analyze the maximum impact force using the EYDROP computer program.

3. Analyze the axial and hoop stresses in the cask shells and lead.

4. Analyze the cask lid for bending, assuming the payload acts as a uniform load on a plate supported by the impact limiters exerting a uniform pressure in the opposite direction. Reanalyze the lid, omitting payload reaction.

5. Analyze the stresses in the cask primary and secondary lid bolts.

6. Analyze maximum bearing stresses in the EnviroSeals^{tm} and adjacent sealing surface.

7. Determine the amount of lead slump.

The flat end free drop event will tend to impose critical loads on the major cask structural components. Lids will generally experience their greatest bending forces, while the cask shells will undergo maximum compressive loading conducive to buckling. In addition, there are a number of cask-specific considerations which could govern component loads and determine which are the most critical. These are as follows:

1. The NuPac 10/140MB cask has two different basic configurations -- a fixed-bottom and a removable-bottom version. Each will respond differently to the same imposed drop load.

2. Drop orientation could be an important factor. Impacts for both top-down and bottom-down end drops must be addressed.

3. The presence of the cask payload may, in certain circumstances, tend to counteract and relieve impact loading on some components. Response of the lids, for example, under uniform loadings applied externally by the impact limiters and internally by the payload will differ from the response where a payload is reduced or constrained from applying an evenly distributed loading. Consequently, two bounding cases are considered: One, where the impact is modelled as though the full 15,000 lb payload were present, and the other with no payload reaction at all.

4. The maximum normal condition internal pressure (6.8 psig, from Section 3.4.4) must be accounted for, when this will result in a worse-case stress condition. Generally, the presence of internal pressure will tend to increase the critical inner shell (containment boundary) buckling strength. Conversely, for lid analysis purposes, internal pressure will result in additional bending stress. Therefore, for the following shell analyses, internal pressure will be conservatively neglected. For lid stress evaluation, internal pressure will be applied.

It should be noted that the analyses below demonstrate that the lead shielding will always slip under Hypothetical Accident Conditions end drop loadings. Assumed lead condition for structural analysis purposes will therefore always reflect this initial state.

In the analyses that follow, worst-case combinations of all the above factors have been evaluated. Where simple geometries and load patterns allow, classical stress analysis techniques are utilized to determine component response to end drop loading. For more complex geometries, the ANSYS finite element program was used to determine maximum stresses.

A summary of all end drop analyses performed in Section 2.7.1.1 is presented in Tables 2.7.1-1 and 2.7.1-2. This summary details each component analysed, the initial conditions assumed, analysis technique utilized, and results. It

TABLE 2.7.1-1

(Page 1 of 2)

Hypothetical Accident Condition

Flat End Drop Structural Component Analysis Parameters

(Foam Temperature of -20°F)

Component	Case Ref. No.	Cask Configuration	Drop Orientation	Payload	Load Status	Internal Pressure	Analysis Technique
INNER SHELL	1	Bottom Loading	Bottom Down	No	Slump	No	ANSYS
	2	Fixed Bottom	Bottom Down	Yes	Slump	No	Classical
	3	Fixed Bottom	Bottom Down	No	Slump	No	Classical
OUTER SHELL	4	Bottom Loading	Bottom Down	No	Slump	N/A	ANSYS
	5	Fixed Bottom	Bottom Down	Yes	Slump	N/A	Classical
	6	Fixed Bottom	Bottom Down	No	Slump	N/A	Classical
TOP LID	7	Both	Top Down	Yes	N/A	Yes	ANSYS
	8	Both	Top Down	No	N/A	No	ANSYS
BOTTOM LID	9	Bottom Loading	Bottom Down	Yes	N/A	Yes	ANSYS
	10	Bottom Loading	Bottom Down	No	N/A	No	ANSYS
BOTTOM PLATE	11	Fixed Bottom	Bottom Down	Yes	Slump	No	Classical
	12	Fixed Bottom	Bottom Down	No	Slump	No	Classical

TABLE 2.7.1-1

(Page 2 of 2)

Component	Case Ref. No.	Cask Configuration	Drop Orientation	Payload	Lead Status	Internal Pressure	Analysis Technique
PRIMARY LID BOLTS	13	Both	Top Down	No	N/A	No	Classical
BOLT LUGS	14	Both	Top Down	No	N/A	No	Classical
SECONDARY LID BOLTS	15	Both	Top Down	Yes	N/A	Yes	ANSYS

TABLE 2.7.1-2
(Page 1 of 2)

Hypothetical Accident Conditon
Flat End Drop Structural Component Stress Evaluation

Component	Case Ref. No.	Location Within Component	Load Combination	Type of Stress	Resultant Stress Component or Stress Intensity (psi)*	Acceptance Criteria	Allowable Value of Stress (psi)	Margin of Safety	SAR Reference Location
INNER SHELL	1	Impact End	Min. Payload Lead Slump	Membrane + Bending	SI = 21695	SI ≤ $3.6S_m$	$3.6S_m$ = 72000	+2.32	2.7.1.1.3(2)
				Membrane	SI = 18427	SI ≤ $2.4S_m$	$2.4S_m$ = 48000	+1.61	2.10.6.3
				Buckling Interaction	σ_h = 7341 σ_a = 18788	**	σ_{hc} = 26042 σ_{ac} = 27593	+0.06	
	2	Impact End	Max. Payload Lead Slump	Membrane	SI = 15558	SI ≤ $2.4S_m$	$2.4S_m$ = 48000	+2.09***	2.7.1.1.3(2)
				Buckling Interaction	σ_h = 6320 σ_a = 15558	**	σ_{hc} = 26042 σ_{ac} = 27593	+0.24***	
	3	Impact End	Min. Payload Lead Slump	Membrane	SI = 20086	SI ≤ $2.4S_m$	$2.4S_m$ = 48000	+1.39	2.7.1.1.3(2)
				Buckling Interaction	σ_h = 6320 σ_a = 20086	**	σ_{hc} = 26042 σ_{ac} = 27593	+0.03	
OUTER SHELL	4	Impact End	Min. Payload Lead Slump	Membrane + Bending	SI = 20007	SI ≤ S_m	S_m = 70000	+2.50	2.7.1.1.3(2)
				Membrane	SI = 13806	SI ≤ $0.7S_m$	$0.7S_m$ = 49000	+2.55	2.10.6.3
				Buckling Interaction	σ_h = 3274 σ_a = 11621	**	σ_{ac} = 36258	+1.43	
	5	Impact End	Max. Payload Lead Slump	Membrane	SI = 17980	SI ≤ $0.7S_m$	$0.7S_m$ = 49000	+1.73	2.7.1.1.3(2)
				Buckling Interaction	σ_h = 0 σ_a = 13820	**	σ_{ac} = 36258	+1.62	
	6	Impact End	Min. Payload Lead Slump	Membrane	SI = 15504	SI ≤ $0.7S_m$	$0.7S_m$ = 49000	+2.16***	2.7.1.1.3(2)
				Buckling Interaction	σ_h = 0 σ_a = 11344	**	σ_{ac} = 36258	+2.20***	

* SI = Stress Intensity, σ_h = hoop compressive stress, σ_a = axial compressive stress
** Buckling Interaction: $[(\sigma_h/\sigma_{hc}) + (\sigma_a/\sigma_{ac})] \leq 1$
*** Not specifically presented herein - not a governing worst case

TABLE 2.7.1-2
(Page 2 of 2)

Hypothetical Accident Condition
Flat End Drop Structural Component Stress Evaluation

Component	Case Ref. No.	Location Within Component	Load Combination	Type of Stress	Resultant Stress Component or Stress Intensity (psi)*	Acceptance Criteria	Allowable Value of Stress (psi)	Margin of Safety	SAR Reference Location
TOP LID	7	Outside Dia.	Max Payload	Membrane	SI = 15923	SI ≤ 2.4S_m	2.4S_m = 48000	+2.01	2.7.1.1.4 2.10.7.4
		Outside Dia.		Membrane + Bending	SI = 34314	SI ≤ S_m	S_m = 68785	+1.00	
	8	Outside Dia.	Min. Payload	Membrane	SI = 14031	SI ≤ 2.4S_m	2.4S_m = 48000	+2.42	2.7.1.1.4 2.10.7.4
		Outside Dia.		Membrane + Bending	SI = 11763	SI ≤ S_m	S_m = 68785	+4.85	
BOTTOM LID	9	Outside Dia.	Max. Payload	Membrane	SI = 15537	SI ≤ 2.4S_m	2.4S_m = 48000	+2.09	2.7.1.1.4 2.10.7.2
		Center		Membrane + Bending	SI = 22453	SI ≤ S_m	S_m = 68785	+2.06	
	10	Outside Dia.	Min. Payload	Membrane	SI = 13919	SI ≤ 2.4S_m	2.4S_m = 48000	+2.45	2.7.1.1.4 2.10.7.2
		Outside Dia.		Membrane + Bending	SI = 11914	SI ≤ S_m	S_m = 68785	+4.99	
BOTTOM PLATE	11	Center	Max. Payload Load Slump	Membrane + Bending	SI = 10517[illegible]	SI ≤ S_m	S_m = 68785	+5.54[illegible]	2.7.1.1.4
	12	Center	Min. Payload Load Slump	Membrane + Bending	SI = 21315	SI ≤ S_m	S_m = 68785	+2.23	2.7.1.1.4
PRIMARY LID BOLTS	13	Shank	Preload	Membrane	SI = 4250	S_y	S_y = 102000	+Large	2.7.1.1.5
BOLT LUGS	14	Weld to Cask Body	Preload	Membrane + Bending	SI = 2665	S_u	S_u = 70000	+Large	2.7.1.1.5
SECONDARY LID BOLTS	15	Shank	Max. Payload	Membrane	SI = 82000	S_y	S_y = 109000	+0.26	2.7.1.1.5 2.10.7.4

is from these Tables that the worst-case end drop stress states detailed in Table 2.7-1 are drawn.

Material properties utilized in the analyses were taken from Table 2.3-1. Stress allowables were drawn from Tables 2.1.2-1 and 2.1.2-2, and buckling allowables came from Tables 2.1.2-5 and 2.1.2-6. Polyurethane foam properties were derived from Figure 2.1.2-3.

The impact limiter is conservatively assumed to resist the impact over its entire footprint area. Tests performed on a variety of packages indicate that loads calculated in this manner are overpredicted. Since the EYDROP program assumes a circular impact limiter, a geometry assumption was made to accurately account for the irregular footprint of the 10/140MB. The impact limiter diameter used for input to EYDROP is adjusted to account for the impact limiter 'flats', which reduce the impact - resisting area of the impact limiter. The equivalent diameter may be calculated as follows:

$$D_e = \left[D^2 - D^2(2/\pi)(\alpha - \sin\alpha\cos\alpha)\right]^{0.5}$$

Where D_e = equivalent diameter.

D = major diameter (101.0 in. in this case)

$\alpha = \cos^{-1}$ (Flat width/D) = $\cos^{-1}(96/101)$ = .316 radians

$$D_e = \left[101^2 - 101^2(2/\pi)[.316 - \sin(0.316)\cos(.316)]\right]^{0.5}$$

= 100.34 inches

The equivalent impact limiter geometry assumed for flat impact evaluation is shown in Figure 2.7.1-1.

2.7.1.1.1 Impact Limiter Deformation

Table 2.7.1-3 presents the results from the EYDROP energy balance program for

FIGURE 2.7.1-1

Impact Limiter Assumed Geometry for Flat End Drop

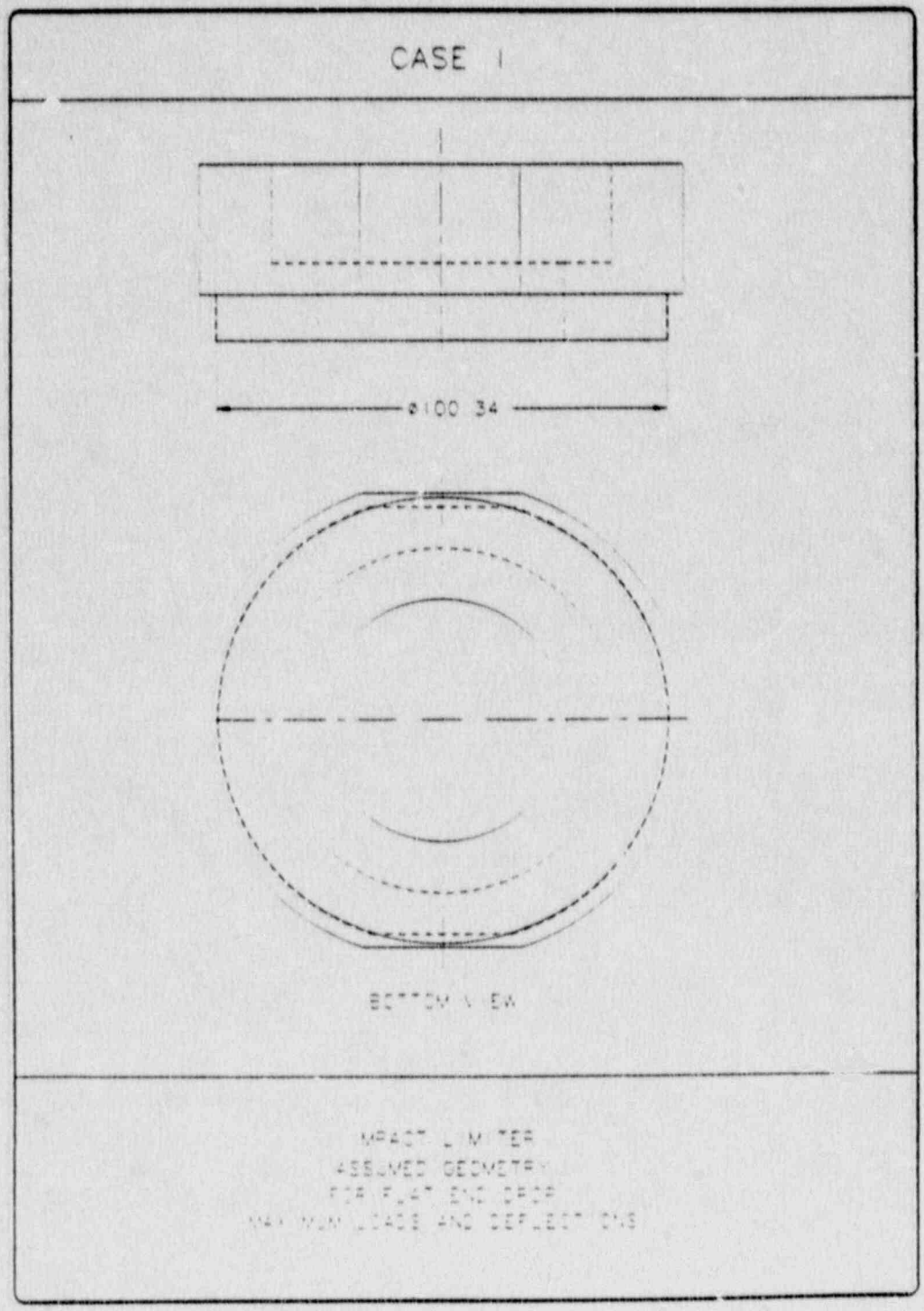

TABLE 2.7.1-3

EYDROP Results for 105°F Foam

EYDROP(END) NUPAC 10/140MB, WARM FOAM (105 DEG), N.A.C.

PACKAGE WEIGHT = 68000. (LBS)
PACKAGE DIAMETER = 100.54 (IN)
HOLE DIAMETER = 55.00 (IN)
OVERPACK DEPTH = 18.00 (IN)
DROP HEIGHT = 30.00 (FT)

CRUSH DEPTH (IN)	STRAIN	++++ IMPACT ++++ FORCE (LBS)	ACCEL. (G)	++++++ ENERGY ++++++ KINETIC (IN-LB)	STRAIN (IN-LB)	RATIO (SE/KE)	
.25	.014	1410882.	20.7	24497000.	176360.	.007	
.50	.028	2821764.	41.5	24514000.	705441.	.029	
.75	.042	3699090.	54.4	24531000.	1520548.	.062	
1.00	.056	4174104.	61.4	24548000.	2504697.	.102	
1.25	.069	4375511.	64.3	24565000.	3573399.	.145	
1.50	.083	4533931.	66.7	24582000.	4687079.	.191	
1.75	.097	4640952.	68.2	24599000.	5833940.	.237	
2.00	.111	4729863.	69.6	24616000.	7005291.	.285	
2.25	.125	4802739.	70.6	24633000.	8196867.	.333	
2.50	.139	4858699.	71.5	24650000.	9404547.	.382	
2.75	.153	4901310.	72.1	24667000.	10624548.	.431	
3.00	.167	4934140.	72.6	24684000.	11853979.	.480	
3.25	.181	4960755.	73.0	24701000.	13090841.	.530	
3.50	.194	4984723.	73.3	24718000.	14334025.	.580	
3.75	.208	5024772.	73.9	24735000.	15585212.	.630	
4.00	.222	5077688.	74.7	24752000.	16848020.	.681	
4.25	.236	5133947.	75.5	24769000.	18124474.	.732	
4.50	.250	5194171.	76.4	24786000.	19415489.	.783	
4.75	.264	5258983.	77.3	24803000.	20722133.	.835	
5.00	.278	5329005.	78.4	24820000.	22045631.	.888	
5.25	.292	5404859.	79.5	24837000.	23387364.	.942	
5.52	.306	5485228.	80.8	24854000.	24748625.	.996	1.000
5.75	.319	5570001.	81.9	24871000.	26130529.	1.051	
6.00	.333	5663261.	83.3	24888000.	27534687.	1.106	
6.25	.347	5766195.	84.8	24905000.	28963369.	1.163	
6.50	.361	5879988.	86.5	24922000.	30419141.	1.221	
6.75	.375	6005825.	88.3	24939000.	31904868.	1.279	
7.00	.389	6144891.	90.4	24956000.	33423708.	1.339	
7.25	.403	6293844.	92.6	24973000.	34978550.	1.401	
7.50	.417	6441017.	94.7	24990000.	36570407.	1.463	
7.75	.431	6608124.	97.2	25007000.	38201550.	1.528	
8.00	.444	6798972.	100.0	25024000.	39877437.	1.594	

an impact limiter at 105°F. This corresponds to the maximum temperature the polyurethane foam that the package might experience prior to the accident conditions tests, as described in 10 CFR 71 (see Section 3.4.6). Note that the 105°F temperature represents the maximum foam temperature, and not the average temperature. The minimum temperature in the impact limiter foam is actually only 101°F. It should also be noted that the foam properties assumed were taken at the lower bound that might be expected at that temperature. That is, foam strength was derated by 15% up to 75% strain, and by 20% thereafter. Refer to Section 2.1.2.4 for further details.

Interpolation of results for the energy balance point yields a maximum impact limiter deflection of 5.52 inches. Since the bottom of the impact limiter is 18 inches deep, it may be seen that this deformation will be of no consequence. The impact load for warm foam is calculated as 80.8 g's, which is less than half of the cold temperature loading derived in the next section.

2.7.1.1.2 End Impact Force Determination

The maximum acceleration imparted to the 10/140MB cask during a flat end impact from 30 feet was also calculated using the EYDROP program. For this bounding case, the highest foam strength possible (15% greater than the average for foam at -20°F, up to 75% strain, and 20% greater thereafter) was assumed.

The results of the EYDROP analysis are presented in Table 2.7.1-4. The accelerations for this case can be interpolated from the appropriate lines of output on the Table. As can be seen, the maximum end drop impact acceleration which might be expected for the 30 foot drop is 164.0 g's.

2.7.1.1.3 Axial and Hoop Stresses in the Shells

Of all impact orientations, the flat end impact causes the greatest acceleration to be imparted to the cask. This acceleration creates a significant compression load to be carried by the inner and outer shells of the package. The lead between the two shells complicates the state of stress,

TABLE 2.7.1-4

EYDROP Results for -20°F Foam

EYDROP(END) NUPAC 10/140MB, COLD FOAM (-20 DEG), M.A.C.

PACKAGE WEIGHT = 68000. (LBS)
PACKAGE DIAMETER = 100.34 (IN)
HOLE DIAMETER = 55.00 (IN)
OVERPACK DEPTH = 18.00 (IN)
DROP HEIGHT = 30.00 (FT)

CRUSH DEPTH (IN)	STRAIN	++++ IMPACT ++++ FORCE (LBS)	ACCEL (G)	++++++ ENERGY ++++++ KINETIC (IN-LB)	STRAIN (IN-LB)	RATIO (SE/KE)
.25	.014	2711659.	39.9	24497000.	338957.	.014
.50	.028	5423317.	79.8	24514000.	1355829.	.055
.75	.042	7592145.	111.6	24531000.	2982762.	.122
1.00	.056	8992200.	132.2	24548000.	5055805.	.206
1.25	.069	9761936.	143.6	24565000.	7400072.	.301
1.50	.083	10289657.	151.3	24582000.	9906522.	.403
1.75	.097	10596713.	155.8	24599000.	12517318.	.509
2.00	.111	10832304.	159.3	24616000.	15195945.	.617
2.25	.125	11003778.	161.8	24633000.	17925455.	.728
2.50	.139	11105777.	163.3	24650000.	20689150.	.839
2.75	.153	11152076.	164.0	24667000.	23471351.	.952 1.000
3.00	.167	11156446.	164.1	24684000.	26259947.	1.064
3.25	.181	11132672.	163.7	24701000.	29046087.	1.176
3.50	.194	11094518.	163.2	24718000.	31824486.	1.288
3.75	.208	11118663.	163.5	24735000.	34601133.	1.399
4.00	.222	11190747.	164.6	24752000.	37389819.	1.511
4.25	.236	11270228.	165.7	24769000.	40197432.	1.623
4.50	.250	11358662.	167.0	24786000.	43026043.	1.736
4.75	.264	11457605.	168.5	24803000.	45878076.	1.850
5.00	.278	11568613.	170.1	24820000.	48756354.	1.964
5.25	.292	11693243.	172.0	24837000.	51664086.	2.080
5.50	.306	11830802.	174.0	24854000.	54604591.	2.197
5.75	.319	11981998.	176.2	24871000.	57581191.	2.315
6.00	.333	12152396.	178.7	24888000.	60597991.	2.435
6.25	.347	12344204.	181.5	24905000.	63660066.	2.556
6.50	.361	12559628.	184.7	24922000.	66773045.	2.679
6.75	.375	12800878.	188.2	24939000.	69943108.	2.805
7.00	.389	13070160.	192.2	24956000.	73176987.	2.932
7.25	.403	13360371.	196.5	24973000.	76480804.	3.063
7.50	.417	13647287.	200.7	24990000.	79856761.	3.196
7.75	.431	13975332.	205.5	25007000.	83309588.	3.331
8.00	.444	14352109.	211.1	25024000.	86850519.	3.471

since it is much softer than the steel. As the acceleration increases, the lead expands radially at a different rate than the steel, and when the lead actually yields, both inner and outer shells support and contain the lead.

The response of the cask steel shells and lead shielding to the accident end drop event is determined using both hand calculations and finite element analyses. The principal concern for the cask shield wall assembly is with buckling of the inner shell. As shown by the following calculations, buckling will not occur as the result of the hoop and axial compressive stresses which develop in the cask inner shell under accident end drop conditions.

Various initial conditions can be assumed for the accident drop event. In particular, a temperature must be assumed in order to establish an initial fabrication stress for the inner shell. A lower assumed temperature will result in a higher initial hoop stress on the inner shell (see Section 2.6.2), but higher allowable stresses. For purposes of this analysis, drops at 128°F (maximum lead normal temperature per Section 3.4.2) and -20°F are considered. To adequately analyze the full consequences of the drop event at the given temperatures, two initial lead conditions are also considered. These are: (1) the lead shielding clings to the cask inner shell for the duration of the drop event, and (2) the lead shielding is free to slump during the drop event.

(1) Stresses in the Cask Shells and Lead Shielding (Maximum Fabrication Stress Condition Assumed)

The first condition assumes that the lead has shrunk onto the inner shell and away from the outer shell. In addition, due to the combined effects of friction between the lead and inner shell, and axial shrinkage of the lead relative to the shells, axial gaps will develop between the lead and the steel structures at the top and bottom end of the lead column. These axial gaps are important in that, until friction is overcome, under increased axial loading, the lead will impose a direct axial load on the inner shell.

Once friction is overcome, the lead will become supported at its base (the bottom of the lead column) and will grow radially outward due to the 'Poisson Effect' under increased axial loading. This radial growth will tend to

relieve the initial fabrication hoop stress as the lead separates from the inner shell. If sufficient axial load develops, the lead would grow out to the outer shell, creating tensile hoop stresses therein. Under further loading, the lead would eventually begin to yield and flow back inward onto the inner shell, thereby developing compressive hoop stresses in the inner shell. Since the primary mechanism of this load case would be to relieve stresses on the critical inner shell, it is not considered to be a worst-case condition.

From Section 2.6.2, hoop stress in the inner shell due to fabrication is as follows:

Temperature (°F)	Inner Shell Hoop Stress (psi)
128	-1,793 (extrapolated)
70	-2,041
-20	-2,642

Note: The outer shell hoop stress is considered negligible since the lead separates from the outer shell upon cooling.

The equivalent pressure at the lead/inner shell interface is as follows:

$$p = \sigma t/r$$

Where:

$t = 0.75$ in

$r = 33.375$ in

Thus, the interface pressures at the different temperatures are:

Temperature (°F)	Interface Pressure, p (psi)
128	40.3
70	45.9
-20	59.4

With a coefficient of friction, f, for lead on stainless steel assumed to fall in the 0.5 to 1.0 range (Refer to Mark's Standard Handbook for Mechanical Engineers, Reference 2.11.12, p. 3-26), the load, P, which can be supported by friction at the lead/inner shell interface, may be determined as follows:

$$P = \pi DLpf$$

Where:

D = 67.5 in (inner shell outside diameter)

L = 77.5 in (lead column height)

p = interface pressure, psi

f = 0.5 to 1.0 (coefficient of friction)

Applying the interface pressures determined earlier, the total load which may be supported is:

Temperature (°F)	Coefficient of Friction	Load Supported (lbs)
128	0.5	331,090
	1.0	662,179
70	0.5	376,885
	1.0	753,769
-20	0.5	487,863
	1.0	975,727

With the total lead weight equal to 15,666 lb., the maximum g-load which can be supported by friction is 975,727/15,666 = 62.3 g's. The Hypothetical Accident Condition g-load's range from 80.8 g's at 128°F to 164.0 g's at -20°F. Since all possible accident condition g-loads are significantly greater than the maximum at which the lead can be supported by friction, the lead will always slip, and this load case will not be of concern here.

(2) Stresses in the Outer Cask Shells and Lead (Zero Fabrication Stress Condition Assumed)

The second initial lead condition assumes that fabrication stresses, as associated with lead shrinkage, have fully crept away resulting in a stress-free column of lead just in contact with the inner and outer shells. This is a potential worst case since any axial load imposed on the lead will directly load, radially, both the inner and outer shells (i.e., the lead need not flow away from the inner shell, into the outer shell and back into the inner shell to develop a compressive hoop stress in the inner shell).

For this condition, initial stresses in the lead and the steel shells are taken as zero. As axial load is applied to the lead and shells, the lead will attempt to move downward and outward and develop pressures on both the inner and outer shells.

Utilizing the analytical technique developed in Section 2.6.7.1.3, inner and outer shell hoop and axial stresses can be calculated. The geometry to be

considered is as follows:

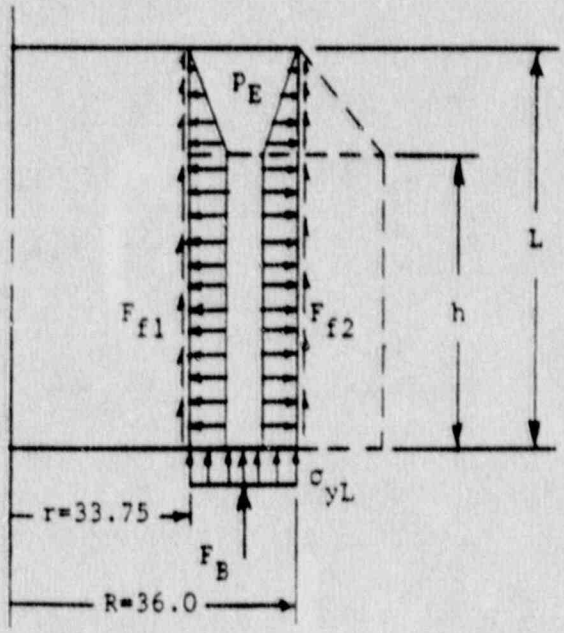

The height, h, at which the lead reaches its yield point is:

$$h = L - \sigma_{yL}/\gamma\rho_L$$
$$= 77.5 - 600/(164.0)(0.41) = 68.6 \text{ in}$$

Static equilibrium of the lead column yields:

$$W_L = F_B + F_{f1} + F_{f2}$$

Where:

$$W_L = (15{,}666)(164.0) = 2{,}569{,}220 \text{ lb}$$

$$F_B = (600)\pi(36.0^2 - 33.75^2) = 295{,}820 \text{ lb}$$

F_{f1} = Frictional Reaction Force on Inner Shell

F_{f2} = Frictional Reaction Force on Outer Shell

Inner and outer shell radial forces are:

$$F_{R1} = F_{f1}/0.5, \text{ or } F_{f1} = 0.5\ F_{R1}$$

$$F_{R2} = F_{f2}/0.5, \text{ or } F_{f2} = 0.5\ F_{R2}$$

Also:

$$F_{R1} = 0.5\ p_E\ \pi D_1\ (L+h)$$

and:

$$F_{R2} = 0.5\ p_E\ \pi D_2\ (L+h)$$

Solving for F_{R1} and F_{R2} in terms of p_E and substituting back into the lead equilibrium equation yields:

$$W_L - F_B = 0.25\ \pi P_E\ (D_1 + D_2)\ (L+h)$$

or:

$$p_E = 4\ (W_L - F_B)/[\pi(D_1+D_2)(L+h)]$$

From which:

$$p_E = 142.0 \text{ psi}$$

Therefore, the inner shell hoop stress is:

$$\sigma_1 = -p_E R_1/t_1$$
$$= -(142.0)(33.375)/(0.75) = -6,320 \text{ psi}$$

The outer shell, tensile hoop stress is:

$$\sigma_2 = p_E R_2/t_2$$

= (142.0)(36.625)/(1.25) = 4,160 psi

To evaluate axial stresses in the shells, a similar approach to that detailed in Section 2.6.7.1.3 is utilized.

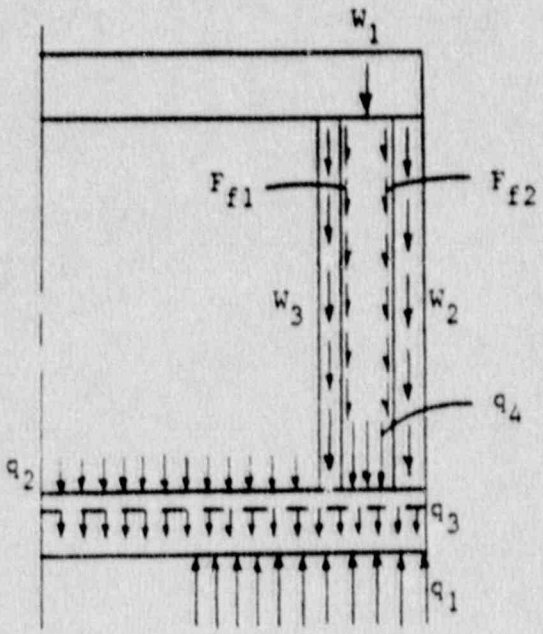

$F_{f1} = 0.25\ \pi\ D_1 p_E\ (L+h)$

$F_{f1} = 1{,}099{,}847$ lb

$F_{f2} = 0.25\ \pi\ D_2\ p_E\ (L+h)$

$F_{f2} = 1{,}173{,}170$ lb

W_1 = (Weight of top impact limiter and cask lid assembly)(164.0 g's)

$= (14,000)(164.0) = 2,296,000$ lb

W_2 = (Weight of cask outer shell, thermal shield, etc)(164.0 g's)

$= (7,790)(164.0) = 1,277,360$ lb

W_3 = (Weight of cask inner shell)(164.0 g's)

$= (3,510)(164.0) = 575,640$ lb

W_L = (Weight of lead)(164.0 g's)

$= (15,666)(164.0) = 2,569,220$ lb

W_B = (Weight of bottom plate)(164.0 g's)

$= (6,460)(164.0) = 1,059,440$ lb

q_2 = (Weight of payload)(164.0 g's)$/\pi(33.375)^2$

$= (15,000)(164.0)/\pi(33.375)^2 = 703.0$ lb/in^2

$q_1 = \left[W_1 + W_2 + W_3 + W_L + W_B + q_2\pi(33.375)^2\right]/\pi(36.625^2 - 27.5^2)$

$= 5,569.3$ lb/in^2

$q_3 = W_B/\pi(36.625)^2$

$= 251.4$ lb/in^2

$q_4 = F_B/\pi(36.625^2 - 33.375^2)$

$= 413.9$ lb/in^2

From the computational technique used in Section 2.6.7.1.3, relative deflection due to the pressure loads is:

$\delta_1 - \delta_2$ = -0.02205 in (positive downward) for no payload reaction
= -0.002945 in with payload reaction

$\delta_1 = R_3 L/A_1E_1 - (W_3 + F_{f1})L/2A_1E_1$

$\delta_2 = R_4 L/A_2E_2 - (W_2 + F_{f2})L/2A_2E_2$

$R_4 = W_1 + W_2 + W_3 + F_{f1} + F_{f2} - R_3$

$= 6,422,220 - R_3$

Solving simultaneously, the inner and outer shell reaction loads become:

R_3 = 3,159,120 lb without payload, and 2,446,920 lb with payload

R_4 = 3,263,100 lb without payload, and 3,975,300 lb with payload

Therefore, axial stresses in the inner and outer shells are:

$\sigma_1 = -R_3/A_1$ = -20,086 psi without payload, and -15,558 psi with payload

$\sigma_2 = -R_4/A_2$ = -11,344 psi without payload, and -13,820 psi with payload

Conservatively ignoring inner shell radial compressive loading, maximum stress intensity in the shell is:

I_1 = 0 - (-20,086) = 20,086 psi

From Table 2.1.2-1, item reference number 1(B), the stress allowable for the inner shell is the lesser of $2.4S_m$ or $0.7S_u$, where S_m = 20,000 psi and S_u = 74,000 psi at 128°F (from Table 2.3-1). For the inner shell material, the allowable is thus (2.4)(20,000) = 48,000 psi (which is less than (0.7)(74,000) = 51,800 psi).

The stress Margin of Safety for the inner shell is thus:

M.S. = 48,000/20,086 - 1 = +1.39

From Table 2.1.2-5, buckling allowables at 128°F are 27,593 psi (axial) and 26,042 psi (hoop). Buckling Margin of Safety is thus:

$$M.S. = 1/\left[(20,086/27,593)+(6,320/26,042)\right]-1$$

$$= +0.03$$

Stress intensity of the outer shell is:

$S.I._2$ = 4,160 - (-11,344) = 15,504 psi for no payload reaction
= 4,160 - (-13,820) = 17,980 psi with payload reaction included

From Table 2.1.2-2, item reference number 1(B), the allowable stress for this non-containment structure is $0.7S_u$, where S_u = 70,000 psi at 128°F. Thus, the stress Margin of Safety is:

M.S. = (0.7)(70,000)/17,980 - 1 = +1.73

From Table 2.1.2-6, the axial buckling allowable at 128°F is 36,258 psi. The buckling Margin of Safety is therefore:

M.S. = 1/(13,820/36,258) - 1 = +1.62

Again, using the same computational technique provided in Section 2.6.7.1.3, bending moment at the center of the end plate is:

M_c = -127,891 in-lb/in (without payload)
= 63,075 in-lb/in (with payload)

where a positive moment indicates tension on the bottom surface of the base plate.

In addition to the hand analysis developed above, a finite element model was

developed to analyze this phenomenon using the common ANSYS structural analysis code. A description of ANSYS is given in Appendix 2.10.2, and details of the analysis are shown in Appendix 2.10.6. The analytical approach to bounding all temperature-related phenomena are the same as for the preceeding classical type analyses, and are recapitulated briefly below.

While the minimum temperature condition for the drop event (-20°F) induces the highest acceleration loading (164.0 g's), the material properties are also at a maximum (refer to Sections 2.1 and 2.3 for details). Likewise, though the maximum temperature case results in lower impact loads (a maximum 80.8 g's), material properties are also reduced at the higher temperature condition. Refer to Section 2.1.2.4, Impact Limiter Design Criteria, as well as Sections 2.7.1.1.1 and 2.7.1.1.2 above for details of the effects of temperature variation on drop loads.

Thus, to conservatively bound the buckling and stress allowable calculations, the maximum g-load (obtained at the minimum temperature condition) was applied to the analysis while utilizing reduced-strength material properties (found at the higher temperature), which will tend to maximize stresses. Therefore the analysis utilized material properties based on an expected Normal Condition of Transport temperature of 128°F at the inner shell. Refer to Section 3.0, Thermal Evaluation, for details of this temperature condition.

For the worst-case loading to be applied to the cask inner shell (the containment boundary), internal pressure and payload reaction pressure were both omitted. Neglecting internal pressure will maximize the compressive loading and buckling effects of lead shielding pressure applied to the outside surface of the inner shell. Neglecting payload reaction, as demonstrated by hand calculations above, and reinforced by the lid analyses below, will result in an inward bowing of the cask lid, resulting in the greater portion of the reaction loading being applied to the inboard portion of the primary EnviroSeal™ plate. This, in turn, will maximize axial loads on the inner shell. A bottom-down drop orientation is assumed, since the top lid, being heavier than the bottom lid or plate, will impose a greater load on the cask shield wall assembly under end drop accelerations.

The finite element analysis was run beyond its theoretical maximum acceleration of 80.8 g's (accident condition end drop load at the upper temperature limit) up to 170.0 g's, to investigate accident condition stresses at normal condition temperature material properties. Further conservatism is thus induced in the analysis, since the Hypothetical Accident Conditions drop, whose maximum anticipated temperature at the critical area during the drop event is only 106°F, was analyzed at the higher normal condition temperature of 128°F, where material properties will be lower and resulting stresses higher.

The results of the stress and buckling analyses for Hypothetical Accident Conditions, detailed in Appendix 2.10.6, are summarized in Tables 2.7.1-5 and 2.7.1-6.

The above analyses used material properties and stress and buckling allowables at the upper temperature extreme (128°F), which conservatively overestimates the stresses and underestimates margins of safety that would actually occur at any hypothetical accident temperature. Additionally, because the actual cold condition drop load was only 164.0 g's and not 170 g's, the high degree of conservatism already inherent in the analyses becomes even greater. The actual margins of safety will therefore be significantly larger than those shown, and it is thus readily demonstrated that the shells will not buckle or exceed allowable stress limits at any temperature in the range of interest.

A comparison of hand calculations and finite element analysis results is presented below. As can be seen, good correlation is achieved for the stress components on both shells. The difference in results can most likely be attributed to end constraint effects in the finite model which were not taken into account in the hand analysis.

As a final note, examination of the finite element results indicates that the inner and outer shell hoop stresses under end drop loading increase gradually from the top (non-impacted) end of the cask to a point approximately one-quarte of the way down. They then tend to remain fairly uniform down to the bottom (impacted) end of the cask. These results support the validity of the

TABLE 2.7.1-5

End Drop Finite Element Analysis Shell Stress Analysis
Results Summary

Drop Load = 170 g's
(Actual Drop Load is 164 g's at -20°F)

Material Properties and Stress Allowables Temperature = 128°F
(Actual Temperature During Drop is 106°F)

Maximum Inner Shell Stress Intensities		Maximum Outer Shell Stress Intensities	
Surface (Element 51)	Membrane (Element 38)	Surface (Element 60)	Membrane (Element 60)
21,695 psi	18,427 psi	20,007 psi	13,806 psi
Stress Intensity Allowables*		Stress Intensity Allowables**	
72,000 psi	48,000 psi	70,000 psi	49,000 psi
Margins of Safety		Margins of Safety	
+ 2.32	+ 1.61	+ 2.50	+ 2.55

* See Table 2.1.2-1
** See Table 2.1.2-2

TABLE 2.7.1-6
(Page 1 of 2)

End Drop Finite Element Shell Buckling Analysis
Results Summary

Drop Load = 170 g's
(Actual load is 164 g's at -20°F)

Material Properties and Buckling Allowables Temperature = 128°F
(Actual Temperature During Drop is 106°F)

Maximum Inner Shell Stresses		Maximum Outer Shell Stress
Axial	Hoop	Axial
(Element 57)		(Element 42)
-18,188 psi	-7,341 psi	-14,896 psi
Buckling Allowables*		Buckling Allowable**
27,593 psi	26,042 psi	36,258 psi
Margin of Safety		Margin of Safety
+ 0.06		+ 1.43

* See Table 2.1.2-5
** See Table 2.1.2-6

TABLE 2.7.1-6
(Page 2 of 2)

Bending (Element 51)	Bending (Element 60)
21,695 psi	20,007 psi
Buckling Allowable*	**Buckling Allowable****
27,754 psi	36,376 psi
Margin of Safety	**Margin of Safety**
+ 0.30	+ 0.82

* See Table 2.1.2-5
** See Table 2.1.2-6

lead slump pattern utilized in the hand calculations.

Stress Component	Hand Analysis	F.E. Analysis
Inner Shell Axial Stress (psi)	-20,086	-18,188
Inner Shell Hoop Stress (psi)	-6,320	-7,341
Inner Shell Buckling M.S.	+0.03	+0.06
Outer Shell Axial Stress (psi)	-13,820	-11,621
Outer Shell Hoop Stress (psi)	4,160	-3,275*
Outer Shell Buckling M.S.	+1.62	+1.43

* Away from end effects, outer shell hoop stresses range from about +4,500 psi to +5,800 psi.

From the preceeding analyses, it is apparent that the cask inner and outer shells will withstand the regulatory Hypothetical Accident Condition end drop event for all applicable temperatures and cask parameters.

2.7.1.1.4 Lid Stress Analysis

Because the end drop impact acceleration at -20°F (164.0 g's, from Table 2.7.1-4) is very much higher than that at the upper temperature bound (80.8 g's, from Table 2.7.1-3), margins of safety in the lid will be conservatively calculated using the acceleration expected at -20°F and material properties taken at the maximum component temperature (top lid, under Normal Conditions of Transport) of 133°F. Stress allowables are likewise conservatively derived at the maximum normal condition temperature for the lids. This is conservative because, at the start of the accident, the maximum lid

temperature is only 110°F.

To accurately predict stress levels under end drop impact conditions for the rather complex lid configurations utilized in the 10/140MB cask, a finite element analysis was undertaken using the ANSYS program described in Appendix 2.10.2. Both the top lid assembly (primary and secondary lids) as well as the bottom lid for the optional bottom loading configuration were evaluated.

Details of this analysis are given in Appendix 2.10.7, and are summarized in Table 2.7.1-7 below.

For the case of the fixed bottom configuration, the previously determined moments (Section 2.7.1.1.3) can be directly used to arrive at the maximum bending stress at the center of the end plate. The maximum moment at the center of the end plate is determined to be:

$$M_c = 127,891 \text{ in-lb/in (no payload, lead slump)}$$

The corresponding stress is therefore:

$$\sigma_B = 6M_c/t^2 = 21,315 \text{ psi}$$

Where t = 6.0 in (average plate thickness)

With an allowable of S_n = 68,785 psi, the corresponding Margin of Safety becomes:

$$M.S. = 68,785/21,315 - 1 = +2.23$$

It is therefore apparent that the cask bottom of either version of the 10/140MB cask is suitably designed to withstand the regulatory drop requirement on the end of the bottom impact limiter.

TABLE 2.7.1-7

End Drop Finite Element Lid Stress Analysis

Results Summary

	Lid	Max. Bending Stress (psi) (Margin of Safety)	Max. Membrane Stress (psi) (Margin of Safety)	Max. Primary Bolt Stress (psi) (Margin of Safety)	Max. Secondary Bolt Stress (psi) (Margin of Safety)
With Payload Reaction	Bottom	22453 (M.S. = +2.06)	15537 (M.S. = +2.09)	2360 (M.S. = +Large)	---
	Top	34314 (M.S. = +1.00)	15923 (M.S. = +2.01)	2406 (M.S. = +Large)	82000 (M.S. = +0.26)
Without Payload Reaction	Bottom	12914 (M.S. = +4.33)	13919 (M.S. = +2.45)	2264 (M.S. = +Large)	---
	Top	11763 (M.S. = +4.85)	14031 (M.S. = +2.42)	3988 (M.S. = +Large)	20242 (M.S. = +4.09)

2.7.1.1.5 Primary and Secondary Lid Bolts

From the finite element lid analysis results presented in Appendix 2.10.7 and summerized above in Section 2.7.1.1.4, it was found that neither the top or bottom primary lid closure bolts exceed their tensile prestress during the end impact event, with or without the full payload present. The primary bolts for both top and bottom lids unload completely at accident condition impact loads, for the case with full payload present. This unloading of primary lid bolts is viewed as a transitory phenomenon, occuring only during the short duration of the impact event. In any case, analysis results indicate that pressure is maintained on the primary EnviroSealtm plates during the impact by reaction forces between the cask and lid.

The primary bolt maximum preload value will thus be taken as a worst case for accident condition end drops. The bolt stress due to the 17,350 lb preload is 17,350/4.0 = 4,340 psi. Since this stress is less than that for normal conditions (refer to Section 2.6.7.1.5), and since the allowable stress is greater for accident conditions than for normal conditions (S_y vs $2.0S_m$), it may be assumed that the Margin of Safety for primary bolts under accident condition loading is even larger than that derived for normal conditions. Primary bolt loads will therefore not be a consideration for accident condition flat end drops.

The loading on the secondary lid bolts may be derived from examination of the finite element results from Appendix 2.10.7, Section 2.10.7.4. Maximum loading occurs for the case with full payload present. The 'smeared' secondary bolt element (element 95) of the axisymmetric model shows a maximum load of 175,710 lb/radian, or an equivalent of (175,710)(2π)/16 = 69,000 lb/bolt. The bolt load due to pressure effects is 10,459 lb. Superposing the two load cases results in a total bolt load of 69,000 + 10,459 = 79,459 lb. As pointed out in Section 2.6.7.1.5, adding pressure effects for this load case is conservative. The total bolt load translates into a bolt stress of:

$$\sigma_{bolt} = 79,459/0.969 = 82,000 \text{ psi}$$

From Table 2.1.2-1, item reference number 7(B), the maximum allowable fastener

membrane stress under accident conditions is the material's specified minimum yield stress S_y. From Table 2.3-1, this value for the bolt material at its maximum temperature of 133°F (top lid under Normal Conditions of Transport) is 103,000 psi. The Margin of Safety in the bolts is then:

M.S. = 103,000/82,000 - 1 = +0.26

From the finite element results for the case without payload applied to the lids, it was found that the secondary lid bolt load was 19,614 lb/bolt. This is less than the case with the payload present, so the secondary bolt Margin of Safety will be greater for this case.

2.6.7.1.6 EnviroSeal[tm] Plate Bearing Stresses

The only other significant consideration for end drop loading is that of bearing stresses on the EnviroSeal[tm] plates. For the primary seal plate, the worst-case assumption would be that the cask lid at the impacted end is supported by the impact limiter at that end, while the combined weight of the cask shield wall and opposite end lid and impact limiter bear directly onto the seal plate under maximum end drop loading. The most critically loaded seal plate will be that for the bottom lid during a bottom-down impact. This is due to the fact that the seal plate dimensions for the optional bottom lid are the same as for the top primary lid, and the top lid assembly weighs more than the bottom lid (8,430 lb vs 6,460 lb, per Section 2.2). Therefore, for the same seal plate surface area, more weight will be bearing on the bottom seal plate during a bottom-down drop than would be acting on the top seal plate during a top-down impact.

The primary lid EnviroSeal[tm] plate basic dimensions are illustrated below:

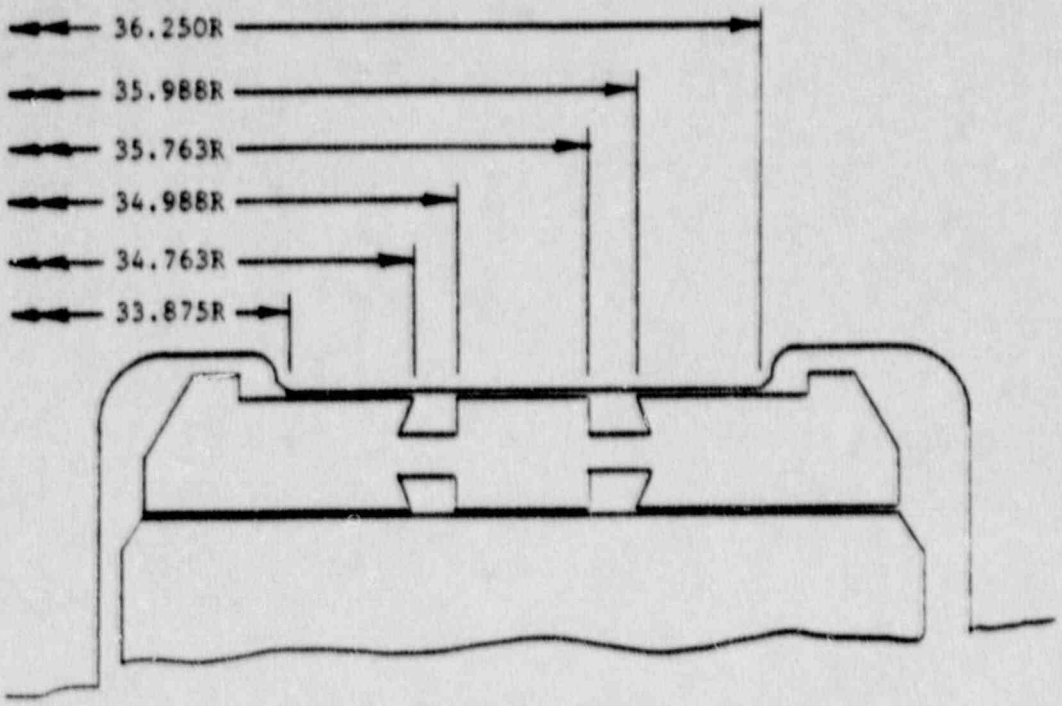

Using this illustration and the drawings in Section 1.3, the minimum bearing surface area of the seal plate can be calculated as 323.0 in^2. This bearing area makes allowance for all chamfers, O-ring grooves, and test gas communication ports and channels. The total weight of the bearing structures is, from Section 2.2, 8,430 lb (top lid assembly) + 26,960 lb (cask body) + 5,575 lb (impact limiter) = 40,965 lb. Under the maximum accident condition end drop loading of 164 g's, the bearing stress on the seal plate and mating surfaces can be calculated as:

$$\sigma_b = (164)(40,965)/323.0 = 20,800 \text{ psi}$$

The maximum allowable bearing stress on seal surfaces is S_y (Table 2.1.2-1, reference case number 4(B)). At the maximum anticipated seal area operating temperature of 133°F, for the lowest-strength seal plate or lid material, S_y = 28,400 psi (ASTM A-240 Type 304 for the seal plate, ASTM A-182 Type F304, or A-351 Type CF8/304 for the lid). The Margin of Safety for bearing stress is:

M.S. = 28,400/20,800 - 1 = +0.37

For the top lid secondary seal plate, the cross-section is illustrated below. For this geometry, the bearing surface is 108.5 in^2.

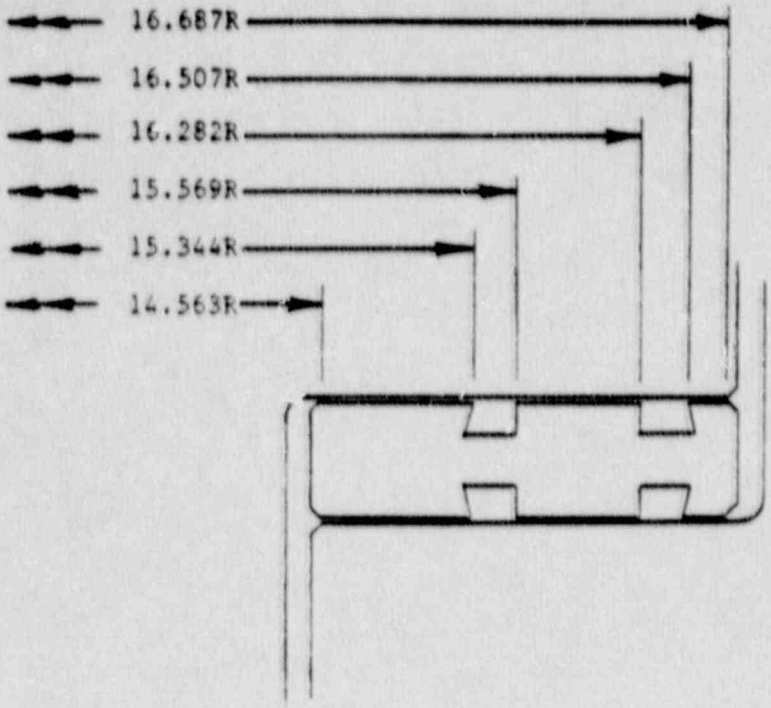

A potential worst-case bearing stress on the secondary EnviroSeal^{tm} plate will occur during a bottom-down end impact. Under this loading condition, the full weight of the 1,700 lb secondary lid, factored by the maximum end drop g-load of 164 g's, will bear on the seal plate. The maximum secondary seal plate bearing stress is thus:

$$\sigma_b = (164)(1,700)/108.5 = 2,570 \text{ psi}$$

Another possible worst-case is that of primary lid bearing on the secondary seal plate during a top-down end drop. An examination of the finite element

results of Appendix 2.10.7 reveals the maximum bearing load on the secondary seal occurs during the end drop case with full payload present. For this case, element 52, one of the gap elements representing the secondary seal plate interface with the primary lid, is closed and under load. The other seal plate gap element (element 51) is open for this load case. The total load acting on the EnviroSeal^{tm} under this condition is 52,841 lb/radian, or (52,841)(2π) = 332,000 lb total load. The bearing stress is then:

$$\sigma_b = 332,000/108.5 = 3,060 \text{ psi}$$

Both these values are considerably less than the bearing stress calculated above for the primary lid seal plate, so the Margin of Safety will be greater for the secondary lid seal plate.

2.7.1.1.7 Lead Slump

The finite element analysis performed in Appendix 2.10.6 demonstrates that the lead might be expected to slump 0.3 inches during end impact at the maximum drop temperature. Due to the stepped configuration of the primary lids, this small amount of lead settlement will not adversely affect the ability of the package to meet the shielding requirements of 10 CFR 71.

2.7.1.2 Oblique Impact

Analysis of the NuPac 10/140MB package behavior during hypothetical oblique impacts from drops of 30 feet has been performed in the following steps:

1. Use the CYDROP computer program in conjunction with the lowest crush strength foam data to determine worst case impact limiter deformation to insure that the package will not 'bottom out'.

2. Use CYDROP with the highest crush strength foam data to determine a conservative estimate of the force-deflection relationship of the 10/140MB impact limiter design at various impact angles.

3. Use the OBLIQUE program to determine a conservative estimate of internal forces in the 10/140MB during impact.

4. Determine the worst case stress state from internal forces in the cask body.

5. Determine lid attachment forces and stresses in the lid closure system under worst-case conditions.

6. Determine impact limiter attachment forces and stresses under worst-case conditions.

2.7.1.2.1 Worst-Case Corner Deformations

Because the containment and shielding structure of the 10/140MB is many times harder than the polyurethane foam impact limiters, it is essential that it may be demonstrated that the cask shield and associated hardware will not actually strike the impact surface. The worst-case drop orientation for impact limiter deformation is that where the center of gravity of the package is directly over the impact point. In this c.g. over struck corner impact, the impact limiter deformation occurs in essentially a state of neutral equilibrium.

Because none of the kinetic energy of the thirty foot drop is dissipated in rotational motion of the package, all the drop energy must be absorbed in strain energy of the deforming foam impact limiters. For this reason, the c.g. over struck corner impact is used to demonstrate maximum possible crush depth. It will be demonstrated that, even with maximum impact limiter deformation, a residual clearance will be maintained between the cask and the impacted unyielding surface.

Additionally, since the mechanical strength of the foam decreases with temperature, greater deformations may be expected with higher temperature foam for a given drop height. Therefore, the energy balance program CYDROP was used in conjunction with the minimum polyurethane foam stress-strain properties at 105°F to determine a conservative estimate of the maximum deflection.

Finally, because CYDROP is written for simple cylinders, the somewhat unorthodox geometry of the 10/140MB impact limiters required that conservative simplifying assumptions be made. To this end, two extreme bounding cases were run. The first case assumes that the impact limiter is a cylinder of 101 inches outside diameter along its full length. This assumed configuration corresponds to the diameter of the 10 inch long end 'cap', and ignores the contribution of the impact limiter beyond the 101 inch diameter base of the impact limiter. This will conservatively overestimate the amount of deflection required to generate enough strain energy to balance the energy of impact. This assumed geometry is illustrated in Figure 2.7.1-2.

The second bounding case assumes a 96 inch impact limiter diameter. This dimension corresponds to the distance across the flats of the end 'cap' portion of the impact limiter. Since larger volumes of crushed foam are ignored, this assumed geometry is even more conservative than that above. The assumed configuration is shown in Figure 2.7.1-3.

The results of the 101 inch diameter case impacting with the package c.g. over the struck corner are presented in Table 2.7.1-8, and results for the 96 inch case are given in Table 2.7.1-9. These results show that the 101 inch diameter impact limiter would deflect 19.78 inches, while the 96 inch diameter case would deflect 19.33 inches.

The impact orientation analyzed above, where the center of gravity is directly over the impact point, is approximately 40° from vertical. The available crush depth or the flattened side of the impact limiter may be determined from the sketch below:

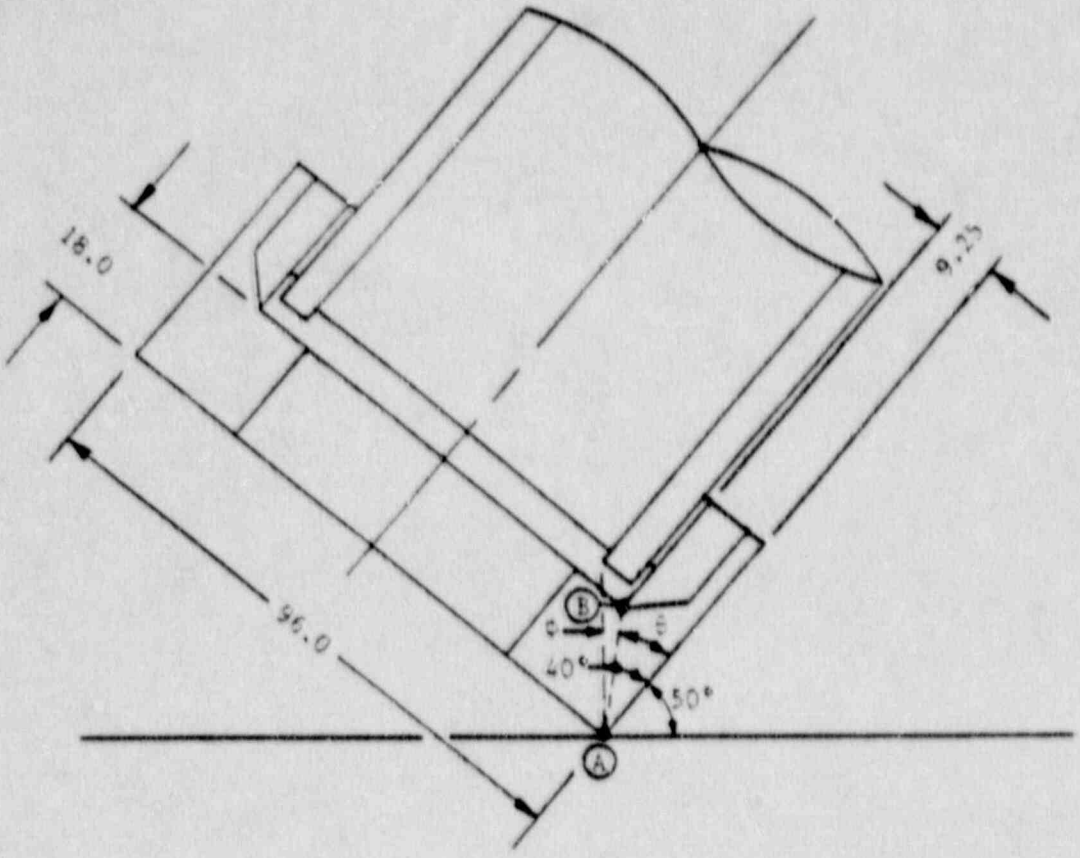

The distance from point A to point B in the figure is:

$$AB = [(9.25)^2 + (18.0)^2]^{0.5} = 20.24 \text{ inches}$$

FIGURE 2.7.1-2

Impact Limiter Assumed Geometry for Center of Gravity Over Struck Corner Drop - 101 Inch Diameter Impact Limiter

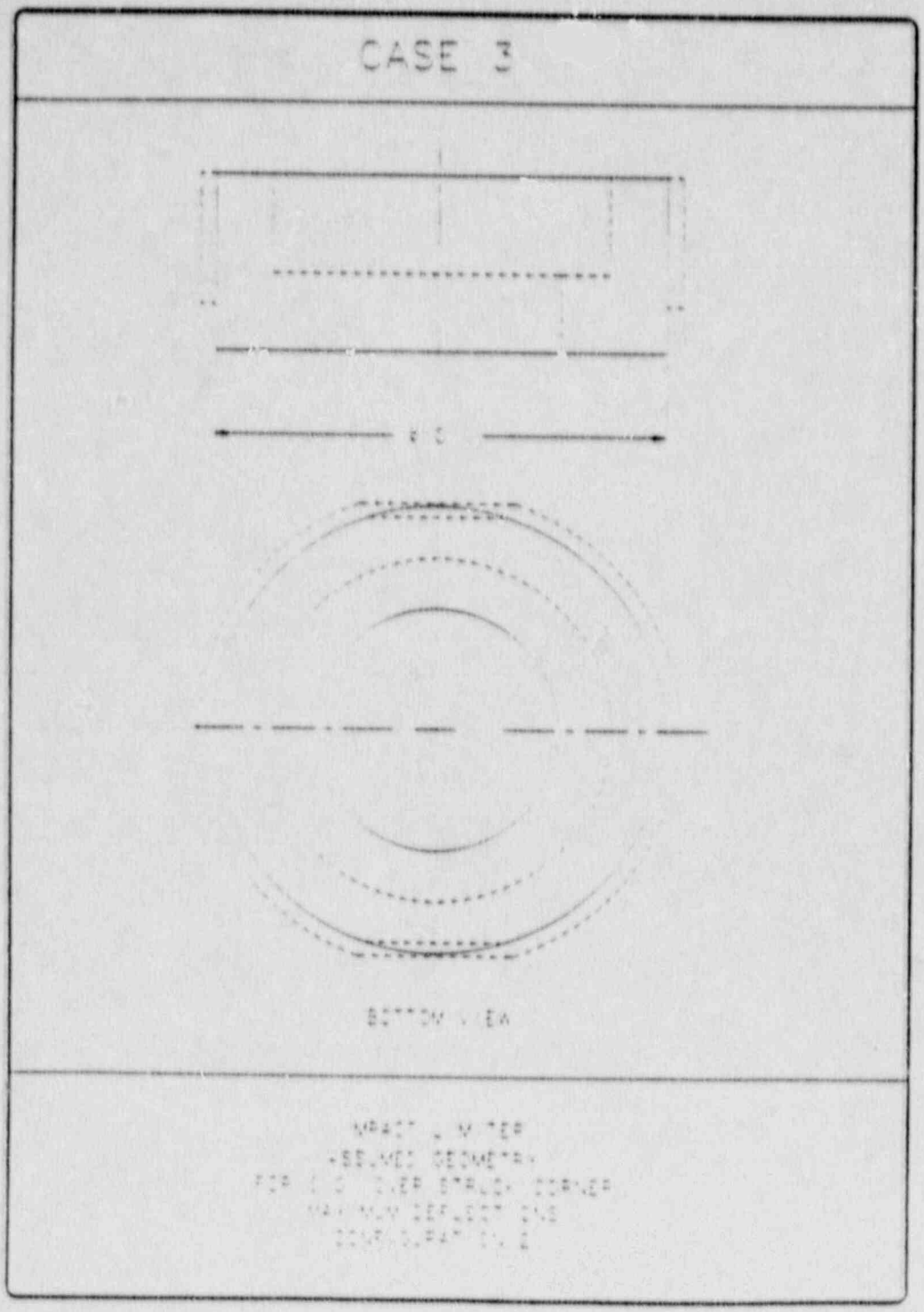

FIGURE 2.7.1-8

Impact Limiter Assumed Geometry for Center of Gravity Over Struck Corner Drop - 96 Inch Diameter Impact Limiter

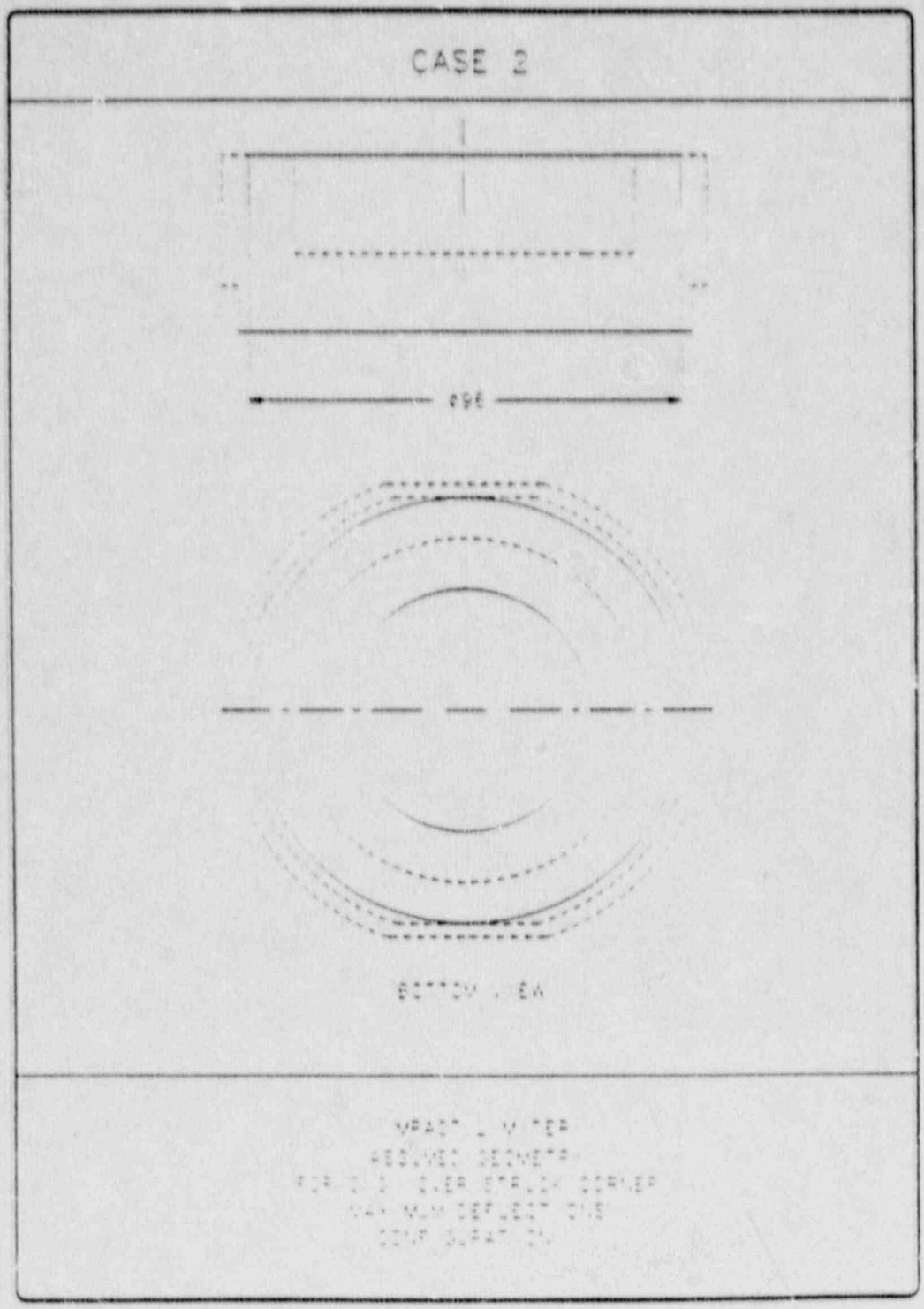

Table 2.7.1-8

Proprietary

Table 2.7.1-9

Proprietary

The maximum possible crush depth (to the point where the cask first contacts the impact surface) can be derived as follows:

$$\delta_{max} = R\theta \cos\theta$$

Where: $\theta = 40^o - \Theta$

$\Theta = \tan^{-1}(9.25/18.0) = 27.2^o$

$$\delta_{max} = 19.74 \text{ in}$$

Since for the 96 inch diameter case only 19.33 inches of deflection is predicted, clearance is maintained between the cask hard point and the impacted surface, even under this extremely conservative analysis approach.

For the 101 inch diameter case, the maximum crush depth that could be allowed prior to 'bottoming out' may be derived in the same manner as above. In this case, the maximum crush depth is 21.50. Since CYDROP predicts only 19.78 inches of deflection under a conservative analysis, there will be an even greater residual clearance remaining during impact on the 101 inch diameter portions of the impact limiter. These results indicate that under the most extreme conditions, the 10/140MB impact limiter is large enough and stiff enough to protect the shield and containment structures from impacting the hypothetical unyielding surface directly.

2.7.1.2.2 Worst-Case Force - Deflection Relationship

In order to obtain a conservative estimate of the internal forces and stresses within the NuPac 10/140MB, assumptions were made regarding the impact limiter geometry input to both CYDROP and OBLIQUE (Nuclear Packaging's oblique impact analysis tools) to maximize both impact reaction forces (in the CYDROP input) and cask body forces (in the OBLIQUE input). These assumptions were required due to the somewhat complicated impact limiter profile used on the 10/140MB.

A conservatively high force-deflection relationship was obtained by assuming the impact limiter is only 13 inches thick on the end of the package, and 13.75 inches thick on the side of the package. This corresponds to an impact

limiter whose outer corner is halfway between the 101 inch diameter corner and the 108 inch diameter corner. The assumed geometry is illustrated in Figure 2.7.1-4.

Because the assumed impact limiter is so much smaller than the actual impact limiter, and because the stress-strain properties of -20oF foam, increased by 15% (increased by 20% at 80% strain) were used, the stresses in the crushed polyurethane foam are predicted to be much higher than would occur in reality. This is due to the fact that foam strains will be greater on a smaller impact limiter for the same crush depth than on an actual, full-size impact limiter. Strain-hardening effects will therefore be more pronounced, resulting in higher reaction forces. Additionally, predicted crush depths will be greater for the small geometry than for the actual configuration, due to the smaller volume of foam available for energy absorption. This will result in an even greater increase in reaction forces than would occur for equal deformations.

The results of this conservative CYDROP analysis, in the form of force-deflection tables at various drop angles, were next utilized in NuPac's OBLIQUE program to determine cask body forces resulting from impacts at the corresponding drop angles.

2.7.1.2.3 Internal Forces during Oblique Impact

Cask internal forces are calculated by NuPac's OBLIQUE computer program discussed in Appendix 2.10.5. OBLIQUE utilizes the force-deflection relationships calculated by CYDROP to determine the rigid-body kinematic response of the cask.

Required input to OBLIQUE includes the cask and impact limiter dimensions, the package mass and mass moment of inertia, the acceleration of gravity, package velocity at impact, and the force-deflection relationship of the impact limiters at various impact angles. OBLIQUE uses inches, pounds and seconds as its primary units of length, force and time. The acceleration of gravity is then 386.4 in/sec^2 and the mass of the 10/140MB in consistent units is 68,000/386.4 = 175.98 lb.-sec^2/in. The package rotational mass moment of inertia, as derived in Section 2.2, 'Weights and C.G.'s', is 265,000 in-lb-

FIGURE 2.7.1-4

Impact Limiter Assumed Geometry for Oblique Drops
to Maximize Impact Forces

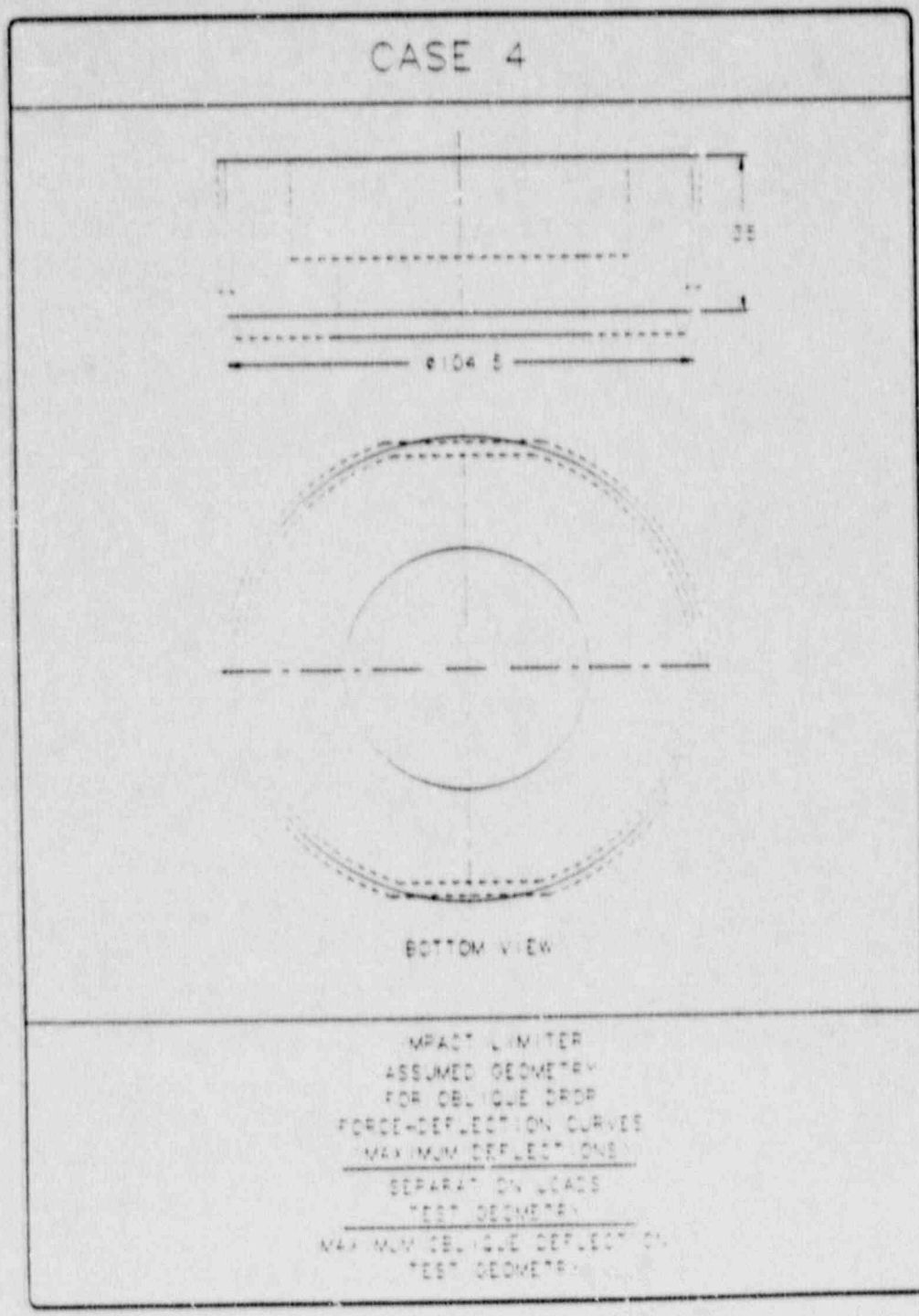

sec^2. Package velocity at impact can be calculated from the following:

$$V = (2gh)^{1/2}$$

Where: g = Acceleration of gravity = 386.4 in/sec^2
h = Drop height = 30 ft = 360 in

$$V = 527.45 \text{ in/sec}$$

For purposes of OBLIQUE input, the impact limiter was taken to be 108 inches in diameter and 40 inches long, extending 18 inches beyond the ends of the lead and steel cask structure. The assumed impact limiter geometry is shown in Figure 2.7.1-5. This assumed geometry causes OBLIQUE to apply the impact forces closer to the cask center of gravity (in the range of impact angles considered critical for body load combinations), resulting in higher internal forces. Also, the load application point is now further from the cask centerline, which will tend to maximize impact limiter separation moments. The logic behind these assumptions is set out below.

As explained in Appendix 2.10.5, the impact reaction force is taken at the geometric center of the elliptical plane defined by the crushed area of the impact limiter. As a result of the impact limiter geometric assumption made herein, the distance between the reaction force vector and the cask center of gravity will decrease. The basis of this logic is illustrated in the following sketch:

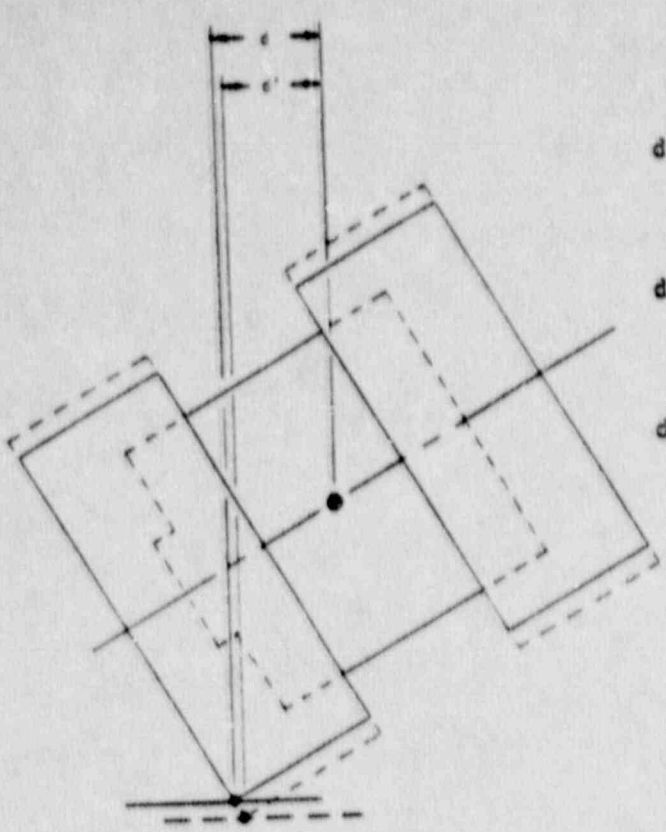

d = Reaction Force Offset from Cask C.G. for Normal Impact Limiter

d' = Reaction Force Offset from Cask C.G. for Extended Diameter Impact Limiter

$d' < d$

From the equations of motion derived in Section 2.10.5.2 of Appendix 2.10.5, it is evident that the result of this reduced offset will be decreased rotational accelleration, $d^2\theta/dt^2$. The implications of this are that more drop energy will have to be dissipated by foam strain energy. This logically implies greater impact limiter deformations are calculated than would actually occur, resulting in higher reaction forces. The net result is an increase in calculated body forces which is conservatively higher than would take place in reality.

So, while the crush 'footprint' and force-deflection characteristics remain the same as conservatively calculated above by CYDROP, the decreased load offset from the cask c.g. means that the final reaction force (which occurs at the point where the combination of foam strain energy and cask rotational energy offset the kinetic energy of the 30 foot drop) will be maximized. The combination of a conservatively derived force-deflection relationship with conservatively simplified impact limiter dimensions makes for an extremely conservative estimate of cask internal forces.

FIGURE 2.7.1-5

Impact Limiter Assumed Geometry for Oblique Drops
to Maximize Cask Body Loads

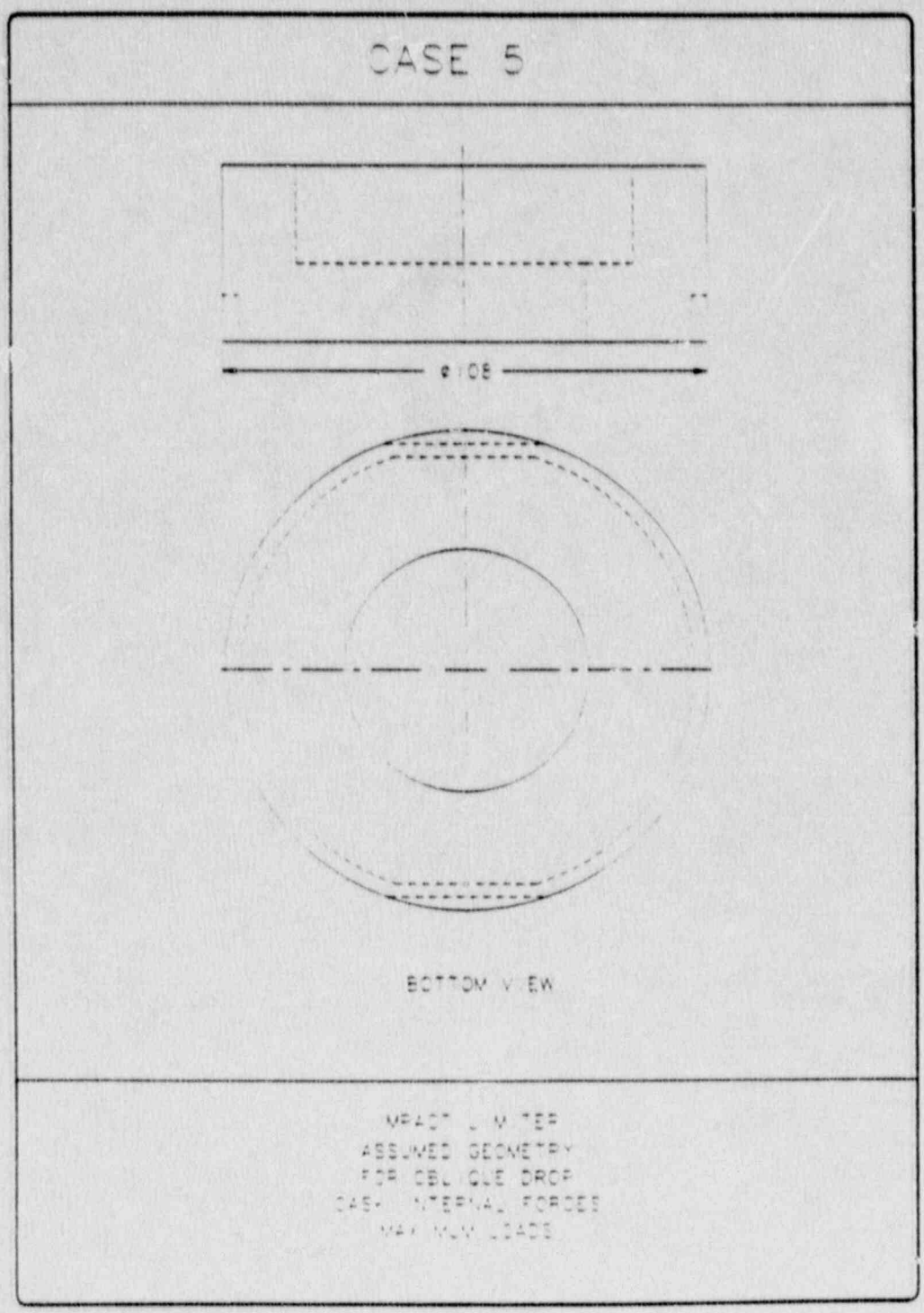

The results from the OBLIQUE computer analysis are presented in Table 2.7.1-10, and the results are shown in graphical form in Figures 2.7.1-6 through 2.7.1-8. Figure 2.7.1-6 illustrates cask body forces (thrust, shear and total forces) throughout the range of drop angles. Figure 2.7.1-7 shows how the bending moment in the cask varies with drop angle. Figure 2.7.1-8 gives the impact limiter separation moment acting at each angle.

From Figures 2.7.1-6 and 2.7.1-7, it is evident that the largest combination of body loads, consisting of thrust force and bending moment, will occur somewhere between drop angles of 35° and 60° with respect to the horizontal. The 'spike' shown in these Figures at the 5° drop angle is a result of relatively sudden foam strain hardening which takes place at lower impact angles, as explained in 2.10.5.2 of Appendix 2.10.5. This results in sharply higher cask bending and shear loading, but the critical combinations of thrust and bending take place at lower angles.

(Note that the maximum bending moment calculated by OBLIQUE is $66.7(10)^6$ in-lb at an impact angle of 5° with respect to the horizontal. It will be demonstrated later, in Section 2.7.1.3, 'Flat Side Impact', that the cask is capable of withstanding a greater bending moment than this).

From the Table, it can be seen that the maximum cask bending moment in the range of interest is $50.1(10)^6$ in-lb, occurring at an impact angle of approximately 40° from horizontal. It should be noted that this moment is derived from slender rod dynamics ($4/27\ F l \cos\theta$) and as such is fairly conservative for the short, squ- 10/140MB. The peak thrust proximate to the peak moment impact angle is $4.47(10)^6$ lb at a 55° from horizontal impact angle.

TABLE 2.7.1-10

OBLIQUE Results for -20°F Foam With Assumed 108 Inch Diameter Impact Limiter

```
PROGRAM OBLIQUE VERSION 8, DATE 8/5/87

12345678901234567890123456789012345678901234567890123456789012*4567890
         V         V         V         V         V         V         V         V
NUPAC 10/140MB SHIPPING CASK ENVELOPE DIMENSIONS, COLD FOAM
     83.50     38.75       40.     15.25       18.
    175.98   265000.     386.4
        .5       18.        .5       25.
       90.       89.      87.5       85.      82.5       80.
       75.       70.       65.       60.       55.       50.
       45.       40.       35.       30.       25.       20.
       15.       10.       7.5        5.       2.5        1.
        0.
   -527.45       85.        5        -5.       0.        5.
```

```
NUPAC OBLIQUE ANALYSIS-NUPAC 10/140MB SHIPPING CASK ENVELOPE DIMENSIONS, COLD FOAM

          PACKAGE GEOMETRY-
               LENGTH                      =        83.500
               RADIUS                      =        38.750
               OVERPACK LENGTH             =        40.000
               OVERPACK SIDE THICKNESS     =        15.250
               OVERPACK BOTTOM THICKNESS   =        18.000
          PACKAGE MASS PROPERTIES-
               MASS                        =       175.980
               MASS MOMENT OF INERTIA      =    265000.000
               GRAVITATIONAL CONSTANT      =       386.400
          SOLUTION CHARACTERISTICS-
               IMPACT VELOCITY (YDOT)      =      -527.450
                               (XDOT)      =         0.000
                               (THETADOT)  =         0.000
               FRICTION COEFFICIENT        =         0.000
               ESTIMATED CRUSH DEPTH       =         5.000
```

THETA0	FMAX	SHEAR	THRUST	MOMENT	DEFLECTION	CLEARANCE
85.0000	6129990.	418773.	6119517.	5180380.	4.78	14.07
80.0000	4743244.	694495.	4698346.	8591164.	6.74	13.16
75.0000	4377977.	982889.	4274388.	12158702.	8.71	12.14
70.0000	4335814.	1320468.	4138563.	16334673.	10.57	11.14
65.0000	4545147.	1757583.	4199215.	21741957.	12.28	10.18
60.0000	4937128.	2331497.	4356556.	28841487.	13.71	9.34
55.0000	5392928.	3018998.	4468705.	37346129.	14.76	8.69
50.0000	5651330.	3650035.	4314484.	45152287.	15.33	8.26
45.0000	5576789.	4032944.	3851745.	49889016.	15.43	8.[illegible]3
40.0000	5127126.	4052769.	3140460.	50134251.	15.18	7.90
35.0000	4527948.	3843712.	2406519.	47548140.	14.64	7.81
30.0000	3976395.	3557122.	1798003.	44002922.	13.83	7.84
25.0000	3614386.	3360504.	1347269.	41570677.	12.78	7.96
20.0000	3421568.	3277377.	1005834.	40542364.	11.54	8.19
15.0000	3362106.	3288658.	728511.	40681922.	10.17	8.43
10.0000	3233386.	3207419.	457189.	39676957.	8.61	8.75
5.0000	5413955.	5394828.	455961.	66736019.	10.58	6.13

FIGURE 2.7.1-6

Oblique Impact Body Forces

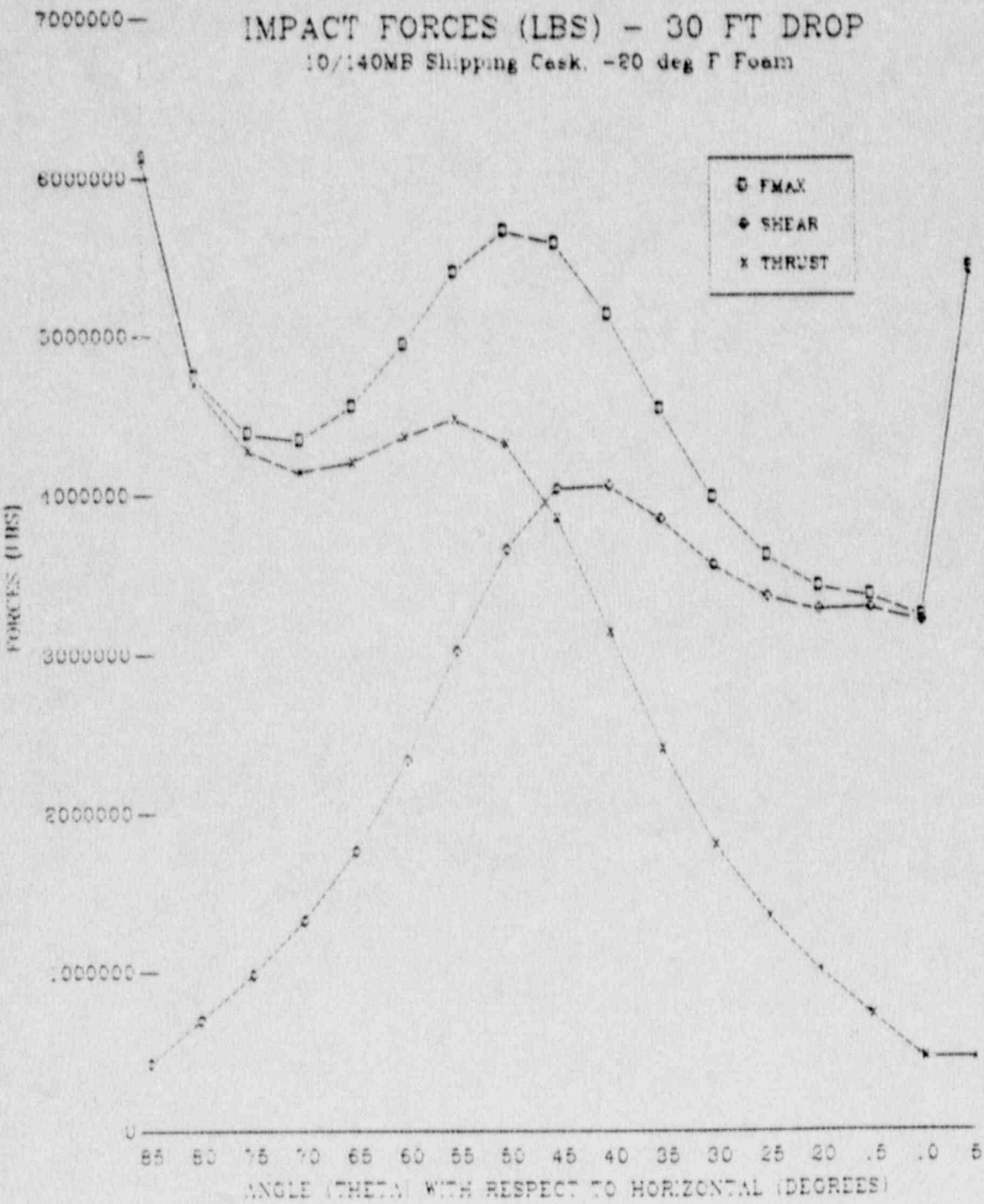

FIGURE 2.7.1-7

Oblique Impact Cask Bending Moment

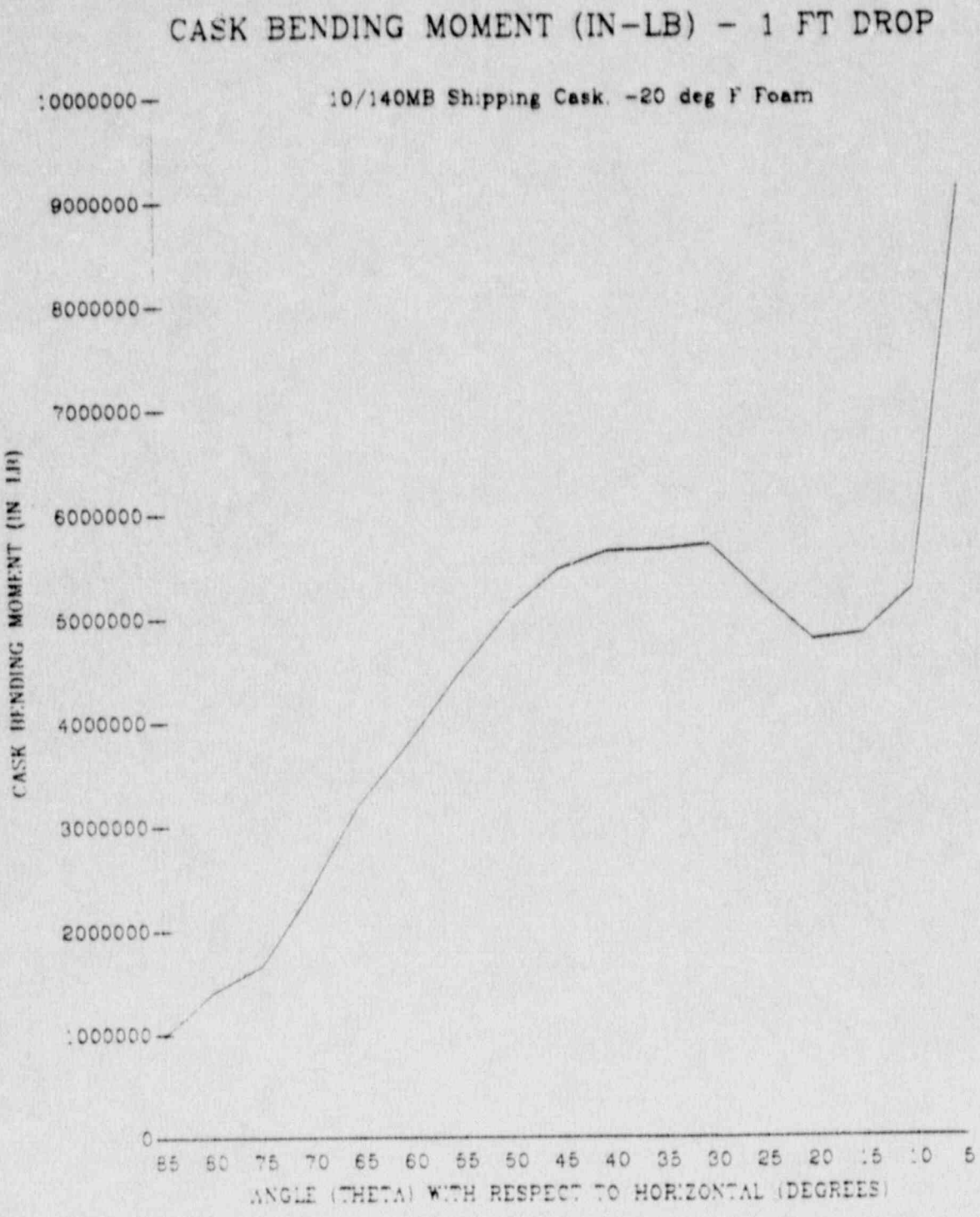

FIGURE 2.7.1-8

Oblique Impact Limiter Separation Moments

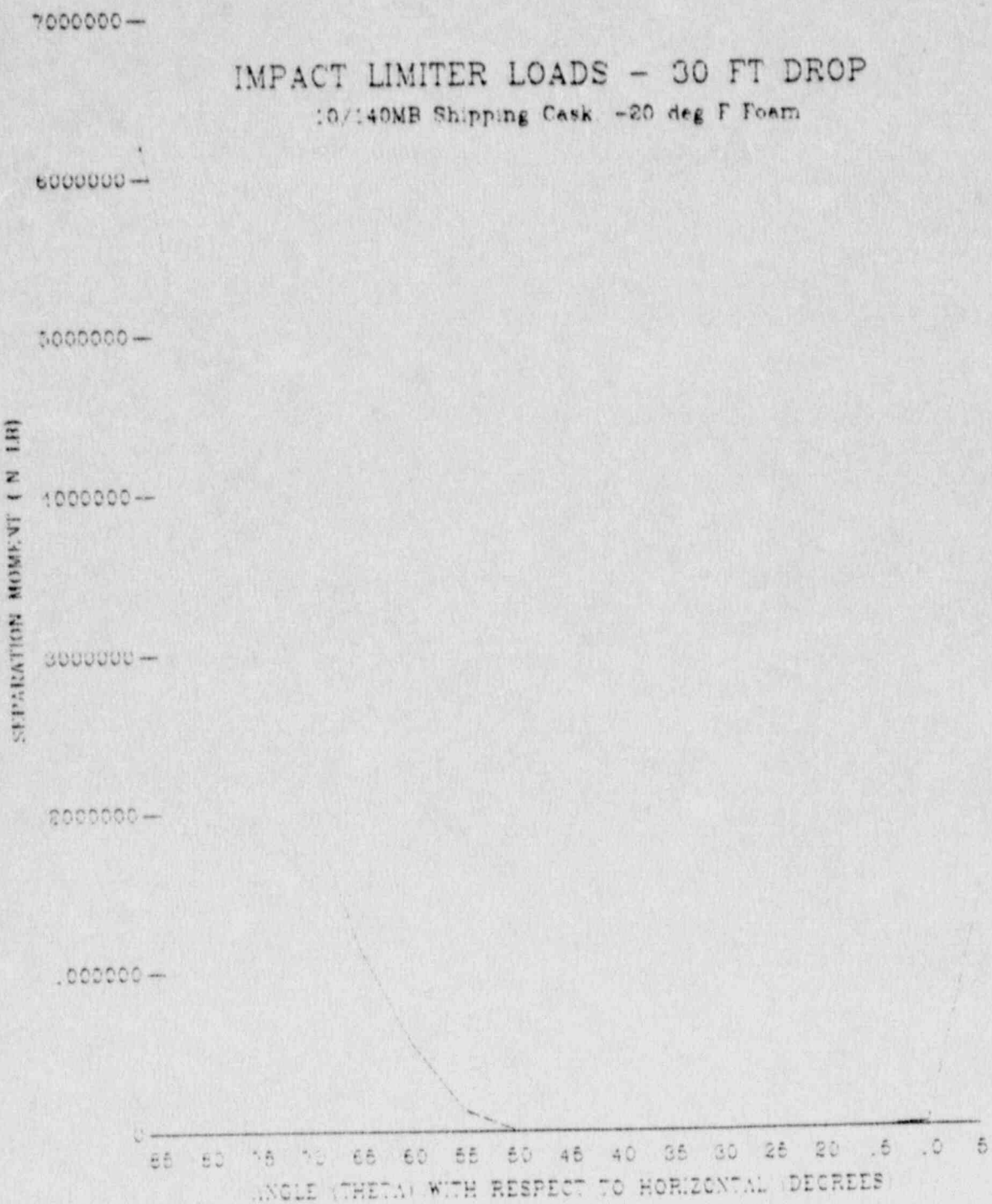

2.7.1.2.4 Stress Calculations in Cask Body

From the summary of internal forces in Table 2.7.1-10, the worst case state of compressive stress may be found. From that Table it is clear that the worst stress state will occur during drops from angles between 60° and 35° from horizontal. Using the standard formula for combined axial and bending stress:

$$\sigma = P/A + Mc/I$$

and conservatively assuming all stress is carried by the outer shell, the following table may be constructed:

Impact Angle	Thrust (10^6 lbs)	Moment (10^7 lb-in)	Stress (psi)
60	4.36	2.884	20724
55	4.47	3.735	22748
50	4.31	4.515	23698
45	3.85	4.989	23013
40	3.14	5.013	20591
35	2.41	4.755	17556

The stresses above were calculated assuming that all of the bending and axial forces are carried by the outer shell. The outer shell compressive area is:

$$A = \pi[(74.5)^2 - (72)^2]/4 = 287.65 \text{ in}^2$$

and the moment of inertia is $1.93(10)^5$ in^4 (see Section 2.7.1.3.3). The maximum combined stress is shown to be 23,698 psi, occuring at an impact angle of 50° with respect to horizontal.

It is important to note that, while the method of calculating the above stresses is fairly straightforward, the assumptions used are very conservative. First, the loads are developed using a conservative envelope of the 10/140MB cask impact limiter. Second, it is assumed that the maximum axial force acts at the same point on the package as the maximum bending

moment for the impact angle. Since the maximum axial force is always at the end of the package and the moment acts at approximately the third point along the length of the package, the moment and axial force maxima never act simultaneously. As stated above and in the discussion of the OBLIQUE program, the moment is based on a slender beam impact, which significantly overpredicts the moment in a short, large radius cylinder such as the 10/140MB. Finally, because the internal forces arise from inertial effects, it is conservative to assume that the stresses are entirely carried by the outer shell. If all these elements of conservatism were removed, the stresses calculated in the cask would be much less than predicted above.

The following margin of safety is calculated using the ASME membrane stress allowable, even though the stresses calculated above include a small fraction which is properly a bending stress. From Table 2.1.2-2, reference case number 1(B), the allowable limit is $0.7S_u$, where, for the outer shell material at the maximum normal operating temperature of 128°F, S_u = 70,000 psi. The allowable stress is thus (0.7)(70,000) = 49,000 psi, and the margin of safety is:

$$M.S. = 49,000/23,698 - 1 = +1.07$$

When the conservative nature of the stresses and allowables used for this analysis are considered, it is clear that oblique impacts from 30 feet will not severely affect the package's containment or shielding capability.

2.7.1.2.5 Lid Attachment Loads

The eight 2-1/2 inch primary lid closure bolts and associated bolt lugs must be strong enough to remain intact during the impact. An analysis of the forces exerted on the lid closure system was performed utilizing results of the the OBLIQUE program.

For this particular OBLIQUE analysis, in order to conservatively maximize lid separation loading, a different assumption regarding impact limiter geometry was made. The general logic behind the choice of impact limiter geometry is set out in Section 2.7.1.2.4 above. The basic criteria is that cask rotational acceleration be minimized, in order to maximize impact limiter

deformations, and thereby maximize loading on the cask. For the near-vertical impact angles at which lid separation loads are greatest, the minimum diameter of 96 inches (corresponding to the distance across the flat areas of the 10 inch long 'cap' portion) is conservatively chosen (refer to Figure 2.7.1-3). This will reduce the distance between the reaction force line of action, and the center of gravity of the cask. As explained above, the result will be less rotational acceleration, greater foam deformation, and hence large reaction forces. The configuration is illustrated below:

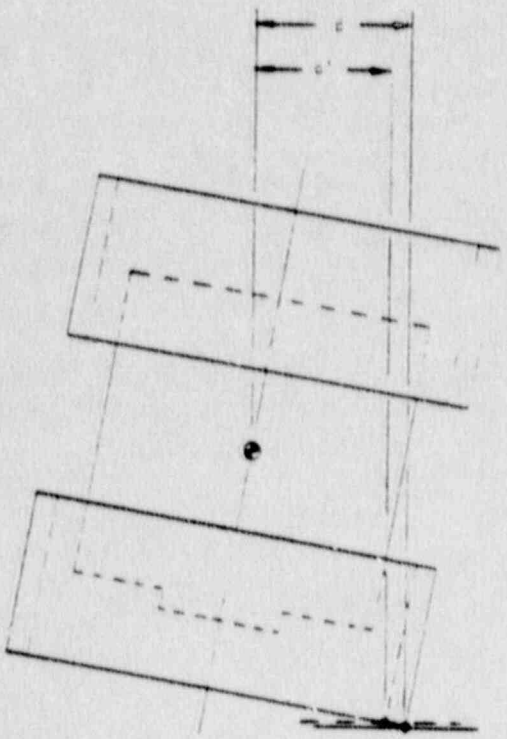

d = Reaction Force Offset from Cask C.G. for Normal Impact Limiter

d' = Reaction Force Offset from Cask C.G. for Reduced Diameter Impact Limiter

d' < d

From the resulting OBLIQUE analysis, shown in Table 2.7.1-11, the maximum thrust load was found to be 6,647,530 lb at an impact angle of 85° from horizontal. The maximum force in the closure system may be conservatively estimated using the assumption that the force acting on the closure bolts varies linearly from the point nearest the impact. The assumed load response of the lid is illustrated below:

TABLE 2.7.1-11

OBLIQUE Results for -20°F Foam
With Assumed 96 Inch Diameter Impact Limiter

```
PROGRAM OBLIQUE VERSION 8. DATE 8/5/87

12345678901234567890123456789012345678901234567890123456789012345678901234567890
         V         V         V         V         V         V         V         V
NUPAC 10/140MB SHIPPING CASK ENVELOPE DIMENSIONS, COLD FOAM
    83.50     38.75       40.      9.25       18.
   175.98   265000.     386.4
       .5       18.        .5       25.
      90.       89.      87.5       85.      82.5       80.
      75.       70.       65.       60.       55.       50.
      45.       40.       35.       30.       25.       20.
      15.       10.       7.5        5.       2.5        1.
       0.
  -527.45       85.        5.       -5.        0.        5.
```

```
NUPAC OBLIQUE ANALYSIS-NUPAC 10/140MB SHIPPING CASK ENVELOPE DIMENSIONS, COLD FOAM

          PACKAGE GEOMETRY-
               LENGTH                        =        83.500
               RADIUS                        =        38.750
               OVERPACK LENGTH               =        40.000
               OVERPACK SIDE THICKNESS       =         9.250
               OVERPACK BOTTOM THICKNESS     =        18.000
          PACKAGE MASS PROPERTIES-
               MASS                          =       175.980
               MASS MOMENT OF INERTIA        =    265000.000
               GRAVITATIONAL CONSTANT        =       386.400
          SOLUTION CHARACTERISTICS-
               IMPACT VELOCITY (YDOT)        =      -527.450
                               (XDOT)        =         0.000
                               (THETADOT)    =         0.000
               FRICTION COEFFICIENT          =         0.000
               ESTIMATED CRUSH DEPTH         =         5.000
```

THETAD	FMAX	SHEAR	THRUST	MOMENT	DEFLECTION	CLEARANCE
85.0000	6659835.	453488.	6647530.	5609813.	5.21	13.31
80.0000	5144713.	749908.	5095985.	9276634.	7.29	11.80
75.0000	4737827.	1072836.	4621534.	13271377.	9.31	10.28
70.0000	4710822.	1456892.	4485039.	18022296.	11.18	8.79
65.0000	4927864.	1953712.	4526784.	24168140.	12.81	7.38
60.0000	5265075.	2562756.	4599271.	31702237.	14.08	6.15
55.0000	5550427.	3196526.	4537561.	39542205.	14.90	5.14
50.0000	5561551.	3665920.	4182329.	45348785.	15.27	4.36
45.0063	5253309.	3840724.	3584145.	47511174.	15.20	3.85
40.0000	4738997.	3775026.	2864832.	46698475.	14.87	3.38
35.0000	4191299.	3565471.	2212235.	44106199.	14.30	3.03
30.0000	3715925.	3328538.	1673234.	41175253.	13.49	2.75
25.0000	3416687.	3179239.	1272243.	39328360.	12.49	2.65
20.0000	3280093.	3143216.	964630.	38882748.	11.31	2.65
15.0000	3270175.	3199265.	709422.	39576098.	9.99	2.73
10.0000	3184542.	3158643.	451377.	39073587.	8.49	2.92
5.0000	5471786.	5452663.	457045.	67451482.	10.61	.11

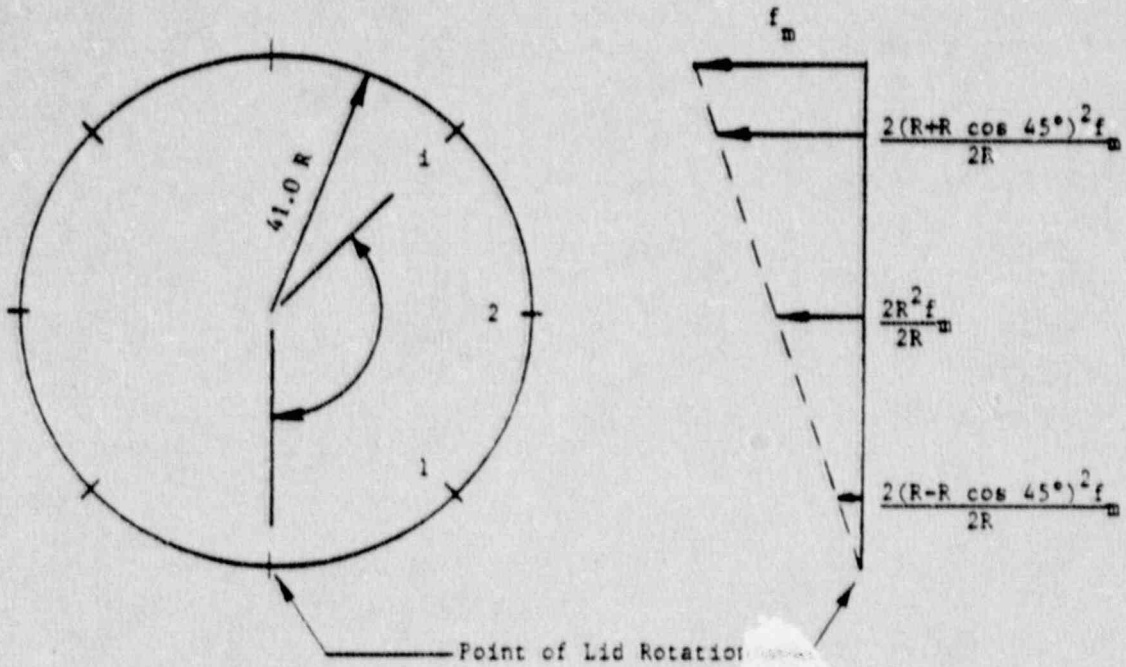

The moment exerted by a set of discrete forces equally spaced around a circumference of radius R, where the force in proportional to its projected distance from the point of rotation nearest the impact point is given by the formula:

$$M = 0.5\, f_m R \sum (1-\cos\theta_i)^2$$

Where: M = Moment to resist (separation moment)

f_m = Maximum force in the lid closure attachments

R = lid bolt circle radius = 41.0 in

θ_i = Angle from point of rotation to attachment i

This formula reduces to:

$$M = 3RNf_m/4$$

Or: $f_m = 4M/3RN$

Where: N = the number of attachments = 8

To derive the separation moment acting on the lid structure, the cask maximum axial g-load is calculated, based on the OBLIQUE results:

$$\gamma_{axial} = 6,647,530/(68,000)(\sin 85^{\circ})$$
$$= 98.13 \text{ g's}$$

The load acting against the lid closure system will consist of the maximum cask payload of 15,000 lb, as well as the weight of the primary lid assembly, 8,430 lb (from Section 2.2). The combined weight is 15,000 + 8,430 = 23,430 lb. The total load will be this combined weight at the axial acceleration of 98.13 g's:

$$P_{max} = (98.13)(23,430) = 2,299,186 \text{ lb}$$

Assuming that the resultant force of this load acts at the center of the lid, a distance of R from the pivot point, the separation moment then becomes:

$$M = (2,299,186)(41.0) = 94.267(10)^6 \text{ in-lb}$$

Therefore:

$$f_m = 4[94.267(10)^6]/3(41.0)(8) = 383,200 \text{ lb}$$

Additionally, there is a maximum normal operating pressure of 6.8 psig, as derived in Section 3.4.4. This will result in a uniform thrust load on each attachment of:

$$f_p = \pi(34.8 \text{ in})^2(6.8 \text{ lb/in}^2)/8 \text{ bolts}$$
$$= 3,234 \text{ lb}$$

Where 34.8 in is the radius of the inner O-ring seal of the EnviroSeal™ plate. The total resultant maximum attachment force is then:

f_T = 383,200 + 3,234 = 386,434 lb

From this resulting maximum bolt load, the maximum stress in the 4.0 in^2 tensile stress area of the 2-1/2 inch diameter bolt may be calculated as 386,434/4.0 = 96,610 psi. The allowable stress for the bolts, from Table 2.1.2-1, reference case number 6(B), is S_y. For the A-320 bolting material at its maximum normal operating temperature of 338°F, the yield stress is 103,000 psi. The Margin of Safety for the closure bolts is thus:

M.S. = 103,000/96,610 - 1 = +0.07

The bolt attachment lugs on the lid and cask body may be evaluated in a manner similiar to that developed in Section 2.5.1. From that Section, the moment of inertia of the section joining the lug to the lid or cask body is 188.68 in^4, and the distance from the tip of the lug gussets to the centroid of the section is (8.0 - 3.2) = 4.8 inches. The moment arm for the upper (lid) lug is 2.50 inches, and for the lower (cask) lug, it is 3.75 inches. Therefore, for the upper lug, the bending stress is:

$$\sigma_B = (386,434)(2.50)(4.8)/188.68$$
$$= 24,577 \text{ psi}$$

Bending stress in the lower lug is:

$$\sigma_B = (386,434)(3.75)(4.8)/188.68$$
$$= 38,866 \text{ psi}$$

Shear stress for both lugs is:

$$\tau = (386,434)/[(2.0)(7.38) + 2(1.5)(6.0)]$$
$$= 11,796 \text{ psi}$$

Combined stress for section is:

$$\sigma_C = \sigma_B + [(\sigma_B/2)^2 + (\tau)^2]^{1/2}$$

For the upper lug:

$$\sigma_C = 41,611 \text{ psi}$$

For the lower lug:

$$\sigma_C = 58,750 \text{ psi}$$

The allowable membrane plus bending stress for these components is the lesser of $3.6S_m$ and S_u (Table 2.1.2-1, reference case number 2(B)). For the stainless steel material of the upper, or lid, lug, at the maximum normal operating temperature of 133°F, S_m = 20,000 psi (Table 2.3-1), and $3.6S_m$ = 72,000 psi. For the same material, the minimum value of S_u = 68,785 psi. The allowable stress is therefore 68,785 psi, and the margin of safety for the upper lug is:

$$M.S. = 68,785/41,611 - 1 = +0.65$$

For the lower lug material, ASTM A-516 Grade 70, or A-537 Class 1, S_m = 23,200 psi, and S_u = 70,000 psi. The allowable is therefore 70,000 psi (less than 3.6 x 23,200 = 83,520 psi). The Margin of Safety is:

$$M.S. = 70,000/58,750 - 1 = +0.19$$

The bearing stress between the bolt head and the lug will now be evaluated. The minimum head diameter of the 2-1/2 inch socket head bolt is 3.717 inches (from Machinerys Handbook, Reference 2.11.18, p. 1202). From the drawings in Section 1.3, the maximum bolt hole diameter is 2.91 inches. The minimum effective bearing area of the bolt head is thus:

$$A_b = 0.25\pi[(3.72)^2 - (2.91)^2] = 4.22 \text{ in}^2$$

Maximum bearing stress on the bolt lug is:

$$\sigma_B = 386,434/4.22$$

= 91,572 psi

The allowable bearing stress on the bolt, washer or nut, from Table 2.1.2-1, reference case number 4(B), is S_u. For the bolting material, ASTM A-320 Grade L43, S_u = 125,000 psi. The Margin of Safety for bolt, nut and washer is:

M.S. = 125,000/91,572 - 1 = +0.37

The minimum outside diameter of the washer under the 2-1/2 inch socket head bolt and mating heavy hex nut is equal to the minimum width of the lug between the support gussets, which is 4.29 inches (refer to Section 1.3). The maximum bolt hole diameter is 2.91 inches. The minimum effective bearing area of the washer on the bolt lug is thus:

$$A_b = 0.25\pi[(4.29)^2 - (2.91)^2] = 7.80 \text{ in}^2$$

Maximum bearing stress on the bolt lug is:

$$\sigma_B = 386,434/7.80$$
$$= 49,543 \text{ psi}$$

The potentially lowest strength lug material is that for the upper lug, ASTM A-182, Type F304, or A-351 Type CF8/304, for which S_u = 68,785 psi at 133°F. The minimum Margin of Safety for both lugs is then:

M.S. = 68,785/49,543 - 1 = +0.39

It should be pointed out that the impact results given in Table 2.7.1-11 for near-horizontal impacts are unrealistic, due to the extremely conservative nature of the assumptions made regarding impact limiter side wall thickness. More realistic results of horizontal impacts, accounting for the impact limiter's true geometry, are given in Section 2.7.1.3, 'Flat Side Impacts'. These Side Drop analyses demonstrate that the cask will be able to withstand greater bending loads than the maximum shown in Table 2.7.1-11 in a worst-case impact situation, while displaying less impact limiter deformation in a worst-case deflection situation.

2.7.1.2.6 Impact Limiter Attachment Loads

As pointed out in Section 2.7.1.2.5 above, the maximum impact limiter separation moment will result from the assumption of a maximum impact limiter diameter, illustrated in Figure 2.7.1-4. The resulting impact limiter separation loading derived from the OBLIQUE analysis performed with this geometry is shown in Figure 2.7.1-8.

The maximum force in the impact limiter retention system may be estimated in a manner similiar to that used above for the lid closure system. Assume that the force varies linearly from the point nearest the impact, and that the eight impact limiter retention lugs are evenly spaced around the circumference of the cask. Refer to the sketch in the previous section for details.

The maximum separation moment was found to be $6.248(10)^6$ in-lb, occuring at an impact angle of 85° with respect to the horizontal. The minimum radius R to the center of the impact limiter attachment pin holes is 40.68 inches. The maximum attachment load is therefore:

$$f_m = 4M/3RN = 4[6.248(10)^6]/3(40.68)(8)$$
$$= 25,600 \text{ lb}$$

With this applied force, tearout of the impact limiter attachment is considered using the 40° shearout equation. The allowable load, P_a, is:

$$P_a = \sigma_{sy}(2t)[E.M. - (d/2)\cos 40^\circ]$$

Where: σ_{sy} = yield shear strength of the gusset material (ASTM A-240 Type 304 stainless steel) = $0.6S_y$
t = 0.75 inch plate thickness
E.M. = 2.00 inch edge margin
d = 1.00 inch attachment pin diameter

For the stainless steel material at a Normal Condition of Transport maximum impact limiter temperature of 169°F (conservative for Hypothetical Accident

Conditions), S_y = 26,550 psi, and σ = (0.6)(26,550 psi) = 15,930 psi. Therefore, the maximum allowable lug load for yield shear is:

$$P_a = (15,930)(2 \times 0.75)[2.00 - (1.00/2)(0.766)]$$
$$= 38,638 \text{ lb.}$$

The Margin of Safety against tearout is:

$$M.S. = 38,638/25,600 - 1 = +0.51$$

Bearing stress at the pin hole is:

$$\sigma_b = f_m/A_b = 25,600/(0.75)(1.0)$$
$$= 34,133 \text{ psi}$$

With an allowable bearing stress of S_u = 72,240 psi at 169°F, the Margin of Safety is:

$$M.S. = 72,240/34,133 - 1 = +1.12$$

The double shear capacity of the 1.0 inch diameter ball-lock pins is 147,000 lb (Carr Lane Model Number CL-16-BLP-S-2BALL). Taking one-fifth of this capacity as a rated working capacity (conservative for the one-time hypothetical accident event) yields 29,400 lb as an allowable load. The Margin of Safety is then:

$$M.S. = 29,400/25,600 - 1 = +0.15$$

The impact limiter retention lug weld consists of two 22-inch long, quarter-inch bevel welds. The total weld area is thus 2 x 22 x 1/4 = 11 in^2. This weld will be essentially loaded in pure shear. The shear stress in the weld is:

$$\tau = 25,600/11 = 2,327 \text{ psi}$$

$$M.S. = 15,930/2,327 - 1 = +5.85$$

The impact limiter attachment gussets on the cask wall will be loaded in bending and shear, and the analysis will proceed per the technique set out in Blodgett, Design of Weldments (Reference 2.11.17), Section 6.3. Total weld length per gusset is 8 inches, and each gusset will take half the total maximum separation load. Weld shear load is thus:

$$f_s = (25,600/2)/8 = 1,600 \text{ lb/in}$$

The center of the attachment pin hole is (40.68 - 37.25) = 3.43 inches from the side of the cask. The moment acting on the weld is thus:

$$M = (25,600/2)(3.43) = 43,904 \text{ lb-in}$$

Weld moment of inertia for a vertical line weld is:

$$S_w = d_w^2/6 = 8^2/6 = 10.67 \text{ in}^2$$

Weld bending load is then:

$$f_b = M/S_w = 43,904/10.67 = 4,115 \text{ lb/in}$$

Resultant weld line load is:

$$f_r = (f_s^2 + f_b^2)^{1/2} = 4,415 \text{ lb/in}$$

Each gusset is welded in place with a half-inch bevel plus a half-inch filet weld, for a total weld shear leg length of L = 0.5 + (0.707)(0.5) = 0.85 inch. The minimum required shear leg length is calculated as:

$$L_w = 4,415/15,930 = 0.28 \text{ in}$$

Margin of Safety on the gusset welds is thus:

$$M.S. = 0.85/0.28 - 1 = +2.04$$

The impact limiter retention system is thus more than adequate to retain its integrity under worst-case Hypothetical Accident Condition oblique drops.

It has therefore been demonstrated with conservative analyses that the 10/140MB package will meet accident condition drop test requirements in any oblique impact orientation.

2.7.1.3 Flat Side Impact

Analysis of the NuPac 10/140MB package behavior during a hypothetical 30 foot side impact is performed in the following steps:

1. Determine worst-case impact limiter deflections using a combination of the SYDROP computer program as well as hand analysis.

2. Determine worst-case impact forces using the SYDROP computer program.

2. Determine stresses in the outer shell assuming it reacts the entire impact bending load. Include ovality effects.

3. Determine stresses in the inner shell assuming it reacts the payload weight and half the lead shielding weight in bending. Include ovality effects.

5. Evaluate the potential for primary and secondary lid shift, and its effects on cask containment integrity; check bearing of primary lid on cask inner wall, and bearing of secondary lid on primary lid; investigate possibility of loading the primary and secondary closure bolts in shear.

Several bounding analyses were performed using the energy-balance program SYDROP, along with appropriate hand calculations, to determine the behavior of the 10/140MB impact limiter system during side impact. The bounding analyses were performed to compensate for the unusual geometry of the 10/140MB impact limiter system. SYDROP was written assuming that a simple rigid cylinder (the cask) is protected by a simple cylindrical foam impact limiter around the sides of the rigid cylinder.

The actual geometry of the 10/140MB package differs from this assumption in three ways. First, the impact limiter extends beyond the end of the rigid cylinder. As a result, some assumptions must be made regarding the effect of the cantilevered (unbacked) foam. Many drop tests have been performed which

indicate that the cantilevered foam contributes a significant part of the package's ability to resist impacts. In general, the effectiveness of the overhang in foam may be estimated by comparing the plateau crush strength of the impacted foam with the shear strength of the foam carrying the load back into the package. The shear strength of the foam in the 10/140MB is more than adequate to assure nearly complete involvement of the impact limiter length in resisting side impacts.

Secondly, the 10/140MB impact limiter employs a stepped design, such that 10 inches from the end of the impact limiter the radius of the impact limiter is reduced 3.5 inches. This step allows the impact limiter to deform much further in the side impact without bottoming out onto one of the protuberances on the side of the cask (e.g., tie down lugs and closure bolts lugs). The impact limiter would be expected to act as if it were only 30 inches long on each end for the first 3.5 inches of impact deflection. After that, the additional 10 inches of impact limiter on each end would begin to be mobilized.

Thirdly, the flat areas on either side of the package will act very little like the cylindrical impact limiter modeled in SYDROP. Additionally, the bolt lug 'pockets' embedded in the impact limiters will effect the manner in which the impact limiters respond to crush on the essentially unyielding surface, even for impacts on the rounded sides of the impact limiters. Accordingly, loads and deflections for impacts on the impact limiter rounded sides, as well as on the flat areas, will be calculated through a combination of simplified geometries which conform with the assumptions of SYDROP, as well as hand calculations for the remaining, non-conforming portions of the impact limiters.

2.7.1.3.1 Side Impact Maximum Deflection

To adequately bound potential maximum deflections, two primary impact limiter orientations will be addressed. These are (1) impact on the rounded portions of the side of the impact limiter, and (2) impact on the flattened sides.

(1) Impacts on Rounded Sides

It is assumed that the worst-case orientation for impacts on the rounded sides of the impact limiters is that where a bolt lug 'pocket' is directly over the impacted surface. The geometry of the resulting impact area is shown below:

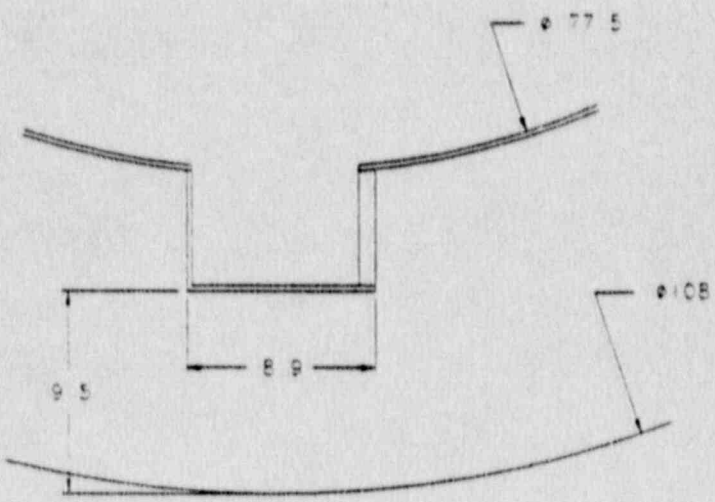

To evaluate the effect of impacts on this region, the impact limiter is divided in four separate components:

1. The 101 inch diameter by 10 inch long end 'cap' of the impact limiter is treated as a cylinder with an outside diameter of 101 inches, and an inside diameter of 77.5 inches (assuming essentially fully-backed response). This portion of the impact limiter, shown shaded in the sketch below, will not have any effect until the main portion, the 108

inch diameter by 30 inch long component, has already deflected a total of (108 - 101)/2 = 3.5 inches.

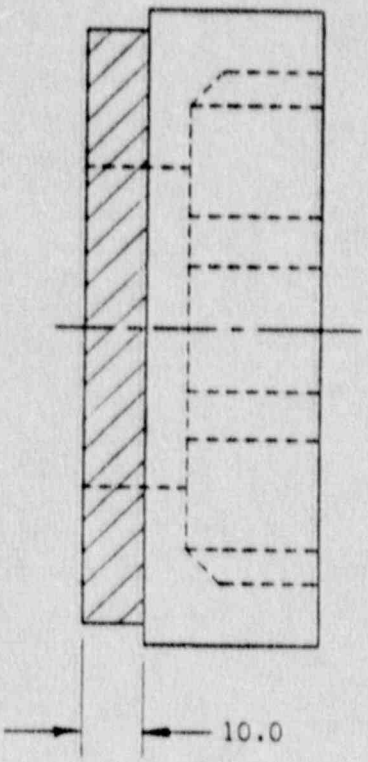

2. The 8 inch long segment of the main portion of the impact limiter (108 inch diameter) which does <u>not</u> include the bolt lug 'pocket' will be treated as a cylinder with an outside diameter of 108 inches, and an inside diameter of 77.5 inches. This portion of the impact limiter is illustrated below:

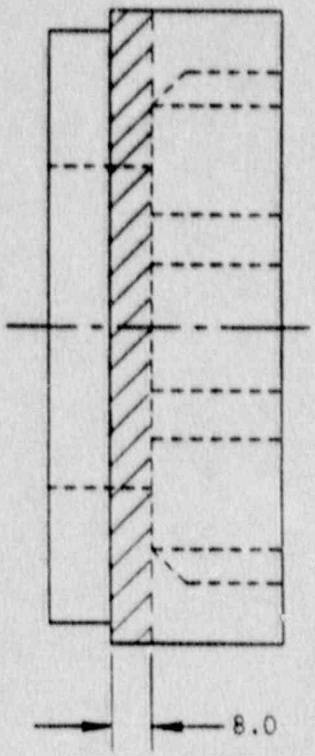

3. The portion of the impact limiter directly 'under' the bolt lug pocket will be treated as a rectangular slab, 8.9 inches wide by 2 x 22 = 44 inches long (where the 'pocket' length is 22 inches for each of the two impact limiters). This portion of the impact limiter will be evaluated with simple hand analysis techniques. The assumed configuration is shown below:

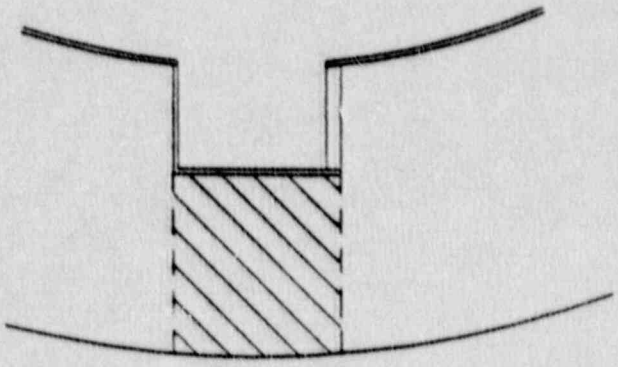

4. The remainder of the major portion of the impact limiter not directly 'under' the lug 'pocket' will be treated as a reduced-diameter cylinder. The method of deriving this equivalent cylinder is simply to subtract the width of the lug 'pocket' (8.9 inches) from the outside and inside diameters of the impact limiter. The outside diameter of this equivalent cylinder is thus 108 - 8.9 = 99.1 inches. The inside diameter is 77.5 - 8.9 = 68.6 inches. The development of this portion of the composite impact limiter is illustrated graphically in Figure 2.7.1-9.

Tables 2.7.1-12 through 2.7.1-14 represent the response of portions 1, 2 and 4 of the composite impact limiters at 105°F, the hypothetical accident maximum temperature for the polyurethane foam. The properties of the foam were degraded 15% from the expected response at 105°F (20% reduction in the 80% strain region, as explained in Section 2.1.2.4, 'Impact Limiter Design Criteria'), consistent with previous analyses presented herein.

FIGURE 2.7.1-9

Impact Limiter Assumed Geometry For Flat Side Drop
on Rounded Side (Maximum Deflections)

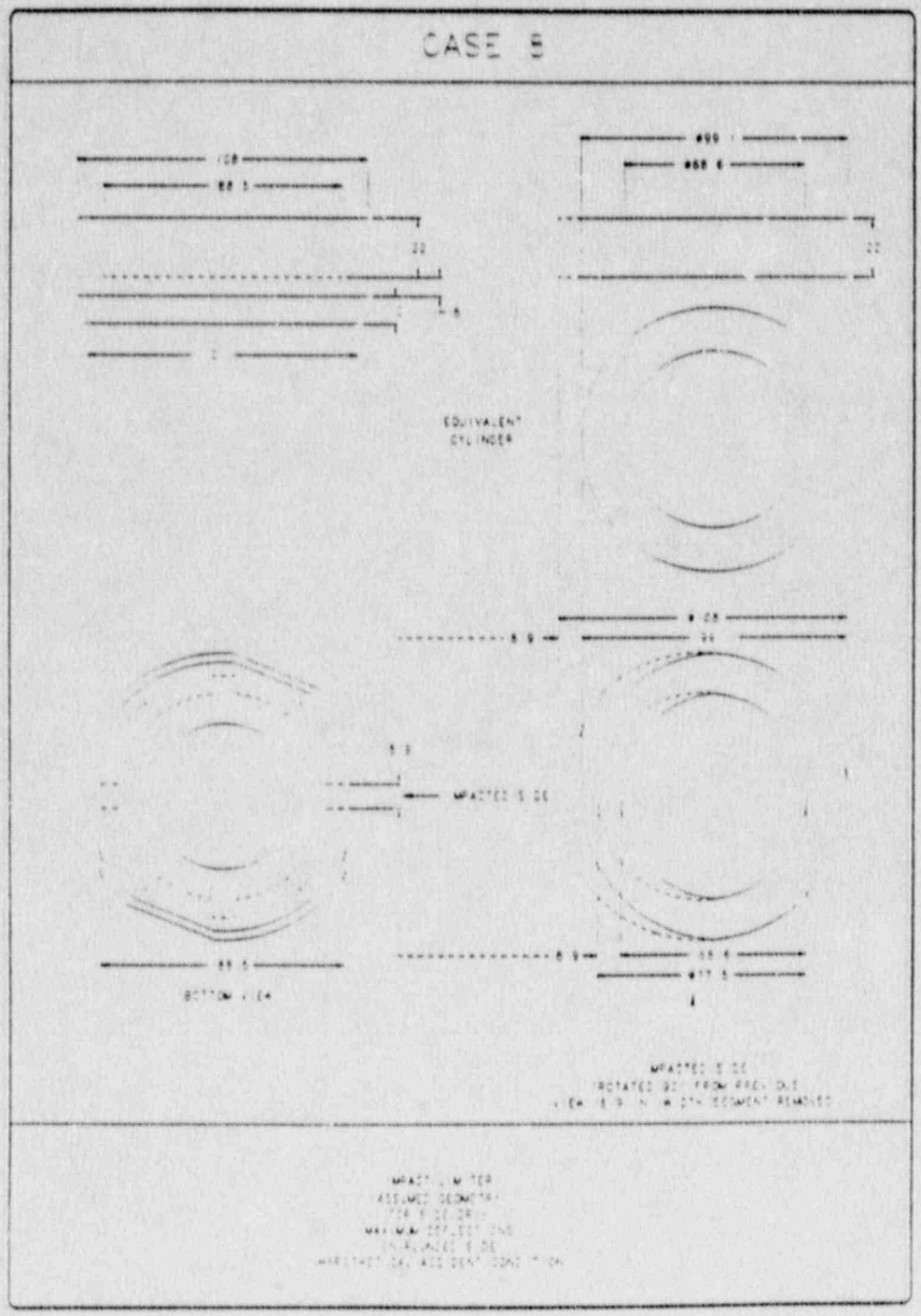

Table 2.7.1-12

Proprietary

Table 2.7.1-13

Table 2.7.1-14

A conservative estimate of the maximum deformation which could be experienced by impact on the curved sides of the impact limiter may be obtained by combining the above elements of the SYDROP runs as follows. Assume that the response of the major diameter portion of the composite impact limiter is correct for the first 3.5 inches of deflection. This portion includes elements 2 and 4, as detailed above. In addition, the hand results indicated by element 3 would be included. After this initial 3.5 inches of deflection, the SYDROP results of element 1 (minor diameter portion of the impact limiter) should be added in to get the combined force and strain energy in the foam. The combined force may be divided by the package weight to determine the effective acceleration. The greatest deflections will result from the 105°F case, and the tables below show how the data from the SYDROP runs can be combined with the hand analysis results to derive total impact limiter deformation, or crush depth.

The following table was developed using hand calculations and the stress-strain relationship for 105°F polyurethane foam. Stresses were assumed to correspond with strain levels as illustrated in Figure 2.1.2-3, 'Foam Stress-Strain Properties Used for Design.' Strains greater than 80% were conservatively represented by the foam stress corresponding to 80%, so that, at no time in the analysis were stress values used which exceeded tested limits.

The columns of the table are related by the following relationships:

Strain = Deflection/9.5 inches
Stress = f(strain), where f(x) is defined by the design stress-strain relationship at this temperature
Force = Stress x 8.9 x 44.0

The total strain energy is obtained by multiplying the average of the force at the given deflection and the force at the previous deflection by the difference in deflections, and adding this to the total strain energy at the previous deflection.

Proprietary

For the 2 x 22 = 44 inch length 'reduced diameter' impact limiter analysis (from Table 2.7.1-14):

Crush Depth	Impact Force	Strain Energy
7.50	2437764	10077395
8.00	2645290	11347275

From the 2 x 10 = 20 inch length minor diameter impact limiter analysis (from Table 2.7.1-12):

Crush Depth	Impact Force	Strain Energy
4.00 (=7.50-3.5)	930325	3837631
4.50 (=8.00-3.5)	1010108	4322398

Combining the four components yields:

Crush Depth	Impact Force	Acceleration	Potential Energy	Strain Energy	Ratio (SE/PE)
7.50	7775787	114.8	24990000	21245811	0.85
8.00	8468419	124.5	2502:000	25305464	1.01

The impact force and crush depth maybe found by interpolation from the combined data:

Crush Depth	Impact Force	Acceleration	Ratio
7.97	8425130	123.9	1.00

Since the crush depth required to contact the bolt lug 'pocket' is 9.5 inches, it can be concluded that the cask will not bottom out on side drop when impact occurs on the rounded sides of the impact limiters.

(2) Impacts on Flattened Sides

As previously stated, impacts on the impact limiter flattened sides cannot be accurately modeled using the program SYDROP alone. However, the impact limiter deformations and impact forces may be estimated from a combination of SYDROP results and hand analyses, similiar to those done above.

The area of the flattened portion of the impact limiter, with corresponding bolt lug 'pockets' shown, is illustrated in Figure 2.7.1-10. To conservatively estimate maximum deflections, the lug 'pockets' and portion of the cask between the 'pockets' are modelled as flat surfaces, shown as dashed lines in the Figure. This assumed configuration will tend to minimize foam strain-hardening effects, and thus maximize deformations. With this conservative approximation, an analysis similiar to that above may now be carried out.

The individual elements of the composite impact limiter remain approximately the same as the previous analysis, with exceptions as follows:

1. The 10 inch long end 'cap' is modelled as a 96 inch diameter cylinder. This is the dimension corresponding to the distance across the flattened areas of this portion of the impact limiter. This assumption conservatively ignores a significant volume of energy-absorbing foam.

2. The major diameter portion of the impact limiter which does not include the bolt lug 'pockets' is modelled as a 102 inch diameter cylinder. This is the dimension corresponding to the distance across the flattened areas of this portion of the impact limiter. This, too, conservatively ignores significant quantities of foam actually available for impact absorption.

3. The flat slab portion is broken down into two separate subsections: That portion of the impact limiter under the lug 'pockets', and that portion backed by the cask wall itself. This assumption is illustrated below:

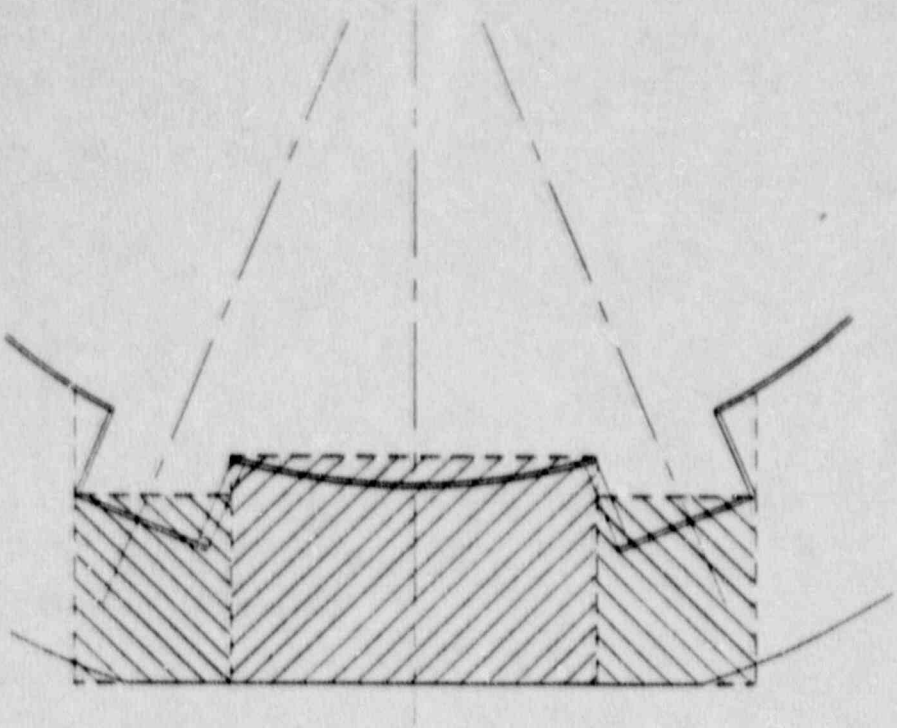

4. The 'reduced diameter' portion has 2 x 11.3 = 22.6 inches removed, leaving an outside diameter of 66.2 inches, and an inside diameter of 35.7 inches. This approximation is illustrated graphically in Figure 2.7.1-11.

It should be noted that, from the above assumptions, the major portion of the impact limiter will now deflect a total of only (102 - 96)/2 = 3.0 inches before the end 'cap' portion will contact the impact surface. Details of the impact response of these segments of the composite impact limiter are given in Tables 2.7.1-15 through 2.7.1-17.

FIGURE 2.7.1-10

Flat Side Drop on Flattened Side
Geometric Details

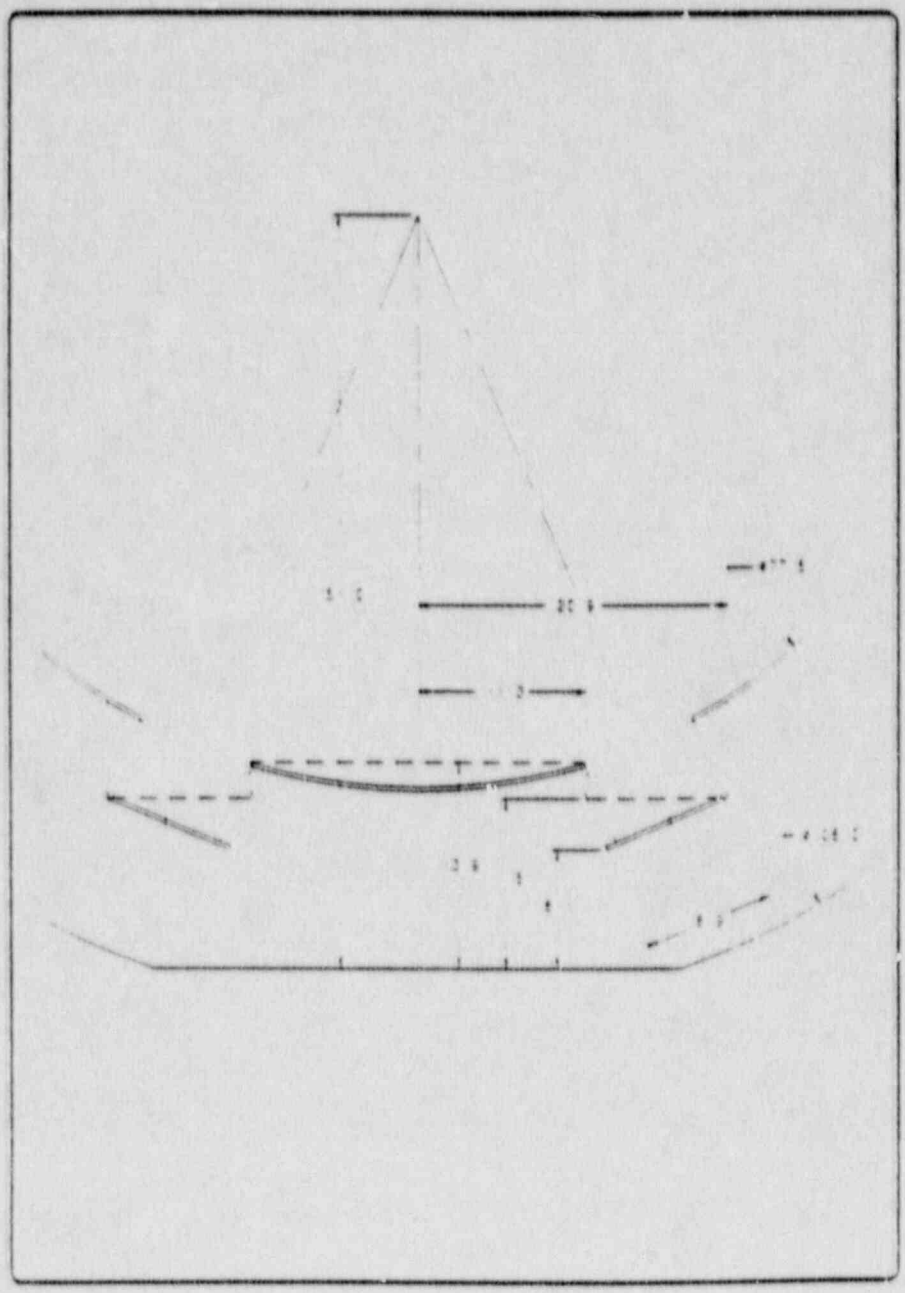

FIGURE 2.7.1-11

Impact Limiter Assumed Geometry for Maximum Deflections
for Flat Side Drop on Flattened Side

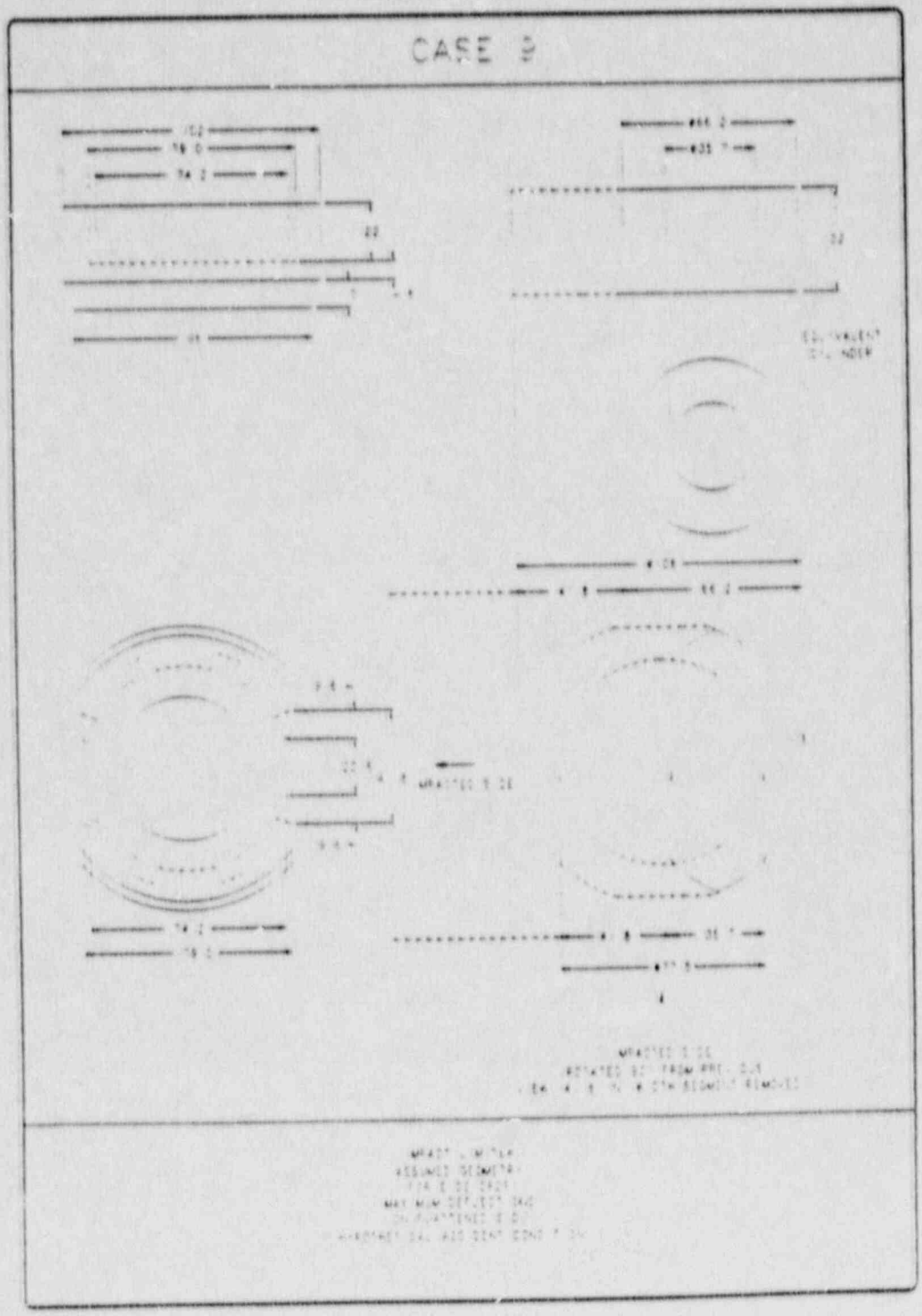

Table 2.7.1-15

Proprietary

Table 2.7.1-16

Propietary

Table 2.7.1-17

Proprietary

Proprietary

Propietary

For the 2 x 22 = 44 inch length 'reduced diameter' impact limiter analysis (from Table 2.7.1-17):

Crush Depth	Impact Force	Strain Energy
6.50	1588740	6220639
7.00	1664308	7033653

From the 2 x 10 = 20 inch length minor diameter impact limiter analysis (from Table 2.7.1-16):

Crush Depth	Impact Force	Strain Energy
3.50 (=6.50-3.0)	671710	1356909
4.00 (=7.00-3.0)	756494	1713683

Combining the four components yields:

Crush Depth	Impact Force	Acceleration	Potential Energy	Strain Energy	Ratio (SE/PE)
6.50	6069176	89.3	24922000	22297601	0.89
7.00	6763835	99.5	24999000	25504374	1.02

The impact force and crush depth maybe found by interpolation from the combined data:

Crush Depth	Impact Force	Acceleration	Ratio
6.92	6656964	97.9	1.00

Since the actual crush depth required to impact the bolt lug 'pocket' is 8.1 inches, it may be concluded that the cask will not bottom out on side drop when impact occurs on a flattened side of the impact limiters.

Again, because the foam properties used in this 105°F analysis were degraded 15% (20% at 80% strain) to account for fabrication variables, the crush depth of 7.97 inches, derived above for impacts on the rounded side of the impact limiter, is the maximum that might be expected assuming a fully effective impact limiter.

The only other possible impact scenario is the situation where side impact could occur at one of the 'pockets' located in an area where the impact limiter transitions from rounded to flattened sides. In this case, because of the unequal distribution of foam under the lug, the resultant center of force of the crushed foam would move away from the centerline of the cask, producing a moment which would roll the cask over onto the flattened side of the impact limiter. Because this rotational acceleration would dissipate a portion of the impact energy, it is expected that this case would be less critical than the two already evaluated.

Additionally, the only protuberance of any significance, aside from the lug 'pockets', which could be affected by a flat side drop is the tie-down lug, which extends 6 inches out from the side of the cask (not including the thermal shield). Each of the four tie-down lugs is located at a position corresponding to the rounded portion of the impact limiter, half-way between two bolt lug 'pockets'. Because the impact limiter extends 15.25 inches outward from the side of the cask, any crush in excess of 9.25 inches would cause the tie-down lug to 'bottom out'. Since it has just been shown that, under a worse-case impact situation (impact on the flattened area between two lug 'pockets') the crush depth is only 6.92 inches, clearly the tiedown lug would not be expected to bottom out.

2.7.1.3.2 Side Impact Maximum Forces

To conservatively estimate maximum impact loads arising from a flat side drop, cold foam properties were utilized in conjunction with impact limiter geometry assumptions illustrated in Figure 2.7.1-12. As detailed in Section 2.1.2.4, foam at the minimum transport temperature of -20°F will exhibit the greatest strength, and results in the highest impact loadings.

FIGURE 2.7.1-12

Impact Limiter Assumed Geometry for Maximum Loads
for Flat Side Drop

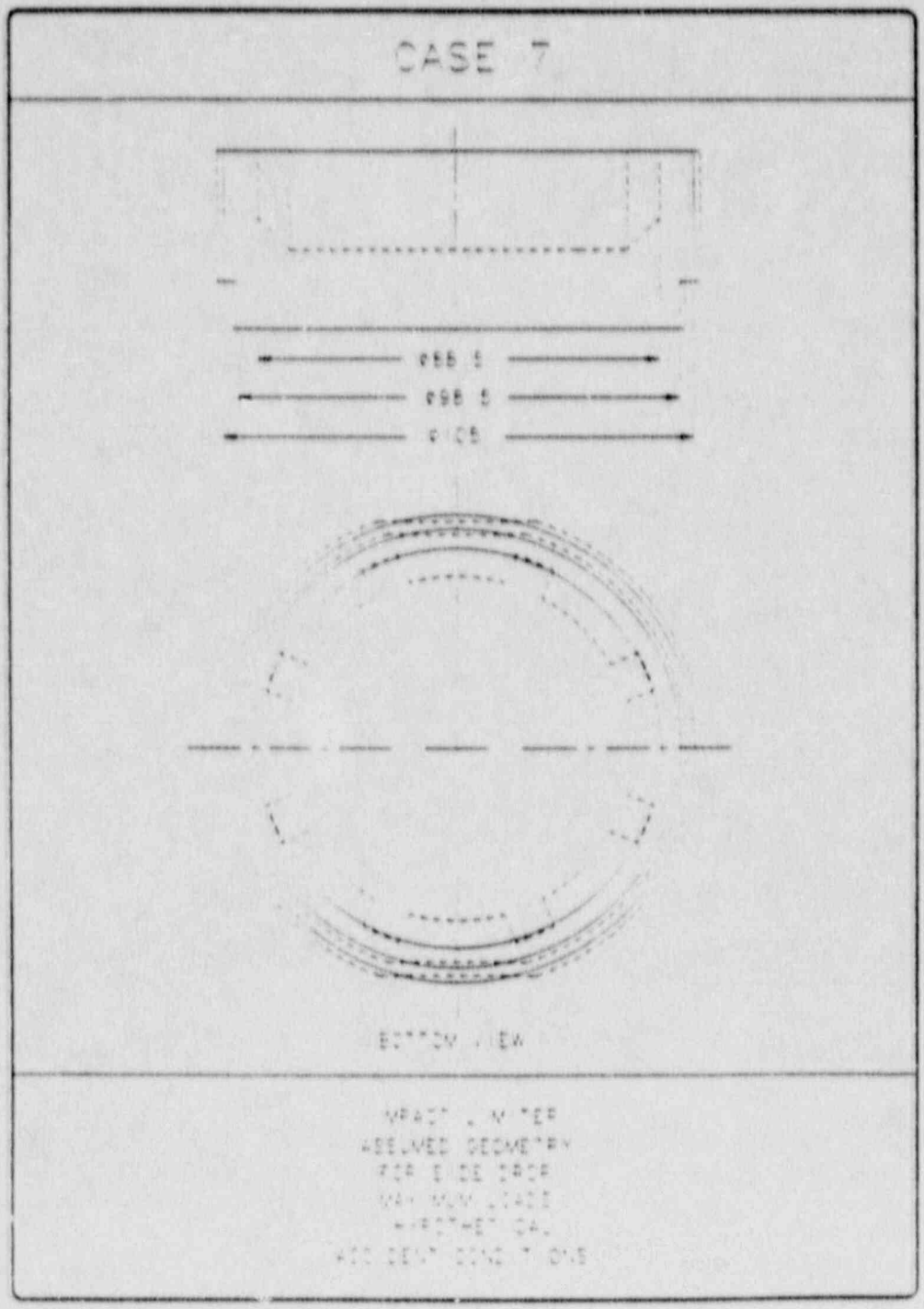

The assumed impact limiter geometry places the inside diameter at the location of the bolt lug 'pockets.' This results in a minimum impact limiter side wall thickness, and ignores the energy absorbing potential of the foam between the 'pockets', causing foam strain hardening effects (and ensuing greater loading) to develop much sooner than would occur in reality. The outside diameters of the major and minor portions of the impact limiter are taken as the average of the maximum diameter and the distance across the flattened areas for each portion. These average diameters are 105 inches for the 30 inch long major diameter segment, and 98.5 inches for the minor diameter 'cap' segment. This assumption will thus be valid and conservative for side impacts on any portion of the impact limiter. The results of the SYDROP analysis are presented in Tables 2.7.1-18 and 2.7.1-19.

Table 2.7.1-18 gives the impact respose for the 30 inch long, major diameter portion of the impact limiter, and Table 2.7.1-19 gives results for the 10 inch long, minor diameter end 'cap.' To evaluate the impact response of the full impact limiter, these results must be combined in a manner similiar to that used in Section 2.7.1.3.1 above. For the assumed outside diameters, the major diameter portion will have to deform a total of (105 - 98.5)/2 = 3.25 inches before the minor diameter portion contacts the impact surface and begins deforming. The results of the two impact limiter components are outlined below:

From the 30 inch length major diameter impact limiter analysis (from Table 2.7.1-18):

Crush Depth	Impact Force	Strain Energy
5.50	9698760	22909497
5.56	10025145	23525869

Table 2.7.1-18

Proprietary

Table 2.7.1-19

Proprietary

From the 10 inch length minor diameter impact limiter analysis (from Table 2.7.1-19):

Crush Depth	Impact Force	Strain Energy
2.25 (=5.50-3.25)	1278719	1634177
2.31 (=5.56-3.25)	1314457	1715214

Combining the two components yields:

Crush Depth	Impact Force	Acceleration	Potential Energy	Strain Energy	Ratio (SE/PE)
5.50	10977479	161.4	24854000	24543674	0.99
5.56	11339602	166.8	24858250	25241083	1.02

The impact force and crush depth maybe found by interpolation from the combined data:

Crush Depth	Impact Force	Acceleration	Ratio
5.52	11098187	163.2	1.00

As can be seen, this impact acceleration is significantly higher than those developed in the geometrically more precise analyses for maximum deflections.

2.7.1.3.3 Outer Shell Bending Stresses

Because the 10/140MB impact limiters extend only 22 inches up the side of the steel and lead radiation shield, the center section of the cask is unsupported during the side impact. A bending moment will develop between the impact limiters.

To evaluate the effects of this bending moment, it will be conservatively assumed that the cask is simply supported at the ends of the lead and steel cylindrical shell. The shell is 79 inches long. The payload is assumed to be

distributed along the middle 73 inches of length, which is the total height of the cask payload cavity. The weight per inch of payload is thus:

$$15000/73 = 205 \text{ lb/in.}$$

The shield linear weight can be calculated as follows:

$$0.25\pi\left[(67.5^2 - 66^2)(0.29) + (74.5^2 - 72^2)(0.283) + (72^2 - 67.5^2)(0.41)\right]$$

$$= 329 \text{ lb/in}$$

Where: 0.29 = Weight density in lb/in^3 of the stainless steel inner shell
0.283 = Weight density of the carbon steel outer shell
0.41 = Weight density of the lead shielding

The total distributed load may be taken as 205 + 329 = 534 lb/in, which conservatively assumes the payload is distributed along the entire 79 inch length of the shell. The maximum moment on a simply supported beam with a distributed load under the 163.2 g maximum side drop acceleration is given by:

$$M = wL^2/8 = (163.2)(534)(79)^2/8 = 68.0(10)^6 \text{ in-lb}$$

The moment of inertia of the outer shell is given by the formula:

$$I = .25\pi (R_o^4 - R_i^4)$$
$$= .25(\pi)(37.25^4 - 36.0^4) = 1.93(10)^5$$

Bending stress is then

$$\sigma = Mc/I$$
$$= (68.0)(10)^6(37.25)/(1.93)(10)^5 = 13,125 \text{ psi}$$

This is a pure tension and pure compression stress on the extreme fibers of the shell. Simultaneous with this stress, a stress due to the shell's tendency to flatten into an oval shape occurs as a bending stress in the hoop direction of the shell. These stresses may be estimated using Roark

(Reference 2.11.11), Case 19 in Table 17 of p. 237, which gives the formula for the bending moment at the top of a circular ring loaded by its own weight and supported by tangential shear:

$$M = W\gamma R^2 (1-k_4)/2$$

Where:

γ = acceleration = 163.2 g's

W = weight of shield per inch of circumference per inch of length
= 329/2πR = 1.429 lb/in

R = Mean Radius of the shell = 36.63

$k_4 = k_2/k_1 = 0.99222$

$k_1 = 1+\alpha+\beta = 1.00424$

$k_2 = 1-\alpha+\beta = 0.99643$

$\alpha = I/AR = .00391$

$\beta = FEI/GAR^2 = 3.33(10)^{-4}$

F = 1.2 (form factor for a rectangular section)

$I = bh^3/12(1-\mu^2)$ (b=1, h=1.25, μ=.3)
$= .1789 \text{ in}^4$

$A = bh$
$= 1.25 \text{ in}^2$

$E = 29(10)^6$ psi at 128°F

$G = E/2(1+\mu) = 11.2(10)^6$

Thus:

$M = (1.429)(163.2)(36.63)^2(1-.99222)/2 = 1,218$ in-lb/in

I = .1789

c = .625

$\sigma = Mc/I = (1,218)(.625)/.1789 = 4,255$ psi

The worst biaxial state of stress may be assumed to occur when the hoop bending stress (ovality) acts in tension and the longitudinal bending stress acts in compression (as at the inner wall of highest point of the shell during impact). The stress intensity under such conditions can be approximated by combining the hoop and longitudinal bending stresses calculated above (under the assumed conditions, there is virtually no shear stress):

S.I. = 4,255 - (-13,125) = 17,380 psi

The maximum allowable membrane stress for the outer shell at the maximum normal operating temperature of 128°F is 49,000 psi (Table 2.1.2-4, reference case number 1(B)). The margin of safety is then:

49,000/17,380 - 1 = +1.82

The buckling allowable stress in bending for the outer shell at 128°F is 36,376 (Table 2.1.2-6), so the margin of safety against buckling is:

M.S. = 32,258/17,380 - 1 = +.86

2.7.1.3.4 Side Impact Inner Shell Stresses

During a side impact, the inner shell of the 10/140MB would be expected to act in conjunction with the outer shell to carry bending load. However, it is conservative to assume that the inner shell must support its own weight, the payload weight, and the weight of the lead above it. As before, the payload weighs 205 lb/in. The inner shell and lead distributed load can be calculated as follows:

$$.25\pi(67.5^2 - 66^2)(0.29) + (.5)(.25)\pi(72^2 - 67.5^2)(0.41)$$
$$= 145 \text{ lb/in}$$

The total distributed load on the inner shell would therefore be 205 + 147 = 352 lb/in. The maximum moment is:

$$M = wL^2/8 = (163.2)(352)(79)^2/8 = 44.82(10)^6 \text{ in-lb}$$

The moment of inertia of the inner shell is:

$$I = .25\pi(33.75^4 - 33^4) = 87,600 \text{ in}^4$$

The stress in the inner shell is then:

$\sigma = Mc/I = 44.82(10)^6(33.75)/87,600 = 17,268$ psi

As in the outer shell, this stress should be combined with the moment in the hoop direction. The following quantities may be calculated using the same method as presented for the outer shell:

$I = .0386$
$A = .75$
$\alpha = .00154$
$\beta = .000144$
$k_1 = 1.001688$
$k_2 = .998601$
$k_4 = .996918$
$E = 28.0(10)^6$ at 128°F
$G = 10.8(10)^6$ at 128°F
$W = 145/2\pi R = .6915$ lb/in
$R = 33.375$
$M = (.6915)(163.2)(1-.996918)(33.375)^2/2$
$= 193.7$ in-lb
$\sigma = (193.7)(.375)/.0386 = 1,882$ psi

Combining (tensile) hoop and (compressive) longitudinal bending stresses to get the stress intensity results in:

S.I. = 1,882 - (-17,268) = 19,150 psi

The allowable stress for the inner shell material at the operating temperature of 128°F is 48,000 psi (Table 2.1.2-1, reference case number 1(B)), so the margin of safety in bending is:

M.S. = 48,000/19,150 - 1 = +1.51

For buckling in bending, the allowable is 27,754 psi (Table 2.1.2-5), so the buckling margin of safety is:

M.S. = 27,754/19,150 - 1 = +0.45

2.7.1.3.5 Lid Deflection Analysis

Under the maximum calculated side drop loading of 163.2 g's, the primary and secondary lids of the 10/140MB cask could potentially slide relative to the cask body and to each other. Because of the face seal arrangement of the EnviroSeal[tm] system, any relative motion of the sealing surfaces would not have any negative impact on the sealing capability of the cask. However, other potential problem areas which might arise under this loading situation must be addressed. These areas of concern specifically include bearing stresses of impacted surfaces, as well as bolt loads.

First, bearing stress between primary lids and the cask body will be investigated. The cask body, top primary and (optional) bottom lids are dimensioned so that, when the lids are centered on the body, an eighth-inch gap will exist between the cask inner shell and the lid inner step. At the same time, a quarter-inch gap will exist between the cask outer wall and the lid outer 'lip'. Thus, any side slippage of the lid will always result in contact between the cask inner shell and the lid inner step.

As can be seen from the drawing details in Section 1.3, the length of the nominal bearing surface of the lid inner step, excluding chamfers and EnviroSeal[tm], is 2.00 inches. The cask inner diameter is 66.0 inches. The projected bearing area will therefore be (66.0)(2.00) = 132 in^2.

A worst-case relative deflection would assume that the cask top primary lid and bottom lid or plate are supported by the impact limiters in a side drop event, and the cask would slide downward and bear against the inner step of the lid(s). Conservatively neglecting the sliding resistance provided by the EnviroSeal[tm] and bolt lug interfaces, the full force of the shield assembly and payload, under a 163.2 g side loading, will produce a bearing stress at the contacting surfaces of the cask and lid(s).

From Section 2.2, the weight of the cask shield assembly is 26,960 lb. This, combined with the 15,000 lb maximum payload, produces a total load of 41,960

lb. Assuming half of this load is supported by each lid, the total bearing stress at the contacting surfaces would be:

$$\sigma_b = (41,960/2)(163.2)/132 = 25,939 \text{ psi}$$

From Table 2.1.2-1, reference case number 4(B), the maximum allowable bearing stress under Hypothetical Accident Conditions is S_u. For the lid and inner shell material (Type 304 stainless steel) at the maximum anticipated operating temperature of 133°F (for the lid), S_u = 68,785 psi (Table 2.3-1). The margin of safety on bearing is thus:

$$M.S. = 68,785/25,939 - 1 = +1.65$$

The nominal width of the bearing area of the secondary lid on the primary lid is 2.63 inches. The lid diameter is 29.0 inches, so that the projected bearing area is (29.0)(2.63) = 76.3 in^2. Secondary lid weight is 1,700 lb. Bearing stress of the secondary lid impacting the primary lid is thus (1,700)(163.2)/76.3 = 3,636 psi. This is less than the bearing stress of the primary lid on the cask wall calculated above, so that the margin of safety will be even greater.

As for the effect of lid shift on primary and secondary lid bolts, it is important that maximum lid movement not result in shearing loads on these fasteners. To this end, all bolt holes have been dimensioned such that, even with the maximum possible lateral lid movement, there will still be clearance between the bolt and the bolt hole. In this manner, shear loads on the bolts will be effectively avoided. Additionally, both primary and secondary lid bolts have sufficient free length inside their respective bolt holes to assure adequate flexibility under the worst-case lift shift scenario.

It is therefore clear from all the preceding analyses in this section that the Hypothetical Accident Condition flat side drop test will have no detrimental effect on the NuPac 10/140MB cask.

2.7.2 Puncture

A 40 inch drop onto a 6 inch diameter pin can occur in three separate regions, e.g., cylindrical body or cask side wall between the impact limiters, top and bottom lids inside the impact limiter center opening, and the impact limiter itself.

2.7.2.1 Side Wall Puncture Resistance

Using ORNL-NSIC-68 (Reference 2.11.12) for the side wall evaluation, the required outer shell thickness for puncture integrity can be calculated as:

$$t = (W/S_u)^{.71}$$

Where: t = Outer Shell Thickness
W = Cask Gross Weight
S_u = Outer Shell Ultimate Strength

From the drawings in the Section 1.3, it can be seen that the external shell for the NuPac 10/140MB cask is fabricated from 1.25 in thick ASTM A-516 Grade 70, or, alternatively, A-537 Class 1 carbon steel. At the 128°F maximum normal operating temperature of the outer shell (conservative for this accident condition test), S_u = 70,000 psi (refer to Table 2.3-1). In Section 2.2, the cask gross weight is calculated as 68,000 lb.

Realizing that the kinetic energy of the 40 inch drop is:

$$E = h W = 40 W$$

this equation may be rearranged as:

$$E/S_u = 40\ t^{1/.71} = 40\ t^{1.41}$$

Assuming that the total kinetic energy of the 40 inch drop is absorbed in stressing the outer shell material just to the point of failure, the minimum energy ratio required to preclude puncture is:

$$E/S_u = 40W/S_u = (40)(68,000)/70,000 = 38.86 \text{ in-lb/psi}$$

From the equation derived above, the actual drop energy ratio is:

$$E/S_u = (40)(1.25)^{1.41} = 54.77$$

The resulting energy Margin of Safety can be calculated as:

$$M.S. = 54.77/38.86 - 1 = +0.41$$

Sakamoto's equation (Reference 2.11.13) for the side puncture event is:

$$E/S_u = [.003 + .047(t/D) + .002(d/D) + .006(r/\delta)]\, t^{(1.585-.11r)} d^{(1.465+.077r)}$$

Where:
- d = Puncture Pin Diameter
- t = Outer Shell Thickness
- D = Cask Outside Diameter
- r = Puncture Pin Edge Radius

all expressed in metric units.

Resolving the equation into English units and utilizing a 6-inch diameter puncture pin with a 1/4-inch edge radius yields:

$$E/S_u = [64.30 + 237.4/D + 929.88(t/D)]t^{.8865}$$
$$= [64.30 + 237.4/74.50 + 929.88(1.25/74.50)](1.25)^{.8865}$$
$$= 101.26 \text{ in-lb/psi}$$

Energy Margin of Safety is:

$$M.S. = 101.26/38.86 - 1 = +1.61$$

Similarly, from Shieh's equation (Reference 2.11.14):

$$\frac{E}{S_u} = \frac{.37[1 + 6/D + (41/D)^2]e^{t/3}t^{1.68}}{1 + .1t^{.87}}$$

can be expressed as:

$$\frac{E}{S_u} = \frac{14.8[1 + 6/D + (41/D)^2]e^{t/3}t^{1.68}}{1 + .1t^{.87}}$$

$$\frac{E}{S_u} = \frac{14.8[1 + 6/74.50 + (41/74.50)^2]e^{1.25/3}(1.25)^{1.68}}{1 + (.1)(1.25)^{.87}}$$

$$= 40.29 \text{ in-lb/psi}$$

for a Margin of Safety of:

$$M.S. = 40.29/38.86 - 1 = + 0.04$$

Finally, intergrity of the cask outer shell has been demonstrated in a quarter-scale test. In this test, the cask was dropped from a height of 40 inches onto a scaled puncture pin, with the pin striking the outer shell midway along the cask length. Results of this test are detailed in Appendix 2.10.4.

In addition to the above discussed concern with local puncture of the cask side wall, the overall bending response of the cask must also be considered. The following calculations demonstrate that the overall bending response of the package due to impacting on a puncture bar at mid-length of the package is of little consequence for the 10/140MB.

For this assessment, the 10/140MB will be idealized as a uniform beam with end masses corresponding to the impact limiter and a center load, F, equal to the force required to flow the puncture bar. The system to be analyzed is therefore as follows:

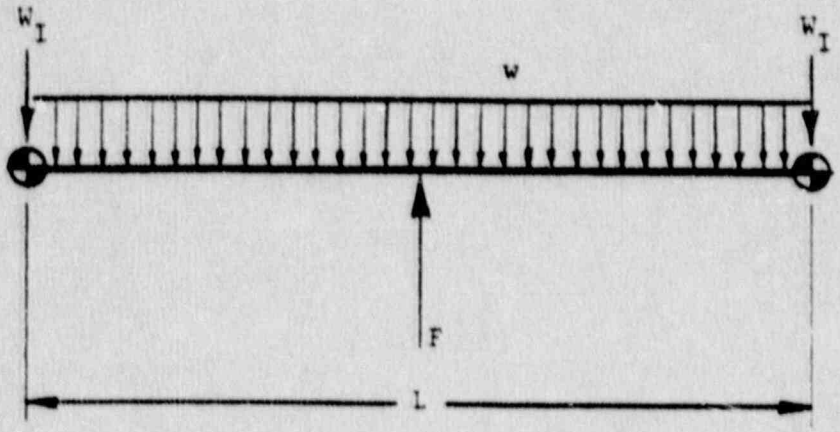

Where:

F = Force to flow the 6-inch diameter puncture pin

= $(\pi/4)(6.0)^2(\sigma_f)$ = $1.329(10)^6$ lb

σ_f = Puncture pin flow stress

= $(1/2)(\sigma_u + \sigma_y)$ = 47,000 psi

σ_u = Assumed mild steel puncture pin ultimate strength

= 58,000 psi

σ_y = Assumed mild steel puncture pin yield strength

= 36,000 psi

L = Length of cask without impact limiters = 83.75 in

W = Gross weight of cask = 68,000 lb

γ = Effective g-load acting on the cask

= F/W = $1.329(10)^6/68,000$ = 19.543

W_I = Concentrated load associated with an impact limiter

= Impact limiter weight time g-load = (5,575)(19.543) = 108,950 lb

w = Distributed load associated with the cask (without impact limiters)
= [68,000 - 2(5,575)](19.543)/83.75 = 13,266 lb/in

Conservatively assuming that the entire bending moment associated with the above loading conditions is reacted by the outer shell of the cask only, the resultant loading and stress in the cask outer shell may be calculated as:

$$M = W_I L/2 + wL^2/8$$
$$= 16.193(10)^6 \text{ in-lb}$$

$$\sigma_B = 16.193(10)^6(37.25)/1.93(10)^5$$
$$= 3,125 \text{ psi}$$

Where $I = 1.93(10)^5$ in^4, as derived in Section 2.7.1.3.3.

This stress is well within the allowable limits for the cask outer shell under Hypothetical Accident Condition loadings, and a large Margin of Safety therefore exists.

Finally, an oblique pin puncture on the cask body could conceivably result in the loss of some of the cask thermal shielding. Such an event, however, would result only in localized and fairly minor damage to the thermal shield. The massive nature of the cask acting as a heat sink would assure that such an occurrance would not result in excessive temperatures in the lead shielding and consequent loss of shielding effectiveness.

It is thus evident that the cask side wall is adequate to resist the regulatory puncture impact requirement.

2.7.2.2 Cask Lid Puncture Resistance

Due to the extremely rigorous leak-tightness requirements for this Type B package, it was determined that a finite element analysis would be required to evaluate the structural response due to post impact on the cask lids within the impact limiter center opening. The secondary lid opening in the top primary lid makes this member potentially the more structurally flexible of

the two lids, and therefore the more prone to high stresses and permanent deformation leading to possible loss of seal integrity. It was therefore this structure which was subjected to the the most intensive analysis. The bottom lid (utilized in optional bottom-loading casks) was evaluated rather than the fixed bottom, since it will be more flexible, and therefore more highly stressed, than the rigidly-attached bottom plate of the baseline fixed-bottom cask model.

In addition to complying with accident condition stress allowables set out in Regulatory Guide 7.6 and outlined in Section 2.7.1 above, lid deflections were to be limited so that a residual compression would be maintained on at least one of the two sets of EnviroSeal^{tm} O-rings at the end of the puncture event. To maintain lid stress levels within regulatory limits while ensuring continued sealing integrity, special lid configurations were developed. These unique designs are shown in the general arrangement drawings in Section 1.3.

For the analysis, the ANSYS finite element routine was utilized. The capabilities of the program are outlined in Appendix 2.10.2 and details of the analysis are given in Appendix 2.10.8. All possible worst case conditions for both stress and deflection were evaluated. These included a center-loaded axisymmetric model of the bottom lid to evaluate center impact, and a three-dimensional model of the top lid with post impact at the center, at the secondary seal location (outside diameter of the secondary lid) and at the inside diameter of the impact limiter center opening.

Material properties for a 133°F temperature condition (maximum normal condition temperature for the top lid) were used in the analysis. Also, the lowest applicable 304 stainless steel material properties from Table 2.3-1 were derived for this temperature to evaluate stress level Margins of Safety. This is conservative, since, from Section 3.0, the maximum anticipated lid temperature for the accident condition drop events is 109°F, for which both material strength and allowable stresses will be higher.

A summary of analysis results is outlined in Table 2.7.2-1 below. To verify the finite element results, a hand analysis for the bottom lid was performed, utilizing Roark, Formulas for Stress and Strain, 4th Edition (Reference 2.11.11), Table 24, Case 16. Assume a lid diameter of 76.0 in, corresponding to the outer diameter of the lid 'lip', so that a = 76.0/2 = 38.0 in. Also assume an average lid thickness of t = 6.0 in.

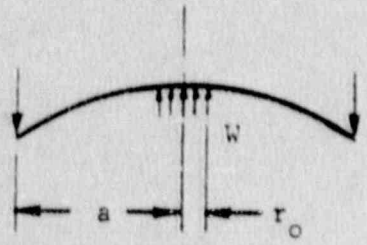

W = $1.329(10)^6$ lb (puncture pin 'flow stress' force, as derived above)

a = 38.0 in.

Since r_o = 3.0 in = 0.5t,

$r_o' = r_o$ = 3.0 in

The maximum bending (surface) stress in the bottom lid finite element model occurs at the location corresponding to the puncture pin radius, $r = r_o$ = 3.0 in. From Roark, the maximum bending moment at this location is:

$$M_{r=3} = (W/16\pi)\left[4(1+\mu)\ln(a/r) + (1-\mu)[4 - (r_o'^2/r^2)]\right]$$
$$= 404{,}597 \text{ in-lb/in}$$

TABLE 2.7.2-1

Pin Puncture Finite Element Lid Stress Analysis Results Summary

Load Case	Max. Bending Stress (psi) (Margin of Safety)	Max. Membrane Stress (psi) (Margin of Safety)	Max. Primary Bolt Stress (psi) (Margin of Safety)	Max. Secondary Bolt Stress (psi) (Margin of Safety)
Center Punch-Bottom Lid	60698 (M.S. = +0.13)	24953 (M.S. = +0.92)	35398 (M.S. = +1.91)	---
Center Punch-Top Lid	56838 (M.S. = +0.21)	29033 (M.S. = +0.65)	14921 (M.S. = +5.90)	0
Punch at Secondary Lid O.D.	65606 (M.S. = +0.05)	47448 (M.S. = +0.01)	22177 (M.S. = +3.64)	6334 (M.S. = +Large)
Punch at Overpack I.D.	45632 (M.S. = +0.51)	43780 (M.S. = +0.10)	15921 (M.S. = +5.47)	16179 (M.S. = +5.37)

For plate bending stress:

$$\sigma_B = 6M_{r=3}/t^2$$
$$= 67,433 \text{ psi}$$

Conservatively neglecting the stiffening effect of the lid attachment system, this result is reasonable and conservative compared to the finite element result of 60,698 psi for the same loading condition. The Margin of Safety resulting from this conservative analysis is:

$$M.S. = 68,785/67,433 - 1 = +0.02$$

As can be seen from Table 2.7.2-1, the worst-case puncture event, resulting in the smallest margins of safety, was that where the pin impacted the cask at the location of the secondary lid outside diameter. As an empirical verification of the above analysis results, a quarter-scale test was conducted. For this test, the cask was dropped from a height of 40 inches onto a scaled puncture pin, with the pin impacting at the secondary lid outside diameter. No significant damage resulted from this test. Details of the test are included in Appendix 2.10.4.

These results indicate that the cask lids are suitably designed to withstand any regulatory puncture event. It should be further noted that the careful design optimization of both lids has lead to structures that are equally strong despite their geometric dissimiliarities. This is evident from the similiar stress results for the top and bottom lids under center punch loading. These results are for the bottom-loading cask configuration. It may be assumed that the fixed-bottom configuration, with its more rigid, essentially clamped-edge bottom plate, will be even stronger and more puncture resistant.

2.7.2.3 Lid Closure System

As shown in Table 2.7.2-1 above, stresses in all primary and secondary lid bolts remain well below their allowable limits during puncture loading. Pin punch on the cask lids will therefore have no detremental effect on the

closure bolts. Additionally, scale testing of a pin impact directly onto a lid bolt lug has demonstrated that pin punch will have no significant effect on the bolt and bolt lug (see Appendix 2.10.4 for detailed test results). This is due in part to the robustness of the lug system itself, as well as dimensional considerations in providing protection for the bolt. The maximum width between lug gussets is only 4.47 inches, which precludes entry of the 6 inch diameter puncture pin into the bolt area. Therefore, the closure arrangement for both top and bottom lids is more than adequate to withstand the effects of regulatory pin punch.

2.7.2.4 Impact Limiter Puncture Resistance

Since it has been demonstrated that the unprotected cask will survive a 40 inch drop onto the puncture pin per 10 CFR 71, damage from such a drop impacting the impact limiters will be less severe on the cask than from the cases already examined. The only additional adverse effect which impact limiter pin penetration might have on cask performance would be the case where the pin strikes the impact limiter at an oblique angle, penetrates the impact limiter, and the tears out some of the polyurethane foam as the cask rolls off of the puncture pin. Recent drop tests on both the 10/140MB quarter-scale model (refer to Appendix 2.10.4), as well as a similiar cask have demonstrated this worst-case loss of foam which could be expected under this impact situation.

The implication of this damaged configuration is a potential loss of some of the foam insulation protection in the vicinity of the EnviroSeal^{tm}. As a result, the temperatures of the O-ring seals could be higher than would otherwise be expected. This damaged configuration has been srbjected to the accident condition fire transient analysis, in conjunction with further damage arising from a 30-foot corner drop at the same location, for maximum loss of impact limiter foam filling. The results of this analysis are given in Section 3.5.3. The peak seal temperature was found to be 296°F, which was maintained for a period of about one-half hour. Recent tests have indicated no loss of sealing capability for the O-ring material used in the EnviroSeals^{tm} under conditions more extreme than those analysed. Refer to Appendix 2.10.7 of the TRUPACT-II Safety Analysis Report (Docket Number 71-9218) for details.

The above results demonstrate that the NuPac 10/140MB cask will survive a 40 inch drop onto the puncture pin per 10 CFR 71 with no adverse affect on cask sealing and shielding integrity.

2.7.3 Thermal

The hypothetical fire transient is analyzed in Section 3.5. From that section, maximum temperatures and pressures are directly available for use.

2.7.3.1 Summary of Pressures and Temperatures

The maximum fire accident condition temperatures for the various cask components are presented in Sections 3.5.3 and 3.5.4. Maximum internal pressure resulting from the fire transient is 17.8 psig.

2.7.3.2 Differential Thermal Expansion

Differential thermal expansions due to the fire accident are of little consequence for the NuPac 10/140MB Cask. All stresses resulting from differential expansions can be classified as secondary, displacement limited stresses. As limits on secondary stresses do not apply for accident conditions (per Section 2.1.2), differential expansions do not compromise the integrity of the cask. Through wall (and through thickness) thermal gradients also result in secondary stresses and again are of little consequence for the cask.

2.7.3.3 Stress Calculations

The concern for accident conditions is with primary, load controlled stresses. The only load controlled stresses during and after the fire transient are those resulting from pressure and dead weight, and are therefore rather modest. Although temperatures associated with the fire transient are typically higher than those associated with other accident conditions, the NuPac 10/140MB Cask design is considered by inspection to be governed by the significantly more severe drop accident events.

2.7.3.4 Comparison with Allowable Stresses

Based on the discussions presented in Section 2.7.3.1 through 2.7.3.3, it is apparent that large margins of safety exist for the fire transient condition.

2.7.4 Immersion - Fissile Material

This section is not applicable to the NuPac 10/140MB, since no fissile material above exempt limits would be transported in it.

2.7.5 Immersion - All Packages

The effect of a 21 psig external pressure due to immersion in 50 feet of water as required by 10 CFR 71.73(c)(5) is analyzed below:

Assuming the pressure is entirely reacted by the outer shell, the component stresses are:

$$\text{Hoop stress} = \sigma_h = pr/t$$
$$\text{Longitudinal stress} = \sigma_L = pr/2t$$
$$\text{Radial Stress} = \sigma_r = p$$

where p = pressure = 21 psig
r = outer shell radius = 36.625 in.
t = outer shell thickness = 1.25 in.

So,

$\sigma_h = (21)(36.625)/1.25 = 615$ psi
$\sigma_L = (21)(36.625)/(2)(1.25) = 308$ psi
$\sigma_r = 21$

The maximum stress intensity in the outer shell is then 615 - 21 = 594 psi and the margin of safety is very large.

Stresses in the 5.25 inch minimum thickness end plates are similarly trivial and completely bounded by the stresses in the lid from the payload pressure during the 164.0g acceleration from end impact from 30 feet at -20°F.

2.7.6 Summary of Damage

From the analyses presented in Sections 2.7.1 through 2.7.5, it can be shown that the accident test sequence will not result in any significant structural damage to the NuPac 10/140MB Cask. Nearly all permanent damage occurs in the external impact limiters as desired. Minor amounts of damage can occur to cask components as follows:

For a 40 inch drop on a 6.0 inch diameter puncture pin, with impact occurring on the side of the cask at midlength, localized cask damage can occur at the impact point, but the outer cask outer shell will not be perforated and the overall bending response of the cask remains elastic. Finally, for a 40 inch drop on a 6.0 inch diameter puncture pin, with impact occurring on the cask top lid, a very slight permanent bow of the 5.25 inch minimum thickness lid may occur.

These permanent deformations are of little consequence for the NuPac 10/140MB Cask as they represent only minor changes in cask geometry. In particular, damage is not sufficient to compromise 'leaktightness' of the containment vessel or cask seals. For these reasons, the integrity of the cask is not considered to be compromised by the accident test sequence set forth in 10 CFR 71.

2.8 Special Form

This section does not apply for the NuPac 10/140MB Cask.

2.9 Fuel Rods

This section does not apply for the NuPac 10/140MB Cask.

APPENDIX 2.10.1

Stability and Buckling Design Criteria

2.10.1 Stability and Buckling Design Criteria

This appendix defines a stability and buckling criteria for radioactive materials packages consistent with the guidelines of Paragraph C.5, NRC Regulatory Guide 7.6, see reference 2.10.1.5.1. The technical rationale for this criteria is presented and discussed in conjunction with appropriate works in the technical literature. This appendix concludes with an analysis of the inherent factors of safety embodied within this criteria and a comparison of these factors of safety with comparable elements of other established forms of design criteria for stability.

Briefly, the criteria establishes the limit (membrane compression) stress at 1/5 or 1/7.5 of the elastic buckling (Euler) stress limits for accident and normal conditions of transport, respectively. In the domain where failure is characterized by yielding or plastic flow, rather than instability, the limit stress is further reduced by consideration of physical material limits for yielding and strength. A parabolic curve provides the transition between the physical material property limits and the elastic stability limits.

The boundary between stability and plastic flow or yielding regimes is set at a point where the elastic buckling load exceeds the yield load by a factor of 5. This boundary criterion is taken from the work of Combescure, reference 2.10.1.5.10. Within this stability design criteria, this boundary is implicitly satisfied, for accident conditions, by setting stress limits at 1/5 of the elastic buckling stress. The corresponding factor of 1/7.5, applied to normal conditions, is attained by application of the conventional ASME factor of 2/3, representing the ratio of (S_m/S_y).

The criteria defined here recognizes that compressively loaded structures behave in different fashions depending upon geometric aspect ratio of the structure. The nature of the criteria is such that the factors of safety vary with this geometric aspect ratio up to asymptotic values of 5 and 7.5, versus elastic buckling stresses, for accident and normal conditions of transport, respectively. These asymptotic factors of safety may be considered conservative for general use as radioactive materials package design criteria. It should be noted that the general form of the criteria allow adjustment of these asymp-

totic factors of safety to any values considered appropriate.

2.10.1.1 Criteria Definition

Direct primary compressive membrane stresses, S, in containment vessels shall be less than the lesser of S_e/R_d or S_j. S_e is defined as the appropriate elastic buckling stress limit considering adjustments resolving theoretical and experimental results, but neglecting plasticity corrections. The reduction coefficient R_d is to be taken as 7.5 for normal conditions of transport and 5 for accident conditions of transport. This reduction coefficient, R_d, corresponds to the intended factor of safety of the method at high aspect ratios of the structure. S_j is a generalized 'Johnson' parabolic transition curve having a value of S_s, at an aspect ratio, G, of zero. This parabolic transition curve is also tangent to the expression S_e/R_d at a stress level of 2/3 S_s. The term S_s denotes the applicable strength limit of the material -- S_m for normal conditions of transport and S_y for hypothetical accident conditions, both as defined within reference 2.10.1.5.1. The details of the criteria, in symbolic form are as follows:

Where G is less than G^*:

$$S \leq S_j,$$

Where G is greater than or equal to G^*:

$$S \leq S_e/R_d.$$

Where: S_e = The classical elastic buckling stress expression cast in the generalized form:

$$= K/G.$$

K = A numerical constant unique to each compressive loading mechanism reflecting materials properties (Young's Modulus, Poisson's ratio) and empirical or theoretical coefficients. See Table 2.10.1.1-1 for a summary versus typical loading mechanisms.

G = A non-dimensionalized geometric aspect ratio unique to each loading mechanism. See Table 2.10.1.1-1 for a summary versus typical loading mechanisms. For example:

= $(L/p)^2$, for column type loadings [Note: $p = (I/A)^{1/2}$],

= (R/t), for external pressures on long cylinders and axial compression loadings of cylinders.

R_d = 7.5, for Normal Conditions,

= 5.0, for Accident Conditions.

S_j = The parabolic transition from S_s to (S_e/R_d):

= $S_s - 4S_s^3G^2/[27(K/R_d)^2]$.

G^* = The aspect ratio, G, where the parabola defined by S_j intercepts and is tangent to the curve defined by (S_e/R_d), in other words, G^* corresponds to the aspect ratio where $S_j = (S_e/R_d)$, or:

= $(3/2)(K/R_d)/S_s$.

S_s = S_m, for Normal Conditions,

= S_y, for Accident Conditions.

S_m = Design Stress Intensity as used within Section III, ASME Boiler and Pressure Vessels Code.

S_y = Yield Stress.

TABLE 2.10.1.1-1

SUMMARY OF NUMERICAL CONSTANTS AND NON-DIMENSIONAL COEFFICIENTS OF S_e = K/G VERSUS LOADING CONDITIONS

Loading Mode	K[1]	G[3]	Reference
Axial Compression and Bending:	Varies:	(R/t)	2.10.1.5.13, pp. 230-5
At (R/t) = 10:	0.5022 E[2]		
At (R/t) = 100:	0.3570 E		
Long Column Compression:	4.9348 E	$(L/R)^2$	2.10.1.5.13, pp. 231
External Pressure - No External Constraints:			
(1) Moderate Length: $(L^2t/R^3 < 11)$	0.9181 E	$(R^{1/2}L/t^{3/2})$	2.10.1.5.13, pp. 236
(2) Long: $(L^2t/R^3 > 11)$	0.2473 E	$(R/t)^2$	2.10.1.5.13, pp. 237
External Pressure - External Constraint:			
	$.0915S\ E$	$\frac{(R/t)^2}{[6.66(R/t)^{.8}-1]}$	2.10.1.5.17, pp. 342, eq. 47-8

Notes:
(1) Poisson's ratio = 0.3 assumed for constant evaluation.
(2) E = Modulus of Elasticity.
(3) Notation:

R = radius
L = length
t = thickness

2.10.1.2 Background

NRC Reg Guide 7.6, reference 1, requires that 'buckling of the containment vessel should not occur under normal or accident conditions'. The ASME NUPACK Committee has proposed a series of rules governing buckling and instability, Section NX-3133, reference 2.10.1.5.2. The NUPACK proposed criteria are of two parts. Sections NX-3133.1 to NX-3133.6 employ charts and 'rote' procedures to establish limits for specific geometries and loading conditions -- most not applicable to typical package geometries or loadings. The second part of this NUPACK criteria, Section NX-3133.8 proposes rules more consistent with the 'design by analysis' approach of NRC Reg Guide 7.6. This particular set of provisions is taken directly from ASME Section III, Division 1 Code Case N-47-21 for Class 1 components in elevated temperature service. Within Section NX-3133.8, constant safety factors are proposed for load-controlled and strain-controlled buckling. The proposed NX-3133.8 factors of safety are as follows:

Condition	Load F. S.	Strain F. S.
Normal (Level A):	3.0	1.67
Accident (Level D):	1.5	1.1

Per NX-3133.8, these factors of safety are applied to the 'load (strain) which would cause instant instability at the design (or actual service) temperature'. Application of these proposed rules has proven difficult due to the diversity of opinion concerning the resolution of these issues:

- 'Instant instability' implies a classic elastic instability failure that is fundamentally inconsistent with the practical geometries of radioactive materials packages. If elastic instability is not of concern for a particular package, are the factors of safety applicable?

- The applicable instability regime is not defined. Does this imply that all compressive loading states are to be treated as potential instability situations?

- 'Instant instability' does not characterize the behavior of structures

whose failure modes are associated with yielding or plastic flow where no loss of load resistance is experienced. What criteria govern the design of these structures? How do these criteria 'mesh' with stability criteria as the aspect ratios of a structure increase?

- The single-valued factors of safety appear both potentially low for 'instant instability' associated with true elastic instability and excessively conservative for plastic flow or yielding situations where no loss of load resistance takes place. In fact, the single-valued factors may be appropriate only within some intermediate regime.

Investigations to resolve these issues have lead to the following findings:

1. ASME Code Case N-47-21 is overly conservative for situations were 'instant instability', or buckling does not represent the failure mechanism of the component, references 2.10.1.5.3 and 2.10.1.5.4.

2. For cylindrical shells, as used for containment vessels of radioactive materials packages, there are three characteristic failure mechanisms associated with compressive loadings, references 2.10.1.5.5 and 2.10.1.5.6. Each of these failure mechanisms is controlled by a different priority set of geometric and material properties, references 2.10.1.5.6, 2.10.1.5.7, 2.10.1.5.8, 2.10.1.5.9 and 2.10.1.5.10. The characteristics of the failure, or safety consequence, in each mechanism differ -- ranging from catastrophic collapse, at one extreme, to controlled plastic flow, at the other extreme, reference 2.10.1.5.5. Thus each, can and should possess differing factors of safety. To illustrate, Johnston, reference 2.10.1.5.6, states (page 265): '...formulas to predict the buckling capacity of thick-walled tubular members under axial compression are much more reliable than formulas to predict the capacity of thin-walled shells. [Thus] .... factors-of-safety used in thick-walled member design should be less than those used with thin-walled shells'.

3. The boundaries between each of the three failure mechanisms can be defined with reasonable accuracy. These boundaries typically are defined in terms of the shell aspect ratio and material properties, for example, see reference 2.10.1.5.11, Section 7.5a. A recent French proposal, reference 2.10.1.5.10, suggests definition of these boundaries in terms of the ratio of elastic buckling stress to yield stress. Both approaches give reasonably consistent results. For example, using a cylindrical shell compression case and assuming a steel with a modulus of 29.5×10^6 psi and a yield of 30 ksi, reference 2.10.1.5.11 gives the inception of plastic buckling at (R/t) = 62, whereas the French approach predicts this boundary at (R/t) = 70.

4. Typical industry design (criteria) codes provide varying factors of safety as a function of aspect ratios, for example, see Paragraph 1.5.1.3 of the AISC Specification, reference 2.10.1.5.12.

The above discussion notes that there are three characteristic failure mechanisms or behavior regimes. They are cataloged below, along with their principal attributes.

o Soft Structures:

a. Stress Range: Elastic.

b. Buckling Type: Local buckling, bifurcation buckling, antisymmetric buckling, diamond (shaped) buckling.

c. Failure Mode: Catastrophic Collapse, oil-canning snap-through.

d. Predictive Sensitivity: Initial imperfections in geometry and material properties lead to large and random variations observed in buckling tests as compared to theory. Large factors of safety are required, reference 2.10.1.5.6. In this range these factors can range from 3 to 10.

- Intermediate Structures:

  a. Stress Range: Elasto-plastic.

  b. Buckling Type: Equilibrium collapse load buckling, bellows type buckling, full-wall buckling, symmetrical (axisymmetric) buckling.

  c. Failure Mode: Controlled plastic deformation, constant or increasing load resistance (for strain-hardening materials, like stainless steels or aluminum).

  d. Predictive Sensitivity: Primarily dependent upon materials properties in the transition regions between fully-elastic and strain-hardening behavior. Relatively insensitive to geometric imperfections and end conditions. Factors of safety should be somewhat greater than those typically applied to strength designs.

- Hard Structures:

  a. Stress Range: Plastic.

  b. Buckling Type: Generally not considered as a buckling phenomena since no instability (loss of load resistance) occurs for a work-hardened material. Yielding, plastic flow.

  c. Failure Mode: Plastic deformation and flow.

  d. Predictive Sensitivity: Completely dependent upon materials properties and strain-hardening behavior. Totally insensitive to geometric imperfections and end conditions. Factors of safety should not exceed those typically applied to strength design.

Boundaries between these three classes of behavior are described in a variety of formats. The most conventional, separating 'Hard' structures from 'Intermediate' and 'Soft' structures is the conventional distinction between thin shells and thick shells, references 2.10.1.5.7, 2.10.1.5.8, 2.10.1.5.9 and 2.10.1.5.13. This is a relatively imprecise distinction with estimates of

(R/t) values ranging from 20 to greater than 100. With a well behaved stress-strain curve, i.e., a smooth transition and strain hardening, the predictive reliability of this boundary determination increases. Thus, from a stability standpoint, stainless steel and some aluminum alloys, with smooth transitions and strain hardening, are preferable to mild steels, with sharp transitions and minimal strain hardening.

Combescure, reference 2.10.1.5.10, suggests that a ratio of elastic buckling stress to yield stress, (S_e/S_y), of 5.0 defines this boundary. Yu, reference 2.10.1.5.11, points out that the AISI Code (Equation 3.8-1), reference 2.10.1.5.14, defines the boundary between 'Hard' (yielding, plastic flow) and 'Intermediate' (plastic buckling) structures at a $(D/t) = 3300/S_y$, or approximately 110 for a 30 ksi steel. Yu also notes that for lesser (D/t) values the design stress need not be reduced below conventional strength allowables. Importantly, the boundary employed by AISI has been developed by extensive tests, references 2.10.1.5.15 and 2.10.1.5.16.

The boundary between 'Intermediate' and 'Soft' structures can be stated in similar terms. For example, Yu gives the AISI boundary estimate as $(D/t) = 13000/S_y$, or approximately 430 for a 30 ksi steel.

2.10.1.3 Criteria Rationale

The proposal of Combescure, reference 2.10.1.5.10, have been adopted as the defining boundary between 'Hard' and 'Intermediate' structures. Thus, this boundary is determined at an aspect ratio defined by the stress ratio $(S_e/S_y) = 5.0$. This boundary is used to define the intercept of the basic strength limit, S_s, and the reduced elastic buckling curve, (S_e/R_d). Of course, in this region the parabolic transition curve, S_j, passes below this intercept value. The primary reason for adoption of this method is that it is independent of loading mode whereas all the aspect ratio methods are mode-specific. Importantly, the Combescure method and the more conventional aspect ratio methods, such as references 2.10.1.5.11, 2.10.1.5.15, and 2.10.1.5.16, all give comparable results, as mentioned in Item 3, Section 2.10.1.2.

At lesser aspect ratios, the basic strength allowables are not reduced significantly. At greater aspect ratios, the allowables are governed by a 'de-

graded' elastic buckling relation, (S_e/R_d). Smooth transition from the 'flat-topped' strength limit to the 'degraded' elastic buckling curve is provided by a traditional 'Johnson' parabola.

The principal attributes of the stability design criteria set forth herein are as follows:

1. At high aspect ratios corresponding to 'Soft' structures, the method provides large factors of safety -- 5 for accident conditions, 7.5 for normal conditions. This is significantly greater than as provided within the NUPACK proposed rules and as provided in other stability related design criteria. Importantly, these increased factors of safety provide a 'penalty-function' for use of 'Soft' structures. This has the effect encouraging use of more robust structural forms that behave in a 'Hard' or 'Intermediate' structural fashion. This penalty-function directly supports the philosophy of Reg Guide 7.6 -- 'buckling ... should not occur'.

2. At low aspect ratios, the method implicitly provides a correction to the elastic buckling relation which conservatively envelopes the plasticity correction factor, see reference 2.10.1.5.13. Using the method, there is no need to calculate this plasticity correction factor. This is a desirable feature because the plasticity correction factor must be derived for each specific material given accurate stress-strain data in the transition region from the proportional limit to the strain-hardening tangent. Such data is difficult to obtain for design purposes, is unique to a particular heat of material and cannot be easily verified or checked by review or Regulatory personnel.

3. For normal conditions, no stresses exceed the proportional limit. This guarantees no instabilities and no inelastic behavior that could invalidate structural demonstrations of adequacy. This condition is assured by the limitation of stresses to values below S_m, which closely approximates the proportional limit stress for all typical package materials.

4. While the bulk of discussion has focused upon axial compressive loadings, it is important to note that the method is fully applicable to column

stability and external pressure (these two are mathematically similar). In fact, the method (for normal conditions) precisely duplicates the column design formulas of AISC and the Column Research Council, see page 64, reference 2.10.1.5.6, when S_m is assumed equal to $0.6*S_y$. In application, this method proves to be considerably more conservative due to the fact that the parabolic transition is tangent to (S_e/R_d) whereas the AISC and CRC parabolic transitions are tangent to S_e itself. Clearly, the reduction factor, R_d, forces a significant and predictable additional measure of conservatism.

2.10.1.4 Safety Analysis

The characteristics of the recommended criteria are analyzed within this section. Three basic loading conditions are examined in a parametric fashion: axial loadings, external pressure loadings and finally, column-type loadings. The analyses are conducted in a parametric fashion, examining results as a function of appropriate aspect ratio. For each examination, two plots are provided. The first is a non-dimensionalized stress plot versus aspect ratio, normalized by yield stress. Shown on this plot is the basic elastic buckling stress with experimental/theoretical corrections, (S_e/S_y), the buckling stress as determined by 'modern' analysis methods including plasticity corrections, Chapter 10, reference 2.10.1.5.13, (S_{cr}/S_y), and finally the stress limits (S_{ai}/S_y) proposed within this criteria, $S_{ai} = S_j$ where $G < G^*$ and $S_{ai} = (S_e/R_d)$ elsewhere, where the subscript 'i' = 'n', for normal conditions and 'i' = 'a', for accident conditions. The second companion plot presents the distribution of the resultant factor of safety (of this method), plasticity correction factor from 'modern' theory, and approximate plasticity correction provided by this method.

Within each of the following paragraphs, the particular characteristics of the inputs to the analysis are described. Resultant output is discussed, where appropriate. For calculation purposes, material properties of 304 stainless at 212 ^{o}F are utilized.

2.10.1.4.1 Axial Compression Behavior

The relations given by Baker, reference 2.10.1.5.13, page 230, are used for

this demonstration and comparison analysis. In the Baker relation an experimental correction coefficient is applied to the basic (Euler) elastic buckling stress value. This coefficient ranges from 0.83 at an aspect ratio, G = (R/t) = 10, to 0.59 at an aspect ratio of 100. For these two aspect ratios, sample criteria evaluation and analysis is provided below (notation follows Section 2.10.1.1).

PARAMETER	Symbol		
Aspect Ratio:	G	10	100
Numerical Coefficient:	K	13910000	9888000
Euler Buckling Stress:	$S_e = K/G$	1391000	98880
Plasticity Factor	-	46.57	4.214
Baker Limit Stress:	S_{cr}	29869	23465
Reduction Factors: (from elastic buckling)	R_d		
Normal		7.5	7.5
Accident		5	5
Strength Limits:	S_s		
Normal	S_m	20000	20000
Accident	S_y	24700	24700
Intercept Aspect Ratio:	G*		
Normal		139.1	98.9
Accident		168.9	120.1
Criteria Stress Limit:	S_{ai}		
Normal	S_{an}	19966	13184
Accident	S_{aa}	24671	18992

PARAMETER	Symbol		
Factors of Safety:			
Normal	S_{cr}/S_{an}	1.50	1.78

Accident	S_{cr}/S_{aa}	1.21	1.24

Comprehensive comparison data is graphically provided in Figures 2.10.1.4-1 and 2.10.1.4-2 for a full range of aspect ratios. The conservatism of the proposed criteria for 'Intermediate' and 'Soft' structures is readily apparent. The graphs are largely self-explanatory, however the difference between normal condition limits and AISI design values requires discussion. For all construction industry codes, including AISI, the working stress limit, F, is set as 3/5 of yield, S_y. The criteria proposed here, sets the normal, or working stress limits at S_m. Normally this provides a value approximating 2/3 of yield, S_y. For the comparison shown in these Figures, data corresponds to properties at 212 ^{o}F. At this temperature, yield is degraded from the room temperature value of 30 ksi to about 24.7 ksi whereas the value S_m remains constant. Room temperature comparisons would have shown both the proposed criteria and AISI nearly coincident, 0.6 versus 0.67, at low aspect ratios.

The Figures clearly show the conservative impact of limiting high-aspect ratio stresses to (S_e/R_d) rather than a constant factor offset (3/5) from S_e, as done by AISI. Figure 2.10.1.4-2 graphically shows how the resultant factors of safety asymptotically approach 7.5 and 5, at high aspect ratios, for normal and accident conditions, respectively. Of note, the plotted plasticity correction shown on this Figure is simply the inverse of that used by Baker, reference 2.10.1.5.13.

FIGURE 2.10.1.4-1

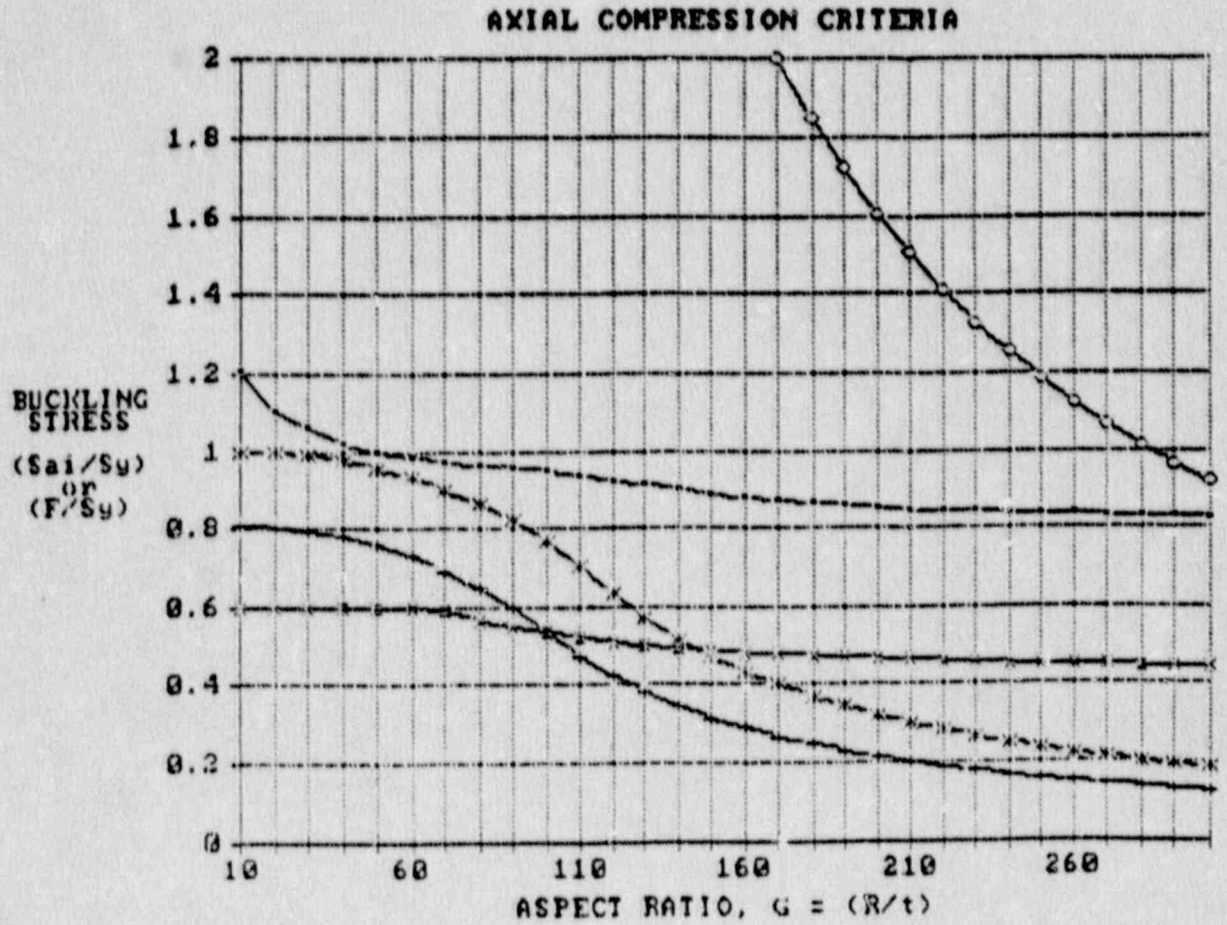

FIGURE 2.10.1.4-2

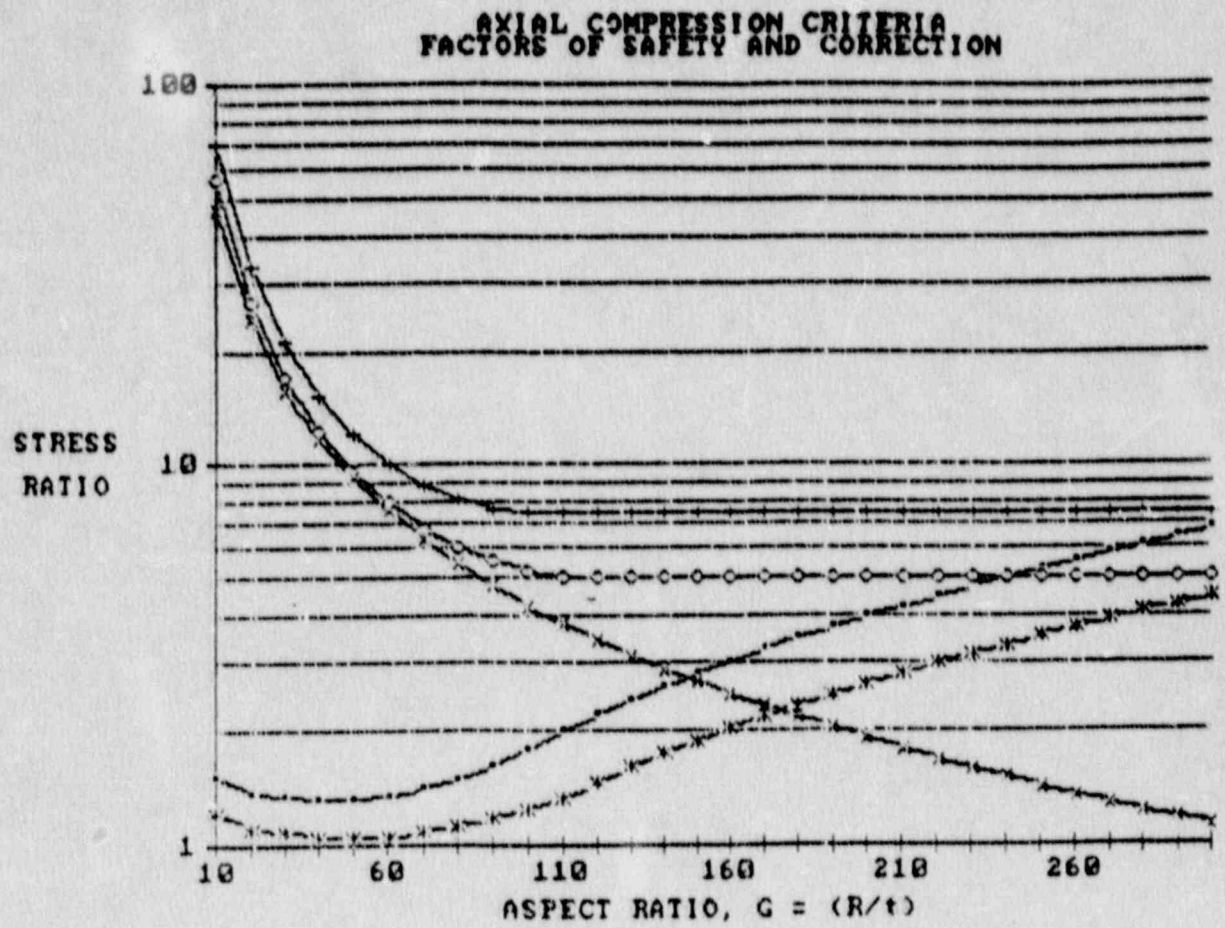

2.10.1.4.3 External Pressure Behavior

These results, Figures 2.10.1.4-3 and 2.10.1.4-4, are essentially identical in form and significance to those discussed for axial compression behavior.

2.10.1.4.3 Column Behavior

Once again, Figures 2.10.1.4-5 and 2.10.1.4-6, display results comparable to the axial compression behavior. The conventional AISC column design formula is shown. For (L/R) values in excess of approximately 60 this design criteria limits stresses to less than 40-60% of the allowable AISC values. This impact is a direct result of the intended high reduction factor, or safety factor of 7.5 and 5 for normal and accident conditions, respectively. This criteria also provides a more sharply defined 'cut-off' of permissible stresses, at the plastic instability boundary ('Hard' to 'Intermediate' structures), due to the fact that the parabolic transition is mapped in the transformed 'G' coordinate system, not the conventional (L/R) coordinate system, as used by AISC. In the case of the column equations this coordinate transformation is given as, $G = (L/R)^2$.

FIGURE 2.10.1.4-3

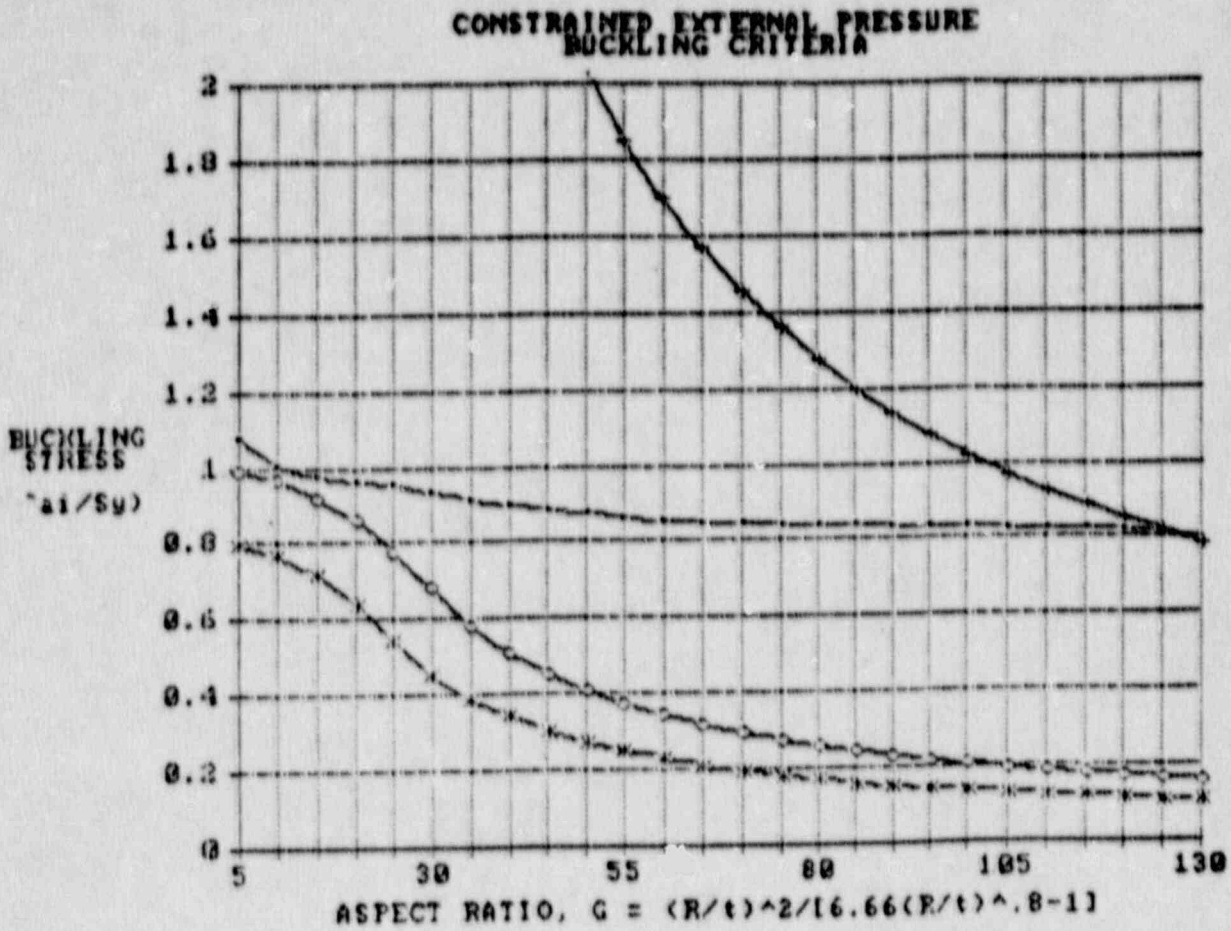

FIGURE 2.10.1.4-4

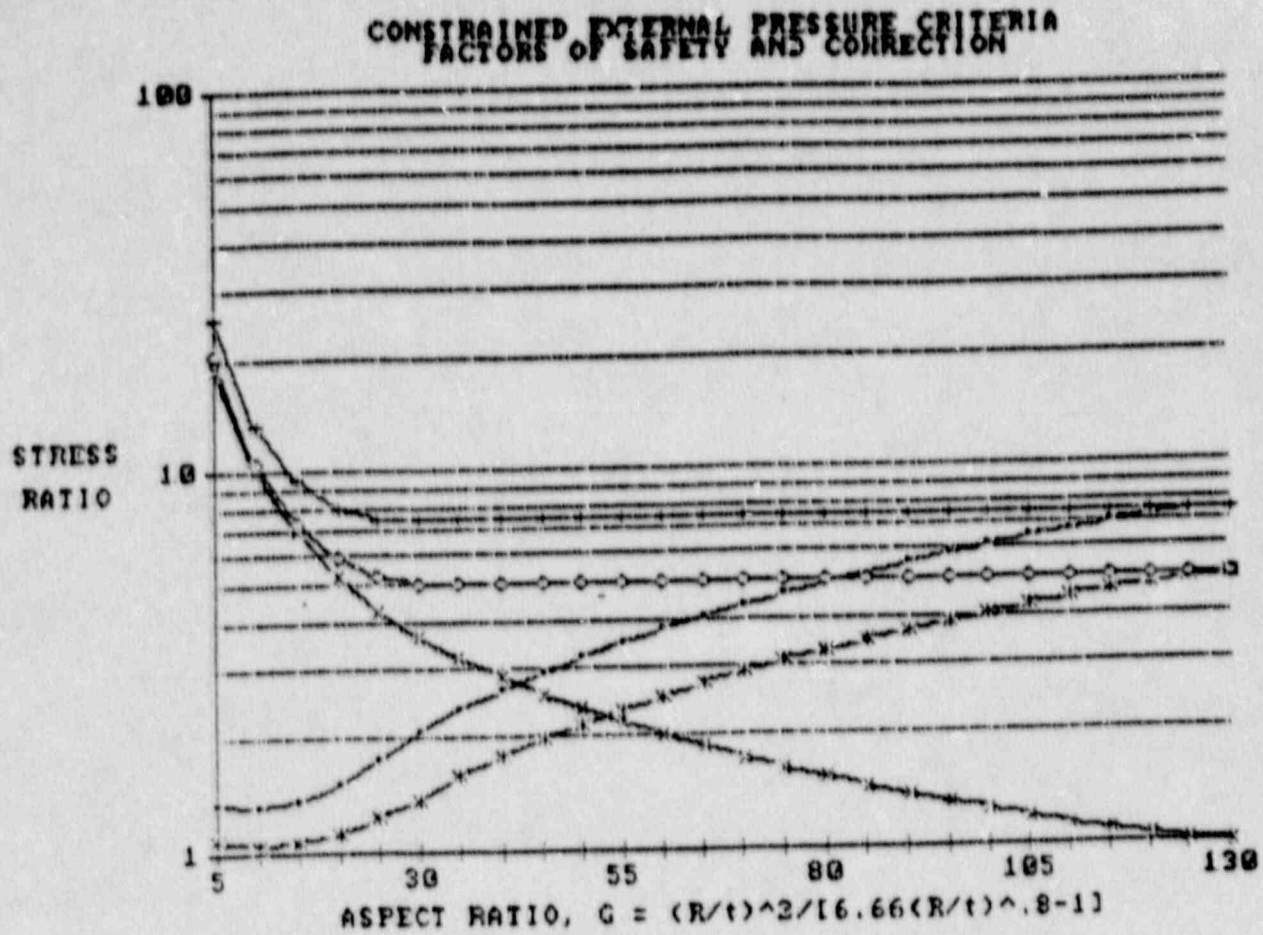

FIGURE 2.10.1.4-5

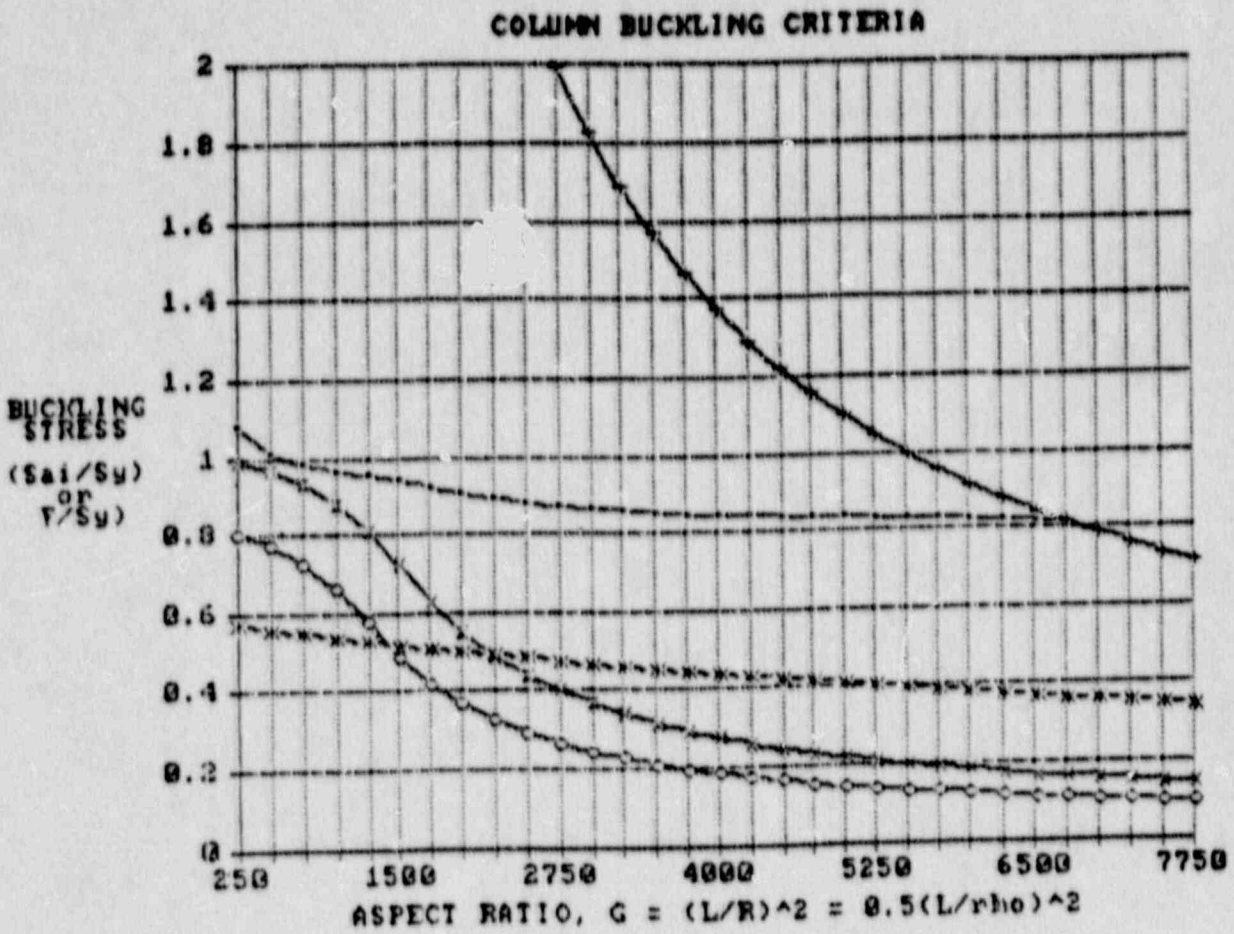

FIGURE 2.10.1.4-6

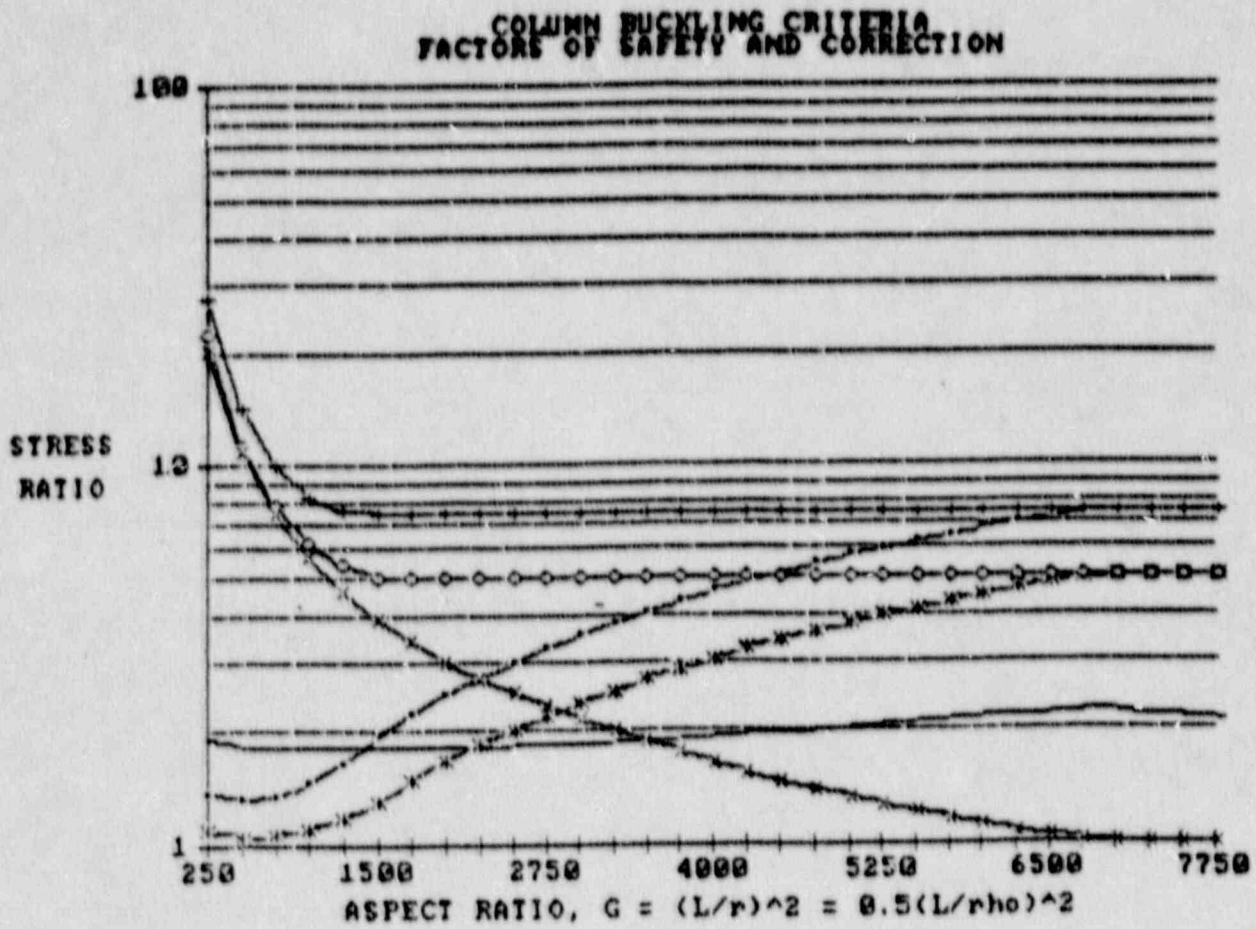

2.10.1.5 References

2.10.1.5.1 U.S. Nuclear Regulatory Commission Regulatory Guide 7.6, Design Criteria for the Structural Analysis of Shipping Cask Containment Vessels, Revision 1, March 1978.

2.10.1.5.2 Design Task Group, ASME Committee on Containment Systems for Nuclear Spent Fuel and High-Level Waste Transport Packagings (NUPACK).

2.10.1.5.3 Personal communications with Code Case N-47-21 Committee member, Dr. Donald Griffin, Westinghouse, Madison, Pennsylvania to Dr. Howard C. Merchant (NuPac consultant).

2.10.1.5.4 Personal communications with Code Case N-47-21 Committee member, Mr. Al W. Dalcher, General Electric, (408) 738-7605 to Dr. Howard C. Merchant (NuPac consultant).

2.10.1.5.5 Bushnell, D., 'Static Collapse: A Survey of Methods and Modes of Behavior', Collapse Analysis of Structures, PVP-Vol.84, ASME, 1984, pp. 7-50.

2.10.1.5.6 Johnston, Bruce G., Editor, Guide to Stability Design Criteria for Metal Structures, Third Edition, John Wiley and Sons, New York, 1976.

2.10.1.5.7 Batterman, S. C., 'Plastic Buckling of Axially Compressed Cylindrical Shells', AIAA Journal, Volume 3, No. 2, January 1965, pp. 316-325.

2.10.1.5.8 Gerard, George, 'On the Role of Initial Imperfections in Plastic Buckling of Cylinders Under Axial Compression', Journal of Aerospace Sciences, Vol. 29, June 1962, pp.744-745.

2.10.1.5.9 Sobel, L. H., S. Z. Newman, 'Plastic Buckling of Cylindrical Shells Under Axial Compression', Journal of Pressure-Vessel Technology, Vol. 102, February 1980, pp. 40-44.

2.10.1.5.10 Combescure, A., 'Design Against Elasto-Plastic Buckling of Shells: Proposition of a Methodology', Recent Advances in Nuclear Component Testing and Theoretical Studies on Buckling, PVP-Vol. 89, ASME, 1984, pp 137-155.

2.10.1.5.11 Yu, Wei-Wen, Cold-Formed Steel Structures -- Design, Analysis, Construction, McGraw-Hill Book Company, New York, 1973.

2.10.1.5.12 Manual of Steel Construction, 6th Edition, American Institute of Steel Construction Inc. (AISC), 1963.

2.10.1.5.13 Baker, E. H., L. Kovalevsky and F. L. Rish, Structural Analysis of Shells, Robert E. Krieger Publishing Company, 1981.

2.10.1.5.14 Cold-Formed Steel Design Manual, 1983 Edition, American Iron and Steel Institute (AISI).

2.10.1.5.15 Plantema, F. J., 'Collapsing Stresses in Circular Cylinders and Round Tubes', Report S.280, 1946, Nat. Luchtvaartlaboratorium, Amsterdam, Netherlands.

2.10.1.5.16 Wilson, W. M., and N. M. Newmark, 'The Strength of Thin Cylindrical Shells as Columns', University of Illinois Engineering Experimental Station Bulletin No. 255, 1933.

2.10.1.5.17 Cheney, James A., Pressure Buckling of Ring Incased in a Cavity, ASCE EM Journal, April, 1971, Vol. 97, EM2.

APPENDIX 2.10.2

ANSYS Program Description

The ANSYS computer program is a large-scale, general purpose computer program for the solution of several classes of engineering analyses. Analysis capabilities include static and dynamic; elastic, plastic, creep and swelling; buckling; small and large deflections; steady state and transient heat transfer, fluid and current flow.

The matrix displacement method of analysis based upon finite element idealization is employed throughout the program. The library of finite elements available numbers more than forty for static and dynamic analyses, and twenty for heat transfer analyses. This variety of elements gives the ANSYS program the capability of analyzing two- and three-dimensional frame structures, piping systems, two-dimensional plane and axisymmetric solids, three-dimensional solids, flat plates, axisymmetric and three-dimensional shells and nonlinear problems including interfaces and cables.

Loading on the structure may be forces, displacements, pressures, temperatures or response spectra. Loadings may be arbitrary functions of time for linear and nonlinear dynamic analyses. Loadings for heat transfer analyses include internal heat generation, convection and radiation boundaries, and specified temperatures or heat flows.

The ANSYS program uses the wave-front (or 'frontal') direct solution method for the system of simultaneous linear equations developed by the matrix displacement method, and gives results of high accuracy in a minimum of computer time. The program has the capability of solving large structures. There is no limit on the number of elements used in an analysis. There is no 'band width' limitation in the analysis definition; however, there is a 'wave-front' restriction. The 'wave-front' restriction depends on the amount of core storage available for a given problem. Up to 2000 degrees of freedom on the wave-front can be handled in a large core. For extremely large analyses, an out-of-core wave-front procedure (which effectively removes the 'wave-front' limit with an increased run time penalty) is available.

The input data for the ANSYS program has been designed to make it as easy as possible to define the analysis to the computer. A preprocessor (PREP7) contains powerful mesh generation capability as well as being able to define all other analysis data (real constants, material properties, constraints, loads, etc.). Geometry plotting is available for all elements in the ANSYS library, including isometric, perspective, section, edge, and hidden-line plots of three-dimensional structures.

ANSYS has the capability of generating substructures (or superelements). These substructures may be stored in a library file for use in other analyses. Substructuring portions of a model can result in considerable computer-time savings for nonlinear analyses.

Postprocessing routines are available for algebraic modification, differentiation, and integration of calculated results. Root-sum-square operations may be performed on seismic modal results. Response spectra may be generated from dynamic analysis results. Results from various loading modes may be combined for harmonically loaded axisymmetric structures. Post routines also plot distorted geometries, stress contours, safety factor contours, temperature contours, mode shapes, time history graphs, and stress-strain curves.

Details of the types of finite elements used in the various analyses of NuPac 10/140MB components can be found in the ANSYS Users Manual, Revision 4.1, Volumes I and II, Swanson Analysis Systems, Inc., Houston, Penn., 1983.

APPENDIX 2.10.3

Tiedown Lug Load and Stress Analysis

THIS SECTION IS PROPRIETARY

APPENDIX 2.10.4

Quarter Scale Drop Test Results

2.10.4.1 Test Objectives

The key objectives of this test program revolved around verification of assumptions used in analyzing the full scale cask design, and confirmation of results derived therefrom, for package response to regulatory requirements set out in 10 CFR 71. Twelve tests were conducted in all -- eight accident condition free drop tests, three puncture tests, and an extra-regulatory bare cask drop.

Specifically, the test objectives included the following:

(1) Comparison of predicted and actual impact limiter deformations at ambient drop conditions.

The differences between calculated and empirical deflections was found to be approximately the same for all drop applicable orientations as occured during the extensive testing program for the 125-B cask (docket no. 71-9200). Since measured loads for that test program were very close to predicted values, and since both casks were analyzed by the same energy balance drop programs (refer to Appendix 2.10.5), it may logically be inferred that predicted loads for the 10/140MB will also correlate well with actual load values.

Drops for true deflections at ambient temperature (impact limiter geometry assumptions not an important consideration):

a. Flat end drop
   Two end drops were performed. These were tests 1 and 1a (1a actually being the third test performed overall in the test series)
b. Flat side drop
   This was test 6
c. Oblique drop - center of gravity over struck corner
   (An indirect comparison, since this drop mobilizes both major and minor diameter portions of impact limiter simultaneously. This situation is not amenable to direct analysis with NuPac's energy balance drop programs. Refer to Section 2.10.4.2 below for details)

This was test 5

(2) Simulation of worst-case impact loadings at critical drop angles

Oblique impacts were evaluated at a near-vertical drop orientation to impose maximum impact limiter and lid separation forces, and at a near-horizontal orientation for cask bending and maximum secondary (slapdown) forces. This simulation of loading due to minimum temperature (-20°F) foam was accomplished at ambient conditions by drops from elevations in excess of the regulatory 30 foot height. For a detailed discussion of the theoretical justification for testing at heights greater than 30 feet to simulate temperature effects on foam properties, refer to Section 2.10.4.6.2.1 of this Appendix.

Drops to induce maximum cask loads were conducted from a 37 foot height, in order to simulate response of minimum temperature (-20°F) impact limiter foam for Hypothetical Accident Conditions initial temperature conditions.

a. Oblique drop -- near vertical
(Maximum impact limiter and lid separation loads)
This was test 2

b. Oblique drop -- near horizontal
(Maximum slapdown and oblique-induced bending loads)
This was test 4

(3) Simulation of worst-case impact limiter deflections

Drop tests were performed to ensure that sufficient energy-absorbing material is available for all drop orientations, to preclude any possibility of the cask body or appurtenances from striking the essentially unyielding impacted surface. This simulation of deformations anticipated at the maximum Hypothetical Accident Conditions impact limiter temperature (105°F) was accomplished at ambient conditions by drops from elevations in excess of the regulatory 30 foot height. Justification for use of non-regulatory drop heights is provided in Section 2.10.4.6.2.2.

Drops to induce maximum impact limiter deflections were conducted at a 40 foot drop height in order to simulate response of warm (105°F) impact limiter foam for Hypothetical Accident Conditions initial temperature conditions.

a. Oblique drop - center of gravity over struck corner
(Corresponds to assumed worst-case deflection situation for Hypothetical Accident Conditions)
This was test 3

b. Flat side drop (on flattened sides of impact limiters)
This was test 7

(4) Simulation of worst-case pin punch drop

The most detrimental result on cask performance arising from a pin punch drop would be possible loss of containment due to damage to top lid or lid retention system (bolts and attachment lugs). Additionally, loss of foam and resultant loss of insulation around seal areas could result in excessive O-ring temperatures resulting from the accident condition fire transient event. Finally, pin puncture through the cask outer shell could result in localized melting of lead shielding during the accident fire. To evaluate the worst-case effects of pin puncture, three orientations were tested.

a. Oblique drop onto lid bolt lug
(To simulate maximum impact limiter foam tear-out and maximum lug damage)
This was test 8

b. Flat side drop
(To simulate worst-case outer shell puncture condition)
This was test 9

c. Flat end drop onto primary lid inside diameter
(To simulate worst-case lid deformation)
This was test 10

(5) Confirmation of lead slump pattern assumed in end drop shell analyses (both classical analysis results and ANSYS finite element results). To maximize lead slump and illustrate exaggerated lead response to impulse loading in the axial direction, a bare cask (no impact limiters) drop was performed from a height of 30 feet. Drop orientation was for a flat end impact on the bottom of the cask. This was test 12.

2.10.4.2 Test Article

The design of the quarter-scale test article adheres to the concepts set out in Section 2.2 regarding equivalent mass and inertial properties. While critical components (closure devices, impact limiters, inner and outer shells, lead shielding, key welds) and component interfaces are scaled precisely, the quarter-scale package in general is composed of simplified equivalent mass shapes which are arranged to duplicate the overall mass and inertial properties of a geometrically-true scaled cask. Additional mass not specifically modelled includes such items as thermal shields, lifting and tiedown lugs, and other relatively minor appurtenances. The equivalent (scaled) mass of these items is conservatively added to the ballast comprising the simulated payload.

Total weight of the test package was 1060.5 lb, for a full scale weight of (64)(1060.5) = 67,872 lb. Maximum estimated full scale weight, from Section 2.2, is 68,000 lb. The payload weight was 279.9 lb, or a full scale total of 17,913.6 lb. Since the actual maximum design payload weight for the 10/140MB Cask is only 15,000 lb, the test was very conservative, particularly with regard to maximum lid separation loading (test 2). The test article payload consisted of dry sand mixed with lead shot, as well as some small lead bricks.

Of particular interest in the quarter-scale model were the impact limiters. The behavior of the cask for the regulatory 30 foot drop at any orientation and within a wide range of temperature extremes, is a direct function of how the impact limiters perform. NuPac's proprietary energy-balance drop programs, EYDROP, SYDROP and CYDROP, detailed in Appendix 2.10.5, have been shown to accurately predict imposed loads, and to calculate resulting impact limiter deformations reasonably well.

These programs assume that all of the kinetic energy arising from the 30 foot drop is converted into strain energy in the polyurethane foam comprising the energy absorbing material in the impact limiters. Extensive drop testing has indicated that, in actuality, a certain percentage of the impact energy is absorbed in plastically deforming the thin-wall shell of the impact limiters. The contribution of the shells has been estimated as a small fraction of the overall energy absorption capacity of the impact limiter. These same tests, however (especially the 125-B quarter-scale tests) indicate that the deformation characteristics of the shell structure tend to match those of the foam contents, resulting in force-defection relationships closely paralleling those predicted by the drop programs.

Additionally, the manner in which the drop programs account for deformation of the foam within the impact limiters makes it difficult to directly correlate analytical and empirical results. The programs present total deformation, which is a combination of elastic and plastic deformation. In actuality, a significant amount of elastic spring-back will generally take place after maximum (elastic plus plastic) deformation has occured. Refer to Section 2.10.4.6.1 of this Appendix for further discussion on this subject.

As a result, measured permanent deformation arising from drop tests will generally be less the total calculated results. High-speed photography utilized in the 125-B test program captured the elastic portion of the impact limiter deformation, thus allowing direct comparisons between calculated and actual deformation results. The correlation was found to be quite good for all drop orientations. The permanent (plastic) foam deformation, as a percentage of calculated (plastic plus elastic) deformation, derived from the 10/140MB test program detailed below, was found to compare well with that arising from 125-B test results. It is thus logically concluded that total deformations of the 10/140MB test cask impact limiters likewise correlate well with calculated results.

The net result is that, both impact loads and total deformations can be predicted with good accuracy, although permanent deformations arising from actual impacts will generally be less than estimated.

The 10/140MB quarter-scale impact limiters contained the same 20 lb/in^3 rigid polyurethane foam that is used in the actual full-size production casks. Refer to Section 2.1.2.4 for further details on the polyurethane foam in particular, and impact limiter design in general.

The 11 gage (0.120 in thick) sheet metal impact limiter shells were simulated on the quarter-scale model with 22 gage (0.030 in thick) sheet. This corresponds precisely with a 1/4 scale thickness. The only difference between the quarter-scale version and full size impact limiters is the fact that, on the full scale impact limiter, all interior sheet metal (directly adjacent to the cask and its appurtenances) will be 0.25 inch thick. The quarter scale model utilized 22 gage material in these areas. This provided a conservative indication that 'inside-out' punch will not be a factor on the 10/140MB cask. Refer to Section 2.10.4.4.6 below for additional discussion of this design consideration.

The quarter-scale cask fabricaton assembly drawing is shown in Figure 2.10.4-1 for reference. Cask components and the assembled cask are shown in Figures 2.10.4-5 through 2.10.4-10.

2.10.4.3 Drop Pad Description

The impact surface used in this test series consisted of a 10 feet square by 6 feet deep concrete foundation, topped by a 3 inch thick steel plate. The facility used is the property of the Tacoma Boatbuilding Company, located in Tacoma, Washington.

2.10.4.4 Test Results

2.10.4.4.1 Predicted vs Actual Impact Limiter Deformations

In order to estimate 10/140MB impact loads by comparison to 125-B test results, similiarities in impact limiter deformation patterns had to be established. Once this was accomplished for the conventional impact orientations (flat end drop, flat side drop on impact limiter rounded sides) for which NuPac's proprietary drop programs provide calculated deflections, it could

then be readily assumed that the very conservative impact limiter geometry assumptions made for impacts on unconventional portions of the 10/140MB impact limiters would result in conservative overpredictions of loads or deformations.

2.10.4.4.1.1 Flat End Drop

For purposes of calculating impact limiter response during flat end drop with the energy balance program EYDROP, an 'equivalent' outside diameter was assumed for the non-circular end of the 10/140MB impact limiter. This resulted in an impacted area exactly equal to the actual area of the end of the impact limiter. Results of the EYDROP analysis were therefore valid for the actual (non-circular) geometry, and could be applied directly. The derivation of this 'equivalent' diameter is presented in Section 2.7.1.1.1. As can be seen, at an ambient temperature of 75°F, an impact limiter deflection of 4.38 inches was predicted by EYDROP. The resulting acceleration was calculated to be 100.2 g's.

Two flat end drop tests were conducted. The first, which was the initial test of the entire test sequence, was judged to be invalid, due to the fact that the steel plate was improperly positioned on the concrete foundation of the drop pad. This resulted in a slight rebound of the plate upon impact of the test cask. Under these circumstances, it was deduced that the pad did not constitute an essentially unyielding surface.

Consequently, another attempt was made, this time on the other impact limiter. In this test, the cask did not strike the drop pad squarely. It struck slightly off-vertical, impacting on one of the flattened sides of the bottom impact limiter. As a result, the cask rebounded, completed one and one-half revolutions in the air, and impacted again on its side. The impacted edge of the impact limiter is shown in Figure 2.10.4-11. A permanent external deformation of approximately 1/8 inch was measured at the point of the primary impact, and an additional 5/16 deformation occured due to inside-out punch, as measured from the reference stripe on the cask at the point where the cask enters the impact limiter. The result was a total permanent impact limiter deformation of approximately 0.44 inch, or (4)(0.44) = 1.75 inches on an

equivalent full-scale cask. This is only about 40% of the calculated deformation. It is reasonable to conclude that a significant part of the drop energy was absorbed in the secondary impact.

It would therefore not be valid to attempt a comparison to 125-B end drop results, as planned. However, a much more severe end drop, without impact limiters, was performed as the last test in the series (refer to Section 2.10.4.4.5 below for details). This test provided evidence that containment integrity of the 10/140MB is maintained for much worse conditions than the impact response predicted for the cask in Sections 2.6.7.1 and 2.7.1.1.

2.10.4.4.1.2 Flat Side Drop

For purposes of calculating impact limiter response during flat side drop (on the rounded sides of the impact limiters), the energy balance program SYDROP was utilized, along with a corresponding hand calculation. This calculation was performed with foam properties derived at ambient temperature (75°F). The method is identical to that used in Section 2.7.1.3 for foam at the maximum accident temperature condition (105°F). Both the major diameter (108 inches) and minor diameter (101 inches) portions of the impact limiter were accounted for, as well as the lid bolt lug 'pocket' embedded in the first 22 inches of the major diameter segment.

For analysis purposes, the impact limiter was separated into four segments. Each segment was evaluated separately, and the results were then combined to determine the overall impact limiter response. The analysis assumes that the minor diameter portion of the impact limiter does not become affected until the major diameter portion had already crushed 3.5 inches ((108 - 101)/2 = 3.5). In this manner, an energy equilibrium point could be calculated to determine the total crush depth and corresponding acceleration, accounting for the full effects of the entire impact limiter.

Results of the 30-foot flat side drop analysis for the composite impact limiter segments are presented in Section 2.10.4.6.3 of this Appendix. A total impact limiter deflection of 7.17 inches was predicted by SYDROP and the associated energy balance hand calculation. The resulting acceleration was

similiarly calculated to be 127.8 g's.

The side drop test, with impact on the rounded side, was performed to verify this result. The cask is shown in Figure 2.10.4-12, just before impact. The cask struck squarely, and the resulting impact limiter damage is shown in Figure 2.10.4-13 at the location marked 'A4 - B4' on the cask (damage on other surfaces of the impact limiters is due to previous drop tests).

The actual measured (plastic) deflection on the 10/140MB quarter-scale model was approximately one inch, or (4)(1.0) = 4.0 inches for a full-scale cask. This is 55% less than the total (plastic plus elastic) deformation predicted by SYDROP. For the 125-B quarter-scale test program, it was found that equivalent full-scale impact limiter permanent deflection was approximately 9.6 inches for nominal temperature conditions (70°F). SYDROP predicted a deflection of 15.92 inches (assuming a fully effective impact limiter at an operating temperature of 70°F). The actual (plastic) deformation value was thus about 66% less than that predicted by SYDROP for that cask. Integration of the cask acceleration indicated an actual total (plastic plus elastic) impact limiter deformation of about 14 inches, showing good correlation with the calculated value.

The corresponding acceleration calculated by SYDROP was 39.6 g's. The average measured value for the quarter-scale 125-B, factored appropriately for a full-size cask, was 44.2 g's.

It can thus be seen that, for the side drop event, SYDROP predictions are quite accurate for accelertions and somewhat underpredict permenant deformations. The same pattern for deflections was noted for the 10/140MB quarter-scale cask (actual plastic deformation approximately 55 - 66% less than calculated). It can therefore be concluded that the acceleration pattern will follow (reasonably good correlation between predicted and actual results). Because of the very conservative assumptions made regarding impact limiter geometry to maximize side drop loads in Sections 2.6.7.3 and 2.7.1.3, impact response accelerations predicted for the 10/140MB can therefore be assumed to be valid and corservative.

2.10.4.4.1.3 Corner Drop

A center of gravity over struck corner drop was performed on the rounded side of the impact limiter. For analytic purposes, a comparison was made to impact results from the same orientation, utilizing an 'average', cylindrical impact limiter with a diameter of 104.5 inches and a length of 35 inches, extending 13 inches beyond the end of the cask. See impact limiter geometry assumption case 4, reproduced in Figure 2.10.4-14, for details of this assumed configuration.

Unlike the previous two analyses, end and side drop, an exact correlation cannot be drawn between this case and test results, since the geometry assumptions made for the impact limiter do not reflect the actual configuration. However, it is instructive to compare results between predicted and actual impact limiter deflections, since the geometry assumption used in this case was the same as that used to derive comparisons between ambient temperature foam and foam at the extreme operating temperatures (see Section 2.10.4.4.2 below) for other oblique drops. The geometry assumptions used to derive final deflection values are illustrated below:

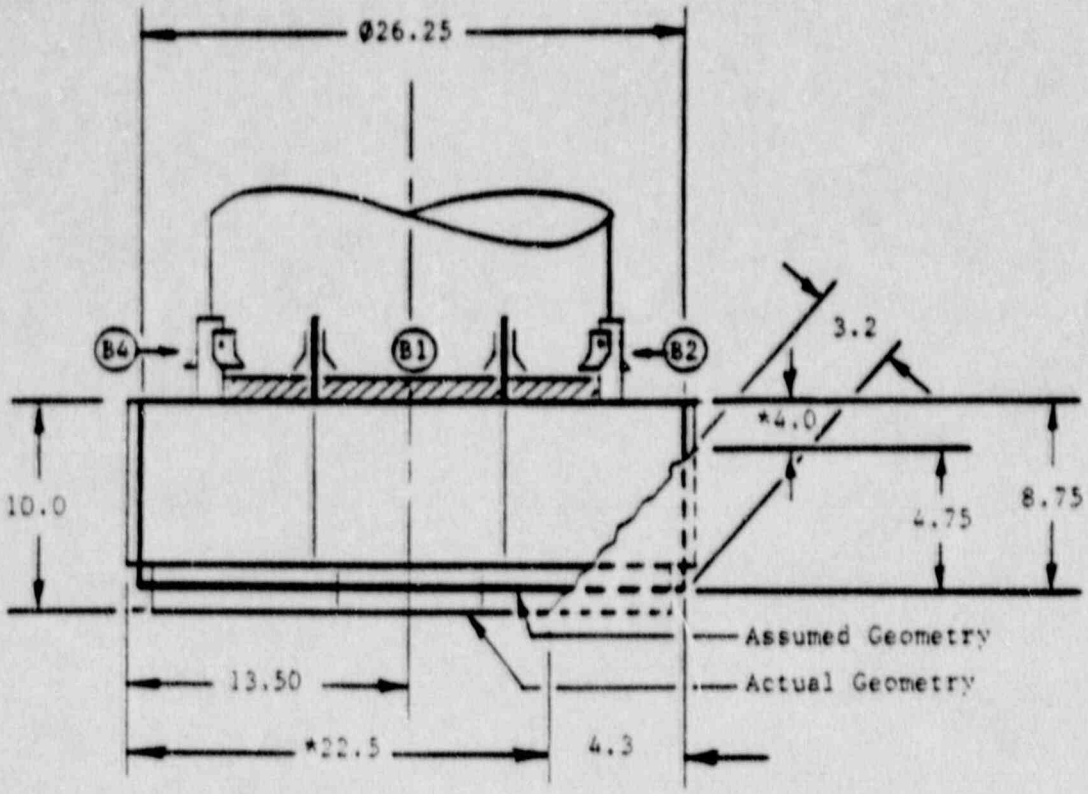

*Measured Dimension

The calculated maximum deflection for this geometry, at ambient temperature, for a 30 foot drop, was 17.4 inches. The corresponding impact load was 97.6 g's. A center of gravity over struck corner drop test was conducted to confirm this result. The cask impact is shown in Figure 2.10.4-15, and the resulting impact limiter damage is shown in Figure 2.10.4-16 and 2.10.4-17.

Test results showed an actual total diagonal deflection of (4)(3.3) = 13.2 inches, full scale, or approximately 76% of the calculated value. The total deformation includes both exterior crush of approximately 3.2 inches, as well as interior ('inside-out') crush of approximately 0.1 inch, as measured from a reference stripe located on the cask at the interface with each impact limiter. This measured deflection indicates that the impact limiter geometry

assumptions made in the analysis result in reasonably good correlation with actual impact deformations.

For purposes of comparison, the 125-B scale test for c.g. over struck corner (at the minimum service temperature of -20°F) induced a 20.0 inch full-scale permanent (plastic) crush depth, with an accompanying average acceleration of 24.7 g's. The value calculated by CYDROP for this impact orientation and temperature was 28.4 inches and approximately 30 g's. The actual (plastic) deflection was therefore about 70% of the predicted total (plastic plus elastic). The total measured (plastic plus elastic) deformation was about 24.9 inches, showing good correlation to the calculated value.

Since, for the 125-B impact limiter geometry, the induced deformation represents a significantly smaller percentage maximum foam strain than that for the 10/140MB (approximately 50% maximum foam strain for the 125-B, vs around 80% maximum strain for the 10/140MB), a direct comparison between impact loads obtained from the two tests would not be valid. However, the 97.6 g impact load predicted for the 10/140MB is conservative, due to the volume of foam neglected in the analysis. Also, it does not impose more critical loading on the cask than those already evaluated at other drop orientations.

2.10.4.4.2 Worst-Case Impact Loads

Since all 10/140MB quarter-scale drops were performed at ambient temperature conditions (approximately 75°F cask components), a method was developed to vary the drop height to conservatively approximate the effects of drops at other component temperatures. Refer to Section 2.10.4.6.2 for details of this method. Of particular interest was the response of the polyurethane foam impact limiters. The foam used exhibits a significant variation in strength characteristics over the range of temperatures anticipated for the 10/140MB arising from temperature conditions imposed at the start of the Hypothetical Accident Conditions drop tests.

At the minimum service temperature of -20°F, the foam is stiffer than would be the case at higher temperatures. Accordingly, the reaction forces arising from crushing of the foam during impact will be highest at reduced tempera-

tures. Cask body loads will accordingly be at their maximum values for this temperature condition.

In this regard, accident condition oblique impacts at near-vertical and near-horizontal impact orientations are of special interest. The former will tend to maximize lid and impact limiter separation forces, and the later will be critical for cask bending and secondary impact ('slapdown') response. Because of the unusual design of the 10/140MB impact limiters, it was not possible to use NuPac's proprietary drop programs, CYDROP and OBLIQUE to accurately evaluate impacts at oblique orientations. Conservative assumptions were made regarding impact limiter response in order to analytically impose maximum worst-case loading, and affected cask components were then evaluated accordingly.

One of the purposes of this test program was to verify that these assumptions are valid, and cask response to worst-case impacts will be no worse than predicted in the relevant analyses.

To simulate response of a cold-foam impact limiter with one at ambient temperature, a elevated drop height was calculated. Drops from this increased height would impose loadings equivalent to drops from 30 feet at the reduced service temperature. Refer to Section 2.10.4.6.2.1 for a background discussion of the method used.

In order to derive this equivalent drop height, conservative assumptions were made regarding impact limiter geometry for the purpose of rendering it into a form compatible with NuPac's energy balance drop programs. That is, a cylindrical impact limiter was assumed, with its diameter equal to the average of the maximum diameters of the major and minor portions of the actual impact limiter. This diameter was (108 + 101)/2 = 104.5 inches. To approximate the height of this assumed equivalent impact limiter, a point was chosen half-way between the end of the major portion of the impact limiter, and the end of the minor portion. This resulted in an overall height of 35 inches, with a 13 inch depth below the bottom of the cask, and a height 22 inches along the cask wall. This assumed geometry is the same as that described in Section 2.10.4.4.1.3 above.

2.10.4.4.2.1 Near-Vertical Oblique Drop

The assumed impact limiter described in the previous section was used in the CYDROP program with cold-foam mechanical properties, for a drop height of 30 feet, to develop force-deflection curves for near-vertical (85 degrees with respect to horizontal) impacts. These force-deflection characteristics were then utilized in the program OBLIQUE to determine cask body loads. A summary of results at the critical angle (85 degrees with respect to horizontal) is given below:

Drop Height (ft.)	Deflection (in.)	Maximum Force (lb.)	Acceleration (g's)
30	4.78	6129990	90.1

Next, the same impact limiter geometry was input with ambient temperature (75°F) foam properties, and CYDROP was again run. This time, drop heights were varied from 35 to 44 feet in one-foot increments, and force-deflection curves were again generated as inputs into OBLIQUE. Body forces were then evaluated at the various drop heights. The results of these analyses are summarized below:

Drop Height (ft.)	Deflection (in.)	Maximum Force (lb.)	Acceleration (g's)
35	7.31	5835298	85.8
36	7.44	5987913	88.1
37	7.56	6163606	90.6
38	7.69	6358876	93.5
39	7.81	6550789	96.3
40	7.93	6739526	99.1
41	8.05	6915621	101.7
42	8.16	7074633	104.0
43	8.28	7232078	106.4
44	8.39	7387586	108.6

From this table, it can be determined that the drop height required at ambient temperature to impart an acceleration equivalent to that of a reduced temperature 30 foot drop (90.1 g's) occurs between 36 and 37 feet for ambient temperature foam. By interpolation of these results at these two points, and equivalent drop height of 36.8 ft can be derived. The actual drop height used in the test was 37 ft.

During the actual near-vertical drop test, the cask impacted on one corner of the top impact limiter, rotated over onto the opposite corner, and then rebounded into the air. The cask made two complete revolutions in the air, then struck the original impact point at approximately the original drop angle. The cask again rolled over on the opposite corner and rebounded. A final impact occured on the bottom impact limiter, diagonally across from the primary impact location.

Cask impact is shown in Figure 2.10.4-18. The resulting primary impact damage is shown in Figure 2.10.4-19, while secondary and tertiary impact damage is shown in Figure 2.10.4-20. A total impact limiter deformation of 1.6 inches was measured. The total deformation includes both exterior crush of approximately 1.3 inches, as well as interior ('inside-out') crush of approximately 0.3 inch, as measured from a reference stripe located on the cask at the interface with each impact limiter. This is equivalent to (4)(1.6) = 6.4 inches total deformation. This corresponds reasonably well with the anticipated deformation of approximately 7.56 inches for ambient foam at a 37 foot drop height.

Exterior damage due to secondary and tertiary (after 2 complete rotations in the air) appear to be similiar in nature to that due to primary impact, though not as extensive. No inside-out type deformation was noted at secondary and tertiary impact locations. From this it may be concluded that the primary impact location on the impact limiter absorbed the majority of the drop kinetic energy.

After this drop test (the second in the full series), the upper impact limiter, lid and payload were removed, and a thorough inspection of the cask

exterior and interior was made. There were no indications of any damage to either the lid closure system, nor to the impact limiter retention system. It may thus be assumed that the analysis indicating no loss of closure or impact limiters is valid.

Measurements were made of the inside diameter of the inner (containment) shell. These measurements indicated a maximum diametral variation of only 0.009 inch, occuring at the upper (impacted) end of the cask inner shell. This provides a clear indication that buckling of the containment boundary will not be a factor for near-vertical impacts of the 10/140MB package. A much more severe loading was imposed when the cask was dropped from a height of 30 feet without impact limiters, and only minor local distortion of the inner shell occcured (refer to Section 2.10.4.4.5 below).

2.10.4.4.2.2 Near-Horizontal Oblique Drop

The same assumptions utilized in the previous section were applied to simulating maximum impact loading at a near-horizontal drop orientation. The cask was dropped from a height of 37 feet at ambient conditions to simulate a 30 foot drop at the minimum service temperature of -20°F. The cask impact is shown is Figure 2.10.4-21.

For the near-horizontal drop orientation, impact-induced deformations were imparted onto both impact limiters. See Figure 2.10.4-22 for primary and secondary impact damage. However, the deformation due to the secondary impact was significantly less than that imparted on the other impact limiter by the initial impact (see Figure 2.10.4-23). It can therefore be concluded that secondary impacts for the 10/140MB will be less severe than primary impacts. This is a reasonable conclusion for a package with a fairly low aspect ratio (approximately 1.0).

2.10.4.4.3 Worst-Case Impact Limiter Deformations

Since polyurethane foam exhibits its lowest strength at elevated temperatures, it is reasonable to assume to maximum impact limiter deformations will be imparted at the maximum service temperature. For the 10/140MB, the maximum

foam temperature expected prior to the start of the accident condition tests is 105°F. To simulate maximum deflections which might arise at this elevated temperature while using foam at an ambient condition, a method of increasing the drop height was developed. This method is very similiar to that used above for maximizing impact loading. Refer to Section 2.10.4.6.2.2 for details.

Anticipated worst-case drop orientations for potential cask 'bottoming-out' are a center of gravity over struck corner drop, and a flat side drop, with impact on the flattened sides of the impact limiter. These cases are evaluated with the programs CYDROP and SYDROP, respectively, for 105°F foam material properties. The same cask geometries were then run for ambient foam, with drop heights varying from 35 to 44 feet, in one-foot increments.

2.10.4.4.3.1 Center of Gravity over Struck Corner

For the center of gravity over struck corner analysis, the same average impact limiter geometry used in the previous oblique drop evaluations above was again utilized. The results of the CYDROP analysis for 105°F foam are presented below:

Drop Height (ft.)	Deflection (in.)	Maximum Force (lb.)	Acceleration (g's)
30	18.59	6754716	99.3

For the CYDROP analyses at ambient conditions (75°F) and various drop heights, the results are summarized below:

Drop Height (ft.)	Deflection (in.)	Maximum Force (lb.)	Acceleration (g's)
35	18.07	7906899	116.3
36	18.17	8145097	119.8
37	18.27	8379367	123.2
38	18.37	8621398	126.8
39	18.46	8855686	130.2
40	18.56	9097368	133.8
41	18.64	9327739	137.2
42	18.73	9558259	140.5
43	18.81	9788940	143.9
44	18.90	10019790	147.3

Interpolation of the ambient temperature data between 40 and 41 feet yields an equivalent drop height of 40.3 ft. A height of 40 feet was actually used in testing.

For purposes of comparison, a CYDROP analysis was also performed using foam properties at -20°F. The results are shown below:

Drop Height (ft.)	Deflection (in.)	Maximum Force (lb.)	Acceleration (g's)
30	15.49	5725768	84.2

It should be noted that, due to the greater deformation of the warm foam case, and resulting strain hardening effects, the impact acceleration is actually greater for warm foam at this impact orientation. In this case, this effect can be at least partially attributed to the conservatively small diameter and length assumed for the impact limiter.

For ambient drops from 40 feet, an impact acceleration of 133.8 g's is expected to develop. Since this is well in excess of the actual maximum anticipated load of 99.3 g's, the 40 foot ambient drop bounds loads as well as impact limiter deformations for this drop orientation.

The center of gravity over struck corner impact is shown in Figure 2.10.4-24. The resulting damage is shown in Figures 2.10.4-25 and 2.10.4-26. The actual impact deformation was measured as approximately 4.0 inches (3.65 inches exterior deformation and 0.35 inch inside-out type deformation). This corresponds to a full-scale total deformation of (4)(4.0) = 16.0 inches. This value compares well with the 18.56 inches of deformation predicted by CYDROP for the assumed impact limiter geometry at a temperature of 75°F and a drop height of 40 feet.

Since extremely conservative calculations in Section 2.7.1.2.1 show a minimum of 19.74 inches would be required to 'bottom out' the cask at this drop orientation, it may be safely assumed that sufficient impact limiter foam is available to absorb all of the worst-case drop energy. As additional assurance, there was no visual evidence of cask 'bottoming out' upon removal and inspection of the affected impact limiter.

2.10.4.4.3.2 Flat Side Drop

To derive an equivalent drop height for maximum deflection side drops (maximum foam temperature and impact on the flattened sides of the impact limiter), the same method used above was again applied.

For this drop case, an impact limiter geometry was assumed which had a major diameter of 105 inches and a minor diameter of 98.5 inches. These dimensions correspond to the average of the maximum diameters and the distances across the flattened areas of the major and minor diameter portions of the impact limiter. The geometry is illustrated in Figure 2.10.4-27. The strain-hardening effects of the bolt lug 'pocket' embedded in the impact limiters were conservatively ignored for maximum deflections.

The major and minor diameter portions were analysed separately, and the results were combined to derive total deflection and load resulting from impacts on the composite impact limiters. It should be noted that the minor diameter portion does not have any effect until the major diameter portion has deformed (105 - 98.5)/2 = 3.25 inches. The method of combining the major and

minor diameter results is similiar to that used in Section 2.10.4.6.3.

For impacts from a 30 ft drop height with elevated temperature foam, the combined impact limiter response is summarized below.

For the major diameter portion of the impact limiter:

Crush Depth	Impact Force	Strain Energy
9.00	5511751	21564251
9.25	5967591	22999169

For the minor diameter portion impact limiter:

Crush Depth	Impact Force	Strain Energy
5.75 (=9.00-3.25)	3625109	3227405
6.00 (=9.25-3.25)	3769362	3507787

Combining the components yields:

Crush Depth	Impact Force	Acceleration	Potential Energy	Strain Energy	Ratio (SE/PE)
9.00	9136860	134.4	25092000	24791656	0.99
9.25	9736953	143.2	25109000	26506956	1.06

The impact force and crush depth maybe found by interpolation from the combined data:

Crush Depth	Impact Force	Acceleration	Ratio
9.04	9222588	135.6	1.00

For comparison purposes, the response of a cold foam impact limiter may be derived in a similiar manner:

Crush Depth	Impact Force	Acceleration	Ratio
6.19	7685081	112.9	1.00

For ambient temperature foam, the following table has been derived:

Drop Height (ft.)	Deflection (in.)	Maximum Force (lb.)	Acceleration (g's)
35	8.59	7684505	112.9
36	8.69	7899793	116.3
37	8.79	8128961	119.8
38	8.90	8403946	123.4
39	8.99	8628934	127.0
40	9.08	8884691	130.9
41	9.17	9144294	134.8
42	9.26	9409365	138.7
43	9.35	9718178	142.9
44	9.43	9992680	147.2

Interpolation of these values results in an equivalent drop height of 39.6 ft. For test purposes, a height of 40 feet was used. Note that the resulting 130.9 g-load is conservatively in excess of the maximum which would be expected at either of the temperature extremes.

The drop test on the flattened sides of the impact limiters from a height of 40 feet indicated that the side of the impact limiter crushed to within approximately 3/8 inch of the impact limiter attachment lug. Elastic rebound of the foam moved the lug somewhat further away from the impact limiter side, but the location of the actual maximum lug deflection is clearly marked by the lug imprint in the impact limiter wall. Refer to Figure 2.10.4-28 for this damage detail. The 3/8 inch residual clearance is equivalent to (4)(3/8) = 1-1/2 inches. This compares favorably with the 2.33 inches residual clearance derived in Section 2.7.1.3.1. General damage arising from the impact is shown is Figures 2.10.4-29 and 2.10.4-30.

Since the impact limiter lug extends out from the cask outer shell the same distance as the lid bolt lug, the residual clearance measured provides proof that none of the cask appurtenances will 'bottom out' under a worst-case side drop impact.

2.10.4.4.4 Pin Punch

2.10.4.4.4.1 Flat Side Pin Impact

Impact of the puncture pin on the side of the cask produced only minor local damage of the cask outer shell at the point of impact. Some shear deformation was induced by the face of the puncture pin, and more general bending around the area of the pin impact was produced. The outer shell remained intact, and not loss of shielding capability due to lead melt would be anticipated during the accident fire transient event. The impact is shown Figure 2.10.4-31. The resulting damage to the outer shell is shown in Figures 2.10.4-32 and 2.10.4-33.

2.10.4.4.4.2 Flat End Pin Impact

The pin punch on the inside diameter of the primary lid produced no measurable deformation in the lid, except for minor local surface embossing by the puncture pin at the point of impact. Since the actual cask lid is reinforced at the inside diameter, and is consequently much stronger than the test version, it may be logically assumed that pin puncture will have no adverse effect on the containment capablity of the 10/140MB cask. The impact is shown in Figure 2.10.4-34. The resulting damage to the lid is shown in Figures 2.10.4-35 through 2.10.4-37.

2.10.4.4.4.3 Oblique Pin Impact

The pin punch at the bolt lug location resulted in a very little foam tear-out. A much greater loss of foam was conservatively assumed for in the thermal analysis for the accident fire condition (Section 3.5.1.1), and the resulting temperatures are shown to have no detrimental effect on the ability

of the package to maintain sealing or shielding integrity. The impact is shown in Figure 2.10.4-38, and the resulting damage is shown in Figures 2.10.4-39 through 2.10.4-41.

No significant effect of pin impact on the bolt lug itself was detectable. The pin impacted directly on the closure nut (Figure 2.10.4-42), leaving a matching indentation in the face of the pin (Figure 2.10.4-43). No detrimental effect was observed upon disassembly and removal of the impacted nut.

From the above tests, it can thus the pin puncture event will have no detrimental effect on the ability of the 10/140MB to survive the accident condition tests.

2.10.4.4.5 Lead Slump

The final test performed was not part of any regulatory requirements, but was done to conservatively verify assumptions made in the end drop analyses regarding the response of the lead shielding to axial impulse loading. The test was a bottom-down drop without impact limiters or payload. This test was conducted in order to determine, under worst possible conditions, how the lead shielding behaves under axial loading.

In the test, the cask did not strike the drop pad squarely. It struck slightly off-vertical, impacted on one edge, rotated over onto the opposite edge, and then rebounded into the air. The cask made one complete revolution in the air, and then struck again on the original impact point at approximately the original impact angle. It may thus be concluded that most of the drop energy was absorbed in local deformation at one location on the cask. The cask was then sliced through this point of maximum deformation in order to observe the lead slump pattern.

The cask impact is shown in Figure 2.10.4-44. The resulting damage is shown in Figures 2.10.4-45 through 2.10.4-47. Figures 2.10.4-48 through 2.10.4-40 show the cut-away section of the cask after the bare drop. Figure 2.10.4-49 is the point of primary impact, while Figure 2.10.4-50 is the point of the secondary impact, on the opposite edge.

Assumptions regarding lead response to this type of loading, characteristic of end drop impacts, have taken into account features inherent in the design of modern lead-lined transport casks. The important design considerations are two:

1. The 10/140MB has relatively thick outer and inner shells, containing a relatively thin layer of lead in between. It is therefore logical to assume that the shells will posses at least some capability of supporting the lead column as it deforms under axial loading and spreads outward, exerting radial pressure on both shells. It naturally follows, then, that the lead pressure acting on the relatively stiff shells will exert some frictional force as it tends to collapse axially, such that the shells will provide some support of the lead in friction.

2. The shield walls of the 10/140 are stiffly supported at each end. At the interface with the primary lid(s), the inner and outer shells are connected by a thick plate. At the interface with the bottom plate on the fixed-bottom version of the cask, the shells are securely welded in place. This fixity of the ends of the inner and outer shells is additional assurance against gross discontinuity effects observed in older and now-obsolete cask designs.

This combination of stiffness and end fixity are important features of the 10/140MB design, and they have considerable influence on lead response to axial loading. As the cutaway section of the cask clearly shows, there was no gross axial deformation of the lead shielding, even under the extreme conditions imposed under a 30 foot bare drop. This finding is in accordance with assumptions made in the Flat End Drop analysis sections of this Safety Analysis Report. These findings are further confirmed by the ANSYS finite element analysis, which predicts maximum stresses at those points where maximum shell deformation has occured. This localized effect is the response that would be expected from a lead column uniformly supported along its length by the shells.

2.10.4.4.6 Discussion of Anomolies

It was observed during the inital cask disassembly following the second drop test that the closure bolts had loosened during the testing, causing the bolts to lose their preload. The bolts had not been lubricated prior to installation, and it was felt that this loss of preload was due to frictional resistance during bolt torquing, which prevented the full torsional force from being translated into axial bolt load. Upon impact, the frictional resistance was released momentarily, causing the bolt to release the torsional component of its preload.

Since surface finish was not scaled on the quarter-scale cask, it is felt that this effect will not be a concern on the full-size casks. To validate this theory, the bolt torquing method for the second series of tests was modified. The bolts were overtorqued to compensate for non-scaleable frictional effects, and then backed off to their actual torque values. This method improved the performance of the bolts, which were checked after each subsequent drop test. While there was some detectable loss of preload in some instances, complete unloading of a bolt occurred only five times in the remaining ten accident condition free drop tests. In no case did more than two bolts ever completely lose preload during any single drop (bolts were retorqued to the stipulated value after each test).

For the second cask reassembly prior to the final drop test (flat end drop of a bare cask), the bolts were also lubricated before being installed in the manner described above. In this case, even the extremely severe impact failed to unload any of the bolts.

Consequently, instructions to lubricate all closure bolts have been inserted into the Operating Procedures (Chapter 7.0). This measure, combined with significantly less frictional effect between surfaces of the full-scale cask, will tend to ensure full bolt preload will always be maintained.

It should be noted that this loss of preload phenomenon has been observed during development tests on other scaled casks. Non-scalable surface finish is felt to have contributed to the same situation in these instances.

A second anomoly involved the retaining pins for the impact limiters. The analyses in Section 2.7.1.2.6 demonstrate that the retaining pins will restrain the impact limiter under worst-case separation loads. These loads occur during oblique impacts at a location opposite the impact point. These calculations were bourne out by the tests described above.

However, shearing of some pins was observed at the impact locations for some oblique drops. The cause of this pin failure was determined to be the inside-out type punch loading, whereby the cask would deform the interior of the impact limiter at the impact location. The resulting relative deflection between cask and impact limiter would sometimes cause adjacent impact limiter pins to shear.

In order to preclude this type of failure on the full scale casks, the interior shell thickness (adjacent to the cask) has been increased from 0.120 inch to 0.25 inch. This will have no effect on impact response of the impact limiters, since none of the thicker skin areas are ever affected by exterior impact loading.

In any case, it is clear from the test results that no loss of impact limiters ever occurred, even under the worst-case impact loadings imposed.

2.10.4.5 Conclusions

The comprehensive test program documented by this Appendix indicates that the NuPac 10/140MB is capable of performing satisfactorily under the most rigorous of regulatory requirements. Additional confirmation has also been given regarding the validity of the analysis techniques used to qualify the cask.

Specifically, no loss of containment will occur, either through lid or closure system failure, or through buckling of the containment shell. The impact limiter design will successfully prevent excessive loading on the package under the full range of service conditions, and the impact limiters will remain attached to the cask. No degradation of shielding capability will take place under the Hypothetical Accident Conditions tests.

2.10.4.6 Discussion of Impact Limiter Foam Response - Theoretical vs Empirical

THIS INFORMATION IS PROPRIETARY

FIGURE 2.10.4-1

Test Cask Fab Assembly Drawing

NOTES: UNLESS OTHERWISE SPECIFIED

[illegible] INTERPRET DRAWING PER ANSI Y14.5

[illegible] FABRICATE IN ACCORDANCE WITH NUPAC SPECIFICATION PS-[illegible]

3. GENERAL ARRANGEMENT DRAWING DEPICTS BASIC DIMENSIONS QUALITY REQUIREMENTS AND GENERAL CONFIGURATION ONLY, AND IS TO BE USED IN CONJUNCTION WITH CONTRACT SPECIFICATIONS

4. EQUIVALENT COMPONENTS AND/OR SOURCES OF SUPPLY MAY BE SUBSTITUTED UPON APPROVAL OF NUPAC ENGINEERING

5. MATCHDRILL IMPACT LIMITERS (ITEMS 1 & 2) TIEDOWN LUGS # 3/4 (8 PLACES) USING THE CASK (ITEM 3) TIEDOWN GUIDE PLATES AS TEMPLATES

8912130040-08

	Item	Part No.	Description	
	4	3238AA034	BALL LOCK PIN #1/4"	MAMASTER CARR
	3	X-102-118-A	CASK	
	2	X-102-117-A	LOWER IMPACT LIMITER	
	1	X-102-116-A	UPPER IMPACT LIMITER	
	A		10-160B / TOP ASSEMBLY	
	ITEM	PART NO.	DESCRIPTION	
	ASSEMBLY & DASH NO.		LIST OF MATERIAL	

NUCLEAR PACKAGING

TOP ASSEMBLY
SHIPPING CASK
10-160B (1/4 SCALE)

SCALE NONE
SIZE D
DWG NO. X-102-115

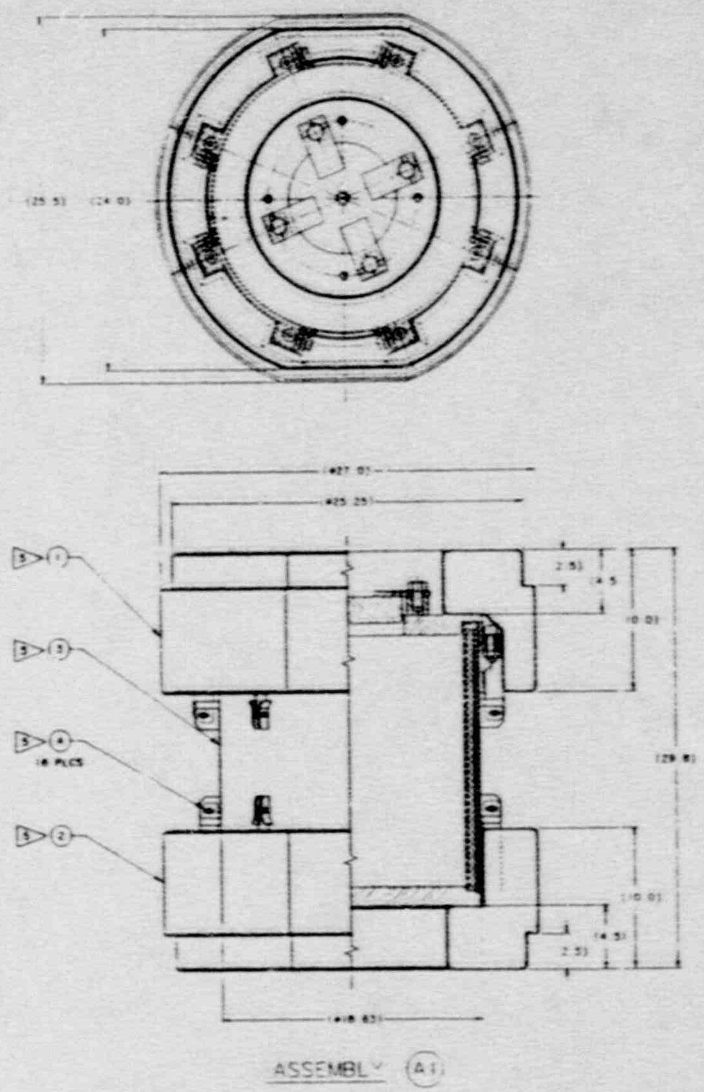

APERTURE CARD

Also available on Aperture Card

8915130040-09

NUCLEAR PACKAGING

TOP ASSEMBLY
SHIPPING CASK
10/140B (1:4 SCALE)

D X-102-115

FIGURE 2.10.4-2

Assembled Cask

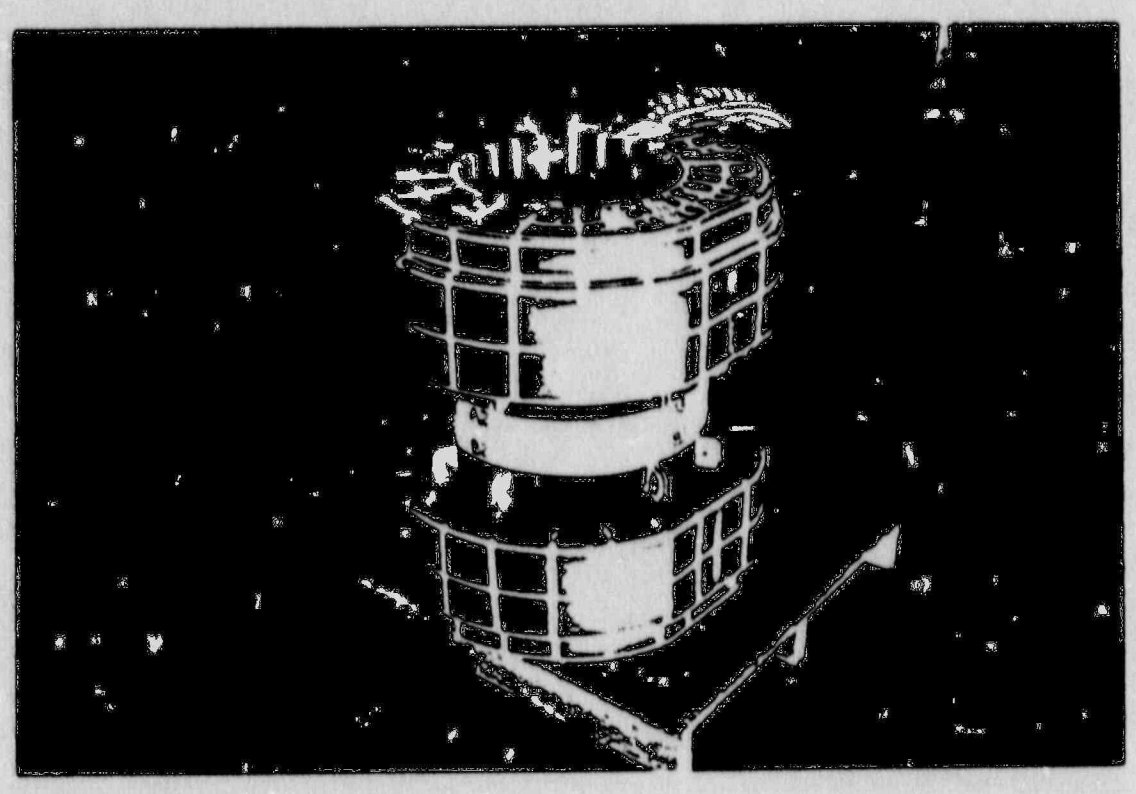

FIGURE 2.10.4-3

Upper Impact Limiter - Outer Surface

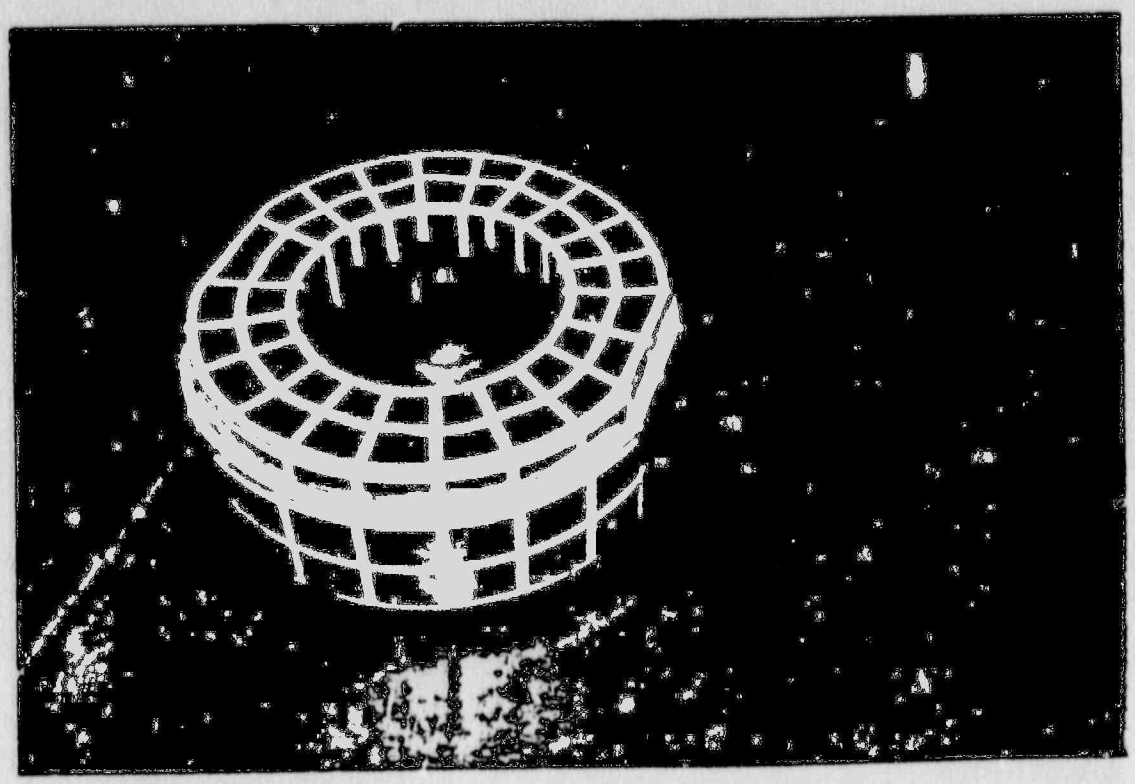

FIGURE 2.10.4-4

Upper Impact Limiter - Inner Surface

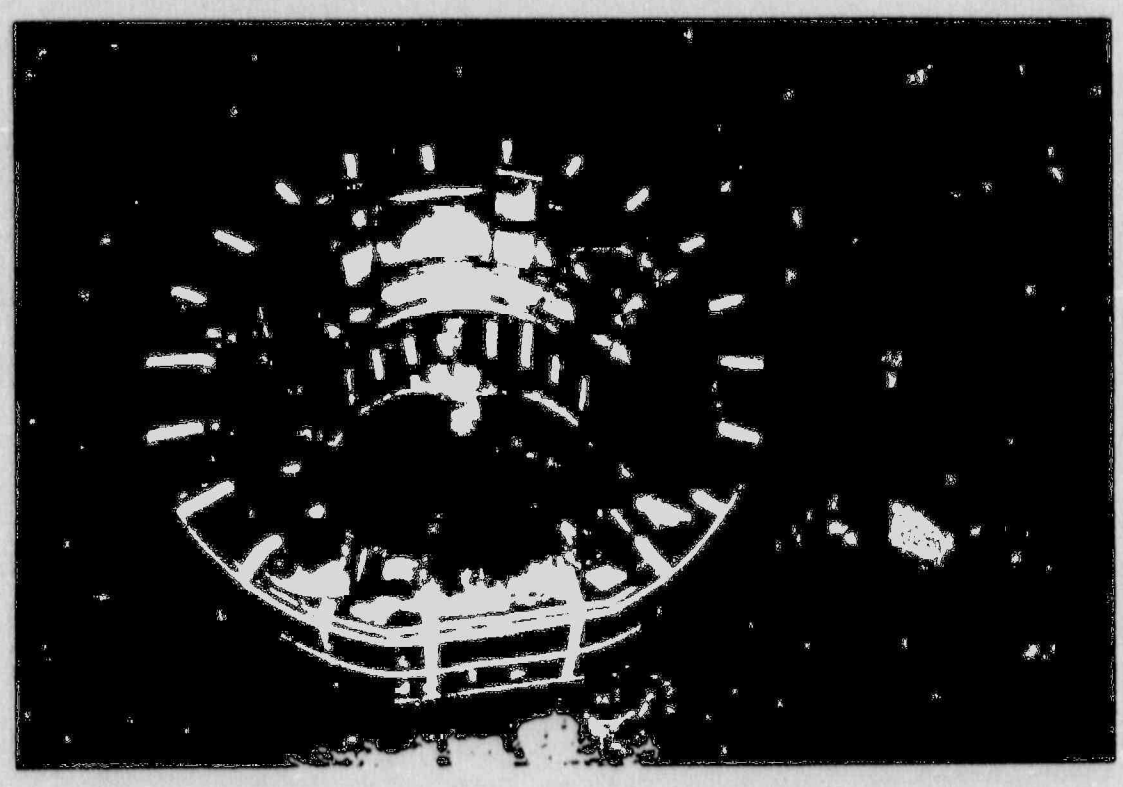

FIGURE 2.10.4-5

Lower Impact Limiter - Outer Surface

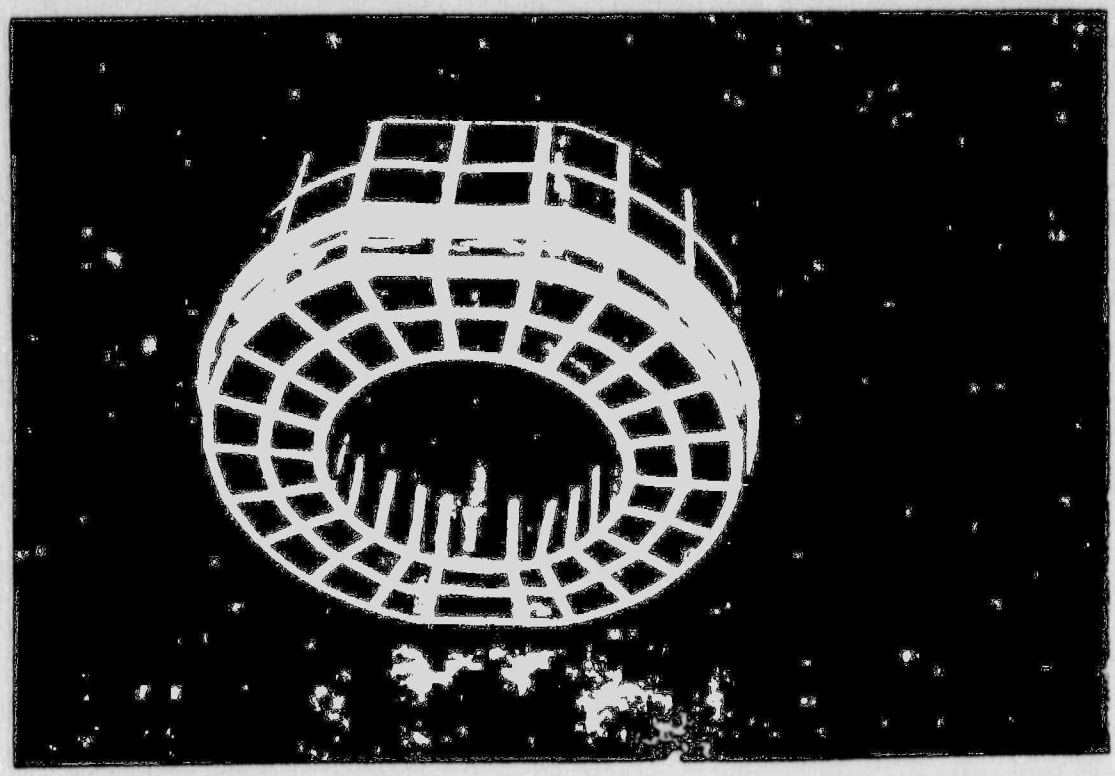

FIGURE 2.10.4-6

Lower Impact Limiter - Inner Surface

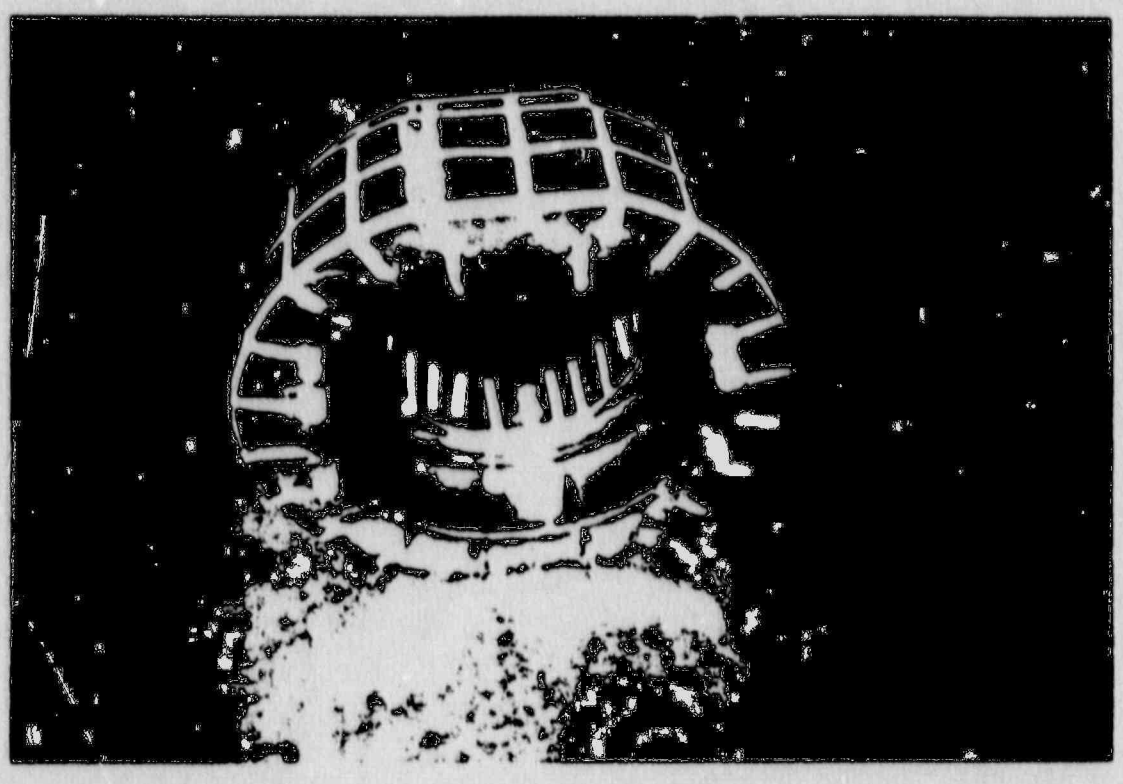

FIGURE 2.10.4-7

Test Cask with Reference Stripes

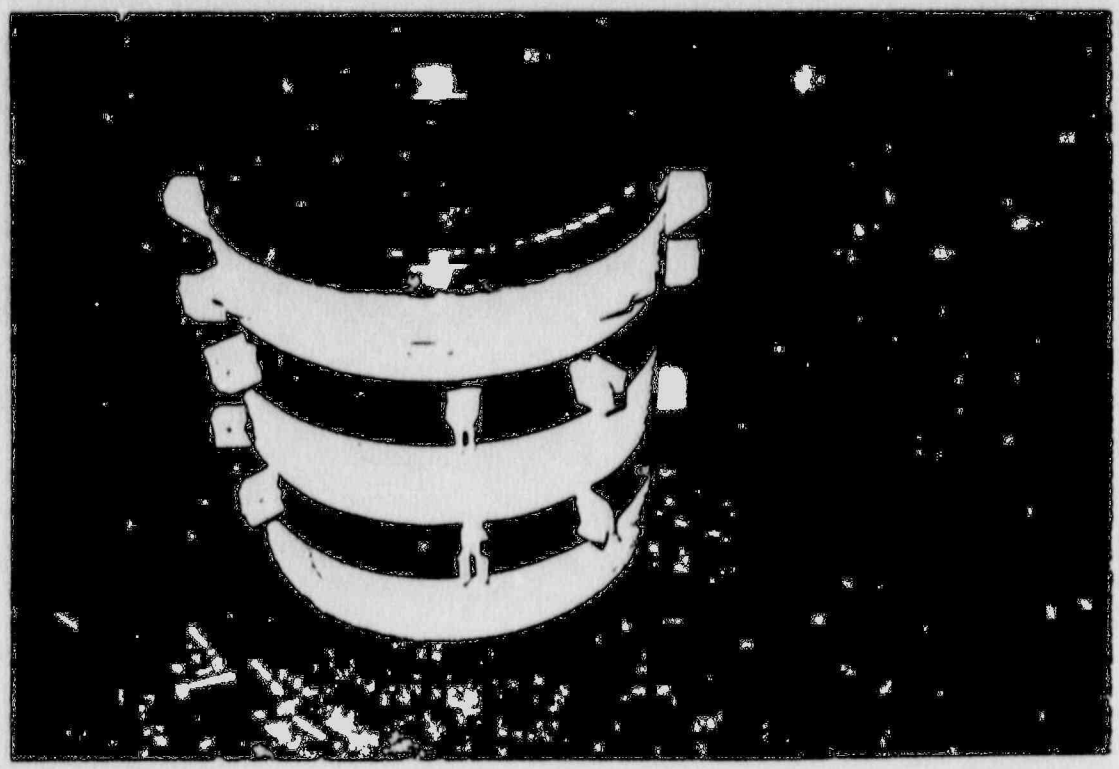

FIGURE 2.10.4-8
Test Cask Lid Assembly

FIGURE 2.10.4-9
Lid Installation

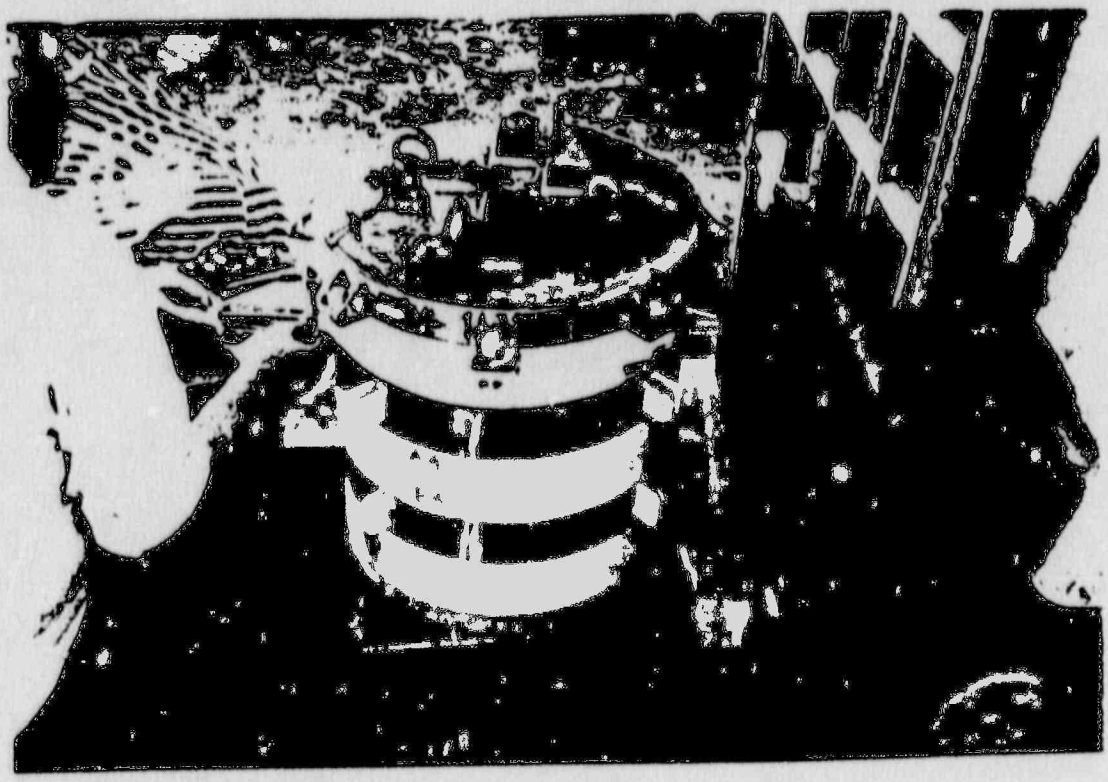

FIGURE 2.10.4-10

Test Package Being Assembled

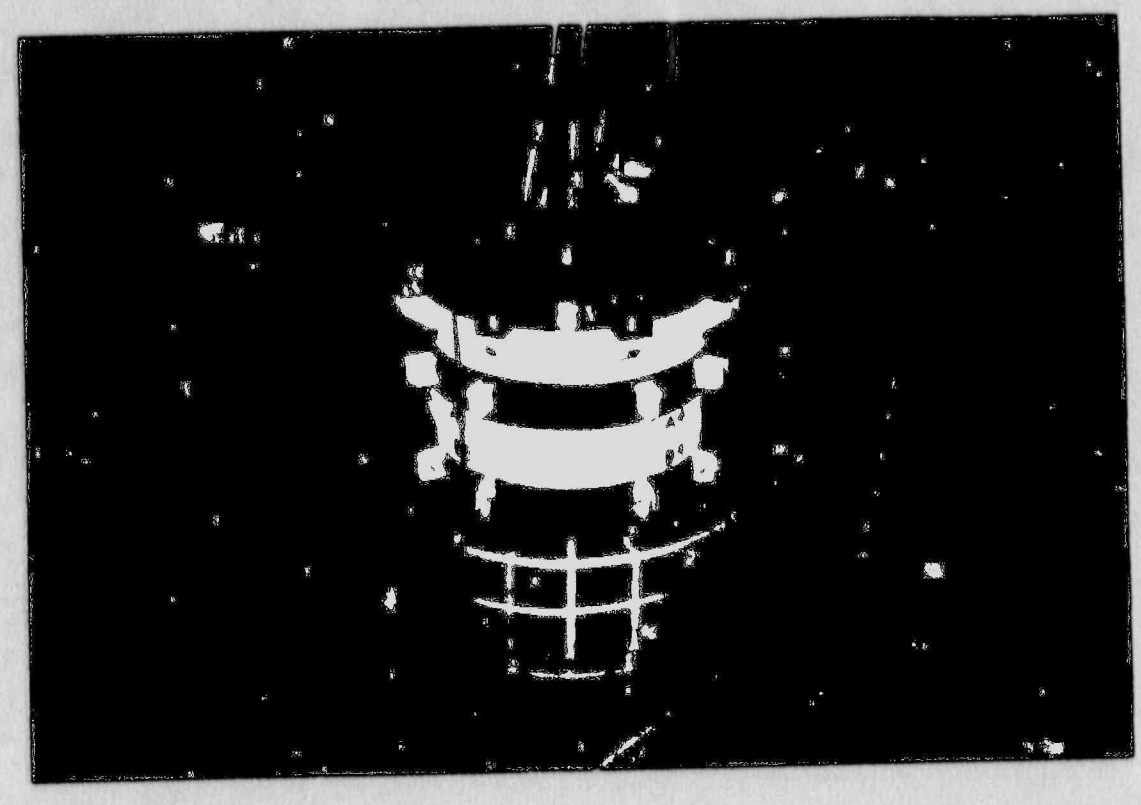

FIGURE 2.10.4-11

End Drop - Damaged Area of Impact Limiter

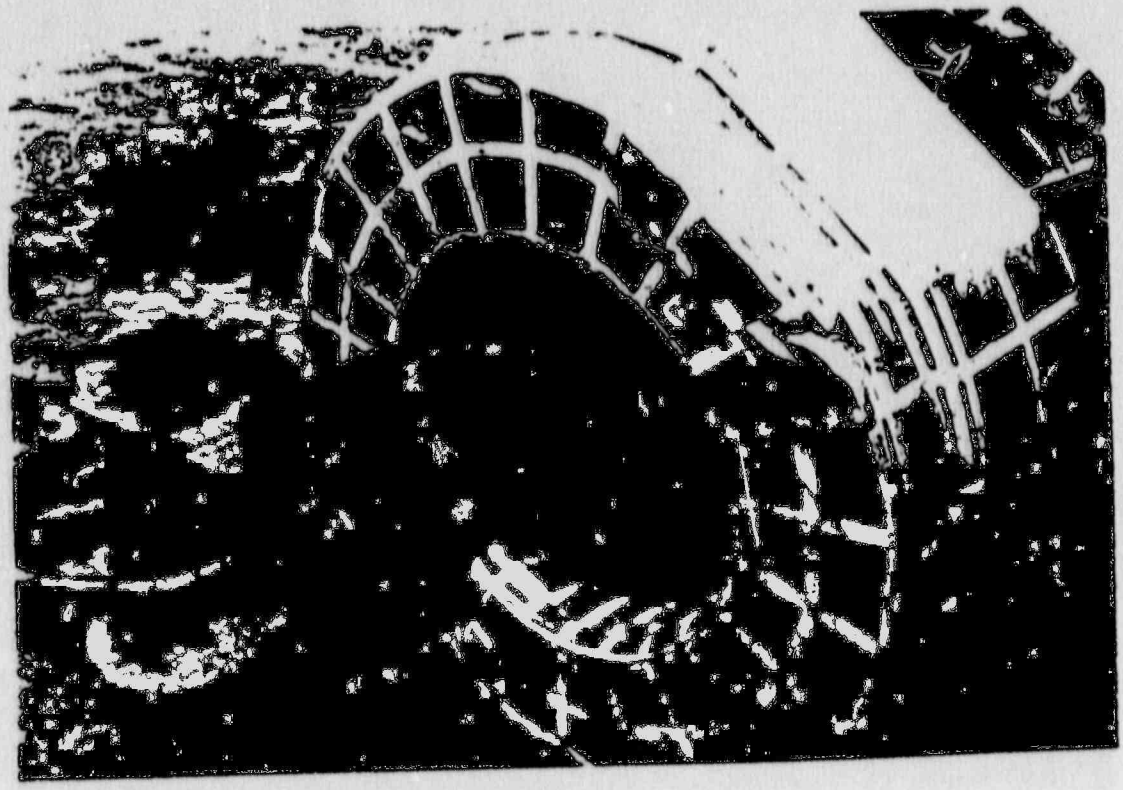

FIGURE 2.10.4-12

Flat Side Drop - Just Before Impact

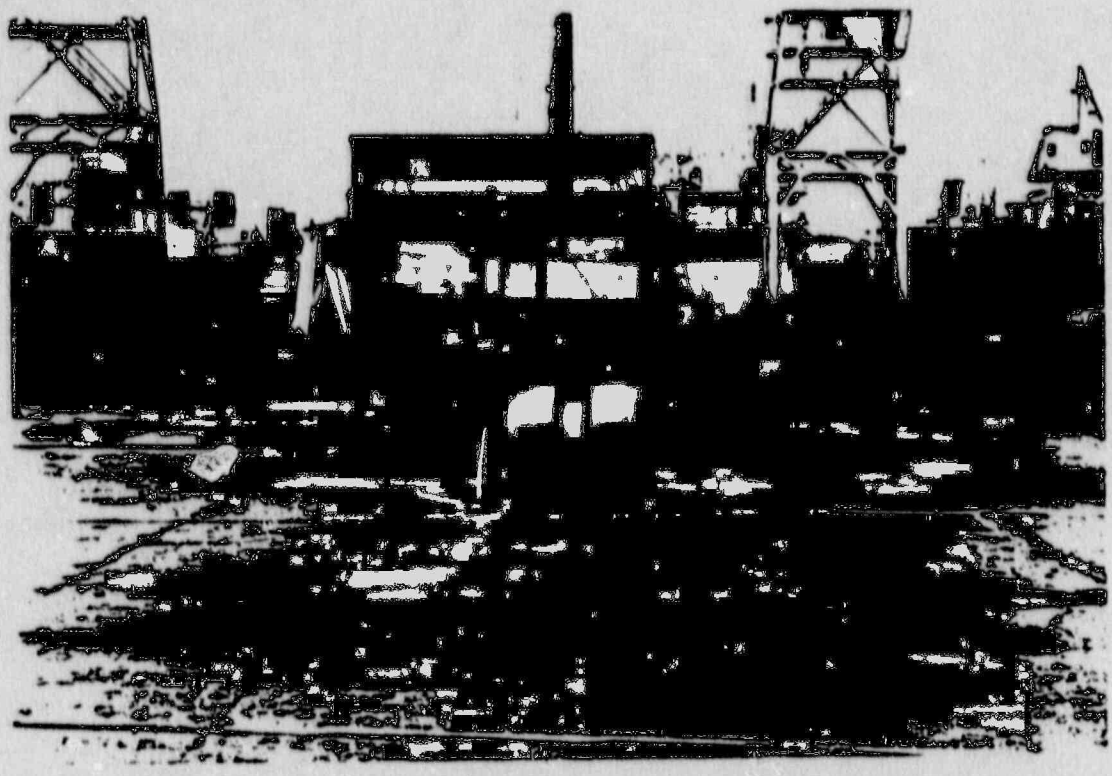

FIGURE 2.10.4-13

Flat Side Drop Impact Damage

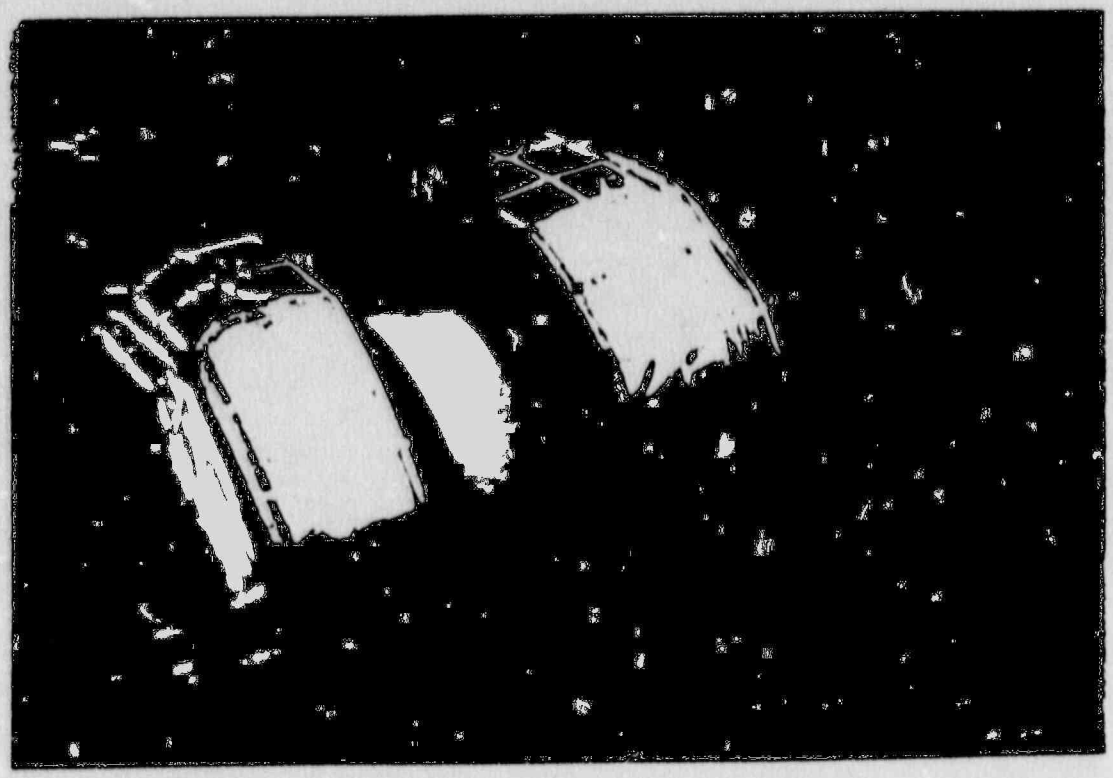

FIGURE 2.10.4-12

Flat Side Drop - Just Before Impact

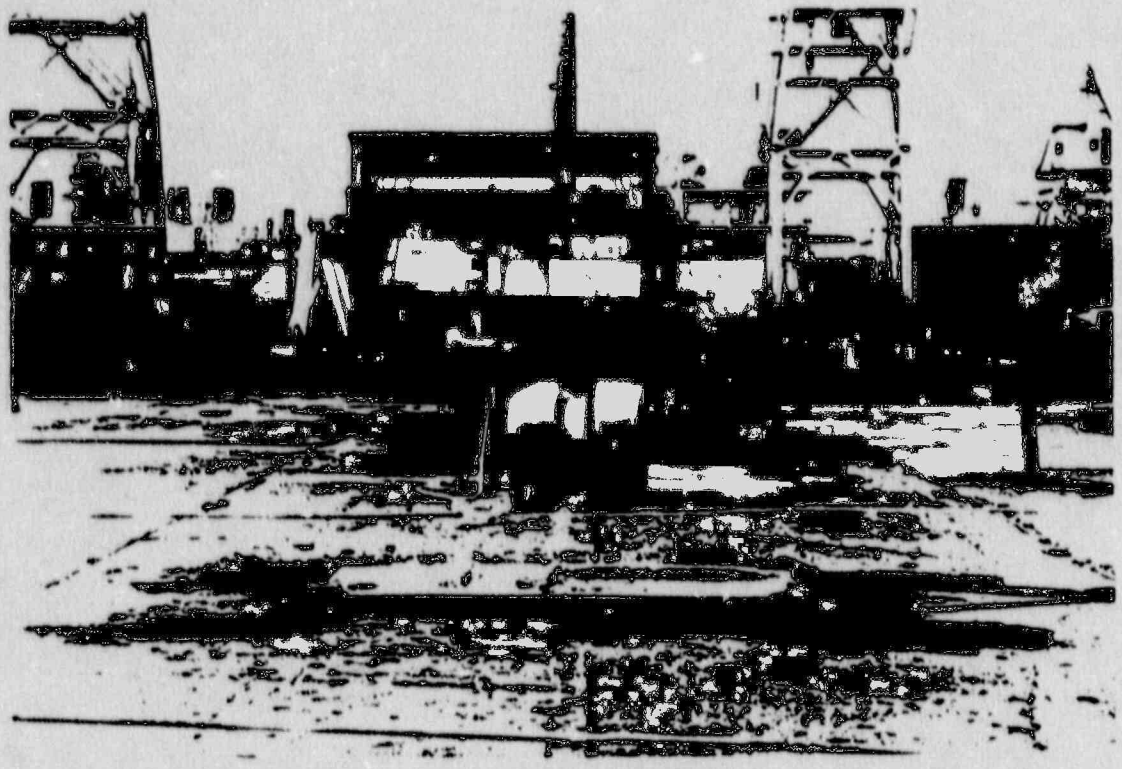

FIGURE 2.10.4-13

Flat Side Drop Impact Damage

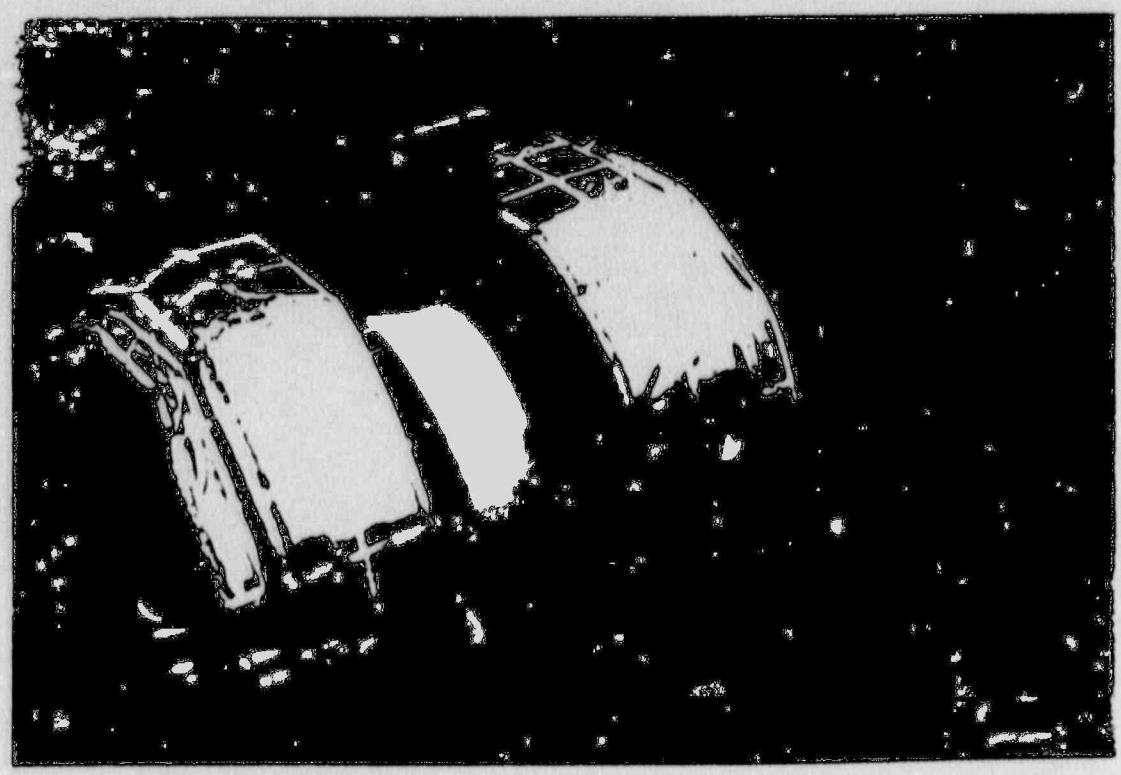

FIGURE 2.10.4-14

Impact Limiter Geometry Assumed for Oblique Drops

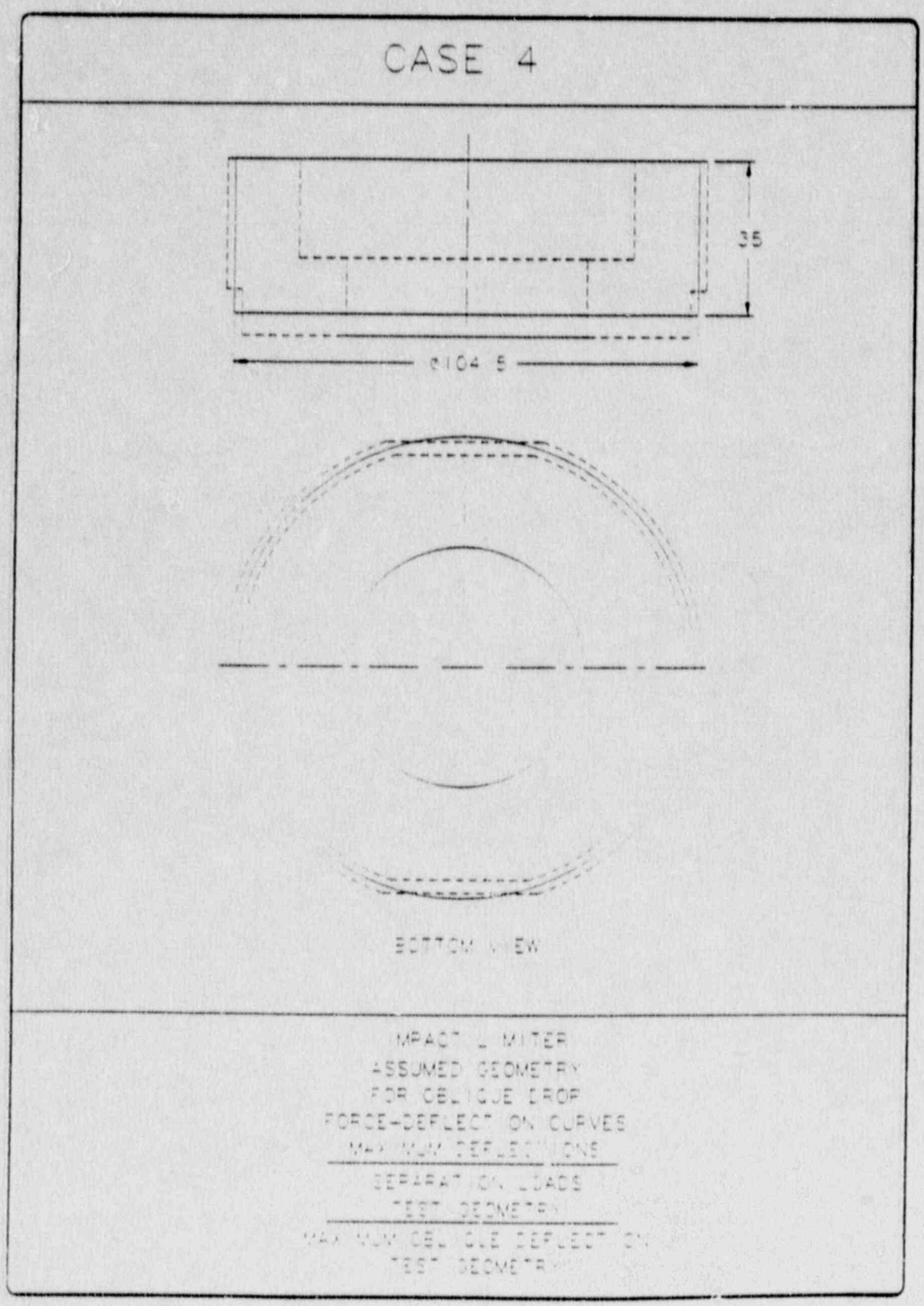

FIGURE 2.10.4-15

Center of Gravity Over Struck Corner Impact

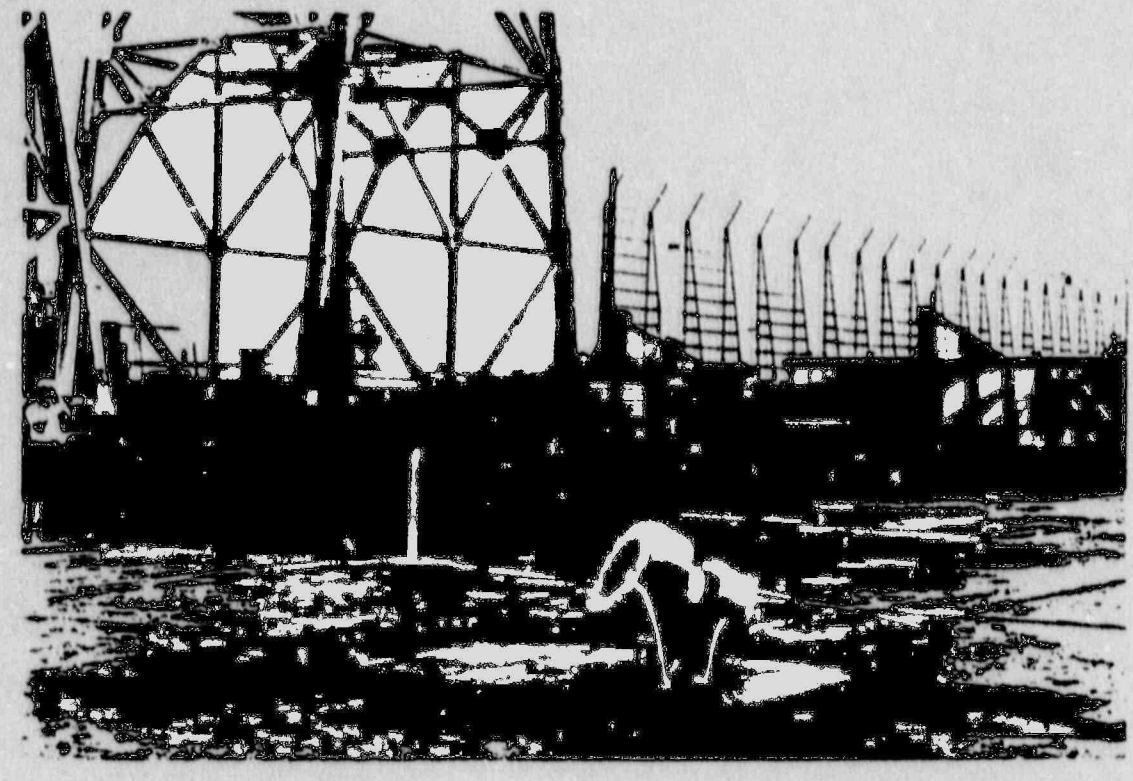

FIGURE 2.10.4-16

Center of Gravity Over Struck Corner—Damaged Area of Impact Limiter

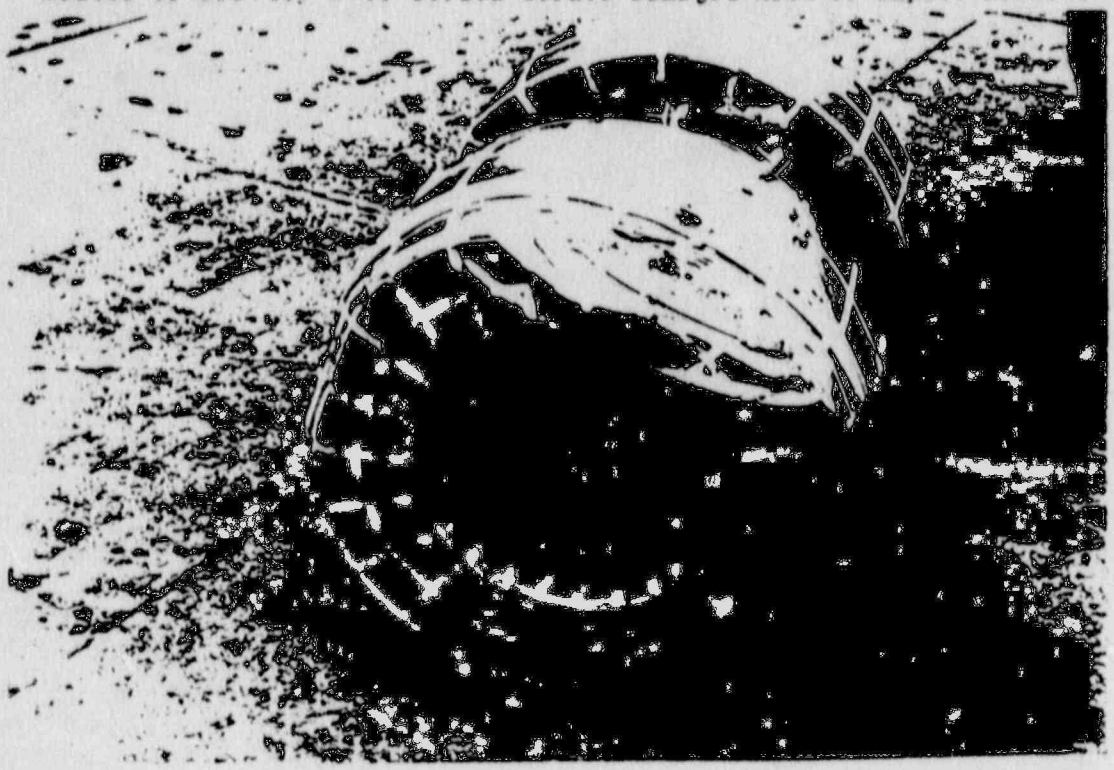

FIGURE 2.10.4-17

Center of Gravity Over Struck Corner-Damaged Area of Impact Limiter

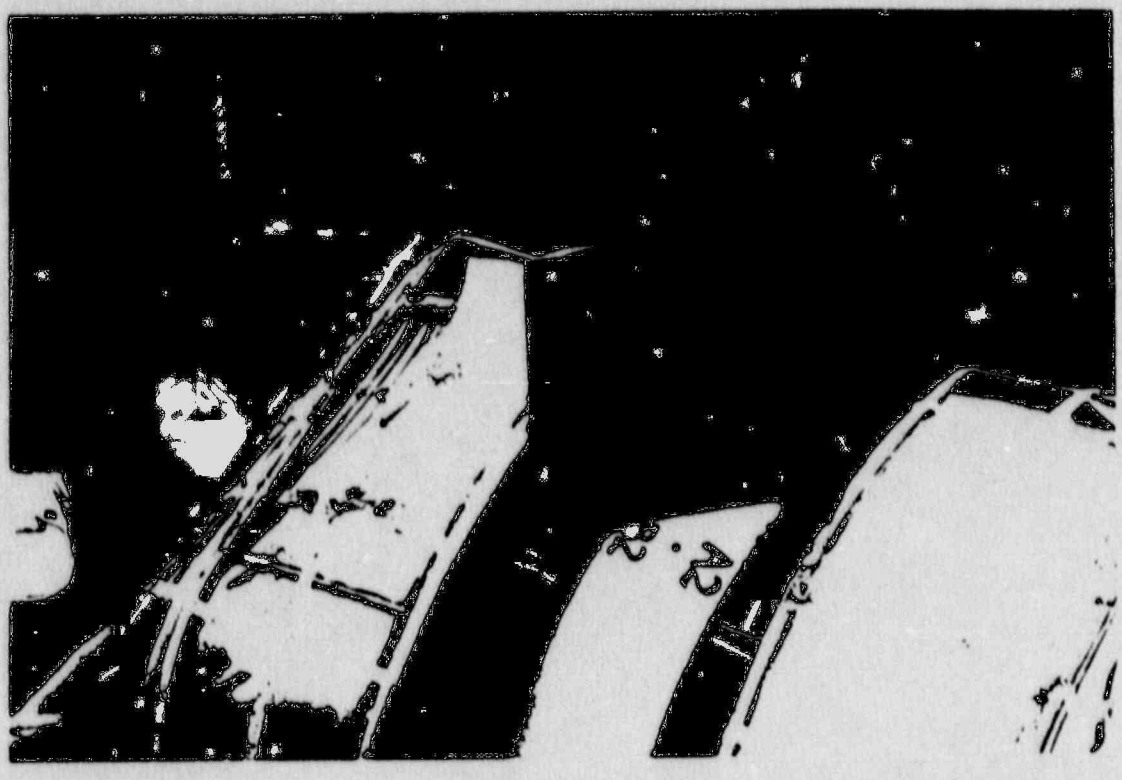

FIGURE 2.10.4-18

Near Vertical Oblique Drop Impact

FIGURE 2.10.4-19

Near Vertical Oblique Drop - Primary Impact Damage

FIGURE 2.10.4-20

Near Vertical Oblique Drop Impact - Secondary (Right Side) and Tertiary (Left Side) Impact Damage

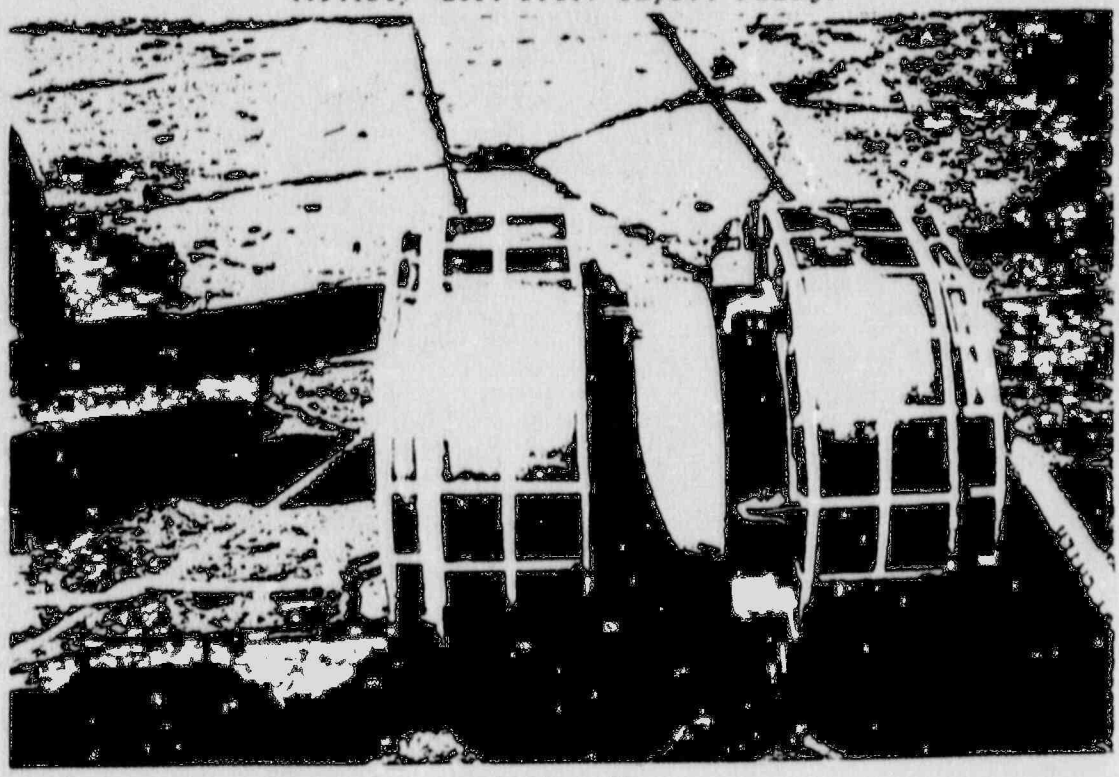

FIGURE 2.10.4-21

Near Horizontal Oblique Drop Impact

FIGURE 2.10.4-22

Near Horizontal Oblique Drop Impact - Primary (Foreground) and Secondary (Background) Impact Damage

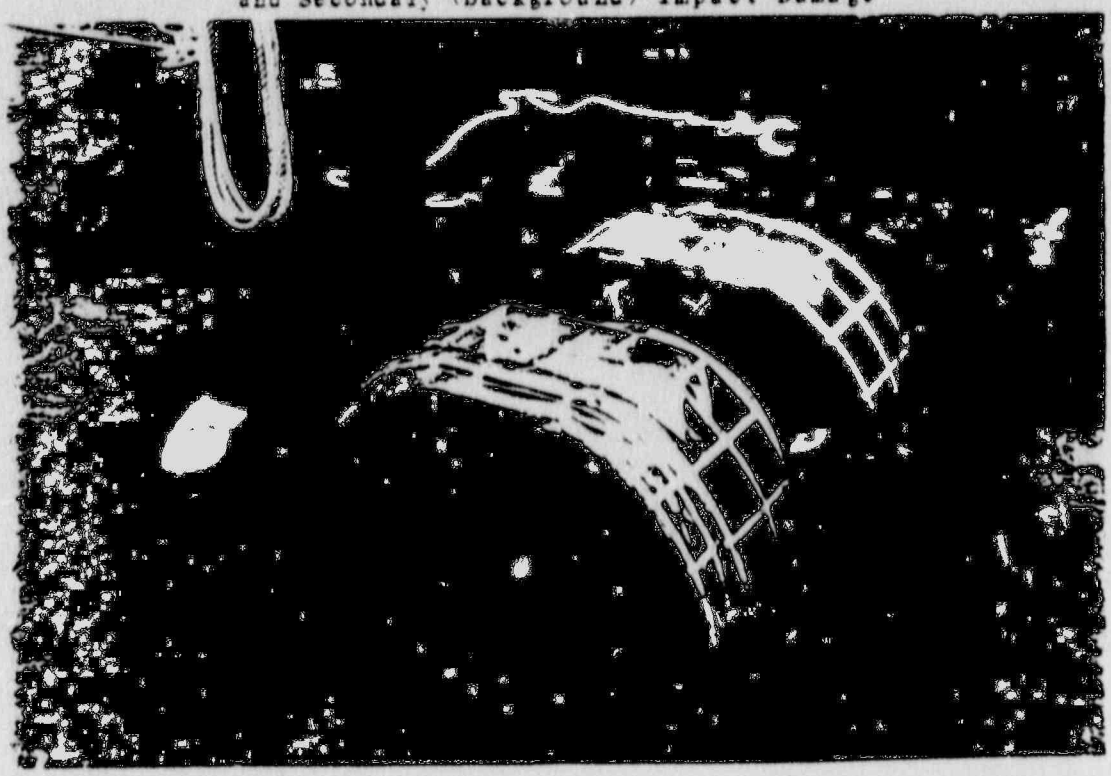

FIGURE 2.10.4-23

Near Horizontal Oblique Drop Primary Impact Damage

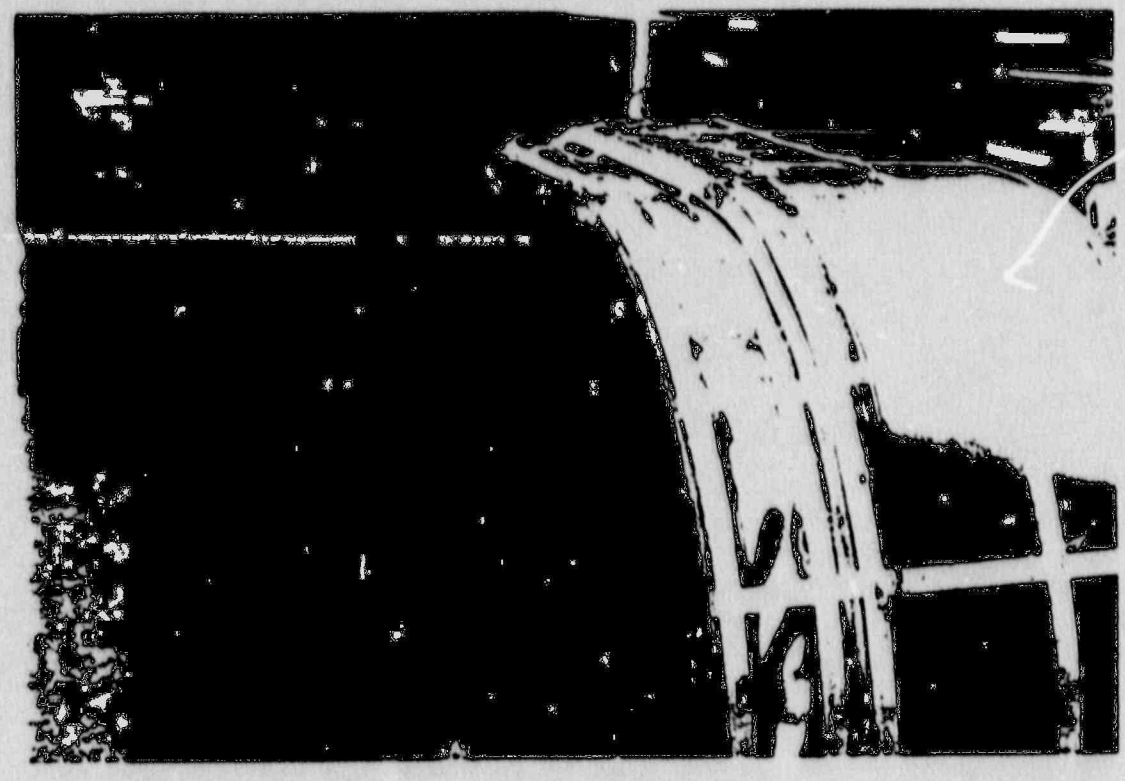

FIGURE 2.10.4-24

Center of Gravity Over Struck Corner Impact

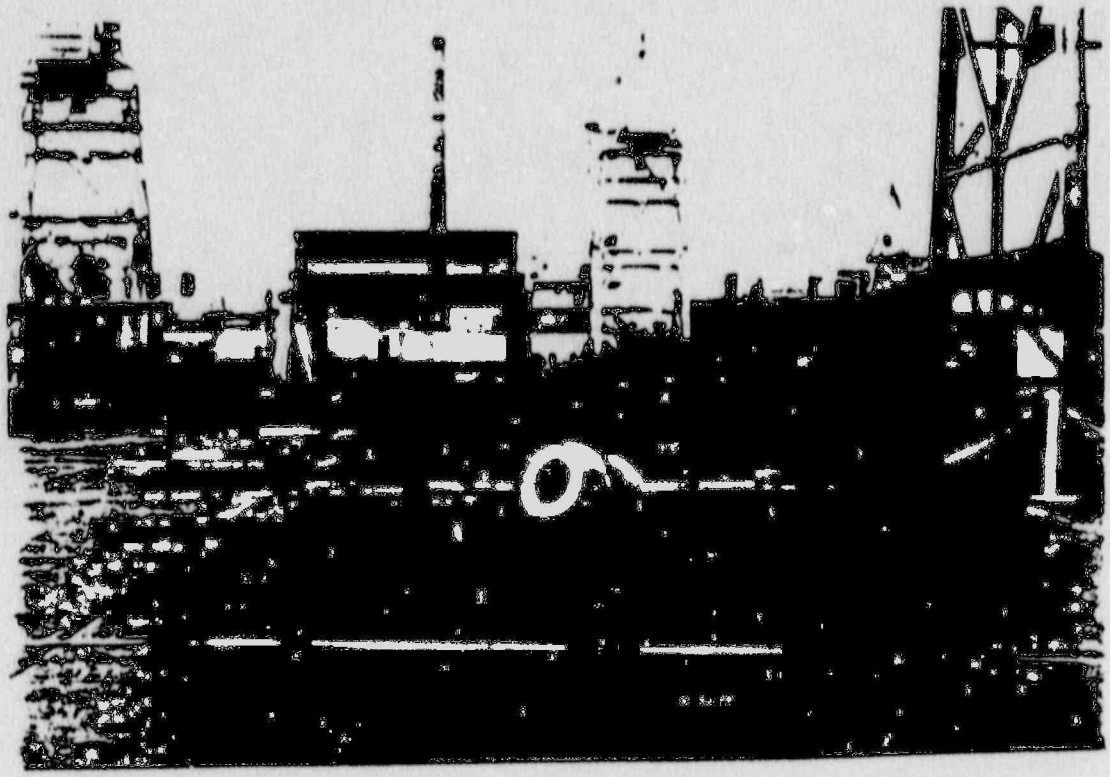

FIGURE 2.10.4-25

Center of Gravity Over Struck Corner Impact - Impact Limiter Damage

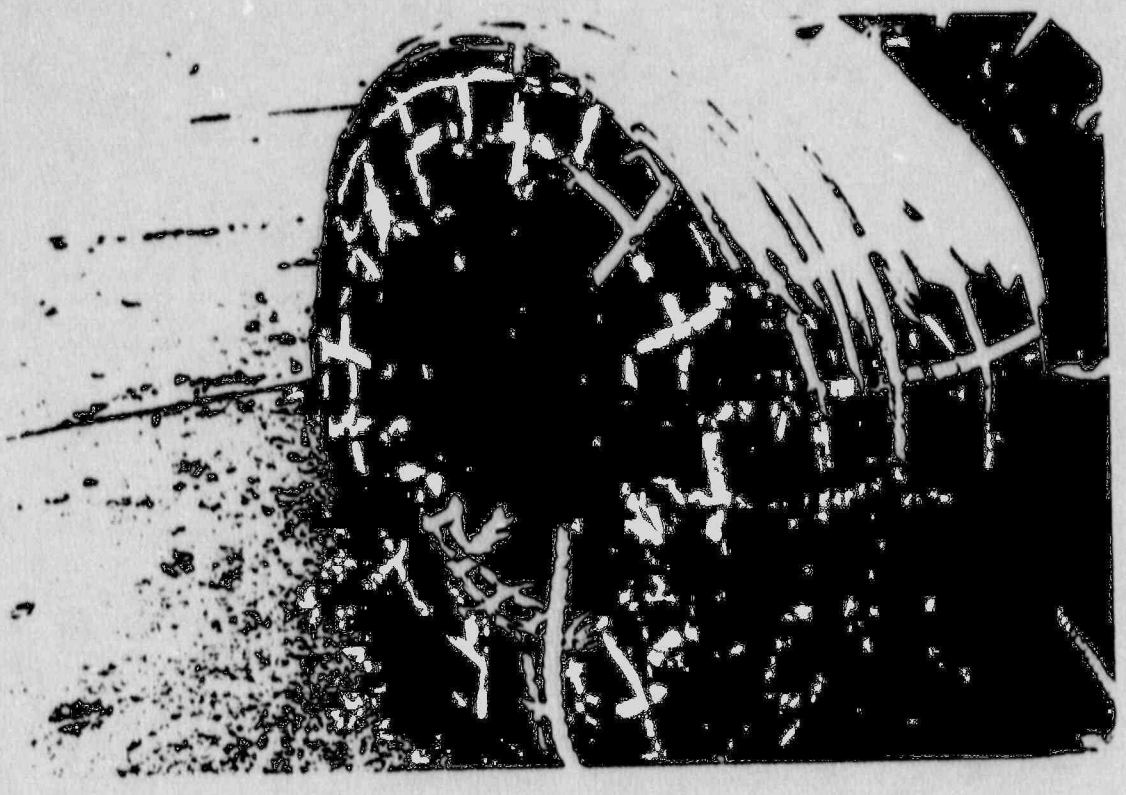

FIGURE 2.10.4-26

Center of Gravity Over Struck Corner Impact - Impact Limiter Damage

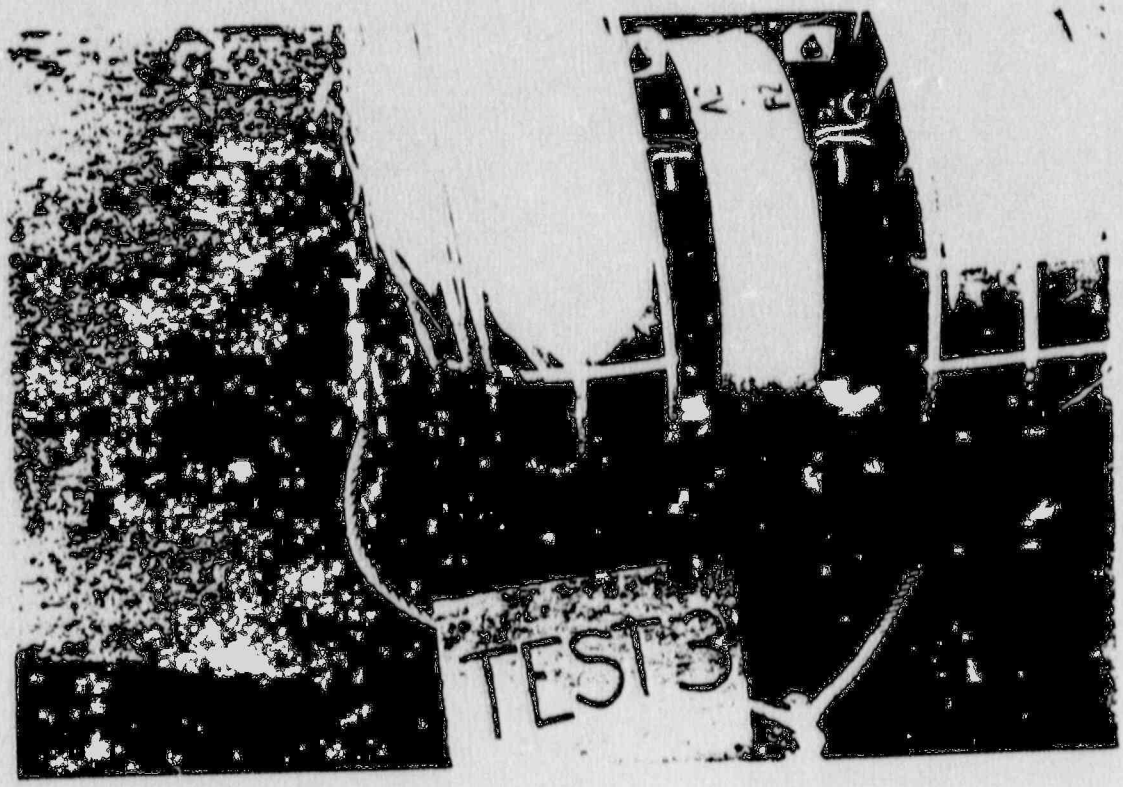

FIGURE 2.10.4-27

Impact Limiter Geometry Assured for Side Drops

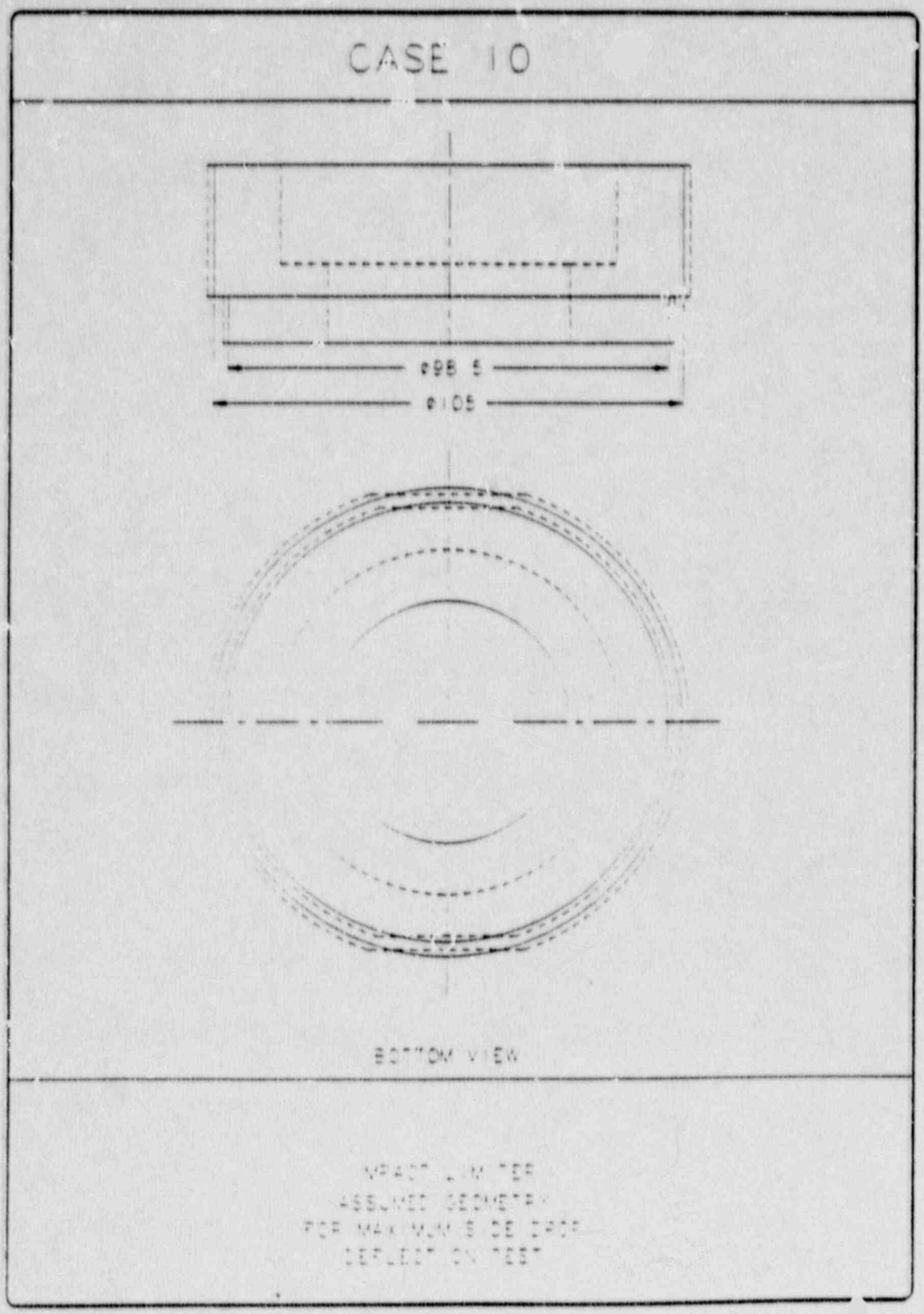

FIGURE 2.10.4-28

Maximum Side Drop Deflection Detail

FIGURE 2.10.4-29

Side Drop Impact Damage

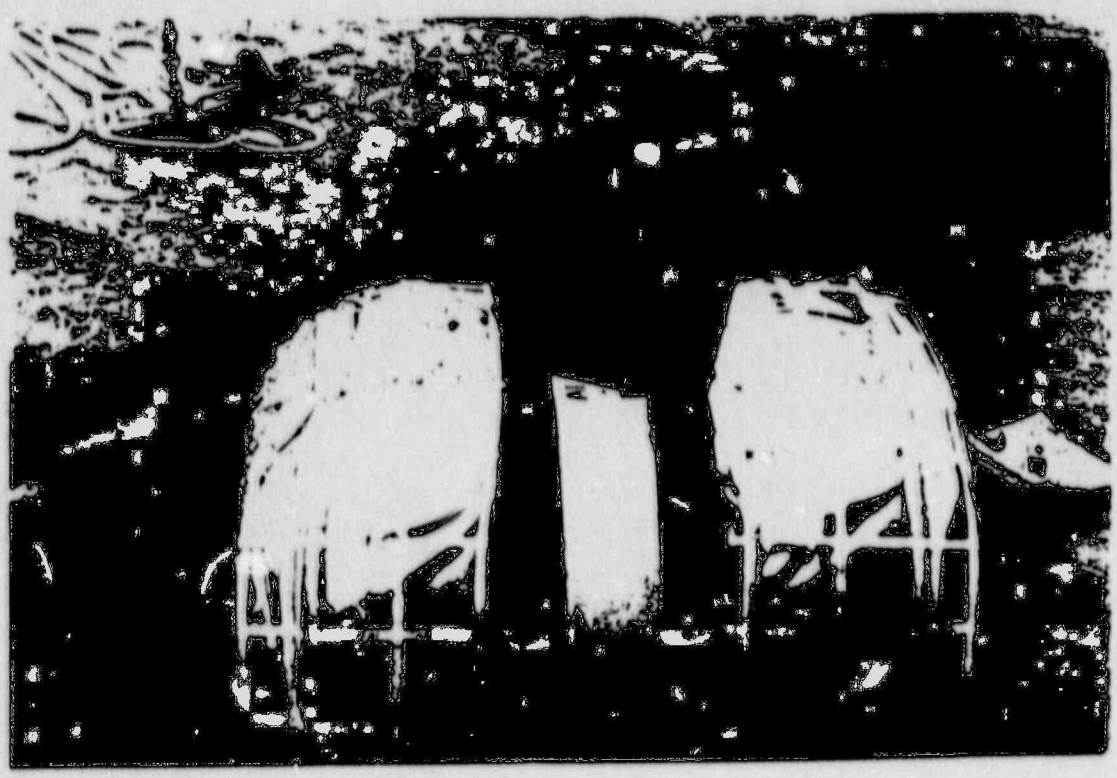

FIGURE 2.10.4-30

Side Drop Impact Damage

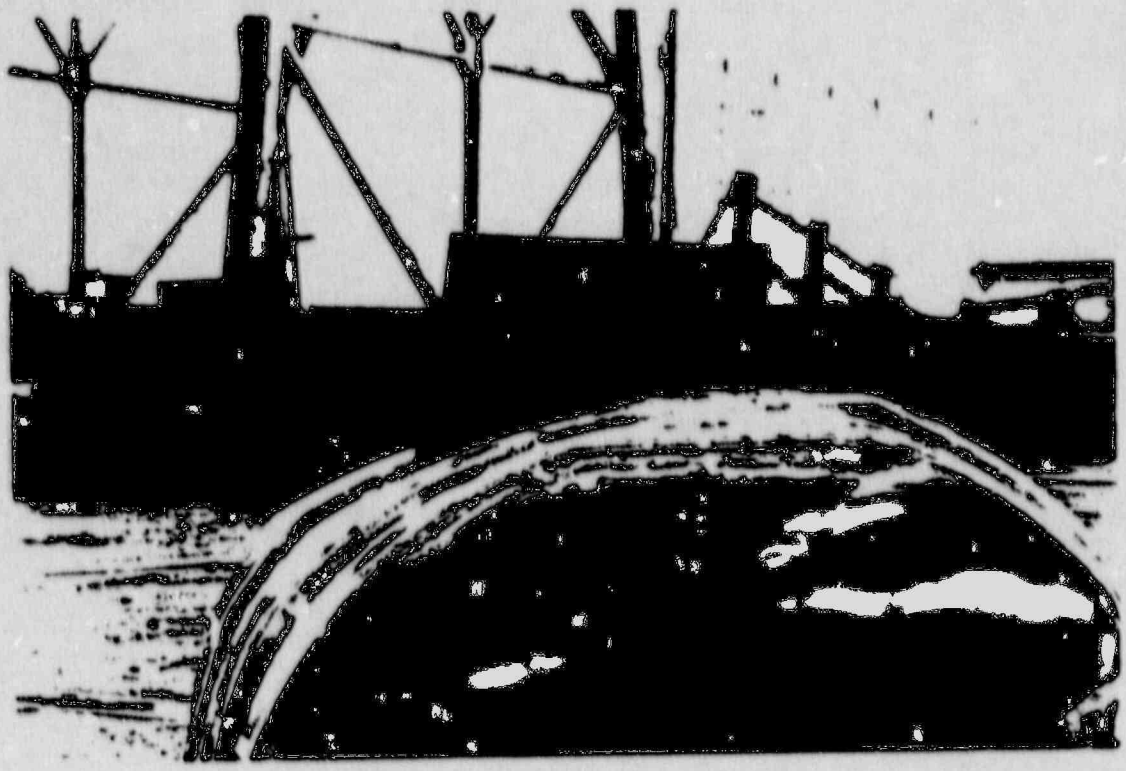

FIGURE 2.10.4-31

Flat Side Pin Impact

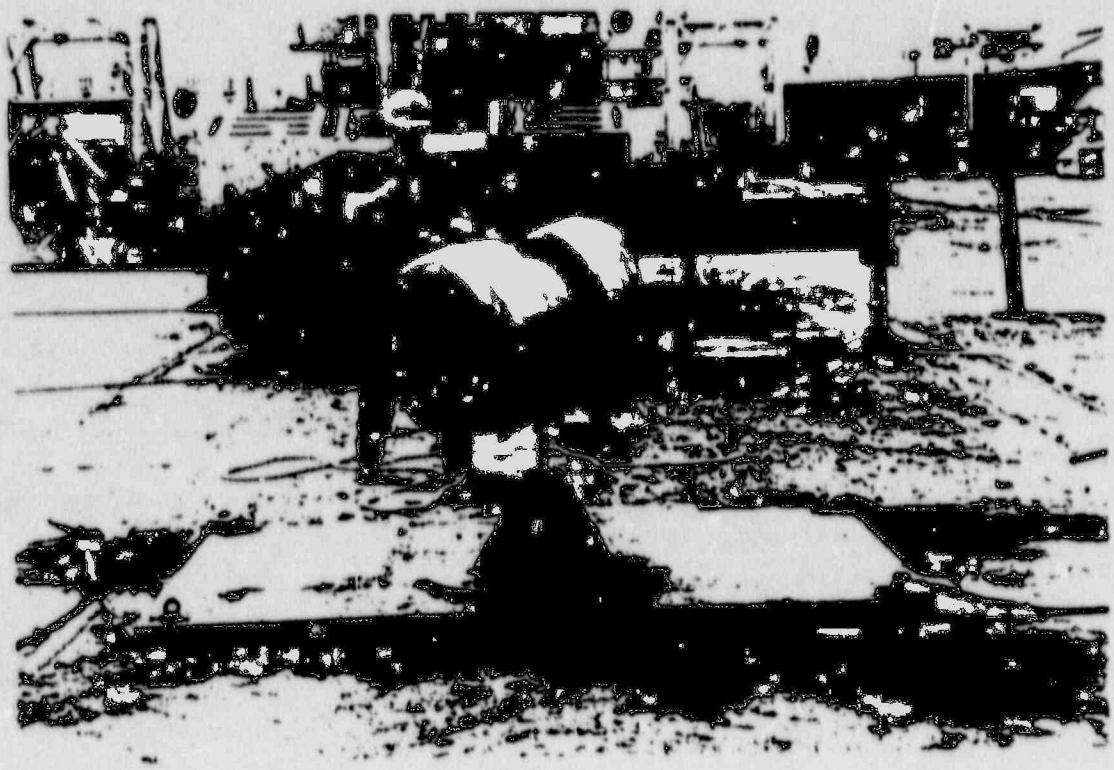

FIGURE 2.10.4-32
Side Puncture Damage

FIGURE 2.10.4-33
Side Puncture Damage

FIGURE 2.10.4-34

Flat End Pin Impact

FIGURE 2.10.4-35

End Puncture Damage

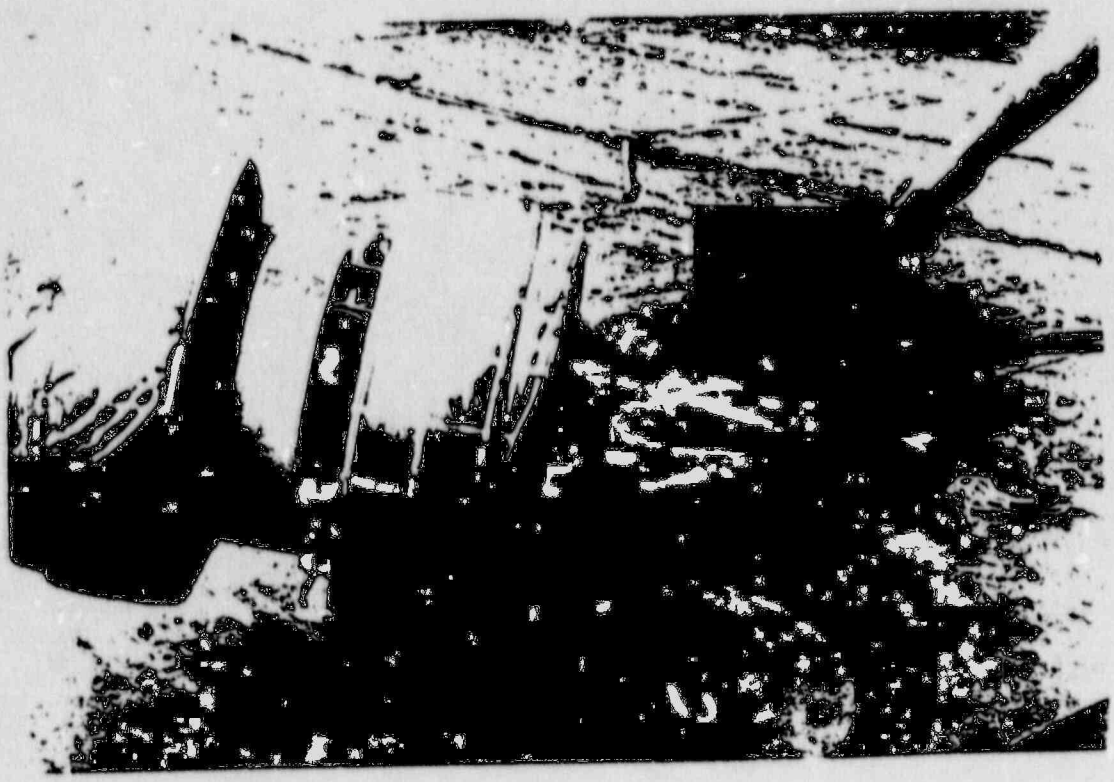

FIGURE 2.10.4-36
End Puncture Damage

FIGURE 2.10.4-37
End Puncture Damage

FIGURE 2.10.4-38

Oblique Pin Impact

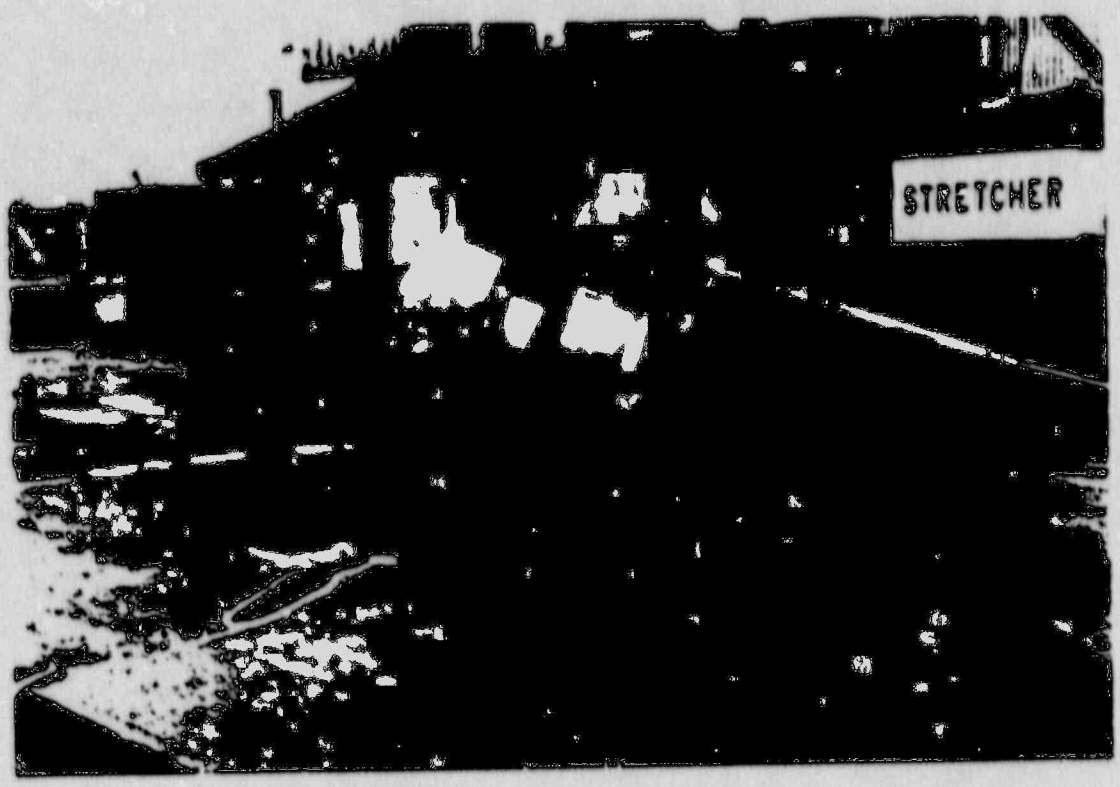

FIGURE 2.10.4-39

Oblique Puncture Damage

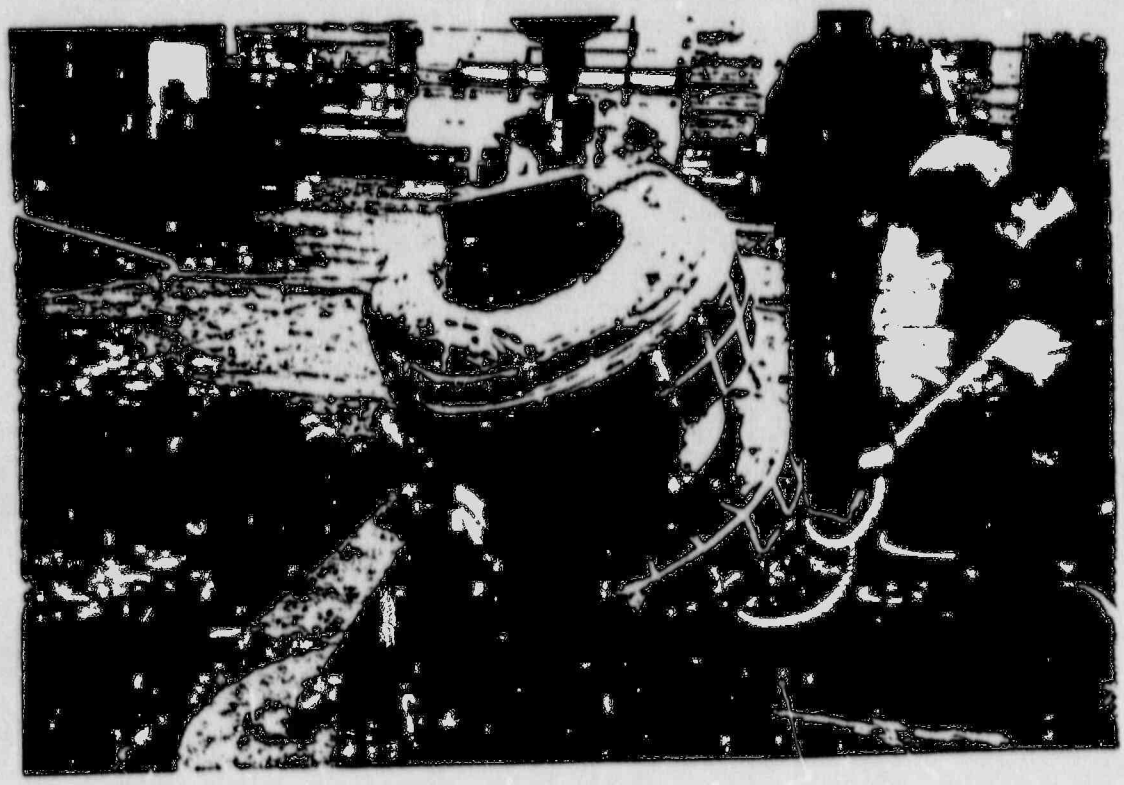

FIGURE 2.10.4-40

Oblique Puncture Damage

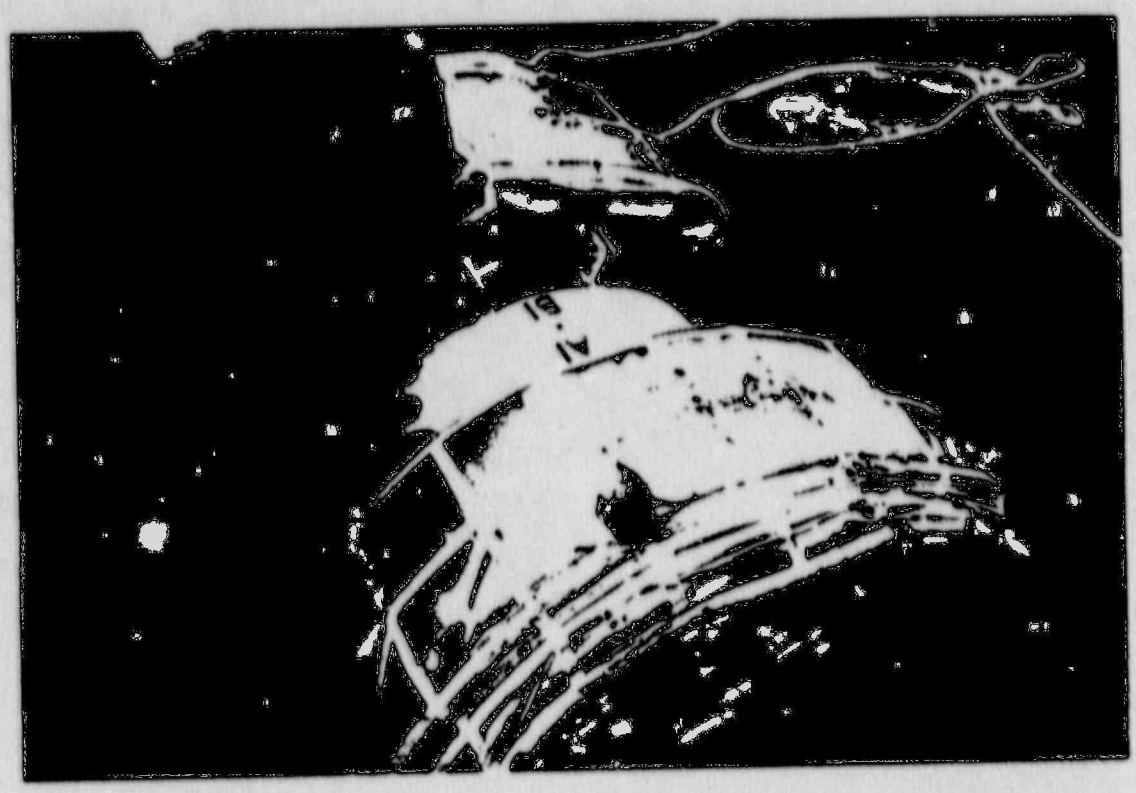

FIGURE 2.10.4-41

Oblique Puncture Damage

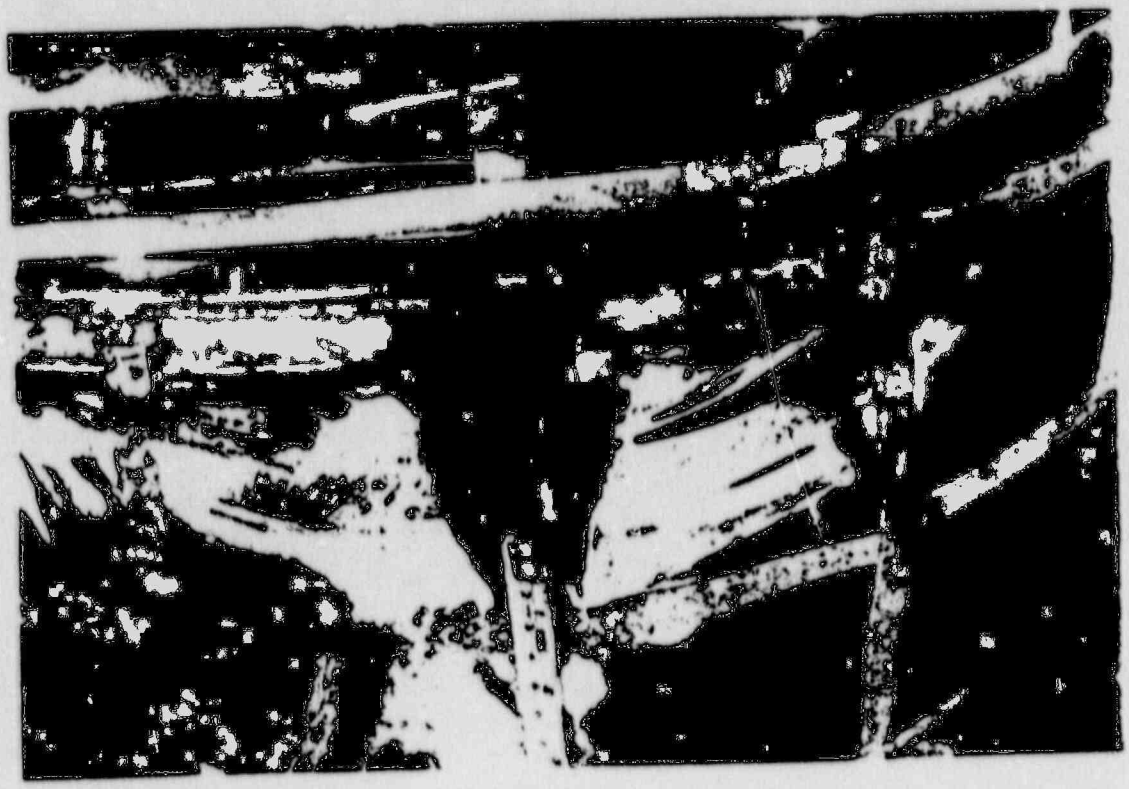

FIGURE 2.10.4-38

Oblique Pin Impact

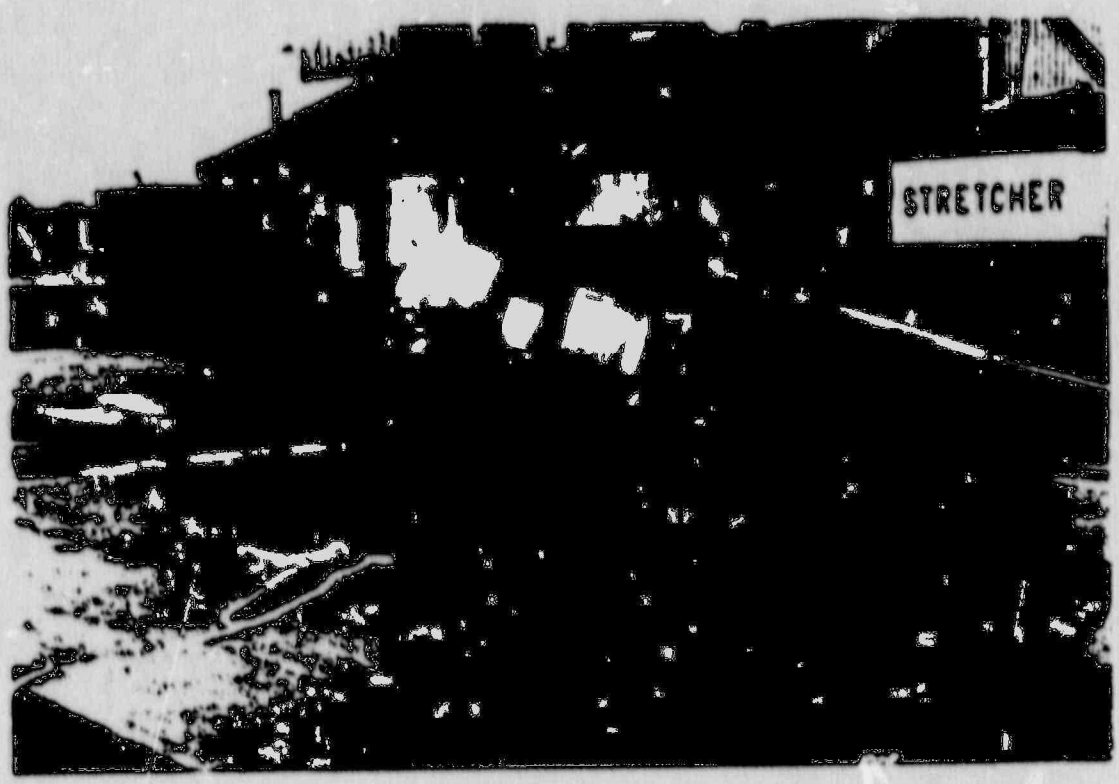

FIGURE 2.10.4-39

Oblique Puncture Damage

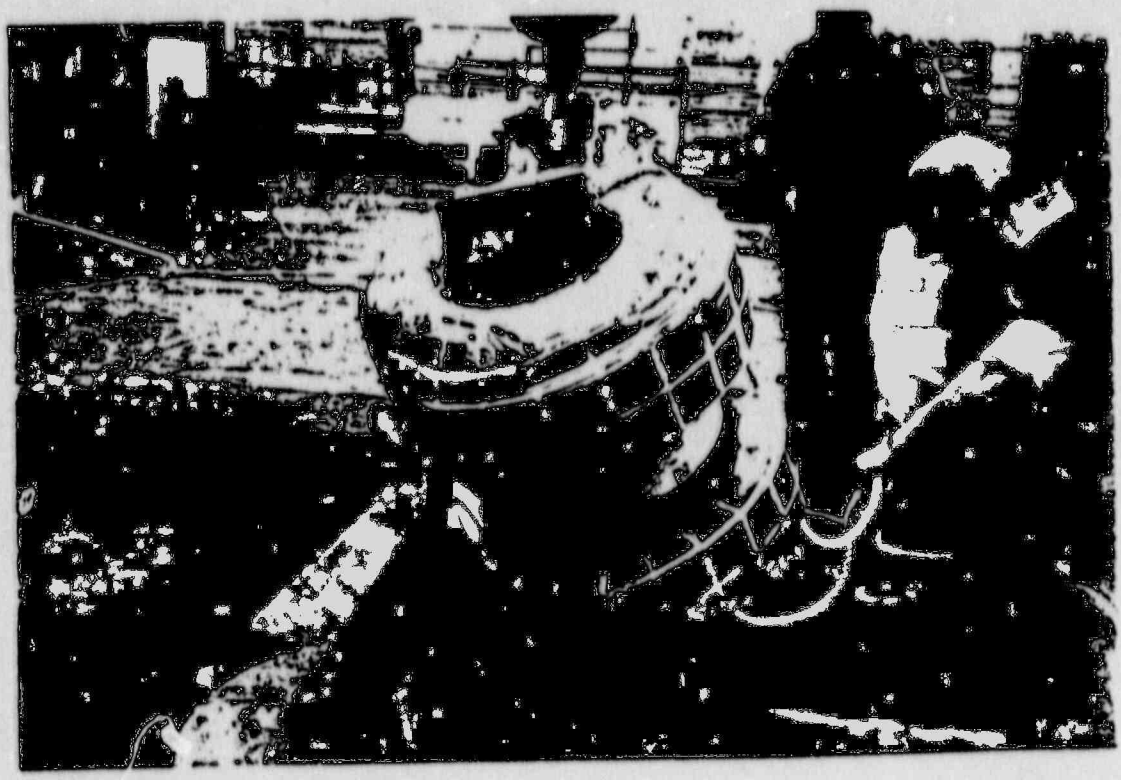

FIGURE 2.10.4-42

Pin Impact Point on Closure Nut

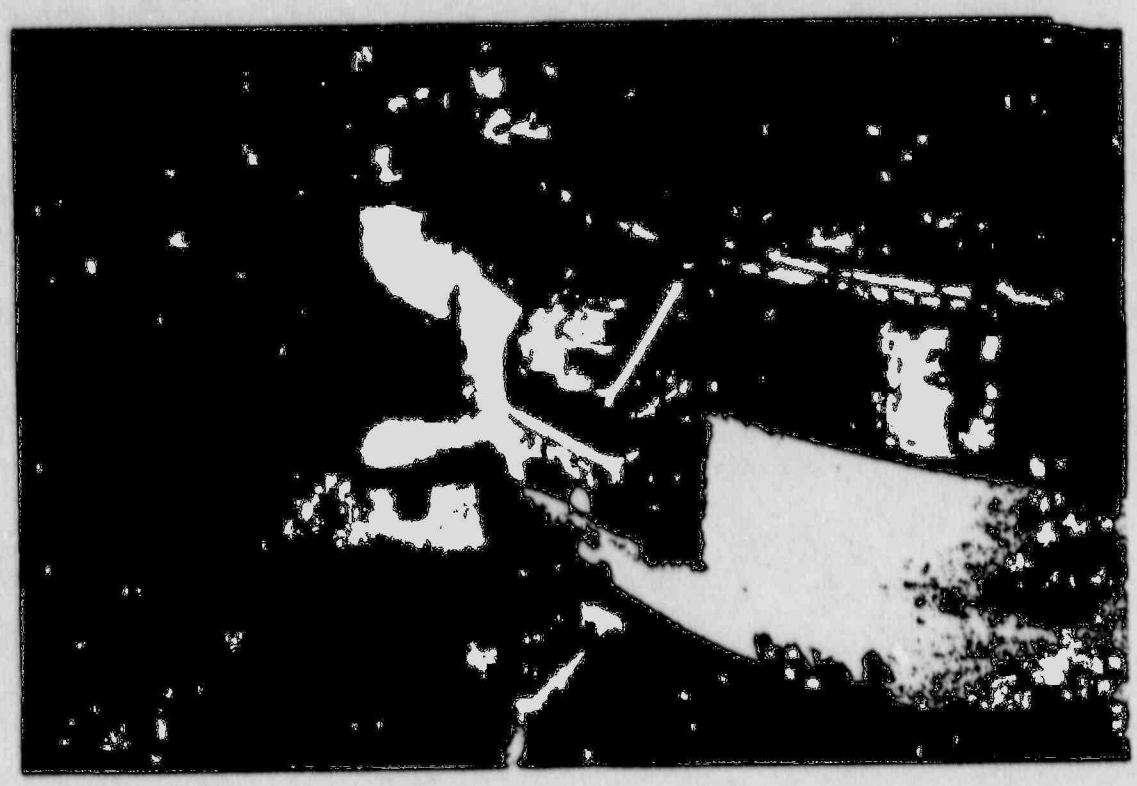

FIGURE 2.10.4-43

Impact Pin Damage

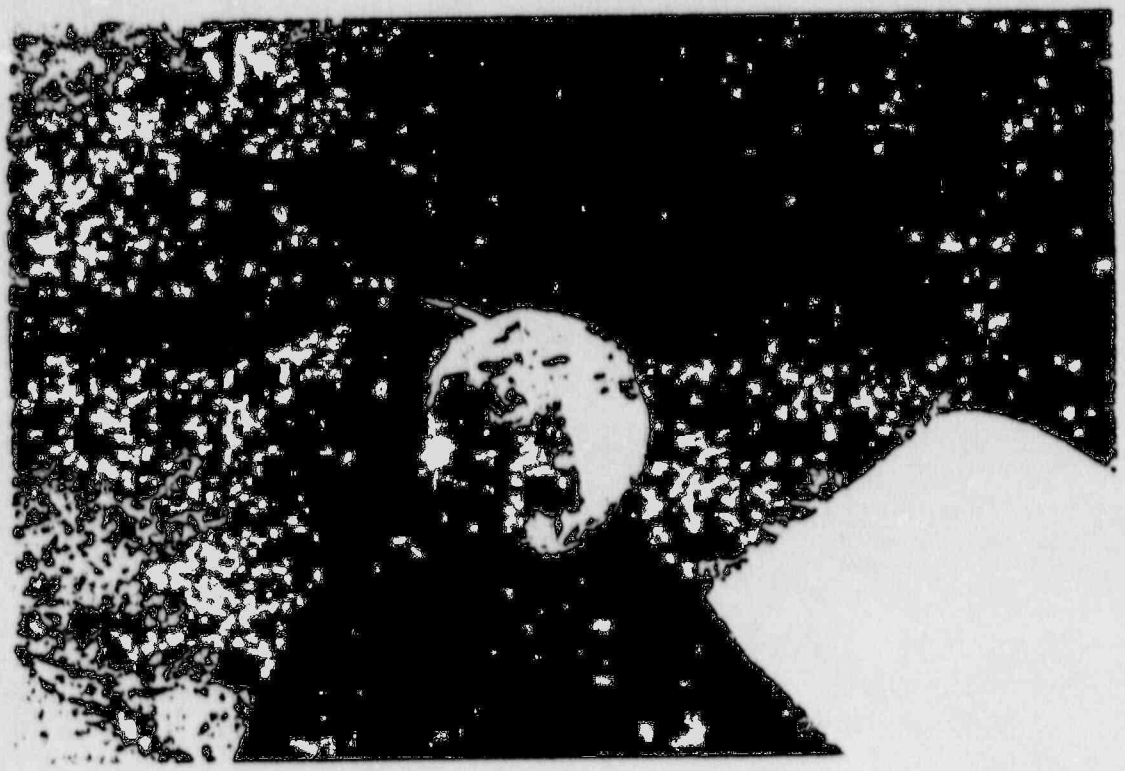

FIGURE 2.10.4-44

Bare Cask Impact

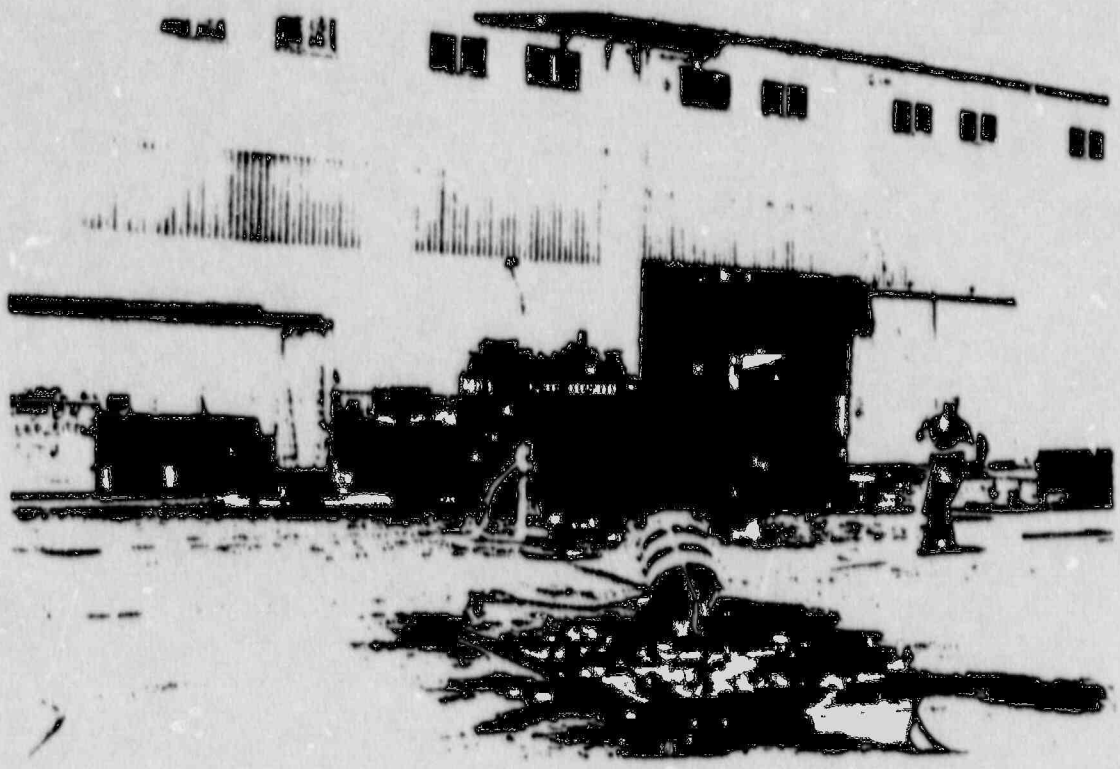

FIGURE 2.10.4-45

Bare Cask Impact Damage

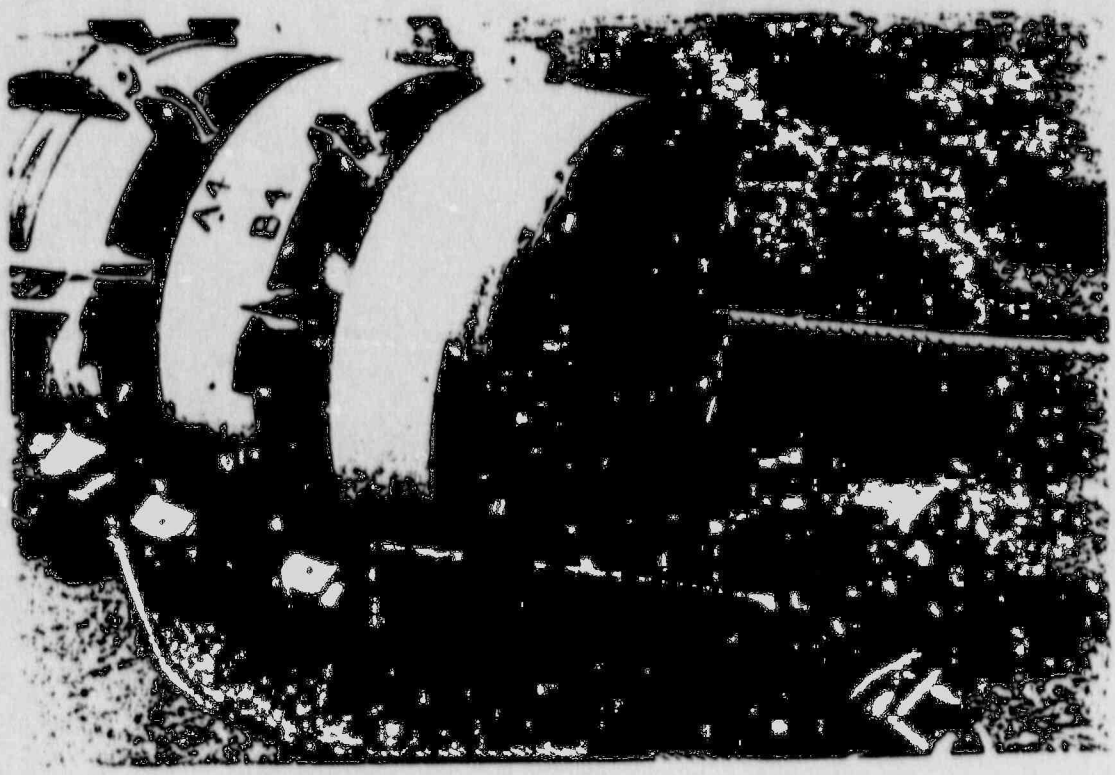

FIGURE 2.10.4-46

Bare Cask Impact Damage

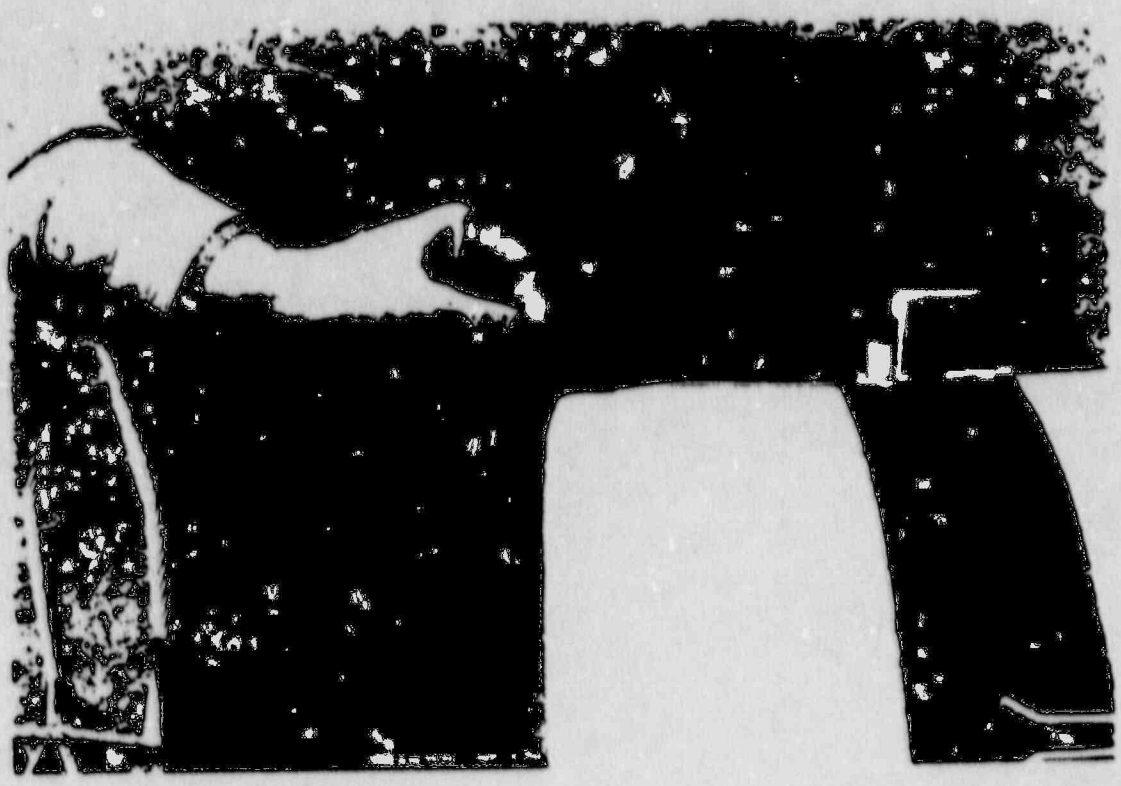

FIGURE 2.10.4-47

Bare Cask Impact Damage

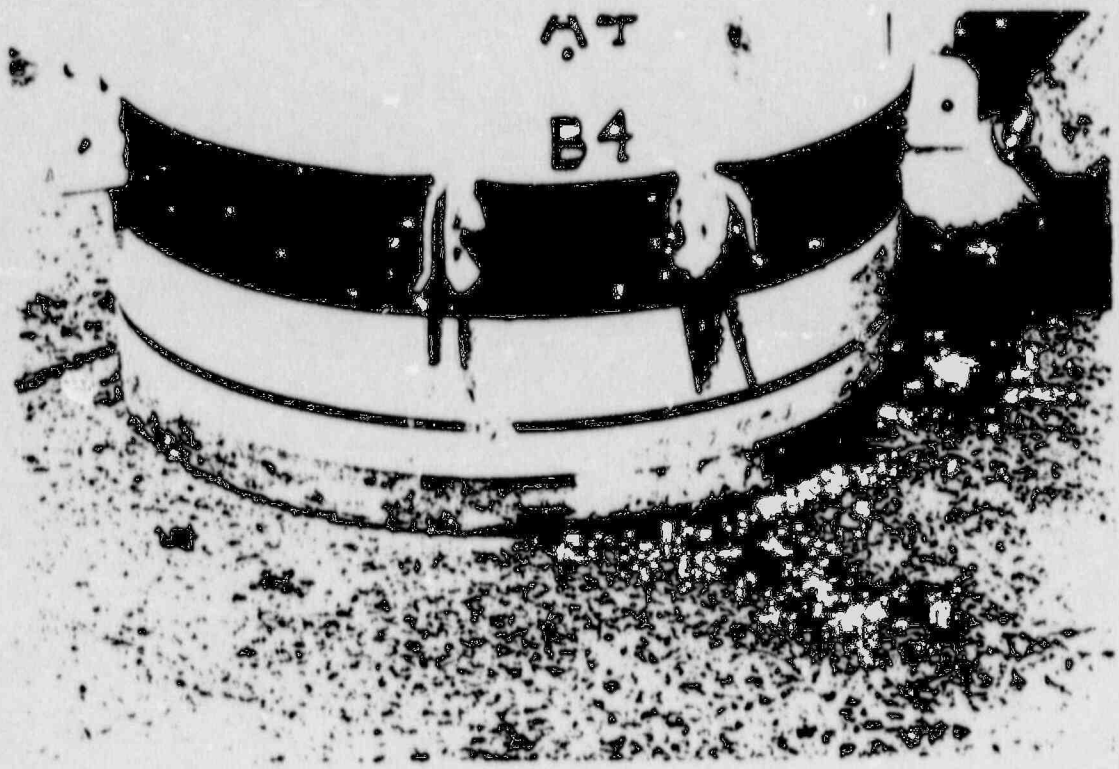

FIGURE 2.10.4-48
Lead Slump Pattern for Bare Cask Impact

FIGURE 2.10.4-49
Primary Impact Damage

FIGURE 2.10.4-50
Secondary Impact Damage

APPENDIX 2.10.5

Description of NuPac Proprietary Drop Programs

2.10.5 Description of NuPac Proprietary Drop Programs

This section briefly documents the methodology employed by the NuPac proprietary computer programs which are used to demonstrate compliance of the package with applicable provisions of 10 CFR 71 for normal and hypothetical accident conditions. The first two subsections deal with the calculation of external and internal forces imposed upon the package, when subjected to drop events. A sample problem is then presented and the NuPac computer code quality assurance program is briefly discussed. These subsections describe techniques and computer programs developed by Nuclear Packaging, Inc. of Federal Way, Washington, as follows:

- 2.10.5.1: Describes derivation of energy absorbing impact limiter load-deflection relations.
- 2.10.5.2: Describes the methods to evaluate the dynamic behavior of oblique impacts and the associated internal forces generated within the cask body.
- 2.10.5.3: Describes a sample problem, and input and output for each of the four computer codes (EYDROP, SYDROP, CYDROP, and OBLIQUE) discussed in this section.
- 2.10.5.4: Describes the quality assurance program utilized to maintain NuPac computer codes.

2.10.5.1 Impact Limiter Deformation Behavior

The package is protected by foam-filled, energy-absorbing end buffers, called impact limiters. For purposes of analysis, the impact limiters are assumed to absorb, in plastic deformation of foam, the potential energy of the drop event. That is, the analyses assume that none of the drop potential energy is transferred to kinetic or strain energy of the target (the unyielding surface assumption of 10 CFR 71), nor strain energy in the package body itself.

There are three orientations of the package where the potential energy of a drop is assumed totally absorbed by plastic deformations of the impact limiters. At other orientations, where rotational effects are important, the methods outlined in Section 2.10.5.2 are employed. The three orientations where rotational (or pitch) motions play no role in the evaluation of the impact event are:

- o End Drop - on the circular end surface of the impact limiters.
- o Side Drop - on the cylindrical side surfaces of the impact limiters.
- o Corner Drop - with package center of gravity directly above the struck corner of the impact limiter.

For these three orientations, the prediction of behavior can be approached from straightforward energy balance principles:

$$E = W(h + \delta) = \int_0^{\delta} F_x \, dx \qquad (1)$$

Where:

W = package weight

h = drop height

δ = maximum impact limiter deformation

F_x = force imposed upon target and package by the impact limiter at a deflection equal to x.

The left-hand term represents the potential energy of the drop. The right hand term represents the strain energy of the deformed impact limiter.

Each of these three orientations is treated by an individual computer program reflecting the differing geometry characteristics of each event. All three computer programs employ common energy balance techniques to assess maximum

impact limiter deformations, including utilizing a common description of the crushable energy absorbing foam. The foam typically exhibits a stress-strain plateau of nearly constant stress up to a total strain of 40-60%. Above this strain value, pronounced strain hardening effects commence which reflect the collapse or consolidation of the entrapped bubbles within the foam. Accordingly, a tabular definition of foam stress-strain relations is employed in each of the three computer programs. This tabular definition is taken directly from measured properties and accurately reflects the strain hardening behavior of the foam up to strains of about 80%.

The following discussion of these three computer programs proceeds from the geometrically simplest (end drop) to the most complex (corner drop).

2.10.5.1.1 End Drop (EYDROP)

EYDROP performs the calculations outlined in Equations (1), (2), and (3) for a trial range of deformation values, δ. For each trial value of total deformation, the energy balance of Equation (1) is monitored and reported. Solution for total impact limiter deformation is found by an interpolated balance of Equation (1). EYDROP assumes a constant foam strain across the crush area, neglecting the affects of any unbacked areas. A sample problem input and output for EYDROP may be found in Section 2.10.5.3.1.

The force produced by the impact limiter is simply:

$$F_x = A\sigma_\varepsilon \tag{2}$$

Where:

$A = \pi D^2/4$, the end area of the package

D = effective diameter of package

$\sigma_\varepsilon = \xi[\varepsilon]$, the foam crush stress at a strain of ε (3)

$\xi[\varepsilon]$ = the tabular definition of foam stress strain properties

$\varepsilon = x/x_u$

x = deformation

x_u = end thickness of impact limiter

2.10.5.1.2 Side Drop (SYDROP)

SYDROP differs from the end drop solution only in the fact that both deformation and strain vary from point to point and total force, at a given crush depth, must be found by geometric integration over these points. The details on this geometry are found in Figure 2.10.5.1-1. SYDROP assumes all foam is backed, exhibiting homogeneous properties along the package length. A sample problem input and output for SYDROP may be found in Section 2.10.5.3.2.

For each trial deformation value, the force is found as:

$$F_\delta = 2L\int_0^{x_{max}} \sigma_{Nx}\, dx$$

Where:

L = effective length of the impact limiter

$x_{max} = [r_o^2 - (r_o - \delta)^2]^{0.5}$

$\sigma_{Nx} = \xi[\varepsilon_x]$, tabular definition of foam stress-strain properties

ε_x = foam strain at location 'x'

Referring to Figure 2.10.5.1-1, the strain at a point 'x' is found by:

$$\varepsilon_x = [\delta - r_o(1 - \cos\theta)]/[r_o(\cos\theta) - r_i(\cos\gamma)]$$

Where:

$\theta = \sin^{-1}(x/r_o)$

$\gamma = \sin^{-1}(x/r_i)$

FIGURE 2.10.5.1-1
Side Impact Geometry (SYLKOP)

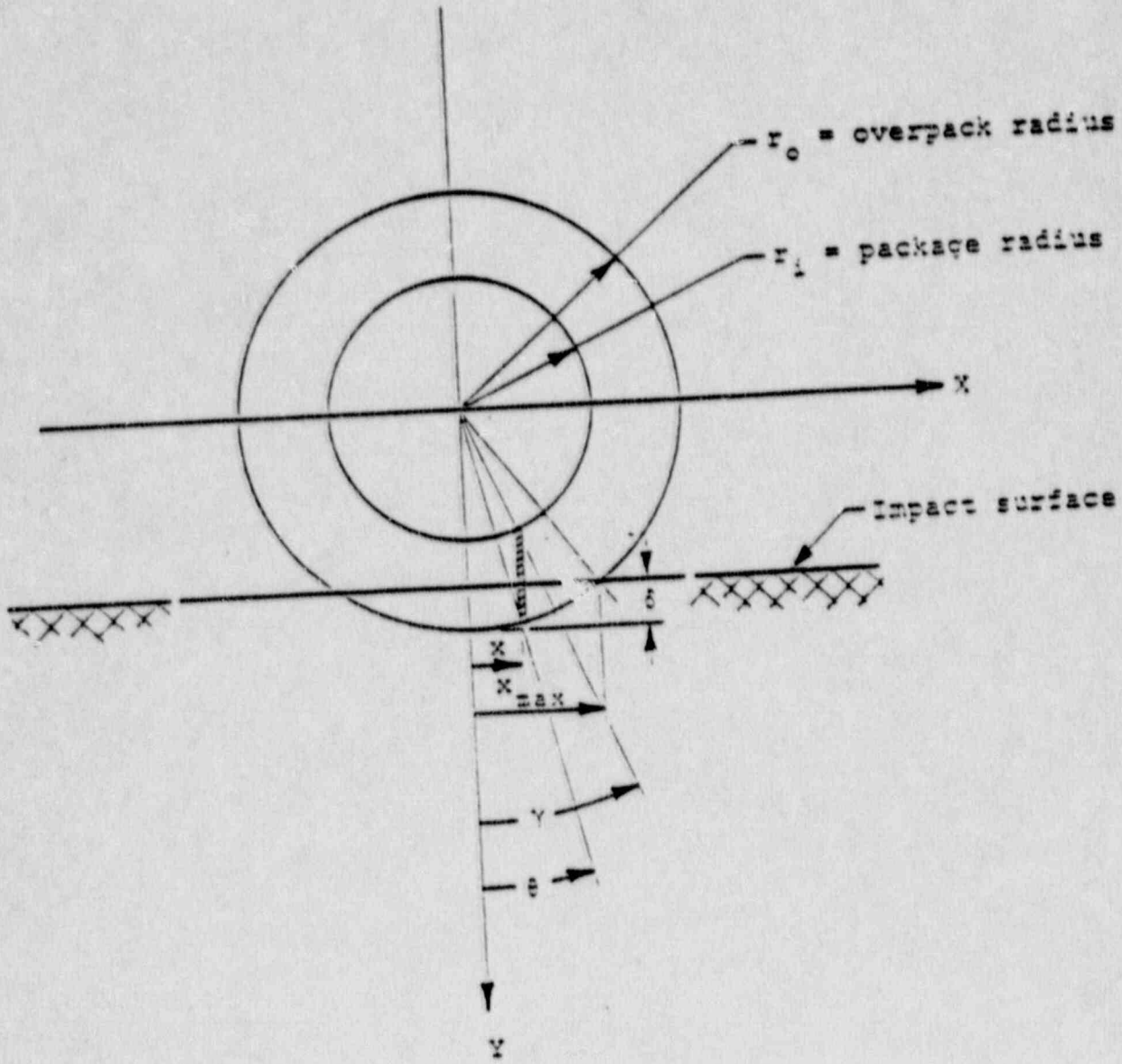

2.10.5.1.3 Corner Drop (CYDROP)

CYDROP is similar to SYDROP, excepting that a two dimensional geometric integration is required to assess the impact limiter crush force at each deformation. A sample problem input and output for CYDROP may be found in Section 2.10.5.3.3.

CYDROP treats the corner impact of a cylindrical package upon an unyielding surface. The package itself consists of a cylindrical payload portion surrounded by a larger cylindrical column composed of a crushable media. So long as the deformations of the crushable media are modest, the problem may be approximately solved by assuming a uniform crush stress exists over the elliptical surface of the crush plane (contact surface). CYDROP was developed specifically to address problems of large deformations of this crushable media and to treat geometries where the cylindrical impact limiter envelope possesses axisymmetric cylindrical voids (e.g., does not completely cover the cylindrical ends of the payload package).

The large deformation behavior of the crushable media is accommodated by determining the actual strain of the crushable media at a point. This strain is used to determine the corresponding stress from an implicit tabular definition of media stress-strain characteristics. The total crush force is found by a double integration over the contact area of the crush plane.

Strain energy absorbed by the crushable media is determined by integrating the crush force and its associated deformation. The package is assumed to be at rest when the computed strain energy value equals the applied drop energy.

The geometric calculations for the contact surface and the associated strains are carried out using a moving (x, y, z) coordinate system in which the x-y plane corresponds to the crush plane, as illustrated in Figure 2.10.5.1-2. The crush plane itself represents a segment of an ellipse. The contact area is this ellipse segment, provided no cylindrical end void exists. When a cylindrical end void exists, the contact area of the crush plane is reduced by the removal of a second elliptical region associated with the projection of this void into the contact plane.

FIGURE 2.10.5.1-2

Corner Impact Geometry (CYDROP)

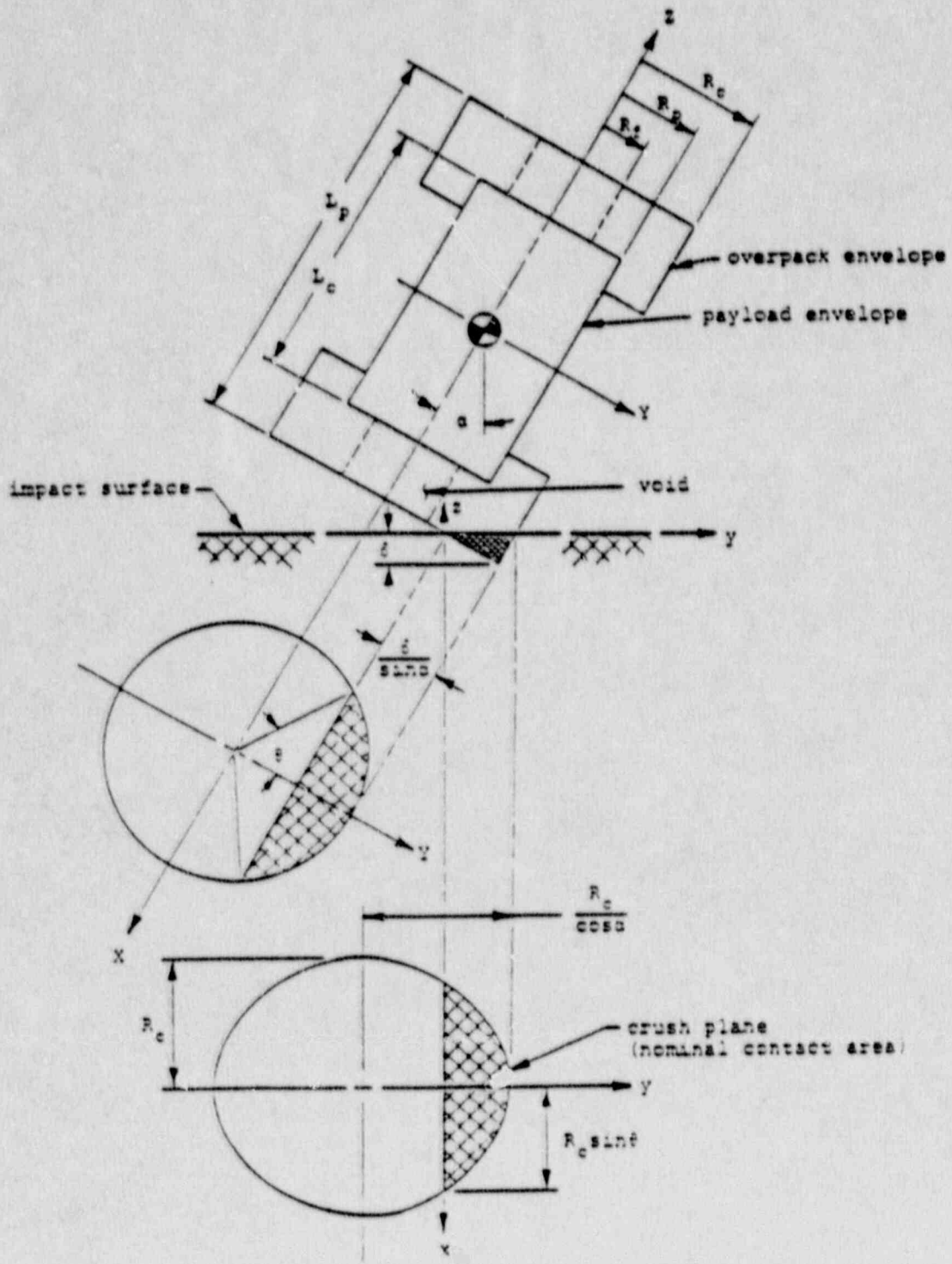

Calculation of strain is somewhat more complex. In principle, the distance from point (x, y) in the crush plane to the payload is found and denoted, Z_{top}. Similarly, the distance to the undeformed external impact limiter envelope is found and denoted, Z_{bot}. The strain represents deformation divided by original thickness, or:

$$\epsilon = Z_{bot}/(Z_{bot} + Z_{top})$$

At any point (x, y), the calculation of Z_{top} may follow three branches, according to location. The three possible branches relate to the payload surface intercepted. They are the circular bottom of the payload, the cylindrical surface of the payload, and the unbacked regions, each of which are separately addressed below:

The Circular Bottom of the Payload:

The bottom of the payload cylinder describes an ellipse in the crush plane. If point (x, y) is inside this ellipse, the point is considered backed by the bottom of the payload. An exception to this general statement is noted in the discussion of the unbacked region, below.

The Cylindrical Surface of the Payload:

The cylindrical surface of the payload describes a rectangular region tangent to the payload bottom ellipse at its major axes. If point (x, y) is outside the bottom ellipse yet possesses an x-coordinate less than the radius of the payload bottom, the point is considered backed by the payload cylinder.

Unbacked Regions:

Unbacked regions are of two forms - those associated with the cylindrical end void and those near the external surface of the impact limiter. The unbacked region associated with the end void is a point in the crush plane which lies within the ellipse defined by the void circle lying in the plane of the payload bottom. The unbacked region associated with points near the impact

limiter extremities is defined by those points (x, y) where the x-coordinate exceeds the radius of the payload volume. Points which are unbacked employ a nominal crush stress for force integration purposes.

The calculation of Z_{bot}, the distance to the undeformed impact limiter envelope, may follow two branches. These branches correspond to intercepts with either the cylindrical surface of the impact limiter or the circular end of the impact limiter.

The analytics describing the geometry discussed above, consists of the sequential application of a series of geometric transformations of surfaces described in the coordinates of the cylindrical package (X, Y, Z)to the coordinates of the contact plane (x, y, z). The surfaces in package coordinates are:

Impact Limiter Cylinder: $X^2 + Y^2 = R_c^2$

Impact Limiter Bottom Circle: $X^2 + Y^2 = R_c^2$, $Z = -L_c/2$

Payload Cylinder: $X^2 + Y^2 = R_p^2$

Payload Bottom Circle: $X^2 + Y^2 = R_p^2$, $Z = -L_p/2$

Void Circle at Payload: $X^2 + Y^2 = R_f^2$, $Z = -L_p/2$

Void Circle at Impact Limiter Exterior: $X^2 + Y^2 = R_f^2$, $Z = -L_c/2$

CYDROP also performs a sensitivity analysis to determine the amount of unbacked foam at each incremental crush depth. Additionally, this calculation is carried over to the impact force and strain energy. The code automatically prints a warning message if the foam strain exceeds 80% and the ratio of foam strain energy to kinetic energy is less than one (SE/KE < 1).

2.10.5.2 Oblique Impact Dynamic Analysis

Impacts at arbitrary orientation angles differ in two major respects from those that occur at angles corresponding to stable or neutral equilibrium (end, side, and center of gravity over struck corner). In the neutral and stable equilibrium conditions, the entire initial kinetic energy of drop is transformed into strain energy associated with plastic deformation of the impact limiter. At arbitrary orientation angles, only a portion of this kinetic energy is transformed into strain energy at the impacted end. The remainder of this kinetic energy becomes rotational motion of the package. The solution approach must properly reflect the continually changing transformation of initial translational kinetic energy into rotational kinetic energy and plastic deformation of the impact limiter energy absorber.

The second major difference between neutral equilibrium impacts and arbitrary angle impacts relates to the rather different load-deflection behavior of the impact limiters at low angle ($<30^{\circ}$ from horizontal) orientations. Under neutral equilibrium conditions, a major portion of the crush footprint is backed by the cylindrical body of the package, allowing strain hardening effects to stiffen the impact limiter load-deflection relation. At low angle orientations ($<30^{\circ}$ from horizontal), much of the impact limiter crush footprint is unbacked. Thus, the low angle load-deflection relations are initially quite soft, then abruptly harden as portions of the crush footprint grow into backed regions. As these low angle orientations approach horizontal attitudes, this terminal stiffening phenomena becomes more pronounced.

There are two potential solution paths to problems of this nature - a momentum formulation or a direct solution of the equations of motion. The momentum approach provides an easy and simple means to assess the transformation of translational initial velocities into rotary velocities, hence, total plastic strain energy absorbed by the impact limiter energy absorber. Unfortunately, this momentum formulation does not produce intermediate values of crush force and crush deformation needed to assess impact limiter attachment forces, nor does it conveniently provide a means to incorporate the varying load-deflection relationships of the impact limiter as a function of orientation angle. Thus, a direct solution of the equations of motion was selected.

The three key problem variables, crush force, F, crush depth, δ, and orientation angle, θ, all vary with time, t, for a given initial orientation angle, θ_o. The crush force is assumed to act at the centroid of the elliptical crush footprint. For the model illustrated in Figure 2.10.5.2-1, three independent second order differential equations of motion can be formed:

$$M(\partial^2 X/\partial t^2) = F_x$$

$$M(\partial^2 Y/\partial t^2) = F_y - Mg$$

$$I(\partial^2\theta/\partial t^2) = \{[\delta(a - c)/c(\sin\theta) + T_B + L/2](\sin\theta)\}F_x + \{\bar{x} - [\delta(a - c)/c(\sin\theta) + T_B + L/2](\cos\theta)\}F_y$$

Where:

M = the package mass = ρL

F = the crush force

g = the gravitational constant = 386.4 in/sec^2

I = the rotational mass moment of inertia (as input)

r_o = the radius of the body

L = the length of the body

T_B = impact limiter bottom thickness

θ = the instantaneous orientation angle of the package with respect to the horizon

ρ = the mass per unit length

$\bar{x}$ = distance to centroid of footprint

a, c = geometric quantities defined in Figure 2.10.5.2-2

FIGURE 2.10.5.2-1
Oblique Impact Geometry

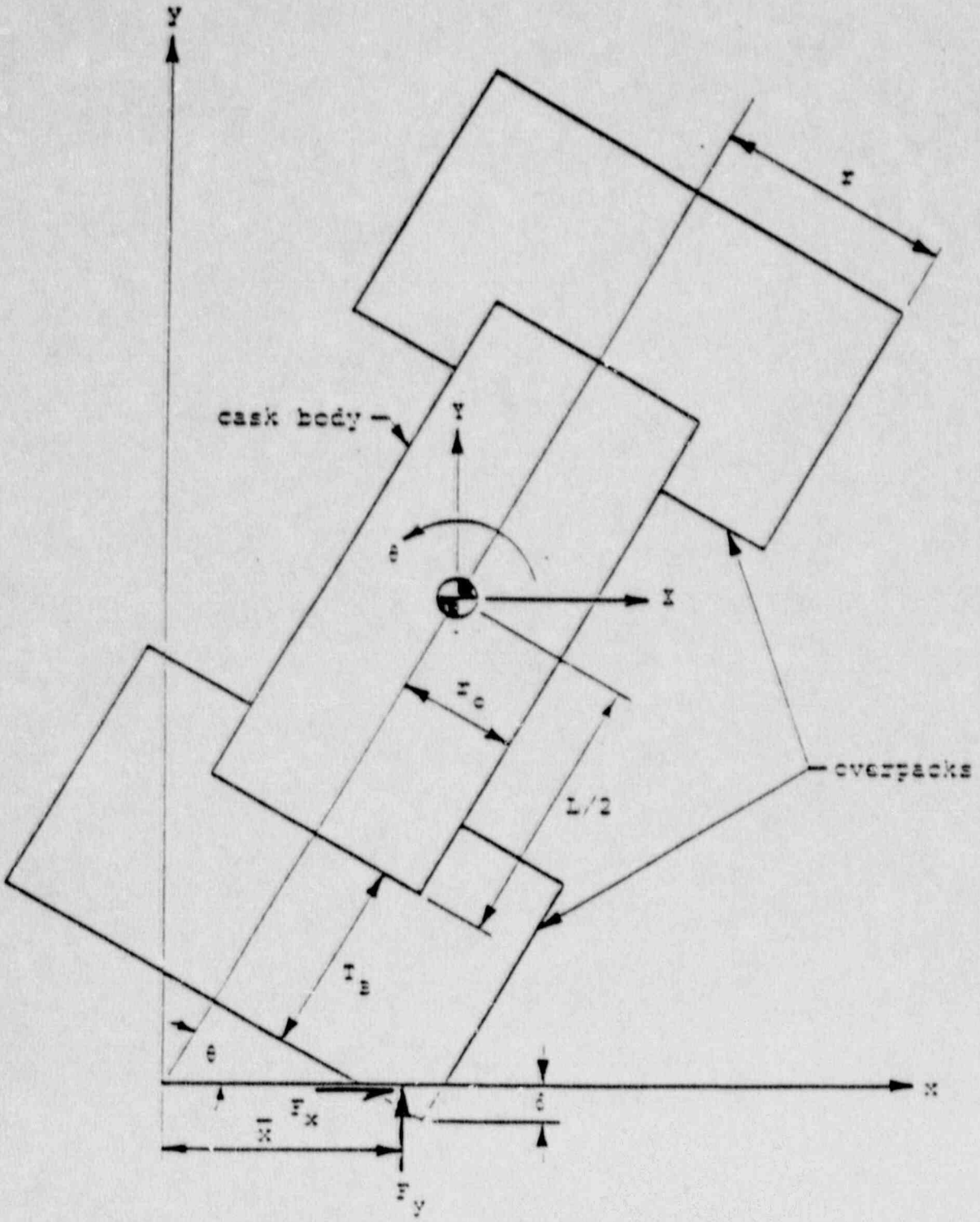

FIGURE 2.10.5.2-2

Elliptical Footprint Geometry

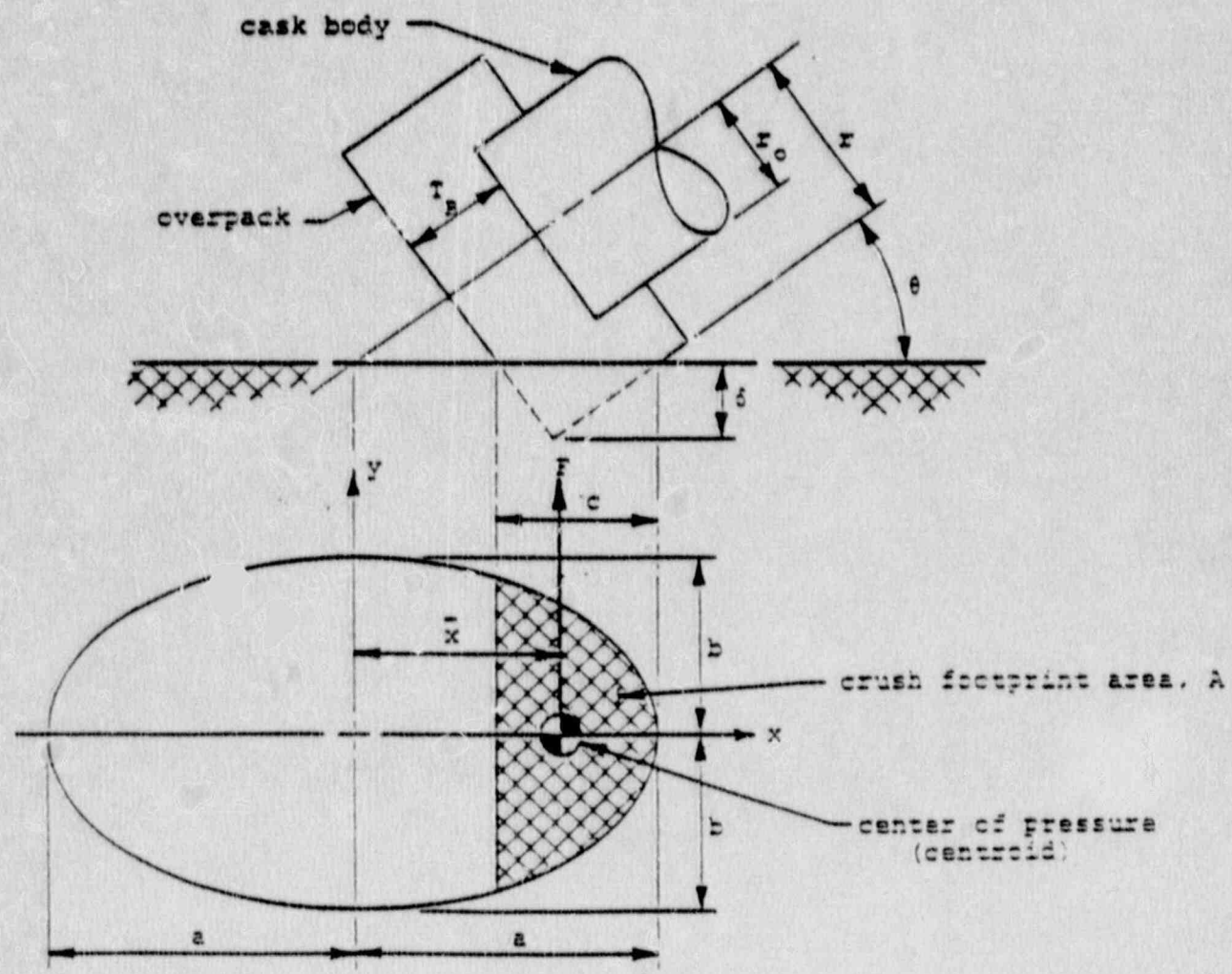

These differential equations are integrated subject to initial conditions, associated with the moment of impact when time, t, equals zero, of:

$$X = 0$$

$$Y = 0$$

$$\theta = \theta_o$$

$$\partial X/\partial t = \partial X_o/\partial t$$

$$\partial Y/\partial t = \partial Y_o/\partial t$$

$$\partial \theta/\partial t = \partial \theta_o/\partial t$$

Where:

θ_o = impact angle (varies with time, t)

$$\partial Y_o/\partial t = (2gh)^{0.5}$$

h = drop height

Each of the above differential equations requires a continuously updated value of the force, F, reflecting both crush depth and package orientation, or:

$$F = \xi(\delta_y, \theta)$$

This continuously updated value of the force, F, is supplied to the integration process by means of a two dimensional Lagrangian interpolation of crush depth, δ_y, and orientation angle, θ. The tabular data used in this interpolation consist of a series of complete force-deflection relations for separate orientation angles developed via the CYDRCP computer program, described in Section 2.10.5.1.3. The deflection, δ_y, is expressed in terms of problem variables as:

$$\delta_y = L(\sin\theta - \sin\theta_o)/2 + r_o(\cos\theta - \cos\theta_o) - Y$$

The foregoing analysis process for evaluating impacts at oblique orientations was consolidated in a NuPac developed computer program, OBLIQUE. OBLIQUE integrates the equations of motion for each value of orientation angle versus time, until maximum values are found for crush force, crush deformation, shear, and body bending moment. At each incremental time step (incremental crush deformation), impact limiter attachment moments are computed, scanned for maximum values and output. By sweeping through a series of initial orientation angles, the maximum values of all internal loads are found. At each specified initial orientation angle, a solution is realized when all internal forces, moments, and deflection have reached a maximum value. Note that these internal forces, moments, and deflections do not necessarily happen at the same instantaneous angle, θ.

2.10.5.2.1 Impact Limiter Force Analysis

This section treats both external and internal forces imposed upon the package. Key to the treatment of external force application locations is an understanding of crush footprint geometry.

The crush footprint is a sector of the ellipse, as illustrated in Figure 2.10.5.2-2. The location of the centroid, $\bar{x}$, is calculated relative to the ellipse origin. The geometric properties of the elliptical crush footprint are:

$$a = r/\sin\theta$$

$$b = r$$

$$c = \delta/[(\sin\theta)(\cos\theta)]$$

The area, A, and the centroidal offset, $\bar{x}$, of the crush footprint are derived as:

When $c \leq a$:

$$A = 2\int_{(a-c)}^{c} y\,dx$$

Where:

$$y = b(a^2 - x^2)^{0.5}/a$$

Then,

$$A = (2b/a)\int_{(a-c)}^{c} (a^2 - x^2)^{0.5}\,dx$$

Solving,

$$A = (b/a)[(\pi a^2/2) - (a - c)(2ac - c^2)^{0.5} - a^2\sin^{-1}[(a - c)/a]]$$

The center of pressure, $\bar{x}$, is:

$$A\bar{x} = (2b/a)\int_{(a-c)}^{c} x(a^2 - x^2)^{0.5}\,dx$$

Then,

$$\bar{x} = (2b[(2ac - c^2)^{1.5}]/3a)/A$$

When $a < c \leq 2a$:

$$A = \pi ab - A'$$

$$\bar{x} = (A'\bar{x}')/A$$

Where A' and $\bar{x}'$ are as defined for A and $\bar{x}$, except that c' replaces c. The value of c' is:

$$c' = 2a - c$$

When $a > 2a$:

$$A = \pi ab$$

$$\bar{x} = 0$$

2.10.5.2.2 Impact Limiter Attachment Forces

For most orientations and crush depths, the impact limiter crush force is transmitted to the cask body in direct compression, hence, the forces transmitted to the circumferential overpack attachments are near zero. this is not true for near vertical and near horizontal orientations of the package, at very modest crush deformations and crush forces. In these very limited situations, the center of pressure of the crush force can lie beyond the outer extremities of the cask body nd exert a resultant moment force upon the impact limiter attachments. Significantly, these moments exist only for very modest crush deformations and crush forces, regardless of orientation angle. This is because larger crush deformations move the center of pressure toward the cask body. At maximum crush depth and maximum crush force, for all angles of orientation, there are no impact limiter attachment moments because the overpack interface forces are all direct compression. The near vertical and near horizontal orientations, where attachment moments exist, are illustrated below:

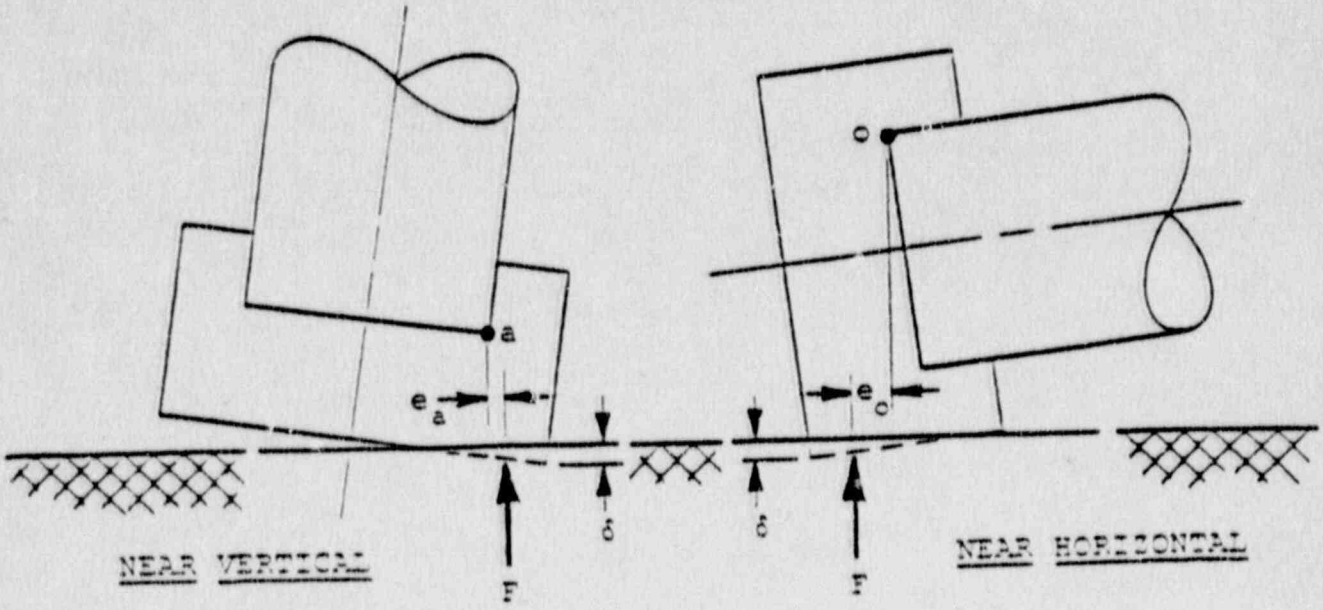

The impact limiter attachment moment is:

$$M = F(e_a) \text{ or } F(e_o)$$

Where:

e_a = moment arm about adjacent corner

e_o = moment arm about opposite corner

The location of the crush force can be approximated as the centroid of the crush footprint area. This approximation is consistently conservative. Specifically, for both near vertical and near horizontal orientations, foam strain-hardening effects tend to move the center of force from the geometric center of the crush footprint toward the cask body. In both instances, this tendency reduces the actual moment arm of the crush force to less than that predicted by the location of the crush footprint centroid. The moment arm, as defined by crush footprint geometry, is derived below. The location of the center of pressure relative to the opposite and adjacent corners of the cask body can be obtained from the geometry as illustrated below:

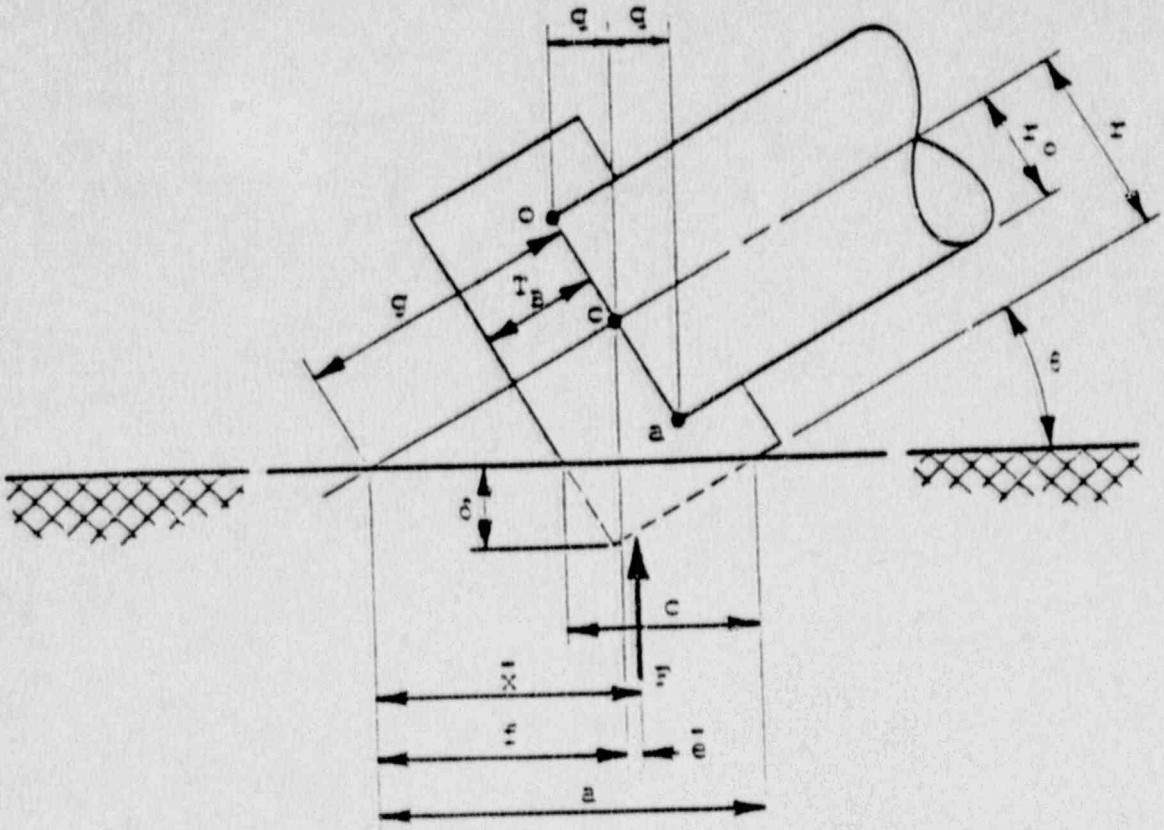

Where:

$$q = r_o(\sin \theta)$$

$$f = g(\cos \theta)$$

$$g = T_B + (a - c)(\cos \theta)$$

$$\bar{e} = \bar{x} - f$$

The location of the center of pressure, measured from a normal to the crush plane passed through the intercept of package center line and body base plane (Point c), is:

$$\bar{e} = \bar{x} - [T_B + (a - c)(\cos \bar{\theta})](\cos \bar{\theta})$$

The moment arms, e_o and e_a, representing the distance from the center of pressure to the corners of the cask body, are thus given as:

$e_o = -(\bar{e} + q)$ = moment arm about opposite corner

$e_a = (\bar{e} - q)$ = moment arm about adjacent corner

Sign convention for these arms is such that the moment, $F(e_o)$, produces a clockwise (separation) moment about the opposite corner and moment, $F(e_a)$, produces a counter-clockwise (separation) moment about the adjacent corner. In other words, a positive moment must be resisted by impact limiter attachment bolts whereas a negative moment implies that the center of pressure is totally resisted by compressive interface forces and there are no attachment bolt loads.

In summary, the forces between the impact limiter and body have been derived in terms of package geometry and three problem variables: orientation angle, crush force, and crush deformation.

2.10.5.2.3 Internal Forces

The package is idealized as a beam impacting on the lower end. The equations of motion are formed and used to define station-wise accelerations. These accelerations, in conjunction with the unit mass of the package, form forces which vary along the length of the package. When integrated, these forces provide a complete definition of internal thrusts, shears, and moments for the package as a function of total impact force and orientation angle.

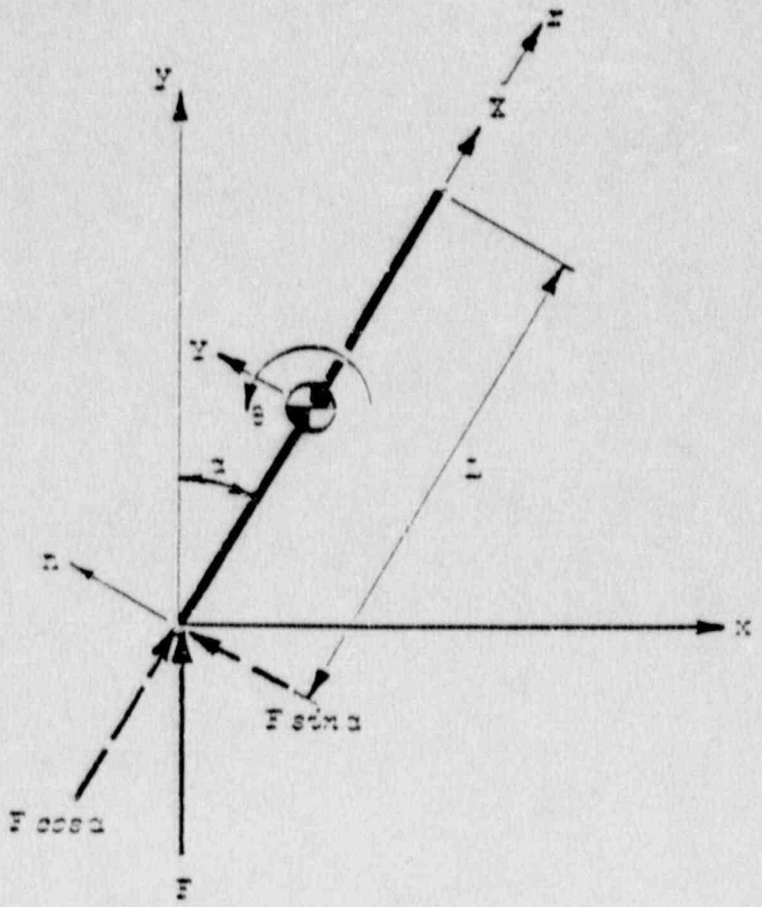

For a planar rigid body system, the behavior is totally defined by a solution of the three equations of equilibrium written at the center of gravity of the rigid body. In the preceding figure, local coordinates are defined at the center of gravity, with axes parallel and normal to the beam. The end impact force is resolved into components parallel to these local axes. Summation of forces at the center of gravity leads to three rigid body equations of motion:

$$\text{Sum of Lateral Forces} - M(\partial^2 Y/\partial t^2) = F(\sin \alpha)$$

$$\text{Sum of Longitudinal Forces} - M(\partial^2 X/\partial t^2) = F(\cos \alpha)$$

$$\text{Sum of Moments} - I(\partial^2 \theta/\partial t^2) = -FL(\sin \alpha)/2$$

Where:

$M = \rho L$, the mass of the body

$I = \rho L^3/12$, the mass moment of inertia of the body

ρ = the mass per unit length of the body

α = the orientation angle with respect to vertical

Note that the mass moment of inertia term given above is valid only for infinitely slender beams of mass. A more accurate mass moment approximation is provided by the equation:

$$I = \rho L(3R^2 + L^2)/12$$

Where:

R = the radius of the cylindrical cask

This increased mass moment of inertia demonstrably decreases the internal moment. Thus, all moments calculated using the slender body approximation are conservative in proportion to the degree with which the cask is not slender. A very squat cask would have an internal moment predicted by OBLIQUE considerably higher than reality.

Substituting for the mass and inertia terms:

$$\partial^2 Y/\partial t^2 = F(\sin \alpha)/\rho L$$

$$\partial^2 X/\partial t^2 = F(\cos \alpha)/\rho L$$

$$\partial^2 \theta/\partial t^2 = -6F(\sin \alpha)/\rho L^2$$

The lateral and longitudinal accelerations at a point 'r' are:

$$\partial^2 S_n/\partial t^2 = \partial^2 Y/\partial t^2 + [r - (L/2)](\partial^2 \theta/\partial t^2)$$

$$= [F(\sin \alpha)/\rho L^2]\{L - 6[r - (L/2)]\}$$

$$= [2F(\sin \alpha)/\rho L^2](-3r + 2L)$$

$$\partial^2 S_r/\partial t^2 = \partial^2 X/\partial t^2 = F(\cos \alpha)/\rho L$$

The lateral inertial force acting on the body at the r^{th} location is:

$$\partial V_r/\partial r = -\rho(\partial^2 S_n/\partial t^2)$$

The corresponding expression for shear is found by integrating this lateral force from the free end to the r^{th} location, or:

$$V_r = [-2F(\sin \alpha)/L^2] \int_L^r (-3r + 2L)\, dr$$

$$= [-2F(\sin \alpha)/L^2]\{-3(r^2 - L^2)/2 + 2L(r - L)\}$$

Rearranging,

$$V_r = [-2F(\sin \alpha)/L^2]\{-3r^2/2 + 3L^2/2 + 2Lr - 2L^2\}$$

$$= [F(\sin \alpha)/L^2][3r^2 - 4Lr + L^2]$$

Similarly, the corresponding moment is found by integration of the shear expression:

$$\partial M_r/\partial r = V_r$$

$$M_r = [F(\sin\alpha)/L^2] \int_L^r (3r^2 - 4Lr + L^2)\, dr$$

$$= [F(\sin\alpha)/L^2]((r^3 - L^3) - 2L(r^2 - L^2) + L^2(r - L))$$

Rearranging,

$$M_r = [F(\sin\alpha)/L^2](r^3 - L^3 - 2Lr^2 + 2L^3 + L^2r - L^3)$$

$$= [F(\sin\alpha)/L^2][r^3 - 2Lr^2 + L^2r]$$

In order to verify these expressions for shear and moment, they are evaluated at the boundaries, r = 0 and r = L:

At r = 0:

$$V_r = [F(\sin\alpha)/L^2][3r^2 - 4Lr + L^2]$$

$$= [F(\sin\alpha)/L^2][L^2] = F(\sin\alpha)$$

$$M_r = [F(\sin\alpha)/L^2][r^3 - 2Lr^2 + L^2r] = 0$$

At r = L:

$$V_r = [F(\sin\alpha)/L^2][3r^2 - 4Lr + L^2]$$

$$= [F(\sin\alpha)/L^2][3L^2 - 4L^2 + L^2] = 0$$

$$M_r = [F(\sin\alpha)/L^2][r^3 - 2Lr^2 + L^2r]$$

$$= [F(\sin\alpha)/L^2][L^3 - 2L^3 + L^3] = 0$$

The maximum moment occurs where the shear, V_r, equals zero. For this to occur, the quadratic term in the shear equation must be solved.

$$0 = 3r^2 - 4Lr + L^2$$

$$r = \{4L \pm [16L^2 - 4(3)L^2]^{0.5}\}/6$$

$$= (4L \pm 2L)/6 = L,\ L/3$$

The maximum moment is found at $r = L/3$, or

$$M_{max} = [F(\sin \alpha)/L^2][L^3/27 - 2L^3/9 + L^3/3]$$

$$= 4FL(\sin \alpha)/27 \quad \text{at } r = L/3$$

The minimum shear occurs where the lateral force equals zero. For this to occur, the linear term in the lateral force equation must be solved.

$$\partial V_r/\partial r = [-2F(\sin \alpha)/L^2][-3r + 2L] = 0$$

$$r = 2L/3$$

The magnitude of the axial (thrust) force can be found as a function of location as:

$$\partial T/\partial r = -\rho(\partial^2 S_r/\partial t^2)$$

$$T = -\rho(\partial^2 S_r/\partial t^2) \int_L^r dr = -\rho(\partial^2 S_r/\partial t^2)(r - L)$$

Then,

$$T = F(\cos \alpha)[1 - (r/L)]$$

For convenience, the package internal forces are summarized below:

PARAMETER	EQUATION	MAXIMUM	MINIMUM
Thrust	$F(\cos \alpha)[1 - (r/L)]$	$F(\cos \alpha)$ $(r = 0)$	0 $(r = L)$
Shear	$F(\sin \alpha)[3r^2 - 4Lr + L^2]/L^2$	$F(\sin \alpha)$ $(r = 0)$	0 $(r = L/3, L)$
Moment	$F(\sin \alpha)[r^3 - 2Lr^2 + L^2r]/L^2$	$4FL(\sin \alpha)/27$ $(r = L/3)$	0 $(r = 0, L)$

These forces are graphically illustrated below:

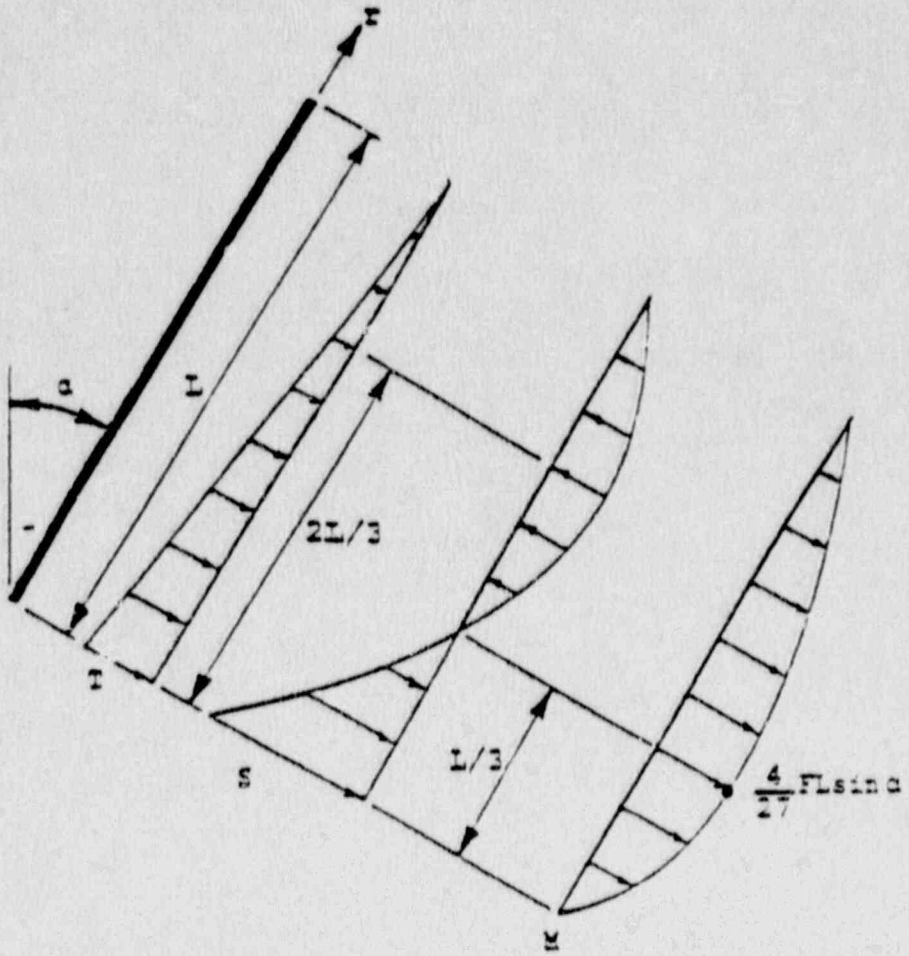

2.10.5.3 Sample Program Input and Output

This section contains sample input and output tables for the computer codes EYDROP, SYDROP, CYDROP and OBLIQUE. As a descriptive illustration, assume a package with the geometry described below in Figure 2.10.5.3-1.

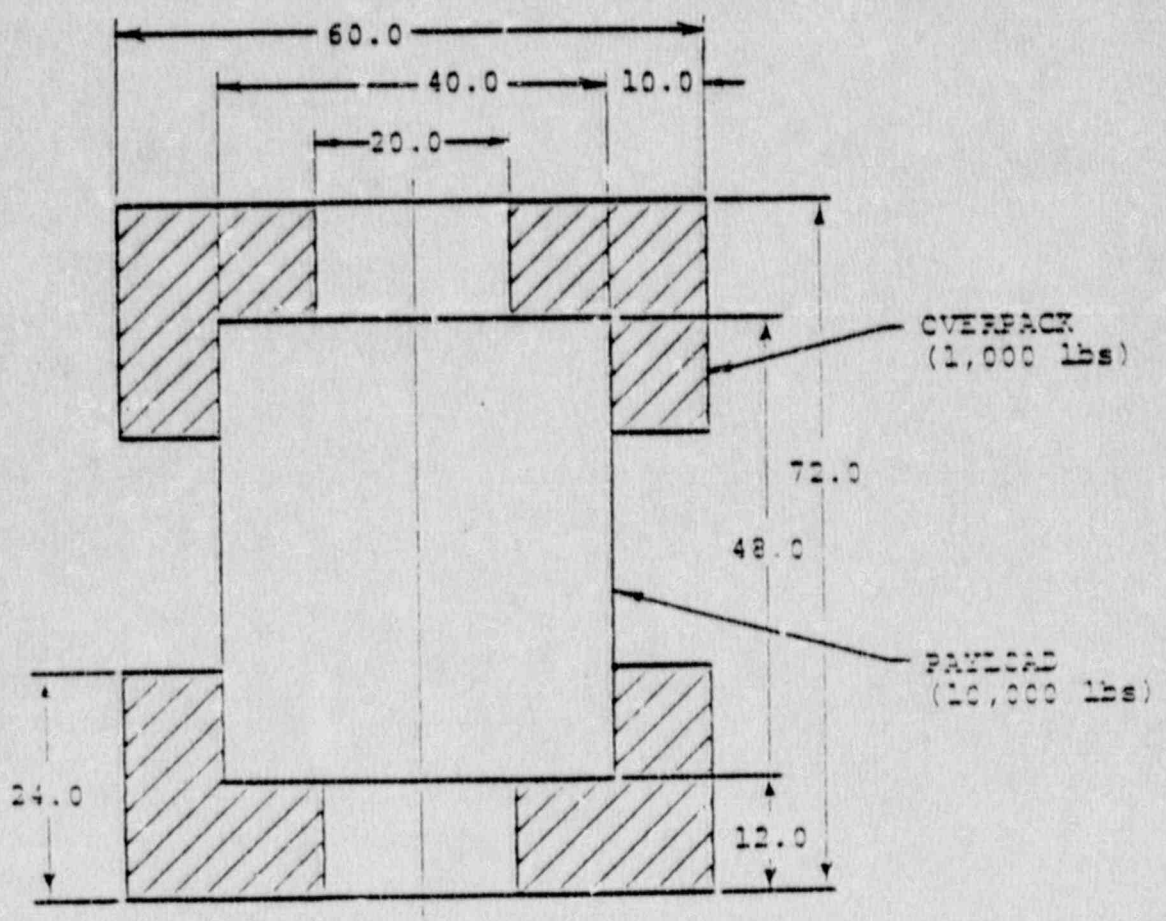

FIGURE 2.10.5.3-1
Sample Problem Package Geometry

2.10.5.3.1 End Drop Sample Problem

Table 2.10.5.3-1 contains the data input to EYDROP for the above geometry.

```
PROGRAM EYDROP, VERSION 2, DATE 5/11/81
12345678901234567890123456789012345678901234567890123456789012345678901234567890
         V         V         V         V         V         V         V         V
EYDROP (END DROP) SAMPLE RUN, 20 PCF FOAM OVERPACKS
    12000.       60.       20.       12.       30.
       .2        3.        .2
  17
      0.00      0.00
      0.05    668.00
      0.10   1337.00
      0.15   1345.00
      0.20   1315.00
      0.25   1347.00
      0.30   1411.00
      0.35   1507.00
      0.40   1673.00
      0.45   1901.00
      0.50   2204.00
      0.55   2627.00
      0.60   3283.00
      0.65   4242.00
      0.70   5908.00
      0.75   9058.00
      0.80  15322.00
```

TABLE 2.10.5.3-1

EYDROP Input Table

A summary of each card is as follows:

Card 1 Problem Title

Card 2 Package weight, package diameter, impact limiter hole diameter, impact limiter end thickness, drop height.

Card 3 Starting crush depth iteration, ending iteration, increment.

Card 4 Number of foam curve data points.

Card 5-N Foam strain, foam crush stress.

All the required input parameters are straightforward. Table 2.10.5.3-2 contains the sample problem output. Information from this table is essentially self-explanatory. A solution is determined when the kinetic energy of the drop is equal to the strain energy (SE/KE = 1) from crushing the foam impact limiters.

EYDROP(END) EYDROP (END DROP) SAMPLE RUN, 20 PCF FOAM OVERPACKS

PACKAGE WEIGHT = 12000. (LBS)
PACKAGE DIAMETER = 60.00 (IN)
HOLE DIAMETER = 20.00 (IN)
OVERPACK DEPTH = 12.00 (IN)
DROP HEIGHT = 30.00 (FT)

CRUSH DEPTH (IN)	STRAIN	←— IMPACT —→ FORCE (LBS)	ACCEL. (G)	←—— ENERGY ——→ KINETIC (IN-LB)	STRAIN (IN-LB)	RATIO (SE/KE)
.20	.017	456640.	38.1	4322400.	45664.	.011
.40	.033	1036803.	86.4	4324800.	195003.	.045
.60	.050	1678367.	139.9	4327200.	466575.	.108
.80	.067	2221210.	193.4	4329600.	866583.	.200
1.00	.083	2902211.	241.9	4332000.	1388925.	.321
1.20	.100	3360248.	280.0	4334400.	2015171.	.465
1.40	.117	3474214.	289.5	4336800.	2698617.	.622
1.60	.133	3461585.	288.5	4339200.	3392197.	.782
1.80	.150	3380354.	281.7	4341600.	4076391.	.939
2.00	.167	3353421.	279.5	4344000.	4749769.	1.093
2.20	.183	3325186.	277.1	4346400.	5417629.	1.246
2.40	.200	3304955.	275.4	4348800.	6080643.	1.398
2.60	.217	3318173.	276.5	4351200.	6742956.	1.550
2.80	.233	3345913.	278.8	4353600.	7409365.	1.702

TABLE 2.10.5.3-2

EYDROP Output

In this case, a linear interpolation of the SE/KE ratio results in a crush depth of approximately 1.38 inches and an acceleration of almost 281 g's. Equations for SYDROP are discussed in Section 2.10.5.1.1.

2.10.5.3.2 Side Drop Sample Problem

Table 2.10.5.3-3 contains the data input to SYDROP for the sample problem package geometry.

```
PROGRAM SYDROP, VERSION 3, DATE 1/28/85
1234567890123456789012345678901234567890123456789012345678901234567890
         V         V         V         V         V         V         V
SYDROP (SIDE DROP) SAMPLE RUN, 20 PCF FOAM OVERPACKS
    12000.       48.       60.       40.       30.
   17
       0.00       0.00
       0.05     668.00
       0.10    1337.00
       0.15    1345.00
       0.20    1315.00
       0.25    1347.00
       0.30    1411.00
       0.35    1507.00
       0.40    1673.00
       0.45    1901.00
       0.50    2204.00
       0.55    2623.00
       0.60    3288.00
       0.65    4242.00
       0.70    5908.00
       0.75    9058.00
       0.80   15322.00
  150   .25   6.0   .25
```

TABLE 2.10.5.3-3

SYDROP Input Table

A summary of each card is as follows:

Card 1 Problem Title

Card 2 Package weight, impact limiter length, package diameter, payload diameter, drop height.

Card 3 Number of foam curve data points.

Card 4-N Foam strain, foam crush stress

Card N+1 Number of integration points, starting crush depth iteration, ending iteration, increment.

As with the end drop problem, all required input parameters are straightforward. The chosen number of integration points (150) is based upon previous parametric study for the side drop geometry. Increasing the number will alter the end results by only a fraction of one percent. As with EYDROP, a solution is determined when the kinetic energy of the drop is equal to the strain energy from crushing the foam impact limiters. Table 2.10.5.3-4 contains the SYDROP output. Equations for SYDROP are discussed in Section 2.10.5.1.2.

TABLE 2.10.5.3-4

SYDROP Output

SYDROP(SIDE) N U C L E A R P A C K A G I N G P R O P R I E T A R Y 18.09.39 85/03/16 PAGE 1

SYDROP (SIDE DROP) SAMPLE RUN, 2" PCF FOAM OVERPACKS

PACKAGE WEIGHT	=	32000. (LBS)
PACKAGE EXTERNAL LENGTH	=	48.00 (IN)
PACKAGE EXTERNAL DIAMETER	=	68.40 (IN)
PAYLOAD DIAMETER	=	40.00 (IN)
DROP HEIGHT	=	30.00 (FT)

STRAIN VS STRESS TABLE

PT	STRAIN	STRESS
1	0.00	0.00
2	.05	668.00
3	.10	1337.00
4	.15	1345.00
5	.20	1315.00
6	.25	1347.00
7	.30	1411.00
8	.35	1507.00
9	.40	1673.00
10	.45	1901.00
11	.50	2204.00
12	.55	2623.00
13	.60	3288.00
14	.65	4242.00
15	.70	5908.00
16	.75	9058.00
17	.80	15322.00

SYDROP(SIDE) N U C L E A R P A C K A G I N G P R O P R I E T A R Y 18.09.39 85/03/16 PAGE 2

SYDROP (SIDE DROP) SAMPLE RUN, 20 PCF FOAM OVERPACKS

CRUSH DEPTH (IN)	** CRUSH PLANE ** AREA (IN2)	VOLUME (IN3)	**** IMPACT **** FORCE (LBS)	ACCEL. (G)	****** ENERGY ****** POTENTIAL (IN-LB)	STRAIN (IN-LB)	RATIO (SE/PE)	DISTRIBUTION OF STRAIN RATIOS BY PERCENT OF CONTACT AREA LE.70	GT.70 LE.80	GT.80 LE.90	GT.90 LE.95	GT.95
[illegible]	371.0	62.	82679.	6.9	4323000.	10310.	.002	100.00	0.00	0.00	0.00	0.00
[illegible]	523.6	175.	232410.	19.4	4326000.	49671.	.011	100.00	0.00	0.00	0.00	0.00
[illegible]	639.9	[illegible]	449672.	37.5	4329000.	134931.	.031	100.00	0.00	0.00	0.00	0.00
1.00	[illegible]	403.	675582.	56.[illegible]	4332000.	273588.	.064	100.00	0.00	0.00	0.00	0.00
[illegible]	822.[illegible]	688.	857486.	[illegible]	4335000.	467222.	.108	100.00	0.00	0.00	0.00	0.00
[illegible]	909.[illegible]	904.	989341.	82.4	4338000.	698075.	.161	100.00	0.00	0.00	0.00	0.00
[illegible]	[illegible]9.3	[illegible]	1096877.	91.[illegible]	4341000.	958852.	[illegible]	100.00	0.00	0.00	0.00	0.00
2.00	1034.[illegible]	1388.	1191309.	99.3	4344000.	1244887.	.287	100.00	0.00	0.00	0.00	0.00
[illegible]	1094.[illegible]	1654.	1281336.	106.8	4347000.	1553979.	.357	100.00	0.00	0.00	0.00	0.00
[illegible]	1151.0	1935.	1370454.	114.2	4350000.	1885452.	.433	100.00	0.00	0.00	0.00	0.00
[illegible]	1204.6	[illegible]	1459288.	121.6	4353000.	2239170.	.514	100.00	0.00	0.00	0.00	0.00
3.00	[illegible]	[illegible]	1549023.	129.[illegible]	4356000.	2615209.	.600	100.00	0.00	0.00	0.00	0.00
[illegible]	1303.5	2857.	1640286.	136.[illegible]	4359000.	3013873.	.691	100.00	0.00	0.00	0.00	0.00
[illegible]	1350.0	3189.	1735198.	144.6	4362000.	3435808.	.788	100.00	0.00	0.00	0.00	0.00
[illegible]	1394.[illegible]	3532.	1837541.	153.1	4365000.	3882401.	.889	100.00	0.00	0.00	0.00	0.00
4.00	1436.8	3886.	1949171.	162.4	4368000.	4335740.	.997	100.00	0.00	0.00	0.00	0.00
4.01	1437.8	3895.	1952158.	162.7	4368074.	4368082.	1.000	100.00	0.00	0.00	0.00	0.00
4.25	1477.[illegible]	4250.	2070772.	172.6	4371000.	4858233.	1.111	100.00	0.00	0.00	0.00	0.00
4.50	1517.[illegible]	4624.	2203828.	183.[illegible]	4374000.	5392358.	1.233	100.00	0.00	0.00	0.00	0.00
[illegible]	1555.[illegible]	5008.	2349512.	195.8	4377000.	[illegible]	1.362	100.00	0.00	0.00	0.00	0.00
5.00	1592.[illegible]	5402.	2510461.	209.2	4380000.	[illegible]	1.500	100.00	0.00	0.00	0.00	0.00
[illegible]	1627.[illegible]	5804.	2688622.	224.1	4383000.	7219177.	1.647	100.00	0.00	0.00	0.00	0.00
[illegible]	1662.[illegible]	6216.	2890243.	240.9	4386000.	7916465.	1.805	100.00	0.00	0.00	0.00	0.00
[illegible]	1695.[illegible]	6635.	3125496.	260.5	4389000.	8668433.	1.975	100.00	0.00	0.00	0.00	0.00
6.00	1728.[illegible]	7063.	3401972.	283.3	4392000.	9484364.	2.159	100.00	0.00	0.00	0.00	0.00

2.10.5.3.3 Corner Drop Sample Problem

Table 2.10.5.3-5 contains the data input to CYDROP for the sample problem package geometry.

```
PROGRAM CYDROP, VERSION 3, DATE 2/07/84
12345678901234567890123456789012345678901234567890123456789012345678901234567890
         V         V         V         V         V         V         V
CYDROP (CORNER DROP) SAMPLE RUN, 20 PCF FOAM OVERPACKS
    12000.       72.       60.       48.       40.       20.       24.
       30.     39.8
     1100.   17
      0.00      0.00
      0.05    668.00
      0.10   1337.00
      0.15   1345.00
      0.20   1315.00
      0.25   1347.00
      0.30   1411.00
      0.35   1507.00
      0.40   1673.00
      0.45   1901.00
      0.50   2204.00
      0.55   2623.00
      0.60   3238.00
      0.65   4242.00
      0.70   5908.00
      0.75   9058.00
      0.80  15322.00
  25   25.512 15.37 .512
```

TABLE 2.10.5.3-5
CYDROP Input Table

A summary of each card is as follows:

Card 1 Problem Title

Card 2 Package weight, package length, package diameter, payload length, payload diameter, impact limiter hole diameter, impact limiter length.

Card 3 Drop height, angle from vertical.

Card 4 Unbacked foam crush stress, number of foam curve data points.

Card 5-N Foam strain, foam crush stress.

Card N+1 Number of integration points along crush plane semi-minor ellipse axis, number of integration points along crush plane semi-major ellipse axis, starting crush depth iteration, ending iteration, increment.

The angle from vertical to execute a center of gravity over struck corner impact is calculated as:

$$\theta = \tan^{-1}(60.0/72.0) = 39.8^{\circ}$$

The unbacked foam crush stress is the foam compressive yield strength, about 1,100 psi for the 20 pcf foam. Program default for this entry is to assume the foam crush stress at 10% strain, a value usually close to the plateau compressive strength.

Similar to SYDROP, the number of integration points chosen for CYDROP (25) have been determined from a parametric evaluation. Additional points are unnecessarily time consuming and provide very little change in the end results.

Table 2.10.5.3-6 contains the CYDROP output for the sample problem. CYDROP also calculates the percentage of foam in the crush area less than and greater than 80% foam strain in the backed and unbacked regions. The foam data used in the drop analyses provide accurate empirical relationships to 80% strain. This calculation is carried into the force and strain energy results to provide the program user with information on solution reliability.

Energy equilibrium for the sample problem may be linearly interpolated to a crush depth of about 10.6 inches and an acceleration of 106.5 g's. The distribution of strain energy ratios for this problem indicate the foam stress data interpolated from the input file never exceeded 70% strain.

Linear interpolation of the sensitivity analysis shows approximately 24.5% of the total crush area was unbacked. Additionally, further interpolation shows the unbacked foam accounted for about 17.5% of the total force and 8.7% of the strain energy at SE/KE = 1. Equations for CYDROP are discussed in Section 2.10.5.1.3.

TABLE 2.10.5.3-6

CYDROP Output

CYDROP(CORNER) NUCLEAR PACKAGING PROPRIETARY 10.11.19 84/02/14 PAGE 1

CYDROP (CORNER DROP) SAMPLE RUN. 20 PCF FOAM OVERPACKS

PACKAGE WEIGHT = 12000. (LBS)
PACKAGE EXTERNAL LENGTH = 72.00 (IN)
PACKAGE EXTERNAL DIAMETER = 60.00 (IN)
PACKAGE EXTERNAL HOLE DIA = 20.00 (IN)
PAYLOAD ENVELOPE LENGTH = 48.00 (IN)
PAYLOAD ENVELOPE DIAMETER = 40.00 (IN)
OVERPACK LENGTH = 24.00 (IN)

DROP HEIGHT = 30.00 (FT)
ORIENTATION ANGLE = 39.800 (DEGREES WRT TO VERTICAL)

PLATEAU CRUSH STRESS = 1100.00 (PSI)
(DEFAULT TAKEN AT 10 PCT STRAIN)

STRESS/STRAIN EVALUATED IN 1/2 CRUSH PLANE ELLIPSE AT:
NX = 25 POINTS PARALLEL TO SEMI-MINOR ELLIPSE AXIS
NY = 25 POINTS PARALLEL TO SEMI-MAJOR ELLIPSE AXIS

EXPERIMENTAL STRAIN VS. STRESS VALUES

PT	STRAIN	STRESS
1	0.00	0.00
2	.05	668.00
3	.10	1337.00
4	.15	1345.00
5	.20	1318.00
6	.25	1347.00
7	.30	1411.00
8	.35	1507.00
9	.40	1673.00
10	.45	1901.00
11	.50	2204.00
12	.55	2623.00
13	.60	3238.00
14	.65	4242.00
15	.70	5968.00
16	.75	9058.00
17	.80	15322.00

TABLE 2.10.5.8-6

CYDROP Output

(continued)

CYDROP(CORNER) N U C L E A R P A C K A G I N G P R O P R I E T A R Y 10.11.20 84/02/14 PAGE 2

CYDROP (CORNER DROP) SAMPLE RUN, 20 PCF FOAM OVERPACKS

CRUSH DEPTH (IN)	CRUSH PLANE AREA (IN2)	CRUSH PLANE VOLUME (IN3)	IMPACT FORCE (LBS)	IMPACT ACCEL. (G)	ENERGY KINETIC (IN-LB)	ENERGY STRAIN (IN-LB)	ENERGY RATIO (SE/KE)	DISTRIBUTION OF STRAIN RATIOS BY PERCENT OF CONTACT AREA LE.70	GT.70 LE.80	GT.80 LE.90	GT.90 LE.95	GT.95
.51	9.6	2.	1386.	.1	4326144.	355.	.000	100.00	0.00	0.00	0.00	0.00
1.02	[illegible]	12.	8775.	.7	4332288.	2956.	.001	100.00	0.00	0.00	0.00	0.00
1.54	49.0	31.	25334.	2.1	4338432.	11688.	.003	100.00	0.00	0.00	0.00	0.00
2.05	74.9	63.	51131.	4.3	4344576.	31263.	.007	100.00	0.00	0.00	0.00	0.00
2.56	103.9	109.	83237.	6.9	4350720.	65666.	.015	100.00	0.00	0.00	0.00	0.00
3.07	133.6	170.	119934.	10.0	4356864.	117683.	.027	100.00	0.00	0.00	0.00	0.00
3.58	169.6	248.	160452.	13.4	4363008.	189462.	.043	100.00	0.00	0.00	0.00	0.00
4.10	205.7	344.	204557.	17.0	4369152.	282904.	.065	100.00	0.00	0.00	0.00	0.00
4.61	243.6	459.	252250.	21.0	4375296.	399847.	.091	100.00	0.00	0.00	0.00	0.00
5.12	283.1	594.	304305.	25.6	4381440.	542325.	.124	100.00	0.00	0.00	0.00	0.00
5.63	324.1	749.	361485.	30.1	4387584.	712767.	.162	100.00	0.00	0.00	0.00	0.70
6.14	366.4	926.	422256.	35.2	4393728.	913405.	.208	100.00	0.00	0.00	0.00	0.00
6.66	409.8	1125.	490795.	40.9	4399872.	1147146.	.261	100.00	0.00	0.00	0.00	0.00
7.17	454.3	1346.	568073.	47.3	4406016.	1418216.	.322	100.00	0.00	0.00	0.00	0.00
7.68	499.7	1590.	648625.	54.1	4412160.	1729691.	.392	100.00	0.00	0.00	0.00	0.00
8.19	545.9	1858.	736216.	61.4	4418304.	2084210.	.472	100.00	0.00	0.00	0.00	0.00
8.70	592.3	2149.	826311.	68.9	4424448.	2484217.	.561	100.00	0.00	0.00	0.00	0.00
9.22	640.2	2463.	927107.	77.3	4430592.	2933092.	.662	100.00	0.00	0.00	0.00	0.00
9.73	688.2	2805.	1046738.	87.2	4436736.	3438397.	.775	100.00	0.00	0.00	0.00	0.00
10.24	736.6	3170.	1181164.	98.6	4442880.	4008740.	.902	100.00	0.00	0.00	0.00	0.00
10.75	785.3	3560.	1322256.	110.2	4449024.	4649615.	1.045	100.00	0.00	0.00	0.00	0.00
11.26	834.2	3976.	1483405.	123.6	4455168.	5367864.	1.205	99.33	.67	0.00	0.00	0.00
11.78	883.3	4414.	1678677.	139.9	4461312.	6177357.	1.385	98.69	1.31	0.00	0.00	0.00
12.29	932.4	4879.	1920373.	160.0	4467456.	7098714.	1.589	96.31	3.69	0.00	0.00	0.00
12.80	981.5	5369.	2246590.	187.2	4473600.	8165457.	1.825	95.07	4.49	.44	0.00	0.00
13.31	1030.5	5884.	2652834.	221.4	4479744.	9419709.	2.103	92.95	5.75	1.30	0.00	0.00
13.82	1079.4	6424.	3155349.	262.9	4485888.	10906604.	2.431	91.07	6.12	2.82	0.00	0.00
14.34	1128.0	6989.	3762296.	313.5	4492032.	12677321.	2.822	88.97	6.72	4.39	.22	0.00
14.85	1176.2	7579.	4496986.	374.7	4498176.	14791897.	3.288	87.74	6.26	4.70	1.30	0.00
15.36	1224.0	8193.	5345237.	445.4	4504320.	17311506.	3.843	85.88	6.02	6.15	1.37	.37

CYDROP(CORNER) N U C L E A R P A C K A G I N G P R O P R I E T A R Y 10.11.27 84/02/14 PAGE 3

CYDROP (CORNER DROP) SAMPLE RUN, 20 PCF FOAM OVERPACKS

SENSITIVITY ANALYSIS OF STRAIN ASSUMPTIONS

CRUSH DEPTH (IN)	CRUSH AREA TOTAL AREA (IN2)	CRUSH AREA PCT DISTRIBUTION UN-BACKED	BACKED MAX STRAIN LT .800	BACKED MAX STRAIN GT .800	IMPACT FORCE TOTAL FORCE (LBS)	IMPACT FORCE PCT DISTRIBUTION UN-BACKED	BACKED MAX STRAIN LT .800	BACKED MAX STRAIN GT .800	STRAIN ENERGY TOTAL STRAIN ENERGY (IN-LBS)	STRAIN ENERGY PCT DISTRIBUTION UN-BACKED	BACKED MAX STRAIN LT .800	BACKED MAX STRAIN GT .800	STRAIN TO KINETIC ENERGY RATIO
.51	10.	0.0	100.0	0.0	1386.	0.0	100.0	0.0	355.	0.0	100.0	0.0	0.000
1.02	27.	0.0	100.0	0.0	8775.	0.0	100.0	0.0	2956.	0.0	100.0	0.0	.001
1.54	49.	0.0	100.0	0.0	25334.	0.0	100.0	0.0	11688.	0.0	100.0	0.0	.003
2.05	76.	0.0	100.0	0.0	51131.	0.0	100.0	0.0	31263.	0.0	100.0	0.0	.007
2.56	105.	0.0	100.0	0.0	83237.	0.0	100.0	0.0	65666.	0.0	100.0	0.0	.015
3.07	128.	0.0	100.0	0.0	119934.	0.0	100.0	0.0	117683.	0.0	100.0	0.0	.027
3.58	173.	0.0	100.0	0.0	160452.	0.0	100.0	0.0	189462.	0.0	100.0	0.0	.043
4.10	[illegible]	0.0	100.0	0.0	204557.	0.0	100.0	0.0	282904.	0.0	100.0	0.0	.065
4.61	[illegible]	0.0	100.0	0.0	252250.	0.0	100.0	0.0	399847.	0.0	100.0	0.0	.091
5.12	292.	.3	99.7	0.0	304305.	.3	99.7	0.0	542325.	0.0	100.0	0.0	.124
5.63	335.	1.0	99.0	0.0	361485.	1.0	99.0	0.0	712767.	.2	99.8	0.0	.162
6.14	380.	1.5	98.5	0.0	422256.	1.5	98.5	0.0	913405.	.4	99.6	0.0	.208
6.66	427.	2.9	97.1	0.0	490795.	2.7	97.3	0.0	1147146.	.8	99.2	0.0	.261
7.17	475.	5.5	94.5	0.0	568073.	5.0	95.0	0.0	1418216.	1.4	98.6	0.0	.322
7.68	524.	7.2	92.8	0.0	648625.	6.4	91.6	0.0	1729691.	2.2	97.8	0.0	.392
8.19	575.	10.6	89.4	0.0	736216.	9.1	90.9	0.0	2084210.	3.1	96.9	0.0	.472
8.70	626.	12.4	87.6	0.0	826311.	10.3	89.7	0.0	2484217.	4.2	95.8	0.0	.561
9.22	679.	[illegible]	[illegible]	0.0	927107.	11.9	88.1	0.0	2933092.	5.3	94.7	0.0	.662
9.73	[illegible]	19.0	81.0	0.0	1046738.	14.6	85.4	0.0	3438397.	6.4	93.6	0.0	.775
10.24	788.	[illegible]	[illegible]	0.0	1181164.	16.7	83.3	0.0	4008740.	7.8	92.2	0.0	.902
10.75	844.	[illegible]	74.[illegible]	0.0	1322256.	17.8	82.2	0.0	4649615.	9.1	90.9	0.0	1.045
11.26	900.	[illegible]	69.[illegible]	0.0	1483405.	[illegible]	79.3	0.0	5367864.	10.4	89.6	0.0	[illegible]
11.78	957.	[illegible]	67.5	0.0	1678677.	[illegible]	79.3	0.0	6177357.	11.7	88.[illegible]	0.0	[illegible]
12.29	1015.	[illegible]	63.[illegible]	0.0	1920373.	[illegible]	78.5	0.0	7098714.	12.9	87.[illegible]	0.0	[illegible]
12.80	1074.	[illegible]	62.[illegible]	[illegible]	2246590.	19.4	[illegible]	3.3	8165457.	13.3	85.[illegible]	[illegible]	[illegible]
13.31	[illegible]	[illegible]	[illegible]	[illegible]	2652834.	28.1	71.6	10.[illegible]	9419709.	14.3	84.[illegible]	[illegible]	[illegible]
13.82	[illegible]	[illegible]	55.[illegible]	[illegible]	3155349.	[illegible]	62.3	20.[illegible]	10906604.	14.9	81.9	[illegible]	[illegible]
14.34	[illegible]	43.9	[illegible]	[illegible]	3762296.	[illegible]	[illegible]	30.4	12677321.	[illegible]	78.3	[illegible]	[illegible]
14.85	1259.	44.1	49.7	6.0	4496986.	[illegible]	46.8	39.3	14791897.	[illegible]	74.4	10.[illegible]	3.288
15.36	1341.	45.4	46.3	[illegible]	5345237.	[illegible]	38.3	48.9	17311506.	14.3	69.7	[illegible]	3.843

2.10.5.3.4 Oblique Impact Sample Input

Table 2.10.5.3-7 contains the data input to OBLIQUE for the sample problem package geometry. Equations for OBLIQUE are discussed in Section 2.10.5.2.

```
PROGRAM OBLIQUE VERSION 7, DATE 9/15/83
12345678901234567890123456789012345678901234567890123456789012345678901234567890
         V         V         V         V         V         V         V         V
OBLIQUE SAMPLE RUN, 20 PCF FOAM OVERPACKS
      48.       20.       24.       10.       12.
  31.056     12574.    386.4
     .25       12.       .25       10.       10.
      5.       10.       20.       30.       40.       50.
      60.       70.       80.       85.
 -527.45       85.        5.       -5.        0.        3.
```

TABLE 2.10.5.3-7
OBLIQUE Input Table

A summary of each card is as follows:

Card 1 Problem title

Card 2 Payload length, payload radius, impact limiter length, impact limiter side thickness, impact limiter end thickness.

Card 3 Package mass, radial mass moment of inertia about the center of gravity, gravitational acceleration.

Card 4 Starting deflection, ending deflection, deflection increment, number of angles, print control.

Card 5-N Angles (6 per card, 24 maximum)

Card N+1 Package free-fall velocity, output starting angle, output ending angle, angle increment, friction coefficient, estimated deflection, package translational velocity, package rotational velocity.

The package mass, assuming a gravitation acceleration of 386.4 in/sec^2, is:

$$m = 12{,}000/386.4 = 31.056 \text{ lb-sec}^2/\text{in}$$

The radial mass moment of inertia of the system is calculated, knowing the payload and impact limiter weights, using composite sections:

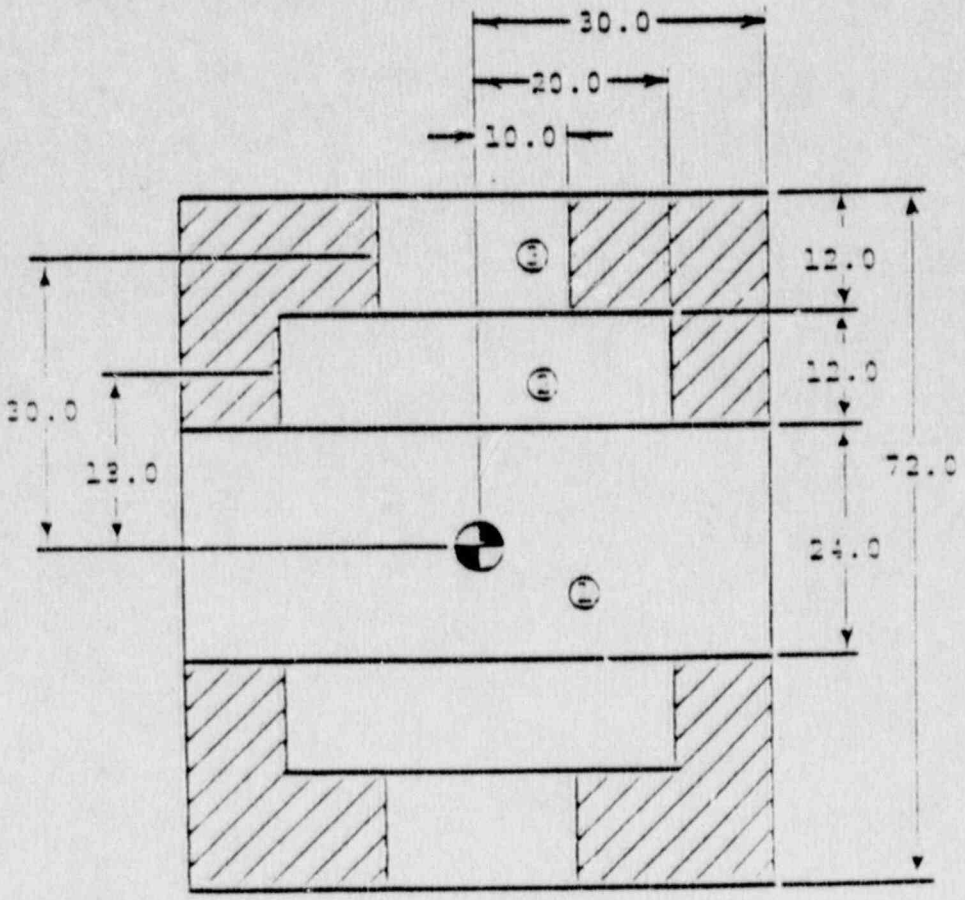

For the Payload:

$$I_p = m(R^2 + L^2/3)/4$$

Where:

$$m = 10,000/386.4 = 25.88 \text{ lb-sec}^2/\text{in}$$

$$R = 40.0/2 = 20.0 \text{ in}$$

$$L = 48.0 \text{ in}$$

Then,

$$I_p = 25.88[(20.0)^2 + (48.0)^2/3]/4$$

$$= 7,557 \text{ lb-in-sec}^2$$

For the impact limiters:

$$I_{op} = m[R^2 + (L^2/3)]/4 - m_1[R_1^2 + (L_1^2/3)]/4 - 2m_2[R_2^2 + (L_2^2/3)]/4 - 2m_2d_2^2 - 2m_3[R_3^2 + (L_2^2/3)]/4 - 2m_3d_3^2$$

Where:

$$m = \bar{m}\pi R^2 L$$

$$\bar{m} = W_{op}/(386.4)V_{op}$$

$$W_{op} = 1,000 \text{ lbs}$$

$$V_{op} = \pi[(30.0)^2 - (20.0)^2]24.0 + \pi[(20.0)^2 - (10.0)^2]12.0$$

$$= 49,009 \text{ in}^3$$

$$\bar{m} = 1,000/[(386.4)49,009] = 5.28(10)^{-5} \text{ lb-sec}^2/\text{in}^4$$

$R = 30.0$ in

$L = 72.0$ in

$m = [5.28(10)^{-5}]\pi(30.0)^2(72.0) = 10.75$ lb-sec^2/in

$m_1 = \bar{m}\pi R_1^2 L_1$

$R_1 = 30.0$ in

$L_1 = 24.0$ in

$m_1 = [5.28(10)^{-5}]\pi(30.0)^2(24.0) = 3.583$ lb-sec^2/in

$m_2 = \bar{m}\pi R_2^2 L_2$

$R_2 = 20.0$ in

$L_2 = 12.0$ in

$m_2 = [5.28(10)^{-5}]\pi(20.0)^2(12.0) = 0.7962$ lb-sec^2/in

$m_3 = \bar{m}\pi R_3^2 L_3$

$R_3 = 10.0$ in

$L_3 = 12.0$ in

$m_3 = [5.28(10)^{-5}]\pi(10.0)^2(12.0) = 0.1991$ lb-sec^2/in

$d_2 = 18.0$ in

$d_3 = 30.0$ in

Then,

$$I_{op} = 10.75[(30.0)^2 + (72.0)^2/3]/4 - 3.583[(30.0)^2 + (24.0)^2/3]/4$$
$$- 2(0.7962)[(20.0)^2 + (12.0)^2/3]/4 - 2(0.7962)(18.0)^2$$
$$- 2(0.1991)[(10.0)^2 + (12.0)^2/3]/4 - 2(0.1991)(30.0)^2$$

$$= 5,017 \text{ lb-in-sec}^2$$

Finally,

$$I = 7,557 + 5,017 = 12,574 \text{ lb-in-sec}^2$$

The starting deflection, ending deflection, and deflection increment are values set to build a uniform force/deflection table for use by OBLIQUE. Prior to use of OBLIQUE, a tape holding force/deflection data (Table 2.10.5.3-8) over the range of angles from 5° to 85° is created by CYDROP. OBLIQUE, in turn, reads the tape and converts the force/deflection data to a uniform table for each specified angle. Note that the angles specified in OBLIQUE are with respect to horizontal whereas CYDROP references vertical. The magnitude of the ending deflection must be chosen such that it is greater than the maximum deflection expected in OBLIQUE, yet need not exceed the maximum possible deflection in the corner drop evaluation.

The print control determines whether the output will be a tabular summary or a time history table.

Package free-fall velocity is based on the drop height. From the equations of motion:

$$V = -(2gh)^{0.5}$$

Where:

$g = 386.4 \text{ in/sec}^2$

$h = 30 \text{ ft} = 360 \text{ in}$

TABLE 2.10.5.3-8

CYDROP Force/Deflection Data

```
12345678901234567890123456789012345678901234567890123456789012345678901234567890
         V         V         V         V         V         V         V         V
       .55     11.01       .55
    32367.   128991.   205207.   334008.   477903.   583552.   677442.   758737.
   845422.   934841.  1038385.  1193477.  1268206.  1515395.  1751333.  2111306.
  2821622.  3527691.  5437239.  8627229.
       .60     11.93       .60
    18240.    67473.   121760.   173898.   258462.   368714.   504353.   634713.
   743455.   842066.   941411.  1049548.  1178914.  1320457.  1509786.  1859217.
  2337319.  3044434.  4269526.  6258679.
       .67     13.49       .67
    12193.    56671.    91499.   113057.   156188.   229526.   313617.   404083.
   501568.   609987.   733768.   880232.  1023319.  1173033.  1357047.  1585754.
  1992534.  2555789.  3396621.  4655222.
       .73     14.65       .73
     5028.    21986.    51813.   100182.   163505.   232741.   304621.   381703.
   465956.   560855.   668431.   792142.   937642.  1114234.  1326595.  1593802.
  1971609.  2595205.  3524784.  4638336.
       .77     15.39       .77
     3109.    20093.    57039.   108821.   168429.   234305.   311057.   394634.
   486876.   592357.   705257.   841622.   999463.  1197891.  1441110.  1764085.
  2248183.  2989067.  4003001.  5295208.
       .78     15.63       .78
     4255.    26380.    68840.   123576.   187139.   259087.   340108.   634086.
   543322.   667914.   804180.   958380.  1156760.  1371183.  1650632.  2040733.
  2621016.  3413833.  4478667.  5815325.
       .77     15.39       .77
     4057.    26494.    76869.   148989.   234526.   330652.   436820.   555823.
   687002.   822086.   979995.  1150114.  1341620.  1566648.  1844710.  2230726.
  2842792.  3730696.  4961650.  6337525.
       .73     14.69       .73
    18772.    68814.   132583.   236890.   366604.   500476.   640691.   801924.
   979105.  1151229.  1316710.  1487169.  1694789.  1946953.  2263342.  2722947.
  3482689.  4608111.  6214733.  8341342.
       .68     13.55       .68
    52820.   216204.   345960.   547724.   819178.  1093308.  1315683.  1515427.
  1750771.  1988978.  2293295.  2677752.  3097958.  3572763.  4040177.  4728886.
  6032544.  8077597. 10828178. 14261926.
       .64     12.83       .64
   132902.   468917.   829010.  1274790.  1673088.  2085488.  2617955.  3024971.
  3080822.  3176792.  3326468.  3552364.  3876190.  4362971.  5134758.  6525535.
  9073079. 12696963. 17334716. 22804149.
```

Then,

$$V = -[2(386.4)(360)]^{0.5} = -527.45 \text{ in/sec}$$

The output starting angle, ending angle, and angle increment specify the OBLIQUE analysis package angles of impact with respect to the horizon. The sample problem specified solutions at angles of 5° to 85° in 5° increments. The friction coefficient is usually set to zero. Package translational and rotational velocities are parameters specified to study the effects of secondary impacts.

The sample problem output for OBLIQUE is found in Table 2.10.5.3-9. For each specified angle of impact the magnitude of FMAX is determined as the maximum value of the vector summation of the thrust and shear forces at some instantaneous package angle during the analysis. Note that the maximum value of the package internal forces, moments, and deflections do not necessarily happen at the same instantaneous angle. When all parameters have achieved a maximum value, the problem terminates for that specified angle of impact. OBLIQUE continues the analysis at each angle of impact.

Additionally, OBLIQUE utilizes the methods delineated in Section 2.10.5.2.2 to determine the maximum impact limiter separation moments about the opposite and adjacent corners in the impact limiter. As before, a solution occurs when the maximum value is found for each moment at some instantaneous angle, not necessarily the same instantaneous angle for each moment. A negative moment denotes impact limiter compression and a positive moment impact limiter separation.

TABLE 2.10.5.3-9

OBLIQUE Output

NUPAC OBLIQUE ANALYSIS-OBLIQUE SAMPLE RUN, 20 PCF FOAM OVERPACKS

PACKAGE GEOMETRY-

LENGTH	=	48.000
RADIUS	=	20.000
OVERPACK LENGTH	=	24.000
OVERPACK SIDE THICKNESS	=	10.000
OVERPACK BOTTOM THICKNESS	=	12.000

PACKAGE MASS PROPERTIES-

MASS	=	31.056
MASS MOMENT OF INERTIA	=	12574.000
GRAVITATIONAL CONSTANT	=	386.400

SOLUTION CHARACTERISTICS-

IMPACT VELOCITY (YDOT)	=	-827.450
(XDOT)	=	0.000
(THETADOT)	=	0.000
FRICTION COEFFICIENT	=	0.000
ESTIMATED CRUSH DEPTH	=	1.000

THETAD	FMAX	SHEAR	THRUST	MOMENT	DEFLECTION	CLEARANCE
85.0000	1710212.	114405.	1727491.	813544.	3.20	9.23
80.0000	1320952.	187846.	1319863.	[illegible]	4.81	8.36
75.0000	1240256.	266781.	1213409.	[illegible]	6.56	7.22
70.0000	1181822.	352957.	1130830.	[illegible]	7.45	6.98
65.0000	1166252.	447885.	1078228.	[illegible]	8.77	6.20
60.0000	1240948.	552237.	1091298.	[illegible]	9.62	5.70
55.0000	1281835.	736041.	1049450.	[illegible]	10.29	5.27
50.0000	1270208.	840096.	948282.	[illegible]	10.57	5.04
45.0000	1180489.	879819.	789060.	[illegible]	10.88	4.91
40.0000	1054731.	854279.	622154.	[illegible]	10.24	4.90
35.0000	940457.	811764.	482942.	[illegible]	9.73	4.96
30.0000	847985.	766511.	371050.	[illegible]	9.06	5.08
25.0000	795586.	748828.	288112.	[illegible]	8.25	5.26
20.0000	723357.	691598.	209484.	[illegible]	7.32	5.68
15.0000	641400.	628788.	136961.	[illegible]	6.30	6.19
10.0000	810749.	805405.	109797.	[illegible]	5.21	5.47
5.0000	879215.	877510.	44411.	[illegible]	3.28	7.62

2.10.5.4 NuPac Computer Code Quality Assurance

NuPac computer analysis programs are maintained in accordance with a formal quality assurance program approved by the Nuclear Regulatory Commission under certificate number 0192 that complies with ANSI N45.2. These provisions are applied to both NuPac authored software and vendor supplied software. Vendors of computer services, such as Boeing Computer Services, have demonstrated that their quality standards are in accordance with the provisions of ANSI N45.2. Documentation of such compliance is maintained in NuPac Quality Assurance files.

The requirements of ANSI N45.2 are interpreted to impose the following stipulations upon computing software:

ANSI N45.2 Section	Requirement
4.3	The supplier shall require the identification and performance of verification/qualification evaluations which demonstrate that computer codes are capable of producing information of sufficient accuracy to satisfy design requirements. All calculations and computer input data shall receive documented, independent, in-house verification.
7.0	The supplier shall establish responsibilities and procedures relating to computer code configuration identification and configuration control.

NOTE:

Configuration identification is the establishment and use of a unique identifier for a code version. Configuration control includes the documentation and preservation of a code version to assure its retrievability and includes similar preservation of input for computer runs to assure that output results can subsequently be reconstructed.

A valid computer solution requires that each of the following tests be satisfied:

- Does the analytic method accurately represent the modeled physical processes?
- Does the computer code fully and accurately implement the analytic method?
- Does the input problem data accurately reflect the physical properties of the situation being analyzed?
- Can the resultant output data be uniquely identified as resulting from a particular input data set?

NuPac procedures assure that each of the above questions is answered in an affirmative fashion. These procedures include the following configuration control elements.

1. Each safety analysis report or design analysis summary provides a complete description of appropriate analysis methods implemented in NuPac developed software.

2. Version identification for each run of the computer code is maintained by the automatic appearance of current code revisions numbers and dates in both output headers and day file listings.

3. All superseded versions of codes are maintained on file.

4. All input data are automatically echoed on output for verification and checking purposes.

5. All output data, including plots, are labeled with a machine generated name, time and date corresponding to the run which generated the reported engineering results.

Verification of methodology and code accuracy involves one or more of the following steps:

1. End-to-end experiments:

These experiments simultaneously test the accuracy of both methodology and code implementation of methodology. For example, a full scale series of 30' drop tests conducted in September, 1980 on the Chem-Nuclear Systems, Inc. CNSI-13C (II) package demonstrated that the overall predictive error of NuPac impact dynamics software is about 6%. (Reference page 2-91, Section 2.7.1.2 of CNSI-13C (II) S.A.R.)

2. Comparison with Alternative Methods:

The method of comparison varies with the particular technology involved. Two examples are described below.

a. Impact Analyses:

Alternative energy balance and momentum methods are used to check point time history impact dynamics solutions. These end-to-end checks have been performed at three orientations where the dynamic equations of motion become simplified: end, side and center of gravity over struck corner. At other orientations, the impact dynamic solution method has been verified by momentum techniques combined with idealized perfectly plastic energy absorber assumptions.

b. Thermal Analyses:

Steady state solutions are checked by independent iteration methods and a careful check of model heat flow balances (equilibrium). Transient analyses are independently checked by Schmidt plot graphical analysis methods.

3. Hand Checks of Code:

Hand checks have been performed to assure that:

- o Equilibrium is always satisfied. Both thermal and all impact solutions have been so tested.
- o Force or heat transfer between points, or nodes, obey the assumptions of the analysis model.
- o Analytic geometry calculations obey the model assumptions. These features have been checked by both descriptive geometry constructions and mathematical checks of the algorithms.
- o Interpolations of non-linear tabular data are correctly performed.
- o Numerical integrations are properly performed.

APPENDIX 2.10.6

Cask Wall Buckling Analysis

THIS SECTION IS PROPRIETARY

APPENDIX 2.10.7

End Drop Lid Analysis

THIS SECTION IS PROPRIETARY

APPENDIX 2.10.8

Lid Puncture Analysis

THIS SECTION IS PROPRIETARY

APPENDIX 2.10.9

ANSYS Analysis Output

(Microfiche)

THIS SECTION IS PROPRIETARY

2.11 References

1. U. S. Nuclear Regulatory Commission Regulatory Guide 7.6, Design Criteria for the Structural Analysis of Shipping Cask Containment Vessels, Revision 1, March, 1978.

2. U. S. Nuclear Regulatory Commission Regulatory Guide 7.8, Load Combinations for the Structural Analysis of Shipping Casks, May, 1977.

3. ASME Boiler and Pressure Vessel Code, Section III, Nuclear Power Plant Components, Division 1, 1983 Edition.

4. NUREG/CR-1815, Recommendations for Protecting Against Failure by Brittle Fracture in Ferritic Steel Shipping Containers up to Four Inches Thick, August, 1981, Lawrence Livermore Laboratory.

5. Baker, E.H., et al, Structural Analysis of Shells, Robert E. Krieger Publishing Co., 1981.

6. Timoshenko, S.P., Theory of Elastic Stability, McGraw-Hill, 1936.

7. Cheney, James A., Pressure Buckling of Ring Incased in a Cavity, ASCE EM Journal, Vol. 97, EM2, April, 1971.

8. ASTM D 1621-63, Test Method for Compressive Properties of Rigid Cellular Plastics, American Society for Testing and Materials.

9. Shigley, Joseph E., and Larry D. Mitchell, Mechanical Engineering Design, 4th Edition, McGraw-Hill, 1983.

10. Tietz, Thomas, Determination of the Mechanical Properties of a High Purity Lead and a 0.058% Copper-Lead Alloy, WADC Technical Report 57--695, ASTIA Document No. 155165, Stanford Research Center, April, 1958.

11. Roark, Raymond J., and Warren C. Young, Formulas for Stress and Strain, 5th Edition, McGraw-Hill, 1975.

12. Baumeister, Theodore, et al, Mark's Standard Handbook for Mechanical Engineers, 8th Edition, McGraw-Hill, 1978.

13. Pilkey, Walter D. and Pin Tu Chang, Modern Formulas for Statics and Dynamics, McGraw-Hill, 1978.

14. Shappert, L. B., Cask Designers Guide - A Guide to the Design, Fabrication and Operation of Shipping Casks for Nuclear Applications, ORNL-NSIC-68, February, 1970.

15. Sakamoto, I., et al, An Experimental Study on Puncture Resistance of Spent Fuel Shipping Cask by Drop Impact Tests, 4th International Symposium on Packaging and Transportation of Radioactive Materials, pp. 262-276, September 22-27, 1984, Miami Beach, Florida.

16. Shieh, R. C., Empirical Equations for Puncture Analysis of Lead-Shielded Spent Fuel Casks.

17. Blodgett, Omer, Design of Weldments, Lincoln Arc-Welding Institute, 1976.

18. Oberg, Erik, et al, Machinery's Handbook, 21st Edition, Industrial Press, Inc., 1980.

19. Knorovsky, G. A., and H. J. Rack, An Assessment of Stress - Strain Data Suitable for Finite Element Elastic - Plastic Analysis of Shipping Containers, NUREG/CR-0481, SAND77-1872, Sept., 1978.

20. ANSI N14.23, Design Basis for Resistance to Shock and Vibration of Radioactive Material Packages Greater than One Ton in Truck Transport, American National Standards Institute, Inc., May, 1980.

3.0 THERMAL EVALUATION

This section identifies and describes the principal thermal engineering design aspects of the NuPac Model 10/140MB shipping cask important to safety and compliance with the performance requirements of 10 CFR 71.

3.1 Discussion

The NuPac Model 10/140MB cask is designed with a totally passive thermal system. As seen from the drawings in Appendix 1.3, the principal physical components of this thermal system consist of a single thickness thermal fire shield surrounding the cask sides, a single thickness thermal fire shield partially covering the cask end plate, and an insulated panel partially covering the cask lid. Additional thermal protection is achieved by the polyurethane foam impact limiters. Together, these various protective devices cover the entire exterior surface of the cask such that direct exposure to external conditions (assuming that no damage has occurred) is minimal.

The cylindrical cask wall consists of a 1.25 inch thick carbon steel plate outer shell with 0.06 inch thick stainless steel cladding in those areas not covered by the thermal shield, a 2.25 inch thick lead shield, and a 0.75 inch thick stainless steel plate inner shell. The cask end plate is fabricated from 6.5 inch maximum thickness stainless steel. The cask lid is fabricated from 5.25 inch norminal thickness stainless steel plate. Twenty lb/cubic foot polyurethane foam impact limiters covering each end of the cask provide protection from accidental impacts.

Four principal heat transfer analyses were run utilizing the NASA/Martin Marietta computer thermal network analyzer program, SINDA/85: 1) steady-state analysis at an ambient temperature of 100°F with solar insolation as prescribed by NRC 10 CFR 71, 2) steady-state analysis at 100°F ambient and no solar insolation, 3) a transient analysis for an undamaged condition with an exposure to an ambient temperature of 1,475°F for thirty minutes followed by exposure to 100°F ambient air to simulate a hypothetical fire accident condi-

tion, and 4) the same fire accident condition for a hypothetical damaged cask configuration. The following table presents the maximum temperatures determined by each of these analyses for selected major components of the cask. Details of the analyses and additional temperature levels are presented in Section 3.4 and 3.5.

Maximum Temperature (°F)

Location	Steady-State		Transient	
	w/ Solar	w/o Solar	No Damage	Corner Drop w/Pin Punch
Cask Inner Shell	128	106	337	341
Lead Shield	128	106	342	345
Cask Outer Shell	128	106	350	352
Thermal Shield	122	104	1240	1241
Impact Limiter Shell	174	100	1417	1416
Impact Limiter Foam	169	105	246	246
Inner Lid Closure Seal	133	108	133	140
Outer Lid Closure Seal	129	106	282	296
Cask Bottom Seal	128	106	202	205
Cask End Plate	129	109	255	255
Tie-Down Lug	114	104	1342	1362

These results are based on a maximum internal decay heat load of 95 watts.

3.2 Summary Of Thermal Properties of Materials

The NuPac Model 10/140MB Cask is fabricated primarily of stainless steel, carbon steel, lead, and polyurethane foam. The void spaces within the package are assumed to be filled with air at a pressure of one atmosphere. Air is also assumed to fill the gap between the cask exterior and the thermal shields.

Since the conductivity and specific heat of the metals and the polyurethane foam varies relatively little with temperature, their values were fixed. However, in the interest of improved accuracy, one conductivity value was used for the steady state analysis, while a second value was used for the higher temperatures seen for the fire accident transient.

In contrast, the thermal properties of air do vary substantially with temperature. As such, the thermal analysis continuously recalculated the value of conductors involving air. This recalculation used the mean fluid temperature.

The following table documents the thermal properties used in the model and the sources from which they were obtained.

	Property			
Material	Conductivity (BTU/hr-ft-^{o}F	Density (Lb/ft^{3})	Specific Heat (BTU/lb-^{o}F)	Reference
Stainless Steel Type 304	9.6 at 120^{o}F 10 at 300^{o}F	488	0.11	3.7.1
Carbon Steel	25.0 at 120^{o}F 24.5 at 300^{o}F	487	0.113	3.7.1
Lead	19.8 at 120^{o}F 18.8 at 300^{o}F	710	0.031	3.7.1
Polyurethane	0.031 at 75^{o}F	20	0.30	3.7.4
Air	-- see below --			3.7.5

The thermal conductivity of air varies significantly with temperature as shown in the following table:

Properties of Air

Temperature (^{o}F)	Conductivity (BTU/hr-ft-^{o}F)	Density (Lb/ft3)	Specific Heat (BTU/lb-^{o}F)
32	.0140	.081	0.2402
100	.0154	.071	0.2402
300	.0193	.052	0.2432
500	.0231	.0412	0.2472
1000	.0319	.0271	0.2622
1500	.0400	.0202	0.2762

Radiation Properties

Component	Material	e	Condition	Ref.
Cask I.D.	S. Steel	0.25	All	3.7.3
Cask O.D.	Carbon Steel w/ S. Steel Cladding	0.25	All	3.7.3
Impact Limiter Shell	S. Steel	0.25	Normal	3.7.
		0.8	Fire	3.7.6
Outer Surface-Thermal Shield	S. Steel	0.25	Normal	3.7.3
		0.8	Fire	3.7.6
Inner Surface-Thermal Shield	S. Steel	0.25	Normal	3.7.3
		.6 to .4	Fire	3.7.2/3.7.7

3.3 Technical Specifications of Components

The O-rings used at the closure seals of the cask are the most temperature sensitive materials within the package. The O-rings are made of butyl rubber and have a sufficient temperature capability to handle the expected peak temperatures to be seen by this cask. This statement is based on recent fire test experience with another cask which showed no loss of sealing capability under more extreme temperature conditions. Refer to Reference 3.7.9 for details.

The stainless steel used in the construction of the cask meets the specifications for ASTM A320 Type 304, while the carbon steel meets ASTM A516 Gr.70. The melting temperatures for lead, carbon steel, and stainless steel are 620, 2750, 2600°F, respectively. The thermal properties are given in Section 3.2.

The foam used in the impact limiters is a rigid polyurethane foam produced under the direction of the Nuclear Packaging, Inc. of Federal Way, Washington. The foam is fire resistant and has been demonstrated to not support a flame. Other technical specifications are given in Reference 3.7.8.

3.4 Thermal Evaluation for Normal Conditions of Transport

This section presents the thermal analyses of the NuPac Model 10/140MB cask for Normal Conditions of Transport. The thermal conditions considered are those specified in 10 CFR 71.71. Per 71.71(c)(1), a 100°F ambient temperature and the solar insolation values given in the table below are to be used for thermal boundary conditions. An assumed solar absorptivity of 0.5 for the stainless steel impact limiter shells and heat shields was used with these solar insolation values.

A 95 watt payload internal heat load was also assumed for the normal transport thermal model.

SOLAR INSOLATION

Form and Location of Surface	Total Insolation for a 12-Hour Period (g cal/c^2)
Flat surfaces transported Horizontally	
- Base	None
- Other surfaces	800
Flat surfaces not transported Horizontally	200
Curved surfaces	400

An additional steady-state case was run using an external ambient temperature of 100°F with internal heat generation, but without solar insolation. This case is to be considered as the initial condition for the Hypothetical Accident Conditions. A final, rather trivial case of -40°F ambient air with no solar insolation and no internal heat generation is also considered herein as another extreme initial condition for other events.

3.4.1 Thermal Model

3.4.1.1 Analytical Model

Figures 3.4.1-1 and 3.4.1-2 illustrate the location of the 88 nodes used in the steady-state analytical model. The location and number of nodes were chosen to permit accurate determination of the temperature distribution in the major cask components. The model utilized the different thermal properties presented in Section 3.2. For simplicity's sake, a fixed value of thermal conductivity and specific heat was used for the metals and polyurethane foam, since their change with temperature is small over the temperature range seen. In contrast, the thermal properties of air were computed as a function of temperature since their variation with temperature is significant.

FIGURE 3.4.1-1

Node Layout - Through Lid Bolt Location

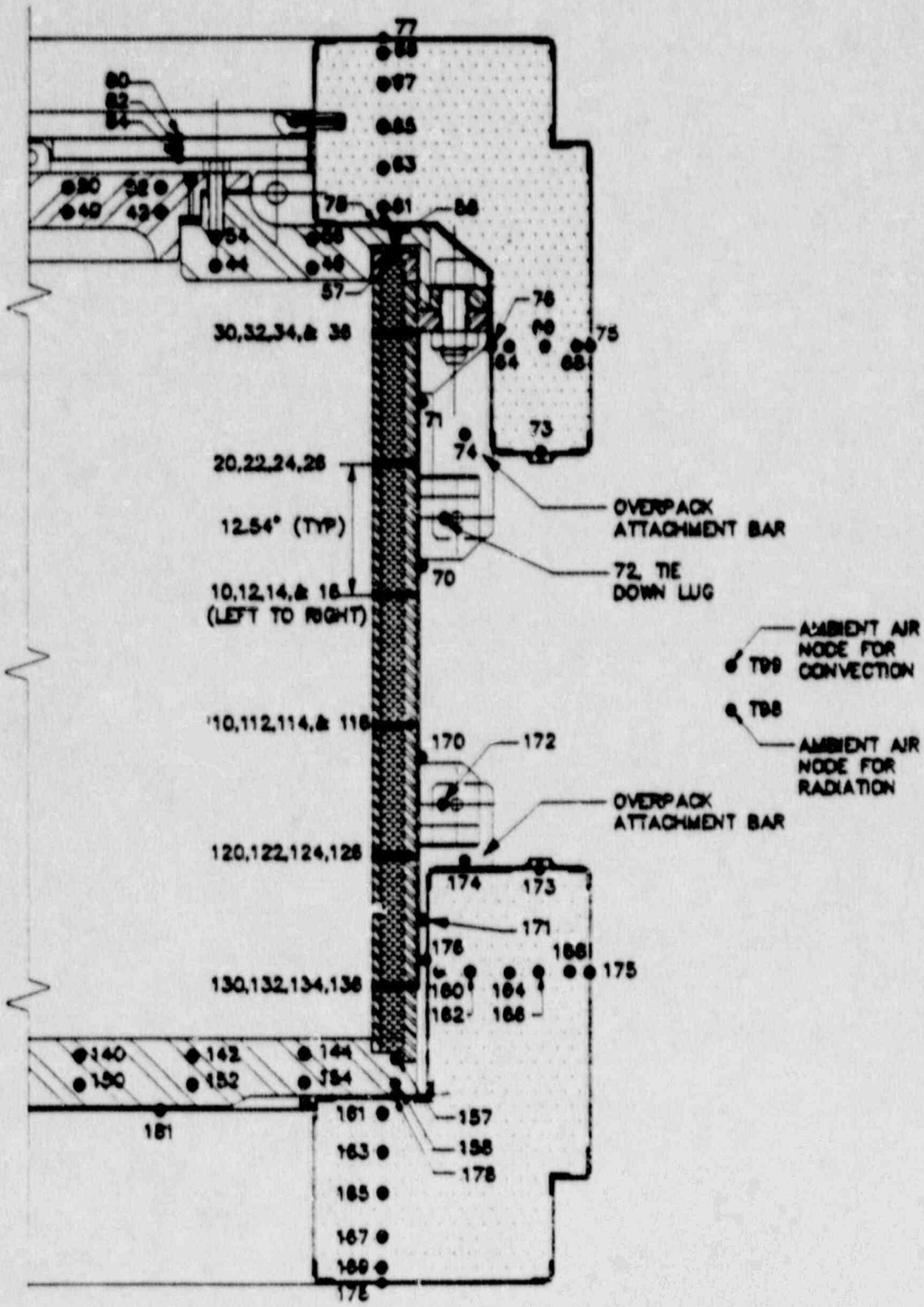

FIGURE 3.4.1-2

Node Layout - In Between Lid Bolts

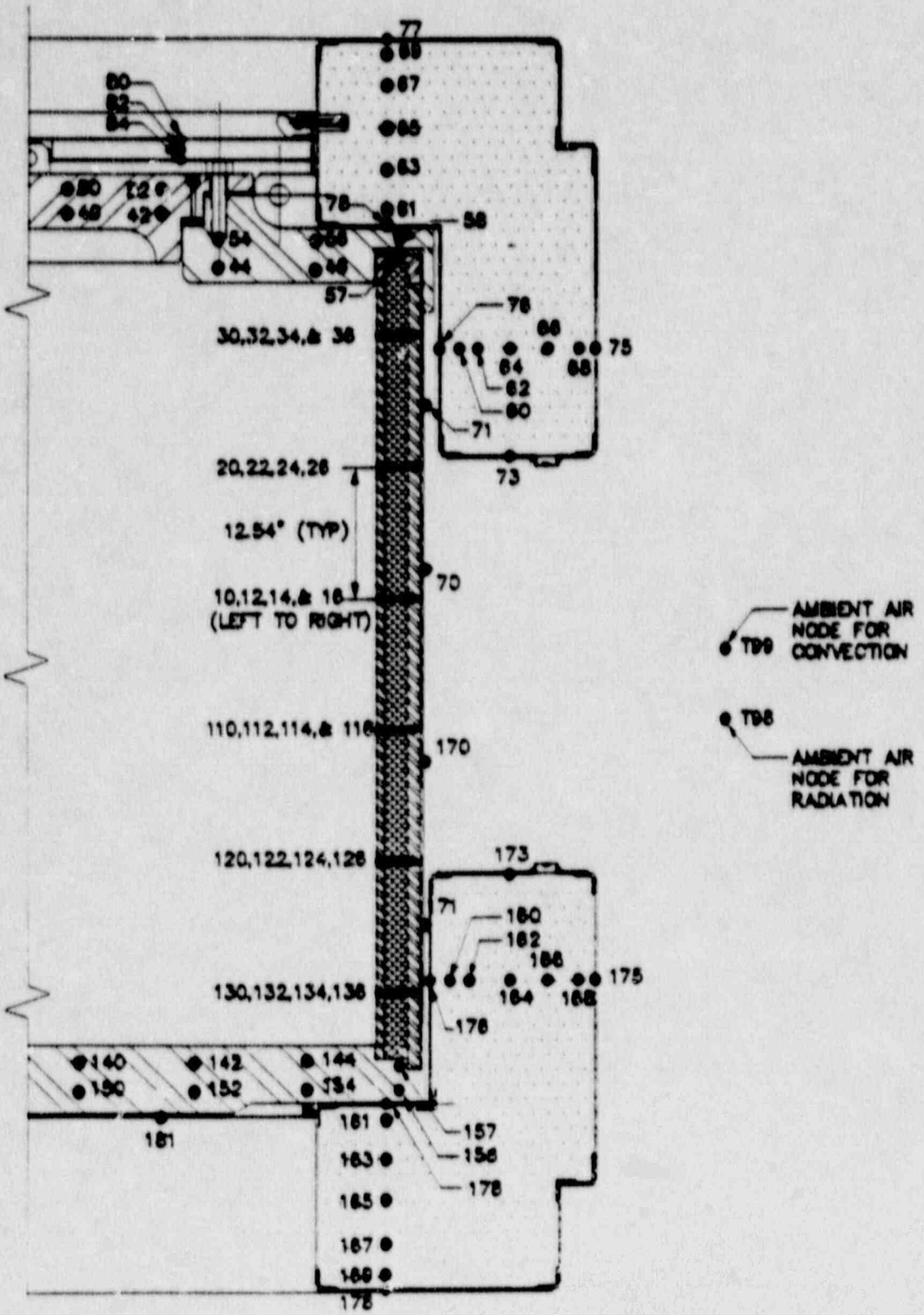

The thermal model represents an axisymmetric segment of a fixed bottom cask configuration. Thermal results for a bottom loading configuration would be similar, except that temperature distributions for the bottom of the cask would be nearly identical to those at the lid because of the additional thermal paths afforded by the lid attachment bolts and the 1-1/4 inch gap between the impact limiter and the cask outer shell. The analysis assumes that the cask is in its normal upright shipping position and that the bottom of the cask sees an adiabatic surface. It is further assumed that the payload within the cask is evenly distributed. The relatively low assumed decay heat rate of 95 watts means that a change in this assumption will not have a serious effect on the peak temperature distributions.

The internal structure within the package was not modeled. Instead, the transfer of heat from the payload to the inner wall of the cask was modeled as a simple heat input to the interior wall nodes.

Heat transfer through all other portions of the cask structure was calculated using a combination of conduction and 'gray-body' radiation heat transfer. The heat transfer across the air gaps within the cask (e.g. between the thermal shield and the cask, cask lid, etc.) was treated as radiation plus pure conduction, since the Grashof number is below that for which free convection occurs. An exception occurs for the air gap between the cask lid and the thermal shield (i.e. node 84) when the cask is in a horizontal orientation, such as occurs for the hypothetical accident scenario (see Section 3.5). Under these conditions the heat transfer across the gap was treated as radiation and free convection within an enclosure.

The free convection of heat from the exterior surfaces was computed as a function of temperature and orientation of the surface using standard equations for free convection from cylinders and vertical or horizontal surfaces. See Appendix 3.6 for the specific equations used in each case.

3.4.1.2 Test Model

This section is not applicable, as no thermal testing was performed for the NuPac Model 10/140MB.

3.4.2 Maximum Temperatures

The maximum temperatures noted for Normal Conditions of Transportation (i.e. 100°F ambient temperature, solar insolation, and 95 decay heat loading) are presented in the following table for the major components of the cask. See Figures 3.4.1-1 and 3.4.1-2 for the location of the various nodes. A complete listing of nodal temperatures is provided in Appendix 3.6.

A point to be considered when reviewing the temperature levels in the table below is that the relatively long time constant of the foam impact limiters (i.e. 50+ hours) means that the steady-state temperatures are conservatively high. This is due to the fact that the impact limiters will isolate the cask components from the effects of solar insolation such that the cask temperatures will not reach a steady-state condition during the typical daily ambient thermal cycle.

Max. Temperatures for NuPac Model 10/140MB
Normal Conditions

Location	Node Number	Temperature °F
Cask Inner Shell	10	127
	30	128
	130	128
Lead Shield	14	127
	34	128
	134	128
Cask Outer Shell	16	127
	36	128
	136	128
Cask Lid	40	133
	46	130
Cask End Plate	140	129
	144	129
Seals - Lid	42	133
- Cover Plate	58	129
- End Plate	158	128
Thermal Shield	70	122
	80	170
	181	129
Impact Limiter Shell	77	174
	75	119

Max. Temperatures for NuPac Model 10/140MB
Normal Conditions
(Continued)

Location	Node Number	Temperature °F
Impact Limiter Foam	69	169
	67	159
	65	150
	63	144
	61	135
	68	119
	66	121
	64	123
	62	127
Tie-Down Lug	72	114

3.4.3 Minimum Temperatures

The minimum temperature distribution for the NuPac Model 10/140MB cask will occur with no decay heat load and an ambient air temperature of -40°F (per 10 CFR 71.71 (c)(2)). Since the steady state analysis of these conditions represents a trivial case, no computerized thermal calculations were performed. Instead, it was assumed that all cask components would reach the -40°F temperature under steady state conditions. This temperature is within the allowable range of all cask components. As a further potential initial condition for normal or accident events, a -20°F minimum uniform temperature was also considered per 10 CFR 71.71(b).

3.4.4 Maximum Normal Condition Internal Pressure

Internal pressures in the NuPac 10/140MB are affected by three physical effects. First, gas laws predict that pressures in a fixed volume are proportional to the absolute temperature of the gas. Second, some anticipated pay-

loads which would be shipped in the 10/140MB exhibit some gas evolution when subjected to a gamma flux. Finally, a change in temperature would change the vapor pressure of water, so that if small amounts of water are present in the package, the internal pressure would increase accordingly.

From the data presented above, it can be seen that the highest inner surface temperature predicted on the lid of the cask is 133°F (node 40) while the remainder of the cask inner surface averages about 128°F. A weighted average of the inner surface temperature can be taken as a means of determining the gas law and vapor pressure effects on the internal pressure.

The inner surface area of the lid can be approximately as:

$$\pi(33)^2 = 3421 \text{ in.}^2$$

The remainder of the internal surface area is:

$$\pi(33)^2+2\pi(66)(73) = 18557 \text{ in}^2$$

So, the average temperature:

$$\left[133(3421)+128(18557)\right]/(3421+18557) = 129^\circ\text{F}$$

Some assumptions regarding the amount of free space present in a loaded container must be made. A typical payload configuration involves a inner waste container (most likely a High Integrity Container, or HIC) filled as much as practical with ion exchange resins. Operational requirements dictate that the HIC may be filled no more than 8 to 10 inches from the top. In addition, the HIC typically is designed with at least 1 inch of clearance on the sides and 2 inches between the top of the HIC and the top of the 10/140MB. For purposes of calculating the internal pressure, assume a void space equivalent to the sum of an 8 inch high cylinder the entire diameter of the cavity, and a one inch thick cylindrical shell the length of the remainder of the cavity:

$$V_{void} = \pi((33)^2(8)+(73-8)(33^2-32^2))/1728 = 23.52 \text{ ft}^3$$

This volume conservatively ignores the interstial volume inherent in the waste form, dewatering plumbing internal volume, and the volume of the domed secondary lid design.

The amount of gas generated may be estimated by assuming that the entire volume of the 10/140MB not counted as void space is filled with ion-exchange resins. BNL-NUREG-51565, p. 27, indicates that the gas generation rate of a typical ion-exchange media exposed to a gamma flux is $1.595(10)^{-8}$ cm^3/gram-Rad. Conservatively assume an average gamma flux through the resin of 300 R/hr (see Section 5).

The volume of the 10/140MB cavity is:

$$\pi\ (33)^2 73/1728 = 144.53\ ft^3$$

So the volume of resin is:

$$144.53 - 23.52 = 121.01\ ft^3$$

The resins may be assumed to be 60 lbs./$ft.^3$ in density so the gas generation rate given above can be converted to British units:

$$(1.595(10)^{-8}\ cc/gram\text{-}Rad)(453.6\ g/lb.)\ 60\ lb./ft^3$$
$$= 4.341(10)^{-4}\ cc/ft^3\text{-}Rad$$

$$(4.341(10)^{-4}\ cc/ft^3\text{-}Rad)(3.5315(10)^{-5}\ ft^3/cc)$$
$$= 1.533(10)^{-8}\ ft^3/ft^3\text{-}Rad$$

The gas generated assuming a 300 R/hr flux for one year can then be calculated:

$$(1.533/10^{-8}\ ft^3/ft^3\text{-}Rad)(121.01 ft^3)(300\ R/hr)(24\ hr/day)(365\ day/yr)$$
$$= 4.88\ ft^3$$

So applying the perfect gas law:

$$P_i V_i / T_i = P_f V_f / T_f$$

P_i = 14.7 psi
V_i = 23.52+4.88 = 28.4 ft^3
T_i = 70°F = 530°R
V_f = 23.52 ft^3
T_f = 124°F = 584°R

Solving for P_f:

$$P_f = P_i V_i T_f / V_f T_i$$
$$P_f = (14.7)(28.4)(584)/(23.52f)(530) = 19.6 \text{ psia}$$
$$= 4.9 \text{ psig}$$

Any water vapor present may be assumed to condense on the surface with the lowest temperature in the cavity. This temperature will be conservatively taken as 130°F. The internal pressure will increase when water is present by the difference in vapor pressure between maximum normal conditions and the conditions at closure. Since the vapor pressure at 70°F is 0.36 psi and at 130°F it is 2.23 psi, the pressure increase due to vapor pressure = 2.23 - 0.36 = 1.87 psi. Therefore, the total pressure increase, assuming a typical payload, is:

4.9 + 1.87 = 6.8 psig, maximum normal condition internal pressure.

3.4.5 Thermal Stresses

An examination of the predicted temperatures in the large steel members of the 10/140MB Cask reveals that through-wall thermal gradients are virtually non-existent. Because of this, and because the overall temperature change from the upper to lower temperature limits is very much less than from the lead pour fabrication temperature to the lowest service temperature, it seems clear that thermal stresses per se are negligible under normal conditions.

3.4.6 Evaluation of Package Performance for Normal Conditions of Transport

The component temperatures found for both the maximum and minimum normal temperature distributions, as described in Sections 3.4.2 and 3.4.3 above, were all well within the allowable limits for the respective material (see Section 3.3). As input to Section 2.6, the minimum temperature for any cask component is taken as -40°F, and the maximum temperature as 128°F for the cask cylindrical outer wall, 133°F for the lid, 130°F for the end plate, and as 169°F for the impact limiter foam.

3.5 Hypothetical Accident Thermal Evaluation

This section presents the thermal analyses of the NuPac Model 10/140MB Cask for the hypothetical fire accident condition specified in 10 CFR 71.73(c)(3). The initial temperature distribution in the cask prior to the fire is taken as that corresponding to the 100°F steady state condition without solar insolation as discussed in Section 3.4. This is in accordance with 10 CFR 71.73(b).

To determine the effect of a hypothetical accident involving a fire, the cask is exposed to a 1475°F flame having an emissivity of 0.90 for one half hour. After this time period, the thermal boundary conditions are returned to 100°F ambient air with no sun. The transient is then continued for a time sufficient for all temperatures within the cask to reach their maximum values. All thermal boundary conditions meet those specified in 10 CFR 71.73(c)(3).

3.5.1 Thermal Model

3.5.1.1 Analytical Model

The analytical model used to evaluate the Hypothetical Accident Conditions was similar to that described in Section 3.4.1.1, except that the cask was divided into six (6) circumferential stations as shown in Figure 3.5.1-1. The node distribution at any circumferential station is identical to that shown in Figures 3.4.1-1 and 3.4.1-2. The distribution of the circumferential stations

was chosen to accurately model the extent of damage and to resolve the circumferential temperature distributions.

The cask is assumed to have been dislodged from its normal upright shipping position and to be resting horizontally at the start of the accident transient. This assumption implies that the cask end is now exposed to the fire conditions as opposed to the adiabatic conditions seen in the cask's normal shipping orientation. This assumption also affects the free convection equations used for each surface. The thermal model also conservatively assumes that the fire conditions will exist around the entire surface of the cask.

An emissivity of 0.80 was used for all external surfaces, while the cask ID and OD surfaces remained at an emissivity of 0.25. Based on data in References 3.7.2 and 3.7.7, the emissivity of the interior surface of the thermal shield was raised to 0.60 during the 30 minute fire and then lowered to 0.40 during the remainder of the transient. This action sought to model the change in emissivity of stainless steel when it has been exposed to temperatures of 1500°F for as little as 15 minutes.

Based on previous fire tests, impact limiter polyurethane foam is assumed to begin to char at temperatures in excess of 400°F, but not support a flame. Therefore, the basic assumption for this analysis is that, although some foam in the direct vicinity of the metal surfaces will be lost, the bulk of the foam will remain intact. For conservatism, the thermal model assumes that three inches of foam in the vicinity of the impact limiter shells is lost due to charring. The charred foam is replaced in the thermal model with an equivalent three inch air gap.

In addition to these assumptions, thermal model modifications were incorporated to account for the Hypothetical Accident Condition damage. The details of this damage are discussed in Section 3.5.2.

3.5.1.2 Test Model

This section is not applicable, as no thermal testing was performed for the NuPac Model 10/140MB cask.

3.5.2 Package Conditions and Environment

Two hypothetical package conditions were examined for the accident thermal environment. The first condition represents undamaged cask. This condition serves as a reference against which to judge the sensitivity of the cask to the damaged condition discussed below.

The second condition evaluated was for a corner drop followed by a puncture impact on the area damaged by the corner drop. The corner drop is conservatively assumed to result in the O.D. of the impact limiter covering the lid end of the cask being crushed inward by approximately 12 inches. This degree of damage would reduce the normal separation distance between the I.D. and O.D. of the impact limiter from 13.5 inches to essentially zero inches at the centerline of the impact zone. Due to this narrow distance, it is conservatively assumed that the polyurethane foam in the impact zone would be completely charred away during a fire transient. For modeling purposes, the charred foam is replaced with air. In addition, it is assumed that the pin puncture would tear a 7.5-inch diameter hole through the outer shell of the impact limiter. The remaining portion of the outer shell of the impact limiter, as well as the entire inner shell, is assumed to remain intact. Note that this simulted damage is actually much worse than occured during the quarter-scale test which attempted to simulate this accident scenario. Refer to Appendix 2.10.4 (Quarter-Scale Drop Test) for details. It is further assumed that, following the free drop and pin punch, the cask would roll over and expose the damaged portion of the impact limiter to the fire conditions.

The line of impact limiter crushing at the other circumferential stations is illustrated in Figures 3.5.2-1 and 3.5.2-2. Based on this schematic, the thermal model assumed that foam nodes 69 and 67 would be crushed and node 65 would be charred at the 45 and 315 degree stations. The cask is assumed to be undamaged at the 75, 180, and 285 degree stations.

FIGURE 3.5.2-1

Damaged Impact Limiter Thermal Model

Cross Section

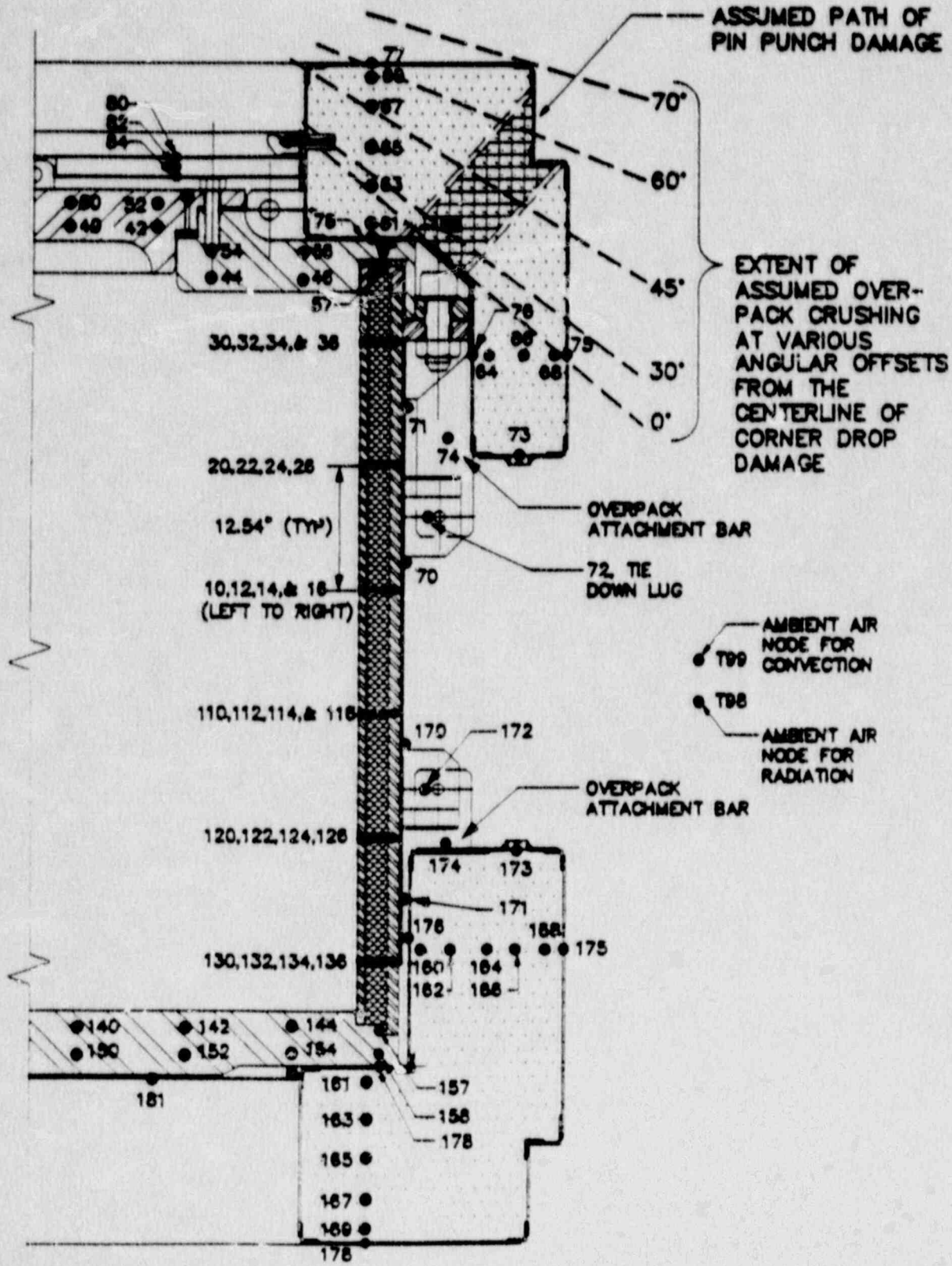

FIGURE 3.5.2-2

Damaged Impact Limiter Thermal Model

Circumferential Stations

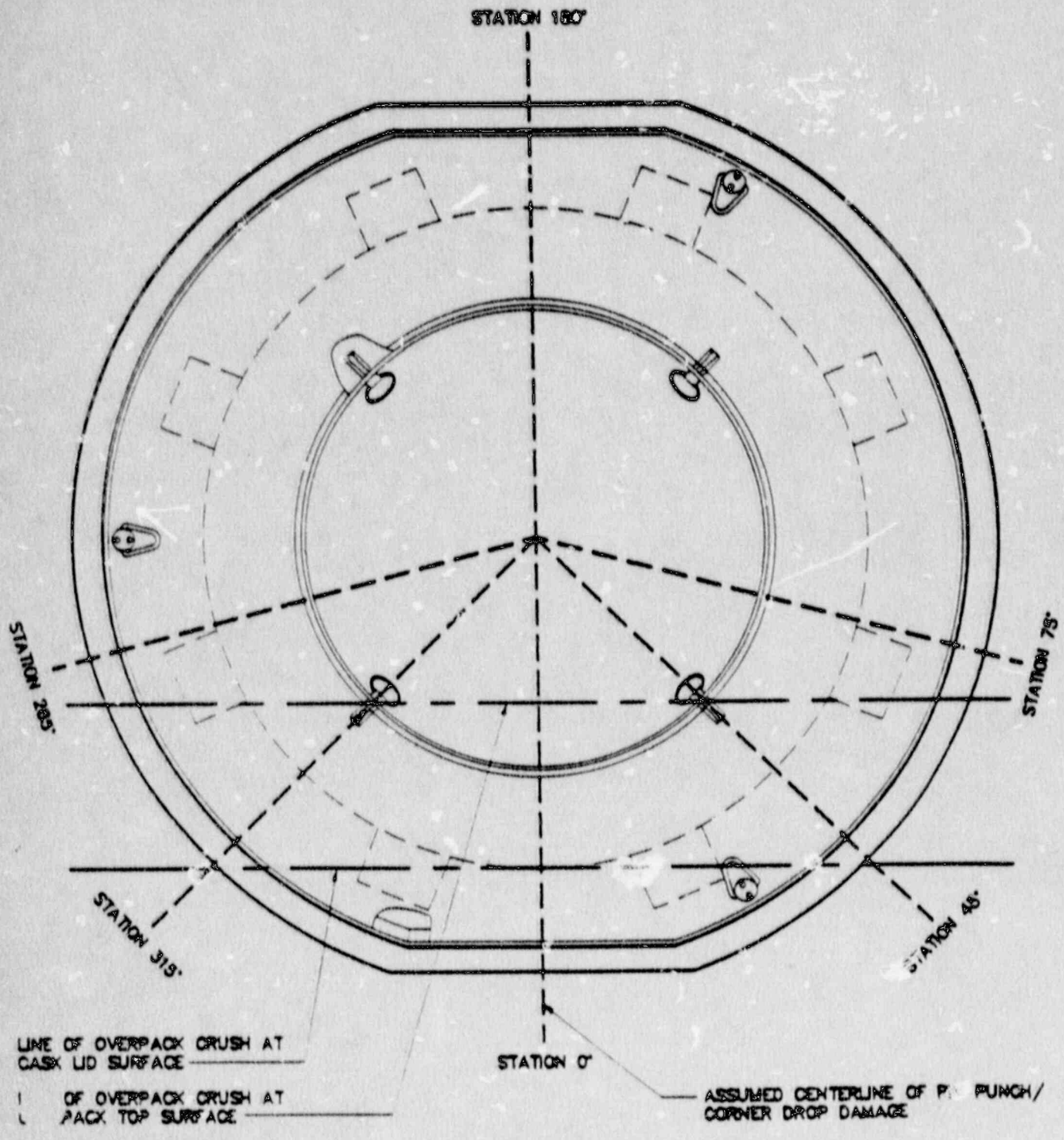

3.5.3 Package Temperatures

The maximum temperatures noted for the Hypothetical Accident Conditions described above are presented in the following table for the major components of the cask. In addition, the initial condition for the transients, as described in Section 3.5, is also given. A complete listing of nodal temperatures is provided in Section 3.6.2. In addition, Figures 3.5.3-1 and 3.5.3-2 illustrate the temperature time histories for typical cask locations for each accident condition. The initial accident condition temperatures were used in Section 2.7 as design temperatures in the analysis of the accident events. Specifically, the impact limiter foam is taken to be 105°.

Maximum Temperatures for NuPac Model 10/140MB Cask
Fire Accident

Location	Node	Initial Condition	No Damage	Corner/Pin Drop
Inner Shell	10	105	338	341
	30	106	290	302
	130	106	203	206
Lead Shield	14	105	342	345
	34	106	290	302
	134	106	203	206
Outer Shell	16	105	350	352
	36	106	291	302
	136	106	203	206
Cask Lid	40	108	130	125
	46	107	165	173
End Plate	40	109	204	205
	144	108	255	255
Seals				
- Lid	42	[illegible]	133	140
- Cover Plate	57	[illegible]	282	296
- End Plate	57	[illegible]	202	205

Location	Node	Initial Condition	No Damage	Corner/Pin Drop
Thermal Shield	70	104	1240	1241
	80	101	1406	1415
	181	108	1066	1066
Impact Limiter	77	100	1414	1395
Shell	75	100	1417	1416
Impact Limiter	69	100	---	---*
Foam	67	101	218	218**
	65	102	127	227**
	63	103	117	118**
	61	105	146	146**
	68	100	---	---
	66	101	246	246**
	64	103	191	191**
	62	103	220	220**
Tie Down Lug	72	104	1342	1362

* - Missing Nodes Represent Charred Foam

** - Foam Nodes At Undamaged Section

FIGURE 3.5.3-1

Fire Transient Time Histories

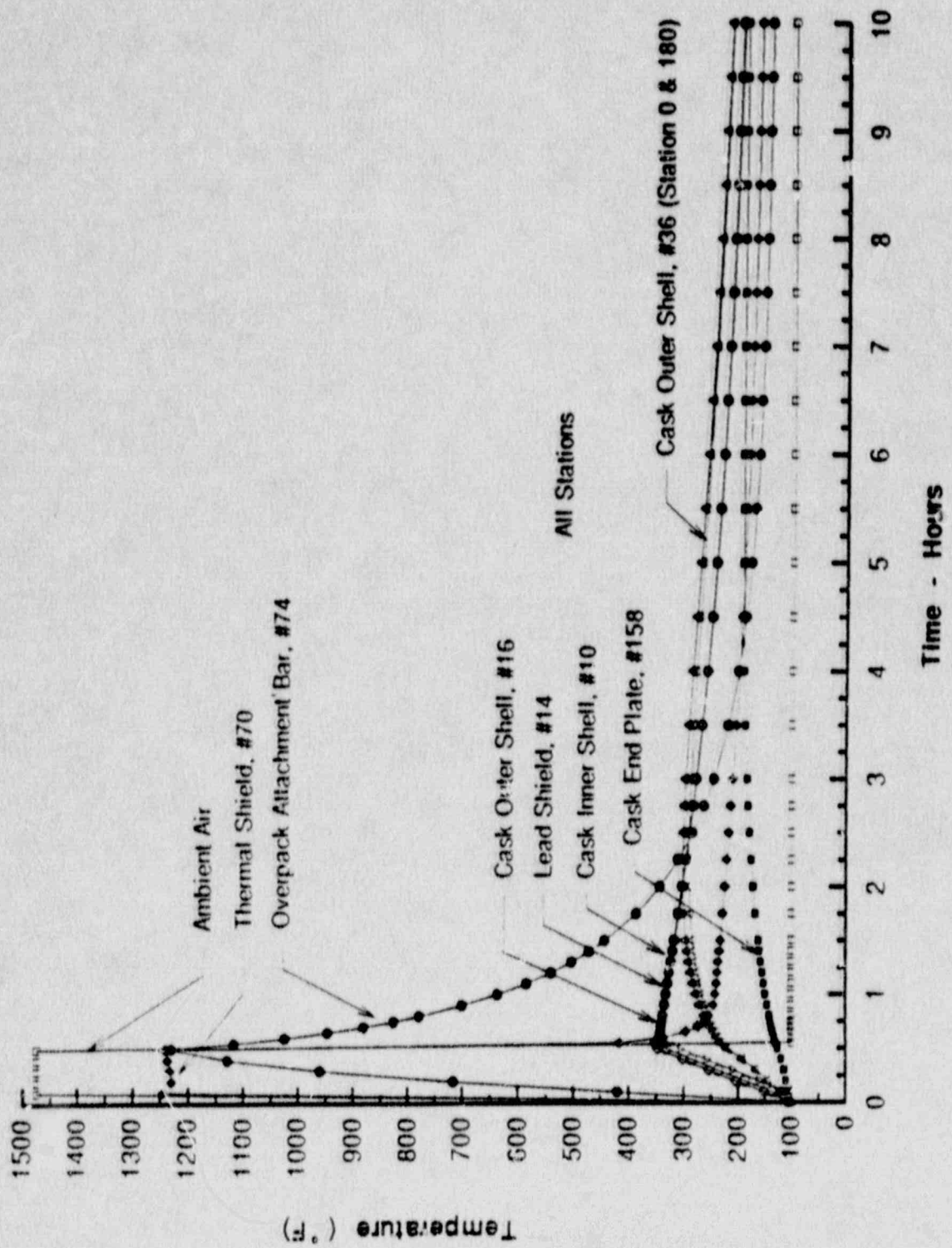

FIGURE 3.5.3-2

Fire Transient Time Histories

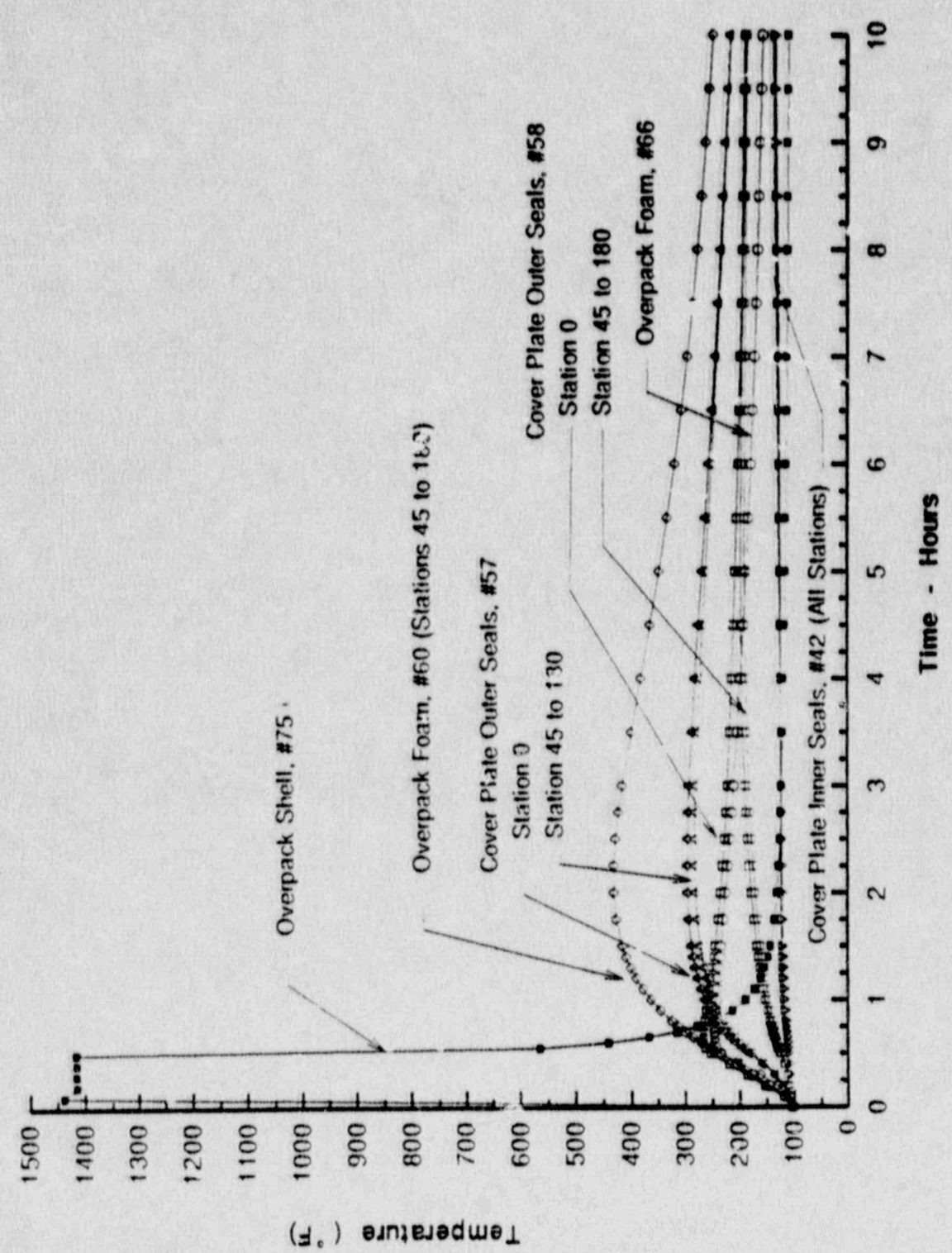

3.5.4 Maximum Internal Pressure

As calculated in Section 3.4.4 above, the maximum normally occurring internal pressure is 6.8 psig. Conservatively assuming the entire internal volume is at the highest temperature predicted for any node on the inner cask surface (341°F at node 10), the maximum internal pressure may be calculated using the perfect gas law:

$$P_1/T_1 = P_2/T_2$$

Assuming the initial temperature is 70°F, the internal pressure may be calculated:

$$(14.7 + 6.8)/(460 + 70) = P_2/(460 + 341)$$

$$P_2 = 32.5 \text{ psia}$$
$$= 17.8 \text{ psig}$$

So, the maximum internal pressure which could occur during the hypothetical accident fire transient is 17.8 psig.

3.5.5 Maximum Thermal Stresses

Through-wall temperature gradients during the accident thermal transient event are never more than about 11°F from the inner steel shell to the outer shell in the center of the cask side wall. Further, the higher temperature shell is the outer shell, so the shells would tend to move apart relative to each other, such that no thermal stresses would arise due to the interaction of the inner and outer shell.

In any case, thermal stresses associated with the fire transient can be classified as secondary, displacement limited stresses. As limits on secondary stresses do not apply for accident conditions (per Section 2.1.2), the magnitude of thermal stresses during the fire transient are of little consequence and are not specifically determined herein.

3.5.6 Evaluation of Package Performance for Hypothetical Accident Thermal Conditions

Of the component temperatures noted from the transient analyses for the undamaged cask condition, none exceeded the temperature limitations of the respective materials as defined in Section 3.3. The highest lead temperature noted is 270°F below the melting point, while the highest seal temperature remains below 300°F. This temperature is within the extended exposure operating limit for the butyl rubber used in the cask O-ring seals.

Similar results were seen for the case of the corner drop with pin puncture damage. In this case, the peak seal temperature was 296°F. This temperature, together with the time of exposure, indicates that the seals will not be adversely affected.

In conclusion, all analyses indicate that no loss shielding or loss of containment will occur as a result of the fire transient for either the undamaged or damaged conditions examined under this study.

APPENDIX 3.6

Thermal Modeling Notes

THIS INFORMATION IS PROPRIETARY

3.7 References

1. Rohsenow and Harvnett, Handbook of Heat Transfer, 1973, McGraw-Hill.

2. General Electric Handbook of Heat Transfer Properties, June 1976. General Electric Co. Section 515.5.

3. 'Emissivity Testing of Metal Specimens', NuPac Coordination Sheet #CHEM 3772, dated August 21, 1986. A copy of this memo is attached.

4. 'Rigid Urethane Foam Thermal Conductivity', letter report from Northwest Laboratories to General Plastics, Tacoma, WA. Laboratory report #E-32611, dated March 29, 1985.

5. Kreith, Frank. Principles of Heat Transfer, 3rd Edition, McGraw-Hill, Table A-3.

6. Nuclear Regulatory Commission, 10 CFR Part 71.73.

7. Thermophysical Properties of Matter, The TPRC Data Series, Purdue University, 1970, IFI/Plenum, New York and Washington.

8. Product Brochure for 'LAST-A-FOAM', General Plastics Manufacturing Company, Tacoma, WA.

9. Appendix 2.10.7 of 'TRUPACT-II Safety Analysis Report', Docket #71-9218, 1988.

4.0 CONTAINMENT

4.1 Containment Boundary

4.1.1 Containment Vessel

The containment boundary of NuPac 10/140MB is formed by an inner 0.75 inch stainless steel cylindrical shell, with ends formed from a varying thickness of heavy stainless steel forged plate. The upper end plate, as well as, optionally, the lower end plate, form removable lids for loading and unloading. The upper end plate features a large secondary lid designed to allow loading without removing the shielding capability of the primary lid.

4.1.2 Containment Penetrations

For models without the bottom loading capability afforded by a removable lower end plate, a testable drain port is provided to facilitate decontamination and other cleaning activities.

4.1.3 Seals and Welds

Each of the closures are equipped with NuPac's EnviroSeal^{tm} (for which patent protection is being pursued), which provide a very high degree of sealing capability while preventing damage from loading and unloading operations in the field. Each EnviroSeal^{tm} consists of a metallic ring, with four O-ring grooves cut into it, two on each side of the ring. Between the inner and outer O-rings on each side, large holes allow the free passage of gasses from either side of the ring. The ring is fixed in place by screws through the ring. Because the seal is fixed in place, the sealing surfaces on the lower half of the ring are protected from possible damage by the ring itself, while the grooves on the top surface are protected by the O-rings. The seal surface on the upper lid is protected by being in a relatively inaccessible location on the underside of the upper lid. For the optional removable lower lid, the EnviroSeal^{tm} stays with the lower lid, and the seal surface on the bottom of the side wall is protected by administrative controls requiring that the side

wall seal surface be kept from bearing against any surface except the seal on the lower lid.

The seals are protected from the effects of normal and hypothetical accident thermal conditions by thick sections of self-extinguishing polyurethane foam. The seal on the secondary lid is protected by a removable thermal shield/pad, and the primary lid seals are protected by the impact limiters. The seals are tested using helium mass spectroscopy to prove that the seals do not exceed a leak rate of 1×10^{-7} standard cubic centimeters per second. The design of the seals is such that a redundant seal is always present. Therefore, the seals provide an unprecedented level of security against leakage.

Prior to first use, the containment vessel welds are radiographed to show their integrity. Also prior to first use, the containment vessel is pressure tested to 1.5 times its design basis pressure, per the requirements of ASME Boiler and Pressure Vessel Code Section III.

4.1.4 Closure

Closure of the containment vessel is effected by a combination of eight ASME A320 Grade L43 bolts on each removable end, and sixteen ASME A320 Grade L43 bolts securing the secondary lid in the center of the upper primary lid. These devices provide for quick and secure closure of the containment vessel.

4.2 Requirements for Normal Conditions of Transport

Prior to each shipment of radioactive material not classified as a Type A quantity or Low Specific Activity (LSA), an assembly leak test meeting the requirements of ANSI N14.5 shall be performed to demonstrate proper assembly of seals. Because the NuPac 10/140MB cask may be used to ship particulate and semi-liquid payloads such as dewatered ion exchange resins, ANSI N14.5 may require that the cask be capable of being sealed to a 'leak tight' condition, or less than 1×10^{-7} standard cubic centimeters per second. This capability shall be demonstrated annually, or whenever the O-rings, EnviroSeal^{tm} ring or other seal elements are changed or reworked.

4.2.1 Release of Radioactive Material

Section 2.6 above demonstrates that normal conditions of transport do not impart loads on any part of the containment vessel in excess of the Regulatory Guide 7.6 design criteria. Because the containment vessel is equipped with NuPac EnviroSeals™, which allow for minor flexure of the seal without loss of containment, there shall be no release of radioactive material to the environment in excess of the tested leak rate of the seals. This leak rate, deemed to constitute 'leak tight' conditions per ANSI N14.5, is extremely insignificant. Assuming a pressure gradient of one atmosphere (14.7 psi), this leak rate would result less than four liters of leakage in 300 years.

4.2.2 Pressurization of Containment Vessel

Section 2.6.3 addresses the structural capability of the NuPac 10/140MB cask for normal pressure. That section demonstrates that the pressures present for normal conditions will not reduce the effectiveness of the package design.

4.2.3 Coolant Contamination

There are no coolants in the NuPac 10/140MB package design, so this section is not applicable.

4.2.4 Coolant Loss

There are no coolants in the NuPac 10/140MB package design, so this section is not applicable.

4.3 Containment Requirements for the Hypothetical Accident Conditions

Section 2.7 above demonstrates that in all hypothetical accident conditions, no significant permanent deformation of the package would be experienced, assuring that the EnviroSeals[tm] remain compressed. Because of the Enviro-Seal[tm]'s double sided seal design, the seal can tolerate an extraordinary amount of seal distortion without significantly affecting the effectiveness of the seal to remain within ANSI N14.5 limits defining leak-tightness. This is well in excess of the leak requirements of ANSI N14.5 accident criteria for any possible payload.

4.3.1 Fission Gas Products

The NuPac 10/140MB package will normally contain negligible quantities of fission gas products.

4.3.2 Releases of Contents

Because the residual seal effectiveness following a hypothetical accident is the same as for normal conditions of transport, there can be no release of radioactive materials in excess of the limits defined in 10 CFR 71.

5.0 SHIELDING EVALUATION

This chapter will describe and quantify the shielding capabilities of the NuPac 10/140MB cask. This is provided merely as a guideline for users to evaluate the package for their particular transport needs. In all cases, a radiation survey will be made prior to the release of a particular cask for shipment to verify that external radiation dose rates fall below the limits set by 10 CFR 71.

5.1 Discussion and Results

Because each shipment may include an indeterminate quantity of various isotopes, it is not possible to fully assess the external dose rate from every possible payload isotope content and distribution. In many cases it is difficult to determine this information even for specific shipments. As a result, shielding calculations have been performed assuming that the source consists entirely of Cobalt-60, an isotope commonly found in power plant waste streams. The use of ^{60}Co as a benchmark case for shielding is justified, since in most shipments, it is the presence of this isotope which controls the external dose rate.

Table 5.1-1 presents the estimated surface dose limits of typical liners filled with dewatered resins loaded to the maximum distributed quantity of ^{60}Co which would remain below 10 CFR 71 limits. In other words, a liner loaded with ^{60}Co resin showing a surface dose rate of that indicated would cause a dose rate at the surface of the 10/14MB cask would not exceed 200 mr/hr, and the dose rate 2 meters from the side of the conveyance would not exceed 10 mr/hr.

TABLE 5.1-1

Total ^{60}Co Curies	Dose (R/hr) Center of Liner	At Liner Surface	At Cask Side	2M From Side of Conv.	Top Surface
160.5*	471.5	76.0	0.060	0.010	0.182

* 160.5 Ci of ^{60}Co is equivalent to 2.5 watts

5.2 Source Specification

5.2.1 Gamma Source

The point-kernel method of calculating shielding effectiveness was used to generate the data presented in Table 5.1-1. It was assumed that the gamma source was ^{60}Co uniformly distributed within a bed of dewatered resins completely filling a typical Enviralloy^{tm} High Integrity Container sized specifically for the NuPac 10/140MB model cask. The ^{60}Co source is assumed to emit two gamma photons per disintegration, one of approximately 1.17 MeV and the other at approximately 1.332 MeV. The quantity of ^{60}Co was determined by scaling a unit quantity by that required to remain within the 10 CFR 71 limits. Self-shielding is accounted for by assuming that the resin exhibits approximately the same attenuation properties as water.

5.2.2 Neutron Source

Since only negligible quantities of neutron emitters would be shipped within the Series B casks, no neutron sources were assumed for this shielding evaluation.

5.3 Model Specification

5.3.1 Description of the Radial and Axial Shielding Configuration

5.3.1.1 Radial Shielding

The radial shielding of the NuPac 10/140MB consists of a 0.75 inch inner stainless steel shell, a 2.25 inch lead thickness, and a 1.25 inch thick outer shell. For the purposes of Table 5.1-1, the 0.375 inch thick wall of the Enviralloy^{tm} High Integrity Container was included in the shielding model, as well as the 0.50 inch thick top plate. This additional element of shielding is considered to be part of a typical configuration. Figure 5.3.1-1 shows schematically how the radial shielding is modeled.

FIGURE 5.3.1-1

Radial Shielding Model Diagram

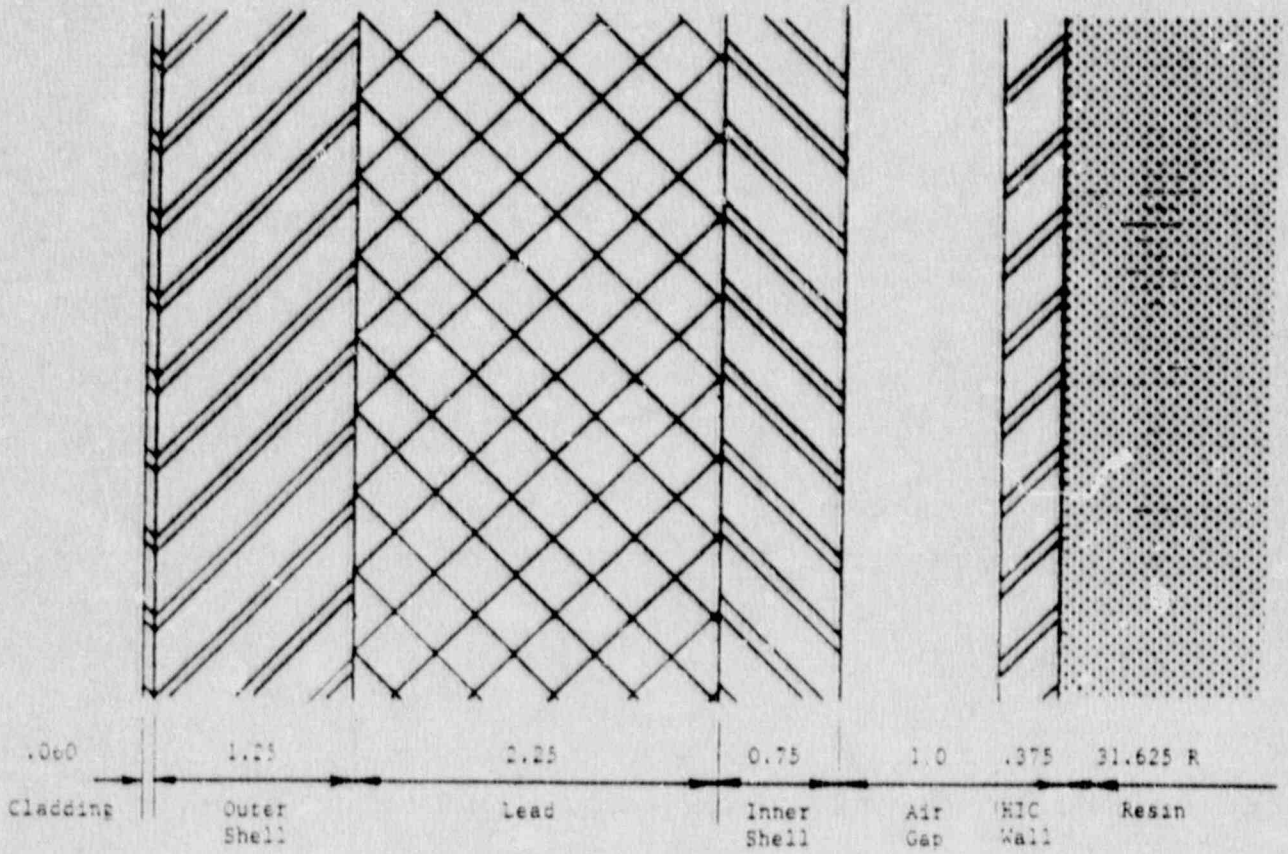

5.3.1.2 Axial Shieldins

Axial shielding in the NuPac 10/140MB cask is provided by thick stainless steel plates on each end. The plates have been sized such that the payload source which would just meet the 10 CFR 71 requirements for radial external dose rates would cause an external dose rate through the end of the cask at or below 200 mr/hr at the package top surface.

5.3.2 Package Regional Densities

The calculational method used for this analysis requires that the mass densities and mass attenuation coefficients for the various regions of the shield be known. The point-kernel build-up factors are also required.

Mass attenuation coefficients and build-up factors are taken from Reactor Handbook, Volume III, Part B, Second Edition. Following the recommendation of N. M. Schaeffer in Reactor Shielding for Engineers, the outermost material greater than two mean free paths thick is used to calculate the build-up factor.

The mass attenuation coefficients and build-up factors for steel were taken to be the same as iron. The properties of water were substituted in regions designated as resin.

The density of steel is assumed to be 490 lbm/ft.^{3} while lead is assumed to be 700 lbm/ft^3. Resin is assumed to be 62.4 lbm/ft.^{3}. The attenuation of air is conservatively neglected.

5.4 Shielding Evaluation

The data presented in Table 5.1-1 above was generated using standard point-kernel techniques on a very simplified model of a possible payload. Because of the uncertainty inherent in the payload to be shipped in this type of cask, the data presented in that table should be considered as reference only. To assure compliance with the requirements of 10 CFR 71, a radiation survey is taken prior to each shipment. The following is a description of the technique used to develop the table.

A computer program was developed by Nuclear Packaging, Inc. to apply these techniques in an iterative fashion to the unique geometric constraints of a right circular cylindrical shield. The program, referred to as 'SAP' for Shielding Analysis Program, breaks up the source term into discrete elements each treated as point sources with no self-shielding. The attenuation of other elements of the source is not ignored, however. The attenuation of photons emanating from each discrete element is calculated, and the dose from all elements are integrated (summed) to arrive at the total dose rate at a given distance from the outside of the shield. To speed calculations, the contribution to the dose rate of elements of source farther than a specified number of mean free paths from the outside of the source are ignored. For the purposes of Table 5.1-1, elements more than 5 mean free paths from the source surface are ignored, since they do not contribute significantly to the total external dose rate at the point in question.

The relative size of the elements of source is controlled by the user. In general, the smaller the elements, the more accurate the results, as in any numerical integration procedure. However, because self-shielding is ignored within calculation of the dose contribution of each individual element, the dose rate calculated is conservatively predicted regardless of the size of the elements.

1

IMAGE EVALUATION TEST TARGET (MT-3)

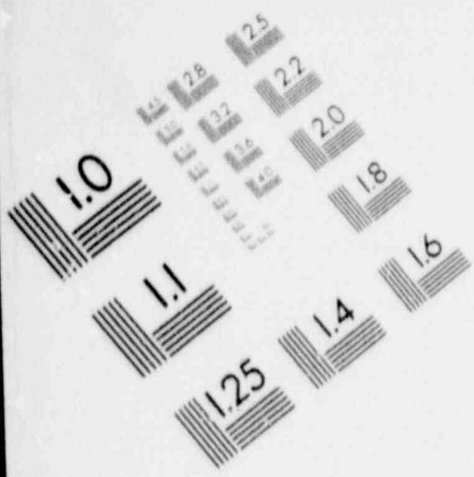

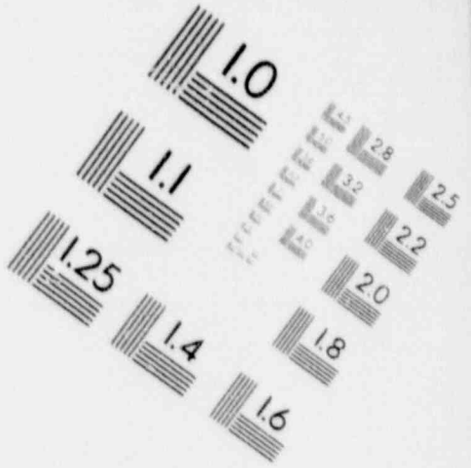

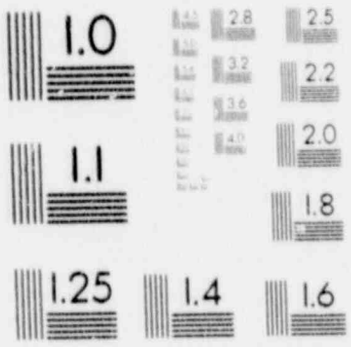

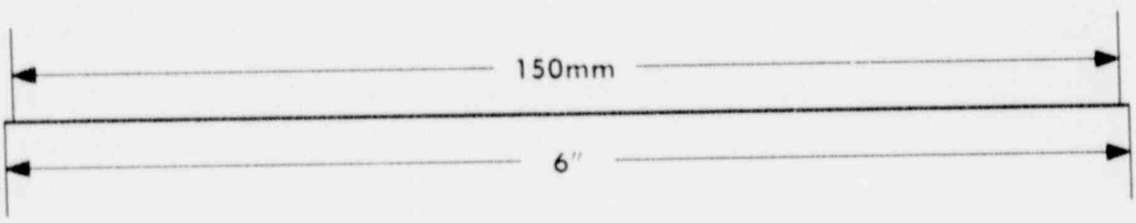

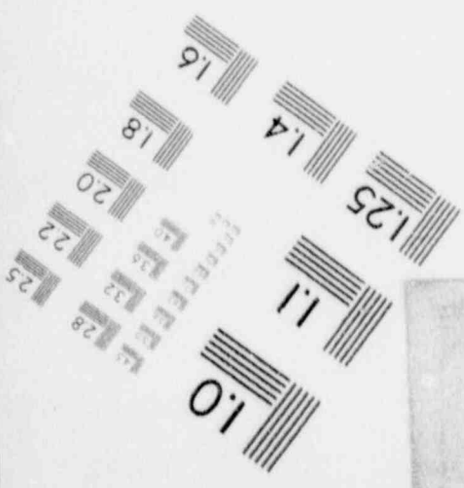

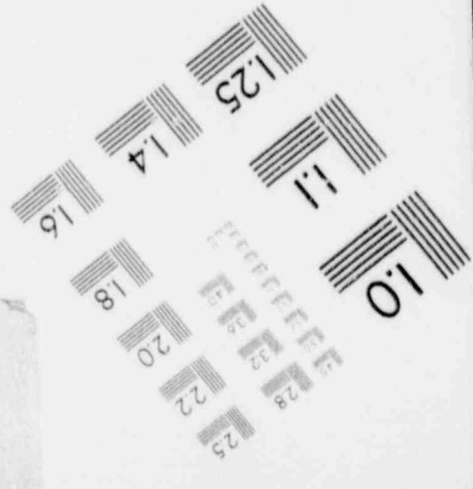

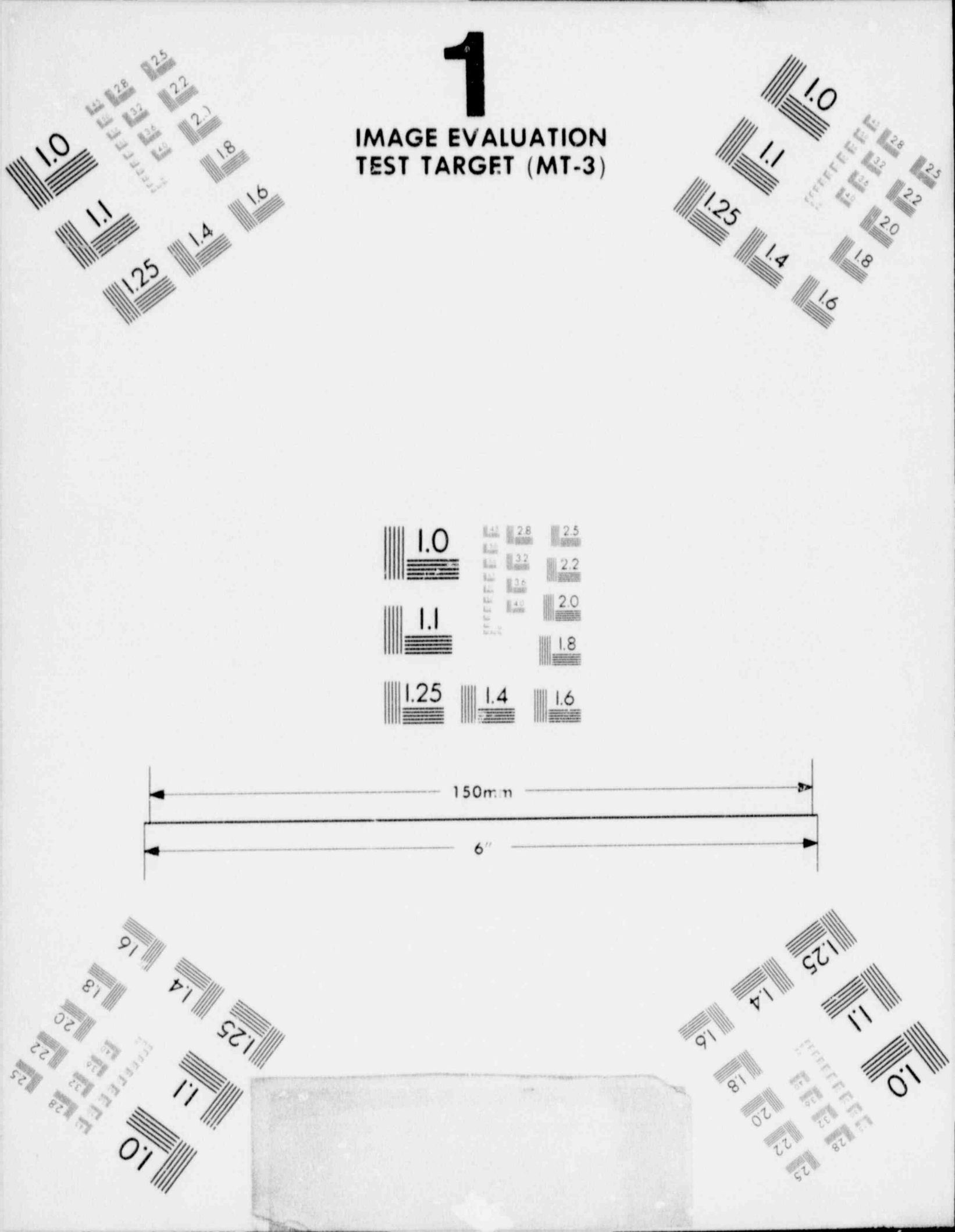
1
IMAGE EVALUATION
TEST TARGET (MT-3)
1.0
1.1
1.25
1.4
1.6
1.8
2.0
2.2
2.5
2.8
3.2
3.6
4.0
150mm
6"

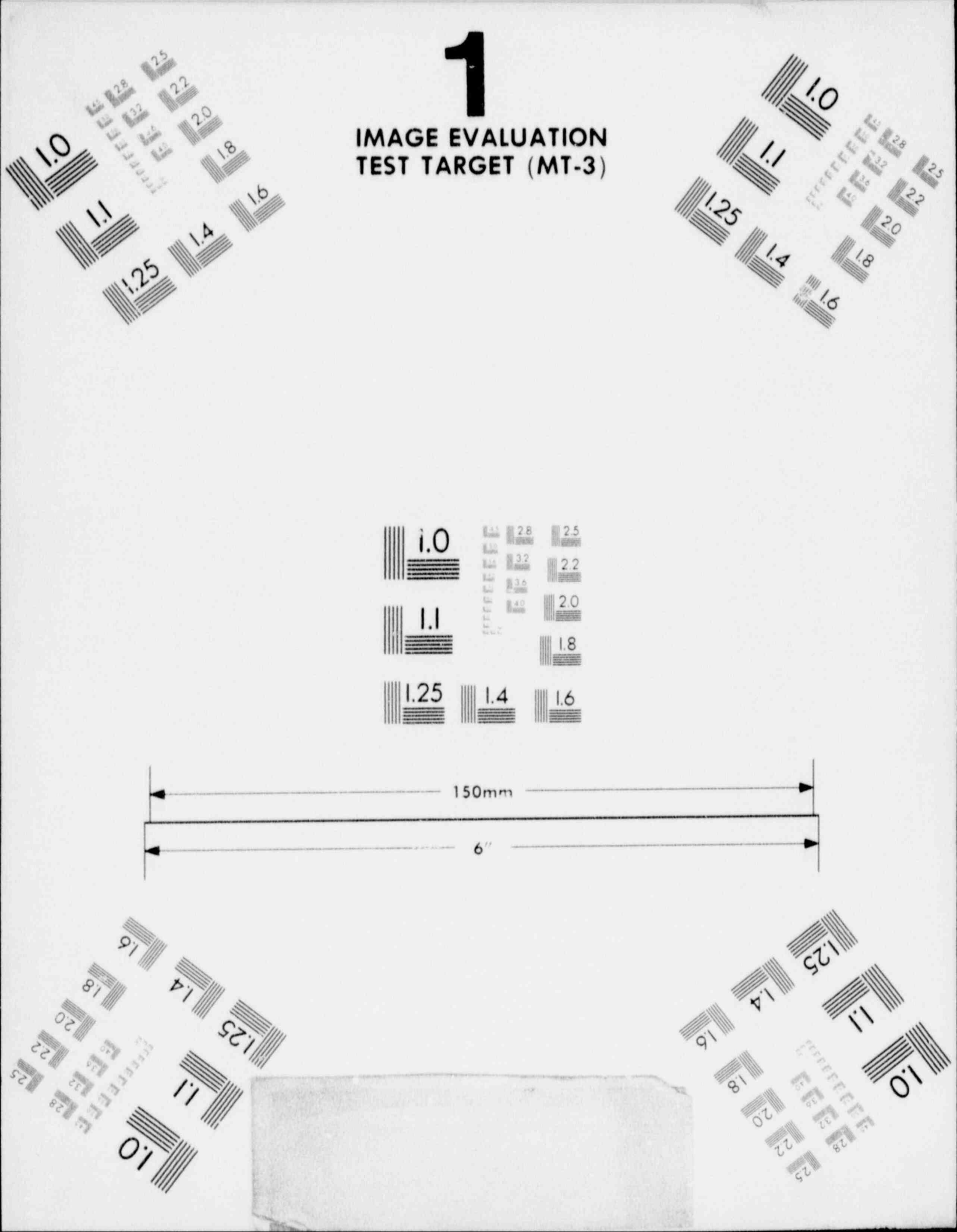
1
IMAGE EVALUATION
TEST TARGET (MT-3)
1.0
1.1
1.25
1.4
1.6
1.8
2.0
2.2
2.5
2.8
3.2
3.6
4.0
150mm
6"

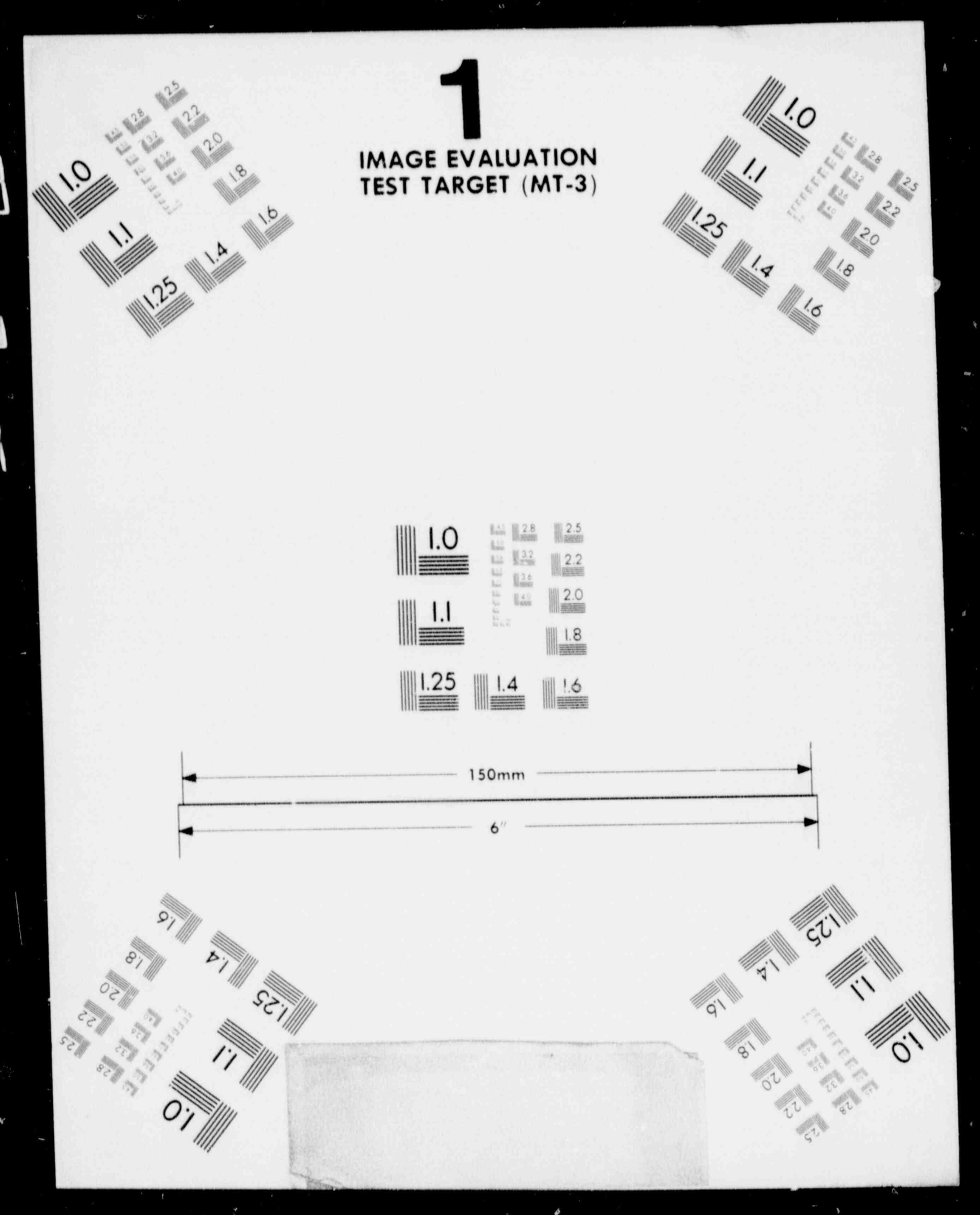
1
IMAGE EVALUATION
TEST TARGET (MT-3)
1.0
1.1
1.25
1.4
1.6
1.8
2.0
2.2
2.5
2.8
3.2
3.6
4.0
150mm
6"

The program evaluates the expression:

$$\phi_A = S\ B\ \exp(-\sum \mu t)\ 4\pi R^2$$

where ϕ_A = Photon flux at the point in question
S = Photon Generation Rate
B = Dose Build-up Factor
μt = Number of mean free paths through material of mass attenuation coefficient μ and thickness t
R = Distance from source element to point in question

for each element of the source and each source photon energy and generation rate. A running total of the contributions to the photon flux at the dose point is kept for all elements less than 5 mean free paths from the edge of the source. From the above expression, it is clear that the other elements will contribute very little to the total flux at the dose point.

The total photon flux from each gamma energy level is then converted to dose rate by means of a standard flux-dose relation from the Reactor Handbook.

The program allows either cylindrical or infinite slab shields to be modeled as well as cylinderical or rectangular source volumes. It allows point and line source calculations as well.

The program has been benchmarked against ANYSN and QAD calculations as well as actual measurements, with good results. Comparisons show the SAP output to be within 10% of other calculational methods, which is well within the accuracy of the point-kernel technique.

As stated in Section 5.1 above, these calculations are presented as a means of approximating the general shielding characteristics of the NuPac 10/140MB cask. In every case, the cask should be surveyed to determine that the regulatory dose rate limits are not exceeded prior to delivery of the package to a carrier for transport. The dose rates and contents limits suggested by Table 5.1-1 are not intended to be used as administratively controlled limits, since many parameters not modeled may affect the actual measured dose rate and permissable radioisotope quantities within any given shipment.

6.0 CRITICALITY

6.1 Discussion and Results

Because the NuPac 10/140MB package will not contain significant quantities of fissile material, this section is not applicable.

7.0 OPERATING PROCEDURES

This section describes the general procedures to be used for loading and unloading the various configurations of the NuPac 10/140MB packaging.

7.1 Procedures for Loading the Package

The following procedure assumes that the cask is in the loading area assembled in its over-the-road configuration. The cask may or may not be on the vehicle used to transport the cask over public roads.

7.1.1 Remove the Thermal Shield Cover from the top of the package. Remove the ball-lock pins securing the top impact limiter to the cask, and remove the impact limiter. Loosen and stow the closure bolts which secure the primary lid.

7.1.2 Remove the lid by attaching suitable hooks to the primary lid lifting lugs. Care should be taken during the operation so as not to damage the lid to body interface seal while setting the lid down. Inspect the EnviroSeal^{tm} plate for signs of damage or wear.

7.1.3 Inspect the inside of the shielded cask to assure there are no loose articles within the packaging. Inspect seal surfaces on underside of lid and clean if necessary. Carefully clean the primary lid seal. Replace O-ring seals at least once a year or upon signs of wear or deterioration.

7.1.4 Place the disposable steel liner into the cask. If the liner is significantly smaller than the internal cavity of the cask, sufficient shoring and/or bracing shall be provided to insure the payload will not shift significantly during shipment.

7.1.5 Replace lid and secure it to the cask body using the closure bolts. Torque primary lid bolts to 455±15 ft-lb torque. Replace top impact limiter and reinstall ball-lock pins. Install lock wire on all three impact limiter hoist rings to preclude their use during transport.

7.1.6 If any loading of material is to be done through the secondary opening in the upper lid of the cask, the secondary lid nuts should be removed and Steps 7.1.7 through 7.1.10 shall be performed.

7.1.7 The lug in the center of the secondary lid may be used to remove the secondary lid from the cask. Care should be taken to avoid damage to the sealing surface on the lip of the secondary lid.

7.1.8 Inspect secondary lid bolts for signs of wear. Damaged threads and excessive corrosion shall be cause for replacement of these items. Measures should be taken to protect the EnviroSeal^{tm} in the secondary lid opening from damage during loading operations.

7.1.9 Load cask through secondary lid. Replace secondary lid and torque bolts to 200±10 ft.-lbs. Install a tamper-indicating seal on the secondary lid.

7.1.10 Survey the loaded cask to assure compliance with 10 CFR 71.47. Inspect for surface contamination per the requirements of 10 CFR 71.81(i).

7.1.11 Perform an assembly verification leak-test per 8.2.5.1 or 8.2.5.2, as required by ANSI N14.5. Undisturbed seals (those which have not been opened since their most recent leak test) need not be tested. This assembly verification test shall demonstrate that all tested seals exhibit leak rates less than $1x10^{-3}$ standard cubic centimeters per second, and any leak actually

detected is less than $1x10^{-7}$ standard cubic centimeters per second. The sensitivity of the assembly verification leak test shall be $1x10^{-3}$ scc/sec.

7.1.12 Replace the top lid Thermal Shield Cover and install tamper indicating device on at least one locking pin.

7.1.13 Inspect the package for proper labeling necessary to meet all applicable regulations.

7.1.14 Using suitable material handling equipment, transfer the package to the transport vehicle, if it is not already on the vehicle.

7.1.15 Check to see that the Thermal Shield Cover lifting lugs are covered for transit.

7.1.16 Install a tamper-indicating seal on one or more of the upper impact limiter ball-lock pins.

7.1.17 Secure package to the transport vehicle using the approporiate tie down devices, if it is not already tied down. If the cask had been previously secured to the vehicle, re-check all tie-down devices for proper security.

7.1.18 NuPac 10/140MB packages may be equipped with bottom loading capability to facilitate remote loading operations in fuel pools or other waste storage facility. The procedures for such operations are similar to those for top loading in Steps 7.1.1 through 7.1.17.

7.2 Procedures for Unloading the Package

7.2.1 The requirements of 10 CFR 20.205 shall be followed whenever greater than Type A quantities of RAM are received.

7.2.2 Move the unopened package to the appropriate unloading area. Place it in a suitable unloading attitude.

7.2.3 Perform an external inspection of the unopened package.

7.2.4 Remove tamper-indicating seals from impact limiter ball-lock pins.

7.2.5 Repeat steps 7.1.1 and 7.1.2 in Section 7.1, above, for removing the primary lid.

7.2.6 Remove the disposable steel liner.

7.2.7 After unloading the entire package, the interior and exterior shall be visually inspected to assure that it has not been significantly damaged i.e., no cracks, punctures, holes or broken welds.

7.2.8 The following configuration checks shall be performed after unloading and prior to any loading activity:

7.2.8.1 Exterior nameplates, stencils, placards and other required identification is in place and legible.

7.2.8.2 Ball-lock pins, bolts and seals are in place and in good operating condition and free of defects.

7.2.8.3 All required documentation is completed and retained/displayed as specified by the regulatory authority and the user.

7.3 Preparation of an Empty Package for Transport

Previously used, empty packages are handled per the requirments of 49 CFR 173.427.

8.0 ACCEPTANCE TESTS AND MAINTENANCE PROGRAM

8.1 Acceptance Tests

The NuPac 10/140MB packaging shall be inspected and released for use by responsible operation personnel prior to loading. The following items shall be included in such inspection:

8.1.1 Before first use, the 10/140MB package shall be subjected to a fabrication verification leak test of the entire containment boundary at $1x10^{-7}$ scc/sec.

8.1.2 All configuration checks described in Section 7.2.8 above.

8.1.3 The cask shall be pressure tested to 1.5 times the maximum normal operating pressure of the cask. This is taken as the pressure given for the Normal Conditions of Transport in Section 3.4.4. In that section, the pressure is given as 6.8 psig., so this test shall be carried out at least 10.2 psig. Following the pressure test, all containment welds shall be liquid penetrant inspected in accordance with ASME Code, Section III, Division I, Subsection NB, Article NB-5000, and Section V, Article 6.

8.1.4 The integrity of the shield shall be demonstrated by means of a gamma scan performed on the lead-filled cylinder during the fabrication process, as described in Appendix 8.3.1 below.

8.2 Maintenance Program

8.2.1 A good sound industrial maintenance program should be followed to assure the integrity of the NuPac 10/140MB packaging. Components such as O-ring seals, ball-lock pins, and bolts shall be inspected prior to each use and repaired or replaced as necessary. A leak test shall be performed when seals are replaced or when damaged seals are suspected. The test shall be performed in accordance with Section 8.2.5 below.

8.2.2 As a minimum, O-ring seals shall be replaced with new O-rings meeting the description in the drawings shown in Appendix 1.3 every twelve (12) months (sooner if visible wear is detected).

8.2.3 Primary lid closure bolts must operate freely and easily. They shall be lubricated as required for installation, and replaced if necessary.

8.2.4 Any damaged or lost fasteners shall be replaced with equivalent grade and strength as shown on the drawings in Appendix 1.3.

8.2.5 Whenever the O-ring seals are replaced, a leak test shall be conducted (see below). Regardless of condition, all O-ring seals shall be replaced every twelve (12) months.

8.2.5.1 The package shall be leak tested utilizing a Mass Spectrometer Leak Detector (MSLD) type test in accordance with ANSI N14.5, Section A3.8. The helium test gas shall be introduced to the fully assembled package through appropriate fittings.

8.2.5.2 The leak test described in section 8.2.5.1 shall be performed at the Primary and Secondary seals and at all ports as appropriate for the particular 10/140MB cask configuration. The acceptance criterion shall be 1×10^{-7} scc/sec. Test sensitivity shall be approximately 5×10^{-8} scc/sec.

APPENDIX 8.3.1

Gamma Scan

8.3 APPENDIX

APPENDIX 8.3.1 DISCUSSION OF GAMMA SCAN PROCEDURE

Lead shielding integrity shall be confirmed via gamma scanning. There are two gamma scan techniques utilized. The main difference is in the method utilized to determine acceptance criteria.

Both gamma scan techniques are exactly the same in all other respects and are conducted as follows.

An Eberline E120 probe or equivalent is used to scan the outer surface of the cask while an Iridium 192 or Cobalt 60 source of sufficient strength is present in the center of the cask. The source is first placed on the bottom of the cask while the surface is scanned around its circumference parallel to the source. The source is then moved up a pre-determined distance and the circumference scanned again. This sequence is repeated until the entire cask surface is scanned.

For these tests, the cask surface is gridded (in this case the grid consists of 4 inch squares) and a chart is made to reflect the gridded cask surface. Readings are taken from each grid square by scanning every point in the grid and recording the maximum reading in the corresponding grid on the chart. This data then serves as the raw gamma scan results. All readings are in Milliroentgens (MR).

The readings are evaluated by comparing them to predetermined MR values for nominal, or as designed, lead thickness and nominal -10% lead thickness.

The two different methods utilized to determine acceptance criteria are discussed below.

The Laboratory Calibration Method utilizes test blocks of the cask wall made up of lead and steel sheets. The test blocks simulate nominal or as designed and -10% lead thicknesses. The source is placed behind the test block at a distance equal to the inside radius of the cask. The probe is then placed on

the outside of the test block and readings are taken. This sequence is repeated on the nominal and -10% test blocks and the data is recorded.

The resultant values are then averaged. A ratio of the values is also developed. Then the average value is multiplied by the ratio. The value so derived is the maximum acceptable value for the shielding to be inspected.

An optional Laboratory Calibration Method can be utilized in lieu of the lead/steel calibration mockup method. In that case, calculations are run to establish acceptance criteria.

To do this, compiled source power data and attenuation characteristics data for steel, lead and distance through air are utilized to calculate the expected readings at the cask surface. The calculations allow for different source powers and are corrected for nominal and -10% shielding configurations.

The following excerpt from NuPac Gamma Scan Procedure No. GS-001 is provided to illustrate the calculation Method of Laboratory Calibration:

1.1 The nominal and -10% shielding calibration MR readings may be obtained via calculation as an option. These calculations shall be performed as follows:

1.1.1 Data and transmission charts found in the Tech/Ops Gamma Radiography Radiation Handbook shall be utilized. Copies of the handbook can be obtained from:

Tech/Ops, Inc.
Radiation Products Division
40 North Avenue
Burlington, Mass. 01803

1.2.2 Attachment A, Table 2, 'Selected Radioisotope Data' from the handbook shall be utilized to obtain source power data. (Copy of Table 2 included as Attachment A.)

1.2.3 Attachment B figures of the handbook shall be utilized to determine the attenuation of Gamma Rays in the shielding materials utilized in the cask to be inspected. (Copy of typical figures included as Attachment B.)

1.2.4 The following is an example of the calculated calibration method using Cobalt 60:

EXAMPLE

Cask O.D. 48 in. Cask I.D. 36 in. I.D. Wall 0.50 in. O.D. Wall 0.50 in. Fe

Lead Shielding = 5.0 in. Less 10% lead shielding = 4.5 in.

Total Fe shielding = 1.0 in.
Source Cobalt 60 strength 15 curies x 14.0 = 210 R/Hr at 12 in. (using Attachment A).

210 R/Hr at 12 in. = 52.5 R/Hr at 24 in. $(210x(12)^2/(24)^2=52.5)$. This would be the outer surface of the cask.

52.5 R/hr at 24 in. x reduction factor for 1.0 in. Fe 0.58 = 30.45 R/Hr.
30.45 R/Hr at 24 in. x reduction factor for 5.0 in Pb 0.0009 = 27.4 mR/Hr.

30.45 R/Hr at 24 in. x reduction factor for 4.5 in. Pb 0.00185 = 56.3 mR/Hr (using Attachment B).

Design thickness reading at cask surface = 27.4 mR/Hr.
Design thickness reading less 10% Pb = 56.3 mR/Hr.

The following is an example of the calculated calibration method using Iridium 192:

EXAMPLE

Cask O.D. 48 in. Cask I.D. 46 in. I.D. Wall 0.25 in. Fe O.D. Wall 0.25 in. Fe

Lead Shielding = 1.5 in less 10% lead = 1.35 in.

Total Fe Shielding 0.50 in.

Source Iridium 192 50 curies x 5.9 = 295 R/hr at 12 in. (using Attachment A).

295 R/Hr. at 12 in. = 73.75 R/Hr at 24 in. ($295x(12)^2/(24)^2$ = 73.75).
This would be the outer surface of the cask.

73.75 R/Hr at 24 in. x Reduction Factor for 0.50 in. Fe 0.55 = 40.56 R/Hr.
40.56 R/Hr. x Reduction Factor for 1.50 in. Pb. 0.0024 = 97.4 mR/hr.
40.56 R/Hr. x Reduction Factor for 1.35 in. Pb. 0.004 = 162.3 mR/hr. (using Attachment B.)

Design thickness reading at cask surface = 97.4 mR/Hr.
Design thickness reading less 10% of Pb = 162.3 mR/Hr.

The calculation values and methods are based on data developed during approximately 300 actual calibrations utilizing the lead sheet/steel plate sandwich technique described in Rev. 4 of the referenced procedure.

Additional correlation has been provided by the use of established attenuation values obtained from the various figures found in the Tech/Ops Radiation Safety Handbook. This reference source is a recognized standard document utilized throughout the NDE industry. This information, together with NuPac's, extensive laboratory data enabled NuPac to develop the current optional calculation method of laboratory calibration for gamma scan.

The calculation method provides a greater degree of accuracy and correlation to the actual gamma scan conditions present in a typical cask than the lead and steel plate setup used in the past. It also reduces operator exposure during the calibration phase. The resultant calibration values for acceptance

of the lead shield are, in fact, slightly more conservative and therefore assure a greater margin of safety for the shield.

The resultant improvement in the calibration of gamma scan acceptance criteria provides greatly improved accuracy and repeatability.

To illustrate this accuracy, correlation and conservativeness, the calibration data for a typical NuPac OH-142 (C of C No. 9073) gamma scan was rerun using the calculation method of Laboratory Calibration. The original calibration technique for this cask had been the lead and steel setup method.

The correlation between the two Laboratory Calibration methods is essentially identical. The variance in the acceptance criteria between the two methods is from .3 mR in the nominal to .1 mR in the -10% values. This equals to more than 2% variance between the Pb/Fe and calculation methods of Laboratory Calibration. The difference in percentage (DIFF, %) between the nominal and -10% values for the two calibrations is also very close with the Pb/Fe at 64% and the Calc at 63%. The calibration results follow:

SUMMARY OF GAMMA SCAN ACCEPTANCE VALUES - NuPac OH-142 (C of C No. 9073)

Source Type	Source Strength (curies)	Calib Type (1)	Nominal Value (mR)(2)	-10% Value (mR)(3)	Diff (%)(4)
Co60	11	Pb/Fe	21.5	33.5	64%
Co60	11	Calc	21.2	33.4	63%

NOTES:

1. Pb/Fe = Laboratory Calibration using lead and steel sheets to simulate the cask wall. Calc = Laboratory Calibration using the calculation method.

2. Nominal Values is the calibrated acceptance value expected if the lead and steel thickness meet the design requirements.

3. The -10% value is the calibrated gamma reading expected if the lead thickness is 10% less than that required by the design. The steel thickness is assumed to be at the nominal. This reading will be larger than the nominal reading. No reading above this value during actual gamma scan inspection is acceptable.

4. DIFF (%) refers to the percentage of difference between the Nominal and -10% values. A variance of approximately 5 to 6% between the nominal and -10% values of separate calibrations is normal. This is attributable to differences in lead density (cast vs. rolled sheet), accuracy of meters and related equipment, as rolled steel thickness variables, etc.

The Field Calibration Method utilizes a specially fabricated test lid which incorporates a holder for various lead and steel sheet thicknesses. This fixture is installed onto the cask to be scanned. The test lid is then set up to simulate the nominal lead thickness, and the source is placed below the test lid in the cask at a distance equal to the inside radius of the cask. Readings are then taken. The test lid is then set up to recreate the -10% lead thickness configuration, and readings are again taken.

Other readings are then taken in 1/8 inch lead thickness increments between and beyond the two base readings until four to eight readings are obtained. The data is then plotted on a chart of readings versus lead thickness. The value for nominal lead -10% is then utilized as the maximum acceptable reading during the actual gamma scan.

GS - 001 - ATTACHMENT A

TABLE 2
SELECTED RADIOISOTOPE DATA

Radioisotope	Halflife	Principal Photon Energies (keV)	Specific Gamma Ray Constant R/hr per curie	
			at 1 foot	at 1 meter
Cesium-137	30y	662	3.4	0.32
Cobalt-60	5.3y	1173, 1332	14.0	1.30
Iridium-192	74d	311, 468, 602	5.9	0.55*
Thulium-170	134d	84 keV x-rays	0.015	0.0014
Ytterbium-169	32d	63, 110, 131 177, 198, 308 Tm x-rays	1.35	0.125

*American National Standards Institute Standard N432 has proposed a value of 0.48R-m²/hr-Ci for the specific gamma ray constant for Iridium 192.

GS - 001 - ATTACHMENT B

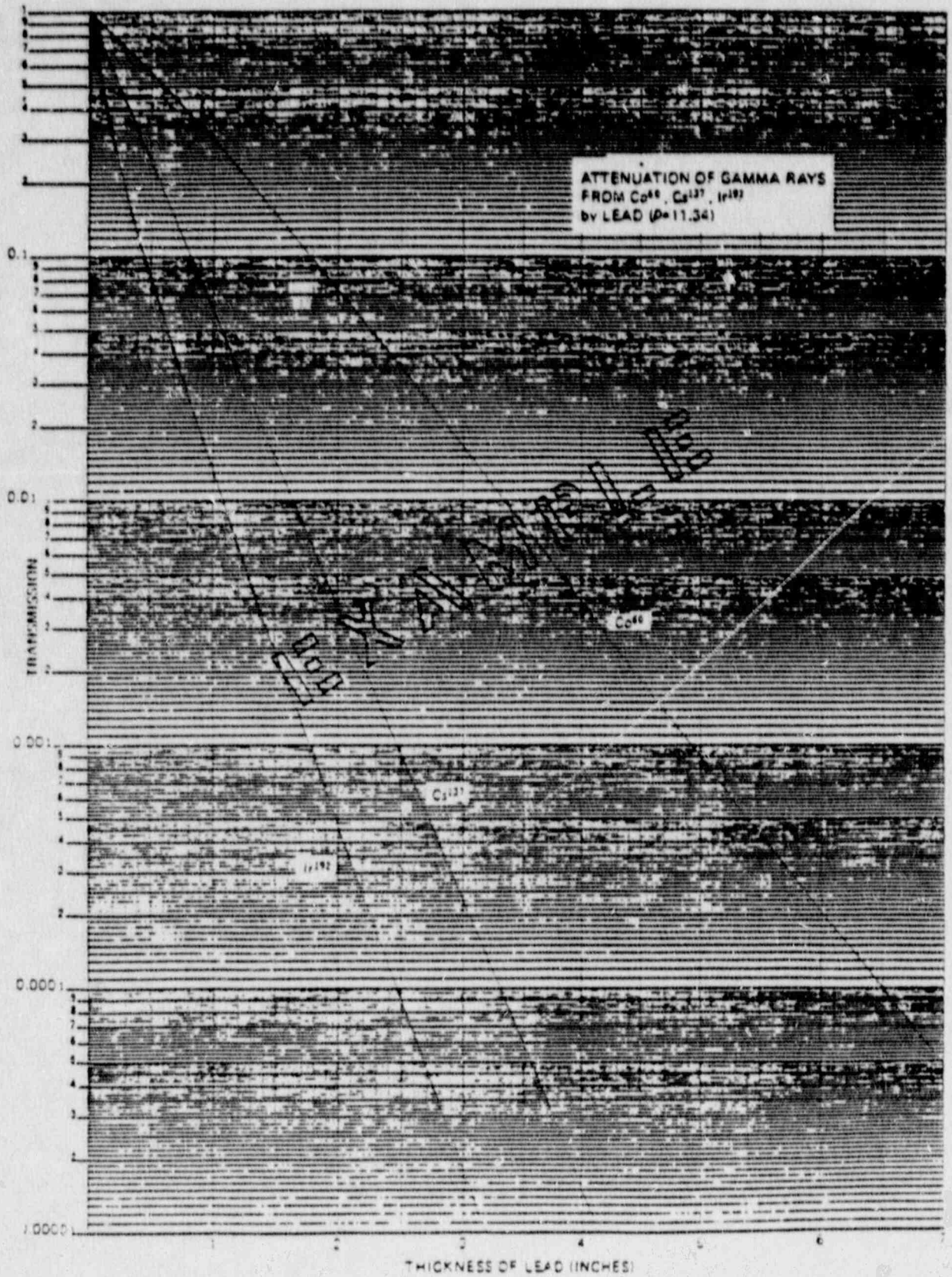

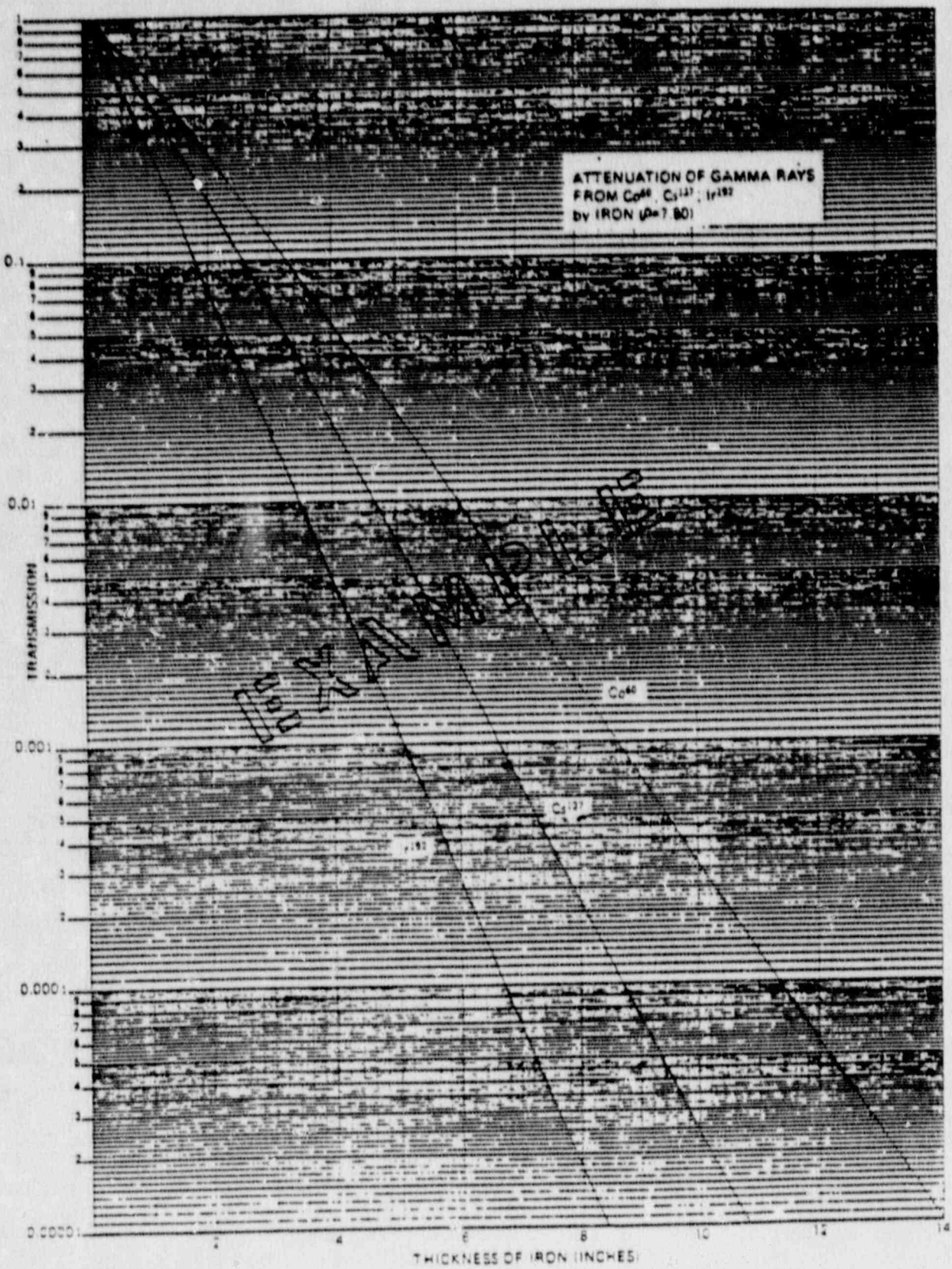
ATTENUATION OF GAMMA RAYS
FROM Co60, Cs137, Ir192
by IRON (ρ=7.80)
TRANSMISSION
THICKNESS OF IRON (INCHES)
Co60
Cs137
Ir192

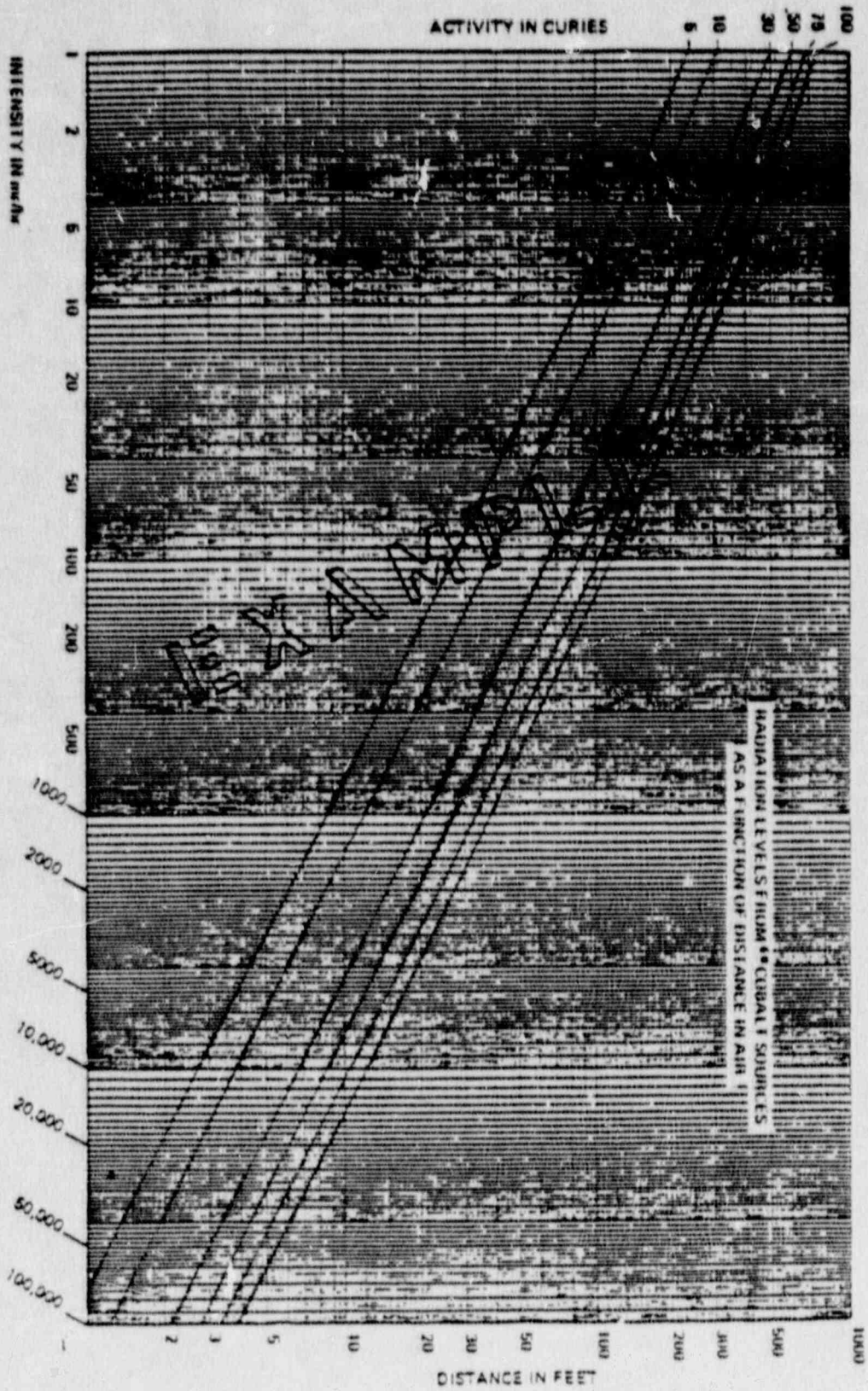
ACTIVITY IN CURIES
0
10
20
30
50
75
100
INTENSITY IN mr/hr
1
2
5
10
20
50
100
200
500
1000
2000
5000
10,000
20,000
50,000
100,000
RADIATION LEVELS FROM 60 COBALT SOURCES
AS A FUNCTION OF DISTANCE IN AIR
1
2
3
5
10
20
30
50
100
200
300
500
1000
DISTANCE IN FEET

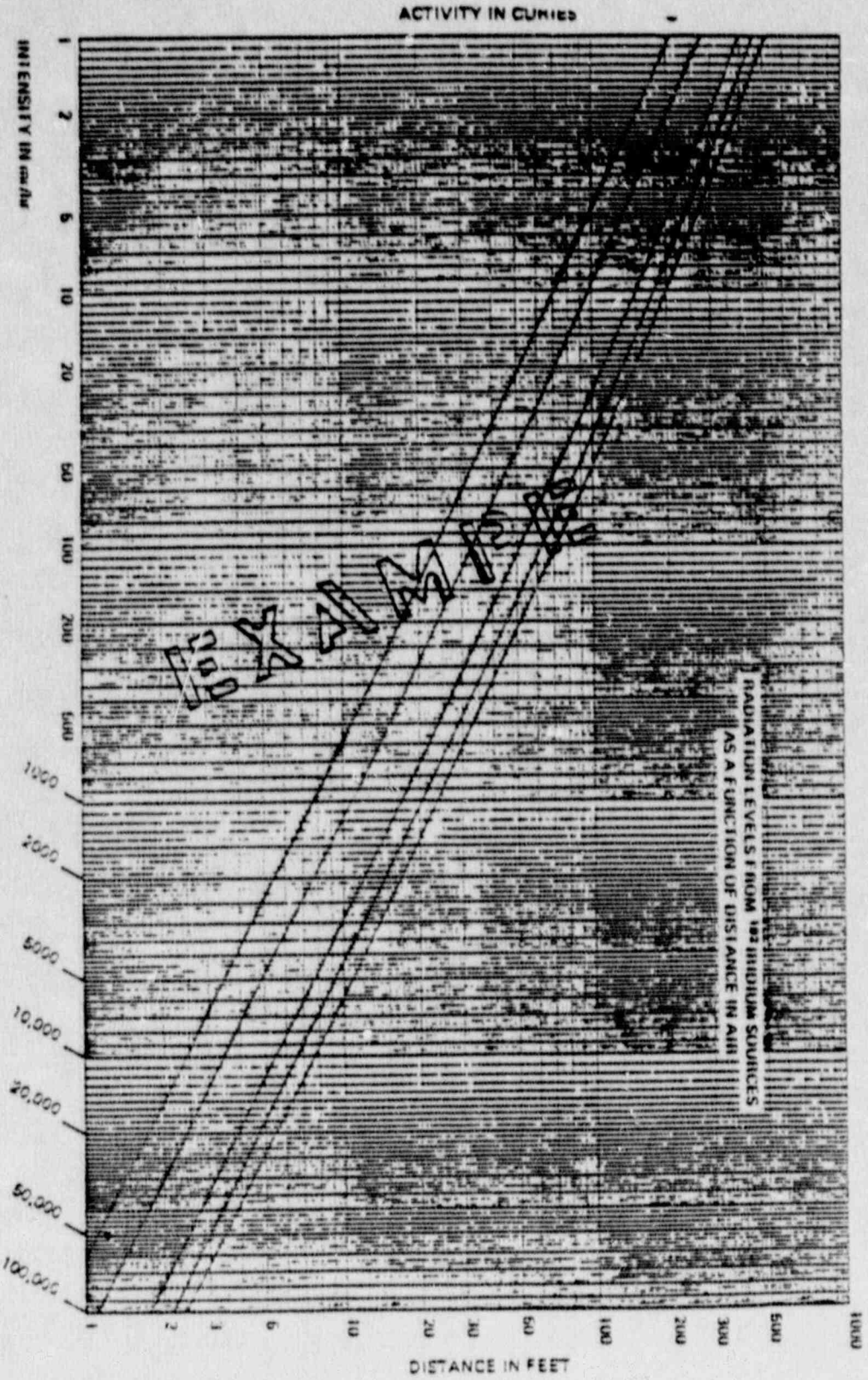
ACTIVITY IN CURIES
INTENSITY IN mR/hr
1
2
5
10
20
50
100
200
500
1000
2000
5000
10,000
20,000
50,000
100,000
1
2
5
10
20
30
50
100
200
300
500
1000
DISTANCE IN FEET
RADIATION LEVELS FROM 192 IRIDIUM SOURCES
AS A FUNCTION OF DISTANCE IN AIR
EXAMPLE

APPENDIX 8.3.2

Helium Leak Testing

The NuPac 10/140MB shielded shipping cask is designed to the Type B criteria of 10 CFR 71. The criteria also places certain requirements for acceptance of the cask during fabrication and after in-service seal maintenance. A major requirement pertains to acceptable leakage past the cask seals. The acceptable leak rate for the seal integrity test is $1x10^{-7}$ atm-cm^3/s or less based on dry air at 25°C. The requirement is delineated in detail in ANSI N14.5, Leakage Tests on Packages for Shipment of Radioactive Materials.

The accepted method for ascertaining leak rates in the $1x10^{-7}$ range is via a Helium Mass Spectrometer Sniffer or Spray test. This test is described in ANSI N14.5 and is utilized for all seal integrity acceptance tests on the 10/140MB cask prior to first use and after any seal maintenance or replacement after the cask is in service.

The test utilizes helium gas as the detector medium and a calibrated helium sniffer or probe as the detector. The helium sniffer or probe is calibrated against a standard leak simulator that produces a known leak rate. This device is traceable to the National Bureau of Standards.

The interior cavity or seal area between the redundant seals is evacuated to an indicated pressure below one atmosphere (vacuum). A special test port tool is utilized for the evacuation. After the evacuation, the special test port tool is adjusted to allow the helium sniffer or probe to monitor the evacuated area between the seals. The exterior of the cask seal area is then loosely enveloped to trap helium gas injected into the enclosed area. If any leaks are present greater than $1x10^{-7}$ scc/sec, they will allow the helium to migrate from the positive exterior pressure to the negative interior pressure. This leak will allow the helium to then be monitored by the helium leak probe. The equipment which monitors the probe's input will indicate when the leak rate exceeds the preset acceptance level. Additionally, the seal in the 10/140MB test ports are also tested to $1x10^{-7}$ scc/sec or less. This is done after the main cask seals are tested. The void between the main seals is flooded with helium at one atmosphere pressure and the test port is then sealed. The area on the outside of the test port seal is evacuated using a special tool and the helium detector is exposed to the evacuated area. If a leak is present, the leak detector will so indicate. If the leak detector indicates a leak rate of

$1x10^{-7}$ scc/sec or less, the seal integrity of the 10/140MB cask is acceptable and the test has been completed successfully.

However, if the leak rate exceeds the acceptance criteria, the test is stopped and the cask seals are re-inspected for proper size, condition and installation. The test should be repeated no more than three times. If the seals do not pass on the third attempt, a Quality Discrepancy Report (QDR) is prepared and submitted to NuPac QA and Engineering for disposition in accordance with the requirements of the NRC approved NuPac QA System.

9.0 QUALITY ASSURANCE

The NuPac 10/140MB Cask has been designed and will be fabricated by Nuclear Packaging, Inc., (NuPac) Federal Way, Washington. The Quality Assurance Program used for the design, fabrication, assembly, testing, use and maintenance of the NuPac 10-140 cask satisfies the eighteen (18) criteria of 10 CFR 71, Subpart H in its entirity. NuPac's Quality Assurance Program meeting these criteria has been submitted to the United States Nuclear Regulatory Commission and has been awarded Approval Number 0192, Revision 2.

In addition, the QA program and the implementation of it during the design and fabrication phases will adhere to NuReg CR-3854, Category III requirements.

A synopsis of the Pacific Nuclear Systems, Inc./Nuclear Packaging, Inc. Quality Assurance Program follows:

9.1 Introduction

Pacific Nuclear Systems, Inc. (PNSI) has developed a quality program to (1) assure traceability, and (2) control the quality of all materials and processes utilized in the production of radioactive shielding, casks, containers, and other equipment pertaining to shipping packages for irradiated fuel, high level waste, and plutonium.

A Quality Manual delineates requirements and procedures necessary to exercise control over design, documentation, procurement, material, fabrication, inspection, operational testing, equipment operation and use, maintenance, repair, modification, inventory, shipment and quality data retention.

The PNSI Quality Program is implemented by Quality Procedures which are designed and administered to meet the 18 criteria of 10 CFR 71, Subpart H. The Quality Program is implemented throughout the company and its subsidiaries. The Subsidiaries include: Pacific Nuclear Systems, Inc., Nuclear Packaging, Inc., NuPac Leasing, Inc., and Pacific Nuclear Systems and Services, Inc.

9.2 Description of the PNSI, 10 CFR 71, Subpart H Quality Program

9.2.1 Organization

Full responsibility for the Quality Assurance (QA) Program adherence to 10 CFR 71, Subpart H criteria rests with PNSI. Quality Program activities include calibration of measuring equipment, non-destructive examination (NDE), and materials testing. PNSI surveys and qualifies all organizations performing these services to assure adherence to the 18 criteria prior to their use. All other quality activities are performed by PNSI quality personnel. However, the responsibility of the control of quality in the other organizations continues to rest with PNSI.

PNSI's President has full authority over all functions of the company, and delegates authority and responsibility for selected functions to other personnel within the company.

The administrative function includes financial, legal, and marketing activities.

Procurement department personnel perform purchasing activities and maintain supplier performance records. The Engineering Department is responsible for research and development of shipping container technology, design of casks for licensing and fabrication, and design documentation.

The PNSI Quality Department has sufficient authority and organizational freedom to identify quality programs, implement corrective action, and verify corrective action effectiveness.

Additionally, the Quality Department is independent from other organizations within PNSI and reports directly to the President of PNSI. The Quality Department is headed by the Corporate Quality Director who is responsible for the development, implementation, and administration of the entire PNSI Quality

Program. He must have sufficient expertise in the entire field of Quality to enable him to direct the entire quality function in close adherence to the 18 criteria of 10 CFR 71 and the PNSI Quality Manual. Responsibility for development of quality acceptance requirements, inspections, and NDE activities rests with the Corporate Quality Director. It is his responsibility to delegate and evaluate the performance of all quality related tasks for PNSI through the authority of the president.

It is delineated in writing through the Corporate Quality Director that designated QA personnel have the authority to prevent the continued processing, fabrication, installation, or delivery of unsatisfactory work.

This authority also extends to the quality monitoring of special processes utilizing PNSI equipment, personnel and procedures such as waste processing, in-service inspections, etc.

Production responsibilities include scheduling or in-service inspection and administration of all fabrication activities, both within PNSI and at qualified suppliers. The shipping and receiving function is also the responsibility of the Production Department.

On-site activities such as waste processing, in-service inspections, etc. are administered as a joint effort of the operations and engineering personnel. Quality supports these activities with written procedures that provide methods, process control, and check points. Inspection personnel perform monitoring activities and verifications of regulatory, contractual, and technical requirements during these operations.

The Corporate Quality Director and all other quality personnel and/or organizations within, or utilized by PNSI, are fully qualified for their quality responsibilities. Qualification records are maintained in the PNSI Quality Record File.